

HIGH-THROUGHPUT APPROACHES FOR THE ASSESSMENT OF FACTORS
INFLUENCING BIOAVAILABILITY OF SMALL MOLECULES IN PRE-CLINICAL DRUG
DEVELOPMENT

By

Megan M. McCallum

A Dissertation Submitted in
Partial Fulfillment of the
Requirements for the Degree of

Doctor of Philosophy
in Chemistry

at

The University of Wisconsin – Milwaukee

May 2013

ABSTRACT

HIGH-THROUGHPUT APPROACHES FOR THE ASSESSMENT OF FACTORS INFLUENCING BIOAVAILABILITY OF SMALL MOLECULES IN PRE-CLINICAL DRUG DEVELOPMENT

by

Megan M. McCallum

The University of Wisconsin – Milwaukee, 2013
Under the Supervision of Professor Alexander (Leggy) Arnold

A bioactive molecule must pass many hurdles to be designated as a “good” pharmaceutical lead or hit compound. It should have a significant activity, selectivity, bioavailability, and metabolic half-life. Many factors have been identified that influence the free drug concentration or bioavailability of orally administered drugs in the earliest development stages. *In vitro* pre-clinical assays have been developed to measure these parameters. The small molecule properties that are investigated here include aqueous solubility, permeability, reactivity (electrophilicity), small molecule-protein binding, and displacement of protein-bound molecules (drug-drug interactions). The development of rapid and miniaturized assays to quantify these factors is presented herein.

First, a 384-well filter plate based assay was developed to determine the aqueous compound solubility to greatly decrease the time and amount of compound necessary for analysis. Secondly, one of the most common and simple permeability assays (parallel artificial membrane permeability assay, PAMPA) was optimized using a filter membrane impregnated with a long chain alkane (hexadecane)

solution as an artificial membrane. Thirdly, permeability was also determined rapidly with the use of Immobilized Artificial Membrane (IAM) and C18 stationary phases by HPLC. The solitary and sequential usage of these columns was compared.

Fourthly, a novel fluorescence-based high-throughput assay was developed to identify electrophilic molecules rapidly, in parallel, among small molecule libraries using only sub-milligram quantities. Subsequently, a filtration-based assay to estimate compound binding with plasma protein was developed for a 384-well plate format. This assay not only increases the throughput, but also addresses non-specific compound binding to the filtration apparatus, which is problematic with other ultra-filtration methods. Finally, a simple high-throughput competitive protein binding assay was developed based on the multiplexing of fluorescent small molecule probes with different spectroscopic and binding properties. The inhibition of probe-protein binding has been identified as a good indicator for plasma protein binding.

© Copyright by Megan M. McCallum, 2013
All Rights Reserved

TABLE OF CONTENTS

LIST OF FIGURES.....	viii
LIST OF TABLES	xiv
CHAPTER I. INTRODUCTION	1
1. Introduction of Drug Discovery and Development	1
2. Bioavailability	2
3. High-Throughput <i>In Vitro</i> Pre-clinical Assays	4
4. Analytical Methods in High-Throughput Screening.....	11
4.1. Absorbance Spectroscopy.....	11
4.2. Fluorescence Spectroscopy.....	14
4.3. High Performance Liquid Chromatography	21
4.4. Mass Spectrometry	25
CHAPTER II. AQUEOUS SOLUBILITY	33
1. Introduction	33
2. Experimental.....	36
2.1. Materials and Instrumentation.....	36
2.2. Solubility Assay.....	37
3. Results and Discussion	39
4. Conclusions.....	42
CHAPTER III. MEMBRANE PERMEABILITY	44
PART 1: PARALLEL ARTIFICIAL MEMBRANE PERMEABILITY ASSAY (PAMPA). 44	
1. Introduction	44
2. Experimental.....	51

2.1. Materials and Instrumentation.....	51
2.2. PAMPA.....	52
3. Results and Discussion	54
4. Conclusions.....	56
PART 2: PERMEABILITY BY HPLC METHODS	58
1. Introduction	58
2. Experimental.....	61
2.1. Materials and Instrumentation.....	61
2.2. HPLC Permeability Assay	63
2.3. Octanol/Water Partitioning	63
3. Results and Discussion	64
4. Conclusions.....	69
CHAPTER IV. ELECTROPHILICITY	71
1. Introduction	71
2. Experimental.....	74
2.1. Materials and Instrumentation.....	74
2.2. Generation of MSTI	75
2.3. Thiol Reactivity Assay.....	76
3. Results and Discussion	78
4. Conclusions.....	91
CHAPTER V. PROTEIN-SMALL MOLECULE BINDING.....	92
PART 1: HIGH-THROUGHPUT ULTRAFILTRATION	92
1. Introduction	92
2. Experimental.....	97
2.1. Materials and Instrumentation.....	97

2.2. High-Throughput Ultrafiltration Assay.....	98
3. Results and Discussion	99
4. Conclusions.....	104
PART 2: COMPETITIVE PROTEIN BINDING	105
1. Introduction	105
2.1. Materials and Instrumentation.....	108
2.2. Protein Binding Assay.....	110
3. Results and Discussion	111
4. Conclusions.....	125
APPENDIX A	127
APPENDIX B	131
APPENDIX C.....	139
APPENDIX D	188
REFERENCES	239

LIST OF FIGURES

FIGURE	PAGE
Figure 1. Drug development pipeline with the general purpose of each stage.	2
Figure 2. The relationship of adsorption, distribution, binding, metabolism, and excretion of a drug on the free drug concentration available to the site of action.	3
Figure 3. In vitro pre-clinical screens studying the absorption, distribution, metabolism, excretion, and toxicity (ADMET) of drug candidates.	5
Figure 4. Incident light, I_0 , passing through the sample of path-length b , resulting in a diminished intensity of light, I , emerging from the sample.	12
Figure 5. Schematic of a UV-Vis spectrophotometer.	14
Figure 6. Jablonski diagram for fluorescence. (i) absorption of a photon to an excited state, (ii) internal conversion to S_1 , (iii) fluorescence, (iv) non-radiative decay, (v) intersystem crossing to T_1 , (vi) phosphorescence, (vii) non-radiative decay.	16
Figure 7. Generic absorbance and fluorescent emission spectra where the Stokes shift is the difference between the peaks in the spectra.	17
Figure 8. Schematic representation of a conventional spectrofluorometer.	19
Figure 9. Schematic of spectrofluorometer used to read microplates.	20
Figure 10. Basic schematic of HPLC.	24
Figure 11. Schematic diagram of a mass spectrometer with HPLC as the sample introduction system.	26
Figure 12. Positive ion generation mechanism by electrospray ionization.	27
Figure 13. Positive ion generation mechanism by atmospheric pressure chemical ionization.	28
Figure 14. Positive ion formation by APCI.	29
Figure 15. Applied RF and DC voltages to the rods in the quadrupole mass analyzer.	30
Figure 16. Ion detection system.	31

Figure 17. Illustration of PAMPA plates. A) 96-well filter plate pre-coated with an artificial membrane with a matched 96-well receiver plate. B) Solutions of the compounds in buffer are added to the filter plate on top of the artificial membrane (donor plate), while buffer is added to the receiver plate (acceptor plate).....	48
Figure 18. Example of a PAMPA assay performed in a multi-well plate.....	48
Figure 19. Functional diagram of the Loc-I-Gut technique used for the determination of human <i>in vivo</i> permeability and absorption.	50
Figure 20. IAM column with immobilized phosphatidylcholine on aminopropyl silica with alkyl endcapping.	59
Figure 21. The partitioning of small molecules through a lipid is hypothesized to be modeled by the retention and/or partitioning of the molecules as they pass through IAM-C18-IAM column in series.....	61
Figure 22. Correlation between the log of the retention factor on a C18 column and the HDM-PAMPA logP at pH 7.2.....	65
Figure 23. Relationship between log k' and log P _{eff} on A) coupled IAM-C18-IAM columns in series, B) coupled C18-IAM columns in series, C) coupled IAM-C18 in series, and D) C18 column.	66
Figure 24. Relationship between A) log P _{eff} and B) log P (HDM-PAMPA at pH 7.2) versus log k' on the IAM column.....	67
Figure 25. Octanol/Water partitioning correlation to A) logP _{eff} B) logP _{HDM-PAMPA} C) logk' _{C18} and D) logk' _{IAM}	68
Figure 26. Correlation between HDM-PAMPA and effective permeability values from intestinal perfusion (P _{eff}).....	69
Figure 27. Formation of glutathione (GS) adducts with electrophilic species. 1) Displacement reaction, 2 and 3) addition to activated double bonds, 4) opening of a strained ring.....	72
Figure 28. <i>In Situ</i> conversion from Acetyl-MSTI to MSTI	76
Figure 29. Electrophilic molecule addition to MSTI.	77
Figure 30. A) Absorbance spectra of 500 μM acetyl-MSTI and MSTI in PBS at pH 7.4. B) Fluorescence spectra of 200 μM acetyl-MSTI and MSTI in PBS at pH 7.4 with an excitation wavelength of 510 nm.....	79

Figure 31. Absorbance spectra dependence of 200 μ M MSTI on buffer composition.....	80
Figure 32. Absorbance spectra dependence of 200 μ M MSTI on buffer pH.....	80
Figure 33. Absorbance spectra dependence of 200 μ M MSTI on buffer ionic strength.	81
Figure 34. Concentration of MSTI versus absorbance and fluorescent intensity.....	81
Figure 35. Compound key for Figures 36, 37, and 38.....	82
Figure 36. Evaluation of the MSTI assay in the presence of small molecules, PBS (50 mM, pH 7.4, 150 mM NaCl), MSTI (30 μ M) and an excitation and emission wavelength of 510 nm and 650 nm, respectively. Change of fluorescence intensity in the presence of small molecules 1-7 (Compound Key, Figure 35) (100 μ M) and different additives (n=3).	83
Figure 37. Change of the fluorescence intensity in the presence of small molecules 1-7 (100 μ M) with 2% DMSO, 5% methanol, and 0.01% NP-40 by volume in PBS at different time points (n=3). PBS (50 mM, pH 7.4, 150 mM NaCl), MSTI (30 μ M) and an excitation and emission wavelength of 510 nm and 650 nm, respectively (Compound Key, Figure 35).....	84
Figure 38. Change of the fluorescence intensity in the presence of small molecules 1-7 (50, 100 and 150 μ M) with 2% DMSO, 5% methanol, and 0.01% NP-40 by volume in PBS. PBS (50 mM, pH 7.4, 150 mM NaCl), MSTI (30 μ M) and an excitation and emission wavelength of 510 nm and 650 nm, respectively (Compound Key, Figure 35).....	85
Figure 39. Results of MSTI-LOPAC screen (1280 compounds), n=3.	86
Figure 40. Summary of the Z' values of each assay plate.....	87
Figure 41. Normalized fluorescence data of a single 384-well LOPAC compound plate in triplicate with their standard deviation.	87
Figure 42. A) Fluorescence intensity (FI) (510nm/650nm) of all LOPAC compounds; B) Structures of fluorescently interfering compounds.	88
Figure 43. Thiol-reactive compound classes identified by the MSTI assay.....	90
Figure 44. Equilibrium dialysis method for the determination of plasma-protein binding.....	93
Figure 45. Ultrafiltration method for determination of drug-protein binding.	94
Figure 46. Diagram of surface plasmon resonance (SPR).....	95

Figure 47. Calibration plot correlating absorbance with concentration of standard molecules at the λ_{\max} at each of the molecules, respectively. Slope of the line for each molecule given in the table with standard deviation.	101
Figure 48. Structures of Mega Red and Nile Red with wavelengths of excitation and emission in PBS with 0.5 mg/mL HSA.....	105
Figure 49. Jablonski diagram describing the fluorescence process including solvent relaxation and (twisted) intramolecular charge transfer. ¹⁴⁶	106
Figure 50. A) Absorbance and fluorescence spectra at 514 nm excitation of Mega Red in PBS with 0.5 mg/mL HSA. B) Absorbance and fluorescence spectra at 570 nm excitation of Nile Red in PBS with 0.5 mg/mL HSA.....	111
Figure 51. Serial dilution of A) Mega Red and B) Nile Red in PBS with varying concentrations of HSA.....	111
Figure 52. Z' value (without HSA, positive control; with HSA, negative control) with changing concentration of HSA and A) Mega Red or B) Nile Red.....	112
Figure 53. Binding response of one standard molecule, naproxen, with changing buffer composition.	113
Figure 54. Standard molecule displacement of 500 nM Mega Red and Nile Red in PBS with 10% glycerol and 0.01% NP-40 in comparison with literature values for <i>in vivo</i> plasma protein binding (n=3). Larger of the values, in gray, for % bound (i.e., probe displaced) is taken for the plot. Dotted line correlates to the cutoff for low protein binding molecules and the dashed line correlates to the cutoff for high protein binding molecules.....	116
Figure 55. Results of the LOPAC screen (1280 compounds) with cutoff for medium and high binding cutoff values at 20% and 40%.	118
Figure 56. P2 receptor antagonists identified as protein binding hit molecules.....	118
Figure 57. Selected hormones identified as protein binding hit molecules.....	119
Figure 58. Prostaglandin synthesis inhibitors (COX 1&2) identified as protein binding hit molecules.	120
Figure 59. A) Fluorescence intensity (514/532 nm and 570/640 nm) of all LOPAC compounds (white points correspond to background at 514/532 nm, grey points correspond to background at 570/640 nm); B) Structures of fluorescently interfering compounds, fluorescent intensity (FI) at 514/532 nm in black and 570/640 nm in grey.	121

Figure 60. Binding dose-response curves for A) naproxen, B) piroxicam, C) β -estradiol, and D) diethylstilbestrol with corresponding IC ₅₀ values.	122
Figure 61. Isothermal titration calorimetry results for the binding of naproxen (350 μ M) and HSA (50 μ M) in fluorescence assay buffer. A) Plot of peak areas for each injection in correlation with analysis time. (n=2) B) Enthalpogram for the titration of naproxen into HSA with 20- 2.02 μ L injections. C) Thermodynamic data from the fit lines in A.	124
Figure 62. Mass spectrum of 2-iodoacetamide-MSTI conjugate; ESI probe, 80 V entrance cone, 3 mV capillary, and 350 °C probe temperature.	182
Figure 63. Fluorescence spectrum of 2-iodoacetamide-MSTI conjugate with an excitation wavelength of 510 nm.	182
Figure 64. Addition of MSTI to small molecule 1 to form adduct molecule 1c.	183
Figure 65. Mass spectrum of adduct molecule 1c formed in Scheme 1. Mass spectrum of the assay mixture in Scheme 1 which confirms the formation of adduct of MSTI with the small molecule (Molecule 1). ESI probe, 120 V entrance cone, 3 mV capillary, and 350 °C probe temperature.	183
Figure 66. Addition of MSTI to small molecule 2 to form adduct molecule 2c.	184
Figure 67. Mass spectrum of adduct molecule 2c formed in Scheme 2. Mass spectrum of the assay mixture in Scheme 1 which confirms the formation of adduct of MSTI with the small molecule (Molecule 2). ESI probe, 40 V entrance cone, 3 mV capillary, and 350 °C probe temperature.	184
Figure 68. Addition of MSTI to small molecule 3 to form adduct molecule 3c.	185
Figure 69. Mass spectrum of adduct molecule 3c formed in Scheme 3. Mass spectrum of the assay mixture in Scheme 3 which confirms the formation of adduct of MSTI with the small molecule (Molecule 3). ESI probe, 40 V entrance cone, 3 mV capillary, and 350 °C probe temperature.	185
Figure 70. Conversion of acetyl-MSTI to MSTI analyzed by LC-MS. A) Chromatogram of acetyl-MSTI B) Chromatogram of MSTI after conversion at pH 12 with approximately 20% acetyl-MSTI remaining.	186
Figure 71. Mass spectra of MSTI (A) and acetyl-MSTI (B), corresponding to the chromatograms in Figure 6. ESI probe, 80 V entrance cone, 3 mV capillary, and 350 °C probe temperature.	187
Figure 72. Standard small molecule displacement of 500 nM Mega Red and Nile Red in PBS with 5% glycerol and 0.01% NP-40 by volume in the presence of 0.2 mg/mL HSA (n=3). Average of literature values for <i>in vivo</i> plasma	

protein binding are given in comparison. Larger % bound values used for the plot.....	188
Figure 73. Standard small molecule displacement of 500 nM Mega Red and Nile Red in PBS with 10% glycerol and 0.01% NP-40 by volume in the presence of 0.2 mg/mL HSA (n=3). Averages of literature values for <i>in vivo</i> plasma protein binding are given in comparison. Larger % bound values used for the plot.	189
Figure 74. Standard small molecule displacement of 500 nM Mega Red and Nile Red in PBS with 20% glycerol and 0.01% NP-40 by volume in the presence of 0.2 mg/mL HSA (n=3). Averages of literature values for <i>in vivo</i> plasma protein binding are given in comparison. Larger % bound values used for the plot.	190
Figure 75. Standard small molecule displacement of 500 nM Mega Red and Nile Red in PBS with 10% glycerol by volume in the presence of 0.2 mg/mL HSA (n=3). Averages of literature values for <i>in vivo</i> plasma protein binding are given in comparison. Larger % bound values used for the plot.	191
Figure 76. Standard small molecule displacement of 500 nM Mega Red and Nile Red in PBS with 10% glycerol and 2% DMSO by volume in the presence of 0.2 mg/mL HSA (n=3). Averages of literature values for <i>in vivo</i> plasma protein binding are given in comparison. Larger % bound values used for the plot.....	192
Figure 77. Standard small molecule displacement of 500 nM Mega Red and Nile Red in PBS with 10% glycerol and 0.001% NP-40 by volume in the presence of 0.2 mg/mL HSA (n=3). Averages of literature values for <i>in vivo</i> plasma protein binding are given in comparison. Larger % bound values used for the plot.	193
Figure 78. Standard small molecule displacement of 500 nM Mega Red and Nile Red in PBS with 500 mM NaCl in the presence of 0.2 mg/mL HSA (n=3). Averages of literature values for <i>in vivo</i> plasma protein binding are given in comparison. Larger % bound values used for the plot.....	194
Figure 79. Standard small molecule displacement of 500 nM Mega Red and Nile Red in PBS at pH 8.0 in the presence of 0.2 mg/mL HSA (n=3). Averages of literature values for <i>in vivo</i> plasma protein binding are given in comparison. Larger % bound values used for the plot.....	195
Figure 80. Standard small molecule displacement of 500 nM Mega Red and Nile Red in 200 mM HEPES buffer at pH 7.4 in the presence of 0.2 mg/mL HSA (n=3). Averages of literature values for <i>in vivo</i> plasma protein binding are given in comparison. Larger % bound values used for the plot.	196

LIST OF TABLES

TABLE	PAGE
Table 1. Preparation of calibration plate for solubility assay.....	37
Table 2. Preparation of solution for solubility assay.....	38
Table 3. Solubility results of the standard small molecules by the standard method in comparison to the miniaturized method.....	40
Table 4. Aqueous solubility of a series of N-((2-methyl-1H-indol-3-yl)(phenyl)methyl)pyridin-2-amine molecules.....	41
Table 5. Aqueous solubility of a series of N-((2-methyl-1H-indol-3-yl)(phenyl)methyl)aniline molecules.....	42
Table 6. Comparison of PAMPA values.....	54
Table 7. HDM-PAMPA (pH 7.2) values for a series of N-((2-methyl-1H-indol-3-yl)(phenyl)methyl)pyridin-2-amine molecules.....	55
Table 8. HDM-PAMPA (pH 7.2) values for series of N-((2-methyl-1H-indol-3-yl)(phenyl)methyl)aniline molecules.....	56
Table 9. Calculated percent bound of standard small molecules after high-throughput ultrafiltration method with varying volumes of 10 mM compound solution in DMSO (n=3) in comparison to literature <i>in vitro</i> values. ($x = A_e$ greater than A_0)	100
Table 10. Calculated percent bound of standard small molecules after high-throughput ultrafiltration method with 2 μ L of 10 mM compound solution in DMSO (n=3) and 0.01% NP-40 and 0.01% NP-40 with 10% glycerol (v/v) in comparison to literature <i>in vitro</i> values. ($x = A_e$ greater than A_0) ...	102
Table 11. Calculated percent bound of standard small molecules after high-throughput ultrafiltration method with 1 μ L of 10 mM compound solution in DMSO (n=3) with 0.01% NP-40, detection by UV absorbance and LC-MS in comparison to literature <i>in vitro</i> values. ($x = A_e$ greater than A_0)	103
Table 12. Solubility assay results of compound library (n=4).....	127
Table 13. Results of HDM-PAMPA assay for compound library (n=3).....	131
Table 14. Results for IAM-C18-IAM coupled columns.....	135

Table 15. Results for C18-IAM coupled columns.	135
Table 16. Results for IAM-C18 coupled columns.	136
Table 17. Results for C18 column.	136
Table 18. Results for IAM column.	137
Table 19. Octanol/water partitioning coefficients at pH 7.2 beginning with 1mg/mL compound solutions in 1-octanol.	137
Table 20. Octanol/water partitioning coefficients at pH 7.2 beginning with 1mg/mL compound solutions in phosphate buffered saline.	138
Table 21. Results of fluorescence-based electrophile screen of the LOPAC library. Values are presented as a percent of the MSTI signal (Avg. %). (n=3).....	139
Table 22. Results of fluorescence-based drug-protein binding screen of the LOPAC library. Values are percent of Mega Red and Nile Red displaced. (n=3)	197

LIST OF ABBREVIATIONS

HTS	High-throughput Screening
HT	High-throughput
ADME	Absorption, distribution, metabolism, and excretion
ADMET	Absorption, distribution, metabolism, excretion, and toxicity
PAMPA	Parallel artificial membrane permeability assay
MDCK	Madin-Darby canine kidney epithelial cells
LC-MS	Liquid chromatography- mass spectrometry
RBC	Red blood cells
CYP	Cytochrome P450 enzymes
CL _{int}	Intrinsic clearance
CHO	Chinese hamster ovary cells
hERG	Human ether-à-go-go related gene
UV	Ultra violet
HPLC	High performance liquid chromatography
NIH	National Institutes of Health
PMT	Photomultiplier tube
HETP	Height equivalent to a theoretical plate
MS	Mass spectrometry
API	Atmospheric pressure ionization
RF	Radiofrequency
DC	Direct current
ESI	Electrospray ionization
APCI	Atmospheric pressure chemical ionization
AC	Alternating current
DMSO	Dimethylsulfoxide
SD or σ	Standard deviation
LLC-PK1	Lewis lung carcinoma – Porcine kidney cells
BCS	Biopharmaceutics classification system
HDM-PAMPA	Hexadecane membrane – parallel artificial membrane permeability assay

PBS	Phosphate buffered saline
IAM	Immobilized artificial membrane HPLC column
ILC	Immobilized liposome chromatography
logP _{o/w}	Log of the octanol/water partitioning
GSH	Reduced glutathione
MSTI	(<i>E</i>)-2-(4-mercaptostyryl)-1,3,3-trimethyl-3 <i>H</i> -indol-1-ium
Acetyl-MSTI	(<i>E</i>)-2-(4-(acetylthio)styryl)-1,3,3-trimethyl-3 <i>H</i> -indol-1-ium
NP-40	Nonylphenyl polyethylene glycol, non-ionic surfactant
LOPAC	Library of Pharmacologically Active Compounds
SPR	Surface plasmon resonance
HSA	Human serum albumin
MWCO	Molecular weight cutoff
ANS	4-Anilinonaphthalene-8-sulfonate
BSA	Bovine serum albumin
ICT	Intramolecular charge transfer
TICT	Twisted intramolecular charge transfer
Mega Red	(<i>E</i>)-1-(5-carboxypentyl)-2-(2-(7-(diethylamino)-4-hydroxy-2-oxo-2 <i>H</i> -chromen-3-yl)vinyl)-3,3-dimethyl-3 <i>H</i> -indol-1-ium-5-sulfonate
Nile Red	9-(diethylamino)-5 <i>H</i> -benzo[α]phenoxazin-5-one
ITC	Isothermal titration calorimetry
K _a	Association constant, 1/K _d
K _d	Dissociation constant

CHAPTER I

INTRODUCTION

1. Introduction of Drug Discovery and Development

The complete drug development process is generally thought to occur in four stages: target identification, drug discovery, clinical trials, and FDA approval before subsequent production (Figure 1). The focus of the drug discovery phase is the identification of potent, selective, and bioavailable drug candidates (lead compounds) that have *in vivo* activity. In the early stages of drug discovery, biochemical assays are applied to enable the screening of diverse compounds against the target protein (high-throughput screening, HTS).¹ With the advent of combinatorial chemistry and parallel synthesis, these small molecule libraries can be produced rapidly.² The characterization of derivatives of hit molecules is done to determine structure-activity relationships for each compound class and develop optimized drug candidates or lead compounds. Because of the vast numbers of molecules that are analyzed for each potential target, high-throughput assays are preferred in the early drug discovery stages.

The pharmaceutical industry and academic drug discovery laboratories rigorously test small molecule drug candidates to ensure that compounds with poor physiological properties do not advance. Failure to do so will consume resources, time, and interest which could have been expended on more promising compounds in the later stages of drug development. Therefore, it is crucial for pre-clinical drug discovery efforts to identify those drug candidates that will be readily absorbed and

distributed throughout the body in an early stage. It can also be argued that it may be more important to identify those compounds that are *not* absorbed or distributed. The characterization is necessary so that a sensible choice can be made as to whether to put forth the effort in formulation or modification of drug candidates. Early *in vitro* pre-clinical screening has been enforced to identify problematic compounds within screening libraries yielding increased efficiency and success.³⁻⁵ This is accomplished by the use of high-throughput (HT) assays that determine pre-clinical small molecule properties, in parallel, for thousands of compounds using low-milligram quantities.⁴ With the continuing development of HT pre-clinical assays, there has been an increasing need for improvements in efficiency and accuracy.

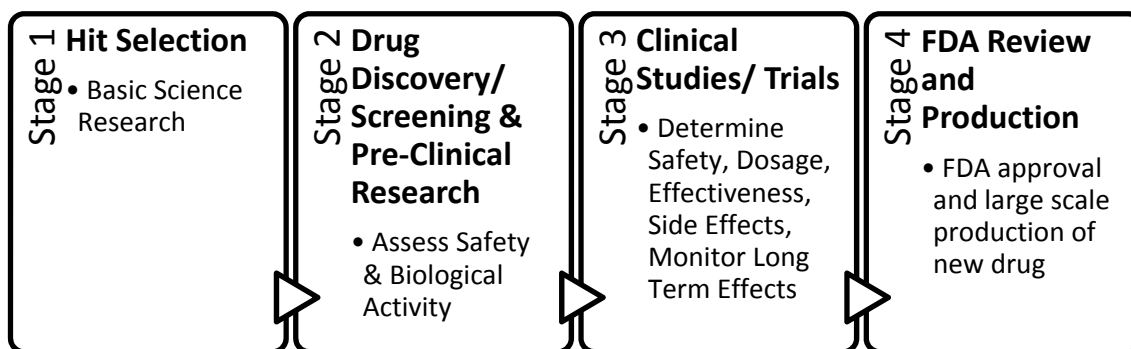


Figure 1. Drug development pipeline with the general purpose of each stage.

2. Bioavailability

Oral bioavailability of a drug is defined as the measure of the rate and extent of the drug reaching the systemic circulation and its availability at the site of action.⁶ Poor oral bioavailability is one of the leading causes of failure for drug candidates in clinical studies. Compounds with low bioavailability exhibit a high variability in free

drug concentrations between individuals.⁷ Bioavailability is a key factor that affects drug efficacy and other adverse effects, which has therefore received considerable attention.⁷

Currently, it is difficult to predict bioavailability because there are numerous factors that are related to the free drug concentration *in vivo*. Some of these factors include physicochemical properties (i.e., dissolution, solubility, and absorption), biological factors (i.e., permeability, protein binding, metabolism, excretion), diet factors (i.e., food-drug interactions), and finally, co-administered drug factors (i.e., drug-drug interactions). Figure 2 depicts the general pathway of an orally administered drug throughout the body. Absorption, distribution, binding, metabolism, and excretion (ADME) of a drug is directly related to its free concentration available at the site of action.⁸

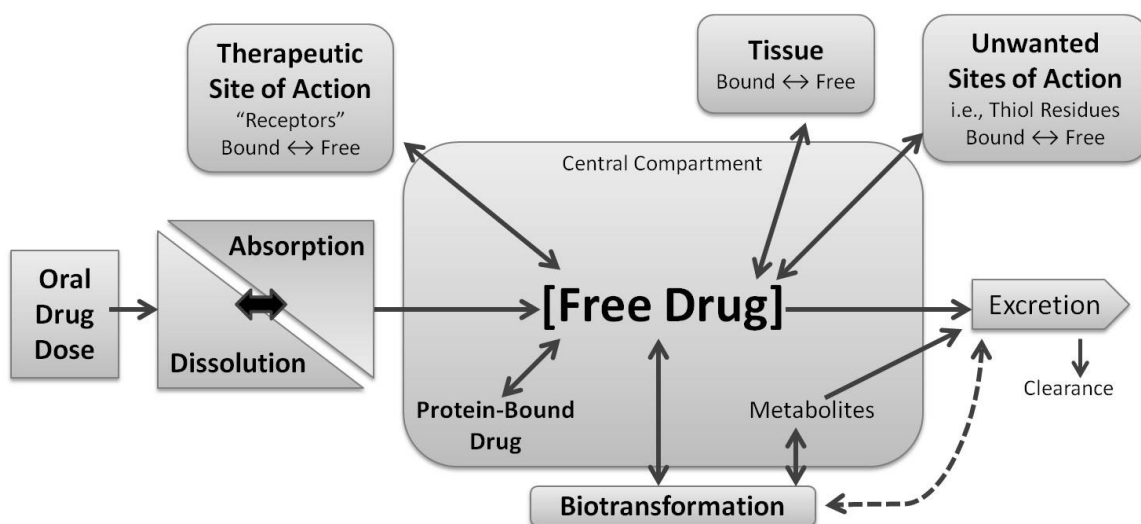


Figure 2. The relationship of adsorption, distribution, binding, metabolism, and excretion of a drug on the free drug concentration available to the site of action.⁸

Because of the numerous factors that affect oral bioavailability, it cannot be fully quantified with the use of *in vitro* assays solely. The most effective alternative is to measure those individual factors influencing bioavailability (solubility, permeability, non-specific binding, metabolism, etc.). Continued progress to develop better assays for the understanding of physicochemical and biochemical profiling of drug or drug-like molecules is therefore needed to improve the characterization of drug candidates with respect to bioavailability.⁷

3. High-Throughput *In Vitro* Pre-clinical Assays

Understanding the interactions between drug candidates and potential molecular targets is essential to estimate *in vivo* safety and to reduce late-stage failures of drugs in the development process.⁹ The pre-clinical development process is a type of risk assessment that extrapolates *in vitro* safety and efficacy information to a potential *in vivo* result.¹⁰ In general, drug candidates are evaluated with respect to absorption, distribution, metabolism, excretion, and toxicity (ADMET) through a number of different assays, as depicted in Figure 3. Even with the current number of primary and secondary screens reported, there is still insufficient *in vitro* information to estimate critical pharmacokinetic variables such as clearance and bioavailability.¹⁰ Therefore, additional assays to predict *in vivo* ADMET properties of drug candidates are needed.

The cellular absorption of molecules is studied with a number of different assays. One of the earliest assays performed during pre-clinical screening is the aqueous solubility assay. The detailed descriptions of the solubility assays are

found in Chapter 2. Aqueous solubility is determined in the earliest stage because poor solubility can have a negative effect on any subsequent screens. Compound solubility can be assessed in buffer solutions with different pH values to mimic the environment of different physiological locations (e.g., stomach, gut, blood). The “gold standard” for solubility determination is the thermodynamic shake flask assay.¹¹

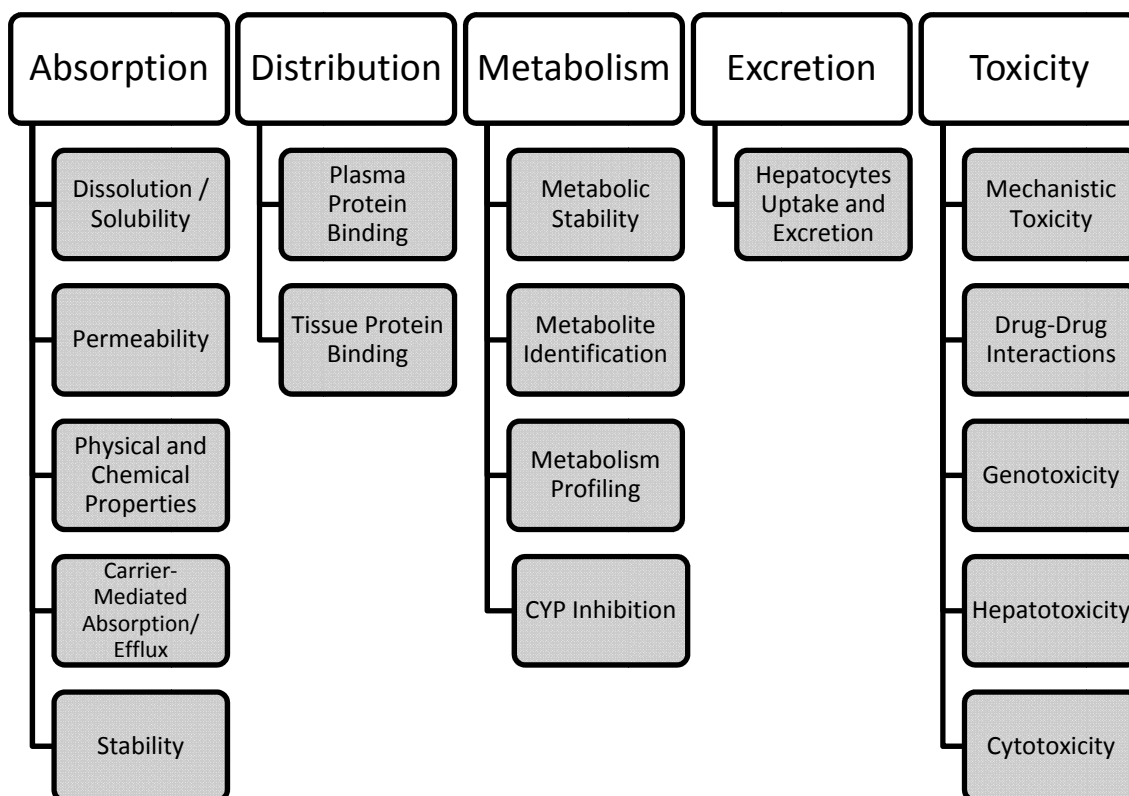


Figure 3. In vitro pre-clinical screens studying the absorption, distribution, metabolism, excretion, and toxicity (ADMET) of drug candidates.⁹

Once the molecule is solubilized, it can be more effectively absorbed by the body. Absorption of molecules is studied by assessing their membrane permeability. The most common permeability assays are discussed in detail in Chapter 3. The “gold standard” of permeability assays uses a layer of human colon epithelial cancer (Caco-2) cells grown on a filter. The diffusion of molecules across this layer is quantified by ultraviolet (UV) absorption.^{12, 13} A different high-throughput assay, called the parallel artificial membrane permeability assay (PAMPA), uses an artificial hydrophobic layer to mimic the cell membrane.¹³⁻¹⁵ Recently, chromatographic methods have been investigated that use immobilized lipids.¹⁶ The lipophilicity of molecules correlates strongly with membrane permeability. Therefore, small molecule partitioning coefficients (i.e., $\log P_{\text{octanol/water}}$ or $\log P_{\text{liposome/water}}$) have also been determined to estimate drug absorption.¹⁷ In addition, computational methods enable the calculation of hydrophobic and hydrophilic compound surfaces, which in turn, enables the calculation of partitioning coefficients.⁶

Additional generalizations about molecules with drug-like properties have been proposed by Lipinski, called Lipinski’s Rules of Five.¹⁸ For example, molecules with more than five hydrogen bond donors, a molecular weight over 500, $\log P_{\text{octanol/water}}$ greater than five, or a sum of nitrogen and oxygen atoms within the molecule over ten indicate poor ADME properties.^{18, 19}

Carrier-mediated transport mechanisms of molecules have been studied as well. All of the before-mentioned permeability assays (i.e., Caco-2, PAMPA,

Lipinski's Rules of Five) are representative of passive diffusion of molecules. Highly lipophilic molecules can traverse the lipid bilayer, whereas highly hydrophobic molecules are absorbed by paracellular transport (i.e., between cells). There are numerous membrane transporter systems in the intestines that facilitate the absorption of essential nutrients and drugs.¹⁰ To study the active transport-mediated efflux and absorption, Madin-Darby canine kidney epithelial (MDCK) cells that stably express membrane transporters have been developed.¹⁹ Everted (inside out) intestinal sacs have also been used, providing information that is most similar to *in vivo* human permeability. Unfortunately, inconsistencies in the tissue as well as time and labor-intensive procedures makes this method difficult for routine use.¹⁹

Understanding the stability of a potential drug is vital in the development process because degraded or metabolized drugs may not have the desired pharmaceutical effects. The stability of the molecule can be assessed at varying physiological pH values, which are simply determined by incubating a molecule at or below its solubility value in buffers over a range of pH values. The solution is then analyzed by liquid chromatography-mass spectrometry (LC-MS) to quantify the compound remaining, determine the stability over time, and identify the decomposition products.^{6, 20}

After absorption into the bloodstream, drugs are distributed all over the body. Drug distribution refers to the reversible relocation of the drug from blood to the various tissues in the body.⁶ There are several factors that affect the rate and extent of drug distribution, such as the physicochemical properties of a drug and the

blood flow to the tissues. The distribution of the drug to different tissues directly affects the duration and magnitude of the therapeutic effect and toxicity.⁶ The binding to tissue and plasma proteins has a large effect on the metabolism and distribution of drugs throughout the body.²¹ The plasma protein binding assays that are most commonly used in pre-clinical screens are described in detail in Chapter 5. Equilibrium dialysis is considered the “gold standard” for protein binding analysis.²² Another common method of protein-binding analysis is ultrafiltration. This method is more simple and less time consuming than equilibrium dialysis.²³ Other higher throughput methods include HPLC with immobilized proteins²⁴ or surface plasmon resonance.²⁵ However, these methods assume that immobilized proteins retain the same binding affinities as native proteins.²⁶ Another method for distribution analysis is blood cell partitioning. The compounds are incubated in whole blood or red blood cells (RBC) suspended in plasma, serum or buffer at physiological pH and temperature.²⁷ The drug concentrations in both the whole blood or RBC solutions are determined by HPLC or LC-MS.²⁷

Drugs are cleared from the body by two general pathways; metabolism and excretion. Many drugs primarily undergo excretion, while some drugs are first metabolized. Drug metabolism is important for the elimination of highly lipophilic molecules because these molecules are more readily excreted after undergoing biotransformation toward more polar metabolites.¹⁰ Drug or drug metabolite toxicity and metabolizing enzyme inhibition are major causes for the termination of drug candidacy.²⁸ To study this, compounds are incubated in liver microsomes, liver homogenate (S9 fraction), hepatocytes, or plasma over multiple time points to

assess the half life ($t_{1/2}$) of molecules in the presence of the drug metabolizing cytochrome P450 enzymes (CYP).²⁹ The drug metabolites are then characterized by LC-MS or LC-MS/MS. Reaction phenotyping assays can be performed to identify the enzymes responsible for the metabolism of the compounds. This is done by incubation of the compound of interest with a single enzyme at a time. The identification of enzymes responsible for metabolism (predominately CYP enzymes) can provide important information for potential drug-drug interactions.³ Potential drugs are likely to be withdrawn if they inhibit the metabolism of co-administered drugs.³ If a reduced amount of metabolite is quantified, by fluorescence techniques or LC-MS, the metabolism of that molecule has been inhibited.^{3, 19, 30-32}

Of all of the ADMET properties, excretion is possibly the least studied *in vitro*. Renal and fecal excretions are generally studied using animals, but there are no *in vitro* surrogates for excretion analysis.¹⁹ All drugs are eliminated, to some extent, via the renal route. Large lipophilic molecules must first be converted to more water-soluble products before elimination. The other major organ for drug elimination is the liver via its capacity for biliary excretion.⁶ To estimate the rate of excretion of drugs, the hepatocyte uptake can be analyzed. Hepatic uptake studies typically measure the rate of appearance of substrate into cells after a relatively short incubation period, which assess the impact of hepatic uptake on unbound drug intrinsic clearance (CL_{int}).^{29, 33}

Identification of potential toxicity at an early stage in drug discovery can save both time and costs, and most importantly reduce the likelihood of late-stage failure.

Cardiotoxicity, hepatotoxicity, and neurotoxicity continue to be the most common underlying issues for drug attrition at all stages of development. The use of human cells with retained organ-specific properties is the most important method for early toxicity screening. Some of the primary human cell cultures include hepatocytes for liver toxicity, renal proximal epithelial cells for nephrotoxicity, vascular endothelial cells for vascular toxicity, neuronal and glial cells for neurotoxicity, and cardiomyocytes for cardiotoxicity.¹⁹ Cytotoxicity endpoints such as membrane integrity³⁴, cellular metabolite content³³, mitochondrial functions³⁵, lysosomal functions³⁶, and apoptosis³⁷ are used for the screening of organ-specific toxicity.¹⁹ Cardiotoxicity is commonly analyzed with HEK293 or Chinese hamster ovary (CHO) cells transfected with the human ether-à-go-go related gene (*hERG*). This gene encodes the inward rectifying voltage-gated potassium channel in the heart which is involved in cardiac repolarization. The effect of drugs on the influx of potassium ions is studied with a patch clamp assay.³⁸

Many of these assays can be related to more than one category of ADMET; as with anything in the body, everything is correlated. For example, CYP inhibition can be related to metabolism and toxicity as drug-drug interactions. The lipophilicity of molecules can be correlated to all ADMET properties (permeability, interaction with proteins, metabolic pathway, etc.). Permeability is not only directly related to absorption, but also affects the rate of distribution in the body. With the development of new assays that study ADMET properties of new molecules *in vitro*, a greater understanding of the risk of the molecules can be reached at earlier stages.

4. Analytical Methods in High-Throughput Screening

For the development of new high-throughput assays, the quality of the method of analysis is crucial. The sensitivity, selectivity, and throughput of the analytical method has a direct impact on the validity of the pharmacological assay.³⁹ One of the largest challenges has been the lack of sample capacity for high-throughput quantitative analysis. Obtaining and processing analytical data is usually the rate limiting step in the development process. The analytical methods should provide as much information as possible in the shortest possible time. Ideally, the best way to achieve this would be through the use of techniques that rapidly provide orthogonal information (i.e., based on independent or non-overlapping methods).⁴⁰ Spectroscopic techniques have greatly contributed to the knowledge of how drugs interact with biological systems. Techniques such as absorption and fluorescence spectroscopy are sensitive and non-destructive.⁴¹ Although, mass spectrometry is also sensitive and selective it is a destructive technique. These techniques will be discussed in detail herein.

4.1. Absorbance Spectroscopy

The use of absorbance spectroscopy to measure concentrations of samples in pharmaceutical research is uncommon due to the inability to handle complex mixtures directly. UV detection is generally much faster than other methods, as speed in analysis is very important for high-throughput screening.⁴² Many drug molecules have strongly ultraviolet or visible absorbing chromophores.⁴¹ Although this method is generally simple and rapid, the purity of the sample is important.

Impurities in the sample can lead to interference in the absorbance spectra and may necessitate purification prior to analysis.

In absorption spectroscopy, the amount of light absorbed as a function of wavelength is measured, which can give qualitative and quantitative information about the sample.^{43,44} Molecular absorption spectroscopy of dilute solutions is described by Beer's Law (Equation 1), where A is the absorbance ($\log(I_0/I)$), Figure 4), ϵ is the molar absorptivity ($M^{-1}cm^{-1}$), c is the concentration (M) of the solution, and b is the path length (cm).

$$\text{Equation 1)} \quad A = \epsilon cb ; \text{ where } A = \log \frac{I_0}{I}$$

Beer's equation is used to quantitatively describe how the amount of attenuation is dependent on the concentration of absorbing molecules through the path-length over which absorption occurs. As the light travels through the sample containing the absorbing analyte, a decrease in intensity occurs as the analyte becomes excited, as illustrated in Figure 4. As the path-length increases, the number of absorbing analytes in the path also increases thereby causing an increase in attenuation.⁴⁴

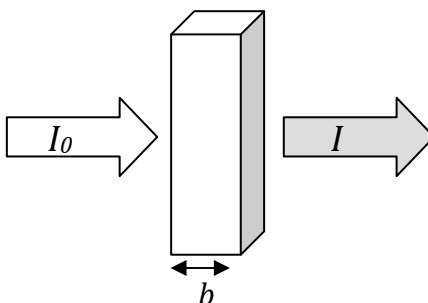


Figure 4. Incident light, I_0 , passing through the sample of path-length b , resulting in a diminished intensity of light, I , emerging from the sample.

Instrumental and chemical interference can cause deviation from Beer's Law. As stated above, Beer's Law describes the absorption of dilute solutions. At concentrations exceeding approximately 10 mM, the average distances between the analyte molecules is diminished by the effect of the charge distribution of neighboring molecules. This effect can also be observed with high concentrations of other species in the sample solution, such as electrolytes. There is also a requirement for monochromatic parallel light and the absence of stray light for Beer's Law to apply. Contaminating light causes the apparent absorbance to be lower than the true absorbance, which has the most significant affect at high absorbance values. The effect of polychromatic or stray light, as well as geometrical factors, can be minimized through better quality instrument design and choice of components.⁴⁴

A representative schematic of a spectrophotometer used as a detector in HPLC is provided in Figure 5. All absorbance spectrophotometers have the same essential components: a light source, monochromator and/or filters, sample cell, and detector. In the example shown in Figure 5, the light sources are deuterium and tungsten-halogen lamps so that the spectral properties can be observed over the ultraviolet and visible wavelength range, respectively. From the source, the light is directed through a monochromator and/or filter to select the wavelength(s) of interest and also to reduce any stray light. The incident light is then passed through the sample in a flow cell (as in Figure 5), cuvette, or microplate with a fixed path-length. Longer path-lengths (typically up to 5 cm) are preferred for dilute solutions,

such as in HPLC. Finally, in certain instruments, the transmitted light is directed through a second monochromator and/or set of filters (used to reduce any stray light again) and finally to the detector. A detector, such as a photomultiplier tube or photodiode array (as in Figure 5) can be used, giving single wavelength or full spectrum absorbance data, respectively.

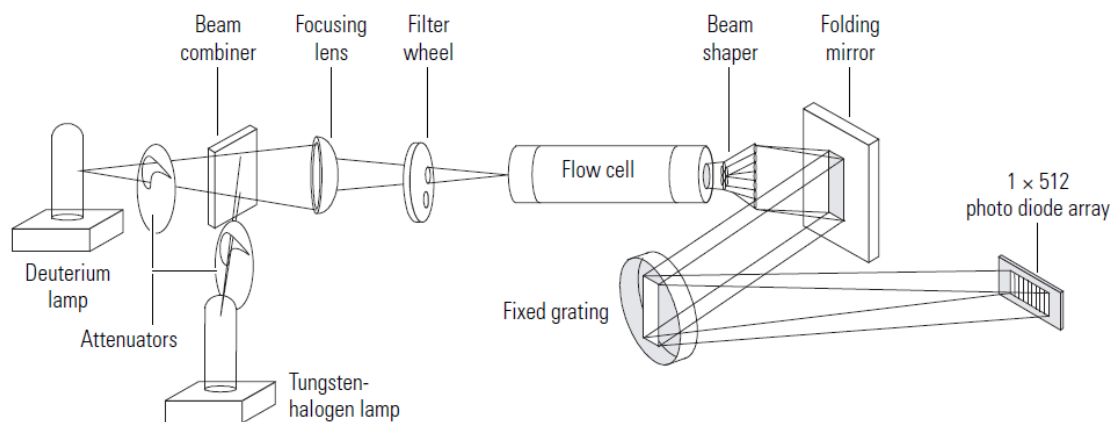


Figure 5. Schematic of a UV-Vis spectrophotometer.⁴⁵

4.2. Fluorescence Spectroscopy

One of the more important features of fluorescence is that it is a highly sensitive and rapid technique. As stated in the previous section, the speed of analysis is very important for high-throughput screening.⁴² It is also selective, as sample impurities should generally not interfere with the analytical wavelength(s) due to the ability to select both the excitation and emission wavelengths. Small fluorescent molecules are an indispensable tool for many bioanalytical methods because they are abundantly used for labeling, substrates, indicators, and stains.

The choice of an ideal fluorophore for a specific purpose can be challenging because of the multitude of molecules available.⁴⁶

The first well-defined small molecule fluorophore identified was quinine. In 1845, Herschel visually observed an emission of a vivid blue color from an aqueous solution of quinine.⁴⁷ Soon after this observation, Stokes was able to show, by the use of rudimentary filters (blue-stained glass and a goblet of yellow-colored wine), that this phenomenon was due to the absorbance and subsequent emission of light. Stokes then coined the term “fluorescence” to describe this process.^{48, 49}

The process of fluorescence is illustrated in the Jablonski diagram⁵⁰ shown in Figure 6. Fluorescence begins when a molecule in its singlet electronic ground state (S_0) absorbs a photon (i). If there is a suitable amount of energy associated with the photon, an electron is then promoted to a higher energy orbital (S_1 or S_2). The energy difference between the S_0 and S_1 energy states is too large for thermal population of the S_1 excited state. Therefore, light is used to induce fluorescence as opposed to heat.⁴⁹ The fluorophore is usually excited to some higher vibrational state within the S_1 or S_2 electronic states. The S_2 excited and higher vibrational states quickly decay (ii) to the lowest vibrational level of the first singlet excited state (S_1) by loss of heat. Then, the decay of the excited state can occur with the emission of a photon (i.e., fluorescence) (iii) or non-radiative decay (iv). The excited state can also undergo intersystem crossing (v) via spin conversion to the triplet excited state (T_1), in which the subsequent relaxation can occur with the emission of a photon (i.e., phosphorescence) (vi) or non-radiative decay (vii). Phosphorescence

is most frequently observed for molecules with heavy atoms, such as iodine or bromine.^{46, 48, 49}

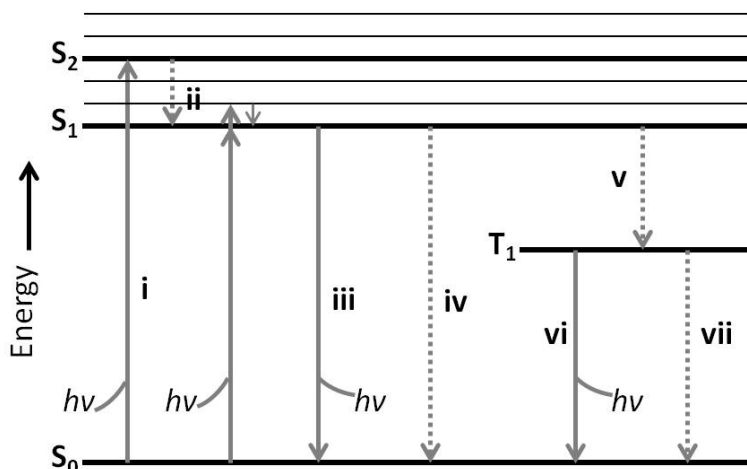


Figure 6. Jablonski diagram for fluorescence. (i) absorption of a photon to an excited state, (ii) internal conversion to S₁, (iii) fluorescence, (iv) non-radiative decay, (v) intersystem crossing to T₁, (vi) phosphorescence, (vii) non-radiative decay.⁴⁶

A generic absorption/emission spectrum is shown in Figure 7. The λ_{max} of the absorbance spectrum is as described in the previous section (4.1). The wavelength of maximum emission (λ_{em}) occurs at a longer wavelength, or lower energy, than the λ_{max} due to the loss of energy as vibrational energy, excited state reactions, solvent effects, and/or energy transfer.^{48, 49} Radiative energy loss between excitation and emission is universally observed for fluorescent molecules in solution. Having first observed this phenomenon with the use of his experiment with simple filters⁴⁸, this difference between λ_{max} and λ_{em} , or energy difference has been subsequently named the “Stokes shift”.⁴⁶

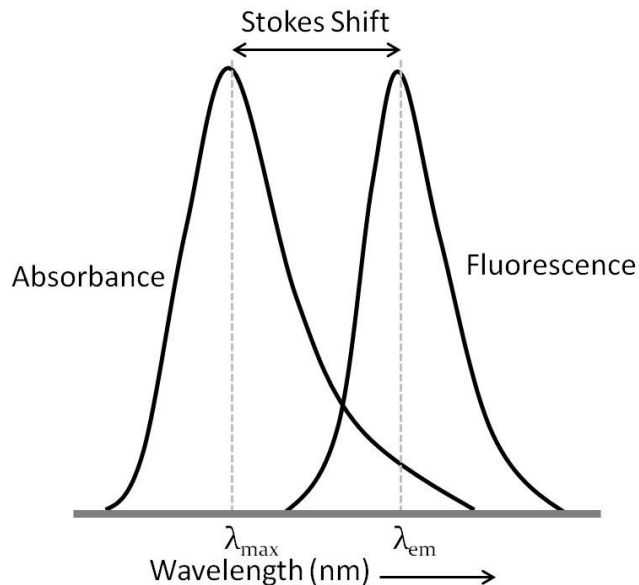


Figure 7. Generic absorbance and fluorescent emission spectra where the Stokes shift is the difference between the peaks in the spectra.⁴⁶

Selection of a fluorophore requires the consideration of a number of different properties. Fluorophores with a very small Stokes shift are susceptible to self-quenching (quenching is generally anything that decreases intensity of emission) and would therefore not be ideal for use with fluorescence detection methods. Fluorescence lifetime and quantum yield are very important characteristics of a fluorophore.⁴⁹ The lifetime of the excited state is characteristically defined as the average time the molecule spends in the excited state before it returns to the ground state. The excited state lifetime is proportional to the fluorescent quantum yield. The fluorescent quantum yield is fundamentally the ratio of photons emitted through fluorescence to those absorbed. The quantum yield of a fluorophore is decreased by non-radiative processes and photochemical reactions, which have a

higher propensity for occurrence with longer excited state lifetimes. Fluorescence intensity is proportionally related to the quantum yield.⁵¹

Discovery of the first fluorophore, quinine, stimulated the development of the first commercially available spectrofluorometer in the 1950s. The first rudimentary instruments were used during World War II for the monitoring of anti-malarial drugs. The National Institutes of Health (NIH) subsequently developed the first practical spectrofluorimeter.^{49, 52} The success of any experiment requires attention to experimental conditions and understanding of the instrumentation. There are many instrumental factors that can affect the quality of excitation and emission spectra.

A spectrofluorometer has the following main components as shown in Figure 8: a light source, monochromator, filters, photomultiplier tube (PMT), and a computer to collect the data as well as control the instrument. This instrument has a xenon lamp as the excitation source. Lamps such as this are useful due to their high intensity at all wavelengths (250 nm and up). The shutters are used to close the light on and off from the sample. The instrument has monochromators at both the excitation and emission side of the sample which are used for the selection of the excitation and emission wavelengths. The concave gratings of the monochromator are used to further reduce any stray light as well as select the wavelength of interest.⁴⁹ Filters may be used to further isolate the wavelength. The monochromators and filters determine the resolution of the instrument. The sample is located at a 90° angle to the source light so that it is not observed by the

detector. After the emitted light, which occurs in all directions, passes through the second monochromator, the fluorescence is detected by a PMT and then quantified with the computer. The results are then presented graphically and stored digitally.⁴⁹

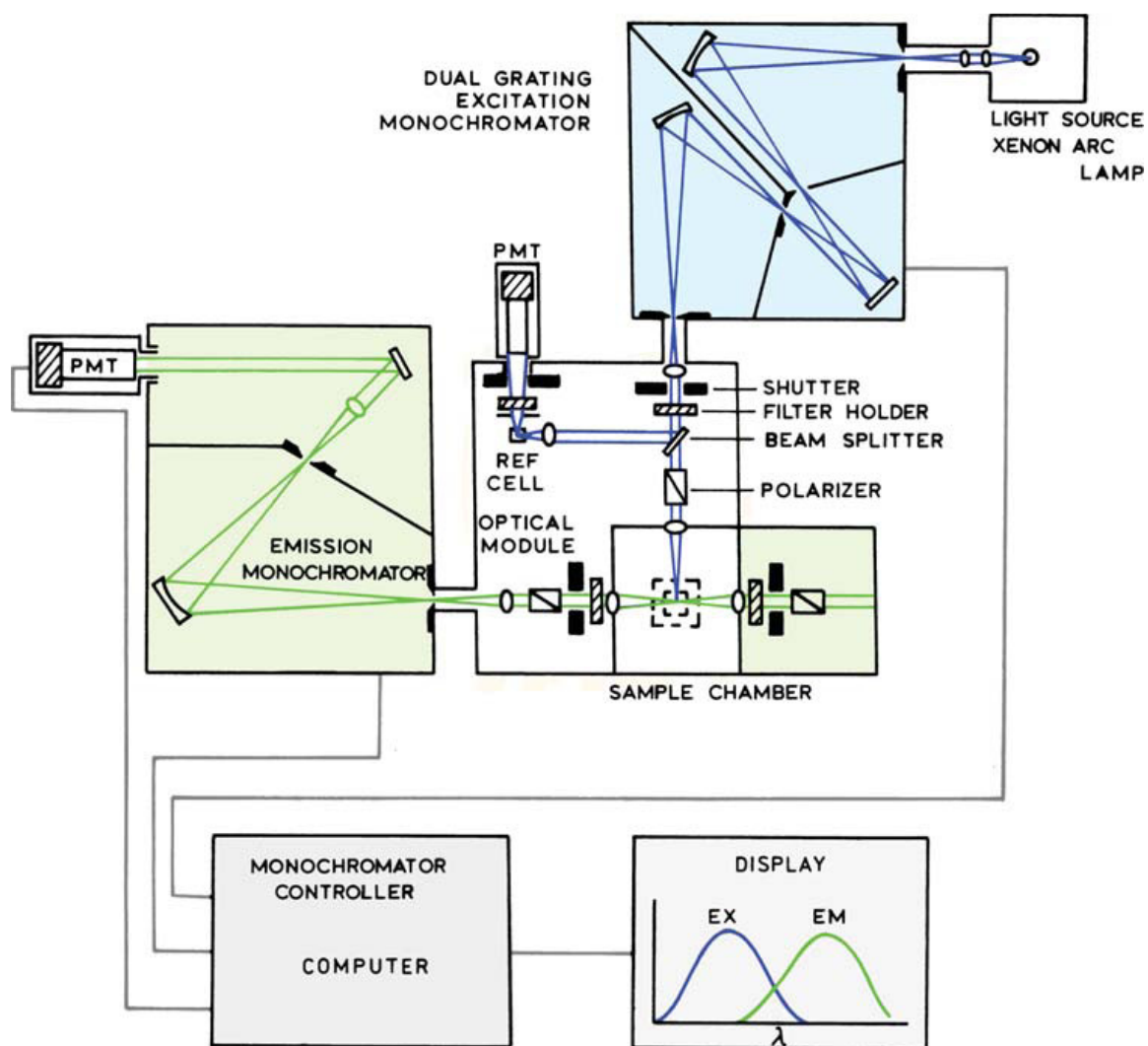


Figure 8. Schematic representation of a conventional spectrofluorometer.⁴⁹

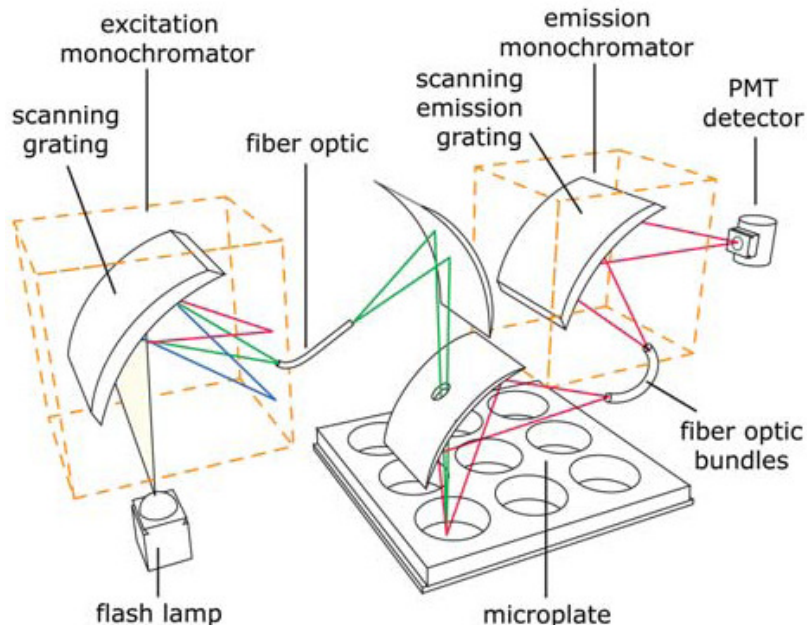


Figure 9. Schematic of spectrofluorometer used to read microplates.⁴⁹

Along with the development of high-throughput techniques, there has become a growing need for high-throughput detection methods. High-throughput screening methods used in drug discovery are usually performed in 96 or 384-well microplates. Measurements of numerous samples can be carried out rapidly using a microplate reader, as was used in the methods presented herein, shown in Figure 9. The optical arrangement in the microplate reader is different than in a conventional instrument. The plate containing the samples is taken into the instrument for analysis and must remain horizontal. Therefore, it is not possible to observe at a right angle as conventionally used. A xenon flash lamp is now commonly used as the light source negating the need for the shutters as in Figure 8. As with a conventional spectrofluorometer, the monochromator is used to select the desired wavelength

and directed with mirrors to the sample. Fluorescence from the sample, which occurs in all directions, is then directed to the emission monochromator and finally to the detector. Lastly, the microplate is typically on an x-y scanning stage in which it will move in order to detect the samples in all of the wells.⁴⁹

4.3. High Performance Liquid Chromatography

High performance liquid chromatography (HPLC) is frequently used in bioanalytical analysis for the separation and characterization of components of complex mixtures. With the implementation of an autosampler capable of introducing samples from microplates, HPLC becomes a necessity for any high-throughput screening lab. Using multiple detectors, such as UV and MS, sample information can be obtained along with the separation. With the increasing number of stationary phases being manufactured, nearly any mixture of compounds can be separated and/or analyzed based on varying retention mechanisms.^{4, 40, 53}

Chromatography was first developed by M. S. Tswett in 1906 during his research on plant pigments. The basis of liquid chromatography is the use of a solid stationary phase and a liquid mobile phase. In the original experiments by Tswett, calcium carbonate in glass tubes was employed as the stationary phase while ether/ethanol mixtures were used as the eluent to separate chlorophylls and other pigments. Using this approach, Tswett was able to observe the separation of the colors on the column, which prompted the term chromatography (Greek for “color writing”).⁵⁴⁻⁵⁶

Classical chromatography is most easily understood with the idea of theoretical plates, introduced by Martin and Synge.⁵⁷ Although high flawed, this concept describes the chromatographic column consisting of a series of hypothetical layers, or theoretical plates, in the direction perpendicular to the direction of sample migration. According to this theory, with every theoretical plate, equilibration of the solute between the stationary and mobile phase occurs. As the analyte moves down the column, it represents the passage from one separation stage or equilibrated mobile phase to the next. The largest shortcoming of this theory is that equilibrium is never reached in the system. The thickness of each of these layers or plates is called the height equivalent to a theoretical plate (HETP, H). With any given chromatographic column, the number of theoretical plates (N) is equivalent to the ratio of the column length (L) to the plate height ($N = L/H$). Improving the separation of compounds can most easily be achieved by increasing the number of theoretical plates.^{53, 56}

Equation 2)
$$H = A + \frac{B}{\bar{u}} + C \bar{u}$$

Several models have been developed to estimate the plate height, one of which is known as the van Deemter equation, Equation 2.⁵⁸ Here, the relationship between the plate height and the linear flow rate, \bar{u} , are related to the eddy diffusion constant, A, longitudinal diffusion, B, and the mass transfer between the mobile and stationary phase, C. The eddy diffusion term, A, results from non-homogeneity of the flow velocities and path lengths around the stationary phase particles. Larger particles lead to larger void spaces between the particles and thus an increase in the

eddy diffusion. Longitudinal diffusion, B , describes the diffusion of the solute away from the center of the sample peak, both with and against the direction of flow. This term is independent of the particle size, but largely dependent upon the time that the sample is on the column. As shown in the equation, it is inversely related to the flow rate (i.e., as flow rate increases, longitudinal diffusion decreases). Finally mass transfer, C , comes from the finite rate of transfer of the analyte molecule between the mobile phase and stationary phase as the sample migrates through the column. The analyte must reach the interface between the two phases to undergo the transfer process. Therefore, mass transfer is primarily dependent upon the particle size and flow rate. Large particles, as with eddy diffusion, leave larger void spaces and therefore increased diffusion time to reach the interface. As shown in the equation, it is directly proportional upon flow rate because with faster flow rates, less time is allowed for the transfer process to occur.⁵⁶

Attempts to increase the flow rate to improve the speed of analysis necessitated improvements in stationary phase materials. Early chromatographic materials were not ideal because they would get crushed under the increased pressure. Therefore, materials with increased mechanical strength have since been introduced. Also, from the van Deemter equation (Equation 2), decreased particle size could also improve the separation at higher flow rates. The combination of increased pressure, increased flow rate, and decreased particle size resulted in faster and more efficient separations.⁵⁶

The basic components of an HPLC system, Figure 10, include a solvent reservoir, pump, injector, analytical column, detector, and data collection. Other optional components include an inlet and in-line solvent filters, sample filter, pre-column filter, guard column, and back-pressure regulator.⁵⁹

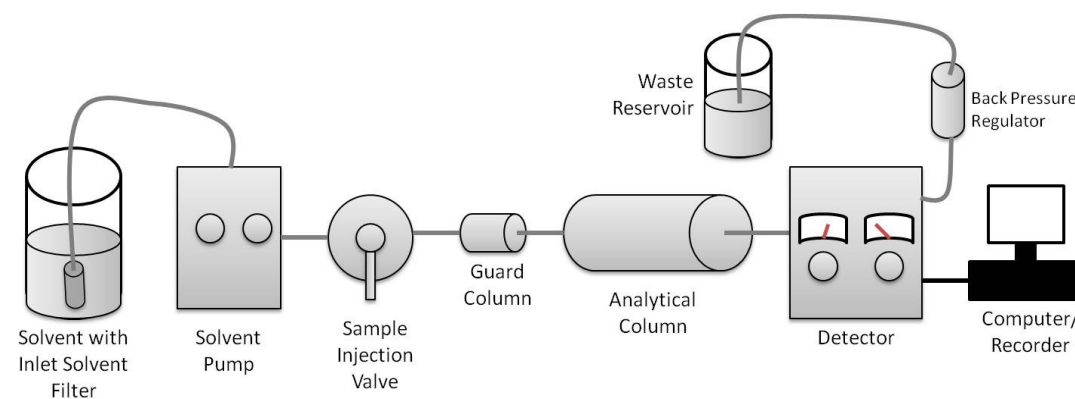


Figure 10. Basic schematic of HPLC.⁵⁹

An HPLC system begins with the solvent reservoir, which contains the solvent used to carry the sample through the system. Many systems use up to four different solvents, which can be mixed in a constant ratio (isocratically) or in changing ratios (gradient). All solvents are filtered with an inlet solvent filter to remove any particles that could potentially damage the system's sensitive components. The solvents are propelled through the system by the pump. This includes internal pump seals, which can slowly break down over time by chemical and mechanical means. As these seals break down and release particles into the flow path, inline solvent filters ideally prevent any post-pump component damage.⁵⁹

The next component in the system is the sample injector. This injection valve is equipped with a sample loop of the appropriate volume for the analyte. The

sample loop allows for the repeatable introduction of sample into the flow path. Because samples often contain particulate matter, it is important to utilize either a sample filter or a pre-column filter to prevent valve and analytical column damage. Following the injector, a sacrificial guard column is often included just prior to the analytical column to chemically remove components of the sample that would otherwise foul the main column. The analytical column allows primary sample separation to occur. The separation is based on the differential attraction of the sample components between the solvent (i.e., the mobile phase) and the packing material (i.e., the stationary phase) within the column.⁵⁹

4.4. Mass Spectrometry

Mass spectrometry (MS) is frequently used in pre-clinical screening due to its ability to separate, quantify, and identify molecules with high selectivity and sensitivity. It is frequently used in combination with HPLC for samples that are highly impure or complex (e.g., biological samples). Liquid chromatography-mass spectrometry (LC-MS) has been shown to be a suitable instrument for HT analysis due to the ease of automation and minimal sample preparation.⁴² Because MS is a destructive method, the sample cannot be recovered, however.

A block diagram of an LC-MS is shown in Figure 11. After the sample elutes from the HPLC column, it is directed to the ionization source, usually atmospheric pressure ionization (API). The vacuum system then draws the vaporized ions into the ion optics where they are then focused and accelerated into the mass analyzer. A common mass analysis system is the quadrupole. In the mass analyzer, the

sample ions are separated according to their mass-to-charge ratios with the use of applied radio frequency (RF) and direct current (DC) fields. The mass analyzer ejects the ions to the ion detection system, where an ion current signal is produced through the detection of the sample ions. The ion current signal that is produced is proportional to the number of ions in the solution. Finally, the signal is amplified and sent to the data system for processing and storage.⁶⁰

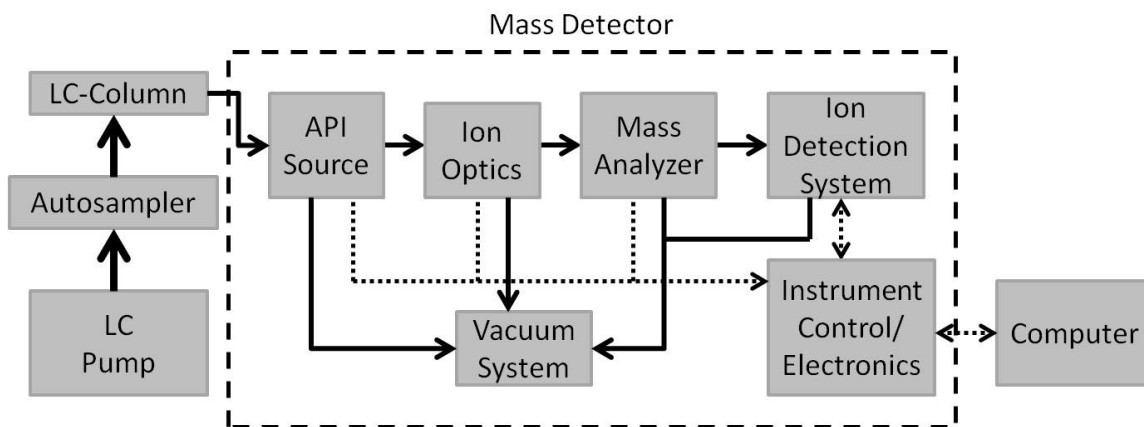


Figure 11. Schematic diagram of a mass spectrometer with HPLC as the sample introduction system.⁶⁰

Among the many different ionization methods, electrospray ionization (ESI) and atmospheric pressure chemical ionization (APCI) are typically used because they are both soft ionization techniques (i.e., most likely to leave the ionized molecule fully intact). ESI is most desirable for large molecules such as proteins or polymers, as this method can yield sample ions with multiple charges. The APCI method only yields singly-charged sample ions and is therefore limited to molecules with masses up to about 2000 atomic mass units (amu). In contrast to ESI, APCI

allows for the ionization of less polar compounds. Although ESI is the method of choice for ionization of very large molecules, both methods provide sufficient ionization for small molecules.

To produce gas phase ions by ESI (Figure 12), a high voltage, usually between 3 and 5 kV, is continually applied to the ESI capillary. The eluent is pumped through the heated capillary, spraying the solution into a fine mist of droplets (aerosol) that have a charged surface. The charge density at the surface of the droplets increases as the solvent evaporates until the critical point, known as the Rayleigh stability limit, is reached. At this point, the droplets divide into smaller droplets due to the electrostatic repulsion being greater than the surface tension. This process continues until very small and highly charged droplets have formed. The electrostatic repulsion from the very small, highly charged droplets ejects the sample ions into the gas phase. The charged capillary repels ions of the same charge and attracts ions of the same charge in the gaseous phase. Finally, the low vacuum produced by the forepump draws the positively charged ions and neutral molecules in the gas phase through the entrance cone and toward the high-vacuum of the mass analyzer.⁶⁰

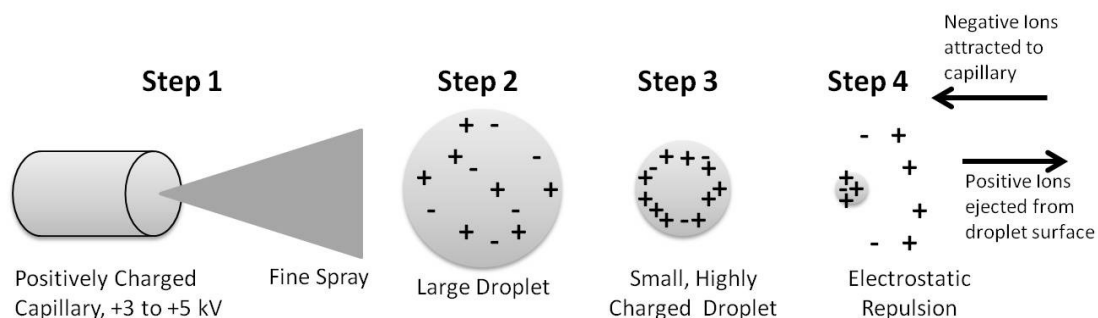


Figure 12. Positive ion generation mechanism by electrospray ionization.⁶⁰

To produce gas phase ions by APCI (Figure 13), the APCI capillary sprays the eluent into a fine mist of droplets. A high temperature tube that surrounds the capillary vaporizes the droplets. Located near the exit of the heated tube, the corona pin with a constant current between 2 and 10 μA creates a corona discharge leading to the formation of ions. The energized electrons produced by the corona discharge ionize the flowing nitrogen gas by primary ion formation. The ionized nitrogen reacts with the solvent molecules (such as water in Figure 14), forming solvent ions through secondary ion formation. The solvent ions then react via a proton transfer reaction with the sample molecules to form sample ions $[\text{M}+\text{H}]^+$. Finally, as with the ESI method, the low vacuum produced by the forepump draws the positively charged ions and neutral molecules in the gas phase through the entrance cone and toward the mass analyzer.⁶⁰

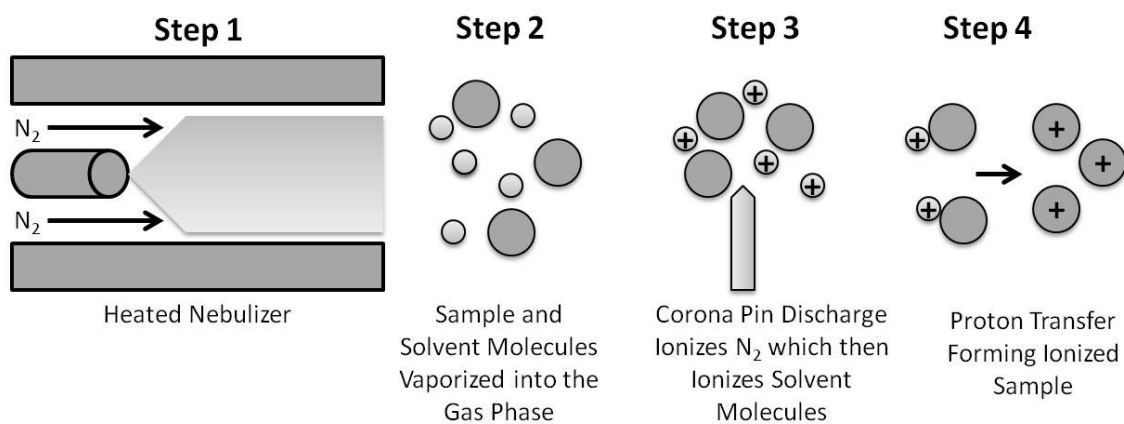


Figure 13. Positive ion generation mechanism by atmospheric pressure chemical ionization.⁶⁰

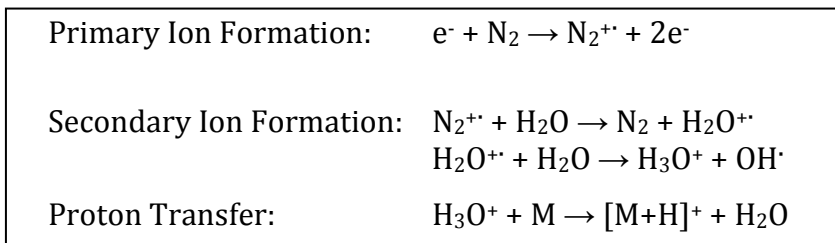


Figure 14. Positive ion formation by APCI.

As the forepump draws the ions and neutral molecules through the entrance cone and toward the mass detector, the neutral molecules are separated from the ions. The ions enter through a second entrance cone and pass through a RF/DC pre-filter (a pre-filter is not necessary in all MS systems). The pre-filter focuses the ions that are produced by the API source and transmits them to the mass analyzer. The pre-filter in the system consists of a square array of square-shaped rods (i.e., a quadrupole of square-shaped rods). During ion focusing and transmission, a positive offset voltage (for analysis of positive ions) is applied to the pre-filter quadrupole. Increasing the offset voltage also increases the kinetic energy of the ions along the axis of the quadrupole.

After focusing and acceleration by the pre-filter, the ions then enter the mass analyzer. The quadrupole mass filter consists of a set of four stainless steel cylindrical rods positioned in a square array (similar to the pre-filter). Rods opposite each other have either a positive or negative direct-current potential at which an alternating-current (AC) potential is superimposed, Figure 15. The AC potential, in the RF region, successively reinforces and overwhelms the DC field. As the ions are introduced into the quadrupole, they begin to oscillate in the plane

perpendicular to the length of the rods as they traverse the filter. At a given instant, one particular set of RF and DC voltages are applied to the mass analyzer rods.

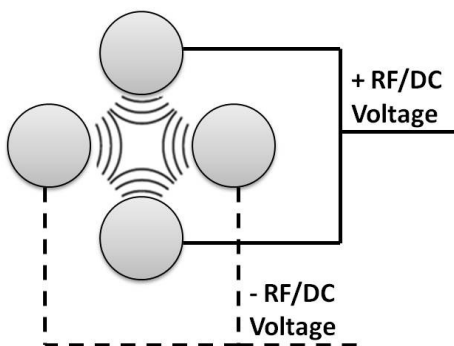


Figure 15. Applied RF and DC voltages to the rods in the quadrupole mass analyzer.

The trajectories of the ions of a particular mass to charge (m/z) ratio, matching a specific RF/DC voltage, are stable and are transmitted toward the detector. Ions with unstable trajectories do not pass through the quadrupole because their oscillation becomes infinite.⁵⁶ These ions strike the surface of one of the rods, become neutralized, and are pumped away by the vacuum. As the mass analyzer scans over the designated mass range by changing the RF and DC voltage, the ions of different m/z ratios are transmitted to the detector. The scanning mechanism of the quadrupole results in a differentiation between ions with similar m/z ratios without the use of filters.⁶⁰

After the ions have been separated by the mass analyzer, they are detected. The ion detection system in the instrumentation used in the analysis herein is an electron multiplier, illustrated in Figure 16. The ions exiting the mass analyzer are directed to the conversion dynode. The conversion dynode is a concave piece of

metal with a potential of -10 kV which is located at a 90° angle to the ion beam. The off-axis orientation greatly reduces the noise by limiting the probability that a neutral molecule will strike the conversion dynode. A high voltage is used to increase the conversion efficiency and thus increase the signal. The conversion dynode shield protects the vacuum manifold from the electric field produced by the conversion dynode.⁶⁰

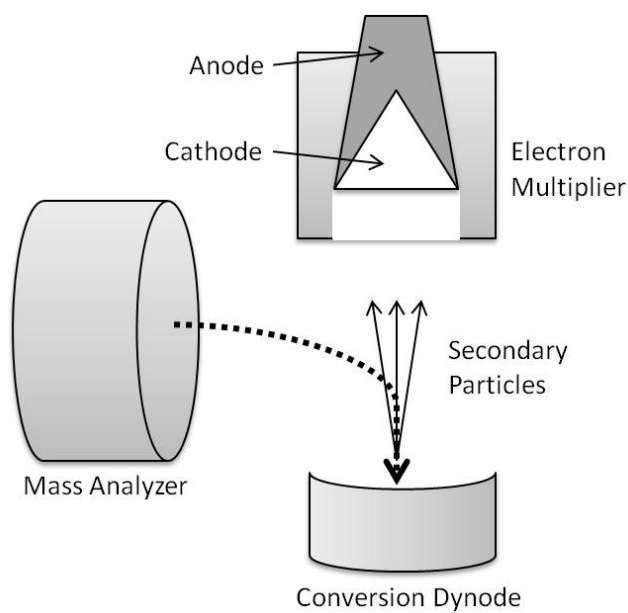


Figure 16. Ion detection system.⁶⁰

When an ion strikes the surface of the conversion dynode, one or more secondary particles are produced (negative ions or electrons from positive ions). The secondary particles are focused by the curved surface and accelerated by a voltage gradient into the electron multiplier. The electron multiplier contains a cathode and an anode. The cathode is a lead-oxide funnel-like resistor. A potential

of up to -2.5 kV is applied by the high voltage ring to the entrance of the cathode, while the exit of the cathode is near ground potential. The anode of the electron multiplier is a small cup that is located at the exit of the cathode and collects the electrons produced by the cathode.⁶⁰

Secondary particles that are produced by the conversion dynode strike the inner walls of the electron multiplier cathode with enough energy to eject electrons. The ejected electrons are accelerated farther into the cathode as they are drawn by the increasingly positive potential gradient. Because of the funnel shape of the cathode, the electrons do not travel far before they strike the surface of the cathode again, causing the emission of more electrons. A cascade of electrons is created as this process continues, creating a measurable current collected by the anode.^{56, 60}

CHAPTER II

AQUEOUS SOLUBILITY

1. Introduction

In a general sense, solubility is an easy concept to understand and measure. It can be defined as the amount of substance that dissolves in a given volume of solvent at a specific temperature. This is different than the concept of dissolution, which measures the time-dependent solvation of a solid. In a more specific sense of the concept, solubility can be defined as un-buffered, buffered, or intrinsic solubility. Un-buffered solubility is normally measured in water at the final pH of the saturated solution. Buffered solubility is measured at a specific pH, neglecting the influence of salt formation with counterions in solution. Finally, intrinsic solubility is the solubility of the neutral form of an ionizable compound.¹¹

Solubility is an essential physiochemical property that must be evaluated during the drug discovery and development process.⁶¹ The oral bioavailability of poorly soluble drugs is highly susceptible to food affects, pH changes, gastrointestinal metabolism, and efflux transporters.⁶² Solubility-limited absorption can influence the effectiveness of a drug and is preferably addressed in the early stages of drug discovery.⁴² Compounds with poor solubility have a high risk of failure with *in vitro* assays due to insufficient solubility to reach effective concentration in solution.^{3, 63, 64} *In vivo*, poor solubility results in a limited absorption of orally administered drugs.⁶⁵

Depending on the design of the solubility assay, the experiment can measure either the kinetic or thermodynamic solubility. The kinetic solubility is often considered a misnomer because it measures the precipitation rate rather than the solubility.⁶⁵ Kinetic solubility values are time-dependent and may be overestimated (with respect to the thermodynamic value) due to pH or co-solvent effects. The results obtained from one particular kinetic solubility assay are not expected to be reproducible between different kinetic methods. Thermodynamic solubility involves the saturation of the compound in solution in equilibrium with an excess of un-dissolved compound. Although thermodynamic solubility is regarded as the 'true' solubility, the values are not absolute. The values depend on a number of different experimental factors such as compound morphology, temperature, and time.

Thermodynamic equilibrium always seeks the overall lowest energy state of the system. Since equilibrium must be reached, it makes the thermodynamic solubility assay a very time consuming assay. Few researchers have the patience to stir the solution for an infinite amount of time in order to ensure equilibrium has been reached. Because of this, a high purity crystalline material gives the best chance that equilibrium can be reached after a reasonable period of time.⁶⁵ As parallel synthesis and combinatorial chemistry have increasingly become the most dominant methods of compound synthesis in the lead discovery stage, there is an increasing probability that the physical form of the compounds will be amorphous due to impurities and solvent residues. This is important to consider when choosing a method of solubility determination because non-crystalline materials are almost

always more soluble in solvents including aqueous media.⁴² In early discovery stages, it is less practical to measure thermodynamic solubility because time, purity, physical form, and quantity are all important factors for accurate solubility determination.

Kinetic solubility, often called “shake flask solubility”, measures the rate of formation of precipitate. Typically, the compound is first dissolved in dimethylsulfoxide (DMSO) to make a stock solution of a known concentration.^{5, 42} This stock solution is then added gradually to an aqueous solution until precipitation of the molecule occurs.⁶⁵ In general, there are two main approaches to determine the kinetic solubility. The first is done by removing the precipitate by filtration through a membrane by vacuum or centrifugation and determining the compound concentration by UV absorption or mass spectrometry. The second approach detects the formation of precipitate by monitoring the scattering of light by the particles using UV absorbance or directly by detecting the light scattering by nephelometric turbidity detection.¹¹

In the discovery stages, a researcher deals with a large number of drug candidates with very small sample sizes and a need to select a limited number of compounds for further investigation based on activity and solubility. In order to accomplish the characterization, a solubility assay must be high-throughput, have minimal sample use, be inexpensive, and fast.⁶⁶ Therefore, a miniaturized kinetic-based high-throughput assay for the determination of the solubility of small molecules has been developed.

2. Experimental

2.1. Materials and Instrumentation

All materials were used as they were received, with no further purification. Five bioactive small molecules; 4,5-diphenylimidazole (Alfa Aesar), β -estradiol (Alfa Aesar), diethylstilbestrol (Spectrum Chemicals), ketoconazole (CalBioChem), 3-phenylazo-2,6-diaminopyridine (Alfa Aesar) were used as standards. Each of the standards were made to a 10 mM solution in DMSO (Acros, Spectroscopic Grade 99.9+%). The buffer was prepared in 18 M Ω water with 90 mM ethanolamine (Alfa Aesar, ACS grade 99+%), 90 mM KH₂PO₄ (J.T. Baker), 90 mM potassium acetate (Fisher Biotech), and 30 mM NaCl (Fisher) and adjusted to pH 7.4 with HCl (Mallinckrodt).

HPLC grade acetonitrile (Columbus Chemical Industries) was used to make a 20% by volume solution in buffer for the preparation of the calibration plate. The calibration solutions (0-300 μ M, 50 μ L each) were read in a 384-well UV plate (Greiner Bio-One, 781801), which was also used for the solubility assay absorbance readings. The incubation and filtration were performed in a 384-well filter plate (Pall, #5071), which was sealed with an aluminum cover (Corning, #6570) during incubation and mixing. The filtration of the plates was performed using a Millipore MultiScreen_{HTS} Vacuum Manifold (MSVMHTS00). All of the absorbance readings were performed on an Infinite M1000 plate reader (Tecan).

2.2. Solubility Assay

Calibration plots were generated to obtain the relationship between solute concentration and absorbance. For each 384-well plate, 16 molecules were serially diluted in a 384-well UV plate according to Table 1, with one compound per row. Once the solutions were added to the wells, they were mixed thoroughly by pipette. The top of the plate was then covered with an aluminum plate cover. The UV plate is then carefully placed in the bench-top sonicator so that it floats on top of the water. It is then sonicated for 1 minute and centrifuged at 1000 rpm for 3 minutes to ensure that all of the solution remains in the wells. The plate is then scanned for absorbance with the Tecan plate reader from 230-800 nm at 5 nm increments with 10 flashes per well.

Table 1. Preparation of calibration plate for solubility assay.

Well Numbers	1, 2, 3, 4	5, 6, 7, 8	9, 10, 11, 12	13, 14, 15, 16	17, 18, 19, 20	21, 22, 23, 24
Volume Buffer	109.13 μ L	16.67 μ L	33.33 μ L	41.67 μ L	45.83 μ L	47.5 μ L
Volume 10 mM DMSO Stock	3.38 μ L					
Volume DMSO						2.5 μ L
Volume from Wells 1,2,3,4		33.33 μ L	16.67 μ L	8.33 μ L	4.167 μ L	
Final Concentration	300 μM	200 μM	100 μM	50 μM	25 μM	0 μM

Once the calibration plates were read, a calibration plot for each compound of adjusted absorbance vs. solute concentration at the maximum wavelength (λ_{\max})

was generated. This was done by subtracting the average absorbance of the buffer (0 μM , background) from the absorbance of each of the other wells. Each of the calibration plots was labeled with the compound name or code and maximum wavelength. Finally, a best fit linear trend line through the origin of the plot with the equation and r^2 value to 6 decimal places was added to the plot.

After the calibration plots were generated at the wavelength of maximum absorbance for each molecule, the solubility assay was performed. The wells in the 384-well filter plate were pre-wetted with 20-40 μL of buffer. The buffer was left to sit in the wells for about 5 minutes and subsequently removed by vacuum. An aluminum plate cover was then adhered underneath the filter plate to prevent wicking out or evaporation of the solvents during the incubation period. The solubility assay was then prepared in the filter plate according to Table 2 with four wells per molecule. With an adhesive plate cover on top and underneath the filter plate, it was sonicated for 1 minute, and shook on a reciprocating plate shaker overnight.

Table 2. Preparation of solution for solubility assay.

500 μM	Blank
47.5 μL buffer	47.5 μL buffer
2.5 μL of 10 mM stock DMSO solution	2.5 μL DMSO

The next morning, the solution was filtered into a collection plate (384-well polystyrene plate). From the filtrate, 30 μL from each well from the collection plate was transferred into a 384-well UV plate using a multichannel pipette. Next, 20 μL of acetonitrile was added to each well by pipette and shaken for 5 minutes on the plate shaker followed by centrifugation at 1000 rpm for 3 minutes. The absorbance was scanned from 230-800 nm at 5 nm increments with 10 flashes per well.

$$\text{Equation 3)} \quad \text{Solubility} = \frac{\text{Adjusted Absorbance at } \lambda_{\text{max}} \left(\frac{3}{5}\right)}{\text{slope}}$$

Finally, the solubility was determined using Equation 3 with the slope from the calibration plot for the molecule. At the maximum wavelength for each compound, the average absorbance from the blank wells (no small molecule) was subtracted from the absorbance of the solution after filtration (Adjusted Absorbance at λ_{max}). The average of the solubility values was calculated and the standard deviation was determined. Five small molecules (4,5-diphenylimidazole, β -estradiol, diethylstilbestrol, ketoconazole, 3-phenylazo-2,6-diaminopyridine) with known solubility values were analyzed as standards on each solubility assay plate.

3. Results and Discussion

The five standard molecules were used for comparison of the miniaturized assay with the standard solubility assay provided by Millipore (96-well plate format). Firstly, the calibration plots exhibited an improved r^2 value (i.e., closer to 1) than those published by Millipore.⁶⁷ Secondly, some solubility values were

similar to those published by Millipore, while others were not. The results of the average solubility concentration with one standard deviation (SD) from the mean for the standard molecules are shown below in Table 3 (standard deviation from the standard method was not reported). The relative standard deviation from the miniaturized solubility assay is less than or equal to 5% in all cases. The values determined by the 384-well solubility assay were very similar to those from the standard method, except for diethylstilbestrol, which was much lower than the reported value. The reported solubility for diethylstilbestrol using the shake flask method was 66 μM ⁶⁷, which is closer to the value determined by the miniaturized method than the standard method. This suggests that the 384-well miniaturized solubility assay is more accurate than the method outlined in the Millipore protocol.⁶⁷

Table 3. Solubility results of the standard small molecules by the standard method in comparison to the miniaturized method.

Name	Standard Method Solubility (μM) ⁶⁷ (n=3)	Miniaturized Method Solubility (μM) (n=4)
4,5-diphenylimidazole	68	67.3 \pm 3.7
β -estradiol	34	43.0 \pm 2.3
Diethylstilbestrol	156	108.3 \pm 5.4
Ketoconazole	141	134.5 \pm 2.4
3-phenylazo-2,6-diaminopyridine	355	357.7 \pm 7.0

Along with the standard molecules, solubility values were determined for an in-house library of small molecules containing hit molecules with varying structures as well as a scaffold library containing molecules with a common structural scaffold. The results are shown in Table 4 and 5 as well as in Appendix A. Generally, a compound with a solubility of 10 μM or less can have problematic oral activity or bioavailability.^{42, 68} In Table 4, a series of 2-indolyl methanamines exhibit very good solubilities. Interestingly, the position of the aromatic chloro-substituent plays an important role with respect to the solubility. The ortho-chloro substituted compound has a solubility of 129 μM , whereas the meta-chloro substituted compound has a solubility of 209 μM . In the case of the methoxy substituent, the position effect on solubility is negligible. This trend is also observed with the series of 2-indolyl methanamines, shown in Table 5. A chloro substituent at the R_1 position leads to a very poor solubility as compared to the non-substituted molecule (bolded in Table 5).

Table 4. Aqueous solubility of a series of N-((2-methyl-1H-indol-3-yl)(phenyl)methyl)pyridin-2-amine molecules.

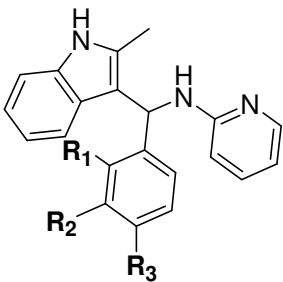
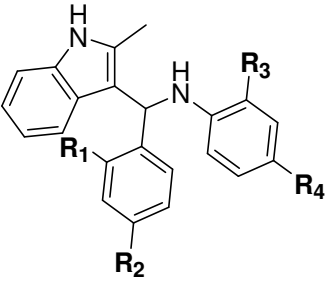
	$-R_1$	$-R_2$	$-R_3$	Solubility \pm 1 SD (μM)
		-H	-Cl	-H
	-Cl	-H	-H	129.3 \pm 0.8
	-H	-OCH ₃	-H	318.2 \pm 21.4
	-H	-H	-OCH ₃	320.1 \pm 5.5

Table 5. Aqueous solubility of a series of N-((2-methyl-1H-indol-3-yl)(phenyl)methyl)aniline molecules.

	-R₁	-R₂	-R₃	-R₄	Solubility ± 1 SD (μM)
	-Cl	-H	-OCH ₃	-H	59.8 ± 8.1
	-Cl	-H	-H	-H	31.6 ± 5.5
	-Cl	-H	-H	-Cl	6.8 ± 1.6
	-Cl	-H	-H	-N(CH ₃) ₂	21.0 ± 2.7
	-Cl	-H	-H	-CH ₃	36.0 ± 6.7
	-Cl	-H	-H	-NO ₂	4.9 ± 1.1
	-Cl	-H	-H	-OCH ₃	84.2 ± 2.7
	-H	-H	-H	-H	252.9 ± 5.6
	-H	-CH ₃	-H	-H	175.2 ± 8.3
	-H	-Cl	-H	-H	94.0 ± 2.6
	-H	-N(CH ₃) ₂	-H	-H	157.8 ± 33.7
	-H	-NO ₂	-H	-H	117.7 ± 1.9
-H	-O(CH ₂) ₂ OH	-H	-H	503.5 ± 16.5	
-H	-OCH ₃	-H	-H	237.6 ± 4.4	

4. Conclusions

For scaffold libraries, as in Tables 4 and 5, the influence of different substituents on the solubility of the molecules can be correlated. This information is crucial for the identification of improved drug candidates and can assist in the design of molecules with improved properties. The solubility information can also be used to determine the optimal concentration for any subsequent screening assays.

A typical high-throughput solubility assay is normally carried out in a 96-well polycarbonate filter plate. In the preparation of the calibration and assay plates

about 76 μL of each compound solution is used. This amount allows for two independent measurements per concentration for the calibration and three independent measurements for the solubility determination.^{61, 67, 69} Only 8 molecules can be analyzed at a time in one calibration plate, while 30 compounds can be analyzed in one assay filter plate.⁶⁷ In the case that milligram quantities of molecules are available, this assay will use about 30% of the stock supply. This leaves little room for error and insufficient material for further studies.

For this novel 384-well filter plate assay, a total of only 23.5 μL of each compound solution was used. This amount was sufficient for four independent measurements for each calibration concentration and four replicates for determination of the solubility concentration. With the 384-well plate format, 16 molecules can be analyzed in one calibration plate and 95 molecules can be analyzed in one assay filter plate.

The small molecules could be studied further by analyzing their solubilities at different buffer pH values. It is understood that the pH at which the molecule is most soluble determines the location where it will most likely be absorbed. For example, drugs that dissolve in acidic solutions are absorbed through the lining of the stomach. Molecules that dissolve readily in alkaline conditions will be absorbed through the walls of the small intestine and into the bloodstream. The understanding of the pH influence on solubility will help to determine other factors influencing permeability and distribution.

CHAPTER III

MEMBRANE PERMEABILITY

PART 1: PARALLEL ARTIFICIAL MEMBRANE PERMEABILITY ASSAY (PAMPA)

1. Introduction

Similar to solubility, permeability is directly related to the bioavailability of a drug. Though, unlike solubility, permeability cannot be manipulated by formulation. Achieving desired permeability must be done through optimization of the molecule itself.⁷⁰ Assays that predict cellular absorption of small molecules have become increasingly important in the drug discovery process. It is essential to have reliable methods of predicting the *in vivo* permeability through the use of *in vitro* methods.⁶

The oral route of the administration of drugs is the most commonly used method as it is the most convenient for patients.⁶ The absorption of an orally administered drug is largely determined by its ability to cross the gastrointestinal tract, its penetration of the blood brain barrier, and its transport across cell membranes.⁷¹ Several mechanisms, such as paracellular transport and active uptake or efflux can also influence the permeability of drugs.⁷² It is generally assumed that sufficiently lipophilic compounds are transported via passive diffusion, while small hydrophilic compounds (<200 Da) are believed to be transported through the paracellular route if not by active transport.⁷³ Active transport of small molecules is difficult to replicate with *in vitro* assays. For this reason, the assessment of passive cellular absorption is the preferred method.

In vitro assays that measure the passive cellular compound absorption often employ artificial or biological membranes such as Caco-2 cells, lipids, or long chain alkanes (dodecane or hexadecane). These methods are based on the passive diffusion process, including paracellular and trans-cellular permeation.⁷⁴ However, *in vivo* permeability cannot be measured by isolation from biological events. All *in vitro* permeability measurements are essentially various forms of lipophilicity analysis.⁵ Although related, permeability and lipophilicity values are not interchangeable, but can correlate significantly.⁵

Many factors based on physiochemical parameters have been recognized to govern the passive absorption of a drug including lipophilicity, molecular weight, polar surface area, ionization state, and hydrogen bonding capacity.^{72, 74} Drug lipophilicity is commonly used as a predictor for membrane permeability because membranes are primarily lipophilic in nature.⁶ Molecular size can also play a distinct role in the permeation process because larger molecules diffuse more slowly than smaller molecules.

Lipids within a membrane that contain hydrogen-bonding acceptor groups can associate with the hydrogen-bonding solutes. This hydrogen-bonding prevents the solutes from penetrating the membrane and slows down the diffusion process. Directly related to the hydrogen-bonding capacity is the polar surface area.⁶ Polar surface area is the molecular surface area associated with hydrogen bonding acceptor atoms (i.e., oxygen and nitrogen) plus the area of the hydrogen atoms. Finally, membranes are more permeable to non-ionized forms of drug than the

ionized species because of their greater lipid solubility and the charged nature of the membranes.⁶

To reduce the time and cost involved with animal models for the estimation of permeability, artificial membranes have long been employed. When screening for passive membrane permeability, artificial membrane models have the advantage of enabling a reproducible and high-throughput format.⁵ The first such artificial membrane permeability assessments was discovered in 1962 when an optically black bilayer lipid membrane was formed over a small hole in a thin sheet of Teflon.⁷⁵ This model, however, had serious drawbacks due to the fragility of the membrane. Nevertheless, membranes such as this have since been viewed as more useful models than the more complex “natural” membranes such as excised tissues.⁴² Since then, passive artificial membrane permeability has been extensively studied and compared with cell-based permeability.^{73, 76, 77}

The Caco-2 cell model has been long considered the “gold standard” technique and has been used as a standard for comparison for other absorption techniques. Caco-2 cells are human colon adenocarcinoma cells which exhibit many *in vivo* intestinal cell characteristics. These cells have tight intracellular junctions, microvilli, and express intestinal enzymes and transporters. Due to these characteristics, the permeation across a layer of Caco-2 cells correlates to human intestinal permeation. This model measures passive diffusion, active transport, and paracellular diffusion. This technique is performed by culturing a layer of cells on a filter support, usually in a microplate.^{5, 6}

Although the Caco-2 model is regarded as a standard technique, it is quite laborious and costly. It can take from days to weeks to generate a fully confluent layer of cells which have gone through enough passages so that they have been fully differentiated.¹² Because of the tedious culture period necessary for Caco-2 cells, other cell-based models had been developed using Madin-Darby Canine Kidney (MDCK) and Lewis Lung Carcinoma-Porcine Kidney (LLC-PK1) cells. Although, the MDCK method correlates closely with transport mediated drug permeability, the LLC-PK1 method has not yet been fully correlated to *in vivo* absorption.⁶

The parallel artificial membrane permeability assay (PAMPA) has been used as an alternative method for predicting passive permeability. It has been regarded as an excellent model because it is amenable to high-throughput, reproducible, and low cost.⁶ Although, PAMPA methods are not completely predictive of *in vivo* permeability, they can identify definitive trends in the ability of a molecule to permeate membranes by passive diffusion.⁴²

The PAMPA is usually performed in a 96-well plate with two parts, the donor plate and the acceptor plate as illustrated in Figure 17. The donor plate has a permeable membrane or filter along the bottom which aligns with the wells in the acceptor plate. The artificial membrane (composed of lecithin, phosphatidylcholine, hexadecane, porcine brain lipid extract, etc. in organic solvents) is impregnated into the filter of the donor plate. Buffer and compound are added to the donor wells while buffer is added to the acceptor wells. With the impregnated filter in contact with both solutions, the assay plates are incubated for a set amount of time, and the

concentration of compound that has passed through the membrane is determined (usually by absorbance spectroscopy, HPLC, or LC-MS). An illustration of the PAMPA method is shown in Figure 18.

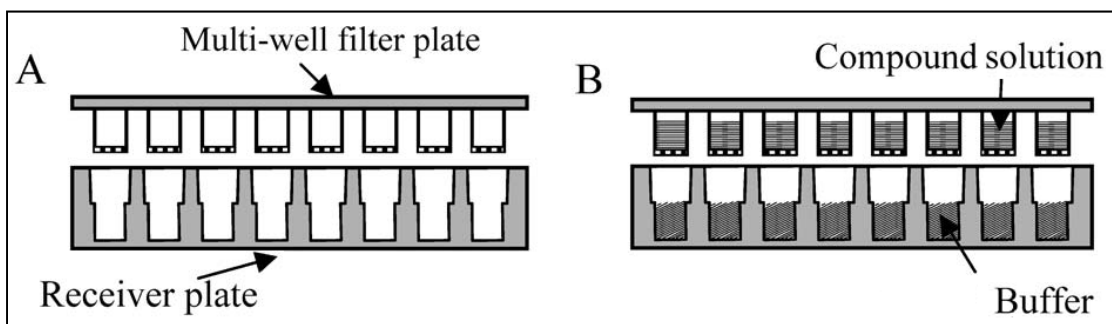


Figure 17. Illustration of PAMPA plates. A) 96-well filter plate pre-coated with an artificial membrane with a matched 96-well receiver plate. B) Solutions of the compounds in buffer are added to the filter plate on top of the artificial membrane (donor plate), while buffer is added to the receiver plate (acceptor plate).⁷⁸

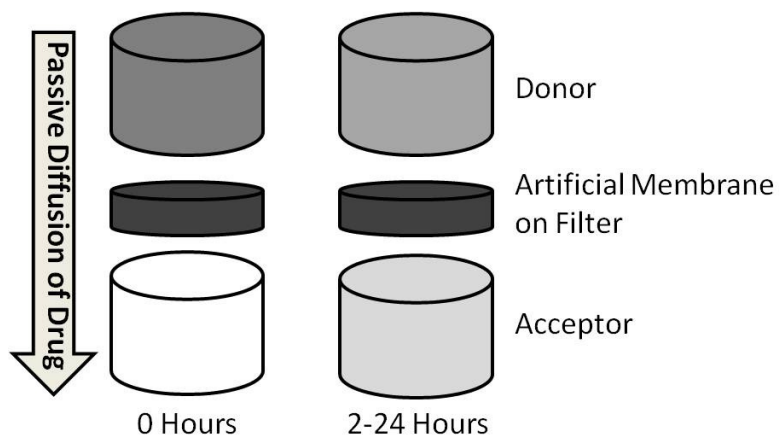


Figure 18. Example of a PAMPA assay performed in a multi-well plate.

The effective permeability determined by cell-based or PAMPA method is calculated using Equation 4. Here, dC_A/dt (mg/s·mL) is the increase of drug

concentration in the receiver chamber over the incubation period. The term A (cm^2) is the surface area of the membrane that is exposed to the compound. V_A (mL) is the volume of the solvent in the acceptor chamber. Finally, C_A and C_D (mg/mL) are the initial drug concentration in the acceptor and donor chambers, respectively.⁶

Equation 4)
$$P_{eff} = \frac{V_a}{A(C_D - C_A)} \left(\frac{dC_A}{dt} \right)$$

Along with PAMPA, other methods have been used to estimate the membrane permeability of small molecules. These alternative methods include HPLC with columns containing immobilized lipids, liposomes, or micellar chromatography. These methods have shown to have a better correlation to permeability than octanol/water partitioning, but are not yet regarded as reliable methods yet. The HPLC method of permeability estimation will be described further in Part 2 of this chapter.

Human *in vivo* P_{eff} values obtained under physiological conditions provide the basis for establishing *in vitro*-*in vivo* correlations, which can be used to make predictions about oral absorption. Therefore, many *in vitro* methods are directly correlated to *in vivo* values in order to assess the accuracy of the assay. One such method is the Loc-I-Gut method, which has been used to establish a Biopharmaceutics Classification System (BCS) database of *in vivo* human permeability values for orally administered drugs.

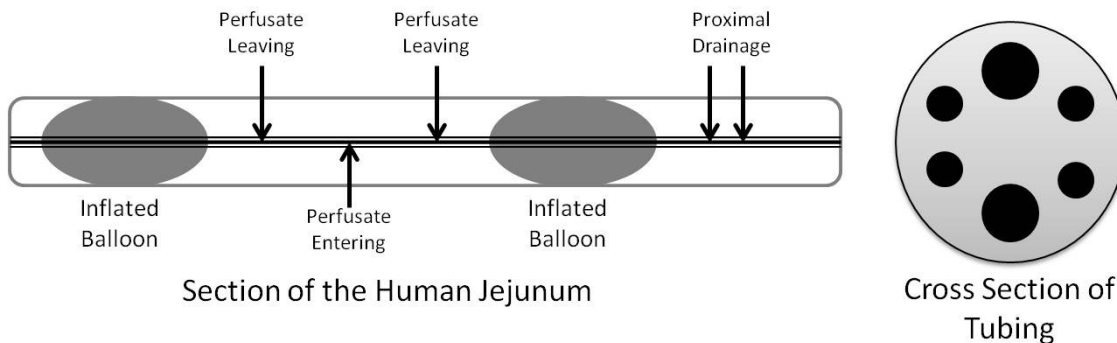


Figure 19. Functional diagram of the Loc-I-Gut technique used for the determination of human *in vivo* permeability and absorption.⁵

The Loc-I-Gut method, shown in Figure 19, is a perfusion technique for the proximal region of the human jejunum (upper intestinal section). It employs a multichannel polyvinyl chloride tube that is 175 cm long and an external diameter of 5.3 mm. The tube contains six channels and also has two 40 mm long, elongated latex balloons which are placed 10 cm apart. Each balloon is separately connected to one of the smaller channels. The two wider channels in the center of the tube are for infusion and aspiration of perfusate. The remaining smaller channels are used for administration of marker substances and/or drainage. A tungsten weight at the far end of the tube aids the passage of the tube into the jejunum. The balloons are then filled with air when the second balloon has passed through the junction between the duodenum and jejunum. Finally, ^{14}C -PEG 4000 is used as a volume marker to detect water flux across the intestinal barrier.^{5, 79-81}

The BCS classifies drugs as having either high or low permeability. It is based indirectly on the extent of absorption of a drug in humans and directly on the measurement of rates of mass transfer across a human intestinal membrane. A drug

is considered highly permeable when the extent of absorption in humans is determined to be 90% or more of the administered dose based on a mass-balance determination or in comparison to an intravenous dose.⁸² Using BCS classified drugs as standards, a hexadecane artificial membrane PAMPA (HDM-PAMPA) was performed with a library of small molecules and the permeability of these molecules was assessed.

2. Experimental

2.1. Materials and Instrumentation

All materials were used as received with no further purification. The following small molecules were used as standards: verapamil hydrochloride (Tocris Bioscience), diethylstilbestrol (Spectrum Chemical Mfg. Corp.), β -estradiol (Alfa Aesar), caffeine (Alfa Aesar), 10,11-dihydrocarbamazepine (Alfa Aesar), D,L-propranolol hydrochloride (MP-Biomedicals), 4,5-diphenyl imidazole (Alfa Aesar), piroxicam (MP-Biomedicals), metoprolol tartarate (LKT Laboratories), naproxen (MP-Biomedicals), atenolol (MP-Biomedicals), and ranitidine hydrochloride (Alfa Aesar). Each of the small molecules were dissolved in DMSO to make a 10 mM solution (Acros, Spectroscopic Grade 99.9+%).

The PAMPA assay was performed with the Millipore MultiScreen filter plates (MAIPNTR10) and Millipore transport receiver plates (MATRNPS50) using a 5% by volume n-hexadecane (Acros) in n-hexane (Fisher) solution to create the artificial layer. The absorbance readings were completed with a Corning Costar 96 well UV plate (3635). 1x Phosphate buffered saline (PBS) was prepared in 1L batches using

18 M Ω water with 3.23 mM K₂HPO₄·7H₂O (J.T. Baker), 7.84 mM KH₂PO₄ (J.T. Baker), 5 mM KCl (Fisher), 150 mM NaCl (Fisher), and adjusted to pH 7.2 with HCl (Mallinckrodt) and NaOH (Fisher). All of the absorbance readings were performed on an Infinite M1000 plate reader (Tecan).

2.2. PAMPA

The artificial membrane was prepared by carefully pipetting 15 μ L of the 5% (v/v) hexadecane in hexane solution to each of the wells of the donor plate (assay plates as shown in Figure 16). The plate was placed into a fume hood for 1 hour to ensure complete evaporation of the hexane. After the hexane had evaporated, 300 μ L of PBS with 5% (v/v) DMSO was added to each of the wells of the acceptor plate. The hexadecane treated donor plate was then placed on top of the acceptor plate taking care that the underside of the membrane is completely in contact with the solution in each of the acceptor wells. Each of the compounds solutions were prepared in triplicate in a separate 96-well plate to 300 μ M (4.5 μ L of 10 mM compound solution in DMSO, 3 μ L DMSO, and 95 μ L buffer). Then, 150 μ L of the compound solution was added to the donor wells. For each plate, carbamazepine (medium-high permeability), verapamil (high permeability), and ranitidine (low permeability) were used as standard molecules for reference.

The lid was placed on the plates and the entire plate sandwich was placed into a closed container with a wet paper towel along the bottom to circumvent evaporation during the incubation process. The container was then placed on a reciprocal shaker for agitation at about 100 rpm. The time at the beginning of the

incubation was recorded, as this is a thermodynamic-based assay. The incubation was then allowed to continue for approximately eighteen hours.

The next day, the plates were removed from the incubation container and the time of the end of the incubation period was noted. The donor plate was removed and 50 μL of the acceptor solution was transferred to the UV plate. Drug solutions at the theoretical equilibrium concentration (300 μM) was also prepared and transferred to the UV plate. The absorbance of the solutions in the UV plate was then scanned from 250-600 nm with 1 nm steps and a 5 nm bandwidth.

$$\text{Equation 5) } \log P = \log \left\{ C \times -\ln \left(1 - \frac{[\text{Drug}]_A}{[\text{Drug}]_E} \right) \right\}; \text{ Where } C = \left(\frac{V_A \times V_D}{(V_D + V_A)A \times T} \right)$$

The relative permeability (cm/s) of the small molecules was calculated with Equation 5, where V_D is the volume of the donor well in cm^3 (150 μL), V_A is the volume in the acceptor well in cm^3 (300 μL), A is the active surface area of the membrane in cm^2 (0.283 cm^2), T is the incubation time of the assay in seconds, $[\text{Drug}]_A$ is the absorbance of the compound in the acceptor well after the incubation period, and $[\text{Drug}]_E$ is the absorbance of the compound at the concentration of the theoretical equilibrium (as if the donor and acceptor solutions were simply combined).⁸³ The equation is derived from Equation 4, described previously, in which the change in concentration of the solute is time dependent.

3. Results and Discussion

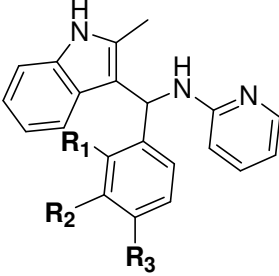
The resulting values of the HDM-PAMPA for the three standard molecules on each assay plate were compared to literature values. This was done to determine the validity of each assay plate as well as to determine the numbers correlating to high and low permeability. The HDM-PAMPA results are shown in Table 6, the literature values were determined using a 2% lipid (2-dioleoyl-sn-glycer-3-phosphocholine) in dodecane as an artificial membrane.⁸³ From the results collected from the standard molecules, it was determined that molecules with a logP value of about -6.75 cm/s and above (i.e., closer to zero) are considered to be highly permeable according to the BCS classification.

Along with the standard molecules, a permeability assay was also performed using an in-house library of small molecules containing molecules with varying structures as well as a scaffold library containing molecules with a common structural scaffold or backbone. The permeability values and structures of the compounds are shown in Appendix B. The average permeability results with standard deviations from two different indole-based scaffolds are summarized in Tables 7 and 8.

Table 6. Comparison of PAMPA values.

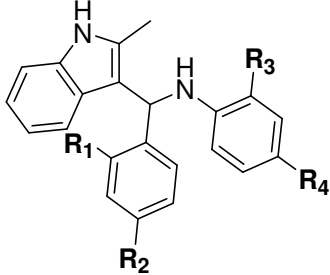
Molecule	BCS Permeability ^{82, 83}	Literature logP ^{42, 83} (cm/s)	Experimental logP (cm/s)
Carbamazepine	High (Medium)	-5.21	-6.81
Ranitidine	Low	-8.00	-8.01
Verapamil	High	-4.40	-5.99

Table 7. HDM-PAMPA (pH 7.2) values for a series of N-((2-methyl-1H-indol-3-yl)(phenyl)methyl)pyridin-2-amine molecules.

	-R₁	-R₂	-R₃	logP (cm/s)
	-H	-Cl	-H	-5.86 ± 0.02
	-Cl	-H	-H	-6.12 ± 0.17
	-H	-OCH ₃	-H	-6.02 ± 0.03
	-H	-H	-OCH ₃	-6.07 ± 0.08

In Table 7, a series of 2-indoyl methanamine molecules with different aromatic substituents exhibit high permeabilities. The position of the aromatic methoxy group (meta or para) does not significantly change the permeability of the compounds. In contrast, the position of the chloro-substituents (ortho or meta) has a strong influence on the permeability. Permeability values for a different series of 2-indoyl methanamines are summarized in Table 8. A chlorine substituent at the R₁ position leads to a poor permeability as compared to the non-substituted molecule (bolded in Table 8). With the substitution of a tertiary amine at the R₁ and R₄ position, the permeability decreases significantly. It is also shown that the electron-withdrawing nitro substituent on the aniline significantly decreases the permeability. In general, any additional substitutions on this molecular scaffold decreases the permeability determined by HDM-PAMPA. This may be due to the increase of molecular weight and therefore size of the molecule.

Table 8. HDM-PAMPA (pH 7.2) values for series of N-((2-methyl-1H-indol-3-yl)(phenyl)methyl)aniline molecules.

	-R₁	-R₂	-R₃	-R₄	logP (cm/s)
	-Cl	-H	-OCH ₃	-H	-6.22 ± 0.08
	-Cl	-H	-H	-H	-6.42 ± 0.02
	-Cl	-H	-H	-Cl	-6.25 ± 0.10
	-Cl	-H	-H	-N(CH ₃) ₂	-7.28 ± 0.16
	-Cl	-H	-H	-CH ₃	-6.46 ± 0.25
	-Cl	-H	-H	-NO ₂	-7.61 ± 0.41
	-Cl	-H	-H	-OCH ₃	-6.31 ± 0.08
	-H	-H	-H	-H	-6.00 ± 0.11
	-H	-CH ₃	-H	-H	-6.34 ± 0.04
	-H	-Cl	-H	-H	-6.04 ± 0.02
	-H	-N(CH ₃) ₂	-H	-H	-6.88 ± 0.08
	-H	-NO ₂	-H	-H	-6.09 ± 0.10
	-H	-O(CH ₂) ₃ OH	-H	-H	-6.83 ± 0.03
-H	-OCH ₃	-H	-H	-6.10 ± 0.02	

4. Conclusions

The HDM-PAMPA has been shown to be a reliable high-throughput method for the estimation of the passive cellular diffusion of small molecules. Molecules that have been well characterized according to BCS classifications were used to determine the range of permeability values to characterized small molecules according their passive absorption abilities.

The determination of permeabilities of small molecules within scaffold libraries, as in Tables 7 and 8, enables the correlation between different substituents and their influence on the compound permeability. This information is essential for further development of drug candidates and the identification of drug candidates for further development. As stated previously, unlike solubility, permeability cannot be improved through the formulation of the drug.

As discussed previously, in the context of aqueous solubility, the permeability of small molecules could be further analyzed at different pH values. This could be done at the body compartment pH, where the molecule is most likely to be absorbed. Also, buffers with different pH values in the donor and acceptor wells can be used to replicate the difference in pH between the gut and blood or intestines and blood. The determination of the pH influence on small molecule permeability will help to understand the complex factors of absorption and distribution of new drug candidates.

PART 2: PERMEABILITY BY HPLC METHODS

1. Introduction

As described in Part 1 of this chapter, there are many different methods for the estimation of cellular permeability of a small molecule. One such method that has recently become of interest is the application of HPLC.⁸⁴⁻⁸⁶ The advantage of HPLC-based permeability assays is the ease of implementation and low cost in contrast to the traditional methods which are time and cost intensive.

The C18 column (octadecane bound to a silica stationary phase) is the most popular stationary phase in reverse phase HPLC methods. During the development of a reliable high-throughput method for the assessment of permeability of small molecules, HPLC methods employing a C18 column have been frequently reviewed. It has been thoroughly established that retention factors obtained by isocratic methods can be related to the lipophilicity of molecules.^{16,85} In fact, the retention factors for purely aqueous mobile phases have been considered to be more representative of lipophilicity than octanol/water partitioning.⁸⁵ Octanol/water partitioning has long been considered the “gold standard” for reporting lipophilicity of molecules.⁵ Although C18 HPLC methods have been shown to model the hydrophobic contribution to drug-membrane interactions, they do not mimic polar lipid head and ionic interactions.¹⁶

Immobilized Artificial Membrane (IAM) chromatography was developed by Dr. Charles Pigeon at Purdue University.^{84,87} Most commonly, an IAM column consists of an aminopropyl-functionalized silica stationary phase that has been

reacted with a lipid, usually phosphatidylcholine, Figure 20. This configuration functions as an “artificial membrane” formed on the surface of the silica particles. The analyte interacts primarily with the polar head groups as it passes through the column. The IAM column has been well studied and retention factors have been shown to have a good correlation with values determined by a Caco-2 permeability assay⁸⁴, liposome/water partitioning¹⁷, and octanol/water partitioning¹⁶. Nevertheless, there is limited contribution of the drug-membrane interactions with the use of either IAM or C18, which may be improved with the use of multiple columns in sequence.

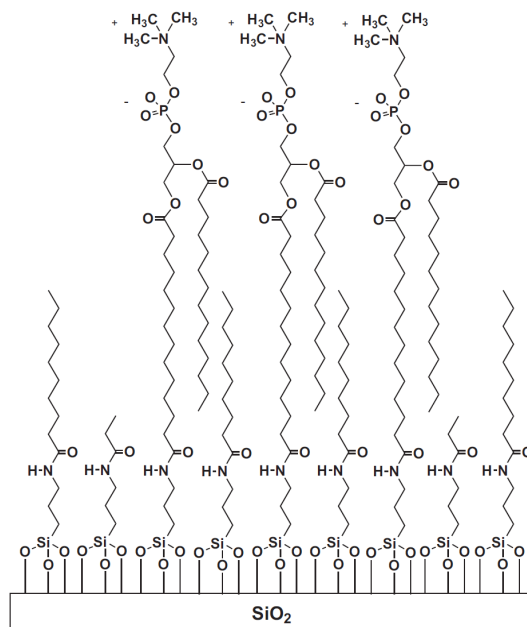


Figure 20. IAM column with immobilized phosphatidylcholine on aminopropyl silica with alkyl endcapping.⁸⁸

For any HPLC-based method, interactions of the analytes with free silanol groups on the silica stationary phase result in increased retention. The mechanism can be attributed to both hydrogen bonding and electrostatic forces between the small molecule and the silanol groups.⁸⁵ To suppress this effect, free silanol groups are reduced by endcapping during manufacturing. For example, IAM columns have been endcapped with aminopropyl groups.⁸⁴ With advances in column manufacturing, the effect on retention from free silanol groups in the stationary phase can be minimized, but not completely eliminated.

Other chromatographic methods for permeability assessment have been developed, such as Immobilized Liposome Chromatography (ILC), as an alternative to IAM chromatography.⁸⁹ In ILC, hydrophobic-functionalized gel beads are used as the stationary phase and treated with phospholipids to form immobilized liposomes. The separations of compounds with the same logP value using this method can sometimes show very different degrees of partitioning, depending on the charge of the compound.^{42, 89} Micellar chromatography methods have also been studied, but do not show an improvement upon the current techniques.⁴²

C18 and IAM column chromatography have been shown to be the most promising chromatographic methods for the determination of permeability. To take advantage of the hydrophobic contribution as well as the polar contribution to the drug-membrane interaction, both types of columns have been employed in the same analysis. The hypothesis of the lipid bilayer partitioning being modeled by HPLC partitioning/retention is shown in Figure 21. The columns were linked together

with column couplers and the retention factors of the standard drugs were compared to those reported HDM-PAMPA (Part 1 of this chapter) as well as human jejunal permeability. The compound retention times of the linked columns were also compared to those determined for the IAM and C18 columns alone.

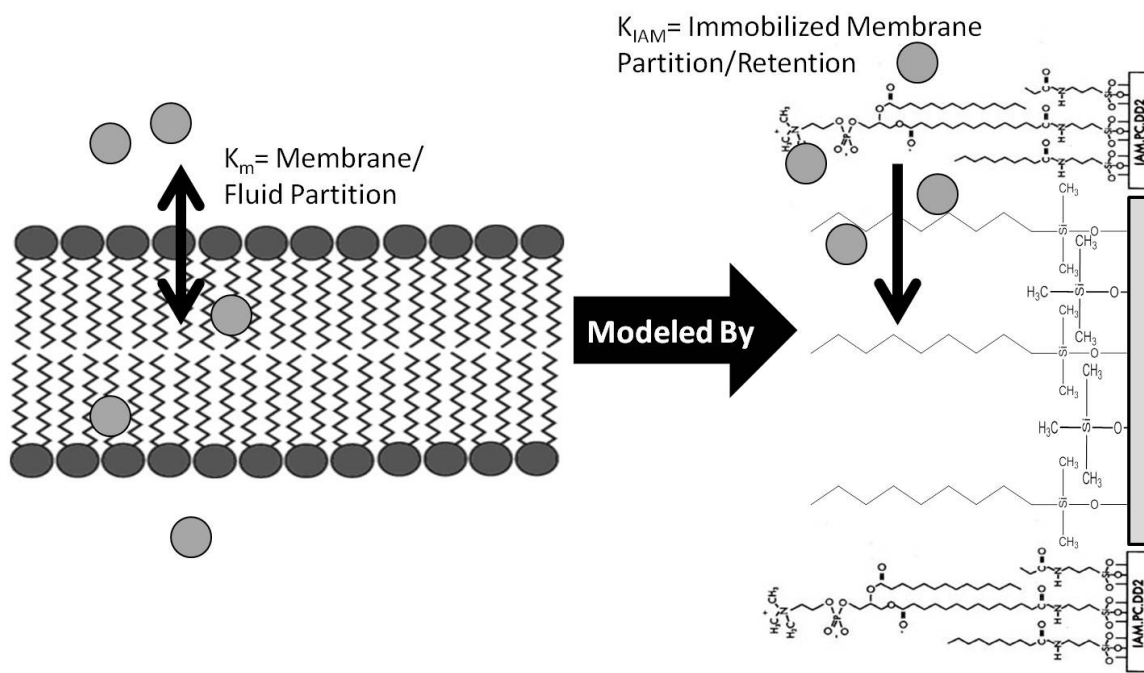


Figure 21. The partitioning of small molecules through a lipid is hypothesized to be modeled by the retention and/or partitioning of the molecules as they pass through IAM-C18-IAM column in series.

2. Experimental

2.1. Materials and Instrumentation

All materials were used as received. The following small molecules were used as standards: verapamil hydrochloride (Tocris Bioscience), diethylstilbestrol

(Spectrum Chemical Mfg. Corp.), β -estradiol (Alfa Aesar), caffeine (Alfa Aesar), 10,11-dihydrocarbamazepine (Alfa Aesar), D,L-propranolol hydrochloride (MP-Biomedicals), 4,5-diphenyl imidazole (Alfa Aesar), piroxicam (MP-Biomedicals), metoprolol tartarate (LKT Laboratories), naproxen (MP-Biomedicals), atenolol (MP-Biomedicals), and ranitidine hydrochloride (Alfa Aesar). Each of the small molecules were dissolved in DMSO to make a 10 mM solution (Acros, Spectroscopic Grade 99.9+%).

Chromatograms and mass spectra were collected using a Thermo Surveyor MSQ LC-MS with an APCI probe with 10 μ A corona, 350°C probe temperature, 80 V entrance cone. Waters XBridge C18, 5 μ m, 4.6x30 mm column and Regis IAM.PC.Fast Screen 1 cm x 3.0 mm with a 1x PBS at pH 7.2 (BDH) and methanol (Fisher) gradient was used for the determination of retention factors. The columns were linked together using Upchurch Scientific column couplers with a 0.007 inch inner diameter stainless steel tubing (U-284).

Octanol/water partitioning was performed in 1.5 mL microcentrifuge tubes (Fisher). The partitioning of the small molecules was analyzed between 1-octanol (Alfa Aesar) and PBS. Phosphate buffered saline (PBS) was prepared in 1 L batches using 18 M Ω water with 3.23 mM K₂HPO₄·7H₂O (J.T. Baker), 7.84 mM KH₂PO₄ (J.T. Baker), 5 mM KCl (Fisher), 150 mM NaCl (Fisher), and adjusted to pH 7.2 with HCl (Mallinckrodt) and NaOH (Fisher). The absorbance readings were completed with a Corning Costar 96 well UV plate (3635). All absorbance readings were performed on a Tecan Infinite M1000 plate reader.

2.2. HPLC Permeability Assay

The standard molecules were analyzed for permeability by HPLC using various combinations of IAM and C18 columns (IAM, C18, IAM-C18, C18-IAM, IAM-C18-IAM). An injection volume of 1 μL from the 10 mM solutions in DMSO was introduced onto the columns and eluted at 500 $\mu\text{L}/\text{minute}$ with 1x PBS and methanol mobile phase. The solvents were held isocratically at 20% (v/v) methanol for 5 minutes followed by an increase to 90% methanol over the next 5 minutes. After each run, the columns were re-conditioned with 20% methanol for 1 minute before the next analysis. All small molecules were analyzed in triplicate. The retention factor, k' , of the compounds were calculated using Equation 6, where t_r is the retention time (minutes) of the compound and t_m (minutes) is the void time of the column(s) (determined by the retention time of DMSO).

Equation 6)
$$k' = \frac{t_r - t_m}{t_m}$$

2.3. Octanol/Water Partitioning

Solutions of each molecule were prepared to 1 mg/mL in 1-octanol and PBS. From these solutions, 100, 300, and 400 μL of the analyte solution were transferred to separate 1.5 mL microcentrifuge tubes. Then, 400, 200, and 100 μL of 1-octanol or PBS were added to each to make the total volume 500 μL . Finally, 500 μL of the other phase (PBS to the vials with 1-octanol solution or 1-octanol to the vials with the PBS solution) was added to each tube.⁹⁰ All of the tubes were securely closed

and put on the reciprocating shaker at 150 rpm for agitation and incubation overnight. Violent shaking was avoided to prevent emulsion formation.

After about 24 hours of incubation, the tubes were centrifuged for 5 minutes at 1000 rpm. From both phases, 50 μ L were transferred to a 384-well UV plate. The UV plate was then centrifuged for 2 minutes at 1000 rpm to ensure a uniform liquid surface in each of the wells. The absorbance for each well was then scanned from 250-500 nm, every 2 nm, with 100 flashes per well. The log of the partitioning between phases ($\log P_{o/w}$) was then calculated using the adjusted absorbance, A , (with the background absorbance of the solvent subtracted) of each phase at the λ_{\max} of each compound, Equation 7.

Equation 7)
$$\log P_{o/w} = \log \left(\frac{A_{\text{Octanol}}}{A_{\text{Water}}} \right)$$

3. Results and Discussion

Given the nature of the C18 column, one would expect that a good correlation would be observed between the retention in C18 HPLC and the permeability values determined by HDM-PAMPA. Both methods are based on hydrophobic interactions between the molecules and long-chain alkanes. The correlation between the two methods is illustrated in Figure 22. As can be seen, there is a very poor correlation between HDM-PAMPA and retention on the C18 column for all compounds tested. This may be due to the partitioning mechanism (i.e. equilibration between the stationary and mobile phases) that occurs between the analyte and the functional groups in a HPLC column. It is concluded that the difference in the interaction

mechanism between the small molecules and the long chain alkyl groups between the two methods is very different and can therefore not be used as equivalent methods of analysis.

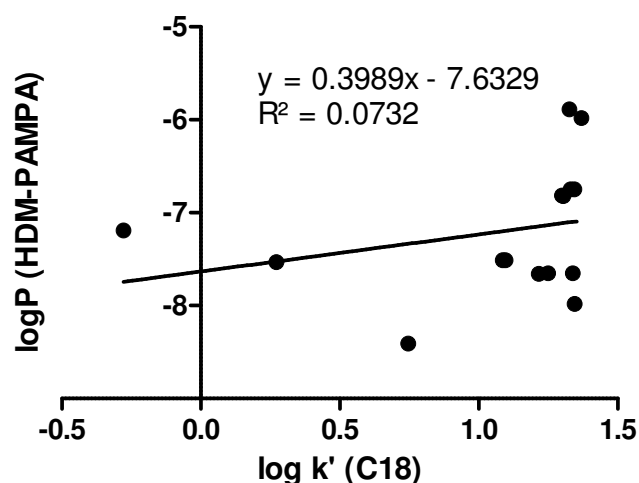


Figure 22. Correlation between the log of the retention factor on a C18 column and the HDM-PAMPA logP at pH 7.2.

Plots of the log of the small molecule retention factors, k' , for the coupled column combination of IAM-C18-IAM (23A), C18-IAM (23B), IAM-C18 (23C), and finally for the C18 column (23D) in relationship to $\log P_{\text{eff}}$ are shown in Figure 23. Tables containing all the values are located in Appendix B. The literature values for $\log P_{\text{eff}}$ were determined as human jejunal permeability^{73, 77, 83} using a single-pass perfusion of a proximal human jejunum between two inflated balloons, as described in part 1 of this chapter.^{73, 79-81} The plots depicted in Figure 23 have a similar pattern, suggesting that the C18 column retention is the limiting factor for these column combinations. The greater hydrophobicity of the C18 column retains the small molecules more than the IAM column. Nevertheless, the R^2 correlation values

of the linear regressions suggest a good correlation between C18 retention and *in vivo* human jejunal permeability values. This shows that the C18 column alone could give a simple and rapid method for the estimation of intestinal permeability.

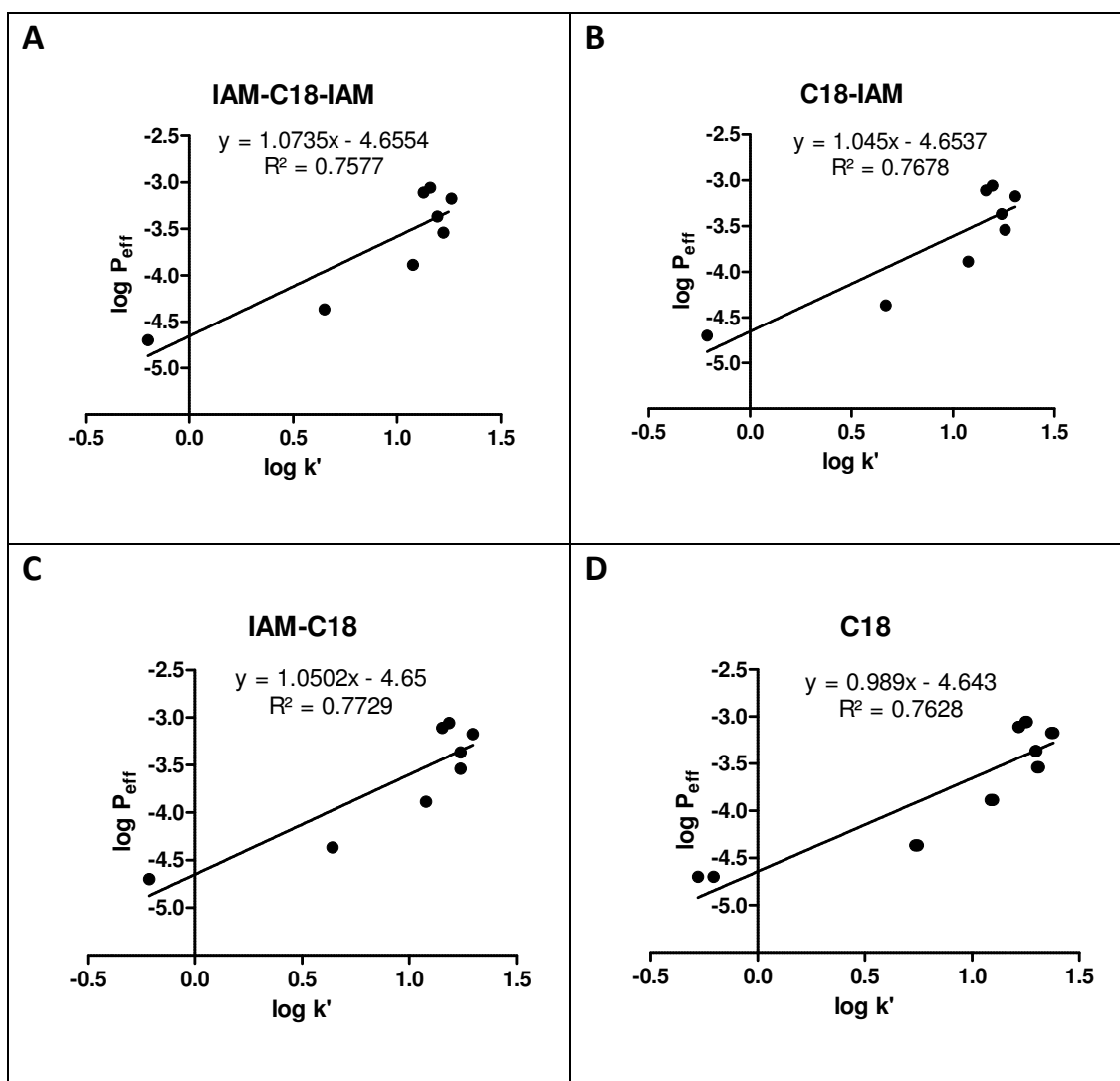


Figure 23. Relationship between $\log k'$ and $\log P_{\text{eff}}^{83}$ on A) coupled IAM-C18-IAM columns in series, B) coupled C18-IAM columns in series, C) coupled IAM-C18 in series, and D) C18 column.

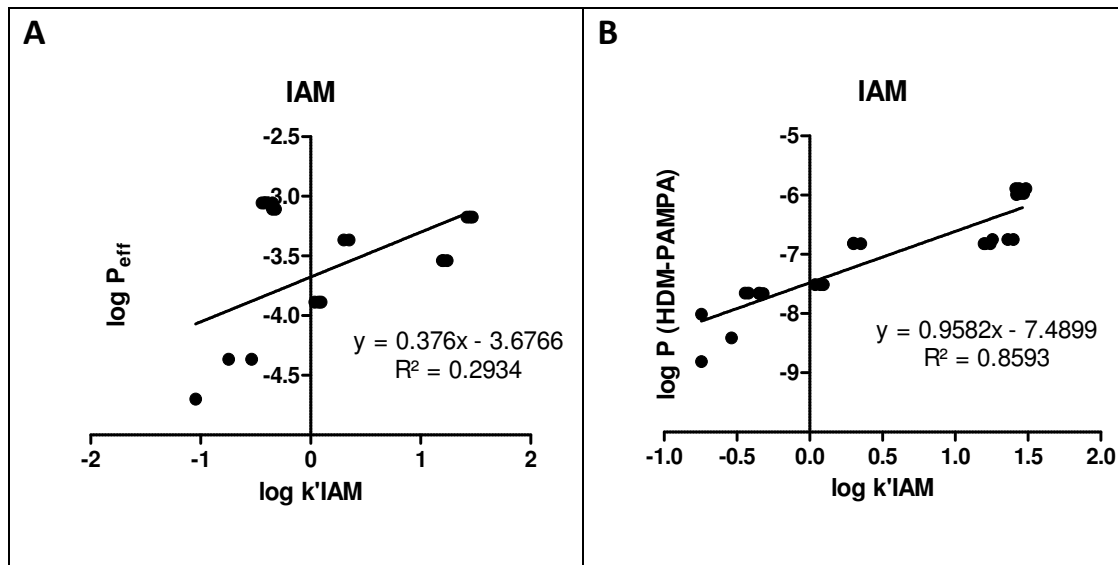


Figure 24. Relationship between A) $\log P_{\text{eff}}$ and B) $\log P$ (HDM-PAMPA at pH 7.2) versus $\log k'$ on the IAM column.

The relationships between the log of the small molecule retention factors for the IAM column with respect to the $\log P_{\text{eff}}$ and $\log P$ by HDM-PAMPA are shown in Figure 24 A and B. These results show that the retention on the IAM column is more closely related to the $\log P$ from the HDM-PAMPA than $\log P_{\text{eff}}$. This suggests that the HDM-PAMPA is based on a mechanism that is predominantly hydrophobic, which has previously been reported for the IAM column.⁹¹

As stated previously, all *in vitro* permeability measurements are based, to some degree, on lipophilicity. Measurements of lipophilicity can be related to *in vivo* permeability, but are not interchangeable with permeability. To determine which of these measurements are more directly related to pure lipophilicity, octanol/water partitioning was measured. The correlation between $\log P$ values and octanol/water partitioning is depicted in Figure 25. There is a strong correlation between $\log P_{\text{eff}}$

and $\log k'(C18)$ with $\log P_{\text{oct/water}}$ (Figure 25 A and C). These results support the correlation between the $\log k'$ for the C18 column and $\log P_{\text{eff}}$ (Figure 23D).

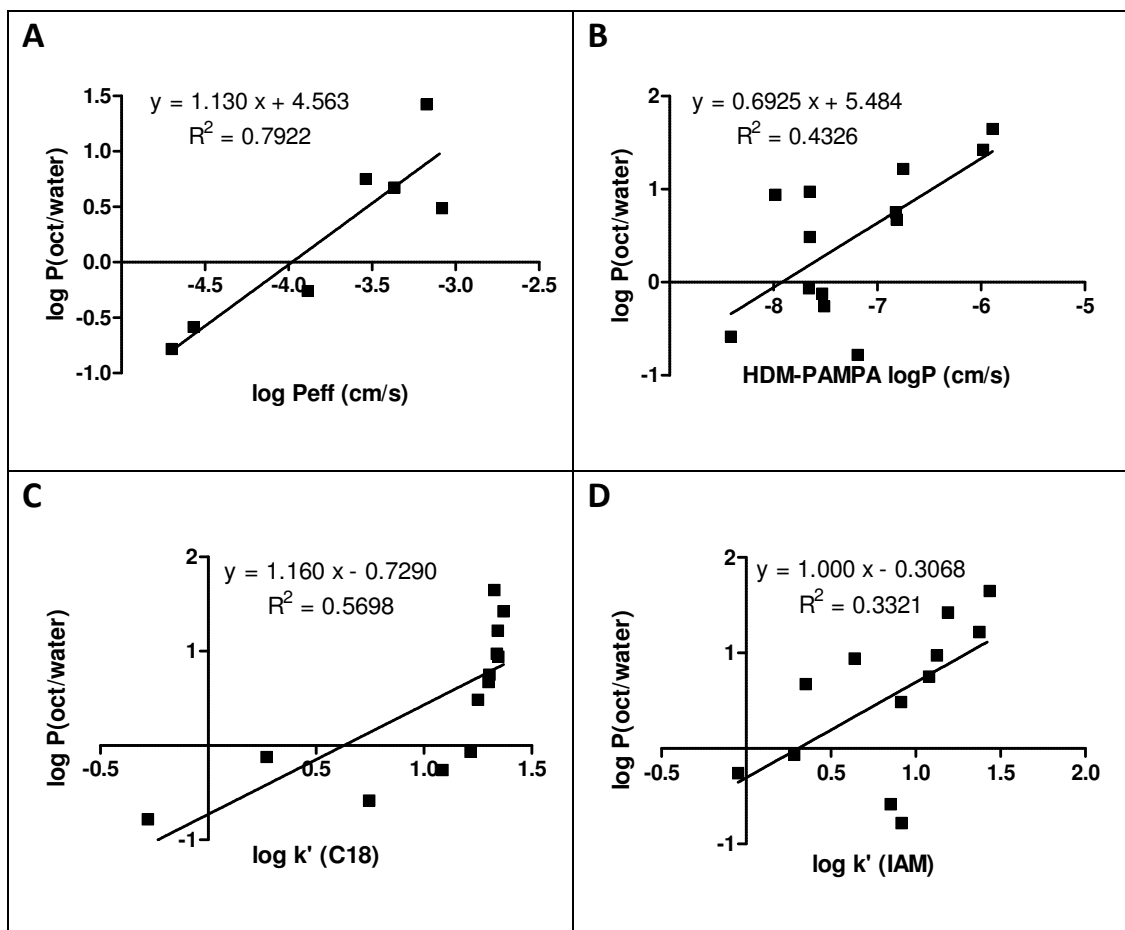


Figure 25. Octanol/Water partitioning correlation to A) $\log P_{\text{eff}}$ B) $\log P_{\text{HDM-PAMPA}}$ C) $\log k'_{\text{C18}}$ and D) $\log k'_{\text{IAM}}$.

The correlation with the octanol/water partitioning also suggests that these measurements are strongly lipophilicity-based measurements. A poorer correlation was observed between $\log P_{\text{oct/water}}$ with $\log k'(\text{IAM})$ and $\log P(\text{HDM-PAMPA})$, shown in Figure 25 B and D. Again, this is consistent with a mechanism of retention on the IAM column based predominantly on hydrophobicity. This also suggests that the

HDM-PAMPA is also dominated by a hydrophobic mechanism as opposed to lipophilicity. The difference in the mechanisms between the P_{eff} and the HDM-PAMPA are shown in Figure 26, with a poor correlation between the two.

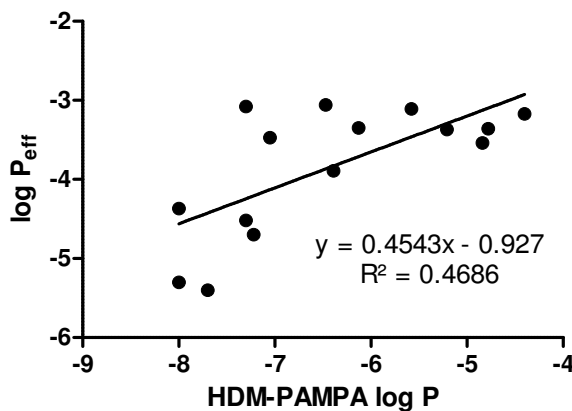


Figure 26. Correlation between HDM-PAMPA and effective permeability values from intestinal perfusion (P_{eff}).⁷³

Using the C18 column HPLC method, an unsatisfactory differentiation between highly lipophilic molecules was observed. This is especially obvious in Figure 25C. It is possible to increase the resolution of these compounds by decreasing the gradient of PBS to methanol and increasing the length of the experiment. In changing the HPLC solvent method, a larger k' difference for highly lipophilic molecules ($\log P_{\text{oct/water}} > 0$) may be achieved. Nevertheless, the current data shows a good correlation between methods to determine the $\log P_{\text{eff}}$ and $\log k'$.

4. Conclusions

The analysis of the retention of compounds using a combination of C18 and IAM columns has no advantage over the analysis using both columns separately. Nevertheless, a strong correlation has been shown between the retention of drugs

on the C18 column and *in vivo* jejunal $\log P_{\text{eff}}$ values. In addition, a good correlation was observed between the retention of the molecules on the IAM column and HDM-PAMPA $\log P$ values.

It was previously reported that the retention on an IAM column is dominated by a partitioning mechanism and thus, represents hydrophobicity.⁹¹ The correlation of the retention on the IAM column with HDM-PAMPA, suggest that both methods are predominately based on a hydrophobicity mechanism. The poor correlation between both of these methods with octanol/water partitioning supports this as well. The correlation of the retention factors on the C18 column with *in vivo* jejunal P_{eff} values for the same compounds suggests that both methods are based on a similar mechanism. The good correlation between both of these methods with octanol/water partitioning suggests that both are based predominately on lipophilicity.

The goal of these methods is to predict the membrane permeability of small molecules in high-throughput. It has been shown that there is a strong correlation between the retention in the C18 column with *in vivo* P_{eff} values, which were obtained using a single-pass perfusion of a proximal human jejunum between two inflated balloons. This research suggests that HPLC analysis on a C18 column may give a greater estimation of actual permeability than most lipophilicity or hydrophobicity measurements.

CHAPTER IV

ELECTROPHILICITY

1. Introduction

Confirmation of activity and selectivity of hit molecules identified by high-throughput screening (HTS) is an essential part of drug discovery. Especially for inhibitor screens, this often results in hundreds to thousands of hit molecules. The characterization of these molecules by secondary screens, which are not always amendable to a higher throughput format, leads to a bottleneck in the discovery pipeline. Frequently, these hit molecule selections contain a large number of promiscuous inhibitors that have a very poor outcome in the following steps of drug discovery.

Multiple underlying non-specific mechanisms have been identified for these inhibitors, such as aggregation⁶⁴, redox activity⁹², protein modification⁹³, and compound interference with the assay signal.⁹⁴ High-throughput assays have been developed to detect compound aggregation⁹⁵ and redox active compounds.⁹⁶ Virtual screening filters are applied to identify reactive molecules among hit compounds.⁹⁷⁻¹⁰¹ Importantly, some FDA approved drugs would be eliminated by these filters, such as irreversible H⁺, K⁺-ATPases inhibitors for duodenal and gastric ulcer.

To deactivate highly reactive and toxic species, the body produces a large amount of glutathione (GSH) to suppress the alteration of vital proteins. Thiol-containing molecules are extremely effective at reducing highly reactive,

electrophilic species. Glutathione donates an electron to reactive species with a high redox potential of -0.33 .¹⁰² It also indirectly regulates the dimerization of proteins that are based on the formation of disulfide bonds.

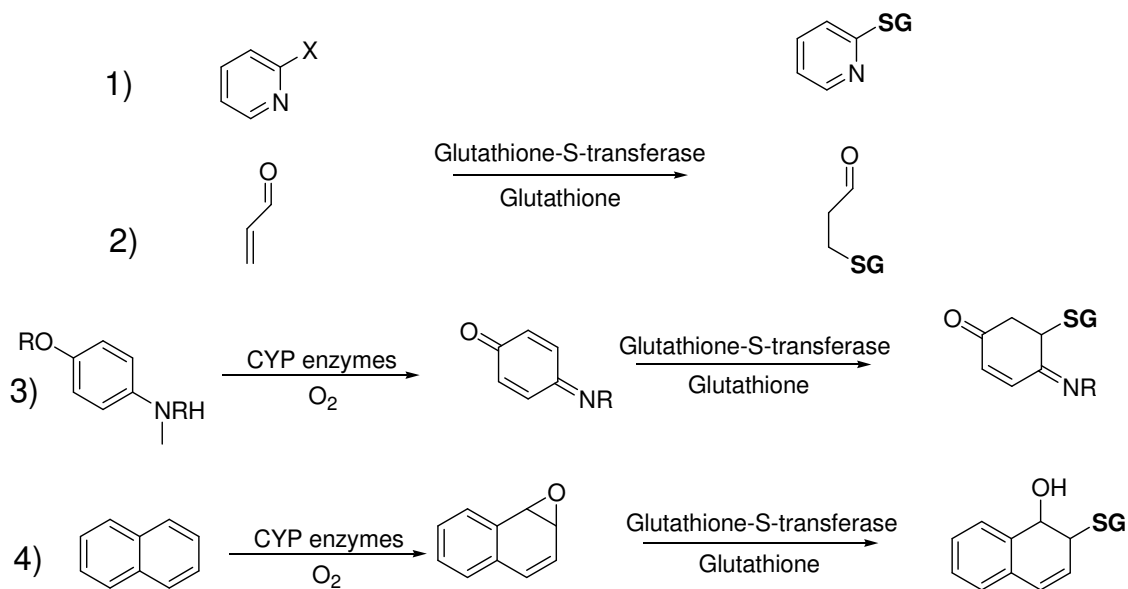


Figure 27. Formation of glutathione (GS) adducts with electrophilic species. 1) Displacement reaction, 2 and 3) addition to activated double bonds, 4) opening of a strained ring.¹⁰³

Highly reactive species can be absorbed by the body or formed by enzymes, such as CYP enzymes (Figure 27 reactions 3 and 4). For example, oxidation by CYP enzymes may result in the formation of a quinones or epoxides. One common example is the oxidation of acetaminophen and subsequent reaction with glutathione.¹⁰⁴ Binding to glutathione not only eliminates the risk of a highly reactive xenobiotics, but also increases the solubility of molecules for excretion.¹⁰⁵ Reactions of glutathione with electrophilic carbons are classified into three types (Figure 27):

displacement reactions, opening of strained rings, and addition to activated double bonds.¹⁰³ After the formation of glutathione adducts, the cell can replenish its glutathione levels within minutes.¹⁰²

Currently, HTS assays that determine the electrophilicity of small molecules and thus the ability to react with naturally occurring thiols have yet to be fully developed. One of the few approaches is a competitive binding assay using glutathione and fluorescein-5-maleimide.¹⁰⁶ Although, this assay could be adapted to high-throughput, it does not allow for the differentiation between electrophilic compounds that react with glutathione and nucleophilic compounds that react with fluorescein-5-maleimide. Additionally, many screening compounds interfere with the yellow/green fluorescence detection at 480/520 nm.⁹⁴ More recently, another lower throughput method has been developed using HSQC NMR by monitoring the ¹³C shift of small molecules that bind to thiol groups in a La antigen protein. The results were compared to the competitive fluorescein-based assay in which it achieves a better validation rate, although the method is far from high-throughput and requires expensive instrumentation.¹⁰⁷ There is still a great need for a simple, high-throughput method that can accurately assess the thiol-binding abilities of small molecules.

Herein, the development of a fluorescence-based (*E*)-2-(4-mercaptostyryl)-1,3,3-trimethyl-3*H*-indol-1-ium (MSTI) assay that enables the identification of thiol-reactive small molecules in a high-throughput manner is presented. In contrast to the very low-throughput detection of small molecule–glutathione adducts using

HPLC, we have developed a nucleophilic fluorescent probe with a discreet fluorescence at 510/650 nm, which enables the detection of thiol-reactive compounds in a 384-well plate format. Strong electrophilic drug candidates can represent a liability in drug discovery because of their elevated toxicity in cell-based assays and *in vivo* studies. Non-specific protein interactions can cause allosteric protein changes and depletion of glutathione levels, which are essential for the redox chemistry of the cell.¹⁰⁸ Therefore, the MSTI assay represents a novel HTS tool to identify compounds that interact with a nucleophilic sulfur group, such as cysteine, and enables the elimination of these compounds in an early stage of drug discovery.

2. Experimental

2.1. Materials and Instrumentation

All materials were used as they were received. Screening was performed with the Library of Pharmacologically Active Compounds; LOPAC-1280 (Sigma Aldrich). Each of the small molecules were dissolved in DMSO to make a 10 mM solution (Acros, Spectroscopic Grade 99.9+%). Phosphate buffered saline (PBS) was prepared in 1 L batches using 18 MΩ water with 3.23 mM K₂HPO₄·7H₂O (J.T. Baker), 7.84 mM KH₂PO₄ (J.T. Baker), 5 mM KCl (Fisher), and 150 mM NaCl (Fisher) and adjusted to pH 7.4 or pH 12 with HCl (Mallinckrodt) and NaOH (Fisher). Nonylphenyl Polyethylene Glycol (NP-40) surfactant (Boston BioProducts) was used as a buffer additive at 0.01% (v/v). The absorbance readings were completed in a 384-well UV plate (Greiner Bio-One, 781801). The assay was performed in a 384-

well, flat bottom, black assay plate (Corning, 3573) which was sealed with an aluminum cover (Corning, 6570) during incubation and mixing.

All of the absorbance and fluorescence readings were performed on a Tecan Infinite M1000 plate reader. Small volume transfers were performed on the Tecan Freedom EVO liquid handling system with a 100 nL pin tool transfer (V&P Scientific). Chromatograms and mass spectra were collected using a Thermo Surveyor MSQ LC-MS with an atmospheric pressure chemical ionization (APCI) probe with 10 μ A corona or electrospray ionization (ESI) probe with 3kV capillary, 350°C probe temperature, and Waters XBridge C18, 5 μ m, 4.6x30 mm column. A Biotage SP1 flash chromatography system and Gilson preparative LC (PrepLC) (215 Liquid Handler, 306 Pump, 112 UV Detector) with a Waters XTerra Prep MS C18 OBD column (5 μ m, 30x50 mm or 19x50 mm) were used for MSTI purification. A BioTek MicroFlo Select instrument was used for the addition of the MSTI probe solution to the assay plate.

2.2. Generation of MSTI

To detect thiol-reactive compounds, and thus electrophiles, a fluorescent probe was designed that exhibits different spectroscopic properties when in the nucleophilic state as opposed to a conjugate with electrophiles. Therefore, an aromatic nucleophilic thiol functionality was bound to a conjugated π -system of a fluorophore. An indolium dye in conjunction with a thiophenol was chosen for the formation of (*E*)-2-(4-mercaptostyryl)-1,3,3-trimethyl-3*H*-indol-1-ium (MSTI), shown in Figure 28.

MSTI, like all thiophenols, is oxygen sensitive and rapidly forms disulfides in non-degassed solvents. Attempts to store MSTI for a prolonged time in the reduced form as a solid or in solution were not successful. Similar difficulties have been reported for fluorescent thiophenols.¹⁰⁹ MSTI was synthesized from acetyl-MSTI under alkaline conditions, and acetyl-MSTI was in turn synthesized from 4-formylbenzyl thioacetate and 1,2,3,3-tetramethyl-3*H* indolium iodide, Figure 28.

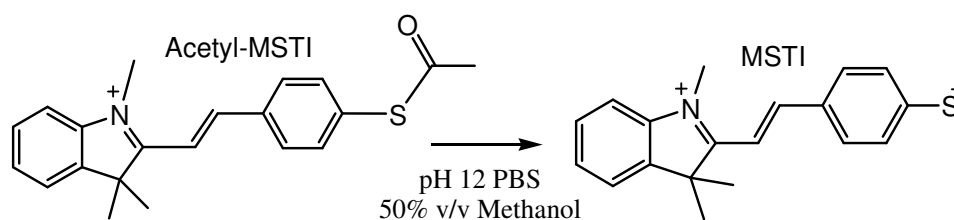


Figure 28. *In Situ* conversion from Acetyl-MSTI to MSTI

Acetyl-MSTI is stable as a solid as well as in solution and represents an excellent precursor for MSTI. Therefore, MSTI was generated *in situ* from acetyl-MSTI for screening purposes. A 10 mM solution of acetyl-MSTI in methanol was diluted in degassed PBS with 50% by volume methanol at pH 12 and stirred for 2 minutes. After that time, the solution became purple in color, and more than 80% of acetyl-MSTI was converted into MSTI as determined by absorbance, fluorescence, and LC-MS. Chromatograms and mass spectra for the conversion of acetyl-MSTI to MSTI are shown in Appendix C, Figures 70 and 71.

2.3. Thiol Reactivity Assay

In the preparation of the “compound plate”, 15 μ L of the 10 mM solution of small molecules in DMSO were dispensed in a 384-well polystyrene plate filling

rows 1 to 18. A second 384-well polystyrene plate, the “control plate”, had rows 19-24 filled with 15 μL DMSO. Acetyl-MSTI was dissolved in methanol as a 10 mM solution and added to a PBS buffered solution at pH 12 with 50% methanol in a ratio of 1:10 creating a dark purple colored solution. After stirring for 2 minutes, the solution was diluted with PBS at pH 7.4 with 2% DMSO, 0.01% NP40, and 5% methanol to form a pink colored, 30 μM solution at pH 7.4 of MSTI.

Next, 20 μL of the 30 μM solution was dispensed in row 1-23 (black polystyrene “assay plate”). A 30 μM solution of acetyl-MSTI (positive control) was made in the same buffer and 20 μL of this solution was dispensed to the assay plate (row 24). With the Tecan liquid handling system, 100 nL from the compound plate and 100 nL from the control plate were transferred into the assay plate using the pin transfer tool. The assay plate was then centrifuged for 2 minutes at 1000 rpm, covered with the aluminum cover, and put on the plate shaker for agitation during the incubation period.

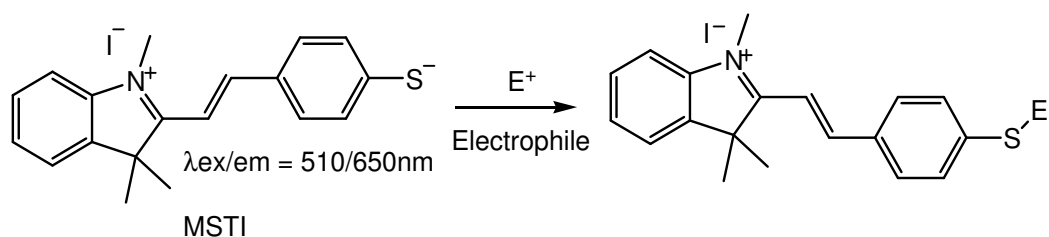


Figure 29. Electrophilic molecule addition to MSTI.

Addition of electrophilic molecules to MSTI occurs as in Figure 29. After 30 minutes of incubation, the assay plate is once again centrifuged for 2 minutes at 2000 rpm to ensure a uniform liquid surface during the reading. The assay plate

was then read using the Tecan M1000 plate reader for the detection of the unreacted MSTI. An excitation wavelength of 510 nm and emission wavelength of 650 nm with a bandwidth of 20 nm and 10 nm respectively, 100 flashes, 25 μ s integration time, optimized gain and z-position (optimized for maximum intensity of the 30 μ M MSTI solution), were used for the quantification of the fluorescence signal. The Z' value, Equation 8, for the assay was then calculated using MSTI as the negative control (0% binding) and acetyl-MSTI as the positive control (100% binding).¹¹⁰ The percent binding of the small molecules at a concentration of 100 μ M was reported as normalized response.

$$\text{Equation 8) } Z' = 1 - \left(\frac{3 \times (\text{Standard Deviation Positive} + \text{Standard Deviation Negative})}{|\text{Average Positive} - \text{Average Negative}|} \right)$$

3. Results and Discussion

At a concentration of 500 μ M in PBS, MSTI at pH 12 and acetyl-MSTI at pH 7.4 show different absorbance and fluorescence spectra (Figure 30 A and B). After changing the pH of the MSTI solution from pH 12 to 7.4, no change in the absorbance spectrum was observed. The wavelength of maximum absorbance (λ_{max}) of acetyl-MSTI was measured at 384 nm, while the λ_{max} of MSTI is at 526 nm (Figure 30A). This absorbance shift is very likely responsible for the appearance of a pink color of the MSTI solution. The fluorescence emission between 530 nm and 750 nm for both compounds at an excitation wavelength of 510 nm was measured for 100 μ M MSTI and 200 μ M acetyl-MSTI, respectively. The gain optimization function of the instrument (Tecan M1000) automatically adjusts the highest

fluorescence value between 40,000 and 50,000 units. The λ_{\max} of fluorescence emission with excitation at 510 nm was 562 nm for acetyl-MSTI and a broad emission peak between 550 nm and 700 nm was observed for MSTI (Figure 30B). Because MSTI was generated *in situ* from acetyl-MSTI, around 20% of acetyl-MSTI remained, which was responsible for the emission peak at 562 nm in the fluorescence spectrum of MSTI. However, a large fluorescent intensity difference between MSTI and acetyl-MSTI was observed.

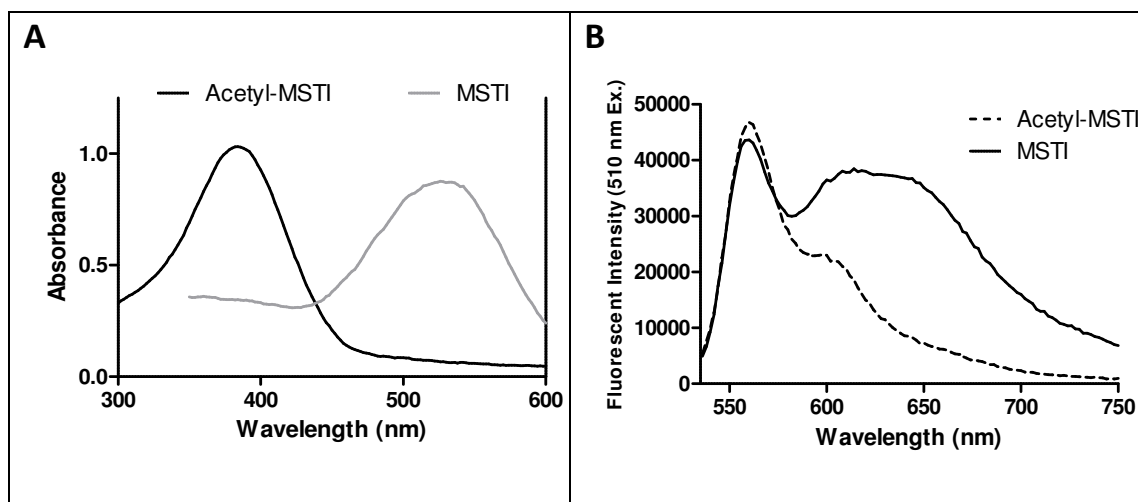


Figure 30. A) Absorbance spectra of 500 μM acetyl-MSTI and MSTI in PBS at pH 7.4. B) Fluorescence spectra of 200 μM acetyl-MSTI and MSTI in PBS at pH 7.4 with an excitation wavelength of 510 nm.

To optimize the fluorescence signal, the composition of the buffer was studied by monitoring the absorbance while varying the buffer reagent, pH, ionic strength (concentration of sodium chloride), or the concentration of MSTI. In each of the absorbance spectra for Figures 31-33, a 200 μM concentration of MSTI was used. A similar absorbance in PBS (50 mM phosphate, 150 mM NaCl, pH 7.0) and

Tris buffer (10 mM Tris base, 150 mM NaCl, pH 7.0) was observed for MSTI (Figure 31). At different pH values (pH = 6-9) in PBS, MSTI showed only a marginal difference in absorbance with the highest values between pH 7.0 and 8.0 (Figure 32). The optimal NaCl concentration was 150 mM giving the highest absorbance for MSTI (Figure 33).

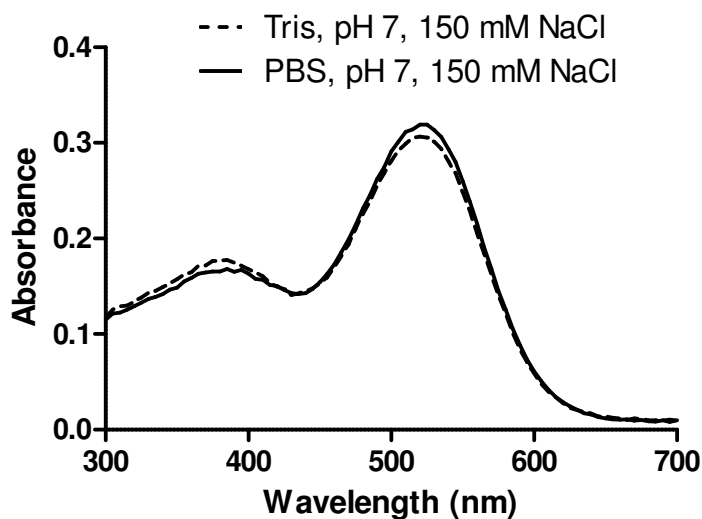


Figure 31. Absorbance spectra dependence of 200 μM MSTI on buffer composition.

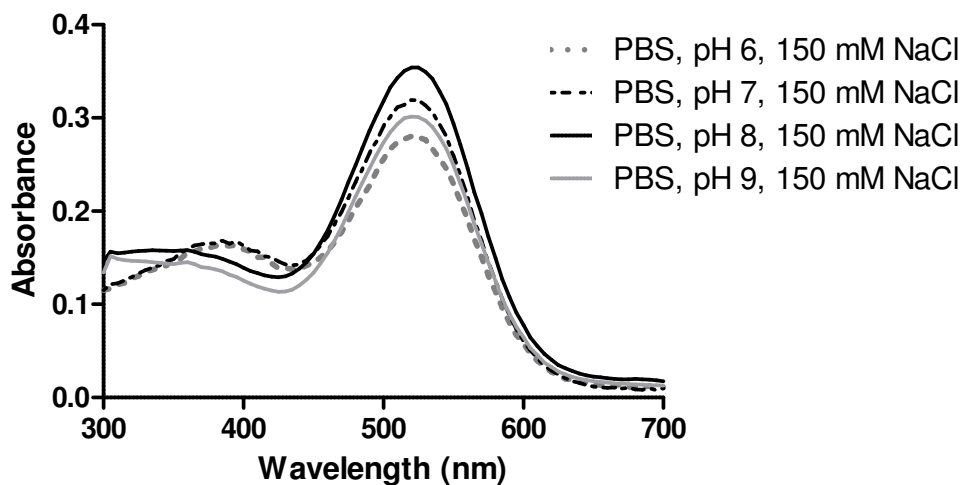


Figure 32. Absorbance spectra dependence of 200 μM MSTI on buffer pH.

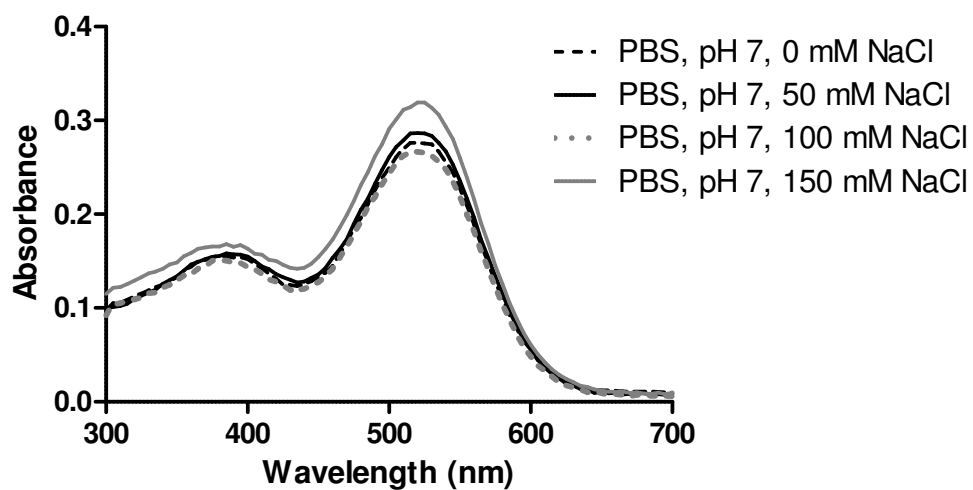


Figure 33. Absorbance spectra dependence of 200 μM MSTI on buffer ionic strength.

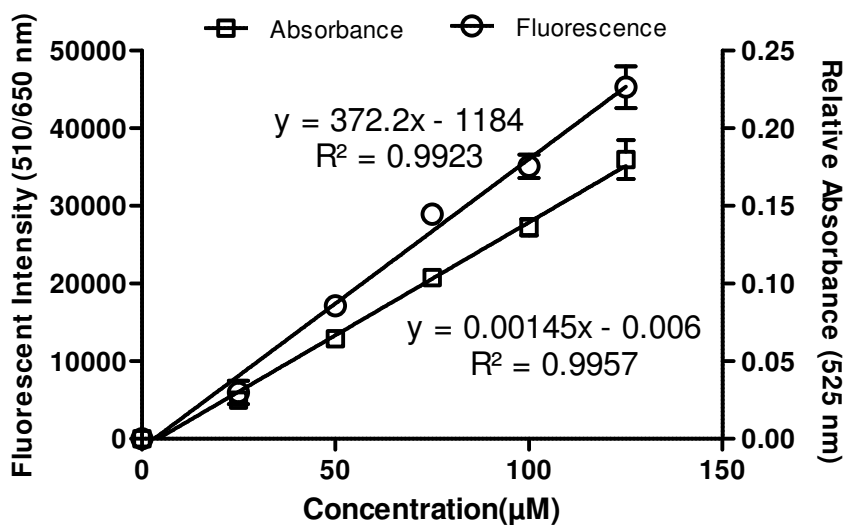


Figure 34. Concentration of MSTI versus absorbance and fluorescence intensity.

The absorbance (525 nm) and fluorescence (510/650 nm) for MSTI in PBS (pH 7, 150 mM NaCl) were measured at different concentrations (Figure 34). Both absorbance and fluorescence intensity were linear between 0.01 and 125 μM MSTI. Relative standard deviations of <5% for the absorbance and fluorescence intensity

were observed for all concentrations used. From this study it was determined that an acceptable Z' value¹¹⁰ of around 0.6 could be achieved with as little as 30 μM of MSTI in the presence of phosphate buffer (50 mM) at pH 7 and 150 mM NaCl.

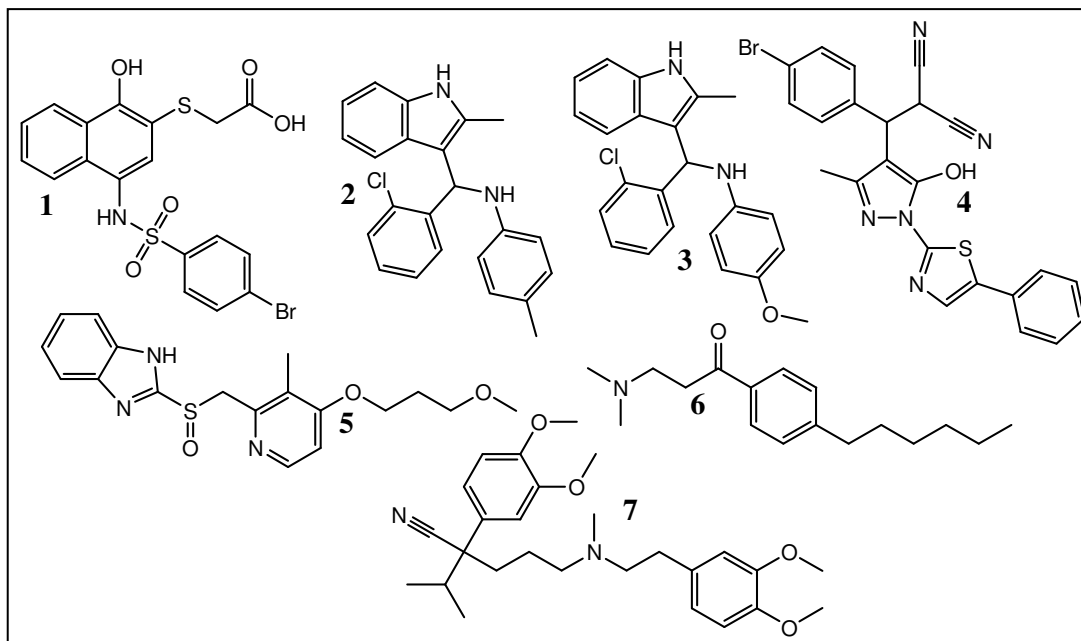


Figure 35. Compound key for Figures 36, 37, and 38.

Compounds 1-6 changed the fluorescence intensity of MSTI, whereas compound 7 did not (Compound key, Figure 35). Compound 1 has been investigated as a proteasome inhibitor with low micromolar toxicity.¹¹¹ The mode of action of this compound has not yet been elucidated, but the formation of the conjugate of compound 1 and MSTI has been confirmed by MS (Appendix C, Figures 64 and 65). Compound 2 and 3 are from a series of 2-indolyl methanamines, which have been recently identified as irreversible inhibitors of the vitamin D receptor (VDR)-co-activator interaction.¹¹² The mode of action of these molecules includes

the formation of an electrophilic species, which is believed to allosterically inhibit the VDR protein-protein interaction with co-regulators. The formation of adducts of compounds 2 and 3 with MSTI have also been identified by MS (Appendix C, Figures 66 and 67 for compound 2, Figures 68 and 69 for compound 3). The electrophilic bisnitrile compound 4 was identified during the assay optimization. Compound 5 is rabeprazole, a proton pump inhibitor that is known to form disulfide bonds with cysteine residues of H⁺, K⁺-ATPases.¹¹³ Compound 6 was identified as an irreversible inhibitor of the thyroid receptor–coactivator interaction by forming an unsaturated ketone that alkylates a cysteine residue in the thyroid receptor-coactivator binding pocket.^{114, 115} Finally, as a negative control, verapamil (compound 7) was used.

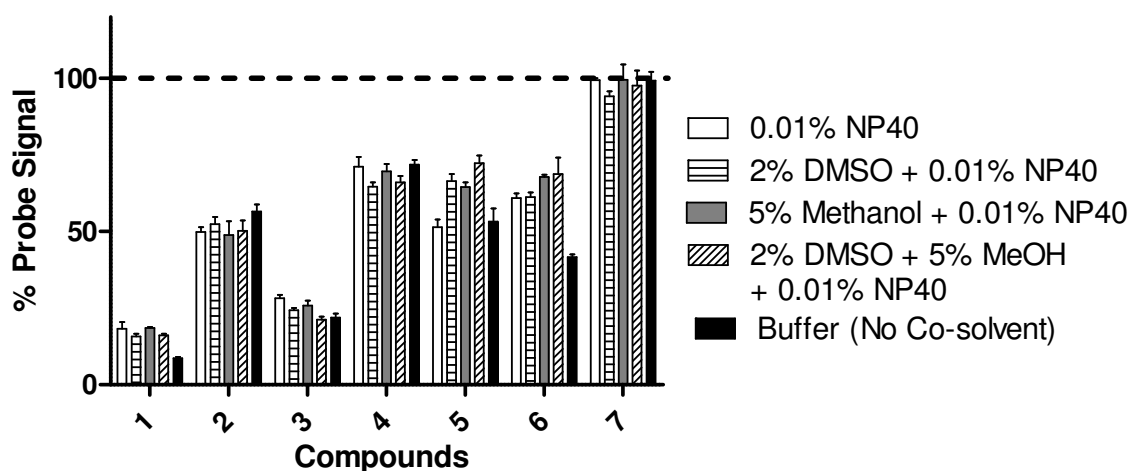


Figure 36. Evaluation of the MSTI assay in the presence of small molecules, PBS (50 mM, pH 7.4, 150 mM NaCl), MSTI (30 μ M) and an excitation and emission wavelength of 510 nm and 650 nm, respectively. Change of fluorescence intensity in the presence of small molecules 1-7 (Compound Key, Figure 35) (100 μ M) and different additives (n=3).

Three different additives (methanol, DMSO and NP-40) and several combinations of additives were investigated (Figure 36). In this study, 30 μM of MSTI and compounds 1-7 (100 μM) in PBS (50 mM, pH 7.4, 150 mM NaCl) were incubated for 30 minutes and analyzed by fluorescence detection (510nm/650nm). As controls, MSTI (negative) and acetyl-MSTI (positive) were used and the signal was normalized to percent of the MSTI signal. Interestingly, only small differences were observed for the compounds 1-7 in the presence of buffer additives. Nevertheless, the addition of NP-40 was preferred to circumvent the possibility of compound aggregation^{64, 95, 116} and the addition of DMSO and methanol to enhance small molecule solubility.

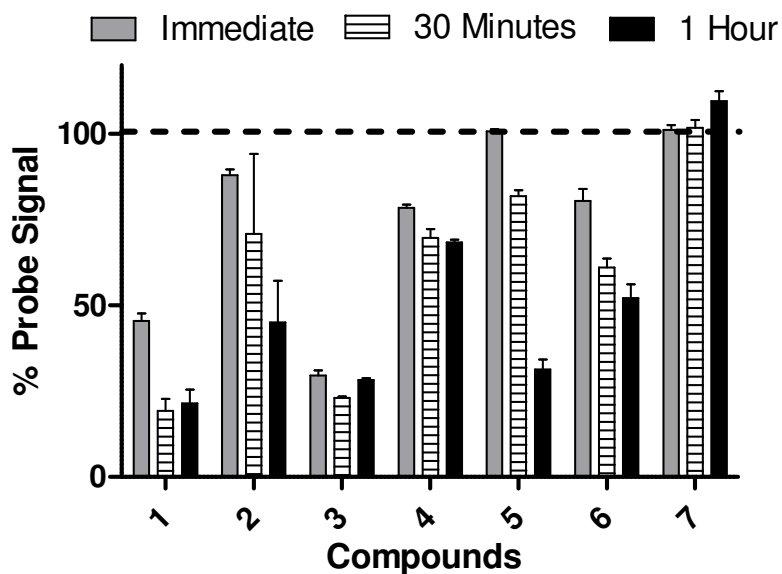


Figure 37. Change of the fluorescence intensity in the presence of small molecules 1-7 (100 μM) with 2% DMSO, 5% methanol, and 0.01% NP-40 by volume in PBS at different time points (n=3). PBS (50 mM, pH 7.4, 150 mM NaCl), MSTI (30 μM) and an excitation and emission wavelength of 510 nm and 650 nm, respectively (Compound Key, Figure 35).

Furthermore, different time points were investigated confirming the time dependency of covalent bond formation between compounds and MSTI. All six active compounds showed a stronger alkylation after 30 minutes than immediately after the addition (Figure 37). Compounds 2, 5, and 6 showed a further decrease after 1 hour. Finally, for the investigation of compound concentrations, for all six compounds a change of the MSTI signal in the presence of more compound (100 μM instead of 50 μM) was observed (Figure 38). Interestingly, no further changes of the signal were observed at the highest compound concentration used (150 μM).

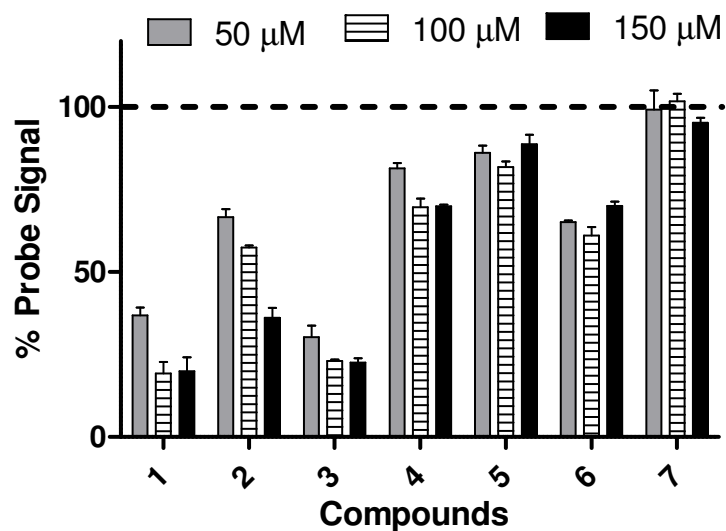


Figure 38. Change of the fluorescence intensity in the presence of small molecules 1-7 (50, 100 and 150 μM) with 2% DMSO, 5% methanol, and 0.01% NP-40 by volume in PBS. PBS (50 mM, pH 7.4, 150 mM NaCl), MSTI (30 μM) and an excitation and emission wavelength of 510 nm and 650 nm, respectively (Compound Key, Figure 35).

With the optimized MSTI assay conditions: PBS (50 mM, pH 7, 150 mM NaCl), MSTI (30 μM), compounds (100 μM), 5% methanol, 2% DMSO, and 0.01% NP-40; a

library of small molecules was screened. The Library of Pharmacologically Active Compounds-1280 (LOPAC) screening collection was used to determine the quality of the assay and the ability to identify compounds that are reactive towards nucleophiles. Each LOPAC compound was measured in triplicate (Figure 39).

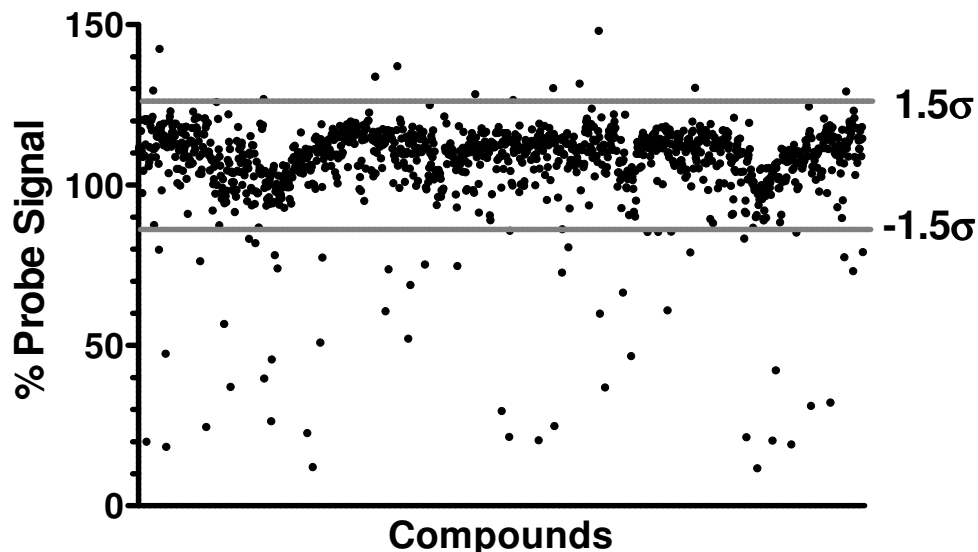


Figure 39. Results of MSTI-LOPAC screen (1280 compounds), $n=3$.

The Z' values of this screen ranged between 0.62 and 0.88 with a mean of 0.75 (Figure 40). The mean fluorescence intensity of all compounds in the presence of MSTI, was 107.0% of the MSTI signal with a standard deviation (σ) of 14.2%. In order to safely distinguish between active and inactive molecules, a cutoff of 1.5 standard deviations from the mean was chosen as indicated with the gray lines in Figure 39. Observing a subset of random 224 LOPAC compounds more closely, the cutoff of 1.5σ represents an acceptable distinction between both populations (Figure 41).

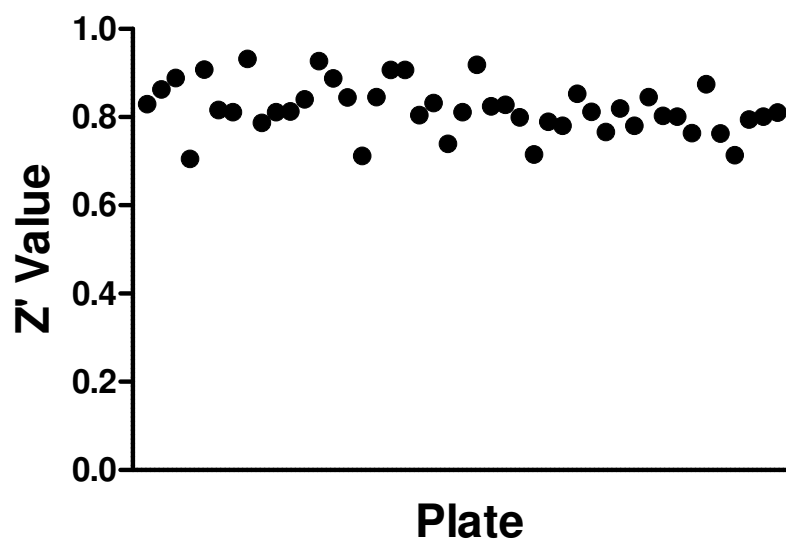


Figure 40. Summary of the Z' values of each assay plate.

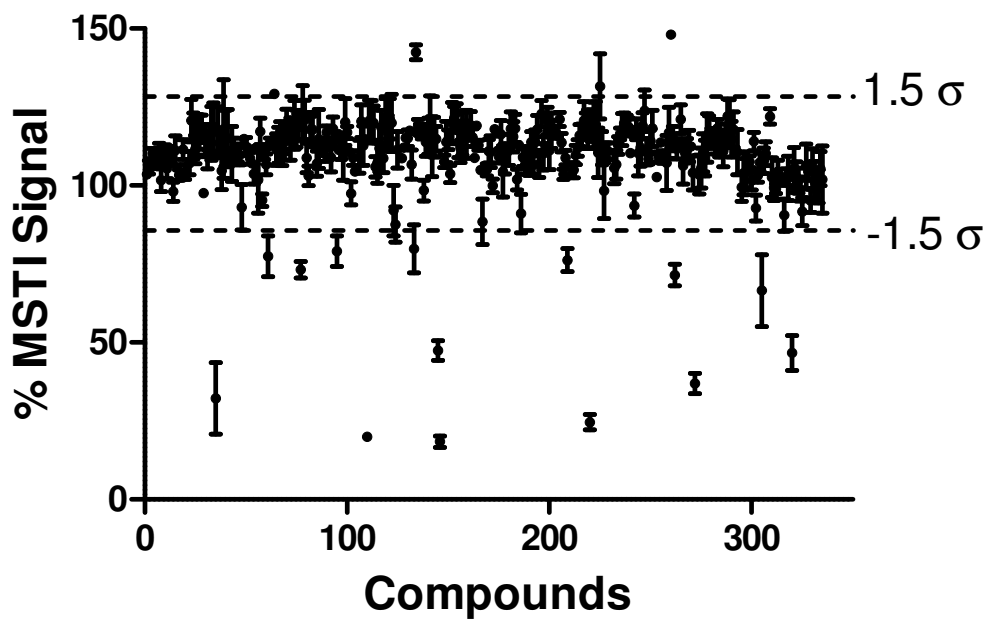


Figure 41. Normalized fluorescence intensity data of a single 384-well LOPAC compound plate in triplicate with their standard deviation.

The background fluorescence was also determined for each LOPAC molecule (100 μ M) in the absence of MSTI at a 510 nm excitation and 650 nm emission wavelength. The vast majority of LOPAC compounds exhibited no fluorescence and gave fluorescence intensity values similar to those measured for the assay media (i.e., background) (Figure 42A). However, eleven compounds exhibit an intrinsic fluorescence intensity of more than 1.5σ of the mean fluorescence signal (21.3%) of MSTI (Figure 42B).

The MSTI-LOPAC screen identified 9 compounds that exhibit a fluorescence intensity of more than 129% of the MSTI fluorescence intensity and 55 compounds with less than 85 % of MSTI fluorescence intensity. The summary of these compounds is provided in Appendix C. Using a cut-off of $\pm 1.5 \sigma$, the hit rate was determined to be 5%. The majority of the hits identified, as predicted, were electrophilic compounds (Figure 43A). These include transition metal complexes bearing ions such as Au^{2+} and Pt^{2+} , α -haloketones, quinones, NO-releasing compounds, halo-alkenes, and unsaturated carbonyl or carbonyl-like compounds. The MSTI conjugates of electrophilic molecules were characterized by $^1\text{H-NMR}$ and MS, such as the 2-iodoactamide-MSTI conjugate (Appendix C). Other compounds identified are those that can undergo a conversion to an electrophilic compound such as β -aminoketones (conversion into unsaturated ketones) and 2-chloroamine derivatives (conversion into aziridines) (Figure 43B). Interestingly, we also identified lansoprazole, a proton pump inhibitor that forms disulfide bonds with cysteine residues. The same mode of action has been reported for positive control compound 5, rabeprazole (Figure 35).

This assay also identified the compound class of apomorphines (Figure 43C). A possible explanation could be the formation of the corresponding diketone, which has been reported under aqueous conditions.¹¹⁷ The diketones, in contrast to the norapomorphines, have a red-shifted absorbance, which might be the underlying mechanism for these false positive hits. Finally, the majority of disulfides and sulfoxides (Figure 43D) were identified by the MSTI assay, confirming the sensitivity of the reduced MSTI probe for other oxidized sulfur species.

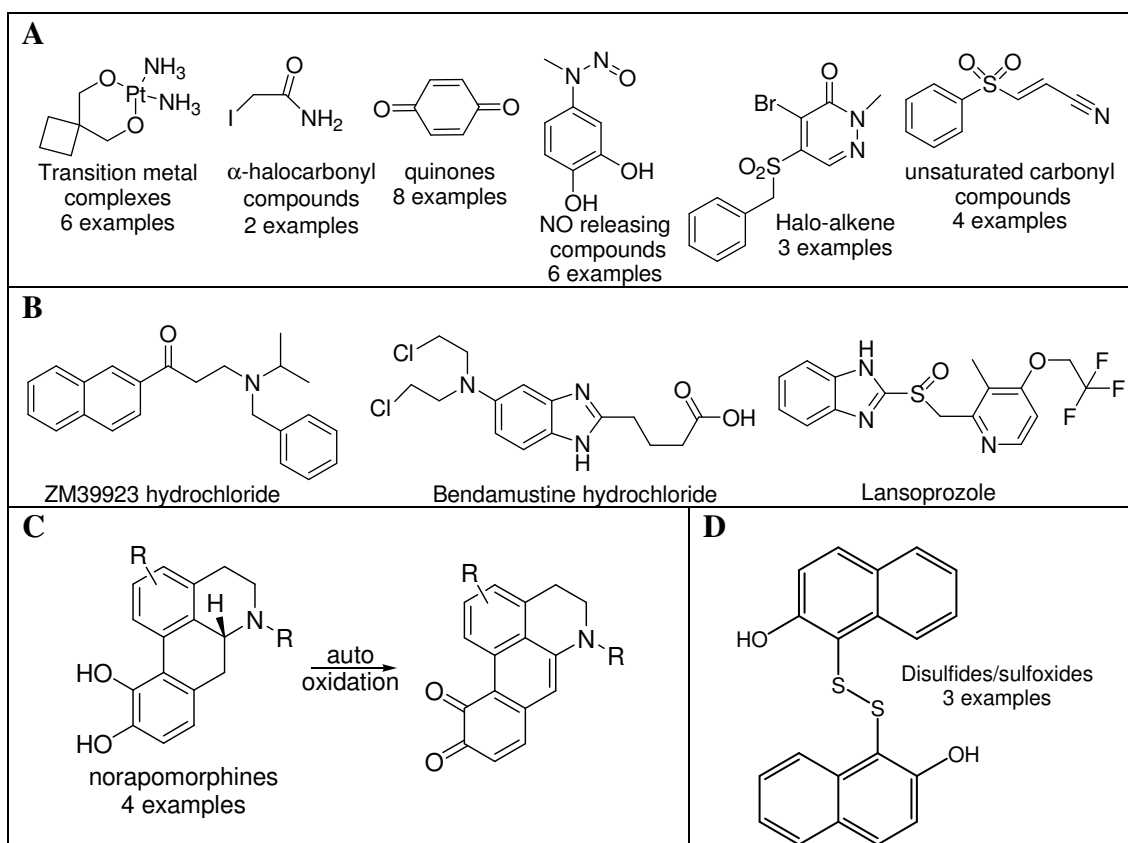


Figure 43. Thiol-reactive compound classes identified by the MSTI assay.

4. Conclusions

Molecules that react with thiols, such as cysteine, have the potential to non-selectively modulate proteins or alter their modes of action, which can be a hallmark of promiscuous inhibition. MSTI, a newly developed molecular probe, can be used to identify thiol-reactive small molecules. MSTI bears a nucleophilic thiol group that can easily react with electrophiles or oxidants to form conjugates or disulfides. The covalent bond formation has a dramatic influence of the fluorescent properties of MSTI, significantly reducing the fluorescence intensity at 650 nm. The MSTI assay only requires an incubation time of 30 minutes and although optimized for a 384-well format, it is easily convertible to 1536-well format.¹¹⁸

The application of a precursor, acetyl-MSTI, has the advantage that the reactive MSTI probe can be reliably produced *in situ*, thus circumventing any challenging storage regimes for MSTI. The MSTI assay is the first HTS assay that identifies thiol-reactive small molecules among screening library compounds. Therefore, this assay can identify their mode of action, as shown for several examples of irreversible inhibitors among the LOPAC screening library. The far-red detection of MSTI limits the number of molecules interfering with the assay, which was 0.85% for the LOPAC screening library. The assay has an excellent reproducibility ($Z' > 0.6$) and standard deviation of $< 5\%$ for each compound. The MSTI assay will be a helpful tool to quickly identify potential promiscuous inhibitors among screening hits and enable the fast identification of the mode of action of hit compounds in regard to their ability to react with nucleophilic protein residues.

CHAPTER V

PROTEIN-SMALL MOLECULE BINDING

PART 1: HIGH-THROUGHPUT ULTRAFILTRATION

1. Introduction

It is widely understood that the extent of drug-plasma protein binding is a major determinant of drug distribution to sites of action as well as metabolism. Only the unbound drug is capable of passing through membranes and bind to metabolic enzymes.¹¹⁹ Non-specific binding of small molecules to plasma proteins causes a decrease in the free drug concentration available to the site of action. Interactions between drugs and plasma proteins may occur through ionic binding, hydrogen bonding, or Van der Waals interactions. Although reversible, drug-plasma protein binding has a significant influence on the pharmacokinetic and pharmacodynamic properties of drugs.^{24, 120} It also can have a large affect on other pre-clinical screens.^{120, 121}

Serum albumin is one of the most abundant blood proteins. It is a carrier for many low polarity metabolites and drugs. The lack of specificity toward particular ligands, multiple binding sites, and allosteric effects complicate the studies of binding to albumin.^{122, 123} Albumin is the major culprit for binding of acidic and neutral drugs.¹²⁴ Basic drugs are bound to a lesser extent to albumin, but bind to globulins.¹²⁵ Protein binding studies are typically studied *in vitro* with either plasma

or serum. Equilibrium dialysis and ultrafiltration are the most commonly used techniques for protein-binding measurements.²⁸

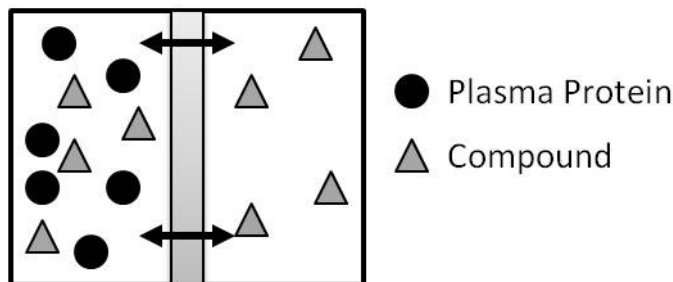


Figure 44. Equilibrium dialysis method for the determination of plasma-protein binding.

Equilibrium dialysis is often considered the “gold standard” method for *in vitro* determination of drug-protein binding. An image illustrating equilibrium dialysis is shown in Figure 44. A plasma solution spiked with drug is placed in one cell of the dialysis apparatus and buffer is placed in the other. The two cells are separated by a semipermeable membrane through which the macromolecule cannot pass. Unbound drug diffuses across the membrane down its electrochemical gradient until equilibrium is reached and the unbound concentration of the drug is equal in both compartments. Usually an incubation period of 6 hours at 37°C is sufficient for most compounds to reach equilibrium (with a 1 mL volume in each cell).²⁸ With equilibrium dialysis, theoretically, non-specific binding to the apparatus is not an issue if equilibrium is reached. Some studies have shown that pre-treatment of the membranes with detergents, such as Tween or NP-40, reduces the extent of non-specific binding.¹²⁶ Equilibrium dialysis continues to be the

benchmark by which other methods are assessed, although it is labor intensive, costly, time consuming, and difficult to automate.²² Recently, developments have been made to improve the equilibrium dialysis method by application in 96-well dialysis blocks, but at least 4 hours of incubation are required to reach equilibrium.^{22, 127, 128}

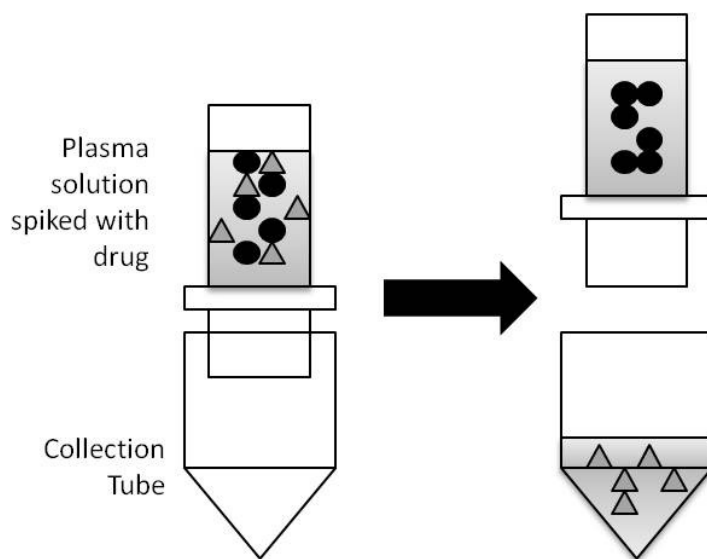


Figure 45. Ultrafiltration method for determination of drug-protein binding.

Ultrafiltration methods have also been readily employed for the determination of plasma protein binding. An illustration of the ultrafiltration method is shown in Figure 45. The ultrafiltration tube contains two parts. The upper part has a semipermeable membrane through which small molecules pass while macromolecules are retained. The plasma is pre-incubated with the drug, typically at 37°C for about 15 minutes. The pre-spiked plasma solution is loaded into the ultrafiltration tube and centrifuged at 500 x g until about 10% of the volume initially loaded is separated out as filtrate in the collection tube.²⁸ The ultrafiltrate is

then analyzed for the drug concentration. It is best to ensure that the volume of the ultrafiltrate does not exceed 10% of the volume loaded to circumvent concentration effects.²⁸ In some methods, the recommended acceptable volume of filtrate is 20–35% percent of the original plasma sample, resulting in minimum disturbance to the protein-binding equilibrium.¹²⁹ Ultrafiltration is a relatively fast and simple method which has been shown to have a good correlation to other methods. Nevertheless, non-specific binding to the filtration apparatus has been a major issue.^{23, 127} The main disadvantage of these techniques is the disturbance of the drug-protein equilibrium by the separation of the free drug.¹³⁰

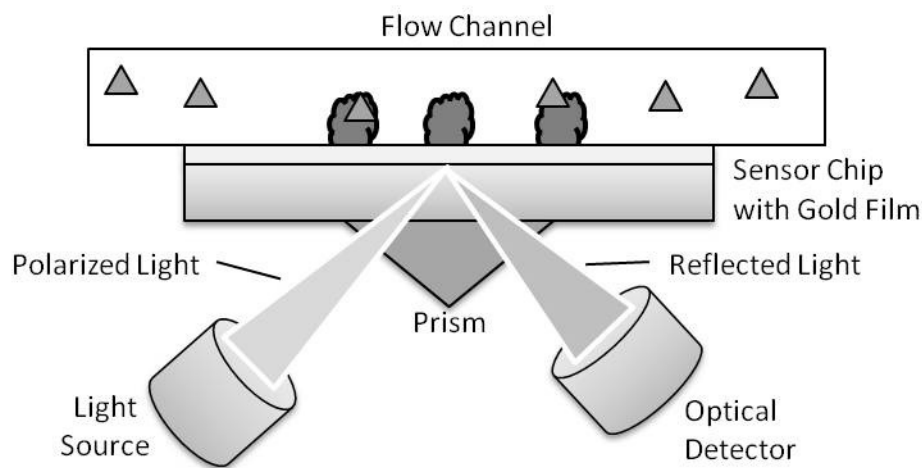


Figure 46. Diagram of surface plasmon resonance (SPR).¹³¹

Surface plasmon resonance (SPR) is an optical biosensor technique that measures binding events at the gold metal surface by detecting changes in the local refractive index (Figure 46).¹³¹ SPR is a surface sensitive technique that is ideal for studying the interactions between immobilized biomolecules and analyte in

solution. Because the measurements are based on changes in refractive index, sensitive and label-free detection is possible. Also, analysis can be performed in real-time, enabling the calculation of kinetic and thermodynamic binding constants.^{25, 131} Finally, SPR is sensitive to the binding of molecules over a wide range of molecular weights and affinities.²⁵ However, this method assumes that the immobilized protein retains its full binding characteristics.²⁶

In effort to increase throughput of plasma protein binding techniques, methods such as LC-MS with an immobilized human serum albumin (HSA) column^{128, 132, 133}, capillary electrophoresis^{128, 134, 135}, or HSA immobilized on silica beads¹³⁶ have been applied with reasonable success. However, as stated before, these methods assume that the immobilized protein retains its full binding characteristics and assumes non-specific binding has no impact.²⁶ Fluorescence methods have also been used for the determination of drug-protein binding. These methods will be discussed in detail in Part 2 of this chapter.

More recently, attempts have been made to increase the throughput of the of ultrafiltration methods. Studies have been published using a 96-well plate with a 10 kDa molecular weight cutoff (MWCO) membrane along the bottom of the wells.^{120, 129} The samples were pooled, four molecules incubated with serum per well, to increase the throughput of analysis.¹²⁰ Sample pooling may cause saturation of the binding sites available on the proteins and therefore yield inaccurate results. Both 96-well plate methods, with analysis of the ultrafiltrate by LC-MS/MS, have a fair correlation to conventional methods.^{120, 129} Concentration effects may play a

significant role in the results.^{28, 120} Also, collection of different volumes at the edges of the filter plate versus the central wells can be an issue with application in 96-well plates.¹²⁹ Another major issue concerning the throughput of these methods is that a centrifugation time of 45-60 minutes was necessary for collection of the ultrafiltrate.^{120, 129} Application of silica-immobilized HSA (TRANSIL-HSA) has also been applied in 96 and 384-well plates and has shown good correlation to equilibrium dialysis methods, with a centrifugation period of only five minutes.¹³⁶ This method has even been marketed recently as a kit for plasma protein-binding analysis.^{137, 138} Development of a 384-well plate with a MWCO membrane that has been shown to have uniform filtration rates across the plate¹³⁹ makes it possible for the development of a higher throughput ultrafiltration assay without the need for sample pooling.

2. Experimental

2.1. Materials and Instrumentation

All materials were used as received. The following small molecules were used as standards: diethylstilbestrol (Spectrum Chemical Mfg. Corp.), β -estradiol (Alfa Aesar), caffeine (Alfa Aesar), D,L-propranolol hydrochloride (MP-Biomedicals), piroxicam (MP-Biomedicals), metoprolol tartarate (LKT Laboratories), naproxen (MP-Biomedicals). Each of the small molecules were dissolved in DMSO (Acros, Spectroscopic Grade 99.9+%) to make 10 mM solutions.

Solutions from lyophilized powder, fatty acid free, globulin free, $\geq 99\%$ human serum albumin (HSA) (Sigma Aldrich) were made in phosphate buffer.

Dialysis of HSA solutions were performed with 10 mL, 50 kDa dialysis tubes (Spectrum Labs, G235070). After dialysis, HSA solutions were stored for no longer than one week at 4°C. Phosphate buffered saline (PBS) was prepared in 1 L batches using 18 M Ω water with 3.23 mM K₂HPO₄·7H₂O (J.T. Baker), 7.84 mM KH₂PO₄ (J.T. Baker), 5 mM KCl (Fisher), 150 mM NaCl (Fisher), and adjusted to pH 7.2 with HCl (Mallinckrodt) and NaOH (Fisher). Nonylphenyl polyethylene glycol (NP-40) 0.01% (v/v) surfactant (Boston BioProducts) and glycerol (Fisher) were used as buffer additives.

The absorbance readings were completed in a 384-well UV plate (Greiner Bio-One, 781801). The assay was performed in a 384-well filter plate with 30 kDa molecular weight cutoff membrane (Pall, 5078) which was sealed with an aluminum cover (Corning, 6570) during incubation and mixing. Separation of the ultrafiltrate was done by centrifugation with an Eppendorf 5810R centrifuge. All of the absorbance readings were performed on a Tecan Infinite M1000 plate reader. Chromatograms and mass spectra were collected for molecules and reaction products using a Thermo Surveyor MSQ LC-MS using electrospray ionization (ESI) with 3 kV capillary, 350°C probe temperature, and Waters XBridge C18, 5 μ m, 4.6x30 mm column

2.2. High-Throughput Ultrafiltration Assay

A 5.0 mg/mL solution of HSA was prepared in PBS and dialyzed exhaustively (4 times, 24 hours each) in 3 L of the same buffer at 4°C. After dialysis, 68 μ L of the HSA solution were added to half of wells in the filter plate. In the other half of the

plate, 68 μL of PBS were added. To both the HSA solution and PBS, 2 μL of the 10 mM standard molecule solutions in DMSO were added in triplicate. As a control, for the background signal, 2 μL of DMSO was added in triplicate to both the HSA solution and PBS. The filter plate was placed on top of a 384-well polystyrene collection plate. The plate was then covered and agitated on the reciprocal plate shaker for ten minutes.

After the incubation period, the plate was centrifuged for 20 minutes at 1500 x g with the collection plate still underneath the filter plate. The ultrafiltrate was collected in the filter plate during centrifugation. After collection, 50 μL of the ultrafiltrate were transferred to the 384-well UV plate. The absorbance was then measured over a range from 250 to 500 nm, every 2 nm, with 100 flashes per well. The percentage of bound compound was then calculated with Equation 9 at the λ_{max} of the molecule, where A_e is the absorbance of the ultrafiltrate at equilibrium after incubation of the small molecules with HSA, $A_{\text{Bkgd},e}$ is the absorbance of the ultrafiltrate at equilibrium after incubation of DMSO with HSA, A_0 is the absorbance of the ultrafiltrate of the small molecules incubated in buffer, and $A_{\text{Bkgd},0}$ is the absorbance of the ultrafiltrate of DMSO incubated in buffer.

Equation 9)
$$\% \text{ Bound} = \left(1 - \left[\frac{A_e - A_{\text{Bkgd},e}}{A_0 - A_{\text{Bkgd},0}} \right] \right) \times 100$$

3. Results and Discussion

To determine the maximum concentration of protein that can be added to the wells of the 384-well filter plate, while still allowing solvent to pass through the

membrane, a dilution of HSA in buffer was performed. Concentrations of 40, 34, 28, 23, 17, 11, 6, and 3 mg/mL HSA were investigated in triplicate at a final volume of 70 μ L. The plate was centrifuged for 20 minutes at 1500 x g. After 20 minutes of centrifugation, only the wells with 6 and 3 mg/mL HSA solutions were filtered completely. After an additional 20 minutes of centrifugation at 1500 x g, the wells containing 11 mg/mL HSA solution were filtered, with minimal to no filtrate collected from the higher HSA concentrations. To retain the highest throughput, a short centrifugation time was preferred. Therefore a maximum concentration of 5 mg/mL (75 μ M) HSA was chosen for subsequent experiments.

Table 9. Calculated percent bound of standard small molecules after high-throughput ultrafiltration method with varying volumes of 10 mM compound solution in DMSO (n=3) in comparison to literature *in vitro* values. ($x = A_e$ greater than A_0)

Molecule	% Bound, Literature Value	Calculated % Bound, 1 μ L Compound	Calculated % Bound, 2 μ L Compound	Calculated % Bound, 3 μ L Compound	Calculated % Bound, 4 μ L Compound
Piroxicam ¹⁴⁰	91	56.6 \pm 2.4	39.8 \pm 2.3	45.2 \pm 1.6	40.8 \pm 1.2
Metoprolol ¹⁴¹	3.5 \pm 32.0	x	x	22.7 \pm 3.5	93.8 \pm 1.3
Propranolol ¹⁴²	87 \pm 6	51.4 \pm 9.9	29.0 \pm 4.3	27.4 \pm 1.1	48.2 \pm 5.0
Naproxen ^{141, 143}	95.3 \pm 1.7	106.7 \pm 5.5	81.2 \pm 5.3	67.2 \pm 1.7	71.0 \pm 0.6
Caffeine ¹⁴²	36 \pm 7	x	37.7 \pm 5.6	22.8 \pm 8.7	41.0 \pm 1.8

Next, the concentration of small molecules with the 5 mg/mL HSA was determined. The concentration must be sufficient for UV detection, but low enough to prevent over-saturation of protein binding sites. Therefore, compound concentrations of 143, 286, 429, and 571 μ M (1, 2, 3, and 4 μ L of the 10 mM

compound solutions in DMSO) were analyzed in triplicate. The resulting calculated percentages of HSA-bound compound in comparison with *in vitro* plasma protein binding values are shown in Table 9. β -Estradiol and diethylstilbestrol were excluded from the table because A_e was greater than A_0 at all concentrations. This was observed for other molecules as well (caffeine and metoprolol), as indicated by an x in the Tables 9, 10, and 11. The reasons for this observation may be the displacement of interfering molecules upon the binding of the drug, breakthrough of the plasma protein during filtration, or low absorbance (Figure 47).

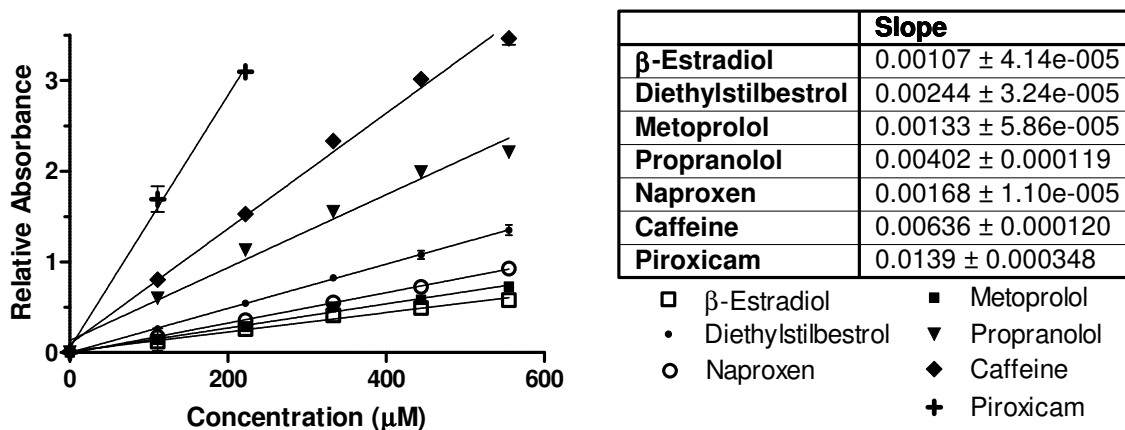


Figure 47. Calibration plot correlating absorbance with concentration of standard molecules at the λ_{\max} at each of the molecules, respectively. Slope of the line for each molecule given in the table with standard deviation.

The co-solvents, NP-40 and glycerol, were investigated for the reduction of non-specific binding during ultrafiltration assays.^{23, 126} NP-40 as well as other surfactants are frequently added to buffers to circumvent aggregation as well as to

increase solubility of proteins and small molecules.^{64, 95, 116} Therefore, 0.01% by volume NP-40 was added to the buffer. The results in Table 10 with the addition of NP-40 showed a much better correlation to the *in vitro* values than those in Table 9, without buffer additives. The addition of glycerol, typically 10% by volume, in protein buffers enhances the solubility and stability of many proteins.¹² Very poor results were observed with the addition of 10% by volume glycerol, which may be due to the increased viscosity of the solution possibly clogging the pores in the membrane.

Table 10. Calculated percent bound of standard small molecules after high-throughput ultrafiltration method with 2 μ L of 10 mM compound solution in DMSO (n=3) and 0.01% NP-40 and 0.01% NP-40 with 10% glycerol (v/v) in comparison to literature *in vitro* values. (x = A_e greater than A_0)

Molecule	% Bound, Literature Value	Calculated % Bound, 0.01% NP-40	Calculated % Bound, 10% Glycerol, 0.01% NP-40
Piroxicam ¹⁴⁰	91	56.7 \pm 0.4	55.9 \pm 8.5
Metoprolol ¹⁴¹	3.5 \pm 32.0	21.0 \pm 1.7	x
Propranolol ¹⁴²	87 \pm 6	32.0 \pm 2.1	x
Naproxen ^{141, 143}	95.3 \pm 1.7	76.7 \pm 3.2	62.5 \pm 23.7
Caffeine ¹⁴²	36 \pm 7	33.4 \pm 7.9	x

To determine if there is a concentration effect with the separation of a large percentage of the initial volume, the plate was only centrifuged for 5 minutes, collecting 10 μ L of filtrate. The calculated percent bound for high-binding molecules (piroxicam and naproxen), both with a λ_{max} greater than 300 nm, were significantly

lower than the *in vitro* literature values. The values for all other molecules were not calculable (A_e greater than A_0) because of the highly dilute solutions.

Table 11. Calculated percent bound of standard small molecules after high-throughput ultrafiltration method with 1 μ L of 10 mM compound solution in DMSO (n=3) with 0.01% NP-40, detection by UV absorbance and LC-MS in comparison to literature *in vitro* values. ($x = A_e$ greater than A_0)

Molecule	% Bound, Literature Value	Calculated % Bound, UV	Calculated % Bound, LC-MS
Piroxicam ¹⁴⁰	91	66.8 \pm 2.1	68.0 \pm 0.2
Metoprolol ¹⁴¹	3.5 \pm 32.0	x	0.9 \pm 0.5
Propranolol ¹⁴²	87 \pm 6	x	17.5 \pm 0.9
Naproxen ^{141, 143}	95.3 \pm 1.7	69.4 \pm 4.4	81.6 \pm 0.5
Caffeine ¹⁴²	36 \pm 7	4.1 \pm 2.3	5.3 \pm 0.2

Many protein-binding methods (equilibrium dialysis and ultrafiltration) use LC-MS or LC-MS/MS for detection due to the sensitivity that can be achieved.^{21, 22, 120, 128, 129, 136} The percent binding of the molecules presented in Table 11 were determined by UV absorbance and LC-MS detection using the ratio of the peak areas of the analytes. The percent binding of β -estradiol and diethylstilbestrol could not be calculated because it co-eluted with DMSO. This could be improved by adjusting the HPLC method. For all other compounds, a similar protein binding was determined by both UV absorbance and LC-MS. With optimization of the LC-MS method, molecules with low absorbance or low maximum wavelengths could be detected more easily.

4. Conclusions

Sieve effects are commonly seen for ultrafiltration methods, in which water molecules are preferentially filtered as compared to the drug molecules giving an underestimation of the free drug concentration.¹⁴⁴ Concentration effects by separation of large amounts of the volume can also have an influence on low-binding molecules such as metoprolol and caffeine. Addition of NP-40 to the assay buffer greatly increases the correlation to reported *in vitro* values for plasma protein binding. This can be due to the decrease in non-specific binding to the filter apparatus^{64, 95, 116} and decreased aggregation of the molecules and proteins.^{64, 95, 116}

It has been discussed previously that ultrafiltration methods are not a sufficient substitute for equilibrium dialysis.¹⁴⁵ There is some variation between *in vitro* methods; for example, equilibrium dialysis has reported 23% plasma protein binding for fleroxacin whereas ultrafiltration has reported 47% plasma protein binding for the same compound.¹⁴⁶ Many high-throughput methods that have been developed for ultrafiltration plasma protein binding that correlate the results to conventional single-tube ultrafiltration values.^{120, 129} Other reports describe the study of the binding of one or two molecules, not multiple.^{120, 129} Application of LC-MS or LC-MS/MS may increase the sensitivity of detection, but can greatly decrease the throughput of analysis. With further optimization, application of the plasma protein binding method in a 384-well filter plate with 30 kDa molecular weight cutoff membrane can be a useful ultrafiltration method for drug-protein binding studies.

PART 2: COMPETITIVE PROTEIN BINDING

1. Introduction

Fluorescence spectroscopy can be applied as a highly sensitive method for protein analysis.^{147, 148} The fluorescent probes can be analogs of natural ligands and drugs or act as binding site markers in competition assays.¹⁴⁸⁻¹⁵⁰ 1-Anilino-8-sulfonaphthalene (ANS) is one of the first fluorophores discovered that displays a change in fluorescence intensity upon interaction with biomolecules.¹⁵¹ ANS and its dimeric form, 4,4'-bis-1-anilino-8-sulfonaphthalene (Bis-ANS) are the most frequently used dyes in protein characterization.^{130, 147, 151-153} Prodran has been used to characterize the warfarin binding site on HSA.¹⁴⁸ Another fluorescence-based method used dansylamide and dansylsarcosine, with fully characterized binding sites on HSA.¹⁴⁸ The decrease in the fluorescence intensity can be interpreted as displacement of the fluorescent probe by an added ligand through a competitive mechanism.^{148, 154} The decrease in fluorescence intensity can also be related non-competitive allosteric inhibition.

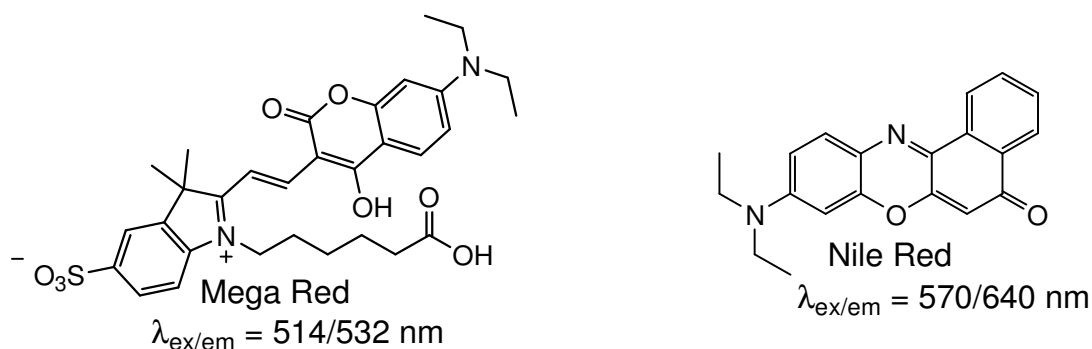


Figure 48. Structures of Mega Red and Nile Red with wavelengths of excitation and emission in PBS with 0.5 mg/mL HSA.

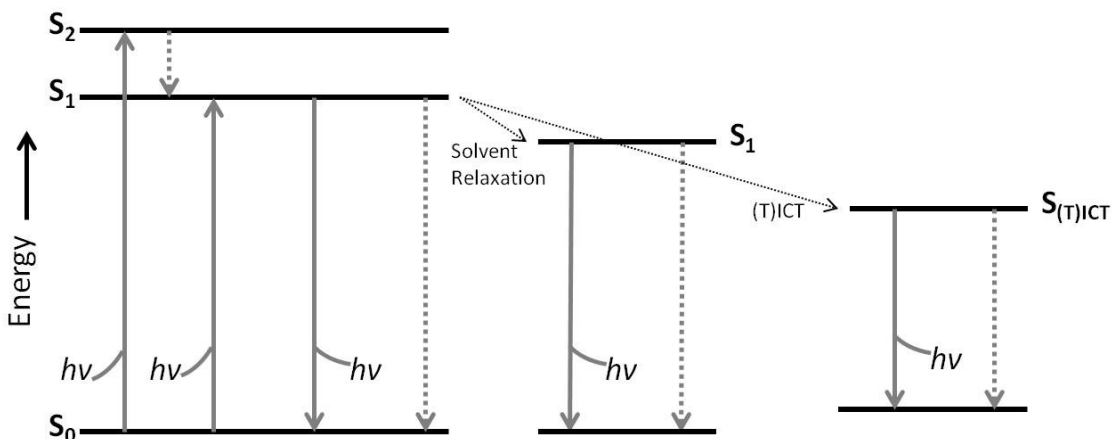


Figure 49. Jablonski diagram describing the fluorescence process including solvent relaxation and (twisted) intramolecular charge transfer.¹⁴⁷

To determine the extent of drug-plasma protein binding, fluorescent molecules were chosen that bind non-specifically and non-covalently with proteins. Some fluorophores have a very low quantum yield in water, but a large quantum yield in the presence of proteins such as bovine serum albumin (BSA). These changes are due to solvent or environmental effects, altering the rates of non-radiative decay.^{149, 155} This phenomenon is observed for many fluorescent molecules including Mega Red and Nile Red, Figure 48. The electron process is described in Figure 49. Upon the absorption of light, electrons are excited from the ground state, S_0 , to a higher energy level. There are several processes that compete with fluorescence, resulting in energy loss. These processes include vibrational relaxation, internal conversion, solvent relaxation, and intramolecular charge transfer (ICT) or twisted intramolecular charge transfer (TICT), illustrated by the dotted arrows in Figure 49. Once the molecule has reached the lowest vibrational

level, S_1 or $S_{(T)ICT}$, the molecule can relax back to the ground state by fluorescence emission of a photon or non-radiative decay. The twisted intramolecular charge transfer, as opposed to normal planar ICT, involves intramolecular rotation and full charge transfer.

Mega Red contains a coumarin moiety which demonstrates the ability to associate non-covalently and non-specifically with proteins.^{156, 157} Nile Red is a non-ionic fluorescent probe that binds non-covalently to protein surfaces. A large Stokes shift, with respect to the emission, makes it useful for observing changes in protein structure.¹⁵⁸ The fluorescence properties of Nile Red are governed by TICT in which an electron transfers from the diethylamino group to the electron-withdrawing aromatic system with rotation around the aromatic-nitrogen bond.^{147, 159} A diethylamino group is also present in Mega Red, causing a similar TICT process, although it has not been fully characterized yet. In polar solvents, the TICT state and non-radiative decay are favored causing the low quantum yield in aqueous solutions. In apolar environments, such as with human serum albumin (HSA) or BSA, the TICT process is thermodynamically unfavorable, which results in a significant increase in fluorescence lifetime and quantum yield.^{147, 159}

Herein, the first high-throughput method to determine drug-protein binding is presented. In contrast to equilibrium dialysis and ultrafiltration methods, this method requires short times and no centrifugation. Importantly, it is carried out in 384-well plate format. The application of fluorescent probes, (E)-1-(5-carboxypentyl)-2-(2-(7-(diethylamino)-4-hydroxy-2-oxo-2H-chromen-3-yl)vinyl)-

3,3-dimethyl-3H-indol-1-ium-5-sulfonate (Mega Red)¹⁵⁷ and 9-(diethylamino)-5H-benzo[a]phenoxazin-5-one (Nile Red)¹⁵⁸, enables the quantification of two independent compound-plasma protein binding constants in one assay at different HSA binding sites. The concept of using multiple fluorescent probes simultaneously for the study of small molecule-protein interactions has been discussed previously, but was not fully developed.¹⁶⁰ Compounds can also be measured in a dose-response analysis to determine the affinity of compound binding. This fluorescence-based assay represents a novel high-throughput screening (HTS) tool for the estimation of plasma protein binding of small molecules.

2.1. Materials and Instrumentation

All materials were used as received. The following small molecules were used as standards: verapamil hydrochloride (Tocris Bioscience), diethylstilbestrol (Spectrum Chemical Mfg. Corp.), β -estradiol (Alfa Aesar), caffeine (Alfa Aesar), D,L-propranolol hydrochloride (MP-Biomedicals), piroxicam (MP-Biomedicals), metoprolol tartarate (LKT Laboratories), naproxen (MP-Biomedicals), atenolol (MP-Biomedicals), ranitidine hydrochloride (Alfa Aesar), ketoconazole (Calbiochem), lansoprazole (Sigma Aldrich), omeprazole (Sigma Aldrich), rabeprazole (Sigma Aldrich), nadolol (Sigma Aldrich), linezolid (Sigma Aldrich), antipyrine (Sigma Aldrich), ofloxacin (Sigma Aldrich), and methotrexate (Sigma Aldrich). Each of the small molecules were dissolved in DMSO (Acros, Spectroscopic Grade 99.9+%) to make 10 mM solutions.

Solutions from lyophilized powder, fatty acid free, globulin free, $\geq 99\%$ human serum albumin (HSA) (Sigma Aldrich) were made in buffer. HSA solutions were stored for no longer than one week at 4°C . Phosphate buffered saline (PBS) was prepared in 1L batches using $18\text{ M}\Omega$ water with $3.23\text{ mM K}_2\text{HPO}_4\cdot 7\text{H}_2\text{O}$ (J.T. Baker), $7.84\text{ mM KH}_2\text{PO}_4$ (J.T. Baker), 5 mM KCl (Fisher), 150 mM NaCl (Fisher), and adjusted to pH 7.2 with HCl (Mallinckrodt) and NaOH (Fisher). Nonylphenyl polyethylene glycol (NP-40) 0.01% (v/v) surfactant (Boston BioProducts) and glycerol (Fisher) were used as buffer additives. Fluorescent molecules, Red Mega 500 (Mega Red) (Fluka) and Nile Red (Acros Organics), were dissolved to 10 mM in DMSO upon receiving and stored at -20°C until used.

The absorbance readings were completed in a 384-well UV plate (Greiner Bio-One, 781801). The assay was performed in a 384-well, flat bottom, black assay plate (Corning, 3573) which was sealed with an aluminum cover (Corning, 6570) during incubation and mixing. All of the absorbance and fluorescence intensity readings were performed on a Tecan Infinite M1000 plate reader. Small volume transfers were performed on the Tecan Freedom EVO liquid handling system with a 100 nL pin tool transfer (V&P Scientific). A BioTek MicroFlo Select instrument was used for the addition of solutions to the assay plate. TA Instruments low volume Nano-isothermal titration calorimeter (ITC) was used for the determination of binding constants of standard molecules to HSA. Analysis of the ITC data for the calculation of thermodynamic data was performed with NanoAnalyze software (Thermo Scientific).

2.2. Protein Binding Assay

In the preparation of the “compound plate”, 15 μL of the 10 mM solution of small molecules in DMSO were dispensed in a 384-well polystyrene plate filling rows 1 to 18. A second 384-well polystyrene plate, the “control plate”, had rows 19-24 filled with 15 μL DMSO. The assay buffer was prepared by mixing 10% by volume glycerol and 0.01% by volume NP-40 in PBS. Next, 20 μL of a 500 nM solution of Nile Red and Mega Red in the assay buffer (positive control) was dispensed to the assay plate (row 24). The rest of the assay plate was filled with 20 μL per well of the assay solution, 0.20 mg/mL HSA and 500 nM Nile Red and Mega Red in the assay buffer.

With the Tecan liquid handling system, 200 nL from the compound plate and 200 nL from the control plate were transferred into the assay plate using the pin transfer tool. The assay plate was then centrifuged for 2 minutes at 2500 rpm and agitated for 5 minutes. The assay plate was read using the Tecan M1000 plate reader. An excitation and emission wavelength of 510 nm and 543 nm for Mega Red and 570 nm and 640 nm for Nile Red, 100 flashes, 20 μs integration time, optimized gain and z-position (optimized to the 500 nM Mega Red and Nile Red solution with 0.20 mg/mL HSA), were used for the quantification of the fluorescence intensity signal. The Z' value for this assay was calculated using Nile Red and Mega Red with HSA as the negative control (0% binding) and Nile Red and Mega Red in buffer without protein as the positive control (100% binding).¹¹⁰ The percent binding of the small molecules at a concentration of 100 μM was reported as normalized

response to the fluorescence intensity of Mega Red and Nile Red in the presence of HSA.

3. Results and Discussion

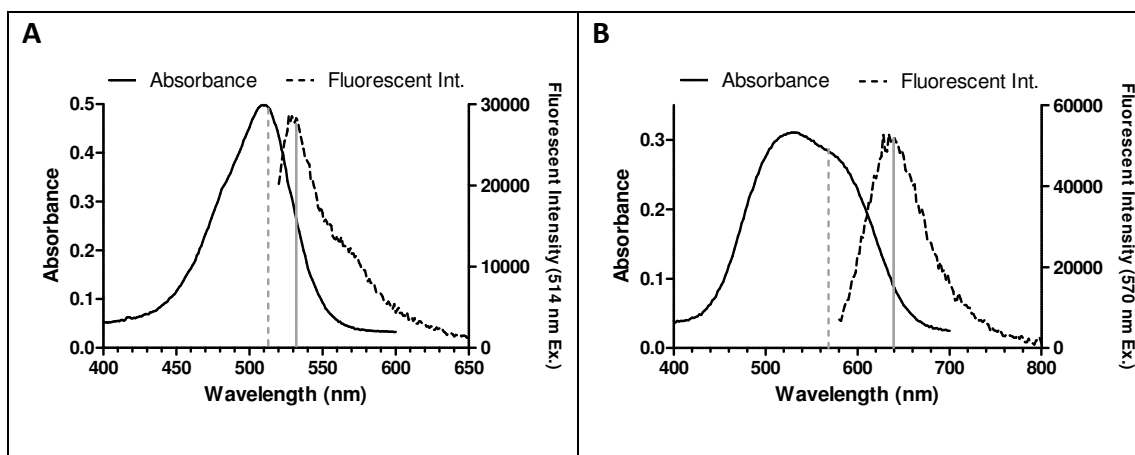


Figure 50. A) Absorbance and fluorescence spectra at 514 nm excitation of Mega Red in PBS with 0.5 mg/mL HSA. B) Absorbance and fluorescence spectra at 570 nm excitation of Nile Red in PBS with 0.5 mg/mL HSA.

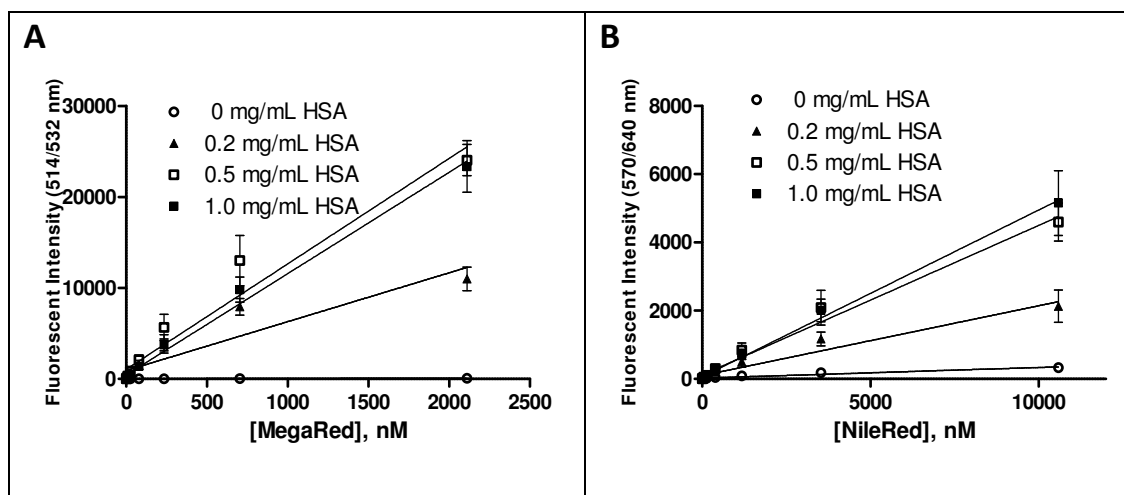


Figure 51. Serial dilution of A) Mega Red and B) Nile Red in PBS with varying concentrations of HSA.

The absorbance and fluorescence spectra of Mega Red and Nile Red in PBS in the presence of 0.5 mg/mL HSA are shown in Figure 50. The different wavelengths for the two fluorophores allow the simultaneous application of both within the same experiment. Serial dilutions of Mega Red and Nile Red with 0, 0.2, 0.5, and 1.0 mg/mL of HSA in PBS are depicted in Figure 51. There is a linear relationship between the concentration of fluorophore and their fluorescence intensity at concentrations below 2.1 μM . The fluorescent intensity also increases with increasing concentration of HSA, reaching a saturation of signal at 0.5 mg/mL for both Mega Red and Nile Red. The Z' values (Figure 52) were calculated for each of the probe concentrations summarized in Figure 51. This data was used to determine the optimal assay concentrations, which were 500 nM of both Mega Red and Nile Red and 0.2 mg/mL HSA.

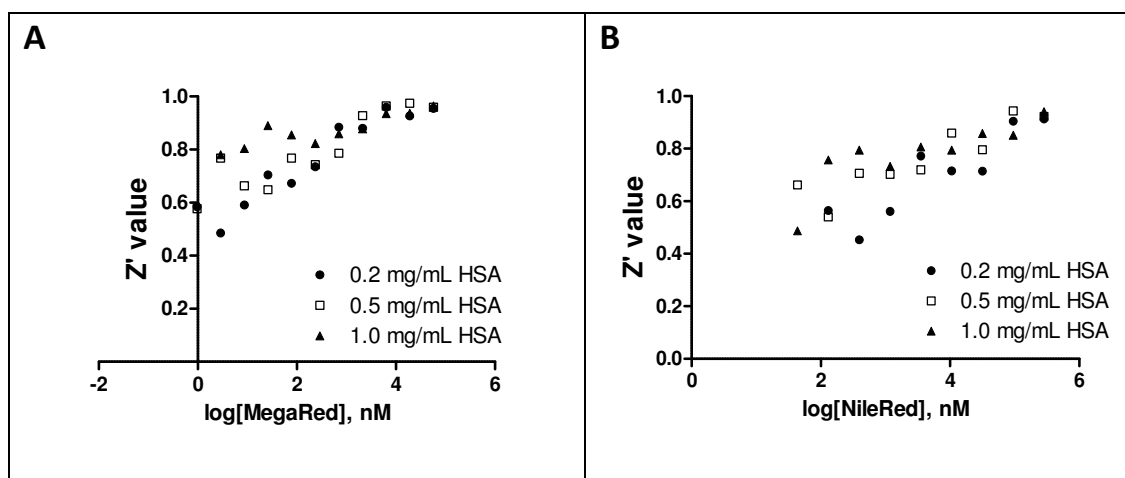


Figure 52. Z' value (without HSA, positive control; with HSA, negative control) with changing concentration of HSA and A) Mega Red or B) Nile Red.

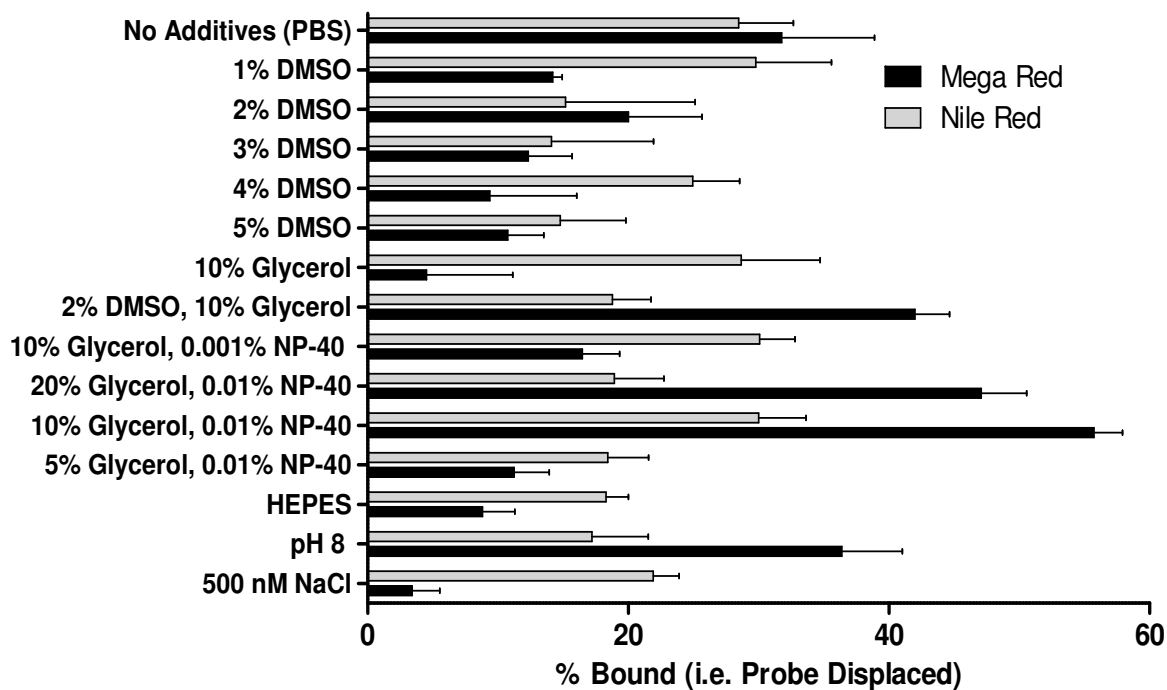


Figure 53. Binding response of one standard molecule, naproxen, with changing buffer composition.

To optimize the fluorescence signal of Mega Red and Nile Red in the presence of HSA and drugs, the buffer composition was varied. For simplicity, the binding response of only one standard molecule, Naproxen, is shown in Figure 53. The data for all standard molecules with changing buffer composition can be found in Appendix D. DMSO is often added to buffers because it can greatly enhance the solubility of small molecules, but may also influence the performance of an assay as it may affect the stability of many biomolecules. DMSO was added at 1, 2, 3, 4, and 5% by volume in PBS. The displacement of Mega Red and Nile Red by naproxen decreased with increasing concentration of DMSO. The strength of electrostatic interactions as well as protein stability can be modulated by varying the ionic

strength of buffers.¹⁶¹ Increasing the NaCl concentration from 150 mM to 500 mM resulted in poor binding of naproxen, as well as other standard molecules. When the pH of the buffer was changed to 8.0, an increase in HSA binding was observed for naproxen, while no improvement was seen with other standard molecules. Changing the buffer to a zwitterionic HEPES buffer at 200 mM and pH 7.2 showed minimal improvements in binding of naproxen as well as other standard molecules. The addition of glycerol, typically 10% by volume, in protein buffers enhances the solubility and stability of many proteins.¹² This is due to the increased hydrophobicity of the buffer with increasing concentration of glycerol. NP-40 as well as other surfactants are frequently added to buffers to circumvent aggregation as well as to increase solubility of proteins and small molecules.^{64, 95, 116} The small molecule binding was determined with varying percent of glycerol, 5%, 10%, and 20% by volume, in PBS with and without the presence of 2% by volume DMSO and 0.01% or 0.001% NP-40. With 5% by volume glycerol, only a minimal HSA binding was observed for naproxen. Increasing the amount of glycerol to 10% and 20% showed a drastic increase in the binding. Little difference was observed between 10% and 20% (v/v) glycerol by volume, therefore 10% was preferred. Decreasing or removing the NP-40 from the buffer with 10% (v/v) glycerol showed a drastic decrease in the HSA binding of naproxen, therefore 0.01% NP-40 was preferred in the buffer. Finally, with the addition of 2% by volume of DMSO to the buffer with 10% glycerol showed an increase in binding of naproxen. Nonetheless, it is preferable to minimize DMSO in assay solutions for concerns of protein stability.¹⁶² For every assay, 1% (v/v) DMSO was added with the transfer of compounds. The

optimized assay buffer consisted of PBS at pH 7.2 with 150 mM NaCl, 10% glycerol, and 0.01% NP-40 by volume.

All standard molecules were screened for the displacement of 500 nM Mega Red and Nile Red and compared with literature values for *in vivo* plasma protein binding, Figure 54. The standard deviations for literature values are given when reported. The standard molecules were screened in triplicate as described in section 2.2. The displacement of the fluorescent molecule resulted in a decrease in fluorescence intensity. The percent binding of the small molecules at a concentration of 100 μ M was reported as normalized response to the fluorescence intensity of Mega Red and Nile Red in the presence of HSA. The larger of the two values was used for the percent bound value in comparison to the literature values (Figure 54).

A good correlation between the experimental and literature *in vivo* plasma protein binding values was observed. Groups of low, medium, and high protein binding molecules were assigned in the plot (Figure 54). Experimental values for 20% (40% *in vivo* binding values) or less binding correspond to low binding molecules, designated by the dotted lines on the plot. Experimental values for 40% (80% *in vivo* binding values) or greater binding correspond to highly binding molecules, designated by the dashed lines on the plot. The values between 20% and 40% (40% and 80% *in vivo* binding values), falling between the dotted and dashed lines, correspond to the medium binding molecules.

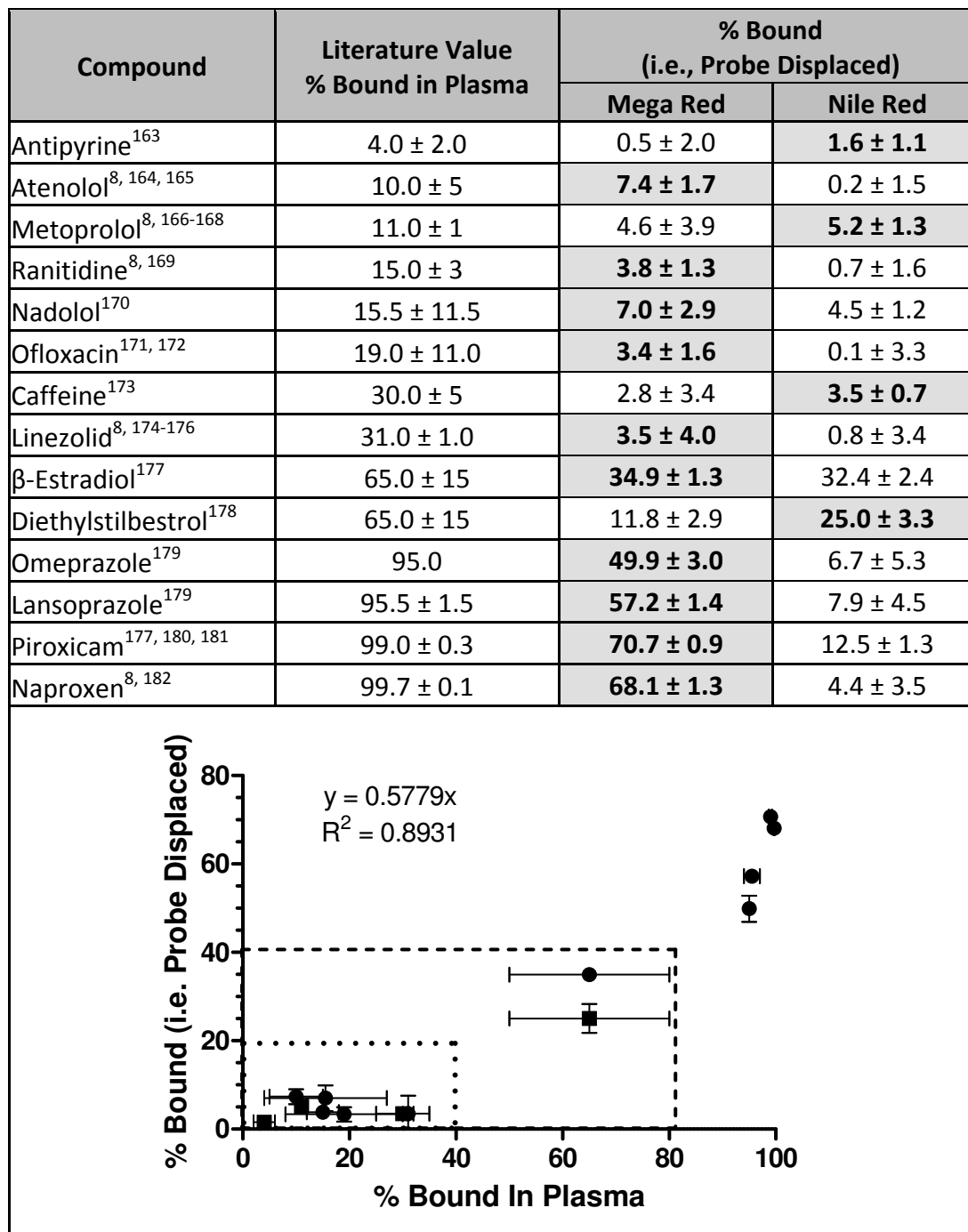


Figure 54. Standard molecule displacement of 500 nM Mega Red and Nile Red in PBS with 10% glycerol and 0.01% NP-40 in comparison with literature values for *in vivo* plasma protein binding (n=3). Larger of the values, in gray, for % bound (i.e., probe displaced) is taken for the plot. Dotted line correlates to the cutoff for low protein binding molecules and the dashed line correlates to the cutoff for high protein binding molecules.

With the optimized assay conditions: PBS (50 mM, pH 7.4, 150 mM NaCl), 500 nM Mega Red and Nile Red, compounds (100 μ M), 0.20 mg/mL HSA, 10% glycerol and 0.01% NP-40; a library of small molecules was screened. The Library of Pharmaceutically Active Compounds-1280 (LOPAC) screening collection (Sigma) was used to determine the quality of the assay and the ability to identify compounds that significantly bind to plasma proteins. Each LOPAC compound was measured in triplet (Figure 55). The results for all of the compounds within the library are summarized in Appendix D. The Z' values of this screen ranged between 0.60 and 0.91 with a mean of 0.93 for Mega Red and 0.72 for Nile Red. The mean fluorescence intensity of all compounds in the presence of Mega Red and 0.20 mg/mL HSA was 10.3% of the Mega Red with HSA signal with a standard deviation of 13.8%. The mean fluorescence intensity of all compounds in the presence of Nile Red and 0.20 mg/mL HSA was 9.0% of the Nile with HSA signal with a standard deviation of 9.5%.

The results of the high-throughput screen identified 82 compounds that displaced Mega Red and/or Nile Red at 40% or greater. This was a hit rate of 6.4% for molecules within the library falling above the high plasma protein binding cutoff limit set by the standard molecules. Of the 82 hit compounds, 75 of these molecules were determined to be moderately to highly lipophilic, with a calculated $\log P_{(o/w)}$ greater than 1.¹⁸³ Within the hit molecules identified by Mega Red, 10 molecules contained negatively charged groups such as sulfate, nitrate, or phosphate groups. Among the group of hits were P2 receptor antagonists, Figure 56, displacing more than 70% of Mega Red. In addition, many hormones were identified, Figure 57, such

as β -estradiol, that exhibit medium and high binding by the displacement of Nile Red.

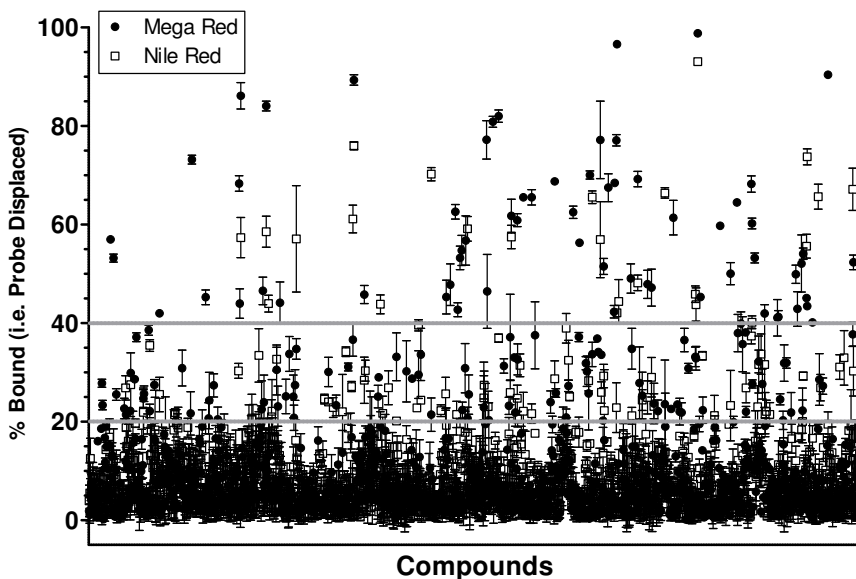


Figure 55. Results of the LOPAC screen (1280 compounds) with cutoff for medium and high binding cutoff values at 20% and 40%.

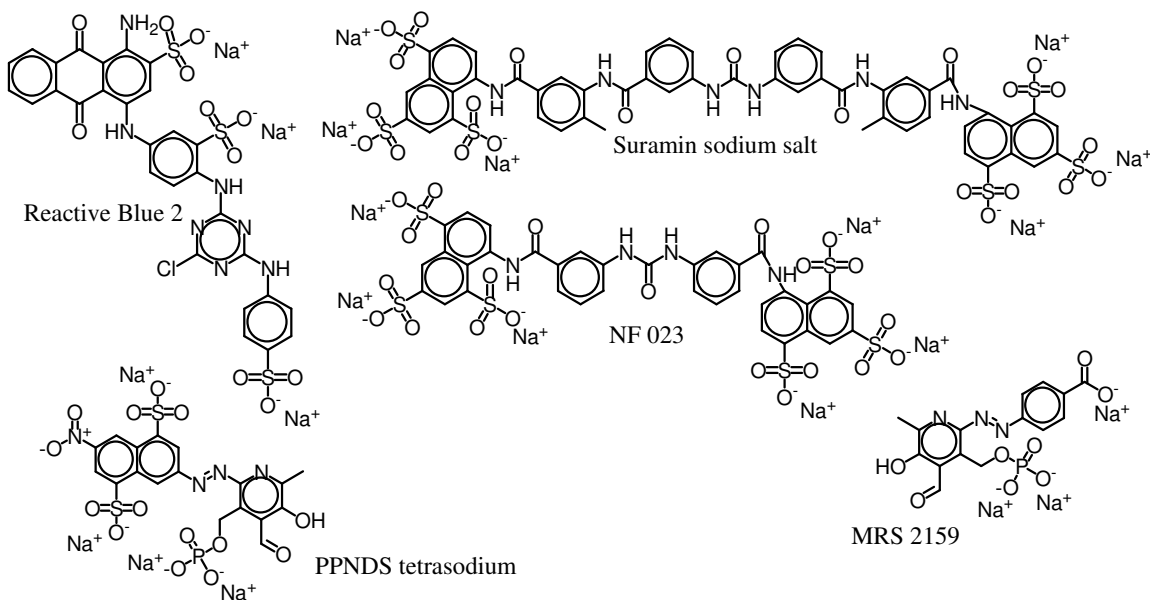


Figure 56. P2 receptor antagonists identified as protein binding hit molecules.

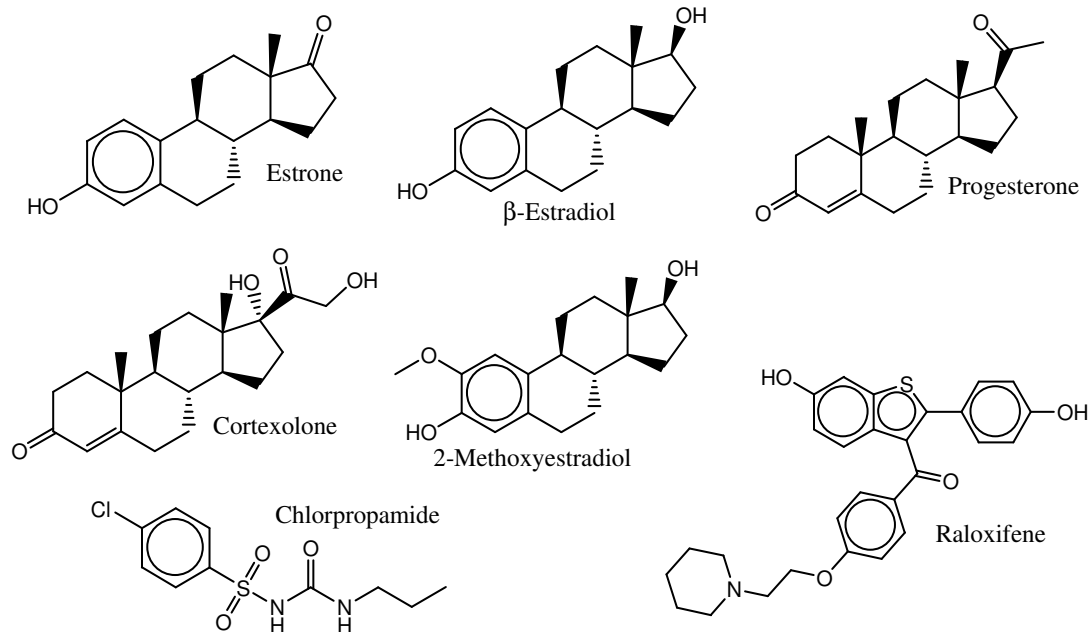


Figure 57. Selected hormones identified as protein binding hit molecules.

With the combination of both Mega Red and Nile Red, 18 of the 20 prostaglandin synthesis inhibitors within the LOPAC library were identified as medium and high-protein binding molecules, Figure 58. Interestingly, two compounds within this family, naproxen and piroxicam, were among the standard molecule used for the optimization of the assay. *In vivo* plasma protein binding values for some of these molecules have previously been studied, such as diclofenac with 99.5% plasma protein binding¹⁸⁴ displaced 43.8% of Nile Red, indomethacin with 90% plasma protein binding¹⁸⁵ displaced 34.2% of Mega Red, ibuprofen with about 99% plasma protein binding^{186, 187} displaced 36.8% of Mega Red, and ketorolac with a 99% plasma protein binding¹⁸⁸ displaced 68.8% of Mega Red and 28.7% of Nile Red.

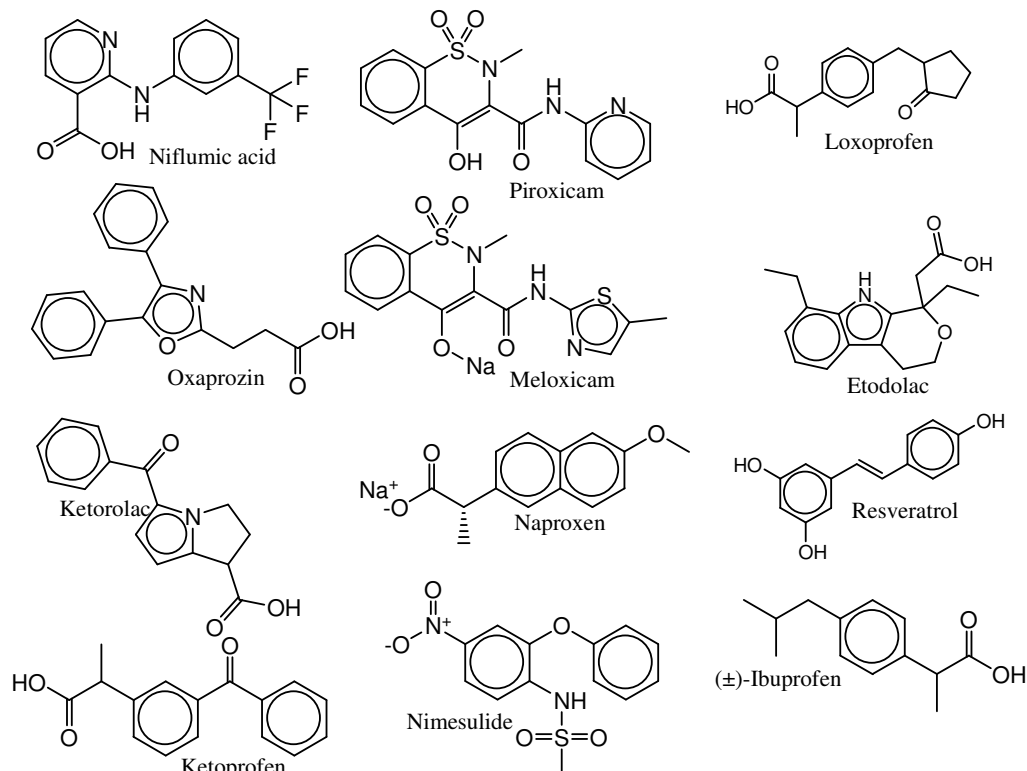


Figure 58. Prostaglandin synthesis inhibitors (COX 1&2) identified as protein binding hit molecules.

The background fluorescence intensity was determined for each LOPAC molecule (100 μM) in the absence of Nile Red and Mega Red with an excitation and emission wavelength of 514 nm and 532 nm as well as 570 nm and 640 nm, respectively. The vast majority of LOPAC compounds exhibited minimal fluorescence intensity and gave a value similar signal to those measured for the assay media (Figure 59A, compound (black), buffer (white/gray)). However, 10 compounds exhibit a fluorescence of more than 1σ of the mean background fluorescence intensity (Figure 59B). Interestingly, the fluorescence intensity for these molecules was decreased in the LOPAC screen in the presence of Mega Red and Nile Red (possibly due to the quenching process).

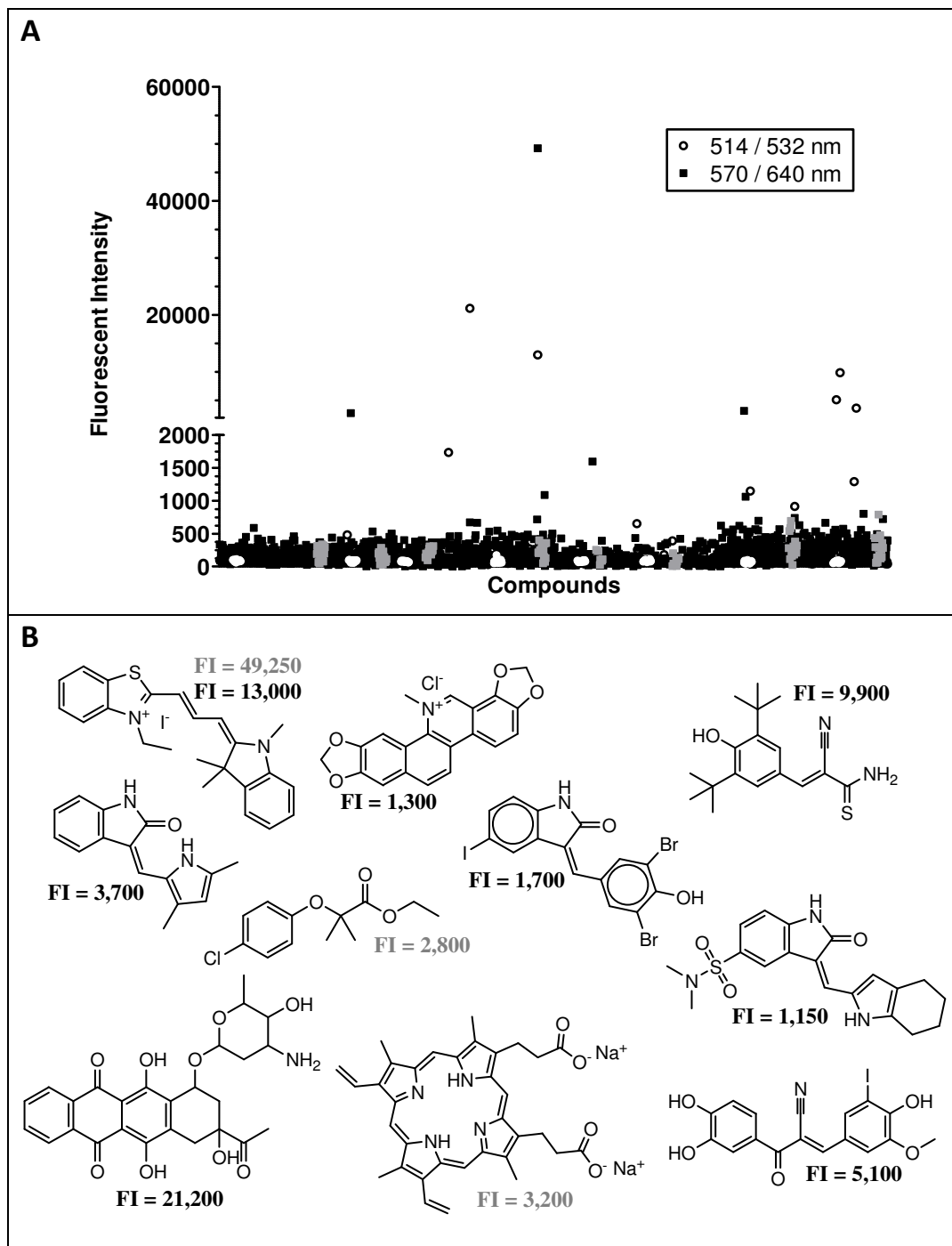


Figure 59. A) Fluorescence intensity (514/532 nm and 570/640 nm) of all LOPAC compounds (white points correspond to background at 514/532 nm, grey points correspond to background at 570/640 nm); B) Structures of fluorescently interfering compounds, fluorescent intensity (FI) at 514/532 nm in black and 570/640 nm in grey.

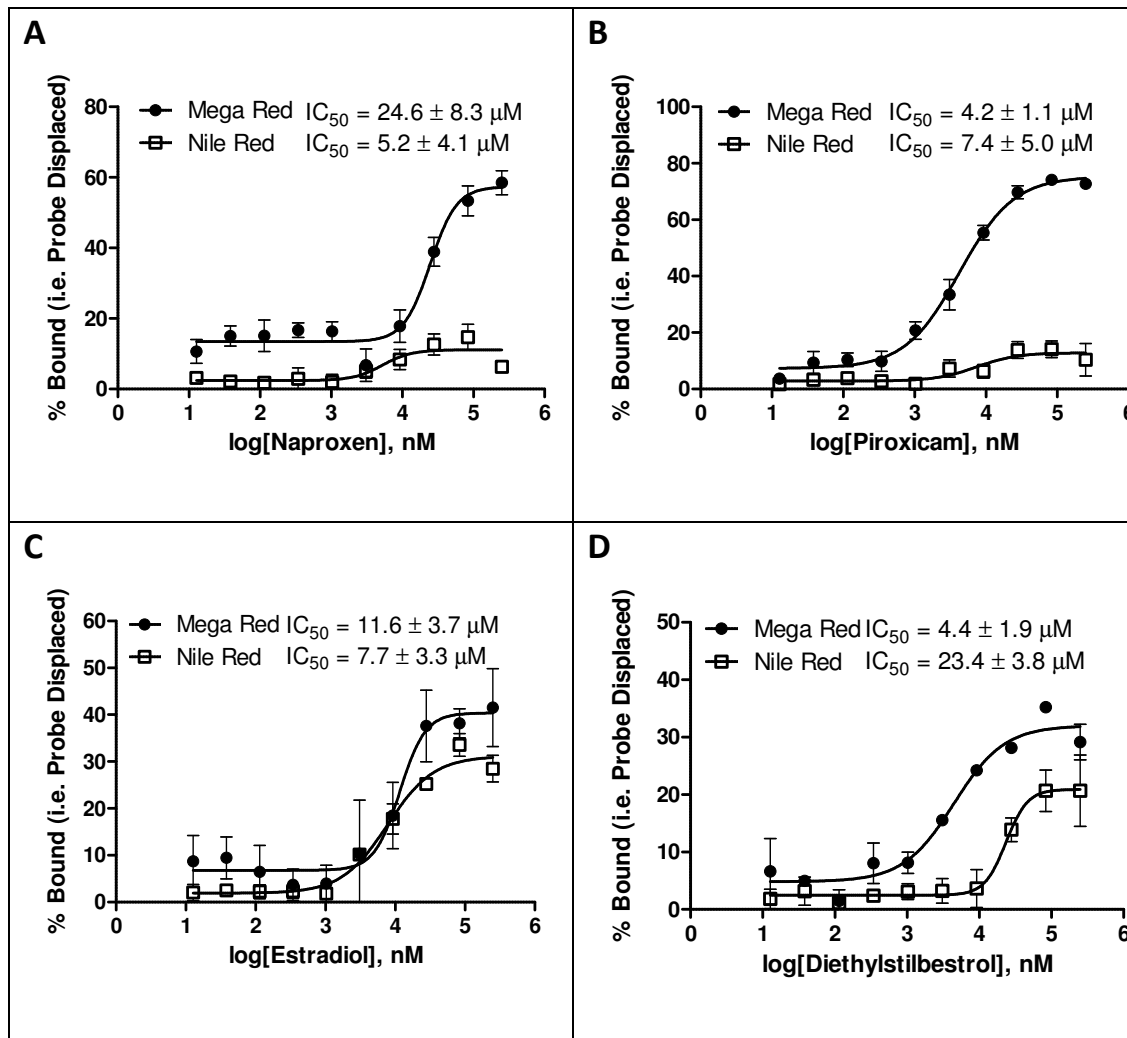


Figure 60. Binding dose-response curves for A) naproxen, B) piroxicam, C) β -estradiol, and D) diethylstilbestrol with corresponding IC₅₀ values.

The standard molecules can also be screened in a dose response manner, giving both the efficacy and affinity of binding. The dose response curves for the standard molecules naproxen, piroxicam, β -estradiol, and diethylstilbestrol are shown in Figure 60. The titration of naproxen resulted with an IC₅₀ of $24.6 \pm 8.3 \mu\text{M}$ for the displacement of Mega Red. The dose response of piroxicam resulted with an IC₅₀ value of $4.2 \pm 1.1 \mu\text{M}$ for the displacement of Mega Red. β -Estradiol displaced

both Mega Red and Nile Red nearly equally, resulting with an IC_{50} of 11.6 ± 3.7 and $7.7 \pm 3.3 \mu\text{M}$. Finally, dose response of diethylstilbestrol resulted with an IC_{50} of $4.4 \pm 1.9 \mu\text{M}$ for the displacement of Mega Red and $23.4 \pm 3.8 \mu\text{M}$ for the displacement of Nile Red.

It has previously been shown that the binding or interaction of Nile Red does not alter the native structure of albumin in aqueous solutions.¹⁵⁸ Isothermal titration calorimetry (ITC) was performed to quantify the direct binding of naproxen with HSA in the absence of Mega Red and Nile Red. All solutions were prepared in the assay buffer optimized for the fluorescence-based assay. A $50 \mu\text{M}$ solution of HSA was added into the cell and a $350 \mu\text{M}$ naproxen solution was loaded into the syringe. A stir rate of 200 rpm at 25°C was used in the analysis with injection volumes of $2.02 \mu\text{L}$ of the naproxen solution with 300 seconds between each of the 20 injections. The resulting data for the binding of naproxen with HSA under these conditions is shown in Figure 61, giving a K_d value of $58.25 \pm 5.06 \mu\text{M}$. An n value of 0.500 was used for the thermodynamic calculations (largest n value, while still achieving a good fit). The K_d value is very similar to the IC_{50} value determined by the fluorescence-based competition assay supporting the observation that the binding of Mega Red and Nile Red does not alter native HSA protein structure.

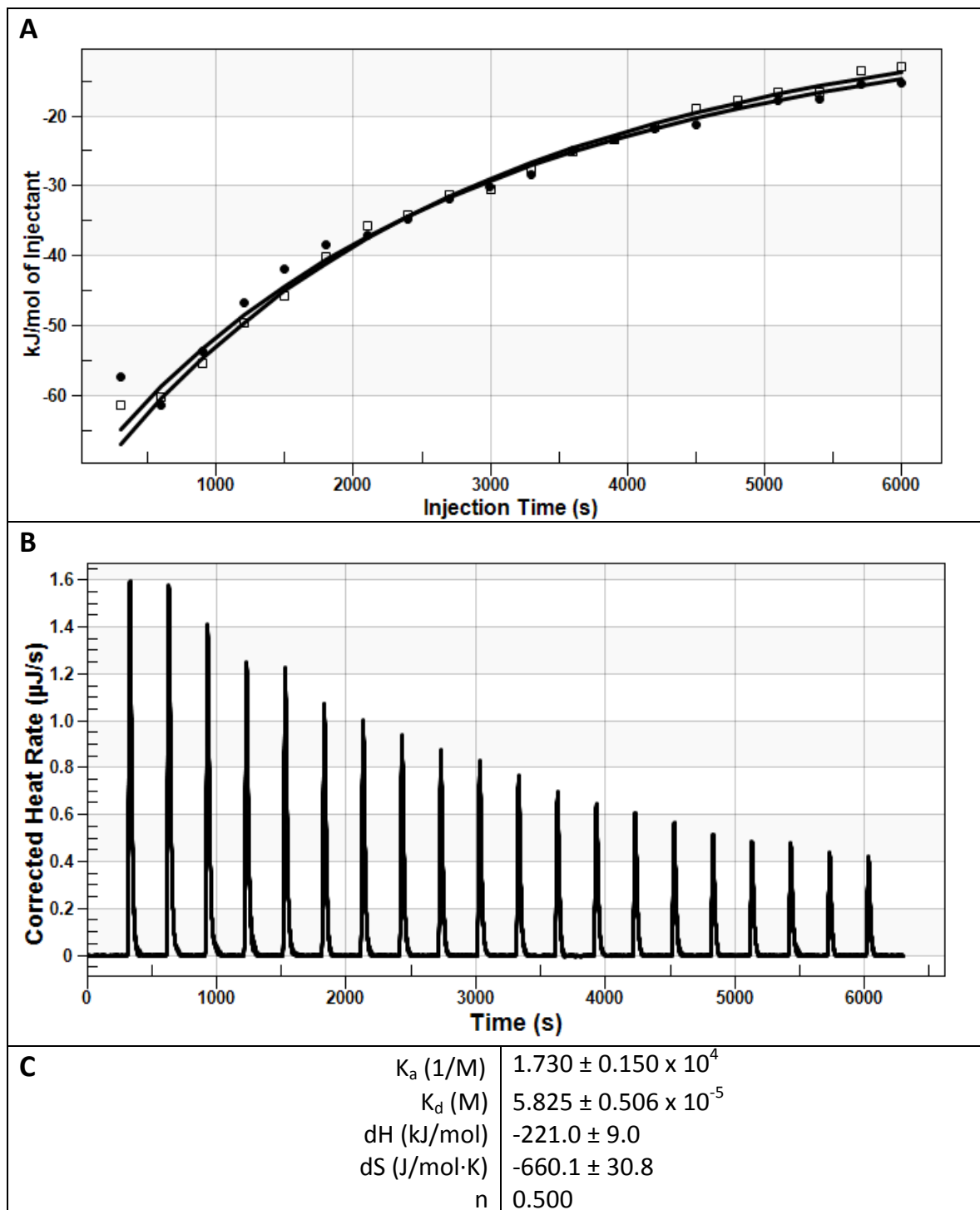


Figure 61. Isothermal titration calorimetry results for the binding of naproxen (350 μM) and HSA (50 μM). A) Plot of peak areas for each injection in correlation with analysis time. (n=2) B) Enthalpogram for the titration of naproxen into HSA with 20-2.02 μL injections. C) Thermodynamic data from the fit lines in A.

4. Conclusions

Molecules that bind strongly to plasma proteins have unique pharmacokinetics that may result in some liabilities in later pre-clinical screens. It is also understood that plasma protein bound molecules have a low available concentration for the site of action and exhibit a limited *in vivo* clearance. Therefore, protein binding is frequently investigated in the early stages of discovery to enable chemical optimization of this property. For the first time, large libraries of molecules can be screened in high-throughput format using the described fluorescence plasma protein binding assay.

The TICT mechanism of both Mega Red and Nile Red results in a very low quantum yield in water that significantly increases once bound to proteins like serum albumin. The identification of competing compounds required minimal incubation time and although optimized for 384-well plates, it could be easily minimized to 1536-well plate format. The far-red detection of both Mega Red and Nile Red limits the number of molecules interfering with the assay, which was 0.78% for the LOPAC screening library. The assay has an excellent reproducibility ($Z' > 0.9$ and 0.7 for Mega Red and Nile Red, respectively) and identifies compounds that bind HSA and are moderately to strongly lipophilic. Importantly, not all lipophilic compounds were able to compete with Mega Red and Nile Red for HSA binding; thus HSA binding is rather specific for each small molecule. This is supported by the fact that dose-dependent inhibition of Mega Red and Nile Red – HSA binding was observed with saturation at higher compound concentrations.

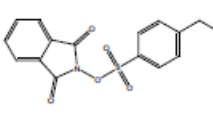
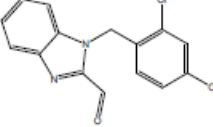
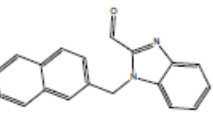
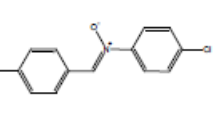
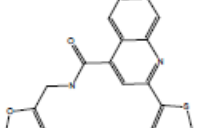
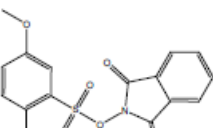
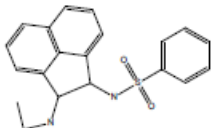
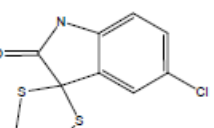
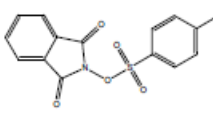
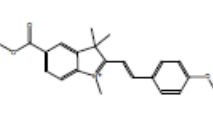
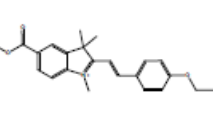
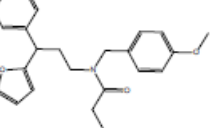
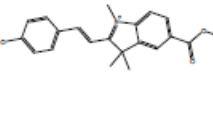
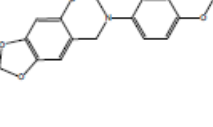
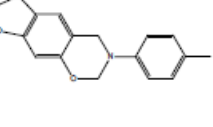
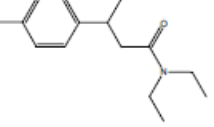
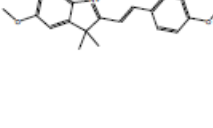
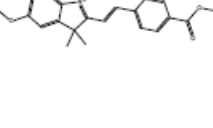
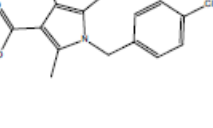
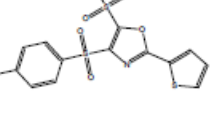
All IC_{50} values measured were between 3-24 μ M and had different efficacies and Hill-slopes. This behavior suggests that different HSA binding for each compound with different affinities, and overlapping binding sites for Mega Red and Nile Red. For naproxen, the measured inhibition constant (IC_{50}) and binding constant (K_a) are similar. Thus, the binding of both fluorescent molecules does not alter native HSA protein structure. This has been shown for Nile Red–HSA binding¹⁵⁸ but here for the first time for the interaction between HSA and Mega Red. In addition, the HTS fluorescence competition assay is capable of producing similar results with the time-intensive label-free ITC measurements.

Overall, a novel HTS assay to determine plasma protein binding was reported. Future studies for the improvements to this method include the investigating of the application of blood plasma instead of HSA as well as other fluorescent probes to improve the detection of small molecule–HSA binding.

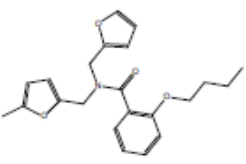
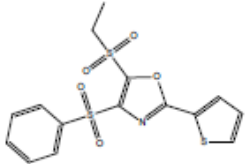
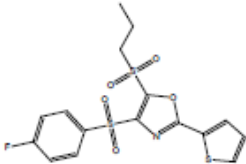
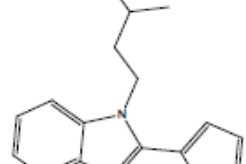
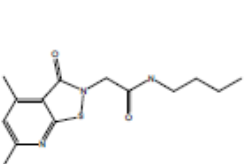
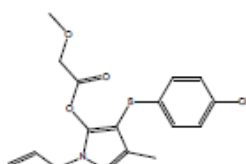
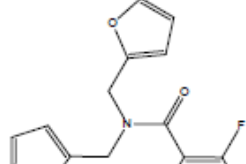
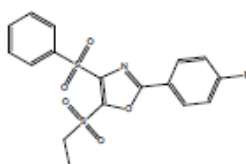
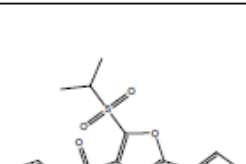
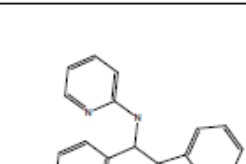
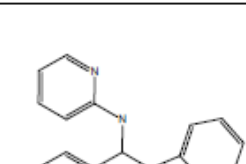
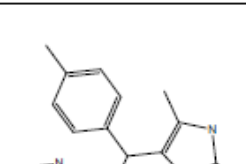
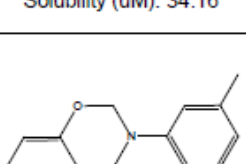
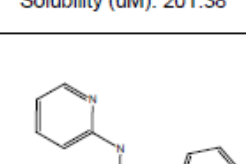
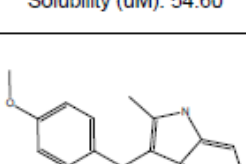
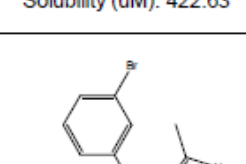
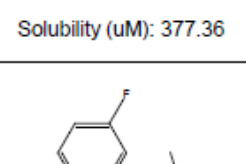
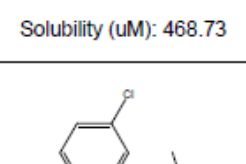
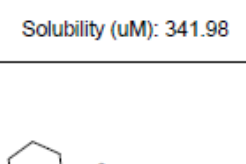
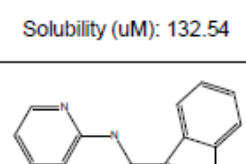
APPENDIX A

SOLUBILITY ASSAY

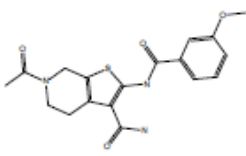
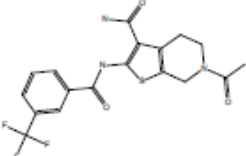
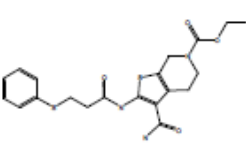
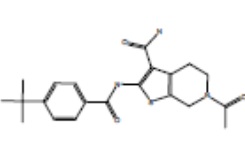
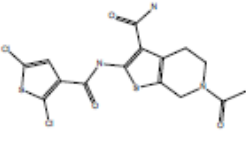
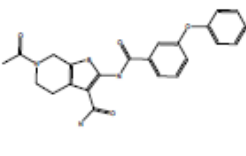
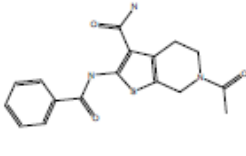
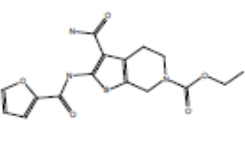
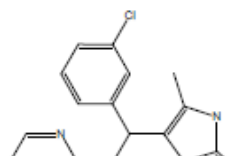
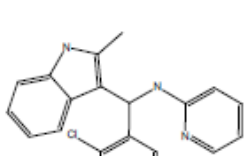
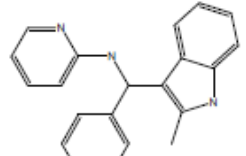
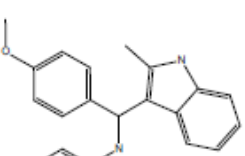
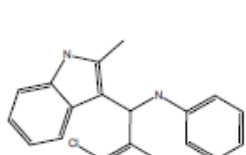
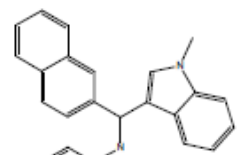
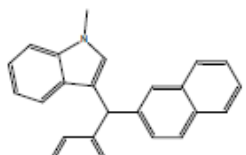
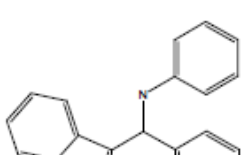
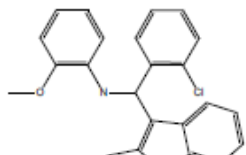
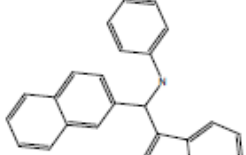
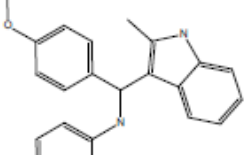
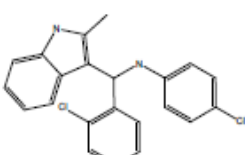
Table 12. Solubility assay results of compound library (n=4).

			
Solubility (uM): 462.04	Solubility (uM): 15.29	Solubility (uM): 42.07	Solubility (uM): 265.69
			
Solubility (uM): 75.76	Solubility (uM): 453.90	Solubility (uM): 20.32	Solubility (uM): 266.38
			
Solubility (uM): 466.75	Solubility (uM): 0.11	Solubility (uM): 0.69	Solubility (uM): 146.39
			
Solubility (uM): 218.66	Solubility (uM):	Solubility (uM): 464.48	Solubility (uM): 300.66
			
Solubility (uM): 273.25	Solubility (uM): 0.23	Solubility (uM): 550.24	Solubility (uM): 17.56

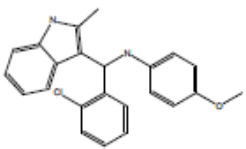
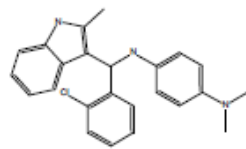
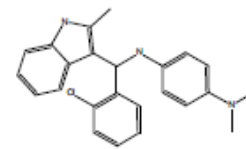
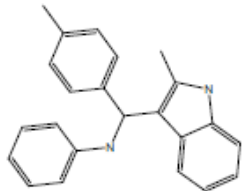
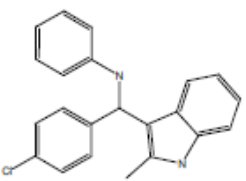
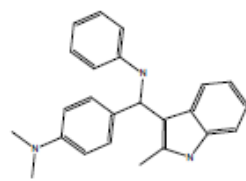
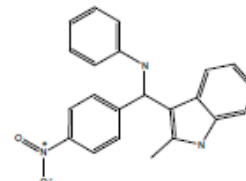
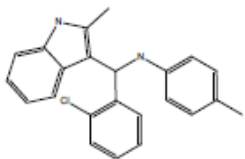
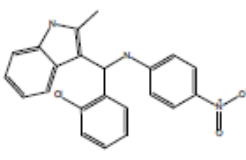
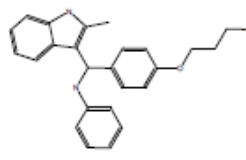
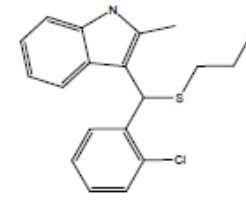
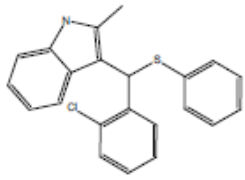
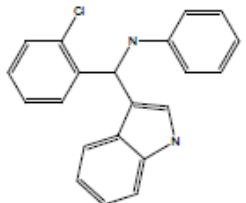
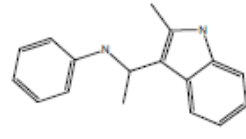
Continued, Table 12. Solubility assay results of compound library (n=4).

 <p>Solubility (uM): 124.20</p>	 <p>Solubility (uM): 49.87</p>	 <p>Solubility (uM): 21.92</p>	 <p>Solubility (uM): 201.86</p>
 <p>Solubility (uM): 486.95</p>	 <p>Solubility (uM): 492.98</p>	 <p>Solubility (uM): 115.23</p>	 <p>Solubility (uM): 5.17</p>
 <p>Solubility (uM): 34.16</p>	 <p>Solubility (uM): 201.38</p>	 <p>Solubility (uM): 54.60</p>	 <p>Solubility (uM): 422.63</p>
 <p>Solubility (uM): 377.36</p>	 <p>Solubility (uM): 468.73</p>	 <p>Solubility (uM): 341.98</p>	 <p>Solubility (uM): 132.54</p>
 <p>Solubility (uM): 427.77</p>	 <p>Solubility (uM): 277.73</p>	 <p>Solubility (uM): 338.78</p>	 <p>Solubility (uM): 403.31</p>

Continued, Table 12. Solubility assay results of compound library (n=4).

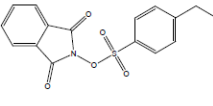
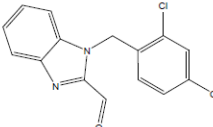
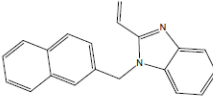
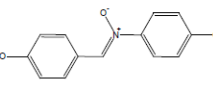
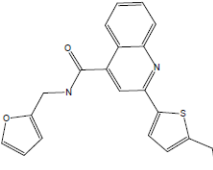
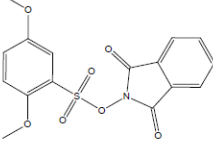
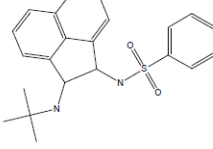
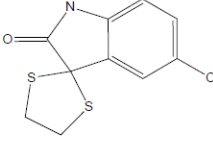
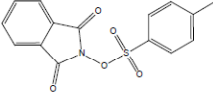
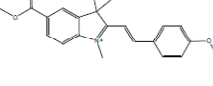
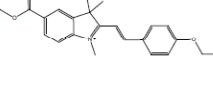
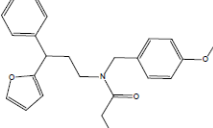
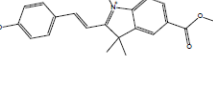
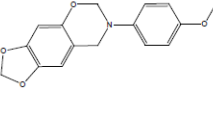
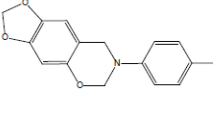
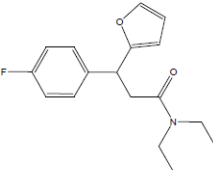
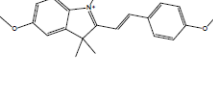
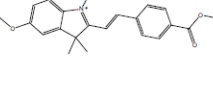
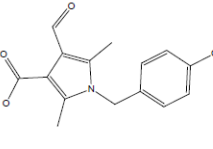
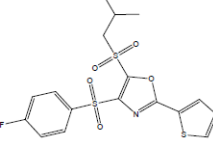
 Solubility (uM): 15.33	 Solubility (uM): 11.61	 Solubility (uM): 30.59	 Solubility (uM): 29.46
 Solubility (uM): 132.68	 Solubility (uM): 5.63	 Solubility (uM): 460.97	 Solubility (uM): 94.11
 Solubility (uM): 209.24	 Solubility (uM): 129.27	 Solubility (uM): 318.25	 Solubility (uM): 320.12
 Solubility (uM): 31.61	 Solubility (uM): 3.75	 Solubility (uM): -2.45	 Solubility (uM): 15.31
 Solubility (uM): 59.76	 Solubility (uM): 67.30	 Solubility (uM): 237.57	 Solubility (uM): 6.84

Continued, Table 12. Solubility assay results of compound library (n=4).

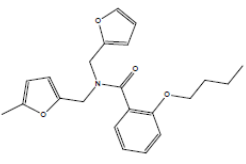
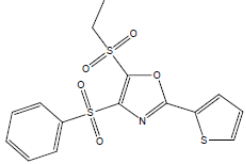
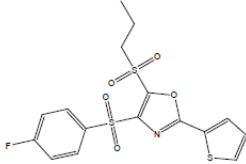
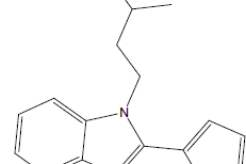
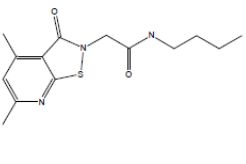
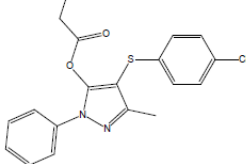
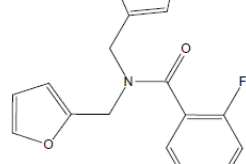
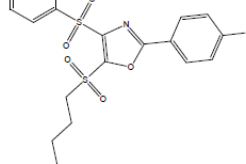
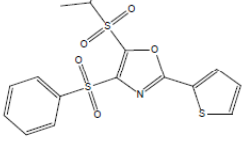
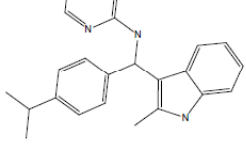
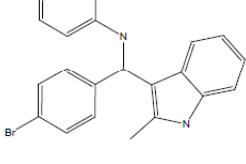
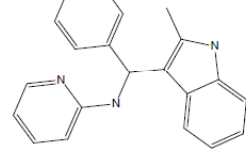
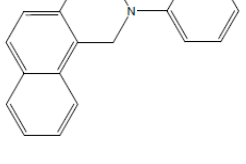
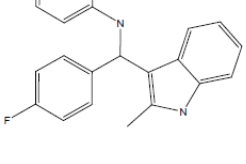
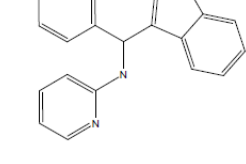
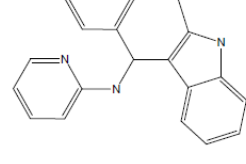
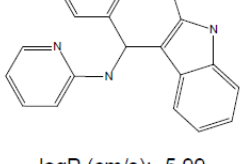
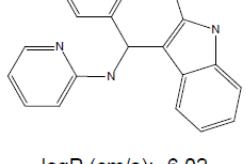
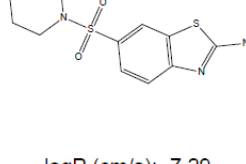
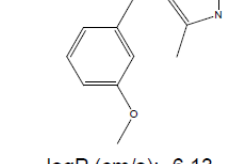
 Solubility (uM): 84.25	 Solubility (uM): 21.04	 Solubility (uM): 252.94	 Solubility (uM): 175.17
 Solubility (uM): 94.00	 Solubility (uM): 157.77	 Solubility (uM): 117.66	 Solubility (uM): 35.97
 Solubility (uM): 4.90	 Solubility (uM): 503.46	 Solubility (uM): 91.38	 Solubility (uM): 11.85
 Solubility (uM): 52.31	 Solubility (uM): 189.04		

APPENDIX B
PERMEABILITY ASSAY

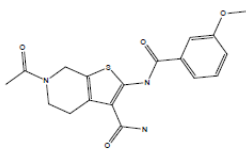
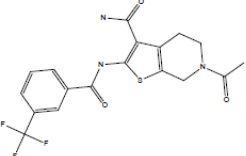
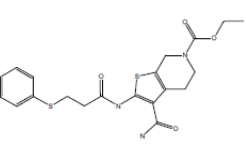
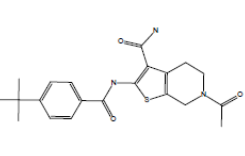
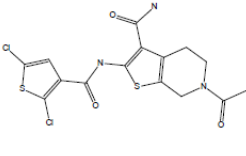
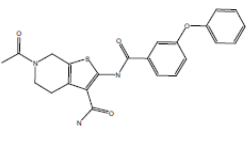
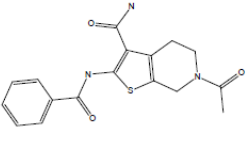
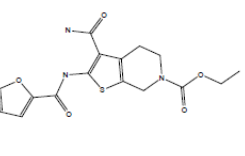
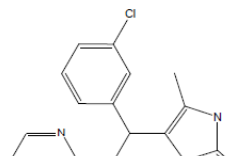
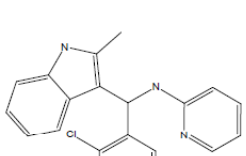
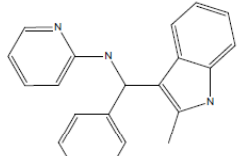
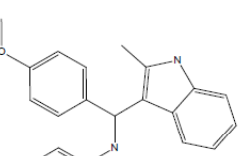
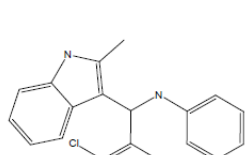
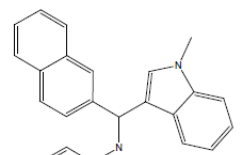
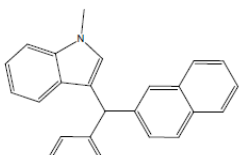
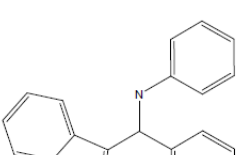
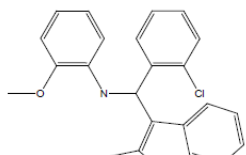
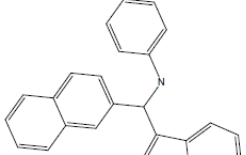
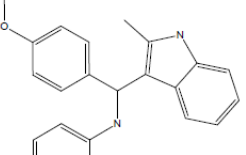
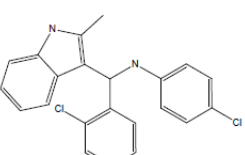
Table 13. Results of HDM-PAMPA assay for compound library (n=3).

 logP (cm/s): -7.84	 logP (cm/s): -6.53	 logP (cm/s): -6.30	 logP (cm/s): -8.47
 logP (cm/s): -6.39	 logP (cm/s): -7.85	 logP (cm/s): -7.25	 logP (cm/s): -5.95
 logP (cm/s): -8.72	 logP (cm/s): -7.87	 logP (cm/s): -8.22	 logP (cm/s): -7.05
 logP (cm/s): -7.71	 logP (cm/s): n/a	 logP (cm/s): -6.72	 logP (cm/s): -6.54
 logP (cm/s): -6.55	 logP (cm/s): -7.94	 logP (cm/s): -8.29	 logP (cm/s): -6.78

Continued, Table 13. Results of HDM-PAMPA assay for compound library (n=3).

 logP (cm/s): -7.25	 logP (cm/s): -6.67	 logP (cm/s): -6.61	 logP (cm/s): -6.49
 logP (cm/s): -6.78	 logP (cm/s): -7.49	 logP (cm/s): -6.89	 logP (cm/s): -6.89
 logP (cm/s): -6.36	 logP (cm/s): -6.13	 logP (cm/s): -6.01	 logP (cm/s): -6.11
 logP (cm/s): -5.95	 logP (cm/s): -6.05	 logP (cm/s): -6.26	 logP (cm/s): -6.11
 logP (cm/s): -5.99	 logP (cm/s): -6.02	 logP (cm/s): -7.29	 logP (cm/s): -6.13

Continued, Table 13. Results of HDM-PAMPA assay for compound library (n=3).

			
logP (cm/s): too low to det	logP (cm/s): -8.43 (n=1)	logP (cm/s): -7.38	logP (cm/s): -6.52
			
logP (cm/s): -7.01	logP (cm/s): -7.95	logP (cm/s): -7.77	logP (cm/s): n/a
			
logP (cm/s): -5.86	logP (cm/s): -6.12	logP (cm/s): -6.02	logP (cm/s): -6.07
			
logP (cm/s): -6.42	logP (cm/s): -6.82	logP (cm/s): -7.54	logP (cm/s): -6.58
			
logP (cm/s): -6.22	logP (cm/s): -6.30	logP (cm/s): -6.10	logP (cm/s): -6.25

Continued, Table 13. Results of HDM-PAMPA assay for compound library (n=3).

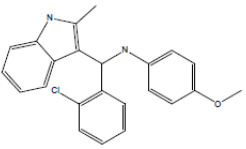
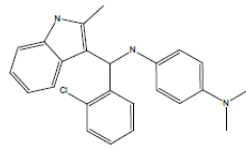
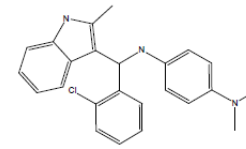
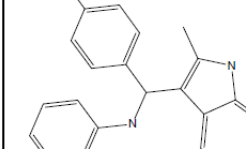
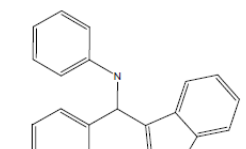
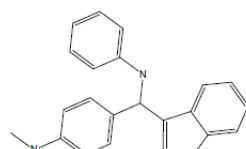
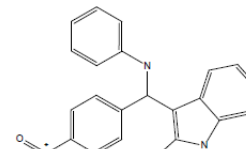
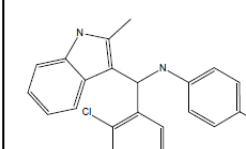
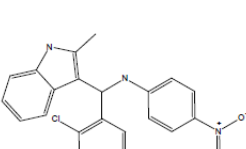
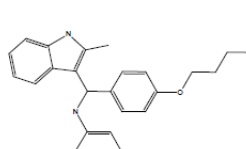
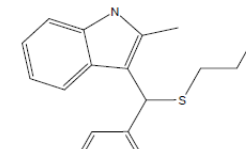
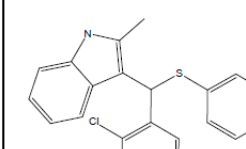
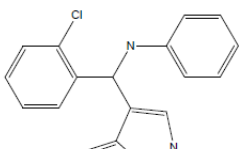
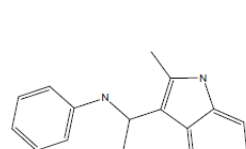
 logP (cm/s): -6.30	 logP (cm/s): -7.28	 logP (cm/s): -6.00	 logP (cm/s): -6.34
 logP (cm/s): -6.04	 logP (cm/s): -6.88	 logP (cm/s): -6.09	 logP (cm/s): -6.46
 logP (cm/s): -7.61	 logP (cm/s): -6.83	 logP (cm/s): -5.77	 logP (cm/s): -6.89
 logP (cm/s): -6.51	 logP (cm/s): -6.41		

Table 14. Results for IAM-C18-IAM coupled columns.

Compound	log k'	HDM-PAMPA logP (cm/s)	log P _{eff} (cm/s)
4,5-diphenylimidazole	1.242	-6.75	n/a
β-Estradiol	1.240	-7.65	n/a
Diethylstilbestrol	1.246	-7.98	n/a
3-phenylazo-2,6-diaminopyridine	1.222	-5.89	n/a
Verapamil	1.263	-5.98	-3.174
Carbamazepine	1.195	-6.82	-3.367
Ranitidine	0.650	-8.41	-4.367
Piroxicam	1.128	-7.66	-3.108
Metoprolol	1.077	-7.51	-3.886
Propranolol	1.223	-6.82	-3.538
Atenolol	-0.199	-7.19	-4.699
Naproxen	1.160	-7.65	-3.056
Caffeine	0.248	-7.53	n/a

Table 15. Results for C18-IAM coupled columns.

Compound	log k'	HDM-PAMPA logP (cm/s)	log P _{eff} (cm/s)
4,5-diphenylimidazole	1.283	-6.75	n/a
β-Estradiol	1.282	-7.65	n/a
Diethylstilbestrol	1.289	-7.98	n/a
3-phenylazo-2,6-diaminopyridine	1.268	-5.89	n/a
Verapamil	1.307	-5.98	-3.174
Carbamazepine	1.240	-6.82	-3.367
Ranitidine	0.669	-8.41	-4.367
Piroxicam	1.161	-7.66	-3.108
Metoprolol	1.075	-7.51	-3.886
Propranolol	1.256	-6.82	-3.538
Atenolol	-0.212	-7.19	-4.699
Naproxen	1.194	-7.65	-3.056
Caffeine	0.260	-7.53	n/a

Table 16. Results for IAM-C18 coupled columns.

Compound	log k'	HDM-PAMPA logP (cm/s)	log P _{eff} (cm/s)
4,5-diphenylimidazole	1.283	-6.75	n/a
β-Estradiol	1.271	-7.65	n/a
Diethylstilbestrol	1.288	-7.98	n/a
3-phenylazo-2,6-diaminopyridine	1.255	-5.89	n/a
Verapamil	1.297	-5.98	-3.174
Carbamazepine	1.240	-6.82	-3.367
Ranitidine	0.642	-8.41	-4.367
Piroxicam	1.154	-7.66	-3.108
Metoprolol	1.078	-7.51	-3.886
Propranolol	1.240	-6.82	-3.538
Atenolol	-0.212	-7.19	-4.699
Naproxen	1.186	-7.65	-3.056
Caffeine	0.276	-7.53	n/a

Table 17. Results for C18 column.

Compound	log k'	HDM-PAMPA logP (cm/s)	log P _{eff} (cm/s)
4,5-diphenylimidazole	1.343	-6.75	n/a
β-Estradiol	1.338	-7.65	n/a
Diethylstilbestrol	1.345	-7.98	n/a
3-phenylazo-2,6-diaminopyridine	1.326	-5.89	n/a
Verapamil	1.369	-5.98	-3.174
Carbamazepine	1.300	-6.82	-3.367
Ranitidine	0.746	-8.41	-4.367
Piroxicam	1.216	-7.66	-3.108
Metoprolol	1.086	-7.51	-3.886
Propranolol	1.304	-6.82	-3.538
Atenolol	-0.279	-7.19	-4.699
Naproxen	1.250	-7.65	-3.056
Caffeine	0.271	-7.53	n/a

Table 18. Results for IAM column.

Compound	log k'	HDM-PAMPA logP (cm/s)	log P _{eff} (cm/s)
4,5-diphenylimidazole	1.375	-6.75	n/a
β-Estradiol	1.124	-7.65	n/a
Diethylstilbestrol	0.640	-7.98	n/a
3-phenylazo-2,6-diaminopyridine	1.436	-5.89	n/a
Verapamil	1.190	-5.98	-3.174
Carbamazepine	0.351	-6.82	-3.367
Ranitidine	0.852	-8.41	-4.367
Piroxicam	0.282	-7.66	-3.108
Metoprolol	-0.048	-7.51	-3.886
Propranolol	1.079	-6.82	-3.538
Atenolol	0.916	-7.19	-4.699
Naproxen	0.913	-7.65	-3.056

Table 19. Octanol/water partitioning coefficients at pH 7.2 beginning with 1mg/mL compound solutions in 1-octanol.

1-Octanol Solutions			
Volume of Drug Solution:	100 μL	300 μL	400 μL
Compound	logP _{o/w}	logP _{o/w}	logP _{o/w}
4,5-diphenylimidazole	1.74	1.76	1.70
β-estradiol	1.08	1.51	1.53
Diethylstilbestrol	1.37	1.88	1.85
3-phenylazo-2,6-diaminopyridine	1.92	1.93	1.72
Verapamil	1.24	1.58	1.40
Carbamazepine	0.770	1.01	0.975
Ranitidine	-0.850	-0.577	-0.492
Piroxicam	-0.0981	-0.0218	-0.0325
Metoprolol	-0.0702	-0.274	-0.299
Propranolol	0.872	0.801	0.459
Atenolol	-0.394	-0.789	-0.663
Naproxen	0.475	0.559	0.513
Caffeine	-0.104	n/a	n/a

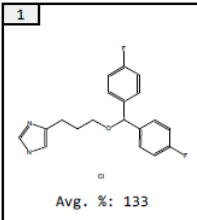
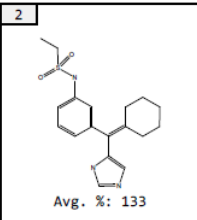
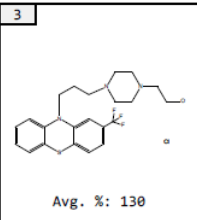
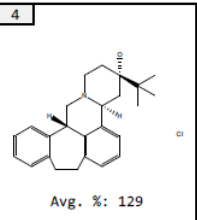
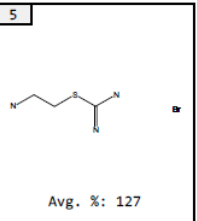
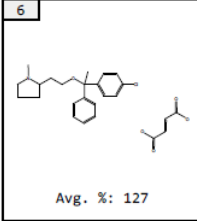
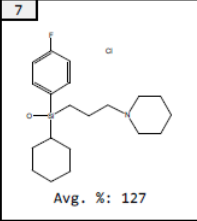
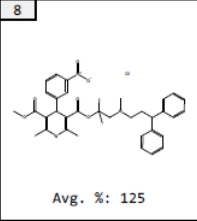
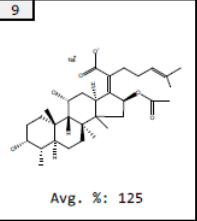
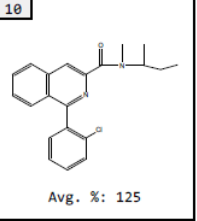
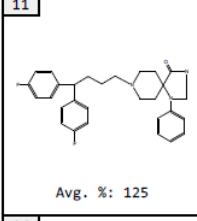
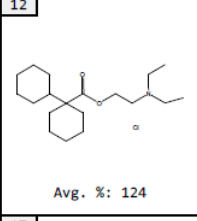
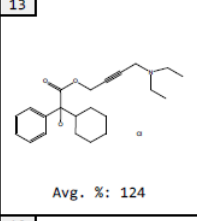
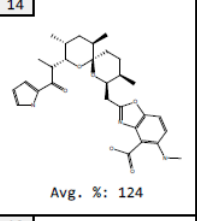
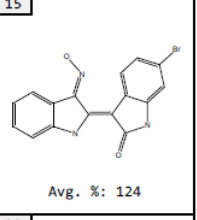
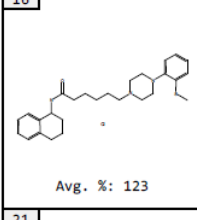
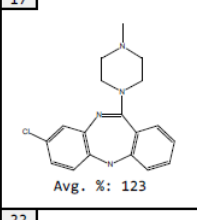
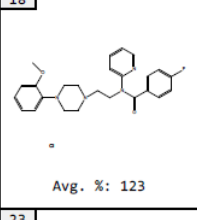
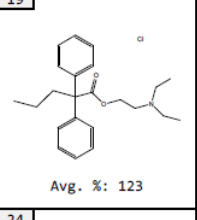
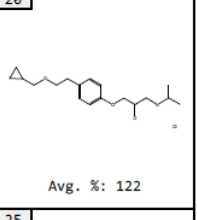
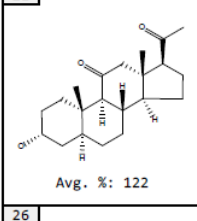
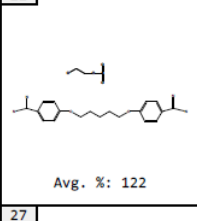
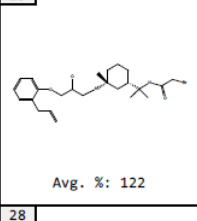
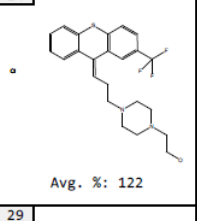
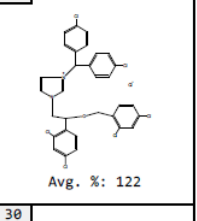
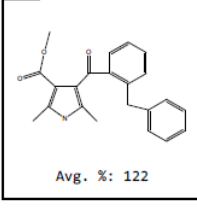
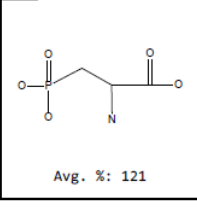
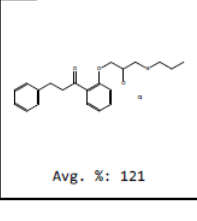
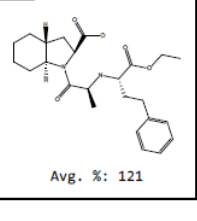
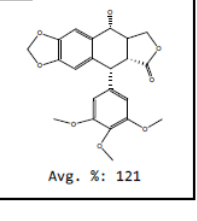
Table 20. Octanol/water partitioning coefficients at pH 7.2 beginning with 1mg/mL compound solutions in phosphate buffered saline.

pH 7.4 PBS Solutions			
Volume of Drug Solution:	100 μL	300 μL	400 μL
Compound	logP_{o/w}	logP_{o/w}	logP_{o/w}
4,5-diphenylimidazole	1.22	1.21	1.64
β -estradiol	0.642	0.930	1.02
Diethylstilbestrol	0.674	0.938	0.946
3-phenylazo-2,6-diaminopyridine	1.66	1.83	1.46
Verapamil	1.33	1.52	1.43
Carbamazepine	0.610	0.693	0.720
Ranitidine	-0.974	-0.647	-0.520
Piroxicam	-0.140	-0.0359	-0.0214
Metoprolol	-0.0706	-0.249	-0.270
Propranolol	0.902	0.599	0.353
Atenolol	-0.446	-0.840	-0.723
Naproxen	0.444	0.508	0.507
Caffeine	-0.120	n/a	n/a

APPENDIX C

THIOL BINDING ASSAY

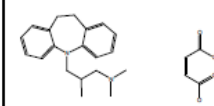
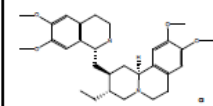
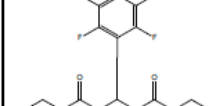
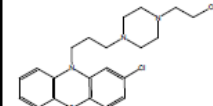
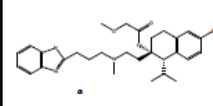
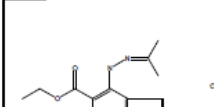
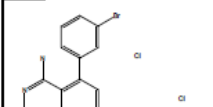
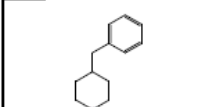
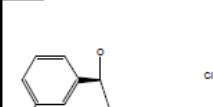
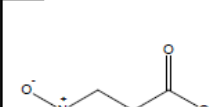
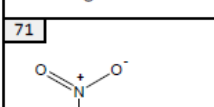
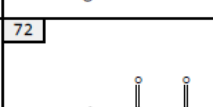

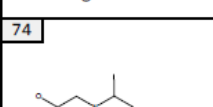
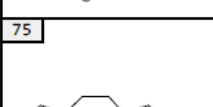
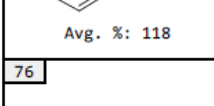
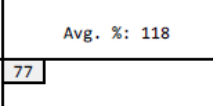
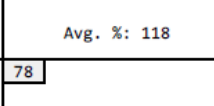
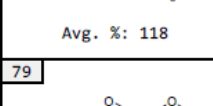
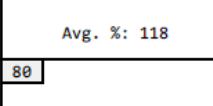
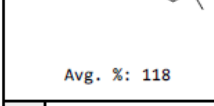
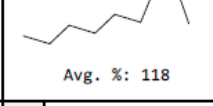
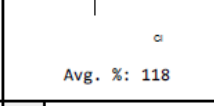
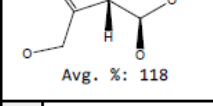
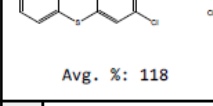
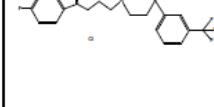
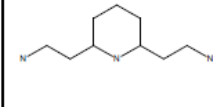
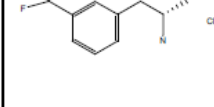
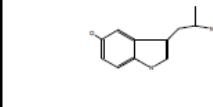
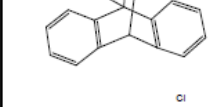
Table 21. Results of fluorescence-based electrophile screen of the LOPAC library. Values are presented as a percent of the MSTI signal (Avg. %). (n=3)

 Avg. %: 133	 Avg. %: 133	 Avg. %: 130	 Avg. %: 129	 Avg. %: 127
 Avg. %: 127	 Avg. %: 127	 Avg. %: 125	 Avg. %: 125	 Avg. %: 125
 Avg. %: 125	 Avg. %: 124	 Avg. %: 124	 Avg. %: 124	 Avg. %: 124
 Avg. %: 123	 Avg. %: 123	 Avg. %: 123	 Avg. %: 123	 Avg. %: 122
 Avg. %: 122	 Avg. %: 122	 Avg. %: 122	 Avg. %: 122	 Avg. %: 122
 Avg. %: 122	 Avg. %: 121	 Avg. %: 121	 Avg. %: 121	 Avg. %: 121

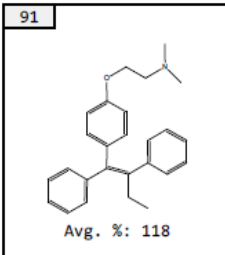
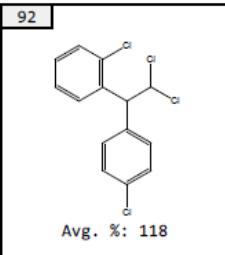
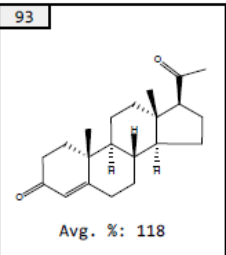
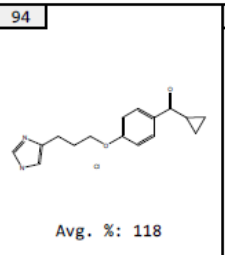
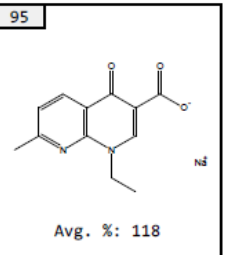
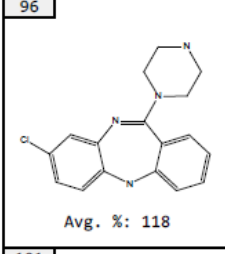
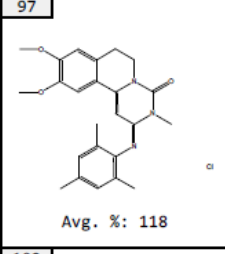
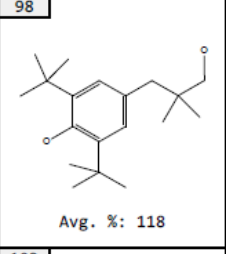
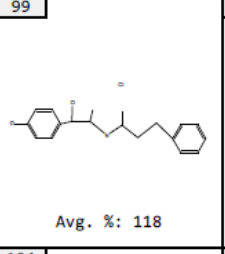
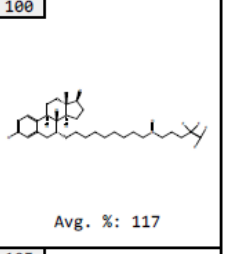
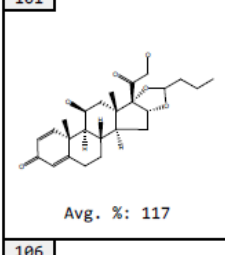
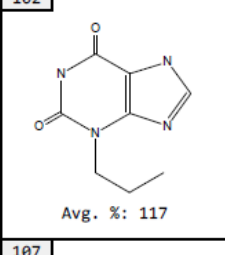
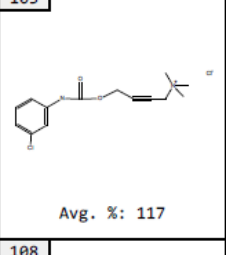
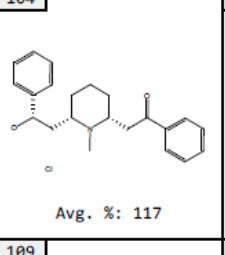
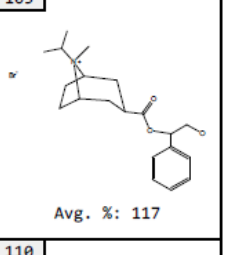
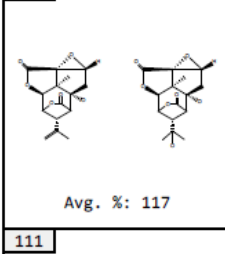
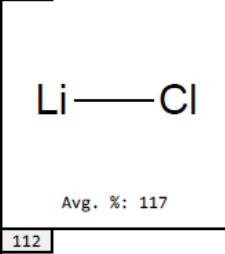
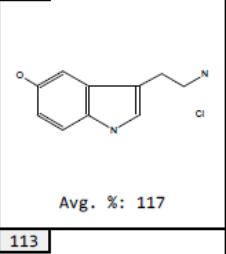
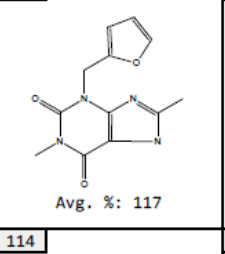
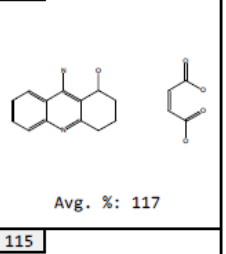
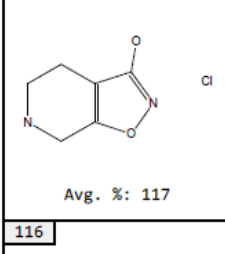
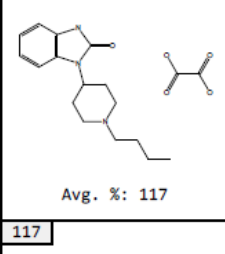
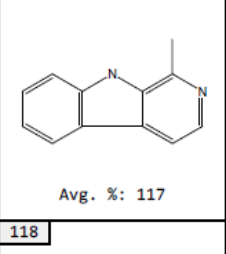
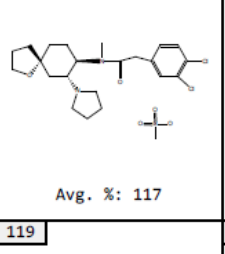
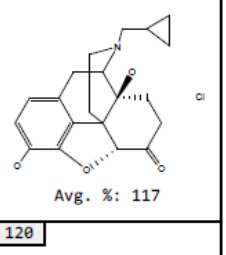
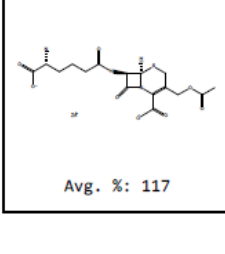
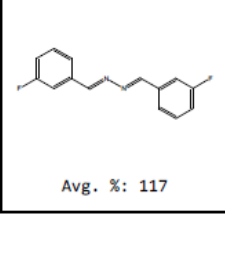
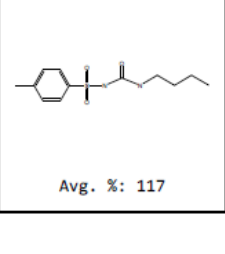
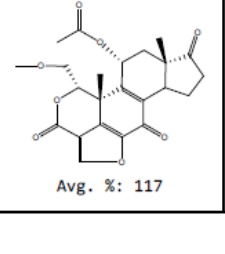
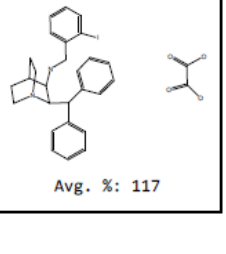
Continued, Table 21. Results of fluorescence-based electrophile screen of the LOPAC library. Values are presented as a percent of the MSTI signal (Avg. %). (n=3)

31 Avg. %: 121	32 Avg. %: 121	33 Avg. %: 121	34 Avg. %: 121	35 Avg. %: 121
36 Avg. %: 121	37 Avg. %: 120	38 Avg. %: 120	39 Avg. %: 120	40 Avg. %: 120
41 Avg. %: 120	42 Avg. %: 120	43 Avg. %: 120	44 Avg. %: 120	45 Avg. %: 120
46 Avg. %: 120	47 Avg. %: 120	48 Avg. %: 120	49 Avg. %: 119	50 Avg. %: 119
51 Avg. %: 119	52 Avg. %: 119	53 Avg. %: 119	54 Avg. %: 119	55 Avg. %: 119
56 Avg. %: 119	57 Avg. %: 119	58 Avg. %: 119	59 Avg. %: 119	60 Avg. %: 119

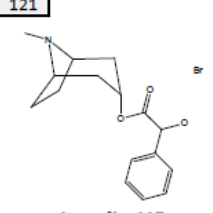
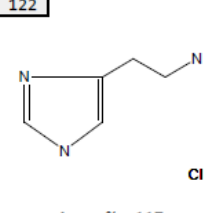
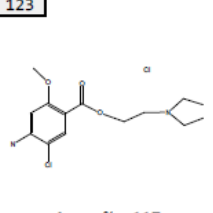
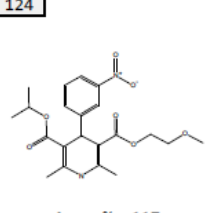
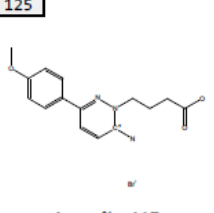
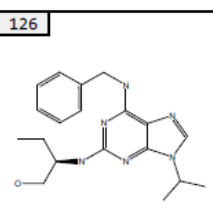
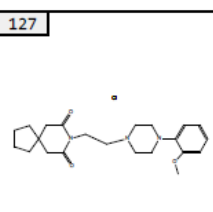
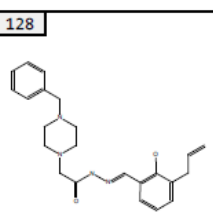
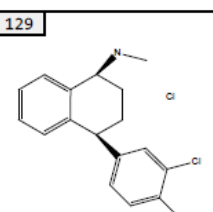
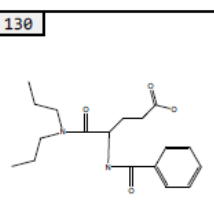
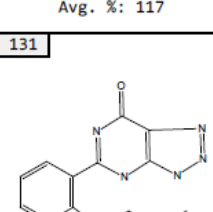
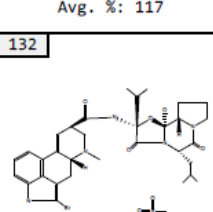
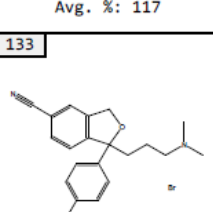
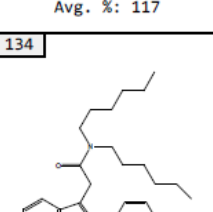
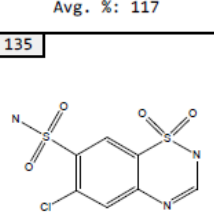
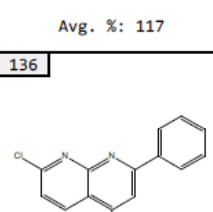
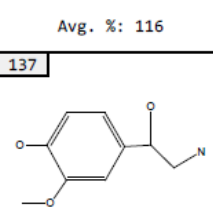
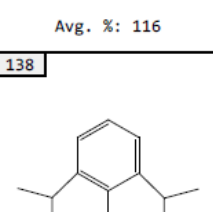
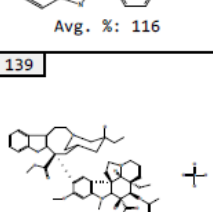
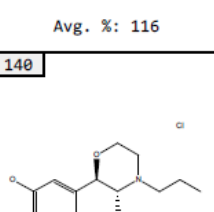
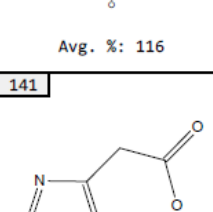
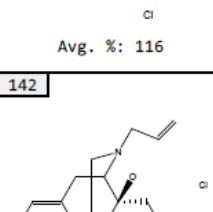
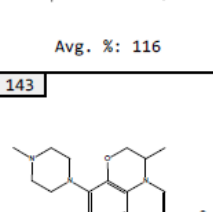
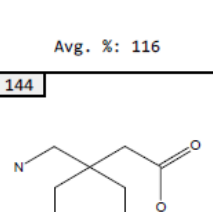
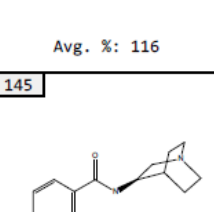
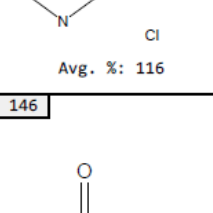
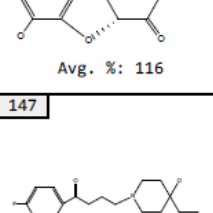
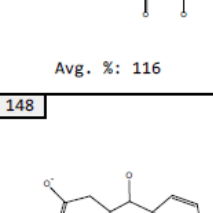
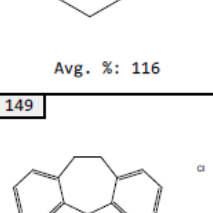
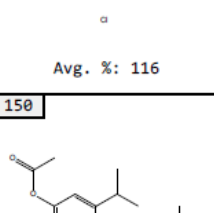
Continued, Table 21. Results of fluorescence-based electrophile screen of the LOPAC library. Values are presented as a percent of the MSTI signal (Avg. %). (n=3)

61  Avg. %: 119	62  Avg. %: 119	63  Avg. %: 119	64  Avg. %: 119	65  Avg. %: 119
66  Avg. %: 119	67  Avg. %: 119	68  Avg. %: 119	69  Avg. %: 119	70  Avg. %: 118
71  Avg. %: 118	72  Avg. %: 118	73  Avg. %: 118	74  Avg. %: 118	75  Avg. %: 118
76  Avg. %: 118	77  Avg. %: 118	78  Avg. %: 118	79  Avg. %: 118	80  Avg. %: 118
81  Avg. %: 118	82  Avg. %: 118	83  Avg. %: 118	84  Avg. %: 118	85  Avg. %: 118
86  Avg. %: 118	87  Avg. %: 118	88  Avg. %: 118	89  Avg. %: 118	90  Avg. %: 118

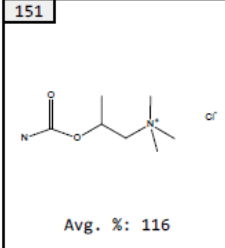
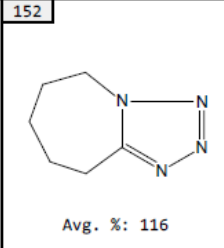
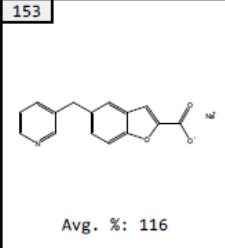
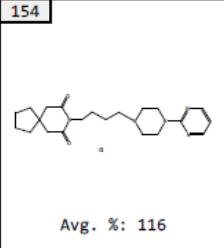
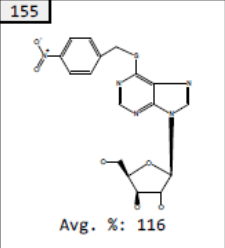
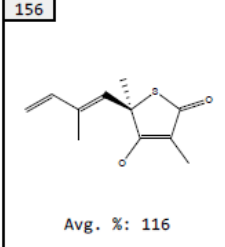
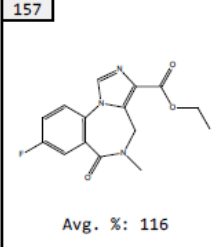
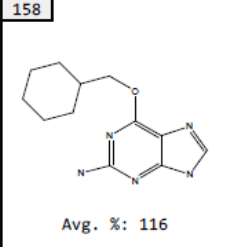
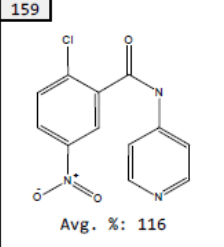
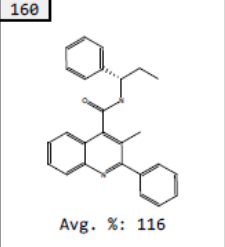
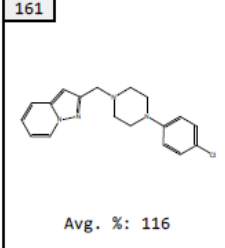
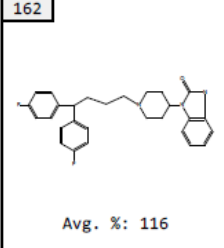
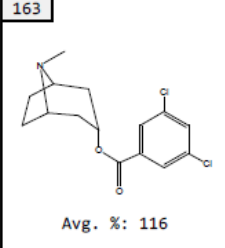
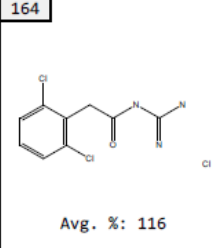
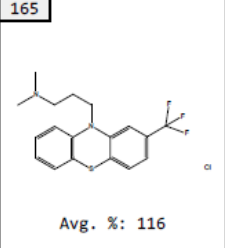
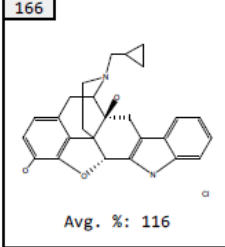
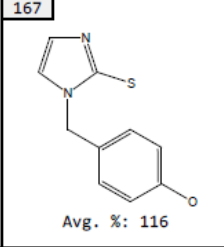
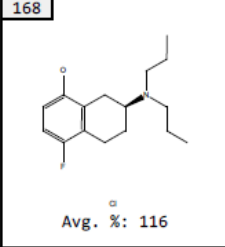
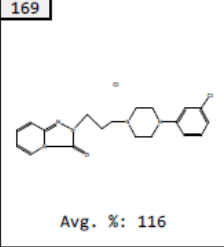
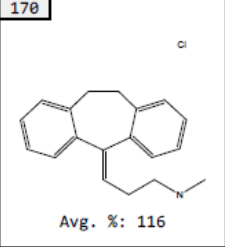
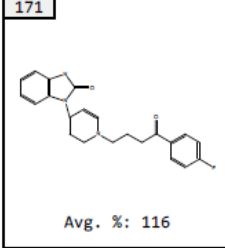
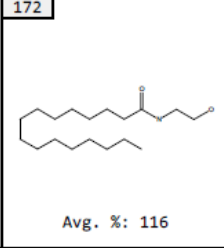
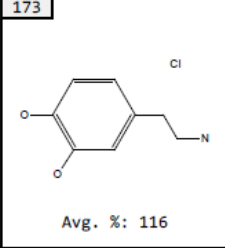
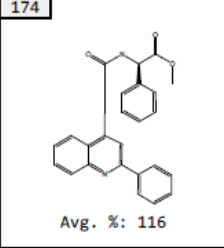
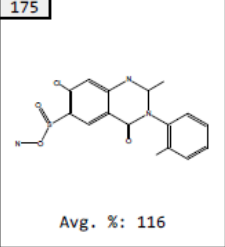
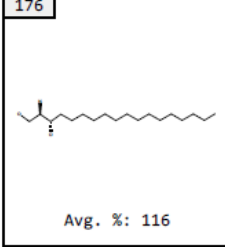
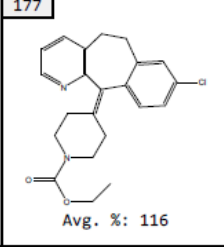
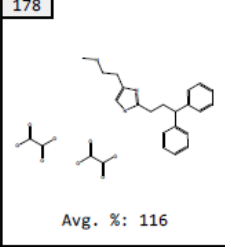
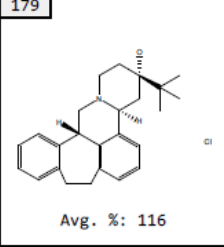
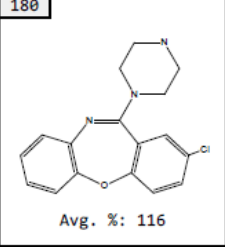
Continued, Table 21. Results of fluorescence-based electrophile screen of the LOPAC library. Values are presented as a percent of the MSTI signal (Avg. %). (n=3)

91  Avg. %: 118	92  Avg. %: 118	93  Avg. %: 118	94  Avg. %: 118	95  Avg. %: 118
96  Avg. %: 118	97  Avg. %: 118	98  Avg. %: 118	99  Avg. %: 118	100  Avg. %: 117
101  Avg. %: 117	102  Avg. %: 117	103  Avg. %: 117	104  Avg. %: 117	105  Avg. %: 117
106  Avg. %: 117	107  Avg. %: 117	108  Avg. %: 117	109  Avg. %: 117	110  Avg. %: 117
111  Avg. %: 117	112  Avg. %: 117	113  Avg. %: 117	114  Avg. %: 117	115  Avg. %: 117
116  Avg. %: 117	117  Avg. %: 117	118  Avg. %: 117	119  Avg. %: 117	120  Avg. %: 117

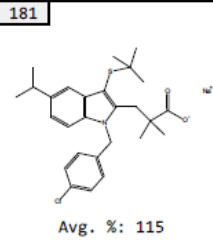
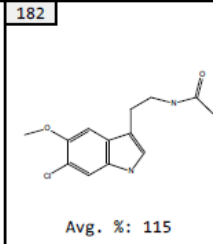
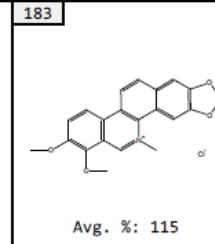
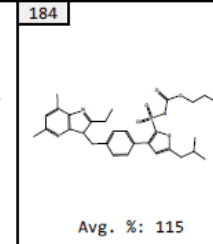
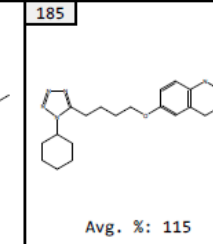
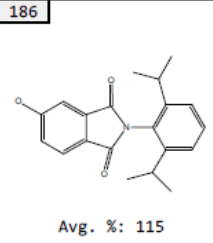
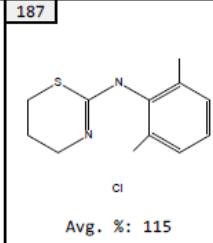
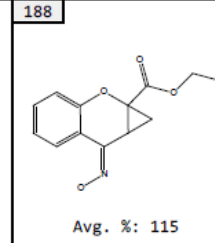
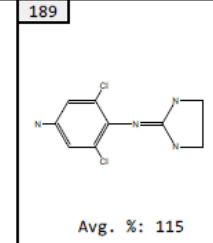
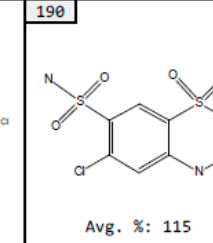
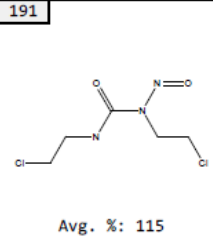
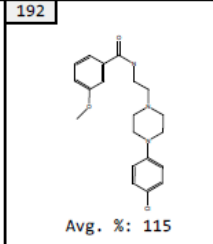
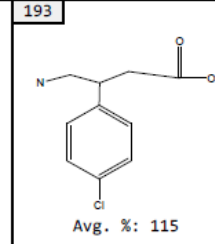
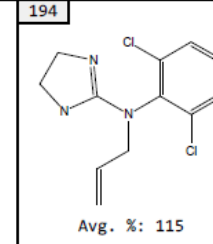
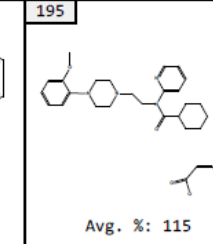
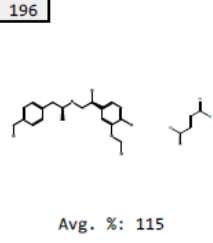
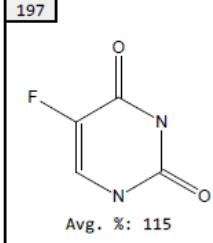
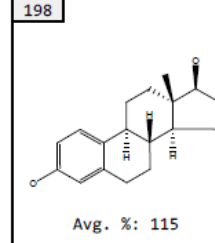
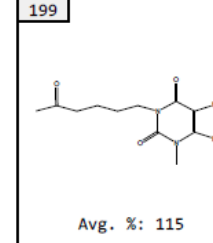
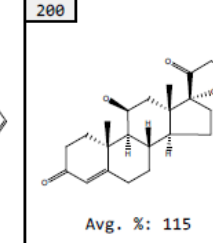
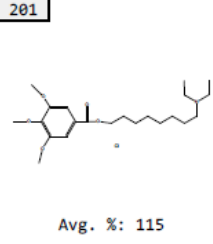
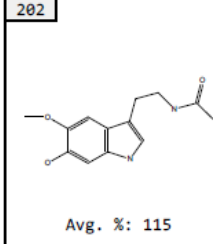
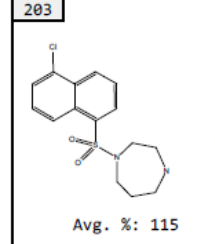
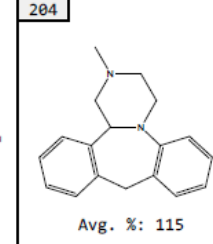
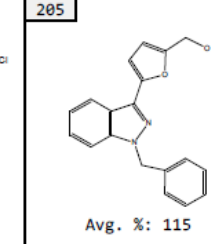
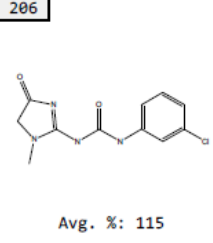
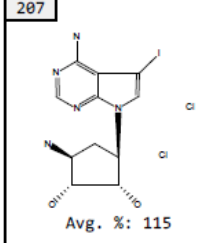
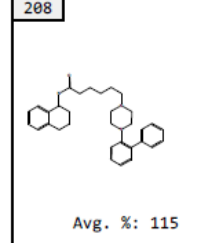
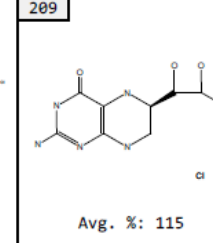
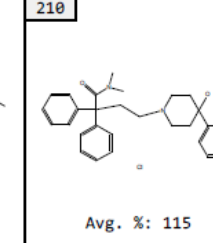
Continued, Table 21. Results of fluorescence-based electrophile screen of the LOPAC library. Values are presented as a percent of the MSTI signal (Avg. %). (n=3)

121  Avg. %: 117	122  Avg. %: 117	123  Avg. %: 117	124  Avg. %: 117	125  Avg. %: 117
126  Avg. %: 117	127  Avg. %: 117	128  Avg. %: 117	129  Avg. %: 117	130  Avg. %: 117
131  Avg. %: 117	132  Avg. %: 116	133  Avg. %: 116	134  Avg. %: 116	135  Avg. %: 116
136  Avg. %: 116	137  Avg. %: 116	138  Avg. %: 116	139  Avg. %: 116	140  Avg. %: 116
141  Avg. %: 116	142  Avg. %: 116	143  Avg. %: 116	144  Avg. %: 116	145  Avg. %: 116
146  Avg. %: 116	147  Avg. %: 116	148  Avg. %: 116	149  Avg. %: 116	150  Avg. %: 116

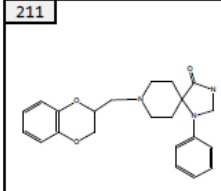
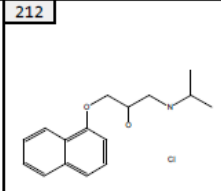
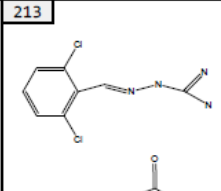
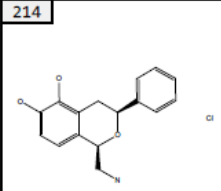
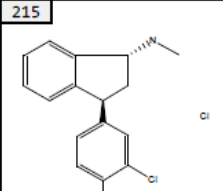
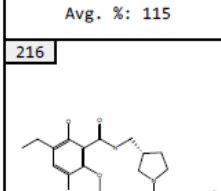
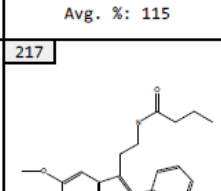
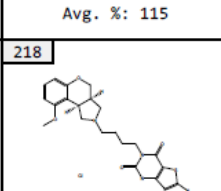
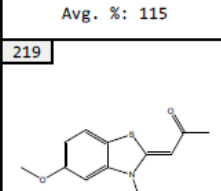
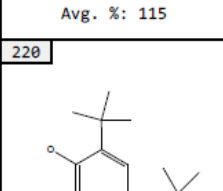
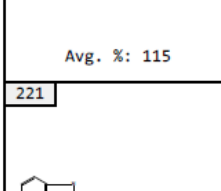
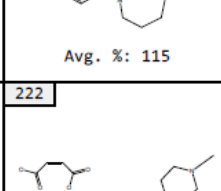
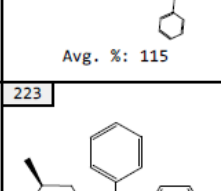
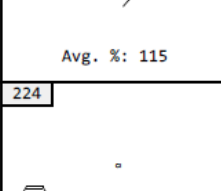
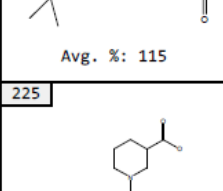
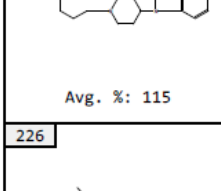
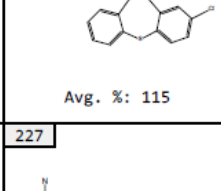
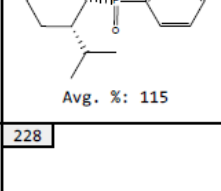
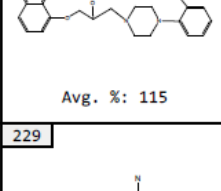
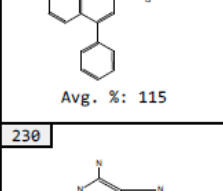
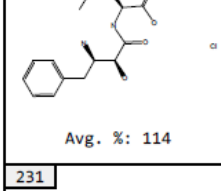
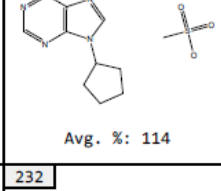
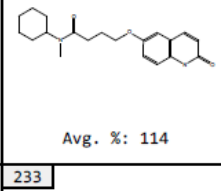
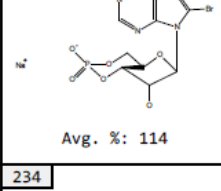
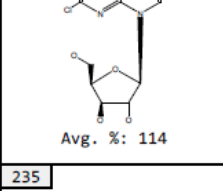
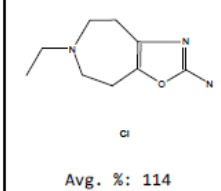
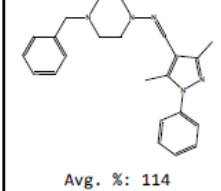
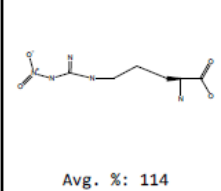
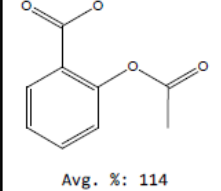
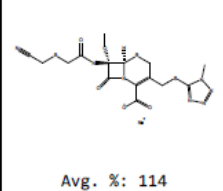
Continued, Table 21. Results of fluorescence-based electrophile screen of the LOPAC library. Values are presented as a percent of the MSTI signal (Avg. %). (n=3)

 <p>Avg. %: 116</p>	 <p>Avg. %: 116</p>	 <p>Avg. %: 116</p>	 <p>Avg. %: 116</p>	 <p>Avg. %: 116</p>
 <p>Avg. %: 116</p>	 <p>Avg. %: 116</p>	 <p>Avg. %: 116</p>	 <p>Avg. %: 116</p>	 <p>Avg. %: 116</p>
 <p>Avg. %: 116</p>	 <p>Avg. %: 116</p>	 <p>Avg. %: 116</p>	 <p>Avg. %: 116</p>	 <p>Avg. %: 116</p>
 <p>Avg. %: 116</p>	 <p>Avg. %: 116</p>	 <p>Avg. %: 116</p>	 <p>Avg. %: 116</p>	 <p>Avg. %: 116</p>
 <p>Avg. %: 116</p>	 <p>Avg. %: 116</p>	 <p>Avg. %: 116</p>	 <p>Avg. %: 116</p>	 <p>Avg. %: 116</p>
 <p>Avg. %: 116</p>	 <p>Avg. %: 116</p>	 <p>Avg. %: 116</p>	 <p>Avg. %: 116</p>	 <p>Avg. %: 116</p>

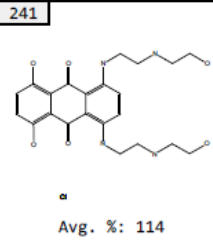
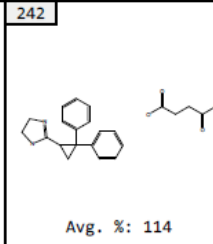
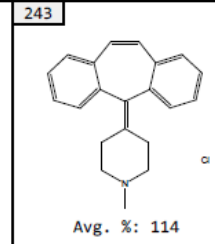
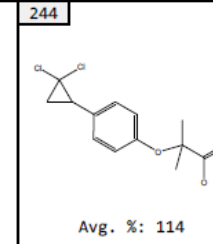
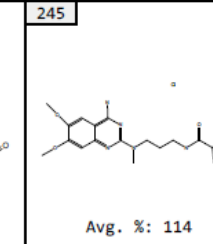
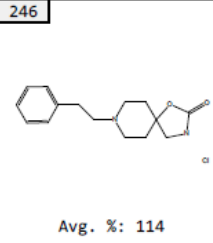
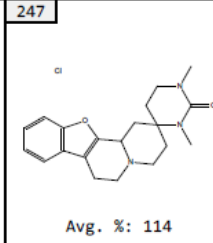
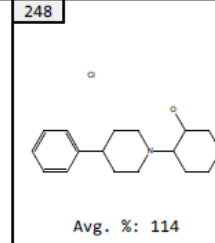
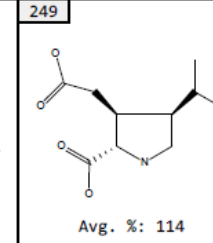
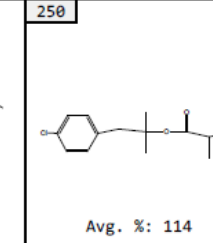
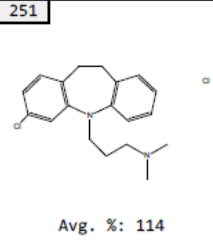
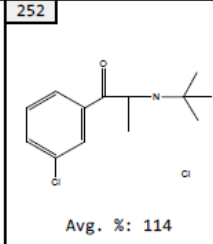
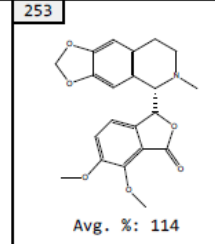
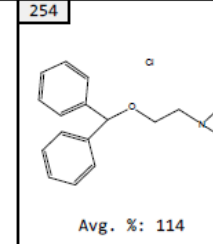
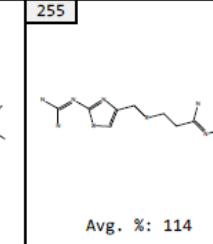
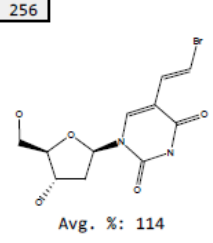
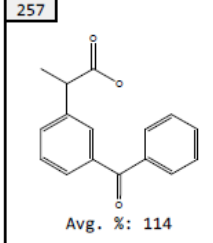
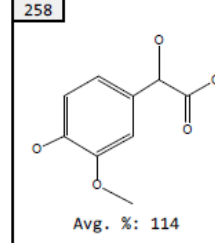
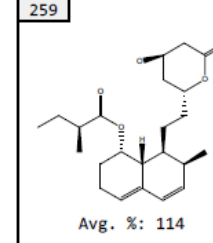
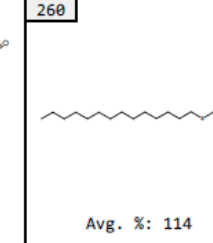
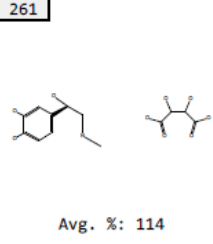
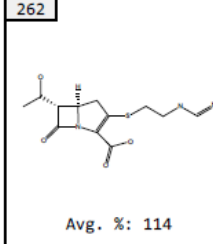
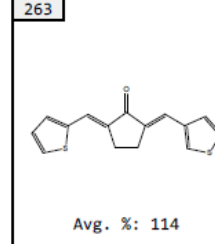
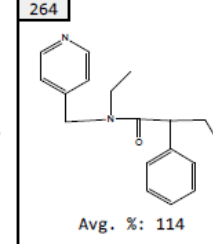
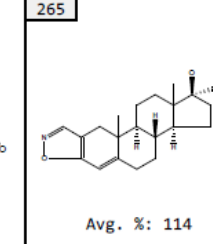
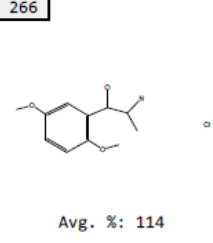
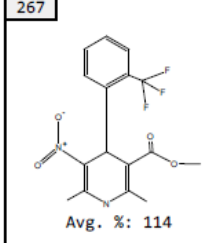
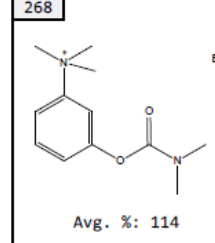
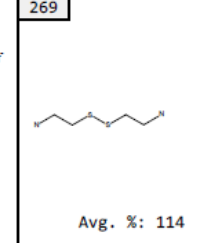
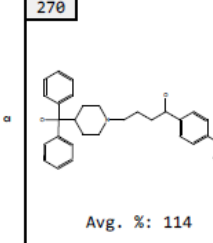
Continued, Table 21. Results of fluorescence-based electrophile screen of the LOPAC library. Values are presented as a percent of the MSTI signal (Avg. %). (n=3)

 <p>Avg. %: 115</p>	 <p>Avg. %: 115</p>	 <p>Avg. %: 115</p>	 <p>Avg. %: 115</p>	 <p>Avg. %: 115</p>
 <p>Avg. %: 115</p>	 <p>Avg. %: 115</p>	 <p>Avg. %: 115</p>	 <p>Avg. %: 115</p>	 <p>Avg. %: 115</p>
 <p>Avg. %: 115</p>	 <p>Avg. %: 115</p>	 <p>Avg. %: 115</p>	 <p>Avg. %: 115</p>	 <p>Avg. %: 115</p>
 <p>Avg. %: 115</p>	 <p>Avg. %: 115</p>	 <p>Avg. %: 115</p>	 <p>Avg. %: 115</p>	 <p>Avg. %: 115</p>
 <p>Avg. %: 115</p>	 <p>Avg. %: 115</p>	 <p>Avg. %: 115</p>	 <p>Avg. %: 115</p>	 <p>Avg. %: 115</p>
 <p>Avg. %: 115</p>	 <p>Avg. %: 115</p>	 <p>Avg. %: 115</p>	 <p>Avg. %: 115</p>	 <p>Avg. %: 115</p>

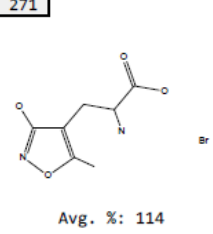
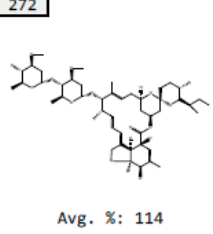
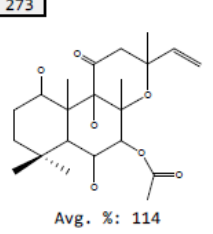
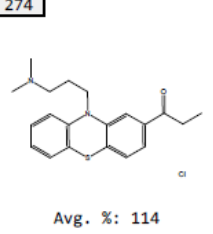
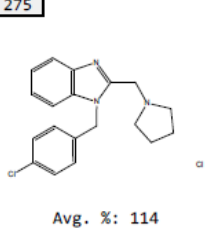
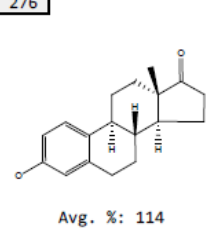
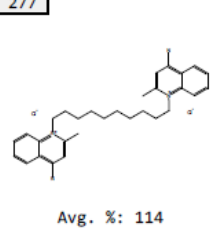
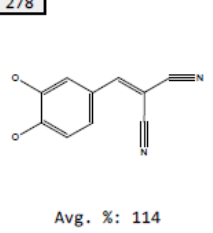
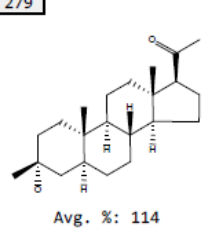
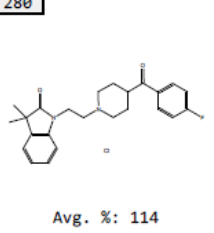
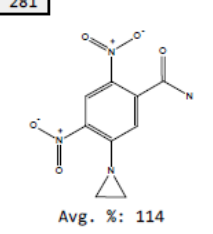
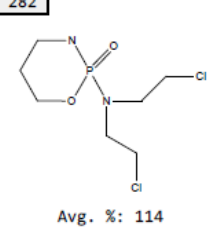
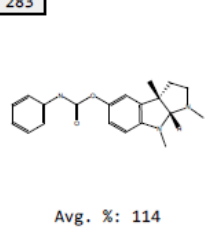
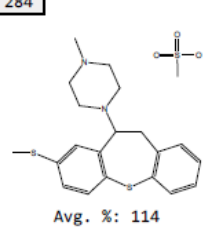
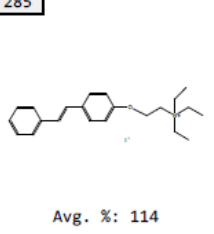
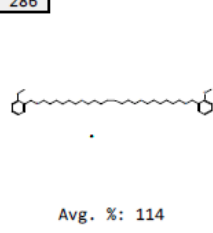
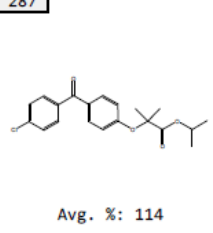
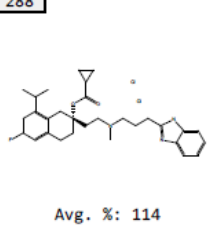
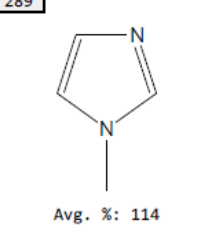
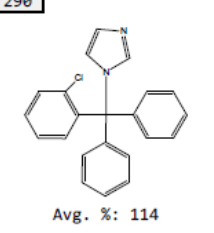
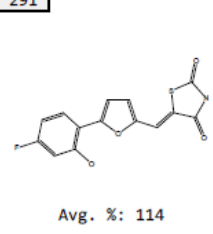
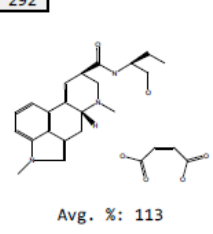
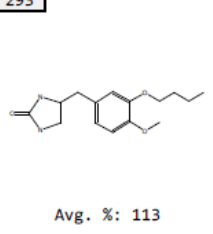
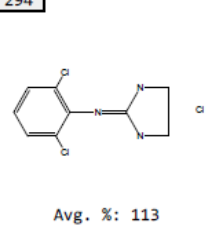
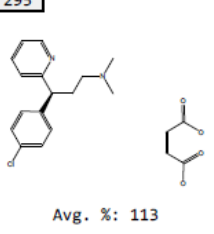
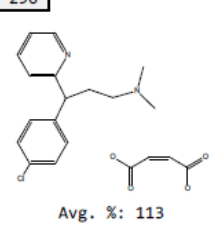
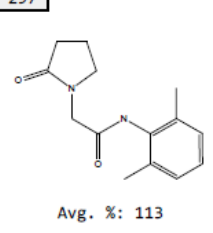
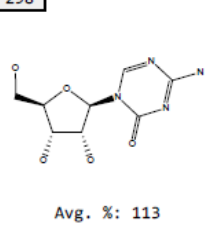
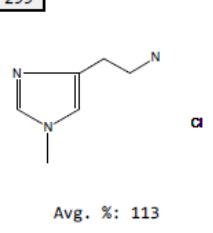
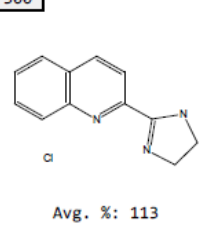
Continued, Table 21. Results of fluorescence-based electrophile screen of the LOPAC library. Values are presented as a percent of the MSTI signal (Avg. %). (n=3)

<p>211</p>  <p>Avg. %: 115</p>	<p>212</p>  <p>Avg. %: 115</p>	<p>213</p>  <p>Avg. %: 115</p>	<p>214</p>  <p>Avg. %: 115</p>	<p>215</p>  <p>Avg. %: 115</p>
<p>216</p>  <p>Avg. %: 115</p>	<p>217</p>  <p>Avg. %: 115</p>	<p>218</p>  <p>Avg. %: 115</p>	<p>219</p>  <p>Avg. %: 115</p>	<p>220</p>  <p>Avg. %: 115</p>
<p>221</p>  <p>Avg. %: 115</p>	<p>222</p>  <p>Avg. %: 115</p>	<p>223</p>  <p>Avg. %: 115</p>	<p>224</p>  <p>Avg. %: 115</p>	<p>225</p>  <p>Avg. %: 115</p>
<p>226</p>  <p>Avg. %: 114</p>	<p>227</p>  <p>Avg. %: 114</p>	<p>228</p>  <p>Avg. %: 114</p>	<p>229</p>  <p>Avg. %: 114</p>	<p>230</p>  <p>Avg. %: 114</p>
<p>231</p>  <p>Avg. %: 114</p>	<p>232</p>  <p>Avg. %: 114</p>	<p>233</p>  <p>Avg. %: 114</p>	<p>234</p>  <p>Avg. %: 114</p>	<p>235</p>  <p>Avg. %: 114</p>
<p>236</p>  <p>Avg. %: 114</p>	<p>237</p>  <p>Avg. %: 114</p>	<p>238</p>  <p>Avg. %: 114</p>	<p>239</p>  <p>Avg. %: 114</p>	<p>240</p>  <p>Avg. %: 114</p>

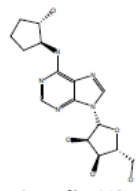
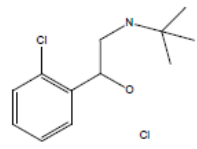
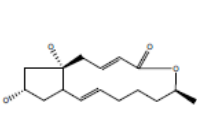
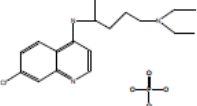
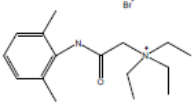
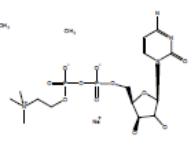
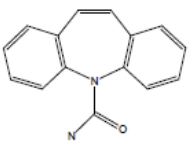
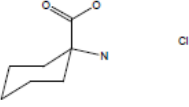
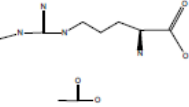
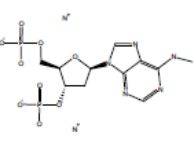
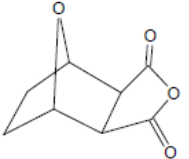
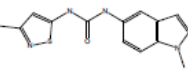
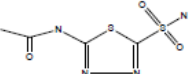
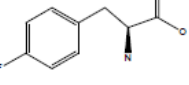
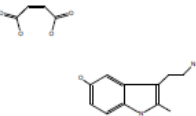
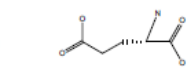
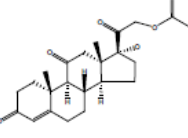
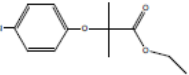
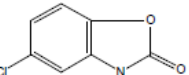
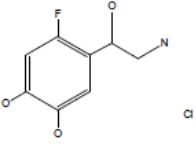
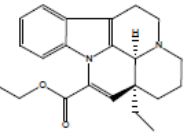
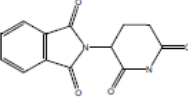
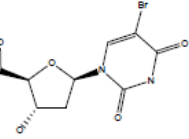
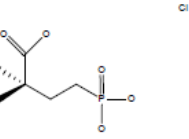
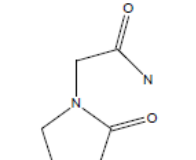
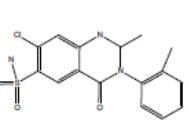
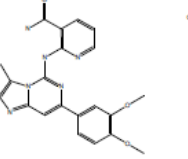
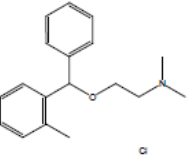
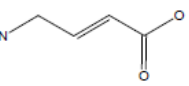
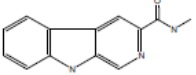
Continued, Table 21. Results of fluorescence-based electrophile screen of the LOPAC library. Values are presented as a percent of the MSTI signal (Avg. %). (n=3)

241	242	243	244	245
				
Avg. %: 114	Avg. %: 114	Avg. %: 114	Avg. %: 114	Avg. %: 114
246	247	248	249	250
				
Avg. %: 114	Avg. %: 114	Avg. %: 114	Avg. %: 114	Avg. %: 114
251	252	253	254	255
				
Avg. %: 114	Avg. %: 114	Avg. %: 114	Avg. %: 114	Avg. %: 114
256	257	258	259	260
				
Avg. %: 114	Avg. %: 114	Avg. %: 114	Avg. %: 114	Avg. %: 114
261	262	263	264	265
				
Avg. %: 114	Avg. %: 114	Avg. %: 114	Avg. %: 114	Avg. %: 114
266	267	268	269	270
				
Avg. %: 114	Avg. %: 114	Avg. %: 114	Avg. %: 114	Avg. %: 114

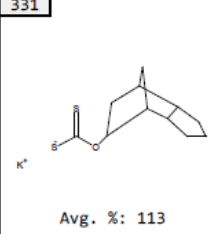
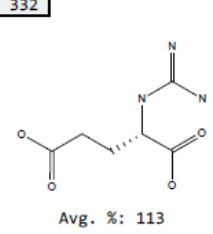
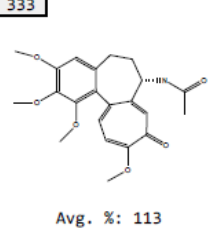
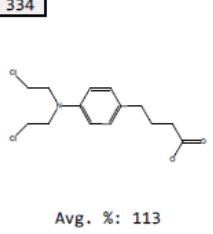
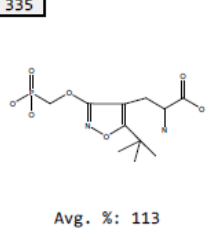
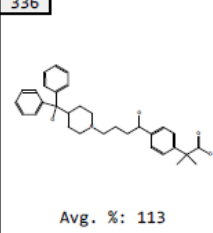
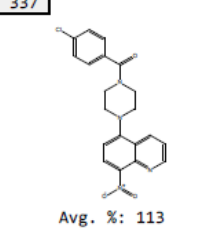
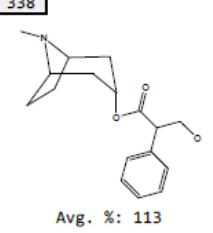
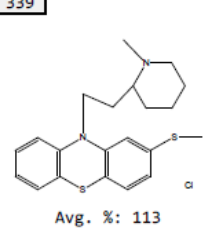
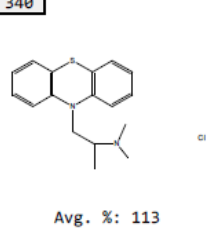
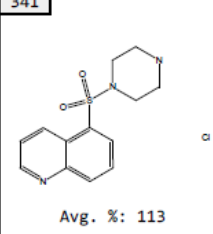
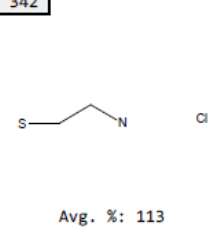
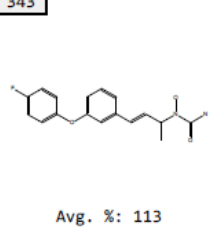
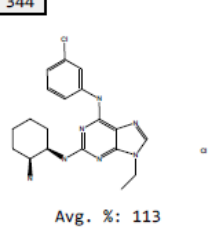
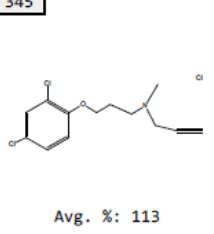
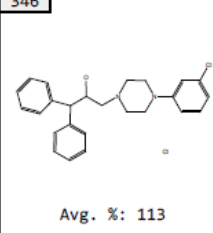
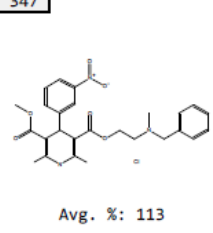
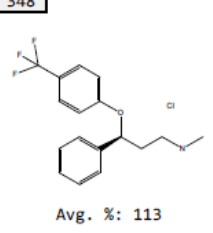
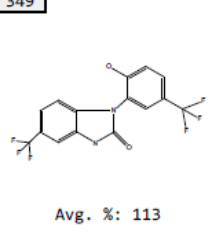
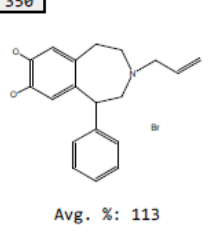
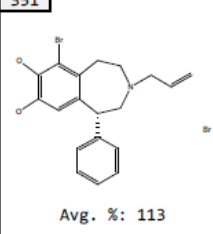
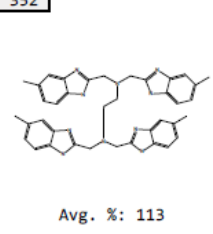
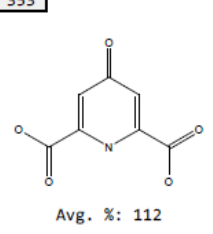
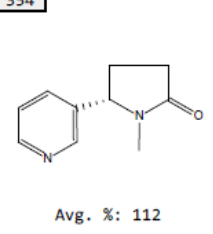
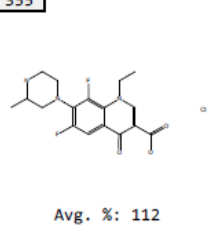
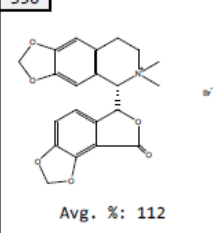
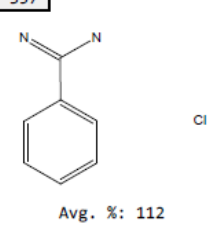
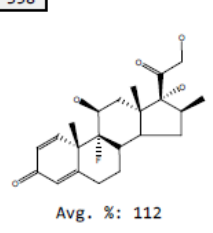
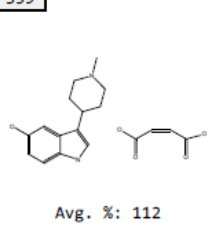
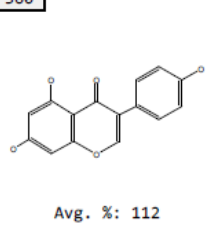
Continued, Table 21. Results of fluorescence-based electrophile screen of the LOPAC library. Values are presented as a percent of the MSTI signal (Avg. %). (n=3)

271	272	273	274	275
				
Avg. %: 114	Avg. %: 114	Avg. %: 114	Avg. %: 114	Avg. %: 114
276	277	278	279	280
				
Avg. %: 114	Avg. %: 114	Avg. %: 114	Avg. %: 114	Avg. %: 114
281	282	283	284	285
				
Avg. %: 114	Avg. %: 114	Avg. %: 114	Avg. %: 114	Avg. %: 114
286	287	288	289	290
				
Avg. %: 114	Avg. %: 114	Avg. %: 114	Avg. %: 114	Avg. %: 114
291	292	293	294	295
				
Avg. %: 114	Avg. %: 113	Avg. %: 113	Avg. %: 113	Avg. %: 113
296	297	298	299	300
				
Avg. %: 113	Avg. %: 113	Avg. %: 113	Avg. %: 113	Avg. %: 113

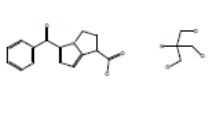
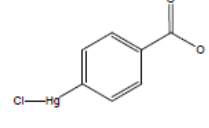
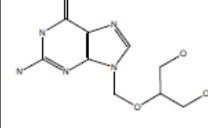
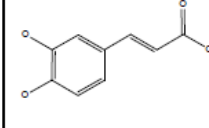
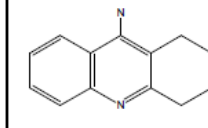
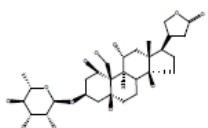
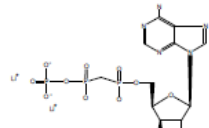
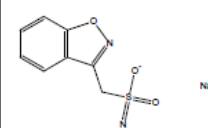
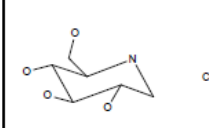
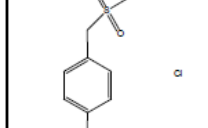
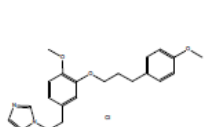
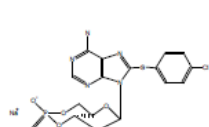
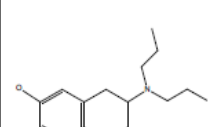
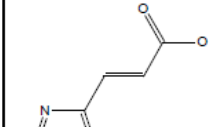
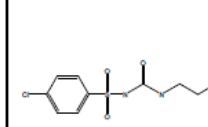
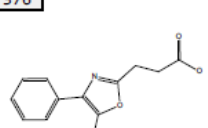
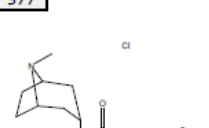
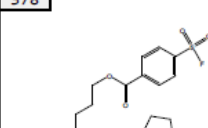
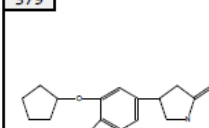
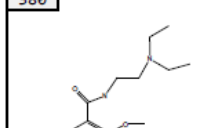
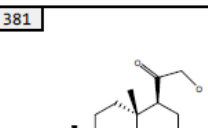
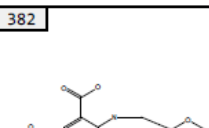
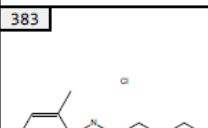
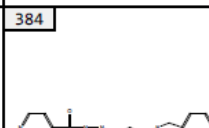
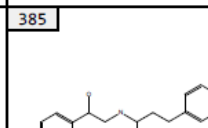
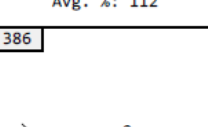
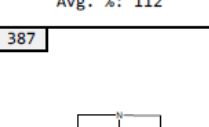
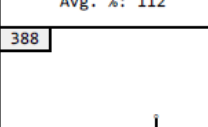
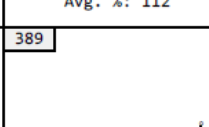
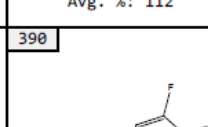
Continued, Table 21. Results of fluorescence-based electrophile screen of the LOPAC library. Values are presented as a percent of the MSTI signal (Avg. %). (n=3)

<p>301</p>  <p>Avg. %: 113</p>	<p>302</p>  <p>Avg. %: 113</p>	<p>303</p>  <p>Avg. %: 113</p>	<p>304</p>  <p>Avg. %: 113</p>	<p>305</p>  <p>Avg. %: 113</p>
<p>306</p>  <p>Avg. %: 113</p>	<p>307</p>  <p>Avg. %: 113</p>	<p>308</p>  <p>Avg. %: 113</p>	<p>309</p>  <p>Avg. %: 113</p>	<p>310</p>  <p>Avg. %: 113</p>
<p>311</p>  <p>Avg. %: 113</p>	<p>312</p>  <p>Avg. %: 113</p>	<p>313</p>  <p>Avg. %: 113</p>	<p>314</p>  <p>Avg. %: 113</p>	<p>315</p>  <p>Avg. %: 113</p>
<p>316</p>  <p>Avg. %: 113</p>	<p>317</p>  <p>Avg. %: 113</p>	<p>318</p>  <p>Avg. %: 113</p>	<p>319</p>  <p>Avg. %: 113</p>	<p>320</p>  <p>Avg. %: 113</p>
<p>321</p>  <p>Avg. %: 113</p>	<p>322</p>  <p>Avg. %: 113</p>	<p>323</p>  <p>Avg. %: 113</p>	<p>324</p>  <p>Avg. %: 113</p>	<p>325</p>  <p>Avg. %: 113</p>
<p>326</p>  <p>Avg. %: 113</p>	<p>327</p>  <p>Avg. %: 113</p>	<p>328</p>  <p>Avg. %: 113</p>	<p>329</p>  <p>Avg. %: 113</p>	<p>330</p>  <p>Avg. %: 113</p>

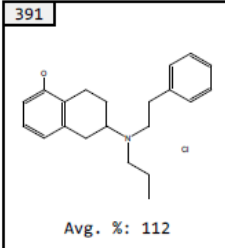
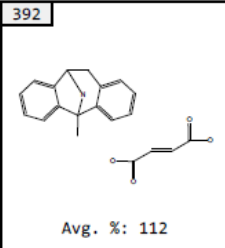
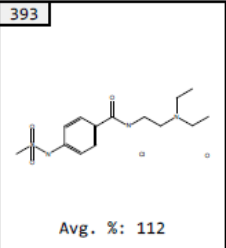
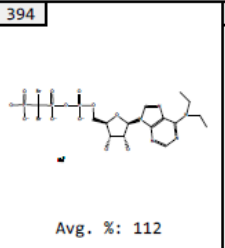
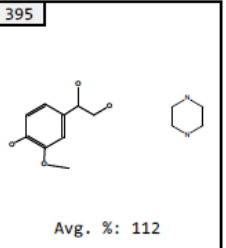
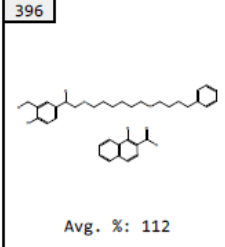
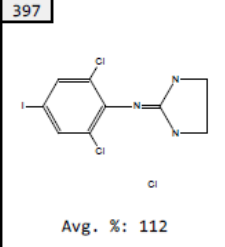
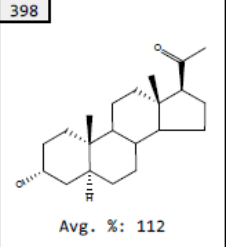
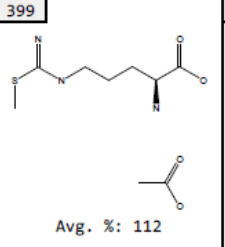
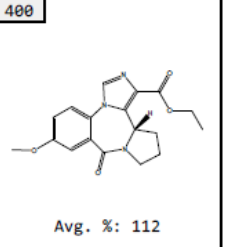
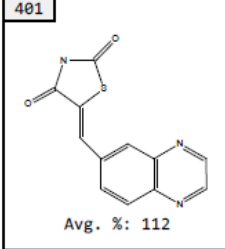
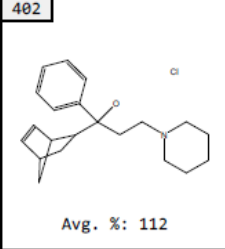
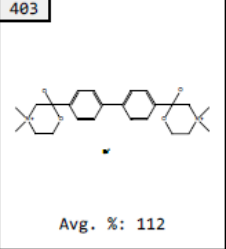
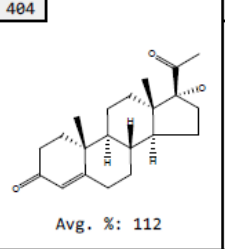
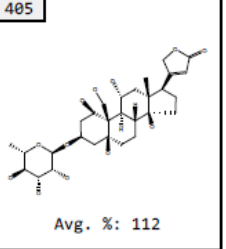
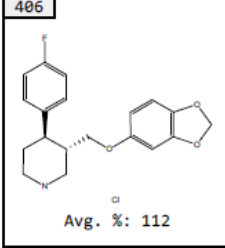
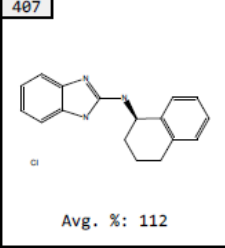
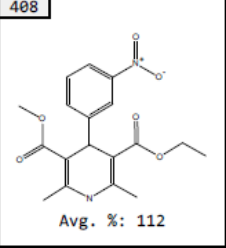
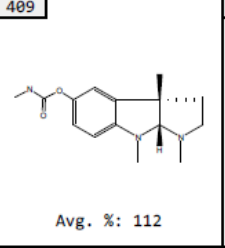
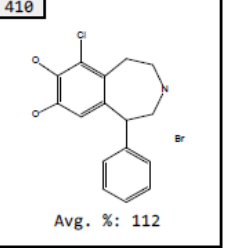
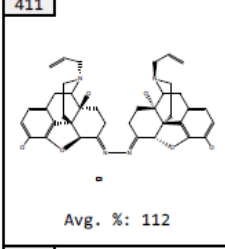
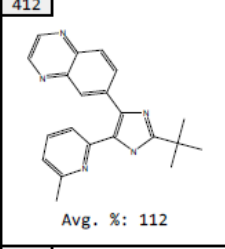
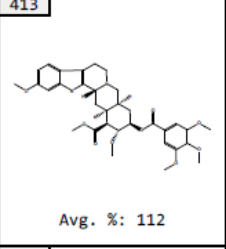
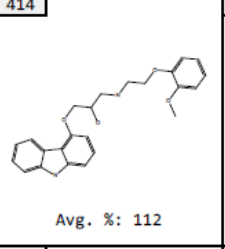
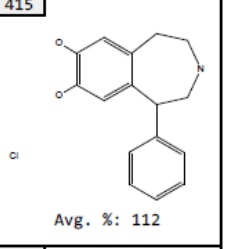
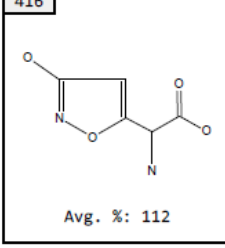
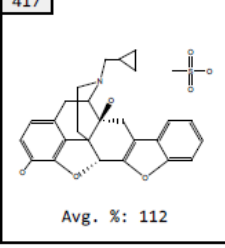
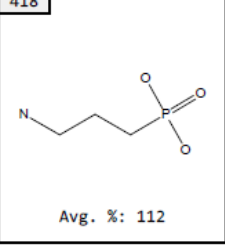
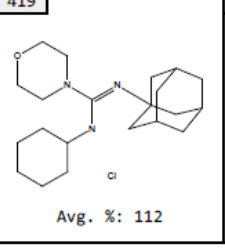
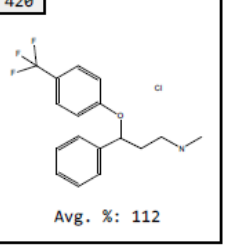
Continued, Table 21. Results of fluorescence-based electrophile screen of the LOPAC library. Values are presented as a percent of the MSTI signal (Avg. %). (n=3)

<p>331</p>  <p>Avg. %: 113</p>	<p>332</p>  <p>Avg. %: 113</p>	<p>333</p>  <p>Avg. %: 113</p>	<p>334</p>  <p>Avg. %: 113</p>	<p>335</p>  <p>Avg. %: 113</p>
<p>336</p>  <p>Avg. %: 113</p>	<p>337</p>  <p>Avg. %: 113</p>	<p>338</p>  <p>Avg. %: 113</p>	<p>339</p>  <p>Avg. %: 113</p>	<p>340</p>  <p>Avg. %: 113</p>
<p>341</p>  <p>Avg. %: 113</p>	<p>342</p>  <p>Avg. %: 113</p>	<p>343</p>  <p>Avg. %: 113</p>	<p>344</p>  <p>Avg. %: 113</p>	<p>345</p>  <p>Avg. %: 113</p>
<p>346</p>  <p>Avg. %: 113</p>	<p>347</p>  <p>Avg. %: 113</p>	<p>348</p>  <p>Avg. %: 113</p>	<p>349</p>  <p>Avg. %: 113</p>	<p>350</p>  <p>Avg. %: 113</p>
<p>351</p>  <p>Avg. %: 113</p>	<p>352</p>  <p>Avg. %: 113</p>	<p>353</p>  <p>Avg. %: 112</p>	<p>354</p>  <p>Avg. %: 112</p>	<p>355</p>  <p>Avg. %: 112</p>
<p>356</p>  <p>Avg. %: 112</p>	<p>357</p>  <p>Avg. %: 112</p>	<p>358</p>  <p>Avg. %: 112</p>	<p>359</p>  <p>Avg. %: 112</p>	<p>360</p>  <p>Avg. %: 112</p>

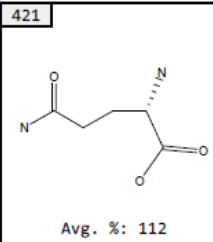
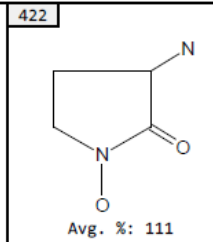
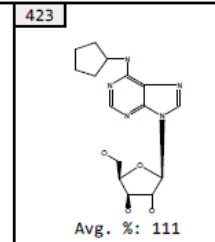
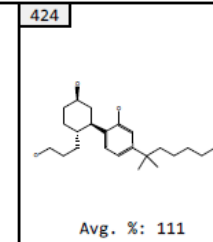
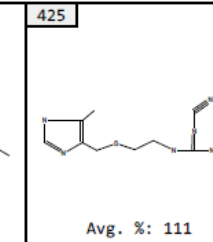
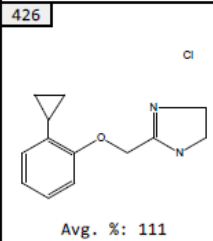
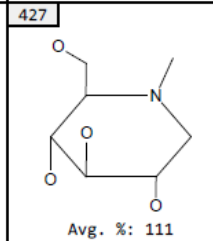
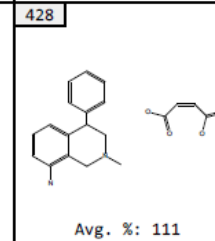
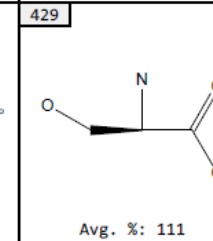
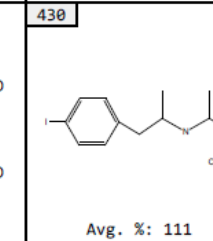
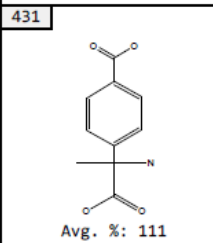
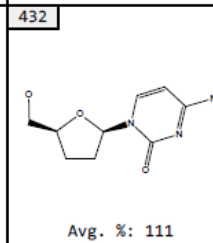
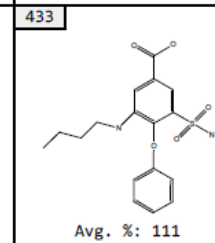
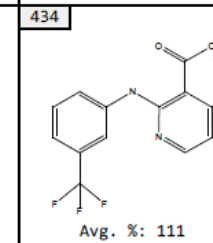
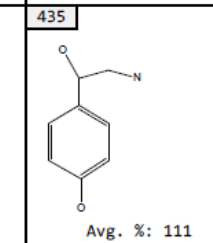
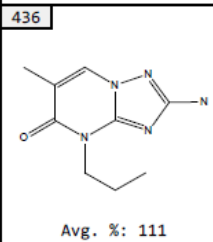
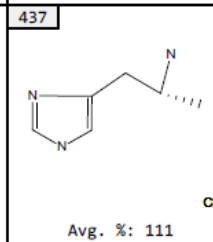
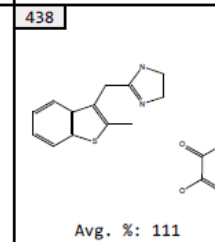
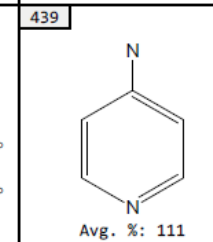
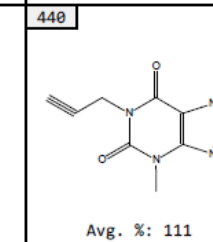
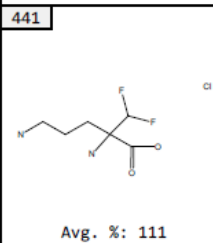
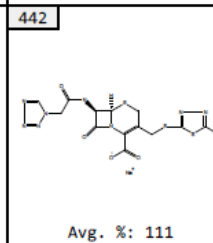
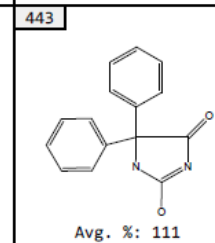
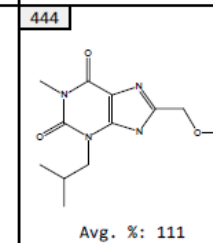
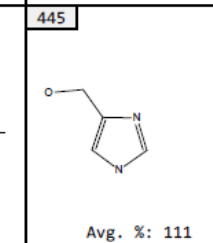
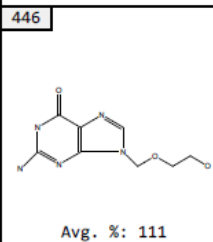
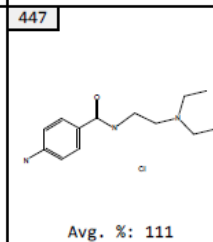
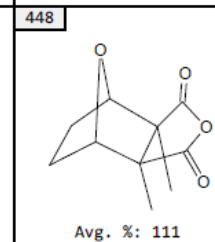
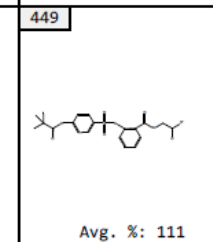
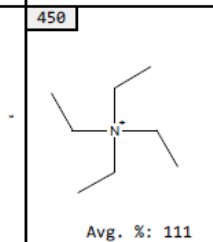
Continued, Table 21. Results of fluorescence-based electrophile screen of the LOPAC library. Values are presented as a percent of the MSTI signal (Avg. %). (n=3)

<p>361</p>  <p>Avg. %: 112</p>	<p>362</p>  <p>Avg. %: 112</p>	<p>363</p>  <p>Avg. %: 112</p>	<p>364</p>  <p>Avg. %: 112</p>	<p>365</p>  <p>Avg. %: 112</p>
<p>366</p>  <p>Avg. %: 112</p>	<p>367</p>  <p>Avg. %: 112</p>	<p>368</p>  <p>Avg. %: 112</p>	<p>369</p>  <p>Avg. %: 112</p>	<p>370</p>  <p>Avg. %: 112</p>
<p>371</p>  <p>Avg. %: 112</p>	<p>372</p>  <p>Avg. %: 112</p>	<p>373</p>  <p>Avg. %: 112</p>	<p>374</p>  <p>Avg. %: 112</p>	<p>375</p>  <p>Avg. %: 112</p>
<p>376</p>  <p>Avg. %: 112</p>	<p>377</p>  <p>Avg. %: 112</p>	<p>378</p>  <p>Avg. %: 112</p>	<p>379</p>  <p>Avg. %: 112</p>	<p>380</p>  <p>Avg. %: 112</p>
<p>381</p>  <p>Avg. %: 112</p>	<p>382</p>  <p>Avg. %: 112</p>	<p>383</p>  <p>Avg. %: 112</p>	<p>384</p>  <p>Avg. %: 112</p>	<p>385</p>  <p>Avg. %: 112</p>
<p>386</p>  <p>Avg. %: 112</p>	<p>387</p>  <p>Avg. %: 112</p>	<p>388</p>  <p>Avg. %: 112</p>	<p>389</p>  <p>Avg. %: 112</p>	<p>390</p>  <p>Avg. %: 112</p>

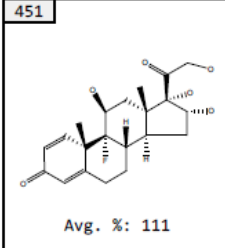
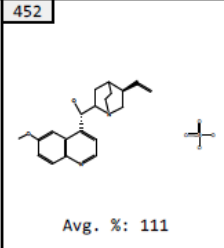
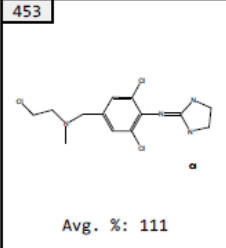
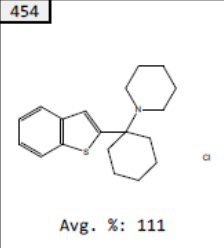
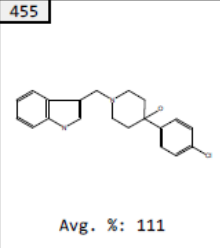
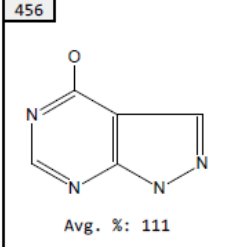
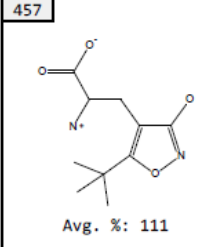
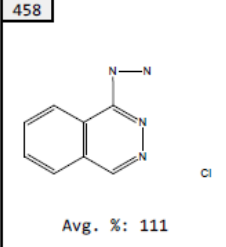
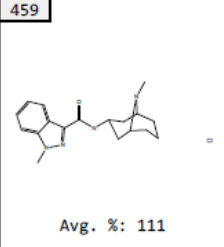
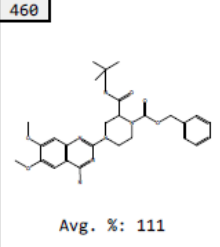
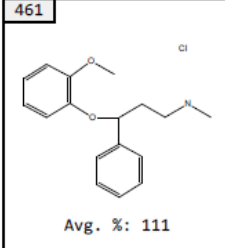
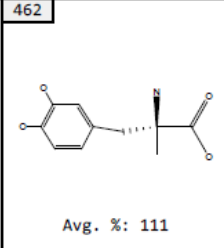
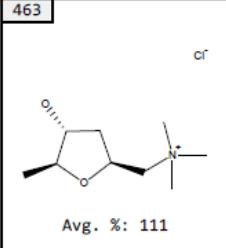
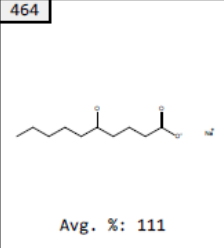
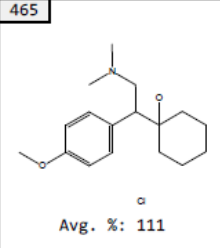
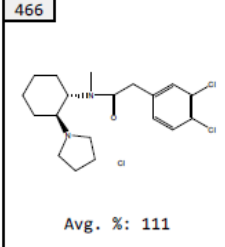
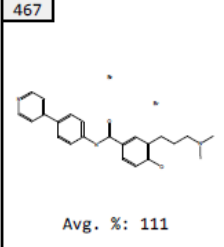
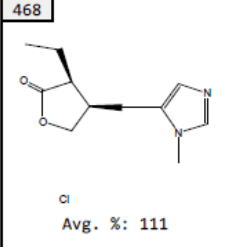
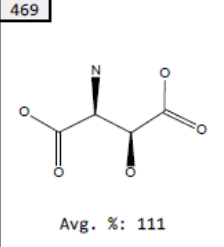
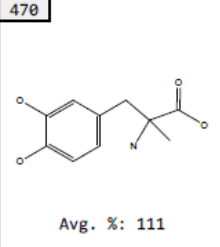
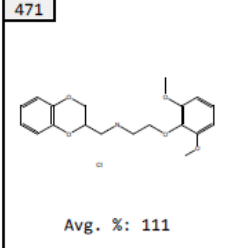
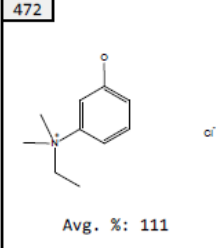
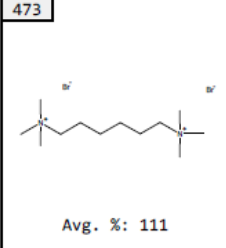
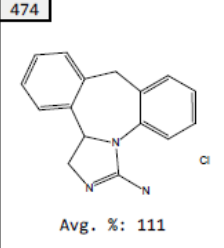
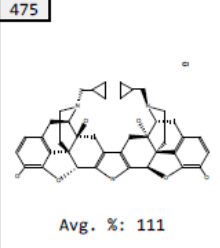
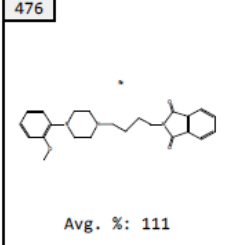
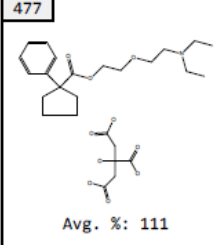
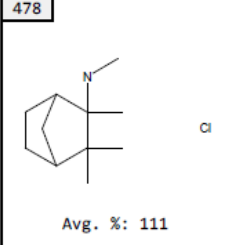
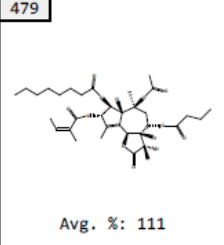
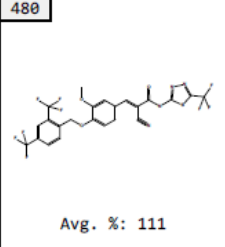
Continued, Table 21. Results of fluorescence-based electrophile screen of the LOPAC library. Values are presented as a percent of the MSTI signal (Avg. %). (n=3)

 <p>Avg. %: 112</p>	 <p>Avg. %: 112</p>	 <p>Avg. %: 112</p>	 <p>Avg. %: 112</p>	 <p>Avg. %: 112</p>
 <p>Avg. %: 112</p>	 <p>Avg. %: 112</p>	 <p>Avg. %: 112</p>	 <p>Avg. %: 112</p>	 <p>Avg. %: 112</p>
 <p>Avg. %: 112</p>	 <p>Avg. %: 112</p>	 <p>Avg. %: 112</p>	 <p>Avg. %: 112</p>	 <p>Avg. %: 112</p>
 <p>Avg. %: 112</p>	 <p>Avg. %: 112</p>	 <p>Avg. %: 112</p>	 <p>Avg. %: 112</p>	 <p>Avg. %: 112</p>
 <p>Avg. %: 112</p>	 <p>Avg. %: 112</p>	 <p>Avg. %: 112</p>	 <p>Avg. %: 112</p>	 <p>Avg. %: 112</p>
 <p>Avg. %: 112</p>	 <p>Avg. %: 112</p>	 <p>Avg. %: 112</p>	 <p>Avg. %: 112</p>	 <p>Avg. %: 112</p>

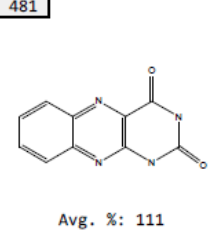
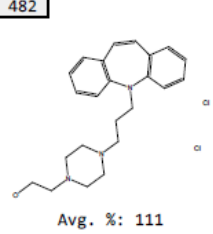
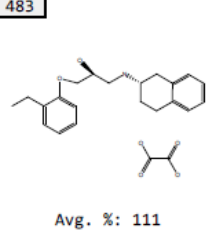
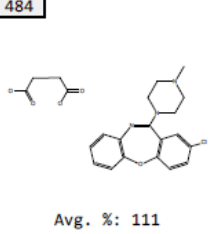
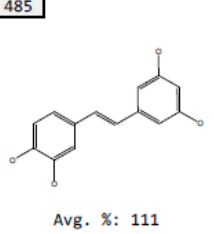
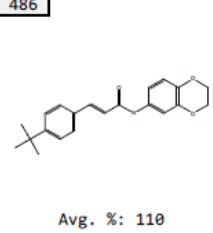
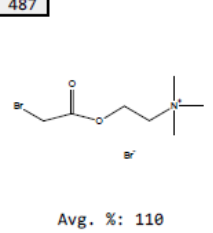
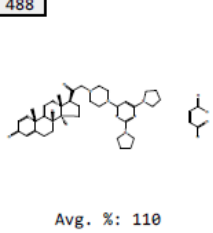
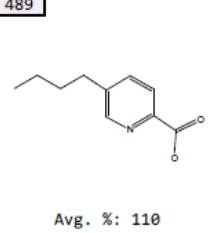
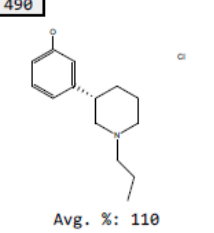
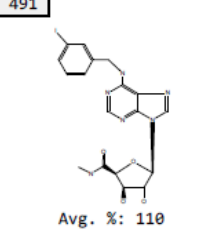
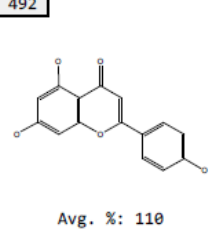
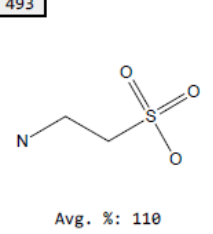
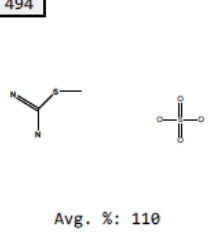
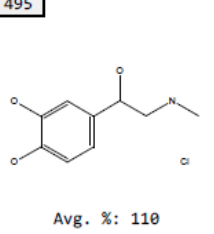
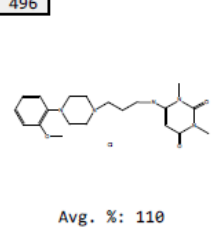
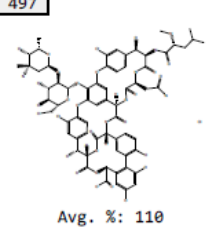
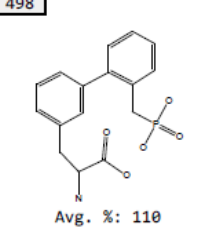
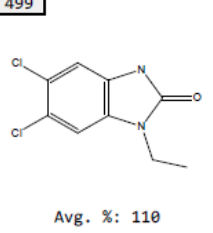
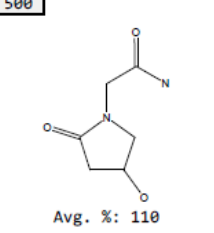
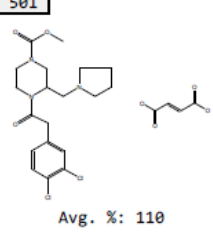
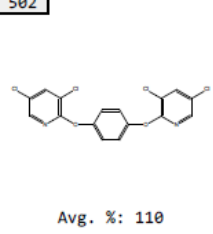
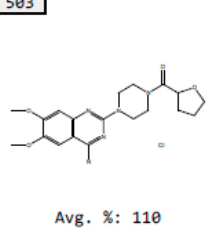
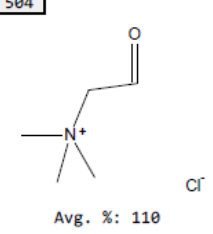
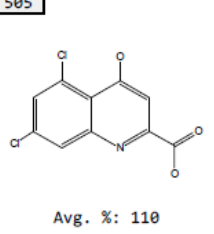
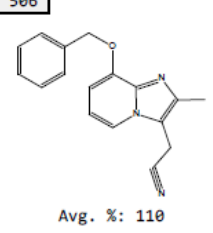
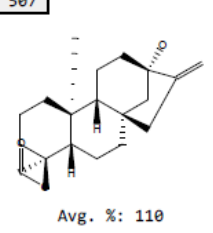
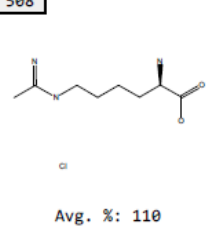
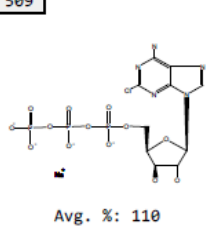
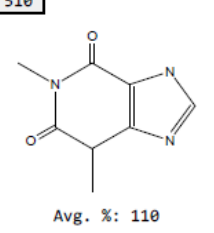
Continued, Table 21. Results of fluorescence-based electrophile screen of the LOPAC library. Values are presented as a percent of the MSTI signal (Avg. %). (n=3)

421	422	423	424	425
				
Avg. %: 112	Avg. %: 111	Avg. %: 111	Avg. %: 111	Avg. %: 111
426	427	428	429	430
				
Avg. %: 111	Avg. %: 111	Avg. %: 111	Avg. %: 111	Avg. %: 111
431	432	433	434	435
				
Avg. %: 111	Avg. %: 111	Avg. %: 111	Avg. %: 111	Avg. %: 111
436	437	438	439	440
				
Avg. %: 111	Avg. %: 111	Avg. %: 111	Avg. %: 111	Avg. %: 111
441	442	443	444	445
				
Avg. %: 111	Avg. %: 111	Avg. %: 111	Avg. %: 111	Avg. %: 111
446	447	448	449	450
				
Avg. %: 111	Avg. %: 111	Avg. %: 111	Avg. %: 111	Avg. %: 111

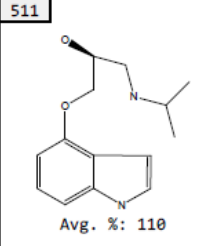
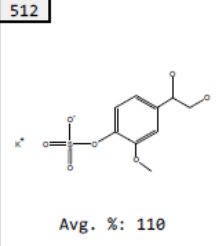
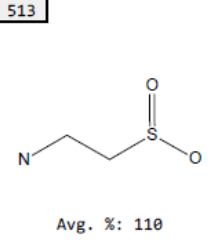
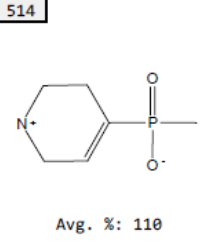
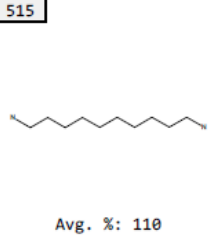
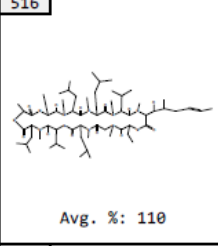
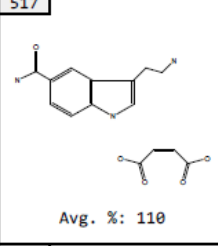
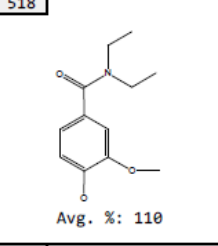
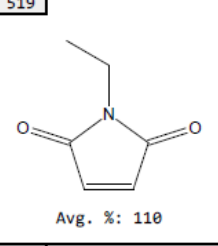
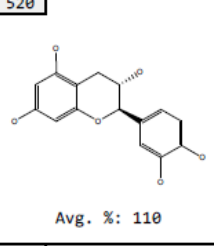
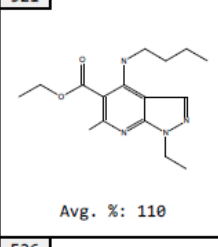
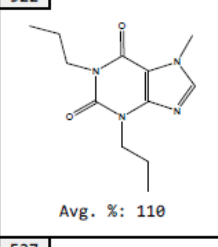
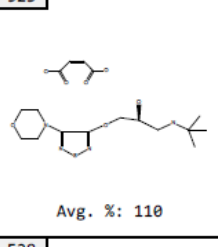
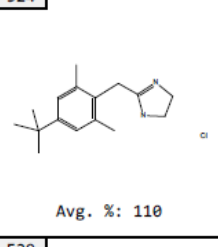
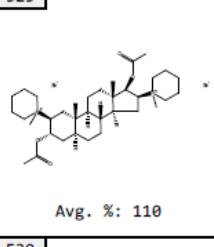
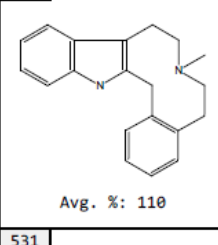
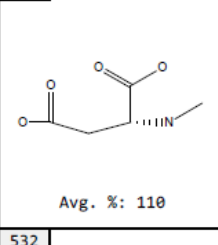
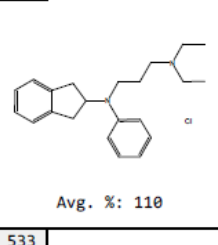
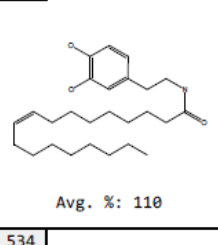
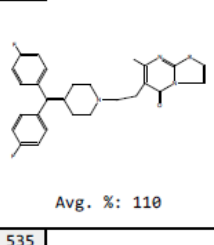
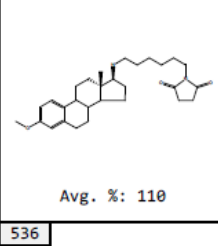
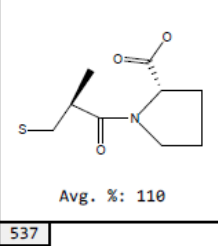
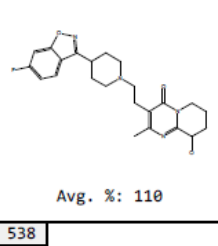
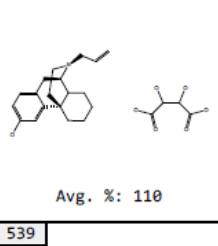
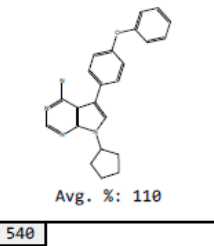
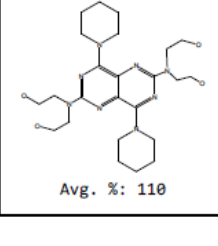
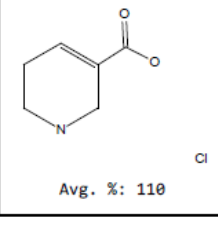
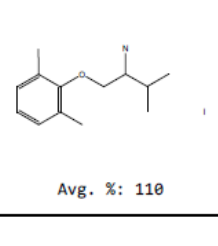
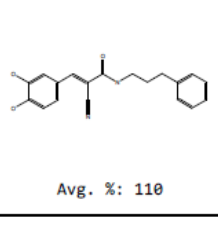
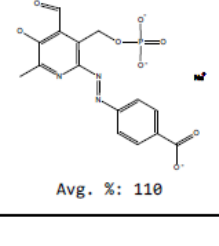
Continued, Table 21. Results of fluorescence-based electrophile screen of the LOPAC library. Values are presented as a percent of the MSTI signal (Avg. %). (n=3)

451	452	453	454	455
				
Avg. %: 111	Avg. %: 111	Avg. %: 111	Avg. %: 111	Avg. %: 111
456	457	458	459	460
				
Avg. %: 111	Avg. %: 111	Avg. %: 111	Avg. %: 111	Avg. %: 111
461	462	463	464	465
				
Avg. %: 111	Avg. %: 111	Avg. %: 111	Avg. %: 111	Avg. %: 111
466	467	468	469	470
				
Avg. %: 111	Avg. %: 111	Avg. %: 111	Avg. %: 111	Avg. %: 111
471	472	473	474	475
				
Avg. %: 111	Avg. %: 111	Avg. %: 111	Avg. %: 111	Avg. %: 111
476	477	478	479	480
				
Avg. %: 111	Avg. %: 111	Avg. %: 111	Avg. %: 111	Avg. %: 111

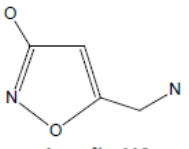
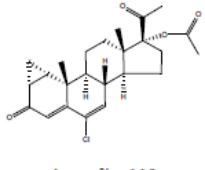
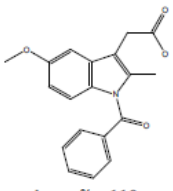
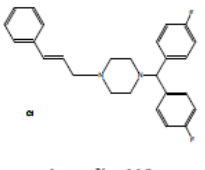
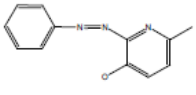
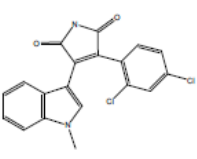
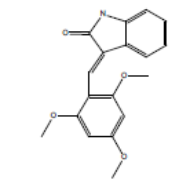
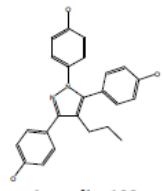
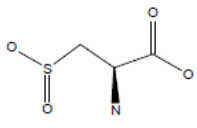
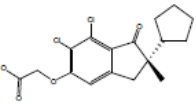
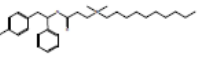
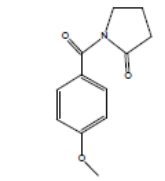
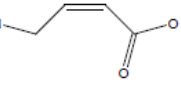
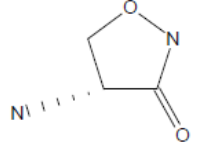
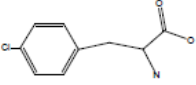
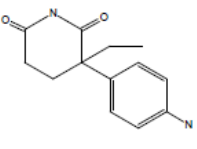
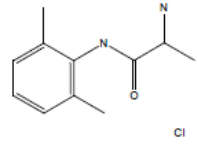
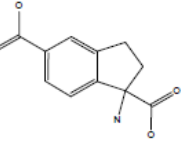
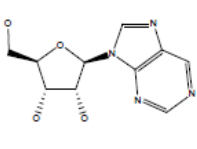
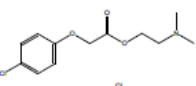
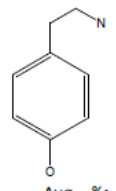
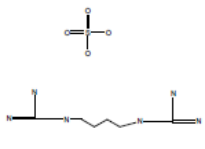
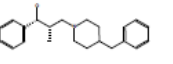
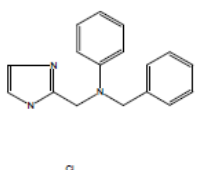
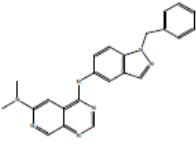
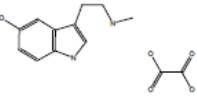
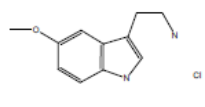
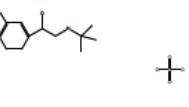
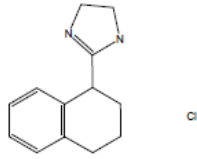
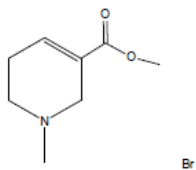
Continued, Table 21. Results of fluorescence-based electrophile screen of the LOPAC library. Values are presented as a percent of the MSTI signal (Avg. %). (n=3)

481	482	483	484	485
				
Avg. %: 111	Avg. %: 111	Avg. %: 111	Avg. %: 111	Avg. %: 111
486	487	488	489	490
				
Avg. %: 110	Avg. %: 110	Avg. %: 110	Avg. %: 110	Avg. %: 110
491	492	493	494	495
				
Avg. %: 110	Avg. %: 110	Avg. %: 110	Avg. %: 110	Avg. %: 110
496	497	498	499	500
				
Avg. %: 110	Avg. %: 110	Avg. %: 110	Avg. %: 110	Avg. %: 110
501	502	503	504	505
				
Avg. %: 110	Avg. %: 110	Avg. %: 110	Avg. %: 110	Avg. %: 110
506	507	508	509	510
				
Avg. %: 110	Avg. %: 110	Avg. %: 110	Avg. %: 110	Avg. %: 110

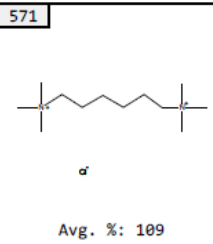
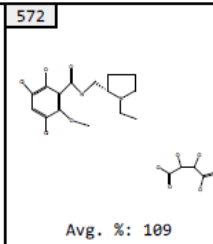
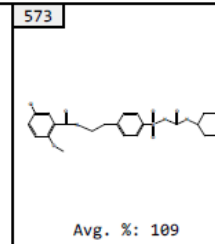
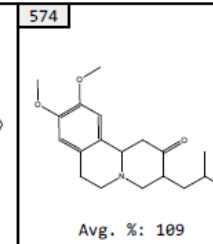
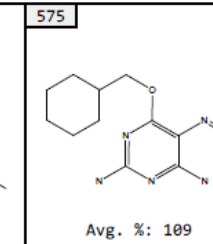
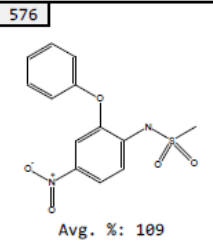
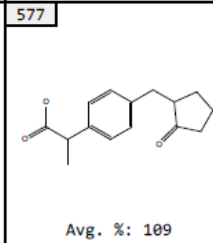
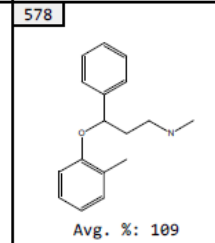
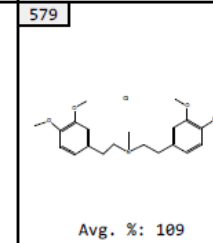
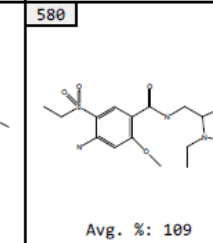
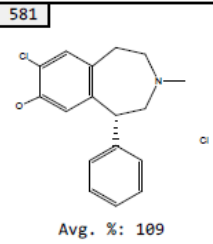
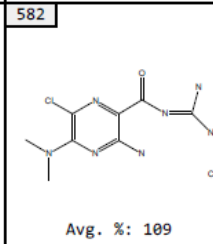
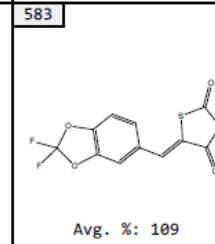
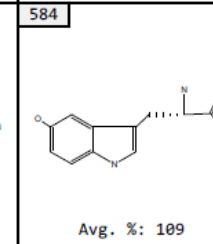
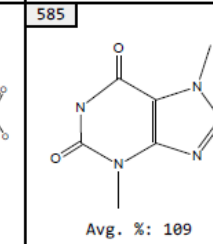
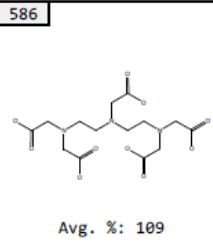
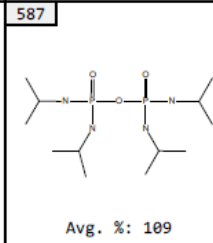
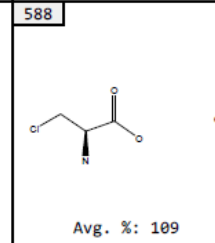
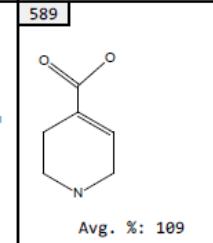
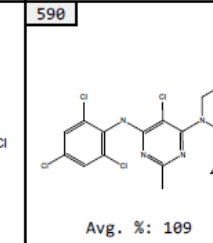
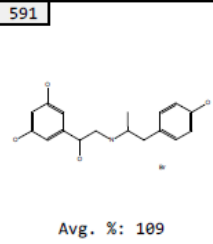
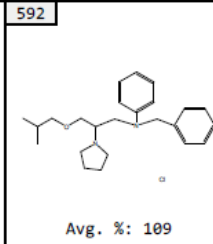
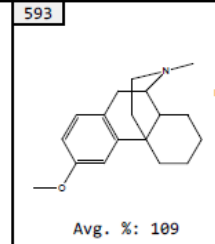
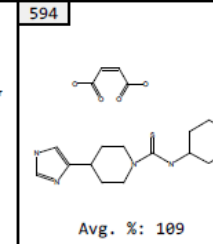
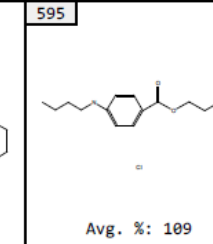
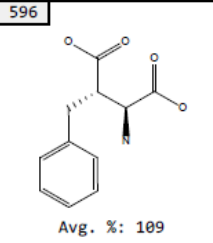
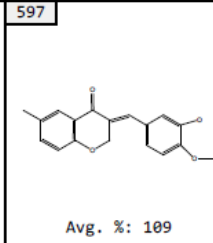
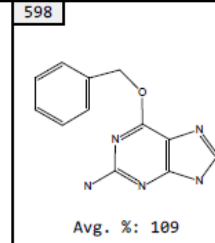
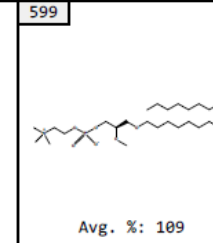
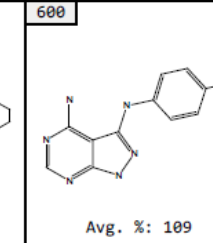
Continued, Table 21. Results of fluorescence-based electrophile screen of the LOPAC library. Values are presented as a percent of the MSTI signal (Avg. %). (n=3)

 <p>Avg. %: 110</p>	 <p>Avg. %: 110</p>	 <p>Avg. %: 110</p>	 <p>Avg. %: 110</p>	 <p>Avg. %: 110</p>
 <p>Avg. %: 110</p>	 <p>Avg. %: 110</p>	 <p>Avg. %: 110</p>	 <p>Avg. %: 110</p>	 <p>Avg. %: 110</p>
 <p>Avg. %: 110</p>	 <p>Avg. %: 110</p>	 <p>Avg. %: 110</p>	 <p>Avg. %: 110</p>	 <p>Avg. %: 110</p>
 <p>Avg. %: 110</p>	 <p>Avg. %: 110</p>	 <p>Avg. %: 110</p>	 <p>Avg. %: 110</p>	 <p>Avg. %: 110</p>
 <p>Avg. %: 110</p>	 <p>Avg. %: 110</p>	 <p>Avg. %: 110</p>	 <p>Avg. %: 110</p>	 <p>Avg. %: 110</p>
 <p>Avg. %: 110</p>	 <p>Avg. %: 110</p>	 <p>Avg. %: 110</p>	 <p>Avg. %: 110</p>	 <p>Avg. %: 110</p>

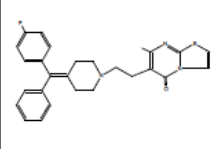
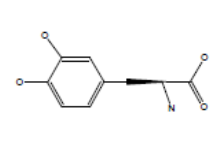
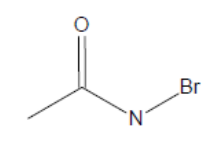
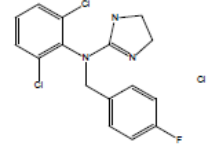
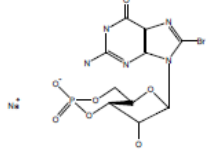
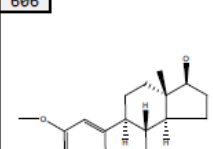
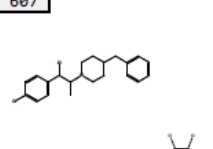
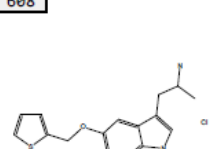
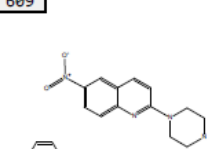
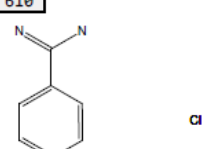
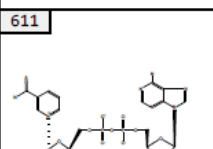
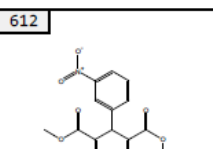
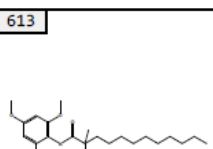
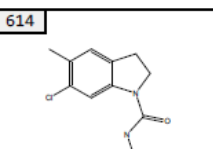
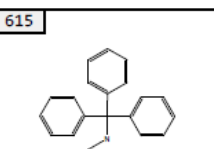
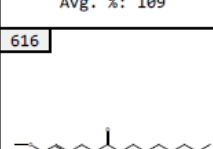
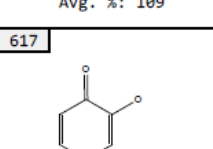
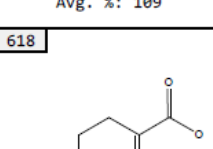
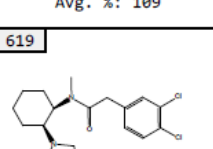
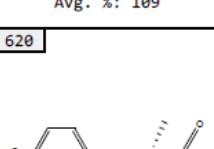
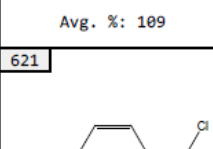
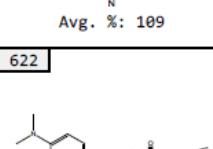
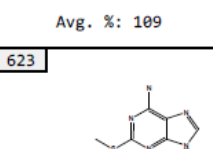
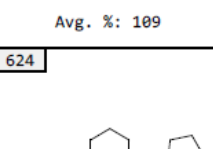
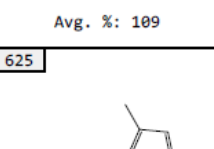
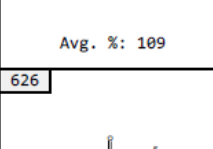
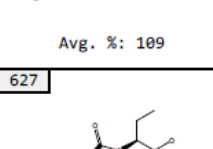
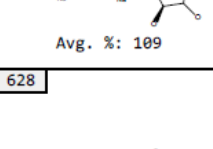
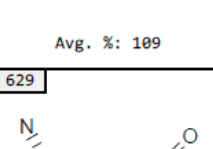
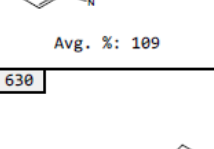
Continued, Table 21. Results of fluorescence-based electrophile screen of the LOPAC library. Values are presented as a percent of the MSTI signal (Avg. %). (n=3)

541  Avg. %: 110	542  Avg. %: 110	543  Avg. %: 110	544  Avg. %: 110	545  Avg. %: 110
546  Avg. %: 110	547  Avg. %: 109	548  Avg. %: 109	549  Avg. %: 109	550  Avg. %: 109
551  Avg. %: 109	552  Avg. %: 109	553  Avg. %: 109	554  Avg. %: 109	555  Avg. %: 109
556  Avg. %: 109	557  Avg. %: 109	558  Avg. %: 109	559  Avg. %: 109	560  Avg. %: 109
561  Avg. %: 109	562  Avg. %: 109	563  Avg. %: 109	564  Avg. %: 109	565  Avg. %: 109
566  Avg. %: 109	567  Avg. %: 109	568  Avg. %: 109	569  Avg. %: 109	570  Avg. %: 109

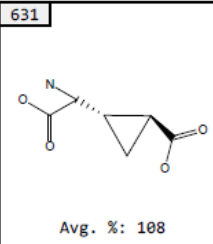
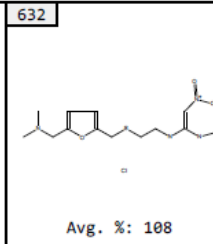
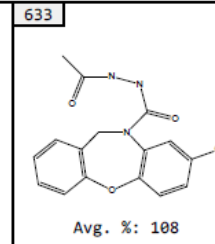
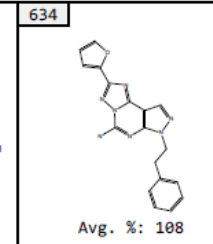
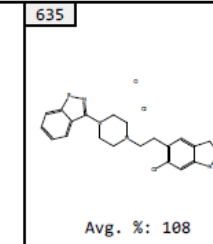
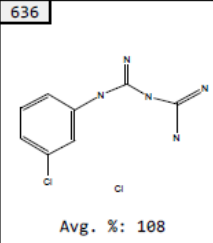
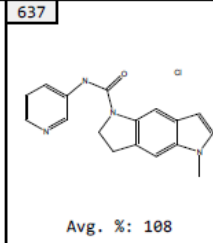
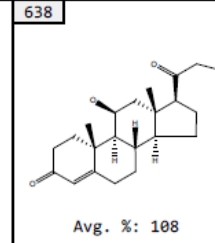
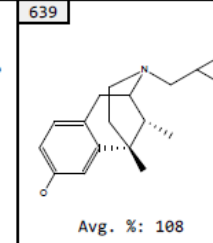
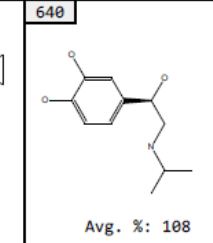
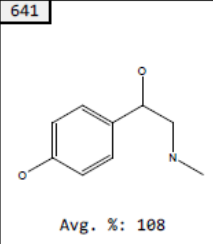
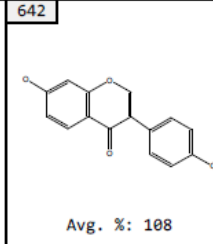
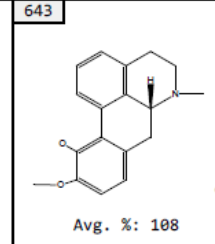
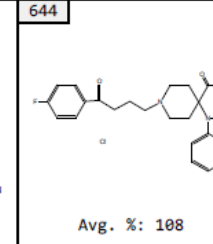
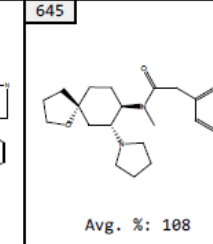
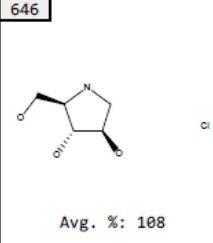
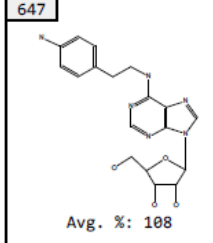
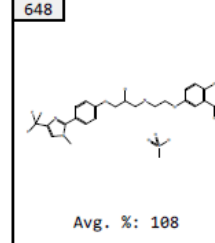
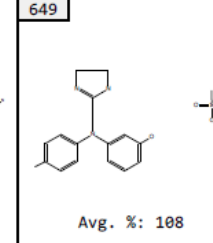
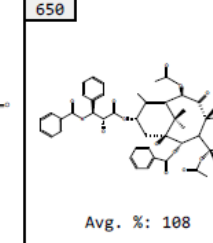
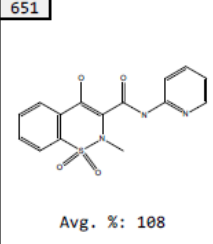
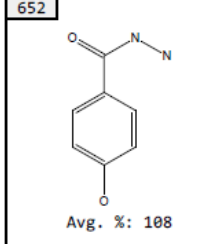
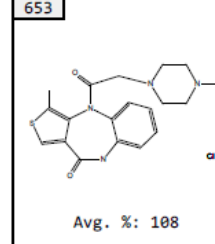
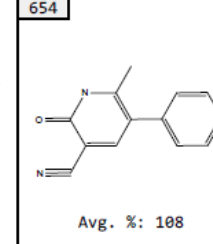
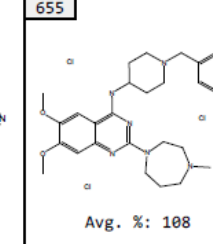
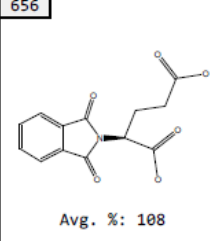
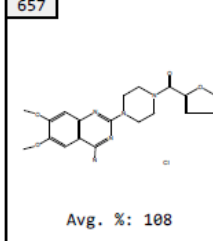
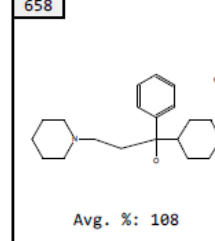
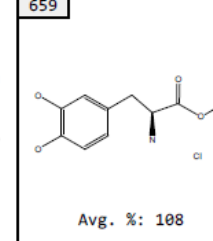
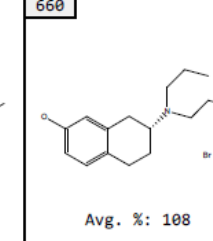
Continued, Table 21. Results of fluorescence-based electrophile screen of the LOPAC library. Values are presented as a percent of the MSTI signal (Avg. %). (n=3)

571	572	573	574	575
				
Avg. %: 109	Avg. %: 109	Avg. %: 109	Avg. %: 109	Avg. %: 109
576	577	578	579	580
				
Avg. %: 109	Avg. %: 109	Avg. %: 109	Avg. %: 109	Avg. %: 109
581	582	583	584	585
				
Avg. %: 109	Avg. %: 109	Avg. %: 109	Avg. %: 109	Avg. %: 109
586	587	588	589	590
				
Avg. %: 109	Avg. %: 109	Avg. %: 109	Avg. %: 109	Avg. %: 109
591	592	593	594	595
				
Avg. %: 109	Avg. %: 109	Avg. %: 109	Avg. %: 109	Avg. %: 109
596	597	598	599	600
				
Avg. %: 109	Avg. %: 109	Avg. %: 109	Avg. %: 109	Avg. %: 109

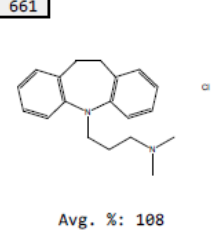
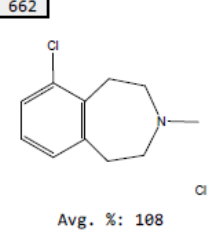
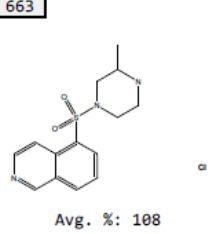
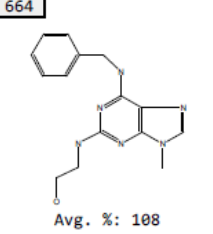
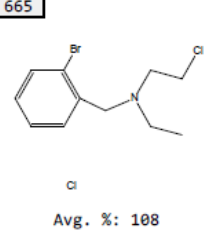
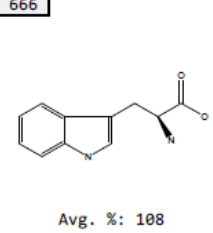
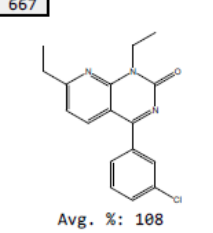
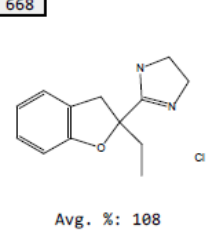
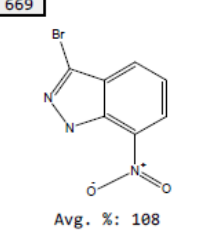
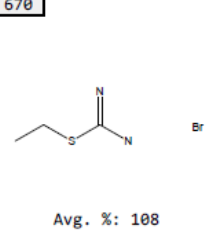
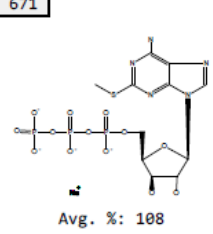
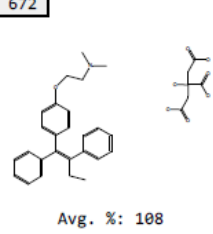
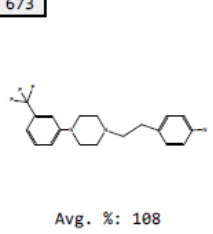
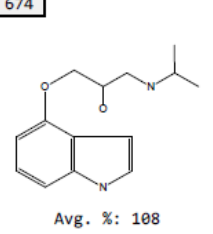
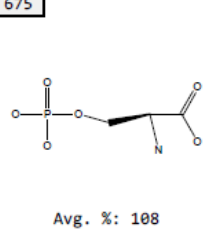
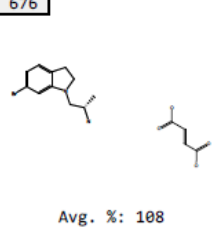
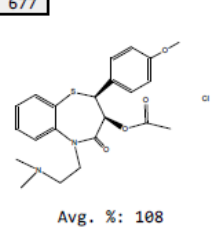
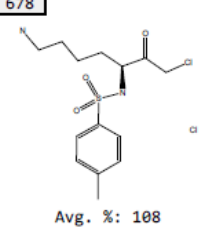
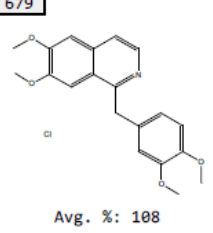
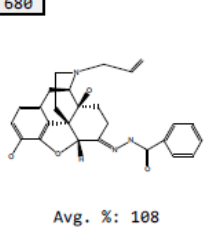
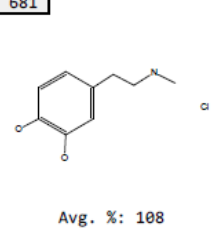
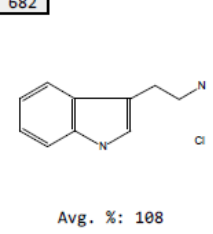
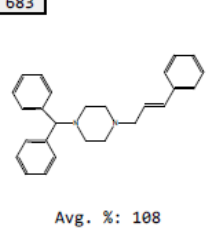
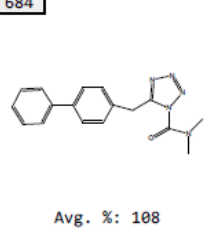
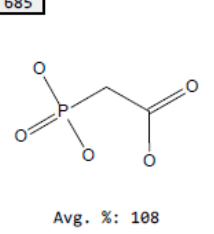
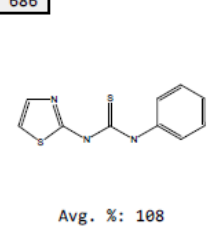
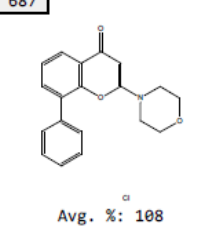
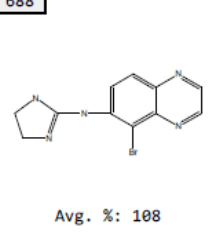
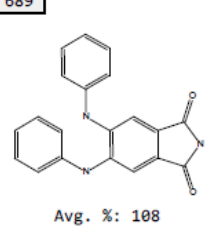
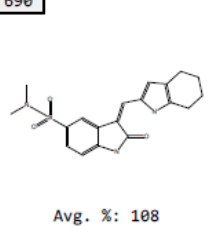
Continued, Table 21. Results of fluorescence-based electrophile screen of the LOPAC library. Values are presented as a percent of the MSTI signal (Avg. %). (n=3)

601	602	603	604	605
				
Avg. %: 109	Avg. %: 109	Avg. %: 109	Avg. %: 109	Avg. %: 109
606	607	608	609	610
				
Avg. %: 109	Avg. %: 109	Avg. %: 109	Avg. %: 109	Avg. %: 109
611	612	613	614	615
				
Avg. %: 109	Avg. %: 109	Avg. %: 109	Avg. %: 109	Avg. %: 109
616	617	618	619	620
				
Avg. %: 109	Avg. %: 109	Avg. %: 109	Avg. %: 109	Avg. %: 109
621	622	623	624	625
				
Avg. %: 109	Avg. %: 109	Avg. %: 109	Avg. %: 109	Avg. %: 109
626	627	628	629	630
				
Avg. %: 108	Avg. %: 108	Avg. %: 108	Avg. %: 108	Avg. %: 108

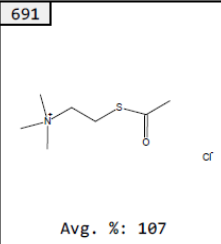
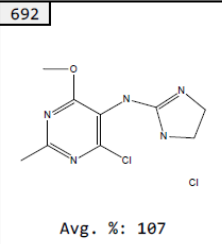
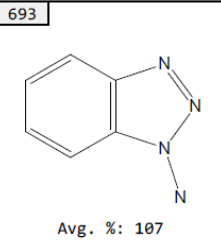
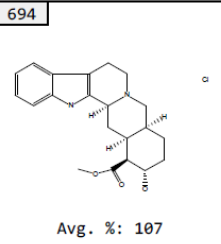
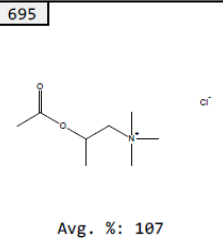
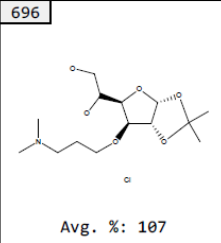
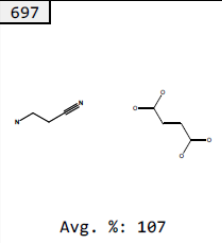
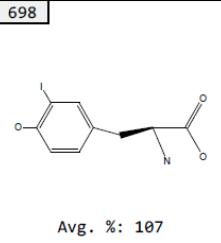
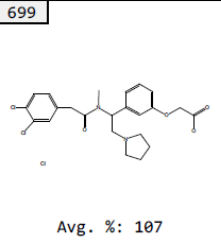
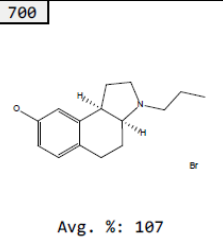
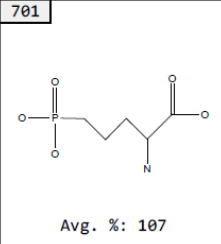
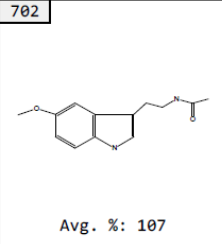
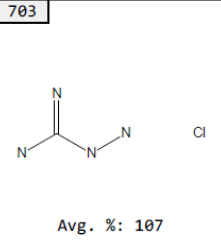
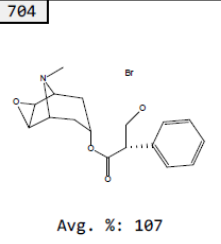
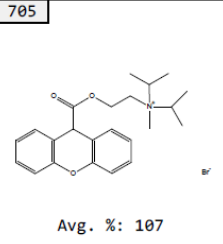
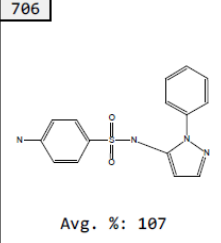
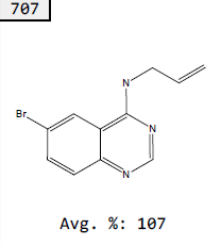
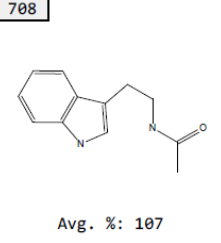
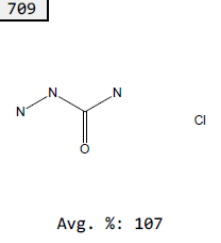
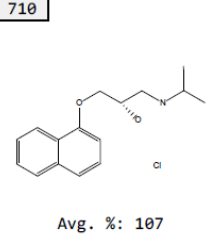
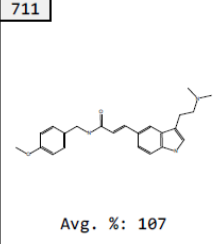
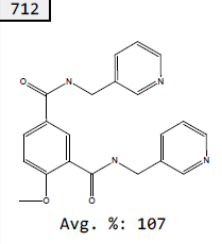
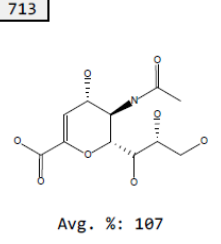
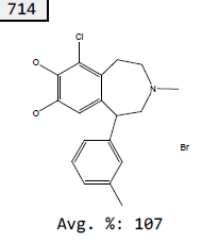
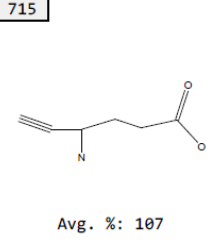
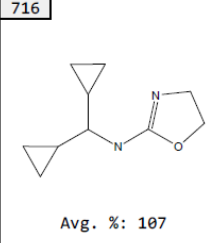
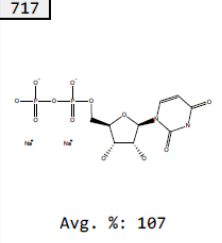
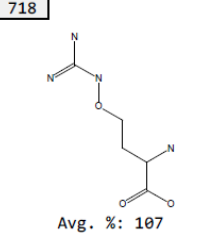
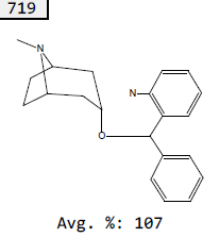
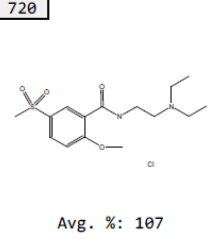
Continued, Table 21. Results of fluorescence-based electrophile screen of the LOPAC library. Values are presented as a percent of the MSTI signal (Avg. %). (n=3)

 <p>Avg. %: 108</p>	 <p>Avg. %: 108</p>	 <p>Avg. %: 108</p>	 <p>Avg. %: 108</p>	 <p>Avg. %: 108</p>
 <p>Avg. %: 108</p>	 <p>Avg. %: 108</p>	 <p>Avg. %: 108</p>	 <p>Avg. %: 108</p>	 <p>Avg. %: 108</p>
 <p>Avg. %: 108</p>	 <p>Avg. %: 108</p>	 <p>Avg. %: 108</p>	 <p>Avg. %: 108</p>	 <p>Avg. %: 108</p>
 <p>Avg. %: 108</p>	 <p>Avg. %: 108</p>	 <p>Avg. %: 108</p>	 <p>Avg. %: 108</p>	 <p>Avg. %: 108</p>
 <p>Avg. %: 108</p>	 <p>Avg. %: 108</p>	 <p>Avg. %: 108</p>	 <p>Avg. %: 108</p>	 <p>Avg. %: 108</p>
 <p>Avg. %: 108</p>	 <p>Avg. %: 108</p>	 <p>Avg. %: 108</p>	 <p>Avg. %: 108</p>	 <p>Avg. %: 108</p>

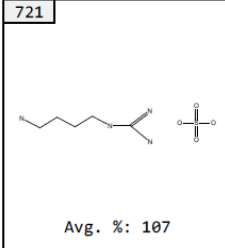
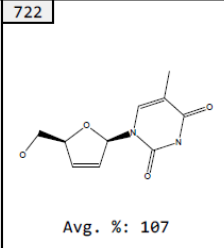
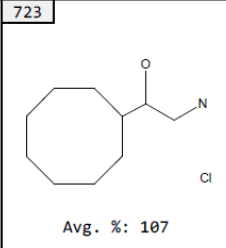
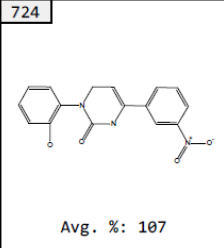
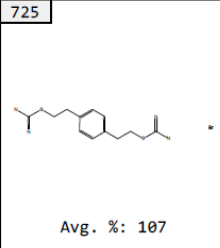
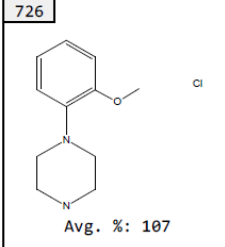
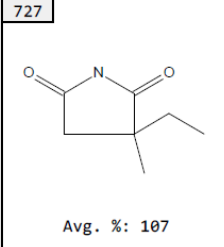
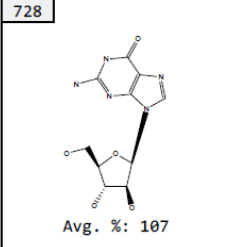
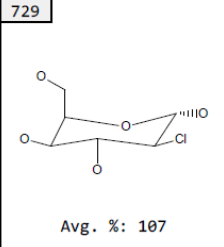
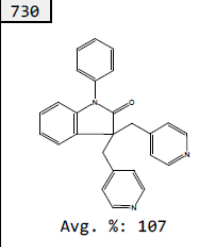
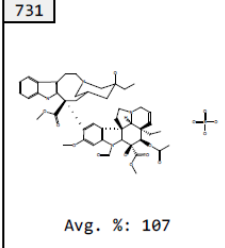
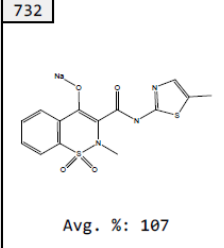
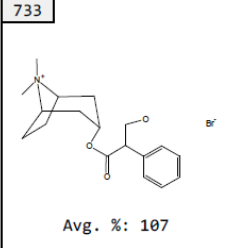
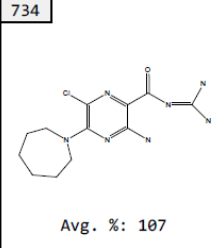
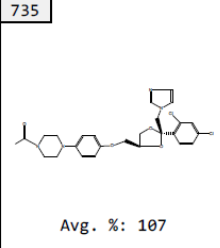
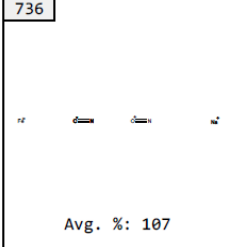
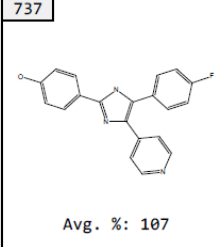
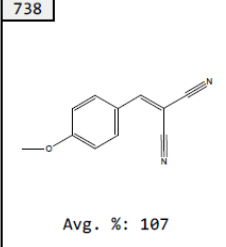
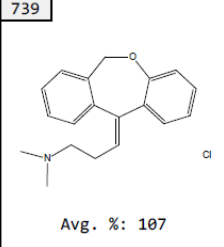
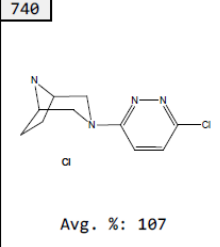
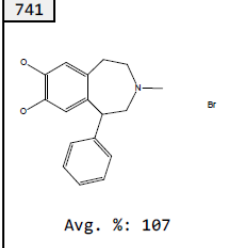
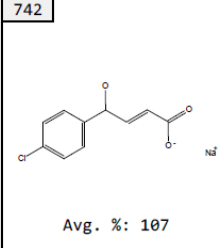
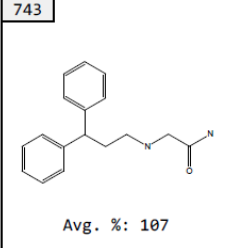
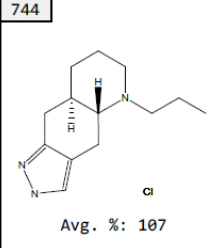
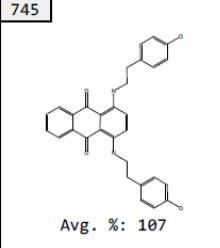
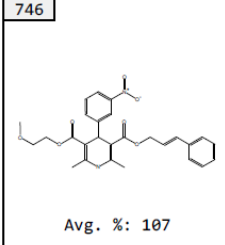
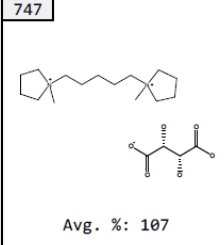
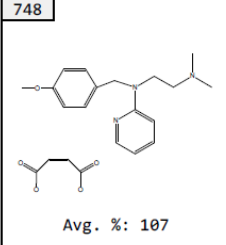
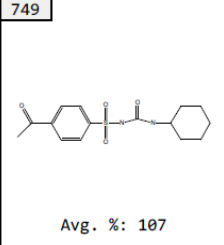
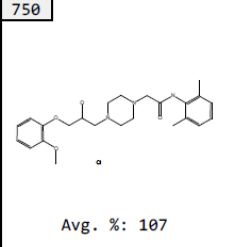
Continued, Table 21. Results of fluorescence-based electrophile screen of the LOPAC library. Values are presented as a percent of the MSTI signal (Avg. %). (n=3)

661	662	663	664	665
				
Avg. %: 108	Avg. %: 108	Avg. %: 108	Avg. %: 108	Avg. %: 108
666	667	668	669	670
				
Avg. %: 108	Avg. %: 108	Avg. %: 108	Avg. %: 108	Avg. %: 108
671	672	673	674	675
				
Avg. %: 108	Avg. %: 108	Avg. %: 108	Avg. %: 108	Avg. %: 108
676	677	678	679	680
				
Avg. %: 108	Avg. %: 108	Avg. %: 108	Avg. %: 108	Avg. %: 108
681	682	683	684	685
				
Avg. %: 108	Avg. %: 108	Avg. %: 108	Avg. %: 108	Avg. %: 108
686	687	688	689	690
				
Avg. %: 108	Avg. %: 108	Avg. %: 108	Avg. %: 108	Avg. %: 108

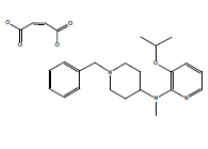
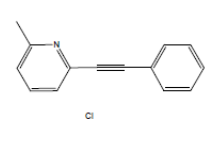
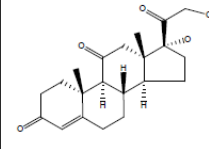
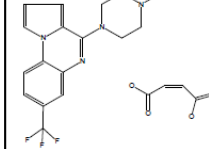
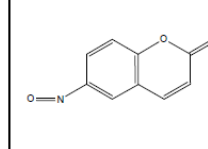
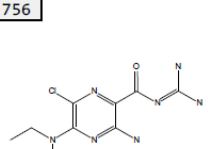
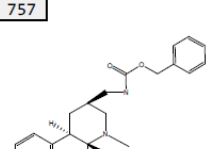
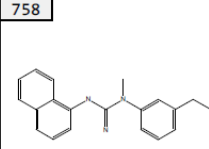
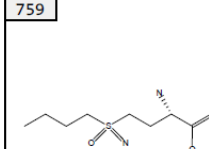
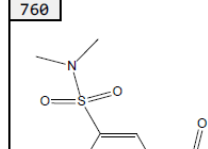
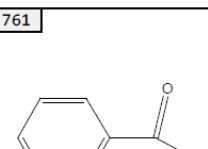
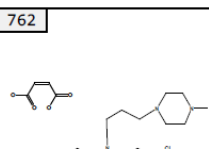
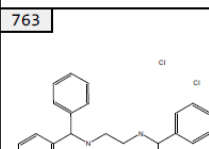
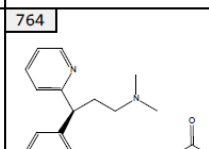
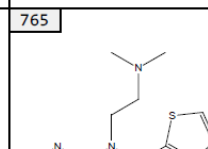
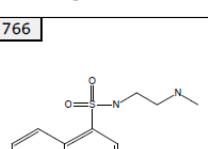
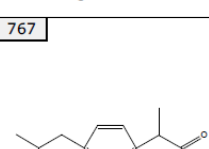
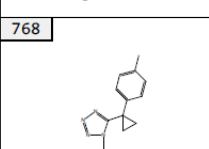
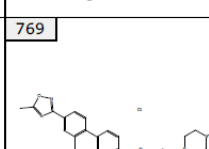
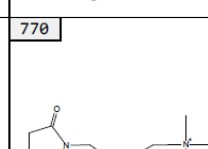
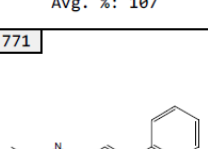
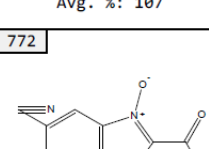
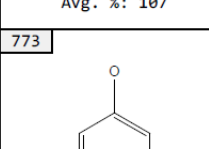
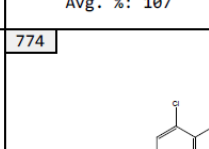
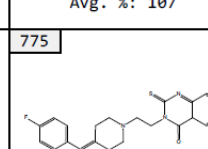
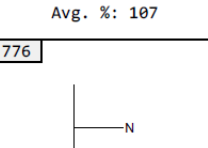
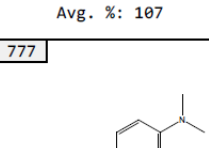
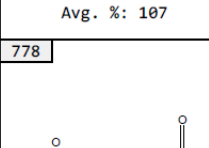
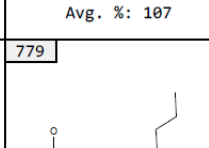
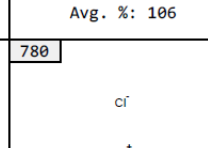
Continued, Table 21. Results of fluorescence-based electrophile screen of the LOPAC library. Values are presented as a percent of the MSTI signal (Avg. %). (n=3)

691	692	693	694	695
				
Avg. %: 107	Avg. %: 107	Avg. %: 107	Avg. %: 107	Avg. %: 107
696	697	698	699	700
				
Avg. %: 107	Avg. %: 107	Avg. %: 107	Avg. %: 107	Avg. %: 107
701	702	703	704	705
				
Avg. %: 107	Avg. %: 107	Avg. %: 107	Avg. %: 107	Avg. %: 107
706	707	708	709	710
				
Avg. %: 107	Avg. %: 107	Avg. %: 107	Avg. %: 107	Avg. %: 107
711	712	713	714	715
				
Avg. %: 107	Avg. %: 107	Avg. %: 107	Avg. %: 107	Avg. %: 107
716	717	718	719	720
				
Avg. %: 107	Avg. %: 107	Avg. %: 107	Avg. %: 107	Avg. %: 107

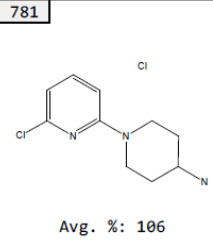
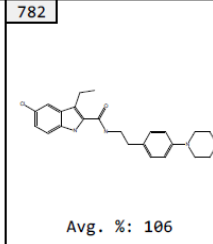
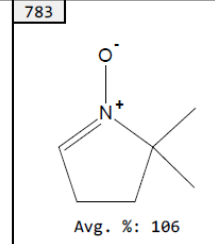
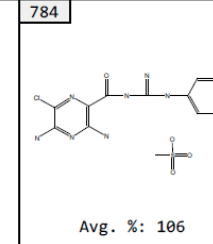
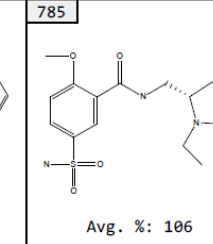
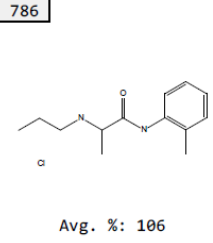
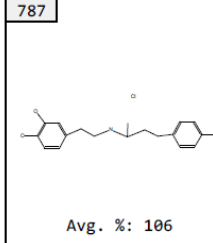
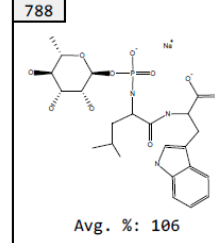
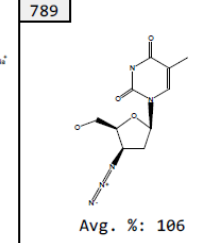
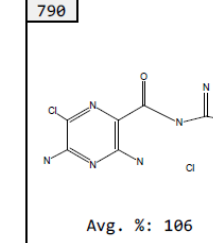
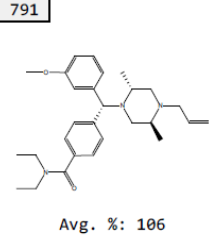
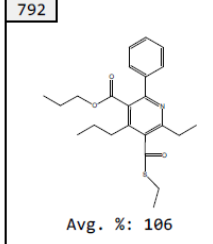
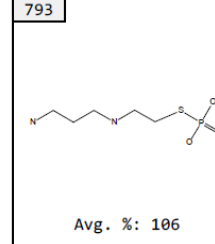
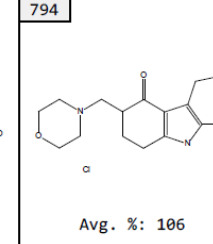
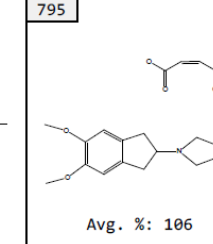
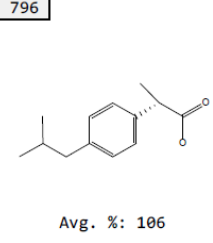
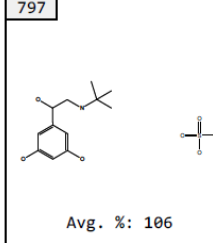
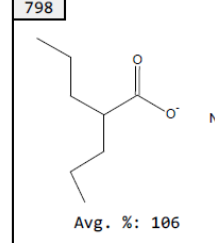
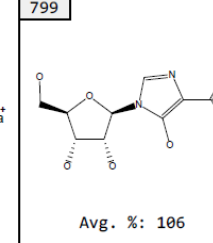
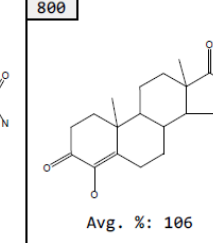
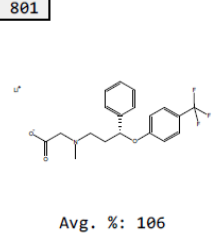
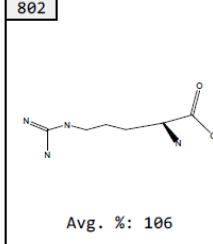
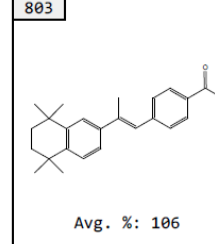
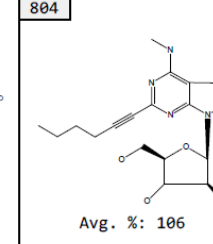
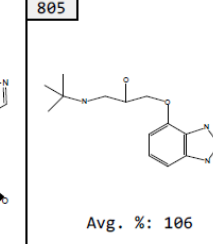
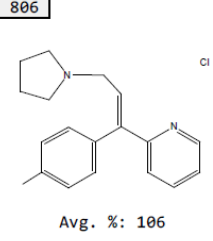
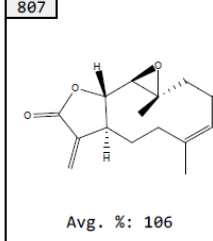
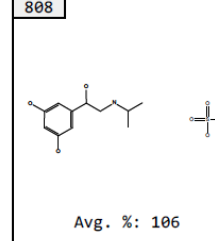
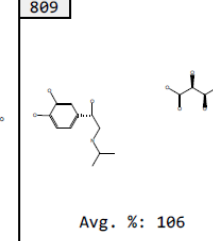
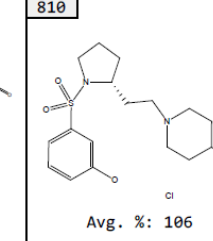
Continued, Table 21. Results of fluorescence-based electrophile screen of the LOPAC library. Values are presented as a percent of the MSTI signal (Avg. %). (n=3)

721	722	723	724	725
				
Avg. %: 107	Avg. %: 107	Avg. %: 107	Avg. %: 107	Avg. %: 107
726	727	728	729	730
				
Avg. %: 107	Avg. %: 107	Avg. %: 107	Avg. %: 107	Avg. %: 107
731	732	733	734	735
				
Avg. %: 107	Avg. %: 107	Avg. %: 107	Avg. %: 107	Avg. %: 107
736	737	738	739	740
				
Avg. %: 107	Avg. %: 107	Avg. %: 107	Avg. %: 107	Avg. %: 107
741	742	743	744	745
				
Avg. %: 107	Avg. %: 107	Avg. %: 107	Avg. %: 107	Avg. %: 107
746	747	748	749	750
				
Avg. %: 107	Avg. %: 107	Avg. %: 107	Avg. %: 107	Avg. %: 107

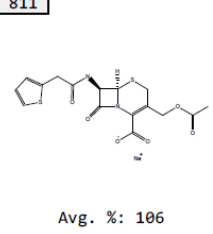
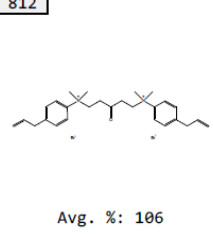
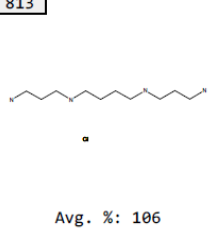
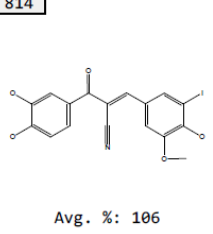
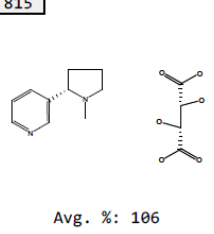
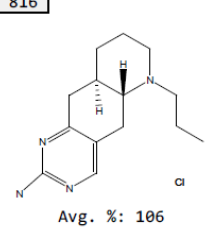
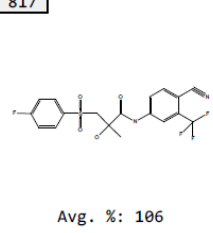
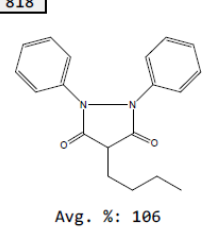
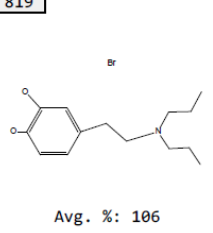
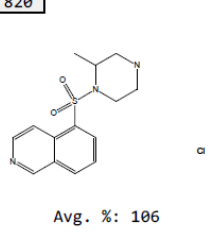
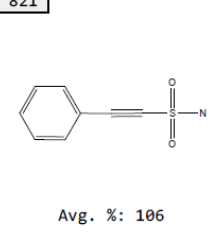
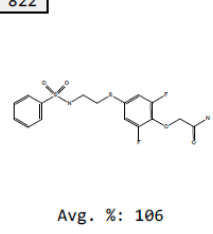
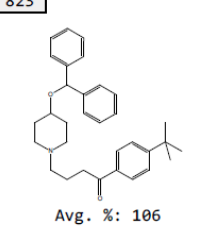
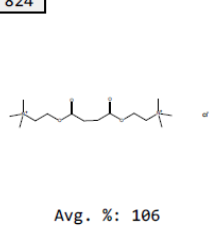
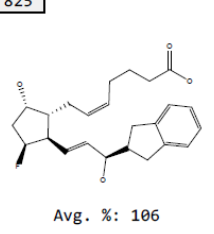
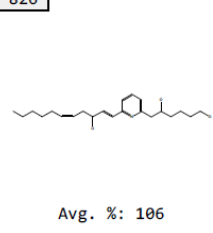
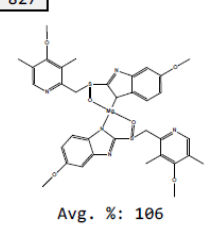
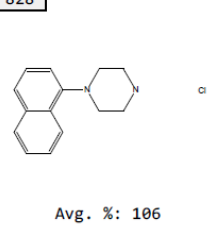
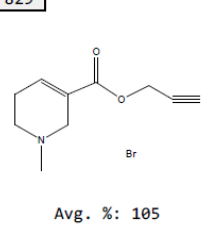
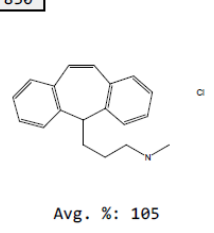
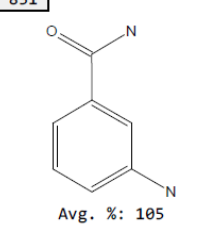
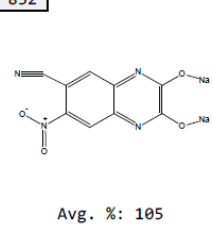
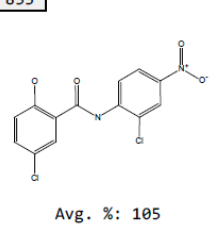
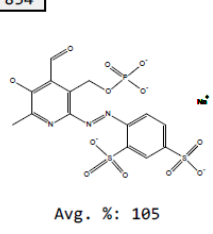
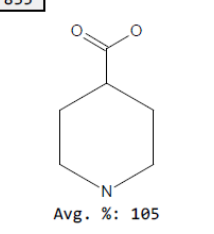
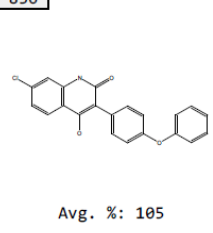
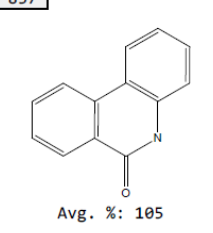
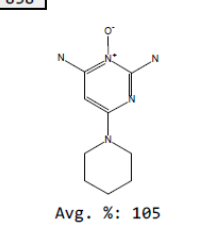
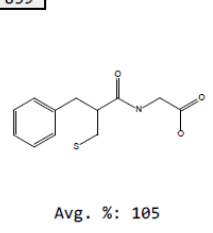
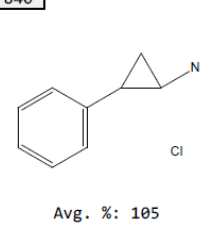
Continued, Table 21. Results of fluorescence-based electrophile screen of the LOPAC library. Values are presented as a percent of the MSTI signal (Avg. %). (n=3)

751  Avg. %: 107	752  Avg. %: 107	753  Avg. %: 107	754  Avg. %: 107	755  Avg. %: 107
756  Avg. %: 107	757  Avg. %: 107	758  Avg. %: 107	759  Avg. %: 107	760  Avg. %: 107
761  Avg. %: 107	762  Avg. %: 107	763  Avg. %: 107	764  Avg. %: 107	765  Avg. %: 107
766  Avg. %: 107	767  Avg. %: 107	768  Avg. %: 107	769  Avg. %: 107	770  Avg. %: 107
771  Avg. %: 107	772  Avg. %: 107	773  Avg. %: 107	774  Avg. %: 107	775  Avg. %: 106
776  Avg. %: 106	777  Avg. %: 106	778  Avg. %: 106	779  Avg. %: 106	780  Avg. %: 106

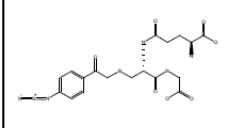
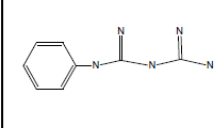
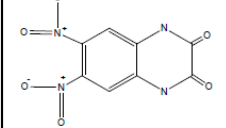
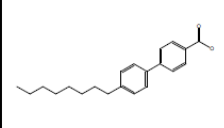
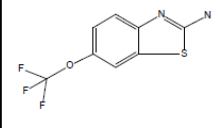
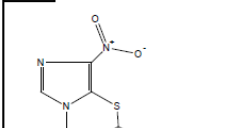
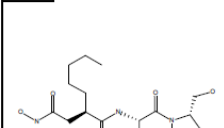
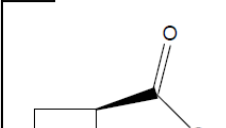
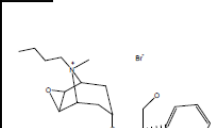
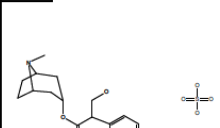

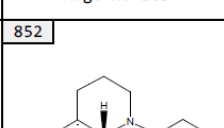
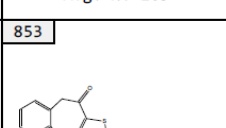
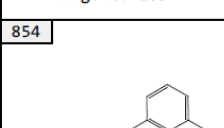
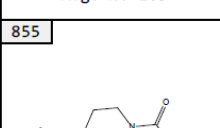
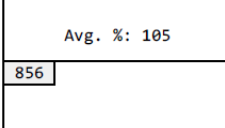
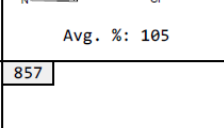
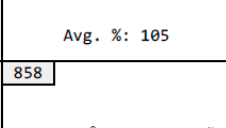
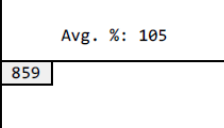
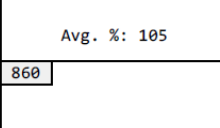
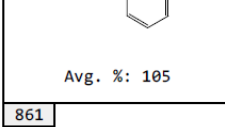
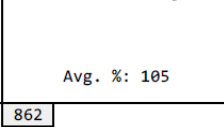
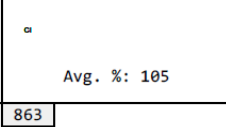
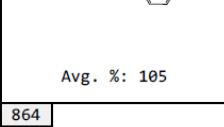
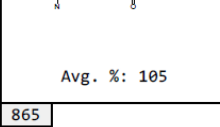
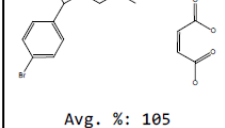
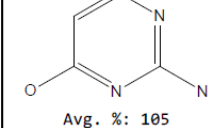
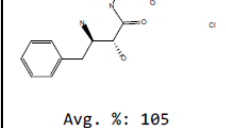
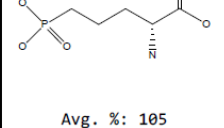
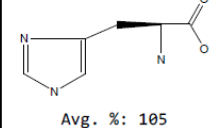
Continued, Table 21. Results of fluorescence-based electrophile screen of the LOPAC library. Values are presented as a percent of the MSTI signal (Avg. %). (n=3)

781	782	783	784	785
				
Avg. %: 106	Avg. %: 106	Avg. %: 106	Avg. %: 106	Avg. %: 106
786	787	788	789	790
				
Avg. %: 106	Avg. %: 106	Avg. %: 106	Avg. %: 106	Avg. %: 106
791	792	793	794	795
				
Avg. %: 106	Avg. %: 106	Avg. %: 106	Avg. %: 106	Avg. %: 106
796	797	798	799	800
				
Avg. %: 106	Avg. %: 106	Avg. %: 106	Avg. %: 106	Avg. %: 106
801	802	803	804	805
				
Avg. %: 106	Avg. %: 106	Avg. %: 106	Avg. %: 106	Avg. %: 106
806	807	808	809	810
				
Avg. %: 106	Avg. %: 106	Avg. %: 106	Avg. %: 106	Avg. %: 106

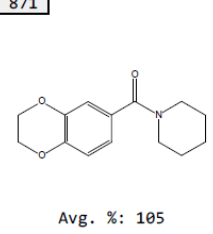
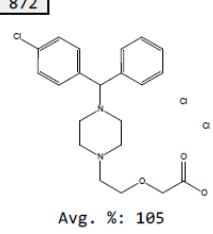
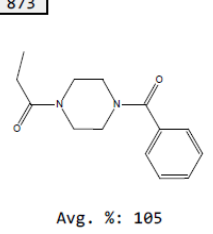
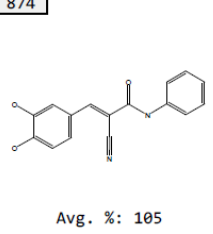
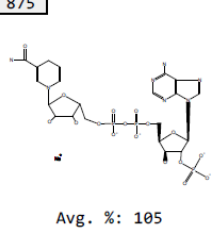
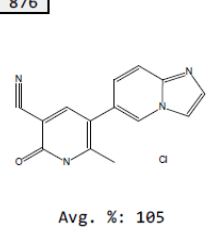
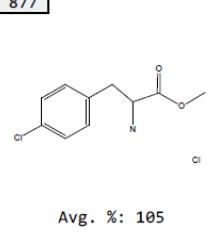
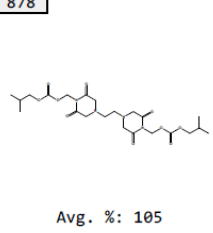
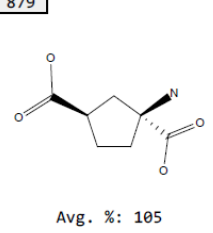
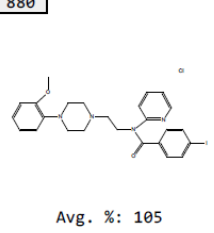
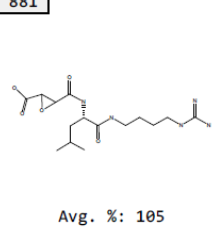
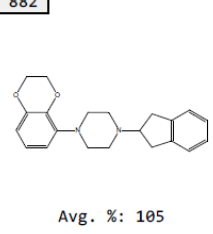
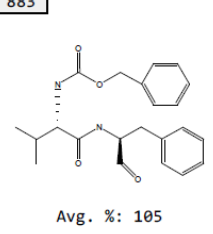
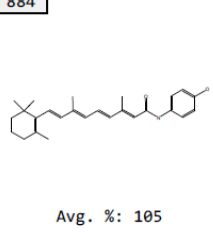
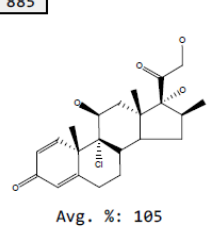
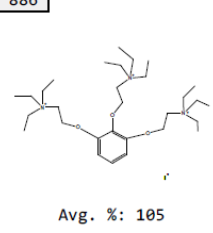
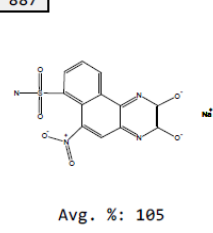
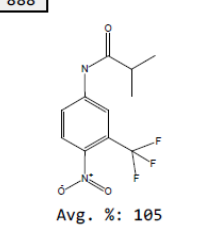
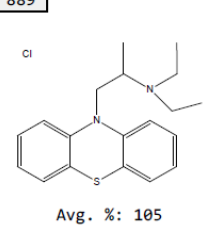
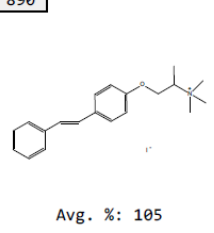
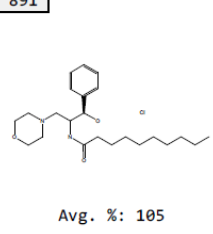
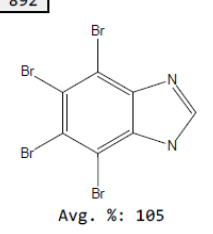
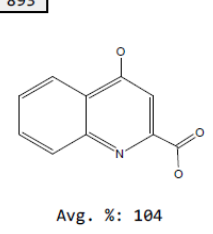
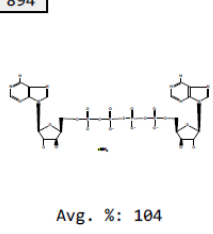
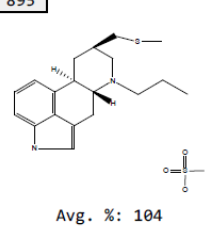
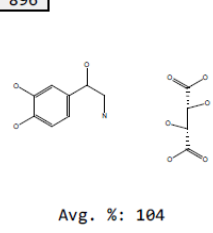
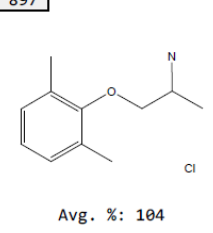
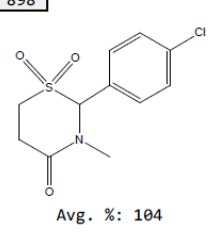
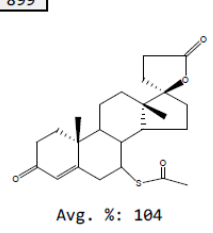
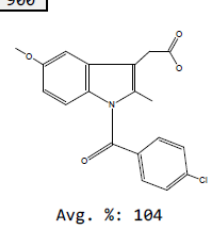
Continued, Table 21. Results of fluorescence-based electrophile screen of the LOPAC library. Values are presented as a percent of the MSTI signal (Avg. %). (n=3)

811	812	813	814	815
				
Avg. %: 106	Avg. %: 106	Avg. %: 106	Avg. %: 106	Avg. %: 106
816	817	818	819	820
				
Avg. %: 106	Avg. %: 106	Avg. %: 106	Avg. %: 106	Avg. %: 106
821	822	823	824	825
				
Avg. %: 106	Avg. %: 106	Avg. %: 106	Avg. %: 106	Avg. %: 106
826	827	828	829	830
				
Avg. %: 106	Avg. %: 106	Avg. %: 106	Avg. %: 105	Avg. %: 105
831	832	833	834	835
				
Avg. %: 105	Avg. %: 105	Avg. %: 105	Avg. %: 105	Avg. %: 105
836	837	838	839	840
				
Avg. %: 105	Avg. %: 105	Avg. %: 105	Avg. %: 105	Avg. %: 105

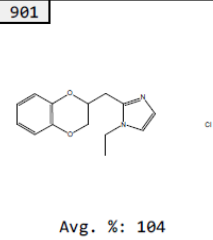
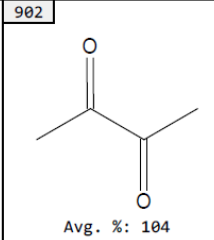
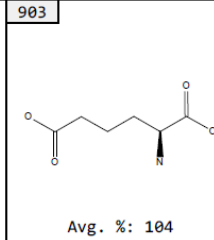
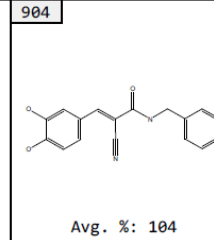
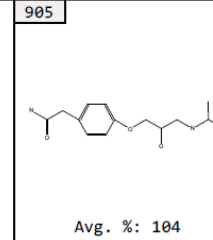
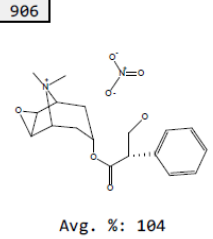
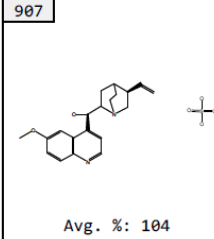
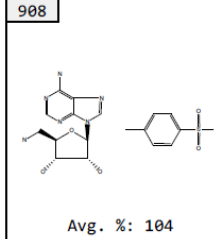
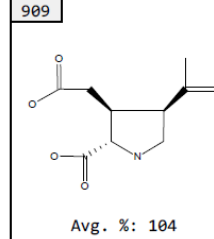
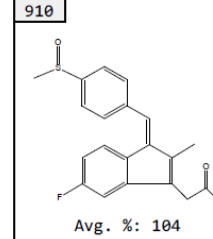
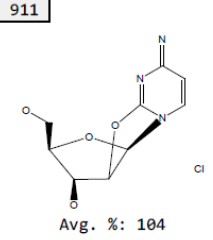
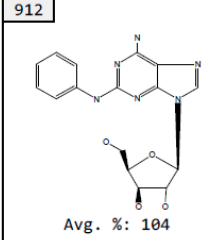
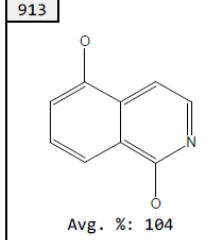
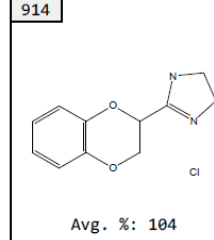
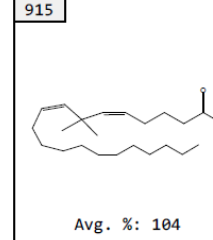
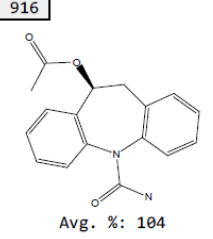
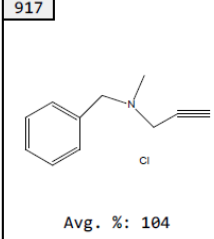
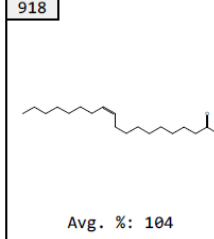
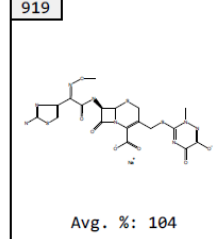
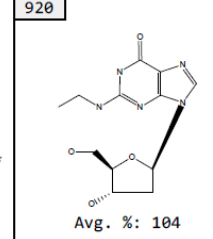
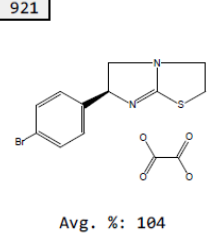
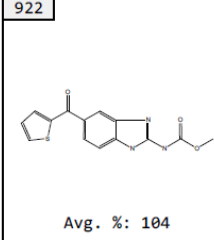
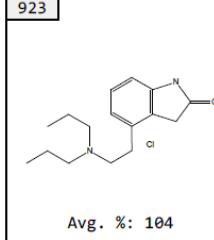
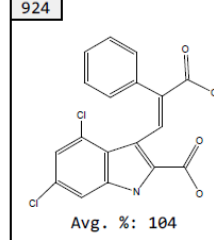
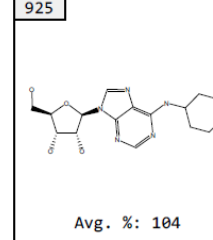
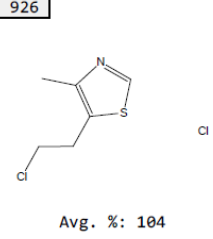
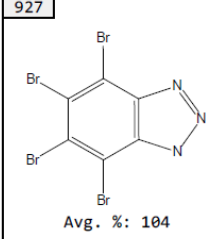
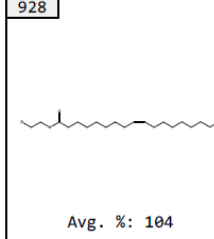
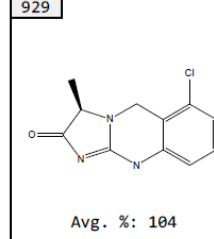
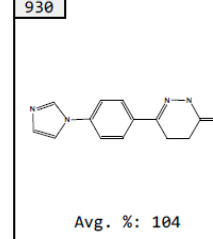
Continued, Table 21. Results of fluorescence-based electrophile screen of the LOPAC library. Values are presented as a percent of the MSTI signal (Avg. %). (n=3)

841	842	843	844	845
				
Avg. %: 105	Avg. %: 105	Avg. %: 105	Avg. %: 105	Avg. %: 105
846	847	848	849	850
				
Avg. %: 105	Avg. %: 105	Avg. %: 105	Avg. %: 105	Avg. %: 105
851	852	853	854	855
				
Avg. %: 105	Avg. %: 105	Avg. %: 105	Avg. %: 105	Avg. %: 105
856	857	858	859	860
				
Avg. %: 105	Avg. %: 105	Avg. %: 105	Avg. %: 105	Avg. %: 105
861	862	863	864	865
				
Avg. %: 105	Avg. %: 105	Avg. %: 105	Avg. %: 105	Avg. %: 105
866	867	868	869	870
				
Avg. %: 105	Avg. %: 105	Avg. %: 105	Avg. %: 105	Avg. %: 105

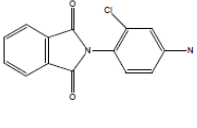
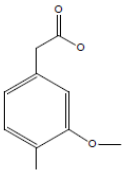
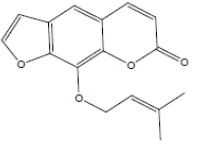
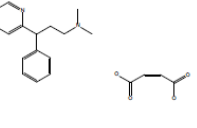
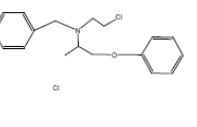
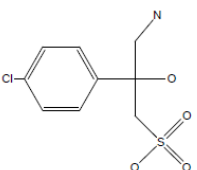
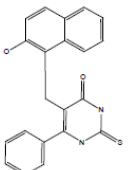
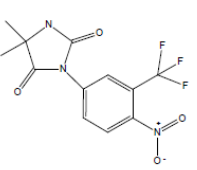
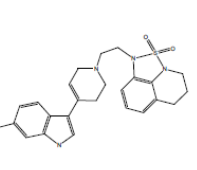
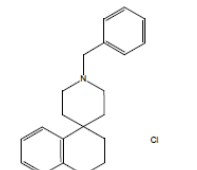
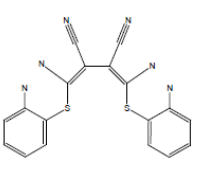
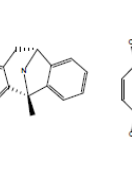
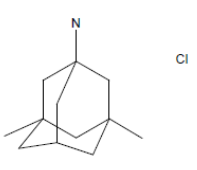
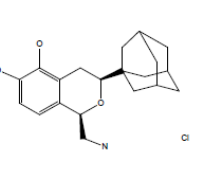
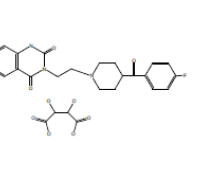
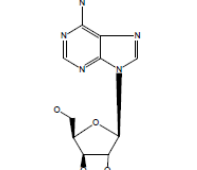
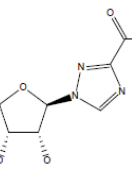
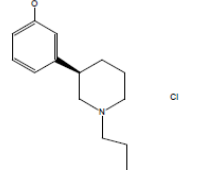
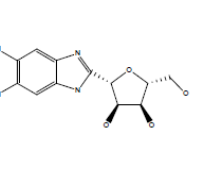
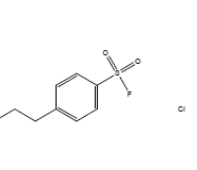
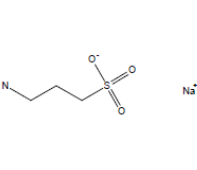
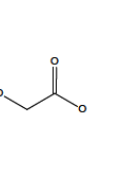
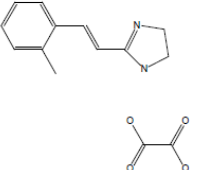
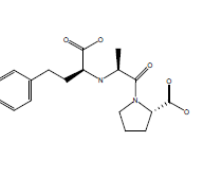
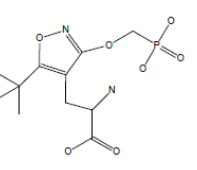
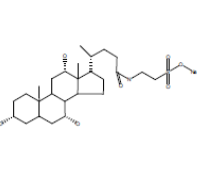
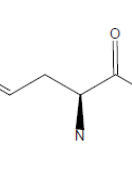
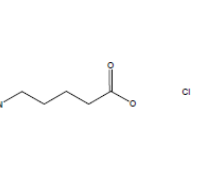
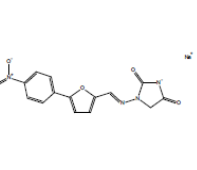
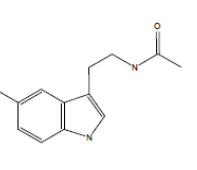
Continued, Table 21. Results of fluorescence-based electrophile screen of the LOPAC library. Values are presented as a percent of the MSTI signal (Avg. %). (n=3)

871	872	873	874	875
				
Avg. %: 105	Avg. %: 105	Avg. %: 105	Avg. %: 105	Avg. %: 105
876	877	878	879	880
				
Avg. %: 105	Avg. %: 105	Avg. %: 105	Avg. %: 105	Avg. %: 105
881	882	883	884	885
				
Avg. %: 105	Avg. %: 105	Avg. %: 105	Avg. %: 105	Avg. %: 105
886	887	888	889	890
				
Avg. %: 105	Avg. %: 105	Avg. %: 105	Avg. %: 105	Avg. %: 105
891	892	893	894	895
				
Avg. %: 105	Avg. %: 105	Avg. %: 104	Avg. %: 104	Avg. %: 104
896	897	898	899	900
				
Avg. %: 104	Avg. %: 104	Avg. %: 104	Avg. %: 104	Avg. %: 104

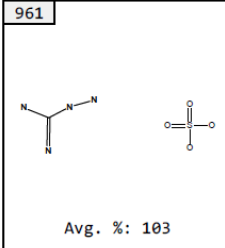
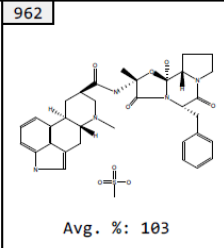
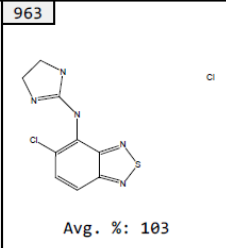
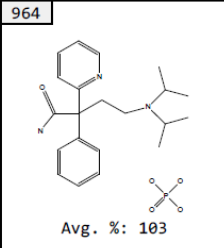
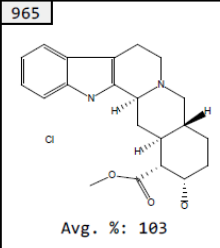
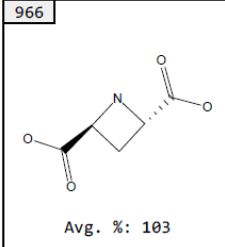
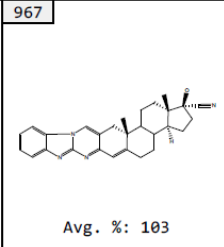
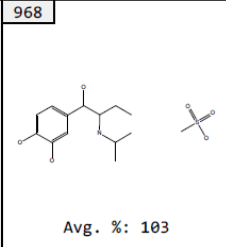
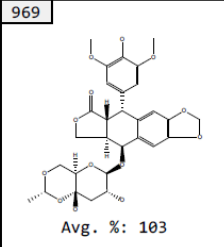
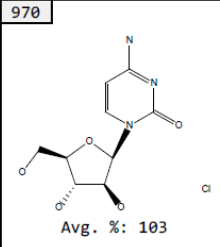
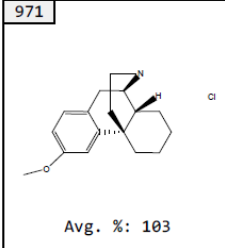
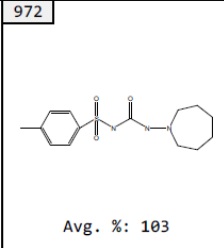
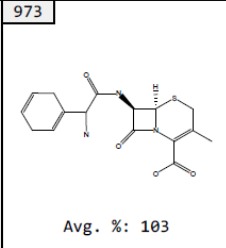
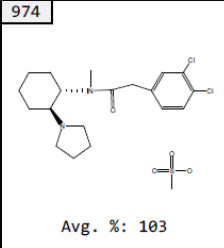
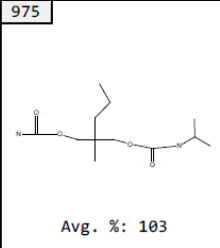
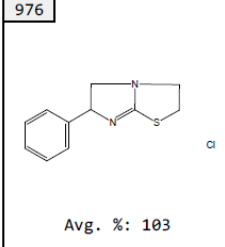
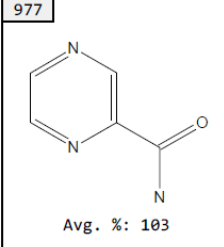
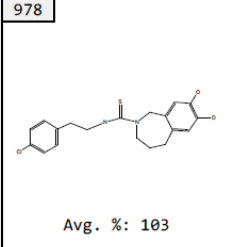
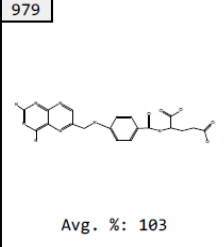
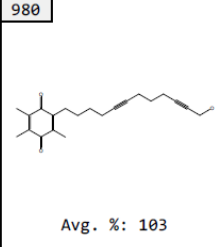
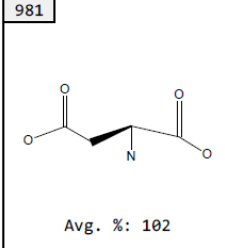
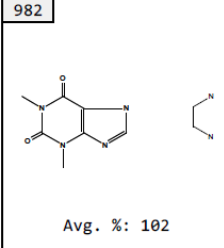
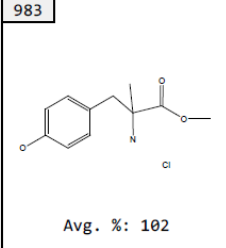
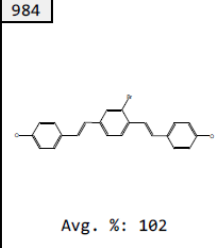
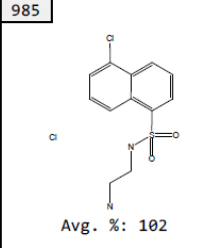
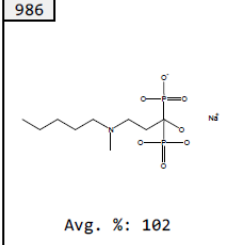
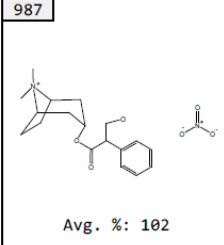
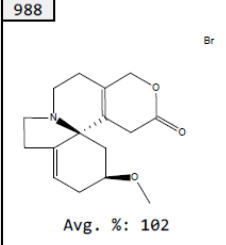
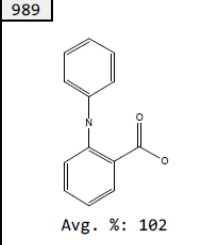
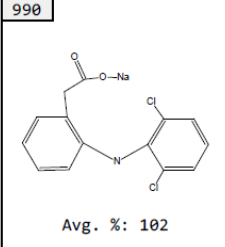
Continued, Table 21. Results of fluorescence-based electrophile screen of the LOPAC library. Values are presented as a percent of the MSTI signal (Avg. %). (n=3)

 <p>Avg. %: 104</p>	 <p>Avg. %: 104</p>	 <p>Avg. %: 104</p>	 <p>Avg. %: 104</p>	 <p>Avg. %: 104</p>
 <p>Avg. %: 104</p>	 <p>Avg. %: 104</p>	 <p>Avg. %: 104</p>	 <p>Avg. %: 104</p>	 <p>Avg. %: 104</p>
 <p>Avg. %: 104</p>	 <p>Avg. %: 104</p>	 <p>Avg. %: 104</p>	 <p>Avg. %: 104</p>	 <p>Avg. %: 104</p>
 <p>Avg. %: 104</p>	 <p>Avg. %: 104</p>	 <p>Avg. %: 104</p>	 <p>Avg. %: 104</p>	 <p>Avg. %: 104</p>
 <p>Avg. %: 104</p>	 <p>Avg. %: 104</p>	 <p>Avg. %: 104</p>	 <p>Avg. %: 104</p>	 <p>Avg. %: 104</p>
 <p>Avg. %: 104</p>	 <p>Avg. %: 104</p>	 <p>Avg. %: 104</p>	 <p>Avg. %: 104</p>	 <p>Avg. %: 104</p>

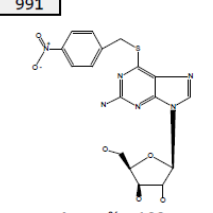
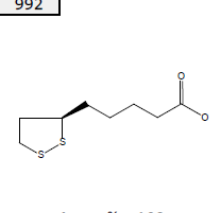
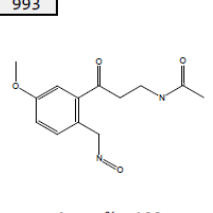
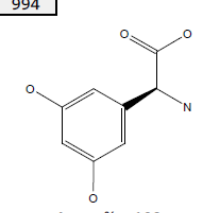
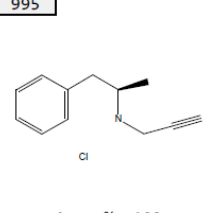
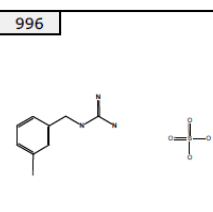
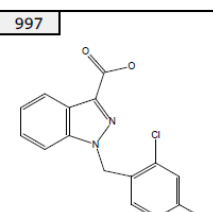
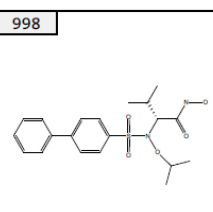
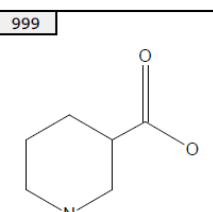
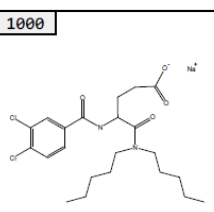
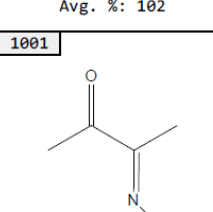
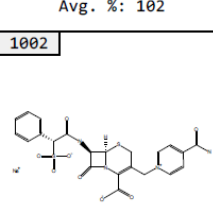
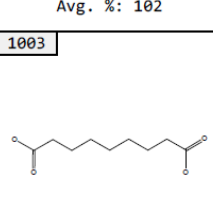
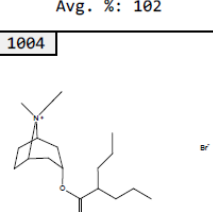
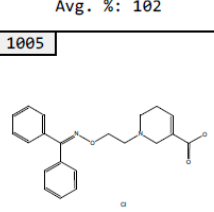
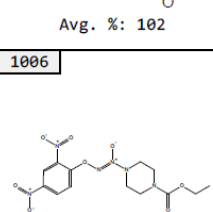
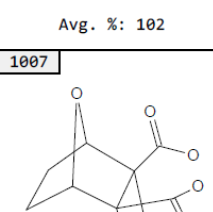
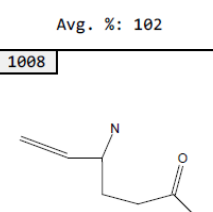
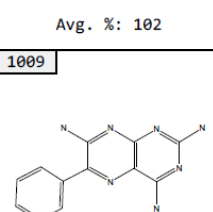
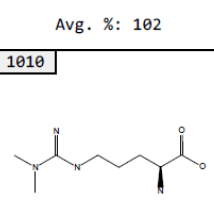
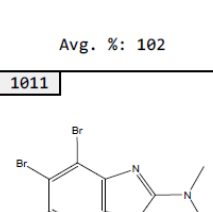
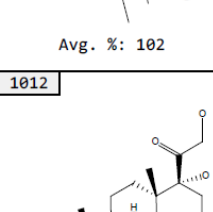
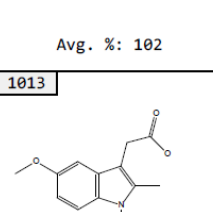
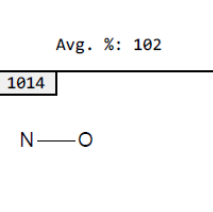
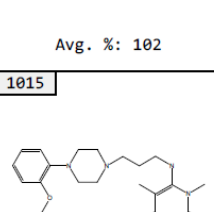
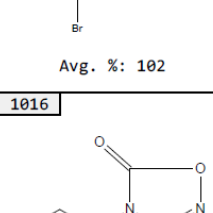
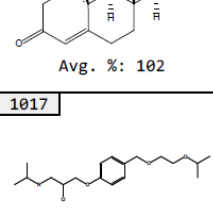
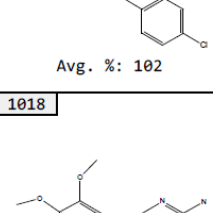
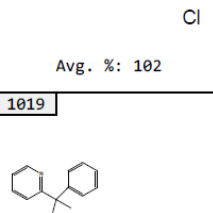
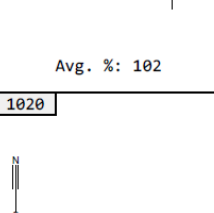
Continued, Table 21. Results of fluorescence-based electrophile screen of the LOPAC library. Values are presented as a percent of the MSTI signal (Avg. %). (n=3)

<p>931</p>  <p>Avg. %: 104</p>	<p>932</p>  <p>Avg. %: 104</p>	<p>933</p>  <p>Avg. %: 104</p>	<p>934</p>  <p>Avg. %: 104</p>	<p>935</p>  <p>Avg. %: 104</p>
<p>936</p>  <p>Avg. %: 104</p>	<p>937</p>  <p>Avg. %: 104</p>	<p>938</p>  <p>Avg. %: 104</p>	<p>939</p>  <p>Avg. %: 104</p>	<p>940</p>  <p>Avg. %: 104</p>
<p>941</p>  <p>Avg. %: 104</p>	<p>942</p>  <p>Avg. %: 104</p>	<p>943</p>  <p>Avg. %: 104</p>	<p>944</p>  <p>Avg. %: 104</p>	<p>945</p>  <p>Avg. %: 104</p>
<p>946</p>  <p>Avg. %: 103</p>	<p>947</p>  <p>Avg. %: 103</p>	<p>948</p>  <p>Avg. %: 103</p>	<p>949</p>  <p>Avg. %: 103</p>	<p>950</p>  <p>Avg. %: 103</p>
<p>951</p>  <p>Avg. %: 103</p>	<p>952</p>  <p>Avg. %: 103</p>	<p>953</p>  <p>Avg. %: 103</p>	<p>954</p>  <p>Avg. %: 103</p>	<p>955</p>  <p>Avg. %: 103</p>
<p>956</p>  <p>Avg. %: 103</p>	<p>957</p>  <p>Avg. %: 103</p>	<p>958</p>  <p>Avg. %: 103</p>	<p>959</p>  <p>Avg. %: 103</p>	<p>960</p>  <p>Avg. %: 103</p>

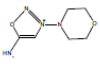
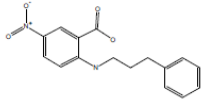
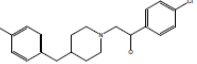
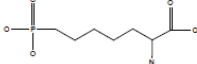
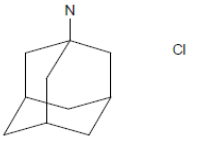
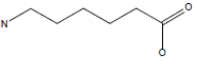
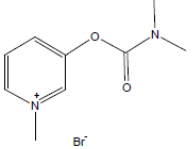
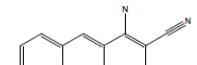
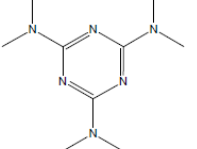
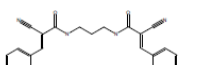
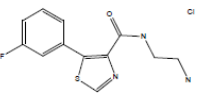
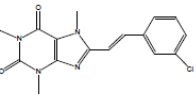
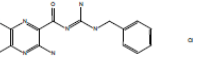
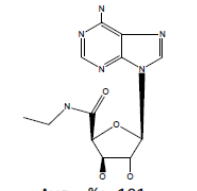
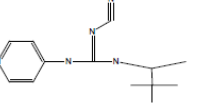
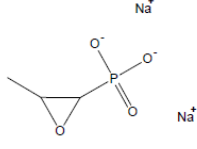
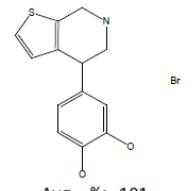
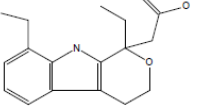
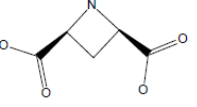
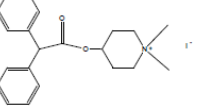
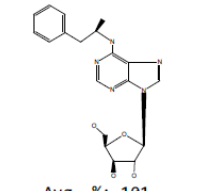
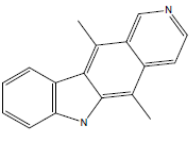
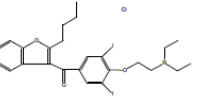
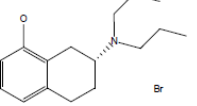
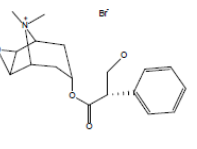
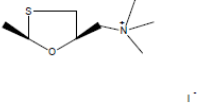
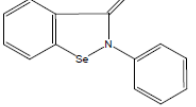
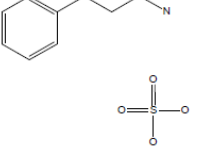
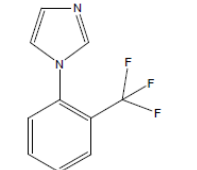
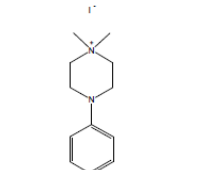
Continued, Table 21. Results of fluorescence-based electrophile screen of the LOPAC library. Values are presented as a percent of the MSTI signal (Avg. %). (n=3)

961	962	963	964	965
				
Avg. %: 103	Avg. %: 103	Avg. %: 103	Avg. %: 103	Avg. %: 103
966	967	968	969	970
				
Avg. %: 103	Avg. %: 103	Avg. %: 103	Avg. %: 103	Avg. %: 103
971	972	973	974	975
				
Avg. %: 103	Avg. %: 103	Avg. %: 103	Avg. %: 103	Avg. %: 103
976	977	978	979	980
				
Avg. %: 103	Avg. %: 103	Avg. %: 103	Avg. %: 103	Avg. %: 103
981	982	983	984	985
				
Avg. %: 102	Avg. %: 102	Avg. %: 102	Avg. %: 102	Avg. %: 102
986	987	988	989	990
				
Avg. %: 102	Avg. %: 102	Avg. %: 102	Avg. %: 102	Avg. %: 102

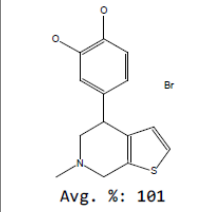
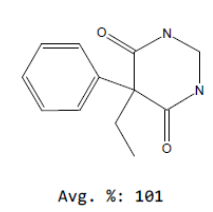
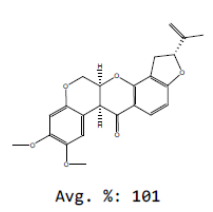
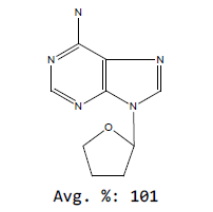
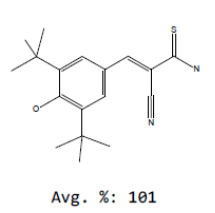
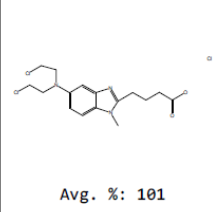
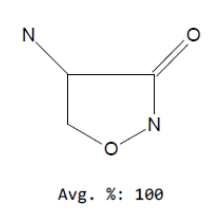
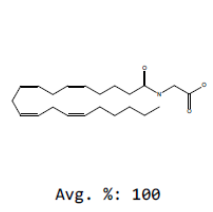
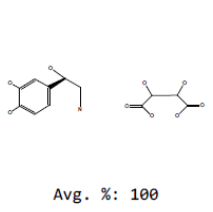
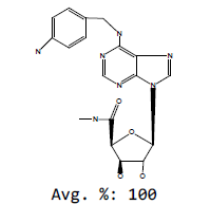
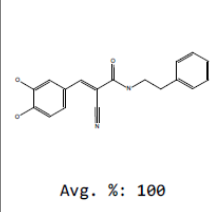
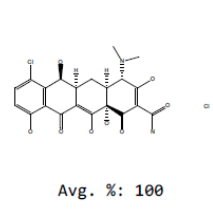
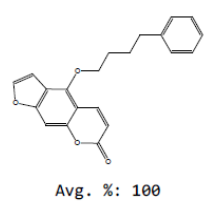
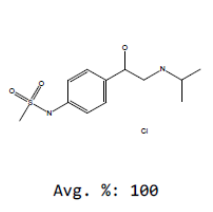
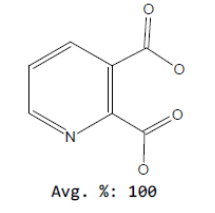
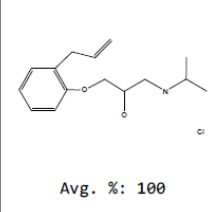
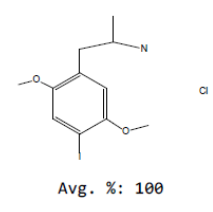
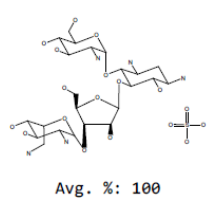
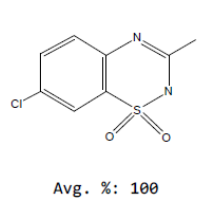
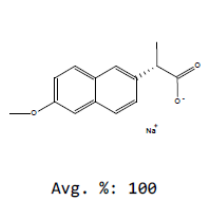
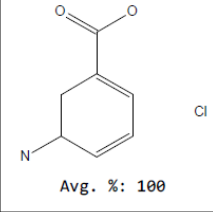
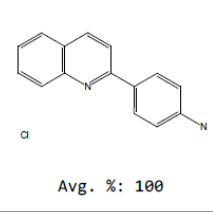
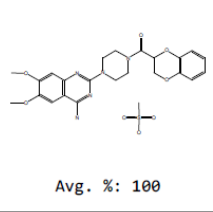
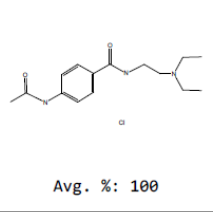
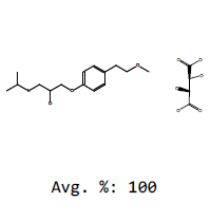
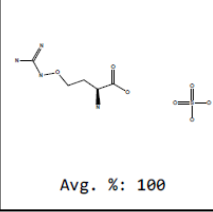
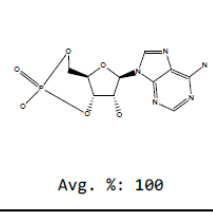
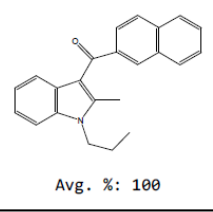
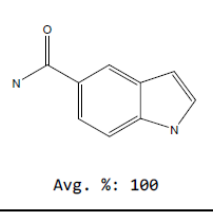
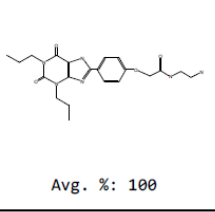
Continued, Table 21. Results of fluorescence-based electrophile screen of the LOPAC library. Values are presented as a percent of the MSTI signal (Avg. %). (n=3)

<p>991</p>  <p>Avg. %: 102</p>	<p>992</p>  <p>Avg. %: 102</p>	<p>993</p>  <p>Avg. %: 102</p>	<p>994</p>  <p>Avg. %: 102</p>	<p>995</p>  <p>Avg. %: 102</p>
<p>996</p>  <p>Avg. %: 102</p>	<p>997</p>  <p>Avg. %: 102</p>	<p>998</p>  <p>Avg. %: 102</p>	<p>999</p>  <p>Avg. %: 102</p>	<p>1000</p>  <p>Avg. %: 102</p>
<p>1001</p>  <p>Avg. %: 102</p>	<p>1002</p>  <p>Avg. %: 102</p>	<p>1003</p>  <p>Avg. %: 102</p>	<p>1004</p>  <p>Avg. %: 102</p>	<p>1005</p>  <p>Avg. %: 102</p>
<p>1006</p>  <p>Avg. %: 102</p>	<p>1007</p>  <p>Avg. %: 102</p>	<p>1008</p>  <p>Avg. %: 102</p>	<p>1009</p>  <p>Avg. %: 102</p>	<p>1010</p>  <p>Avg. %: 102</p>
<p>1011</p>  <p>Avg. %: 102</p>	<p>1012</p>  <p>Avg. %: 102</p>	<p>1013</p>  <p>Avg. %: 102</p>	<p>1014</p>  <p>Avg. %: 102</p>	<p>1015</p>  <p>Avg. %: 102</p>
<p>1016</p>  <p>Avg. %: 102</p>	<p>1017</p>  <p>Avg. %: 102</p>	<p>1018</p>  <p>Avg. %: 102</p>	<p>1019</p>  <p>Avg. %: 102</p>	<p>1020</p>  <p>Avg. %: 102</p>

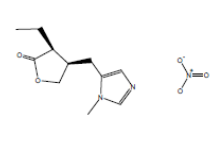
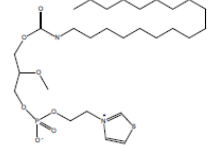
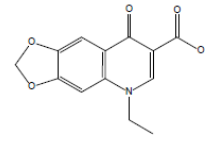
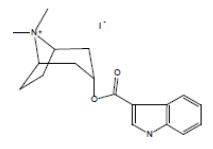
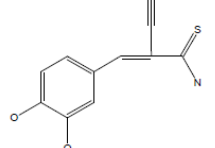
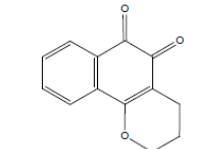
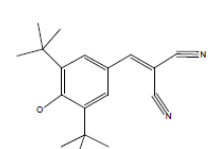
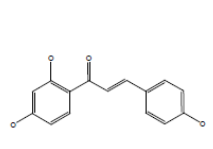
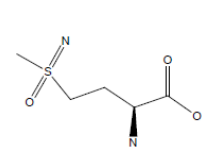
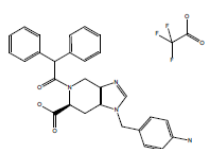
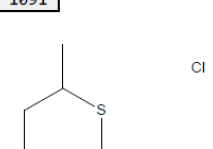
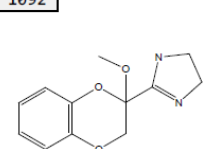
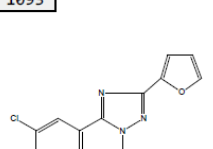
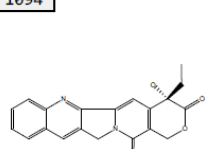
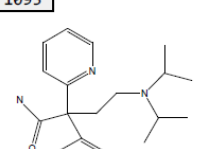
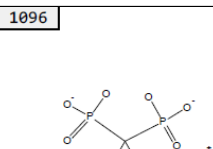
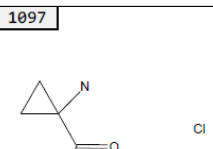
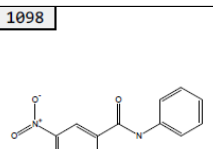
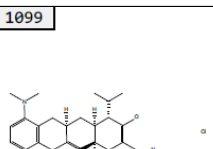
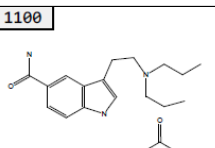
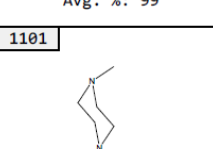
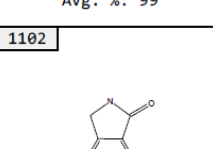
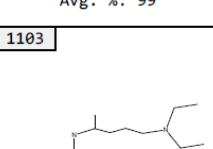
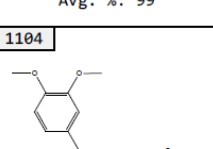
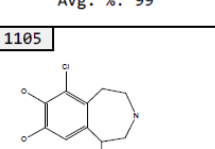
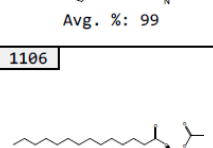
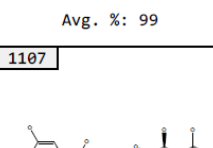
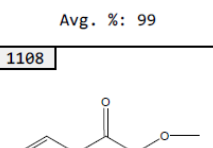
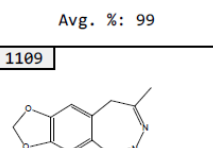
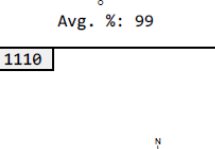
Continued, Table 21. Results of fluorescence-based electrophile screen of the LOPAC library. Values are presented as a percent of the MSTI signal (Avg. %). (n=3)

<p>1021</p>  <p>Avg. %: 102</p>	<p>1022</p>  <p>Avg. %: 101</p>	<p>1023</p>  <p>Avg. %: 101</p>	<p>1024</p>  <p>Avg. %: 101</p>	<p>1025</p>  <p>Avg. %: 101</p>
<p>1026</p>  <p>Avg. %: 101</p>	<p>1027</p>  <p>Avg. %: 101</p>	<p>1028</p>  <p>Avg. %: 101</p>	<p>1029</p>  <p>Avg. %: 101</p>	<p>1030</p>  <p>Avg. %: 101</p>
<p>1031</p>  <p>Avg. %: 101</p>	<p>1032</p>  <p>Avg. %: 101</p>	<p>1033</p>  <p>Avg. %: 101</p>	<p>1034</p>  <p>Avg. %: 101</p>	<p>1035</p>  <p>Avg. %: 101</p>
<p>1036</p>  <p>Avg. %: 101</p>	<p>1037</p>  <p>Avg. %: 101</p>	<p>1038</p>  <p>Avg. %: 101</p>	<p>1039</p>  <p>Avg. %: 101</p>	<p>1040</p>  <p>Avg. %: 101</p>
<p>1041</p>  <p>Avg. %: 101</p>	<p>1042</p>  <p>Avg. %: 101</p>	<p>1043</p>  <p>Avg. %: 101</p>	<p>1044</p>  <p>Avg. %: 101</p>	<p>1045</p>  <p>Avg. %: 101</p>
<p>1046</p>  <p>Avg. %: 101</p>	<p>1047</p>  <p>Avg. %: 101</p>	<p>1048</p>  <p>Avg. %: 101</p>	<p>1049</p>  <p>Avg. %: 101</p>	<p>1050</p>  <p>Avg. %: 101</p>

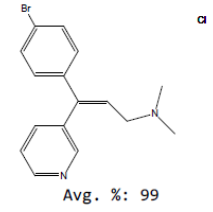
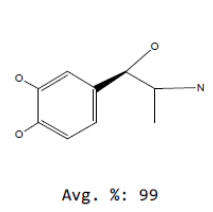
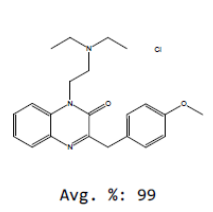
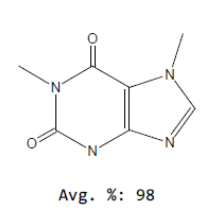
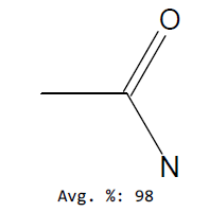
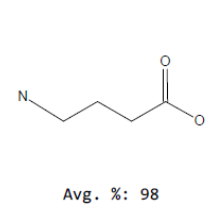
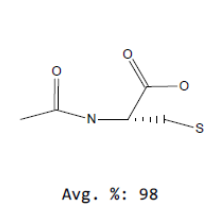
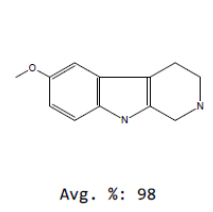
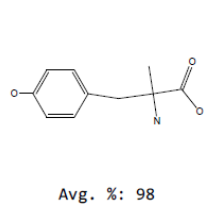
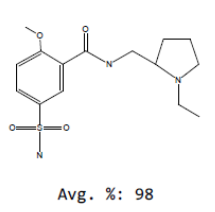
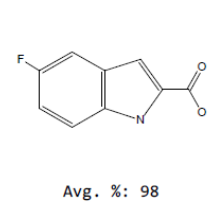
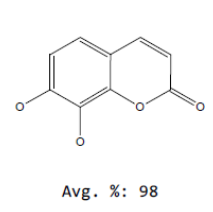
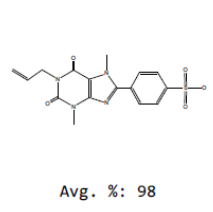
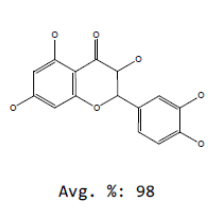
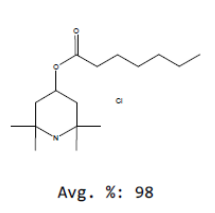
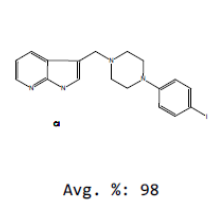
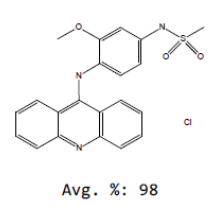
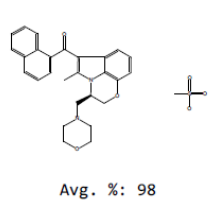
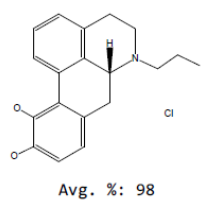
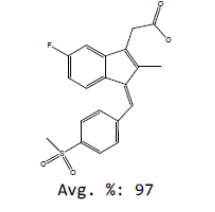
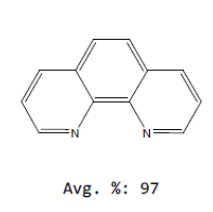
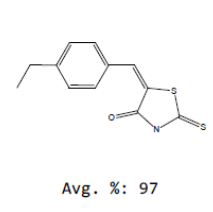
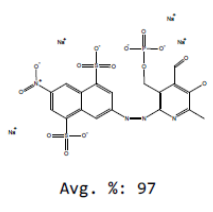
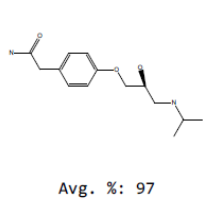
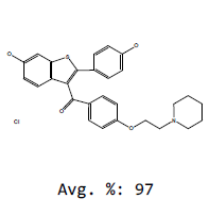
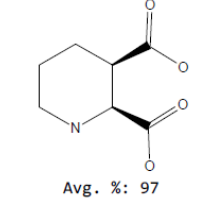
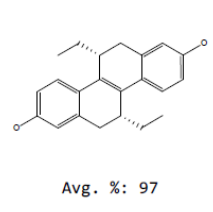
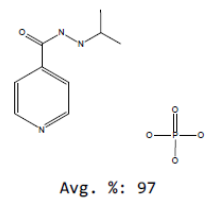
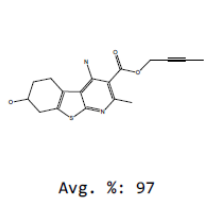
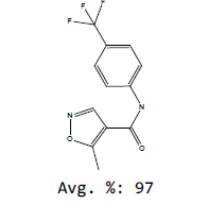
Continued, Table 21. Results of fluorescence-based electrophile screen of the LOPAC library. Values are presented as a percent of the MSTI signal (Avg. %). (n=3)

<p>1051</p>  <p>Avg. %: 101</p>	<p>1052</p>  <p>Avg. %: 101</p>	<p>1053</p>  <p>Avg. %: 101</p>	<p>1054</p>  <p>Avg. %: 101</p>	<p>1055</p>  <p>Avg. %: 101</p>
<p>1056</p>  <p>Avg. %: 101</p>	<p>1057</p>  <p>Avg. %: 100</p>	<p>1058</p>  <p>Avg. %: 100</p>	<p>1059</p>  <p>Avg. %: 100</p>	<p>1060</p>  <p>Avg. %: 100</p>
<p>1061</p>  <p>Avg. %: 100</p>	<p>1062</p>  <p>Avg. %: 100</p>	<p>1063</p>  <p>Avg. %: 100</p>	<p>1064</p>  <p>Avg. %: 100</p>	<p>1065</p>  <p>Avg. %: 100</p>
<p>1066</p>  <p>Avg. %: 100</p>	<p>1067</p>  <p>Avg. %: 100</p>	<p>1068</p>  <p>Avg. %: 100</p>	<p>1069</p>  <p>Avg. %: 100</p>	<p>1070</p>  <p>Avg. %: 100</p>
<p>1071</p>  <p>Avg. %: 100</p>	<p>1072</p>  <p>Avg. %: 100</p>	<p>1073</p>  <p>Avg. %: 100</p>	<p>1074</p>  <p>Avg. %: 100</p>	<p>1075</p>  <p>Avg. %: 100</p>
<p>1076</p>  <p>Avg. %: 100</p>	<p>1077</p>  <p>Avg. %: 100</p>	<p>1078</p>  <p>Avg. %: 100</p>	<p>1079</p>  <p>Avg. %: 100</p>	<p>1080</p>  <p>Avg. %: 100</p>

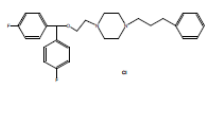
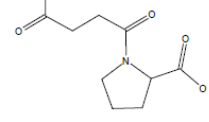
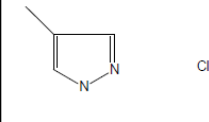
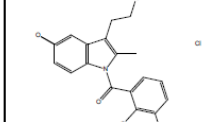
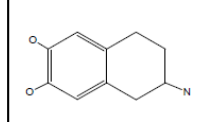
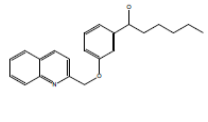
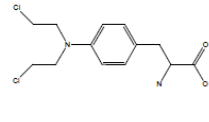
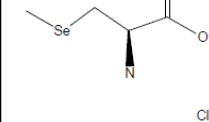
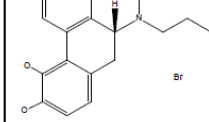
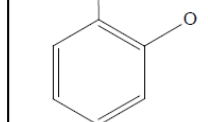
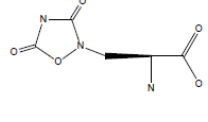
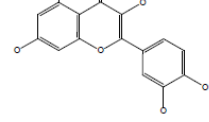
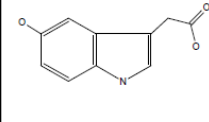
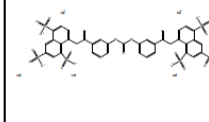
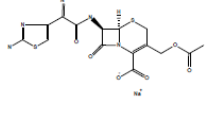
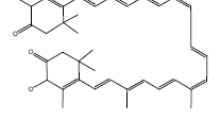
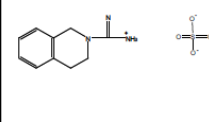
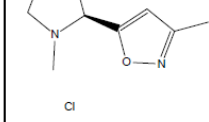
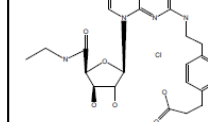
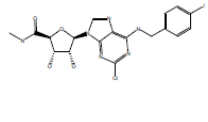
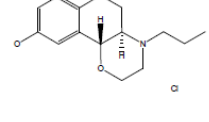
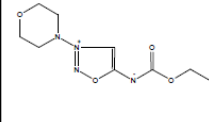
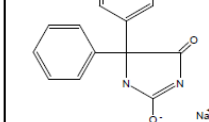
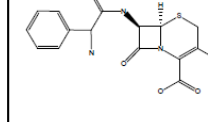
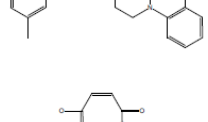
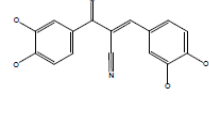
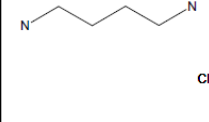
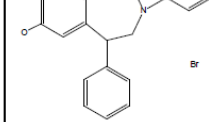
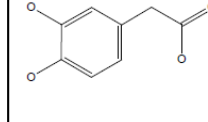
Continued, Table 21. Results of fluorescence-based electrophile screen of the LOPAC library. Values are presented as a percent of the MSTI signal (Avg. %). (n=3)

<p>1081</p>  <p>Avg. %: 100</p>	<p>1082</p>  <p>Avg. %: 100</p>	<p>1083</p>  <p>Avg. %: 100</p>	<p>1084</p>  <p>Avg. %: 100</p>	<p>1085</p>  <p>Avg. %: 100</p>
<p>1086</p>  <p>Avg. %: 100</p>	<p>1087</p>  <p>Avg. %: 100</p>	<p>1088</p>  <p>Avg. %: 99</p>	<p>1089</p>  <p>Avg. %: 99</p>	<p>1090</p>  <p>Avg. %: 99</p>
<p>1091</p>  <p>Avg. %: 99</p>	<p>1092</p>  <p>Avg. %: 99</p>	<p>1093</p>  <p>Avg. %: 99</p>	<p>1094</p>  <p>Avg. %: 99</p>	<p>1095</p>  <p>Avg. %: 99</p>
<p>1096</p>  <p>Avg. %: 99</p>	<p>1097</p>  <p>Avg. %: 99</p>	<p>1098</p>  <p>Avg. %: 99</p>	<p>1099</p>  <p>Avg. %: 99</p>	<p>1100</p>  <p>Avg. %: 99</p>
<p>1101</p>  <p>Avg. %: 99</p>	<p>1102</p>  <p>Avg. %: 99</p>	<p>1103</p>  <p>Avg. %: 99</p>	<p>1104</p>  <p>Avg. %: 99</p>	<p>1105</p>  <p>Avg. %: 99</p>
<p>1106</p>  <p>Avg. %: 99</p>	<p>1107</p>  <p>Avg. %: 99</p>	<p>1108</p>  <p>Avg. %: 99</p>	<p>1109</p>  <p>Avg. %: 99</p>	<p>1110</p>  <p>Avg. %: 99</p>

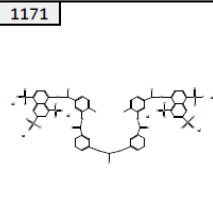
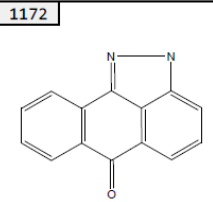
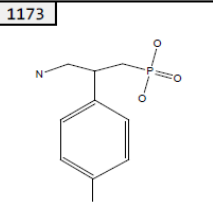
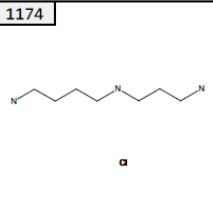
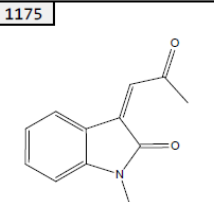
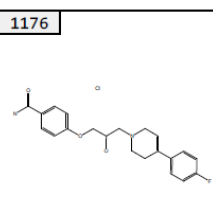
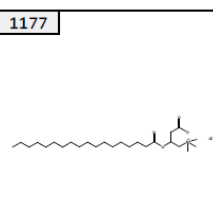
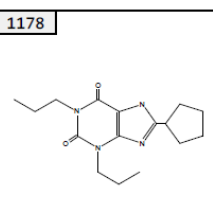
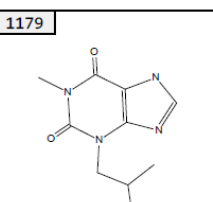
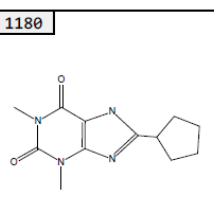
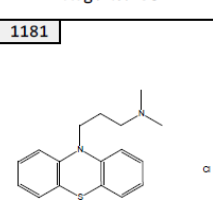
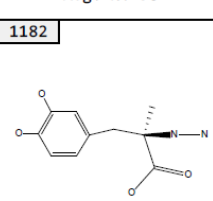
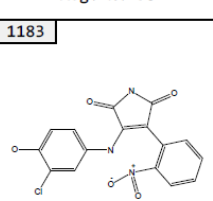
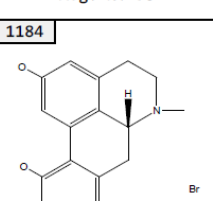
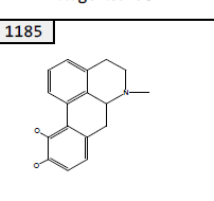
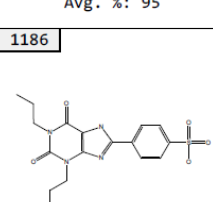
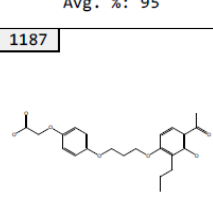
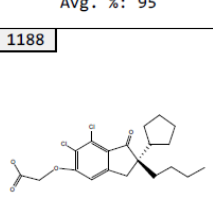
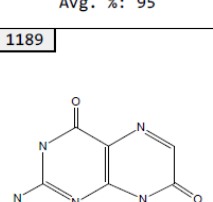
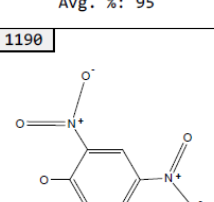
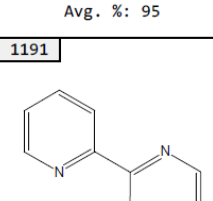
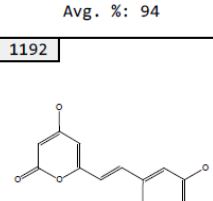
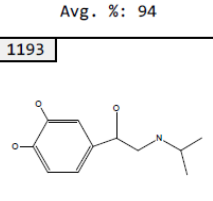
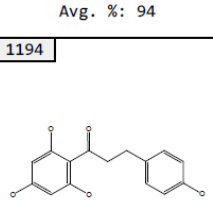
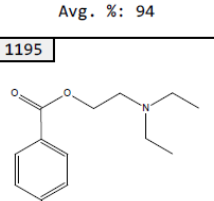
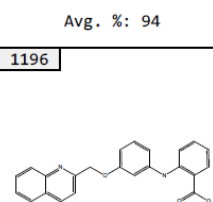
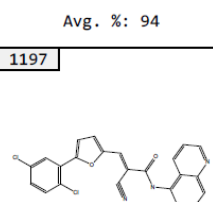
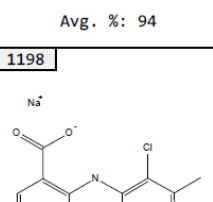
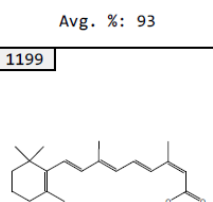
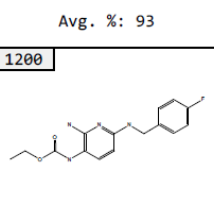
Continued, Table 21. Results of fluorescence-based electrophile screen of the LOPAC library. Values are presented as a percent of the MSTI signal (Avg. %). (n=3)

<p>1111</p>  <p>Avg. %: 99</p>	<p>1112</p>  <p>Avg. %: 99</p>	<p>1113</p>  <p>Avg. %: 99</p>	<p>1114</p>  <p>Avg. %: 98</p>	<p>1115</p>  <p>Avg. %: 98</p>
<p>1116</p>  <p>Avg. %: 98</p>	<p>1117</p>  <p>Avg. %: 98</p>	<p>1118</p>  <p>Avg. %: 98</p>	<p>1119</p>  <p>Avg. %: 98</p>	<p>1120</p>  <p>Avg. %: 98</p>
<p>1121</p>  <p>Avg. %: 98</p>	<p>1122</p>  <p>Avg. %: 98</p>	<p>1123</p>  <p>Avg. %: 98</p>	<p>1124</p>  <p>Avg. %: 98</p>	<p>1125</p>  <p>Avg. %: 98</p>
<p>1126</p>  <p>Avg. %: 98</p>	<p>1127</p>  <p>Avg. %: 98</p>	<p>1128</p>  <p>Avg. %: 98</p>	<p>1129</p>  <p>Avg. %: 98</p>	<p>1130</p>  <p>Avg. %: 97</p>
<p>1131</p>  <p>Avg. %: 97</p>	<p>1132</p>  <p>Avg. %: 97</p>	<p>1133</p>  <p>Avg. %: 97</p>	<p>1134</p>  <p>Avg. %: 97</p>	<p>1135</p>  <p>Avg. %: 97</p>
<p>1136</p>  <p>Avg. %: 97</p>	<p>1137</p>  <p>Avg. %: 97</p>	<p>1138</p>  <p>Avg. %: 97</p>	<p>1139</p>  <p>Avg. %: 97</p>	<p>1140</p>  <p>Avg. %: 97</p>

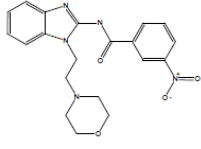
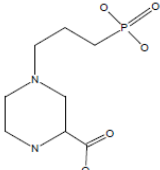
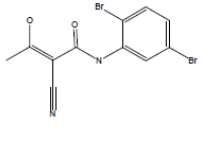
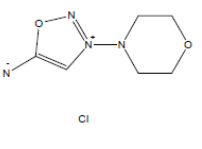
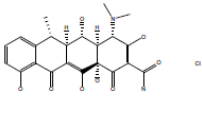
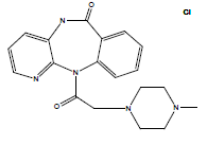
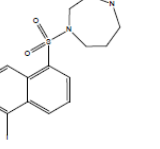
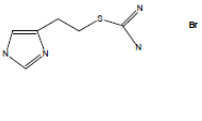
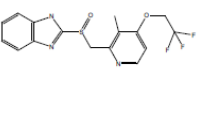
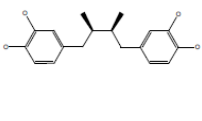
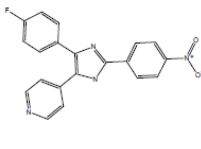
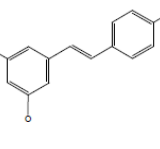
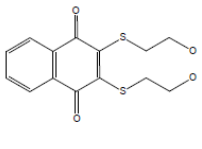
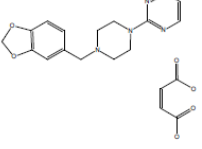
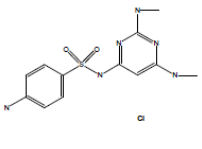
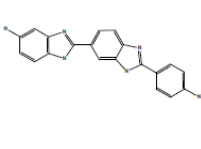
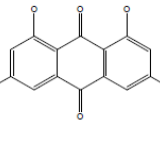
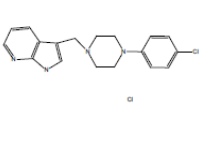
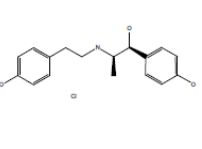
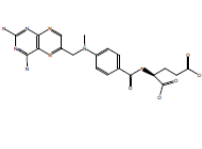
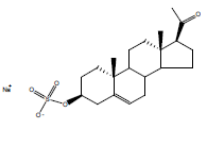
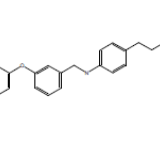
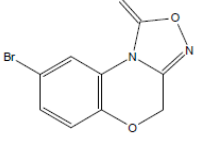
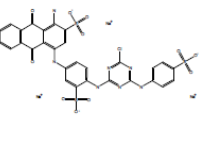
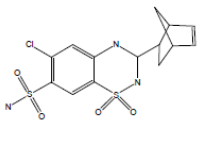
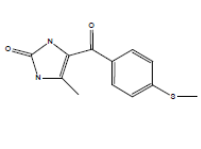
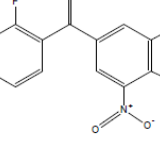
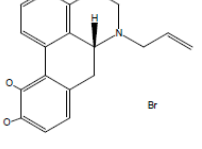
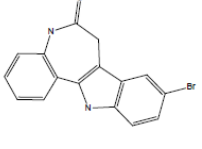
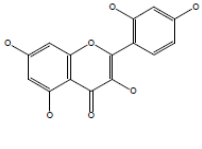
Continued, Table 21. Results of fluorescence-based electrophile screen of the LOPAC library. Values are presented as a percent of the MSTI signal (Avg. %). (n=3)

<p>1141</p>  <p>Avg. %: 97</p>	<p>1142</p>  <p>Avg. %: 97</p>	<p>1143</p>  <p>Avg. %: 97</p>	<p>1144</p>  <p>Avg. %: 97</p>	<p>1145</p>  <p>Avg. %: 97</p>
<p>1146</p>  <p>Avg. %: 97</p>	<p>1147</p>  <p>Avg. %: 97</p>	<p>1148</p>  <p>Avg. %: 97</p>	<p>1149</p>  <p>Avg. %: 97</p>	<p>1150</p>  <p>Avg. %: 97</p>
<p>1151</p>  <p>Avg. %: 97</p>	<p>1152</p>  <p>Avg. %: 97</p>	<p>1153</p>  <p>Avg. %: 97</p>	<p>1154</p>  <p>Avg. %: 96</p>	<p>1155</p>  <p>Avg. %: 96</p>
<p>1156</p>  <p>Avg. %: 96</p>	<p>1157</p>  <p>Avg. %: 96</p>	<p>1158</p>  <p>Avg. %: 96</p>	<p>1159</p>  <p>Avg. %: 96</p>	<p>1160</p>  <p>Avg. %: 96</p>
<p>1161</p>  <p>Avg. %: 96</p>	<p>1162</p>  <p>Avg. %: 96</p>	<p>1163</p>  <p>Avg. %: 96</p>	<p>1164</p>  <p>Avg. %: 96</p>	<p>1165</p>  <p>Avg. %: 96</p>
<p>1166</p>  <p>Avg. %: 96</p>	<p>1167</p>  <p>Avg. %: 96</p>	<p>1168</p>  <p>Avg. %: 96</p>	<p>1169</p>  <p>Avg. %: 96</p>	<p>1170</p>  <p>Avg. %: 96</p>

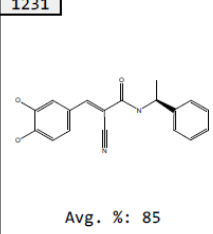
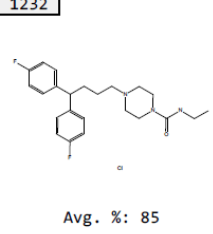
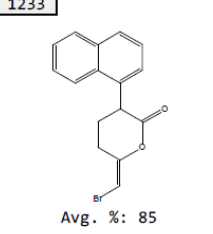
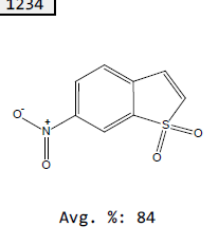
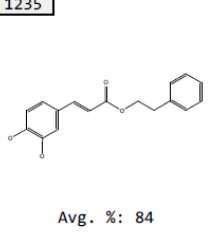
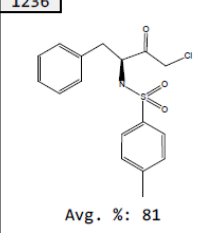
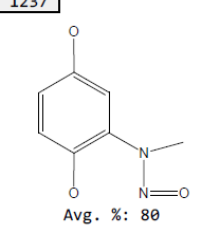
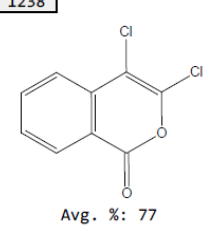
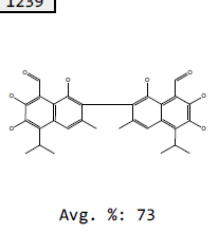
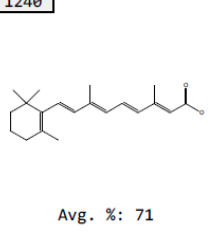
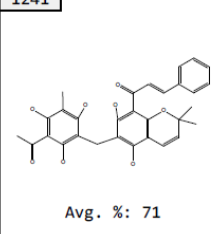
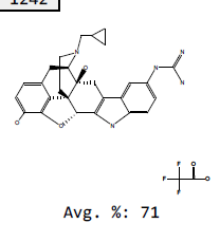
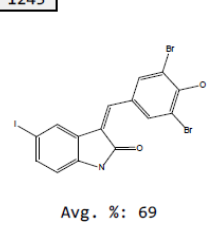
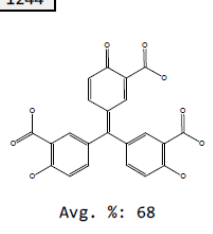
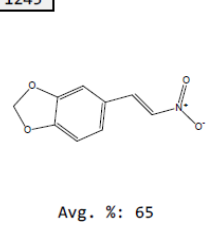
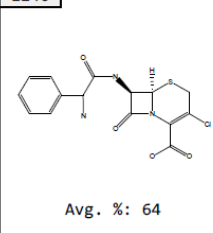
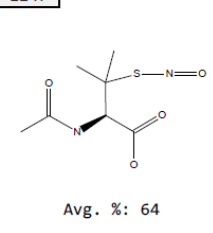
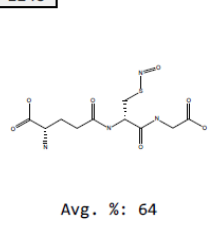
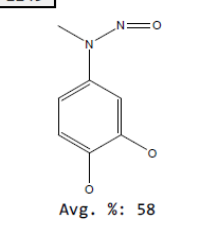
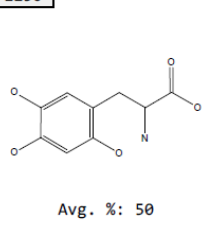
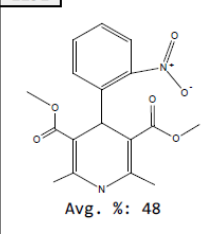
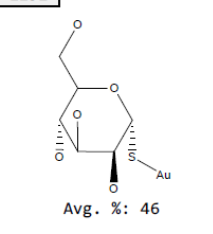
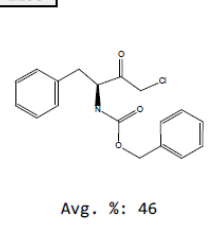
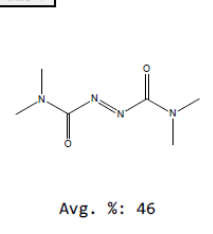
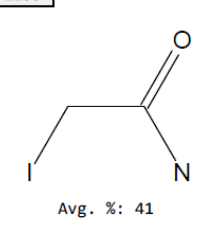
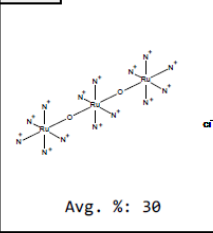
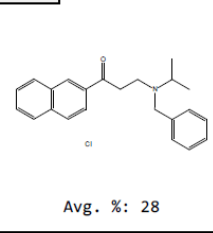
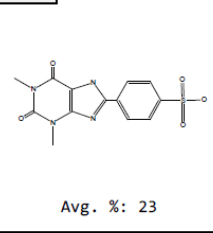
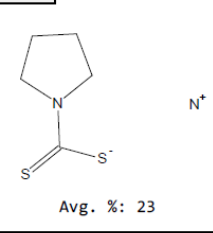
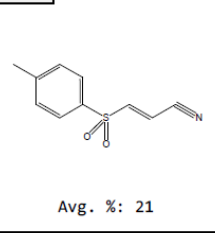
Continued, Table 21. Results of fluorescence-based electrophile screen of the LOPAC library. Values are presented as a percent of the MSTI signal (Avg. %). (n=3)

<p>1171</p>  <p>Avg. %: 95</p>	<p>1172</p>  <p>Avg. %: 95</p>	<p>1173</p>  <p>Avg. %: 95</p>	<p>1174</p>  <p>Avg. %: 95</p>	<p>1175</p>  <p>Avg. %: 95</p>
<p>1176</p>  <p>Avg. %: 95</p>	<p>1177</p>  <p>Avg. %: 95</p>	<p>1178</p>  <p>Avg. %: 95</p>	<p>1179</p>  <p>Avg. %: 95</p>	<p>1180</p>  <p>Avg. %: 95</p>
<p>1181</p>  <p>Avg. %: 95</p>	<p>1182</p>  <p>Avg. %: 95</p>	<p>1183</p>  <p>Avg. %: 95</p>	<p>1184</p>  <p>Avg. %: 95</p>	<p>1185</p>  <p>Avg. %: 95</p>
<p>1186</p>  <p>Avg. %: 95</p>	<p>1187</p>  <p>Avg. %: 94</p>	<p>1188</p>  <p>Avg. %: 94</p>	<p>1189</p>  <p>Avg. %: 94</p>	<p>1190</p>  <p>Avg. %: 94</p>
<p>1191</p>  <p>Avg. %: 94</p>	<p>1192</p>  <p>Avg. %: 94</p>	<p>1193</p>  <p>Avg. %: 94</p>	<p>1194</p>  <p>Avg. %: 93</p>	<p>1195</p>  <p>Avg. %: 93</p>
<p>1196</p>  <p>Avg. %: 93</p>	<p>1197</p>  <p>Avg. %: 93</p>	<p>1198</p>  <p>Avg. %: 93</p>	<p>1199</p>  <p>Avg. %: 93</p>	<p>1200</p>  <p>Avg. %: 93</p>

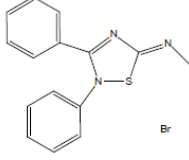
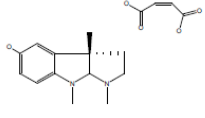
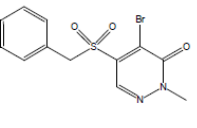
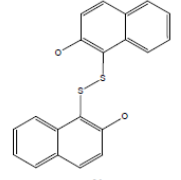
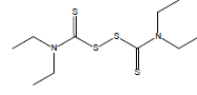
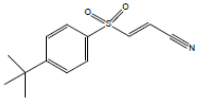
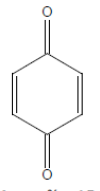
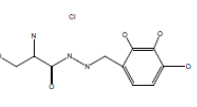
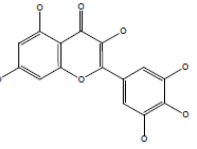
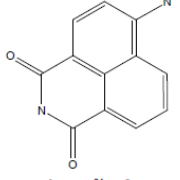
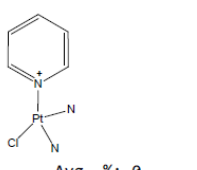
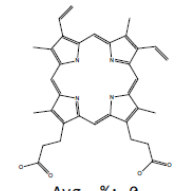
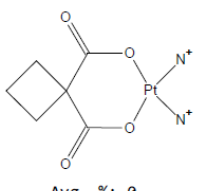
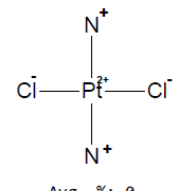
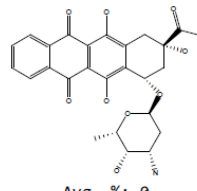
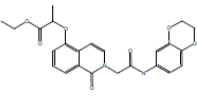
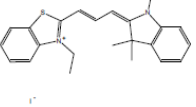
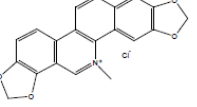
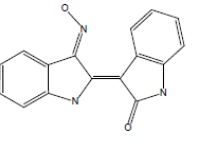
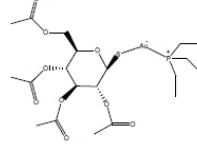
Continued, Table 21. Results of fluorescence-based electrophile screen of the LOPAC library. Values are presented as a percent of the MSTI signal (Avg. %). (n=3)

<p>1201</p>  <p>Avg. %: 93</p>	<p>1202</p>  <p>Avg. %: 93</p>	<p>1203</p>  <p>Avg. %: 93</p>	<p>1204</p>  <p>Avg. %: 93</p>	<p>1205</p>  <p>Avg. %: 92</p>
<p>1206</p>  <p>Avg. %: 92</p>	<p>1207</p>  <p>Avg. %: 92</p>	<p>1208</p>  <p>Avg. %: 92</p>	<p>1209</p>  <p>Avg. %: 92</p>	<p>1210</p>  <p>Avg. %: 92</p>
<p>1211</p>  <p>Avg. %: 91</p>	<p>1212</p>  <p>Avg. %: 91</p>	<p>1213</p>  <p>Avg. %: 91</p>	<p>1214</p>  <p>Avg. %: 90</p>	<p>1215</p>  <p>Avg. %: 90</p>
<p>1216</p>  <p>Avg. %: 89</p>	<p>1217</p>  <p>Avg. %: 89</p>	<p>1218</p>  <p>Avg. %: 89</p>	<p>1219</p>  <p>Avg. %: 89</p>	<p>1220</p>  <p>Avg. %: 89</p>
<p>1221</p>  <p>Avg. %: 88</p>	<p>1222</p>  <p>Avg. %: 88</p>	<p>1223</p>  <p>Avg. %: 87</p>	<p>1224</p>  <p>Avg. %: 87</p>	<p>1225</p>  <p>Avg. %: 87</p>
<p>1226</p>  <p>Avg. %: 87</p>	<p>1227</p>  <p>Avg. %: 86</p>	<p>1228</p>  <p>Avg. %: 86</p>	<p>1229</p>  <p>Avg. %: 85</p>	<p>1230</p>  <p>Avg. %: 85</p>

Continued, Table 21. Results of fluorescence-based electrophile screen of the LOPAC library. Values are presented as a percent of the MSTI signal (Avg. %). (n=3)

1231  Avg. %: 85	1232  Avg. %: 85	1233  Avg. %: 85	1234  Avg. %: 84	1235  Avg. %: 84
1236  Avg. %: 81	1237  Avg. %: 80	1238  Avg. %: 77	1239  Avg. %: 73	1240  Avg. %: 71
1241  Avg. %: 71	1242  Avg. %: 71	1243  Avg. %: 69	1244  Avg. %: 68	1245  Avg. %: 65
1246  Avg. %: 64	1247  Avg. %: 64	1248  Avg. %: 64	1249  Avg. %: 58	1250  Avg. %: 50
1251  Avg. %: 48	1252  Avg. %: 46	1253  Avg. %: 46	1254  Avg. %: 46	1255  Avg. %: 41
1256  Avg. %: 30	1257  Avg. %: 28	1258  Avg. %: 23	1259  Avg. %: 23	1260  Avg. %: 21

Continued, Table 21. Results of fluorescence-based electrophile screen of the LOPAC library. Values are presented as a percent of the MSTI signal (Avg. %). (n=3)

<p>1261</p>  <p>Avg. %: 20</p>	<p>1262</p>  <p>Avg. %: 19</p>	<p>1263</p>  <p>Avg. %: 19</p>	<p>1264</p>  <p>Avg. %: 19</p>	<p>1265</p>  <p>Avg. %: 18</p>
<p>1266</p>  <p>Avg. %: 18</p>	<p>1267</p>  <p>Avg. %: 15</p>	<p>1268</p>  <p>Avg. %: 13</p>	<p>1269</p>  <p>Avg. %: 5</p>	<p>1270</p>  <p>Avg. %: 0</p>
<p>1271</p>  <p>Avg. %: 0</p>	<p>1272</p>  <p>Avg. %: 0</p>	<p>1273</p>  <p>Avg. %: 0</p>	<p>1274</p>  <p>Avg. %: 0</p>	<p>1275</p>  <p>Avg. %: 0</p>
<p>1276</p>  <p>Avg. %: 0</p>	<p>1277</p>  <p>Avg. %: 0</p>	<p>1278</p>  <p>Avg. %: 0</p>	<p>1279</p>  <p>Avg. %: 0</p>	<p>1280</p>  <p>Avg. %: 0</p>

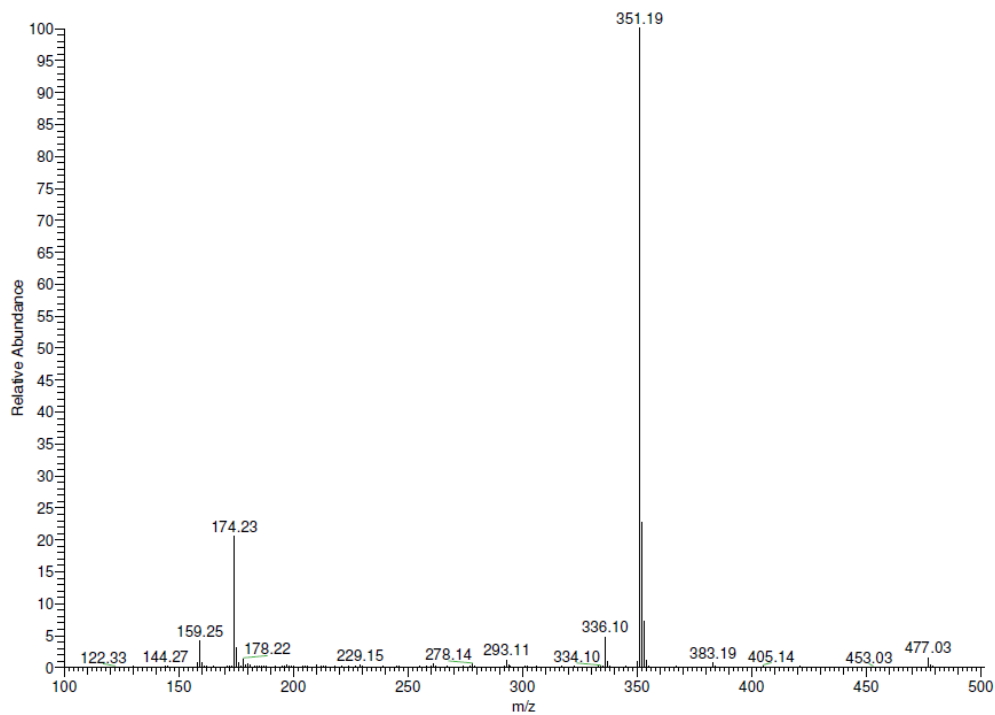


Figure 62. Mass spectrum of 2-iodoacetamide-MSTI conjugate; ESI probe, 80 V entrance cone, 3 mV capillary, and 350 °C probe temperature.

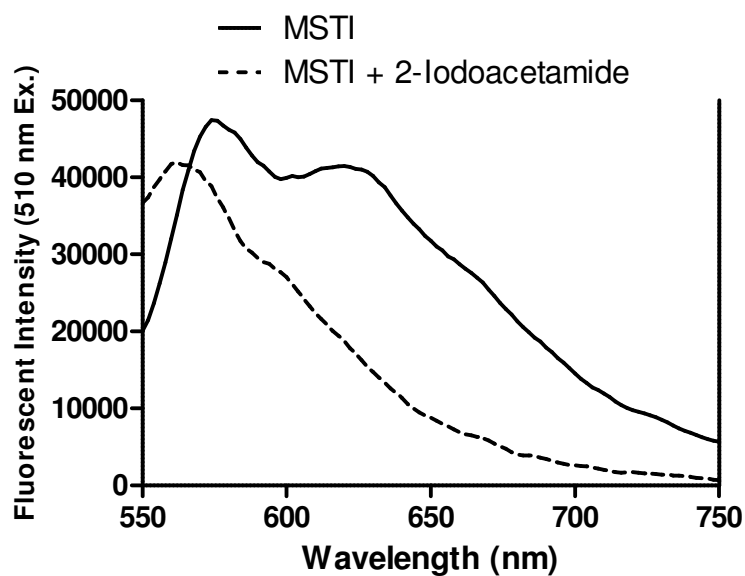


Figure 63. Fluorescence spectrum of 2-iodoacetamide-MSTI conjugate with an excitation wavelength of 510 nm.

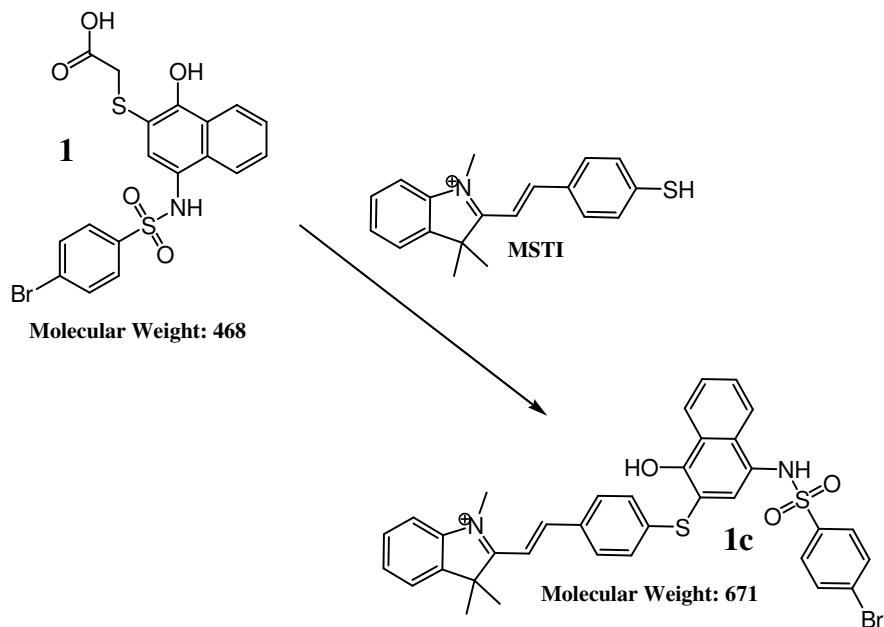


Figure 64. Addition of MSTI to small molecule 1 to form adduct molecule 1c.

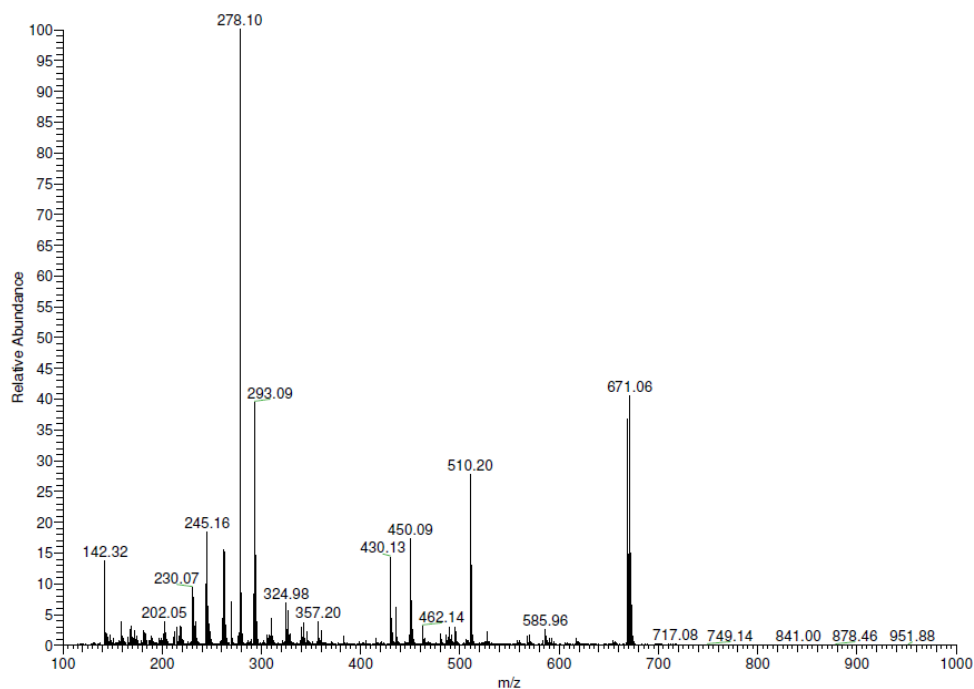


Figure 65. Mass spectrum of adduct molecule 1c formed in Scheme 1. Mass spectrum of the assay mixture in Scheme 1 which confirms the formation of adduct of MSTI with the small molecule (Molecule 1). ESI probe, 120 V entrance cone, 3 mV capillary, and 350 °C probe temperature.

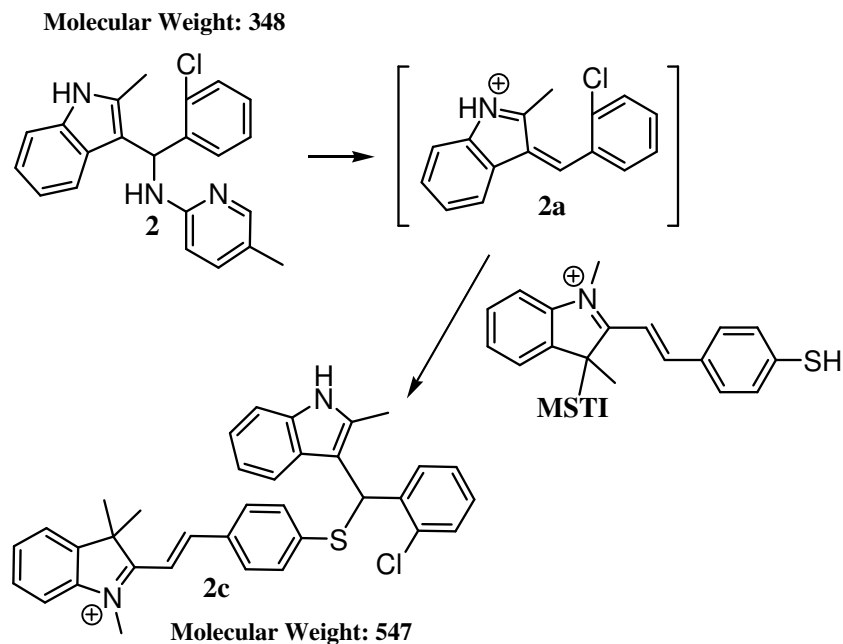


Figure 66. Addition of MSTI to small molecule 2 to form adduct molecule 2c.

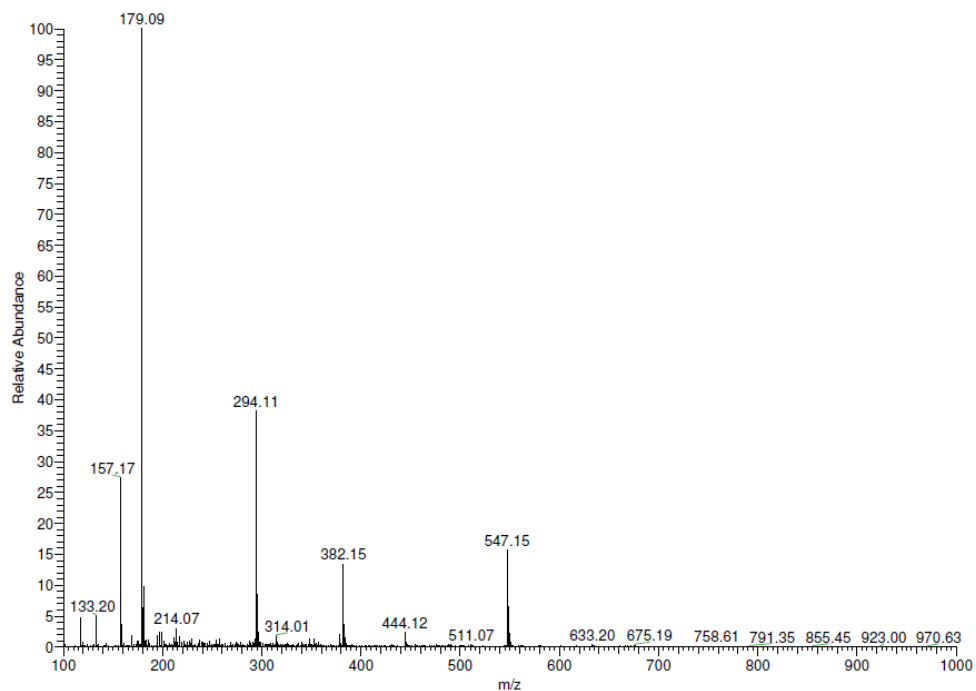


Figure 67. Mass spectrum of adduct molecule 2c formed in Scheme 2. Mass spectrum of the assay mixture in Scheme 1 which confirms the formation of adduct of MSTI with the small molecule (Molecule 2). ESI probe, 40 V entrance cone, 3 mV capillary, and 350 °C probe temperature.

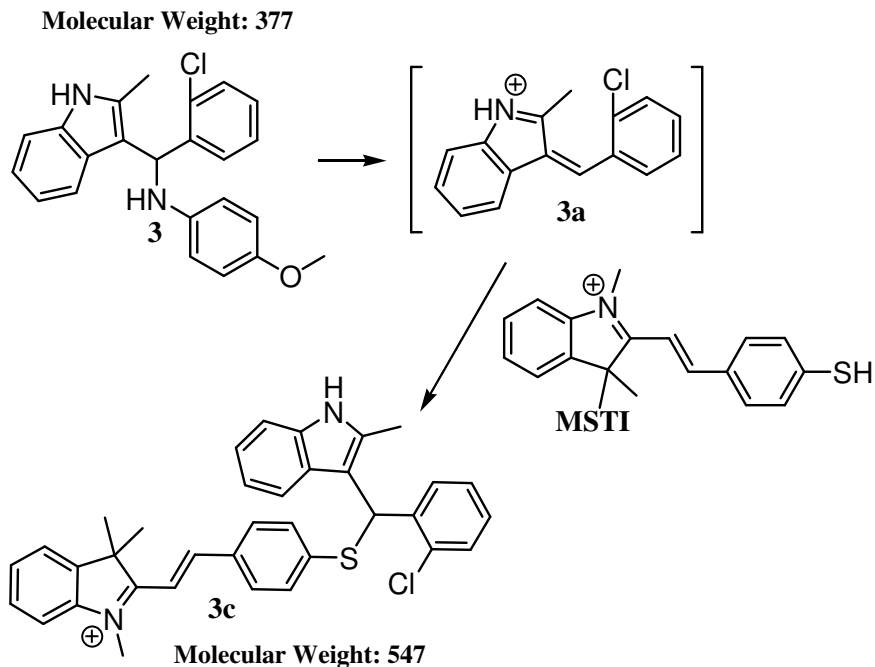


Figure 68. Addition of MSTI to small molecule 3 to form adduct molecule 3c.

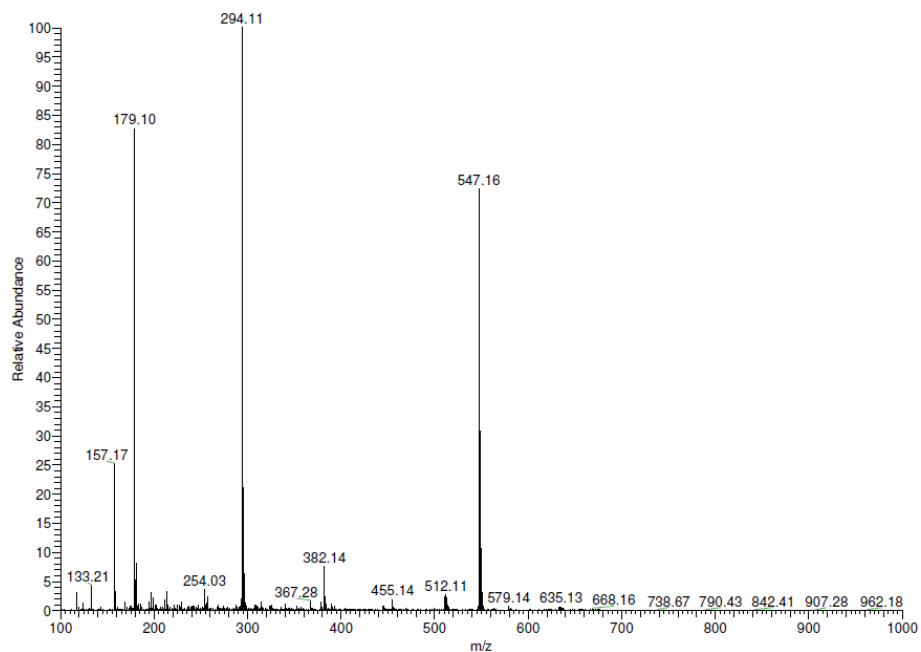


Figure 69. Mass spectrum of adduct molecule 3c formed in Scheme 3. Mass spectrum of the assay mixture in Scheme 3 which confirms the formation of adduct of MSTI with the small molecule (Molecule 3). ESI probe, 40 V entrance cone, 3 mV capillary, and 350 °C probe temperature.

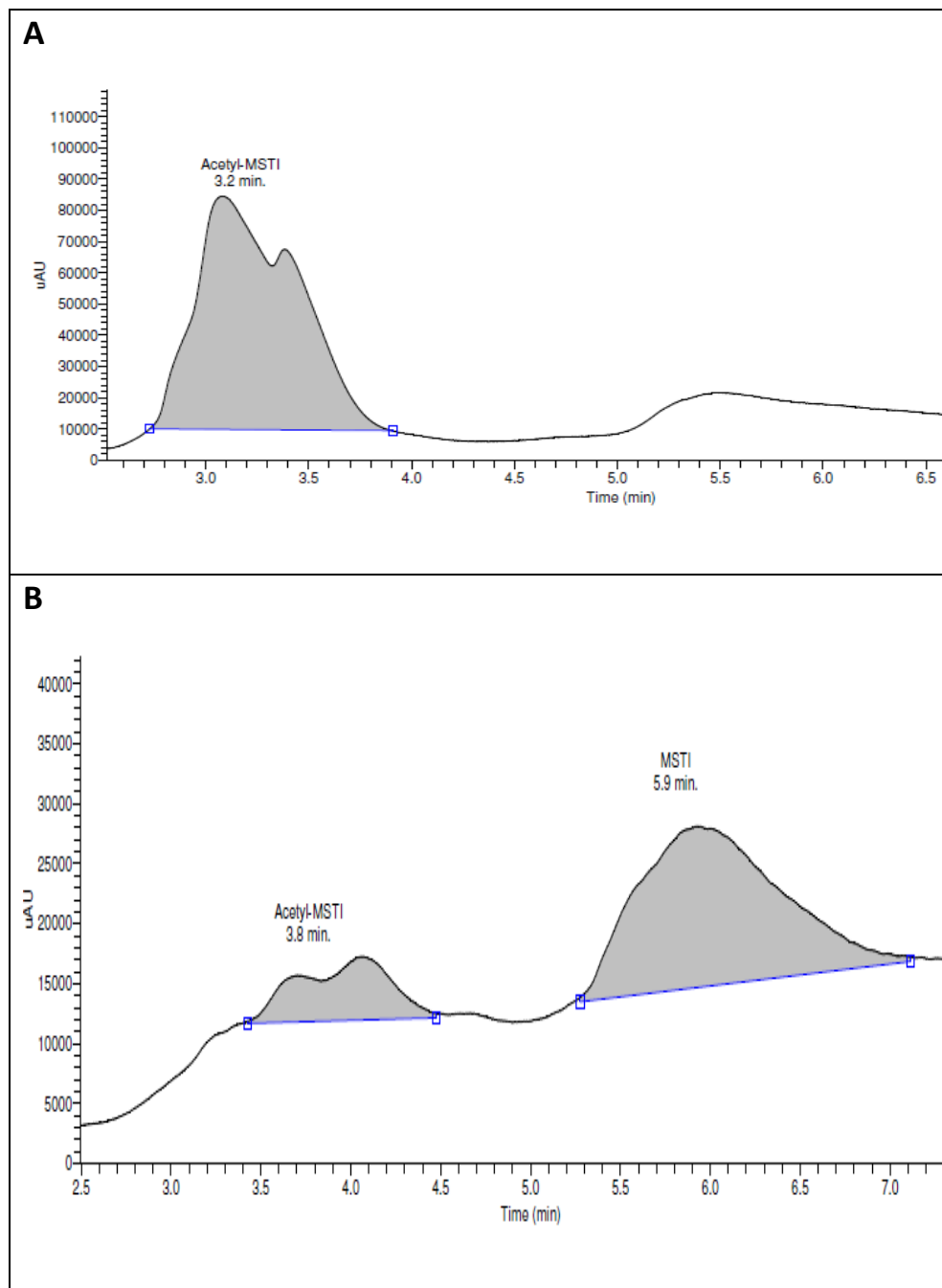


Figure 70. Conversion of acetyl-MSTI to MSTI analyzed by LC-MS. A) Chromatogram of acetyl-MSTI B) Chromatogram of MSTI after conversion at pH 12 with approximately 20% acetyl-MSTI remaining.

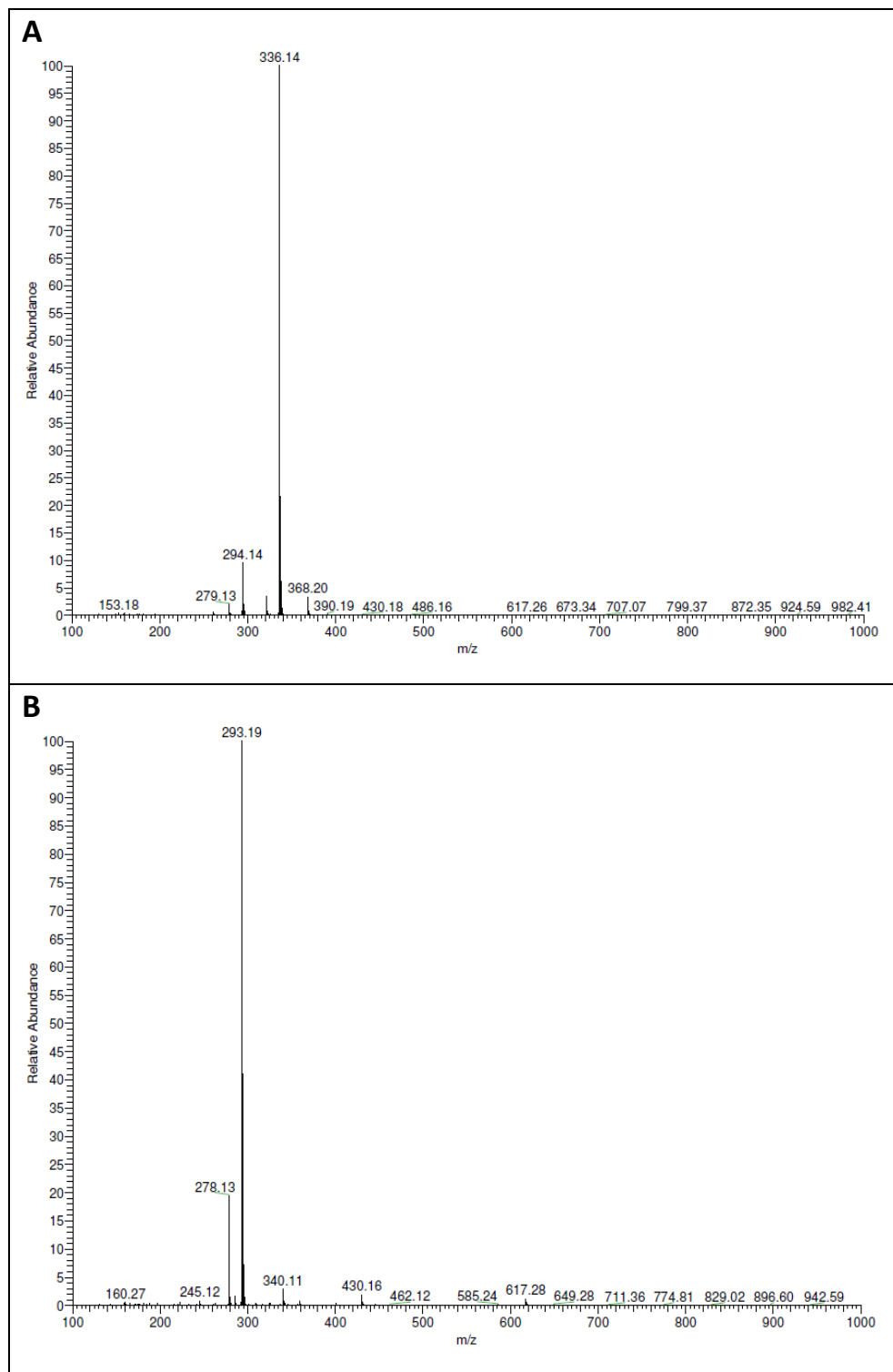


Figure 71. Mass spectra of MSTI (A) and acetyl-MSTI (B), corresponding to the chromatograms in Figure 6. ESI probe, 80 V entrance cone, 3 mV capillary, and 350 °C probe temperature.

APPENDIX D

COMPETITIVE PROTEIN BINDING

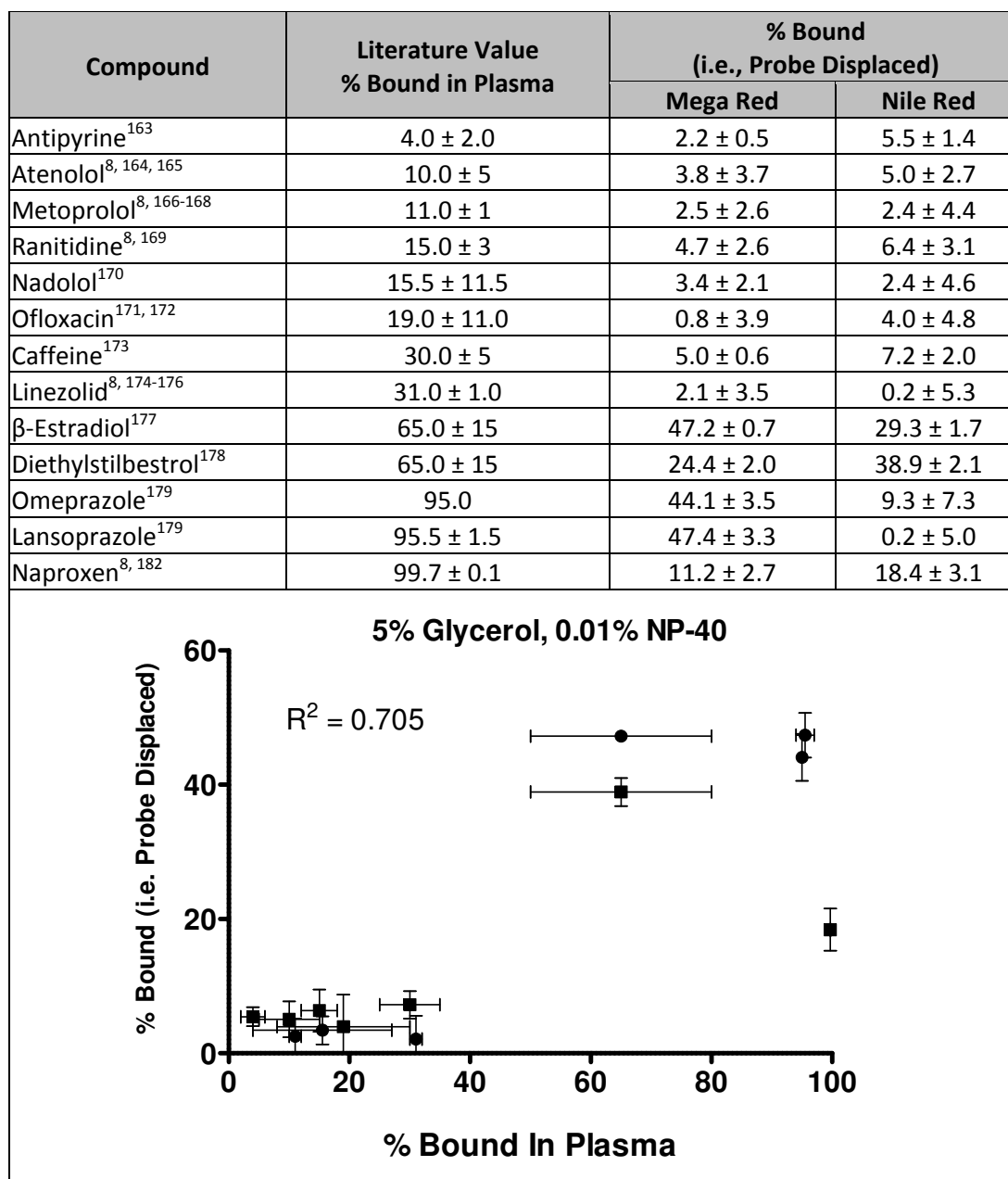


Figure 72. Standard small molecule displacement of 500 nM Mega Red and Nile Red in PBS with 5% glycerol and 0.01% NP-40 by volume in the presence of 0.2 mg/mL HSA (n=3). Average of literature values for *in vivo* plasma protein binding are given in comparison. Larger % bound values used for the plot.

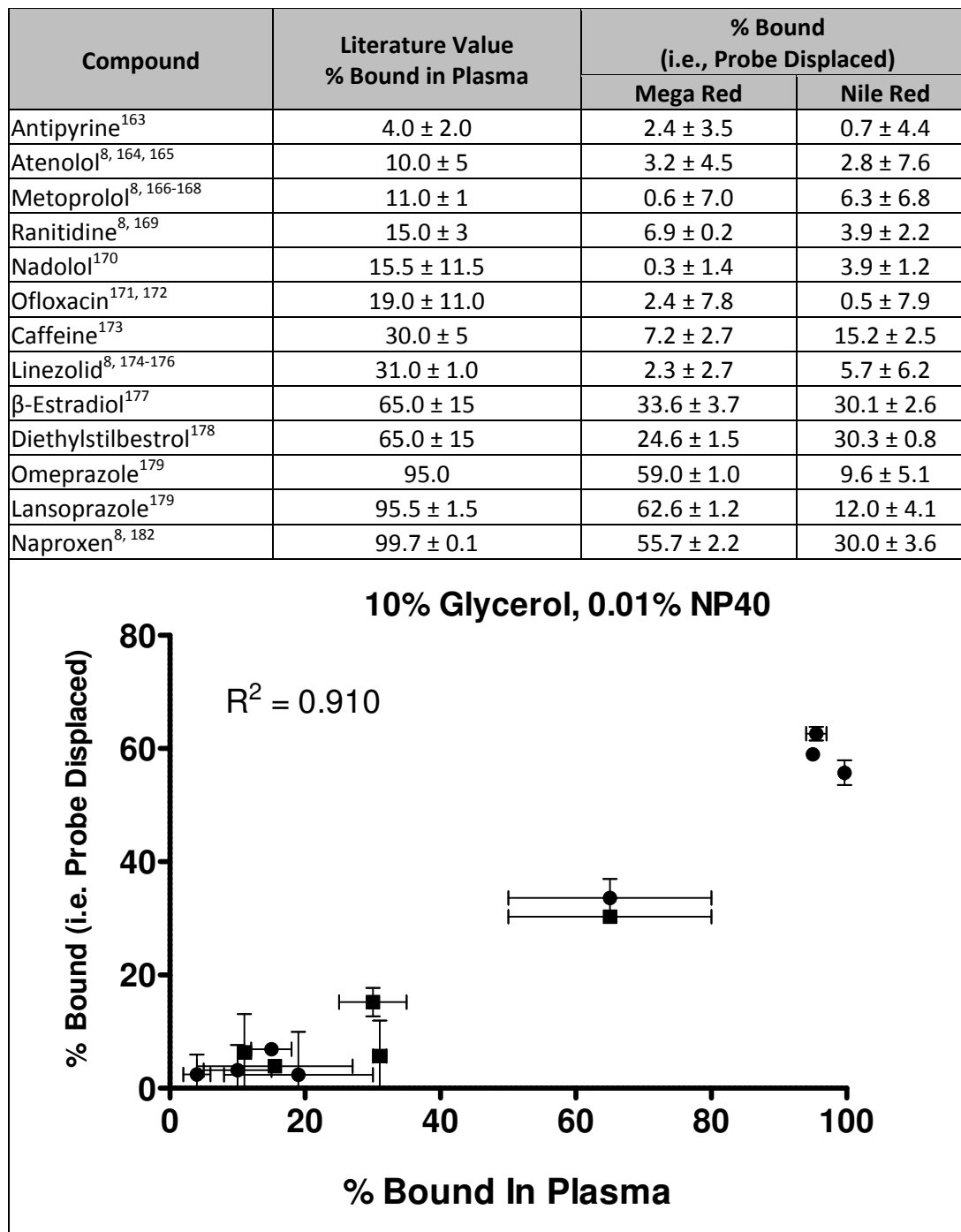


Figure 73. Standard small molecule displacement of 500 nM Mega Red and Nile Red in PBS with 10% glycerol and 0.01% NP-40 by volume in the presence of 0.2 mg/mL HSA (n=3). Averages of literature values for *in vivo* plasma protein binding are given in comparison. Larger % bound values used for the plot.

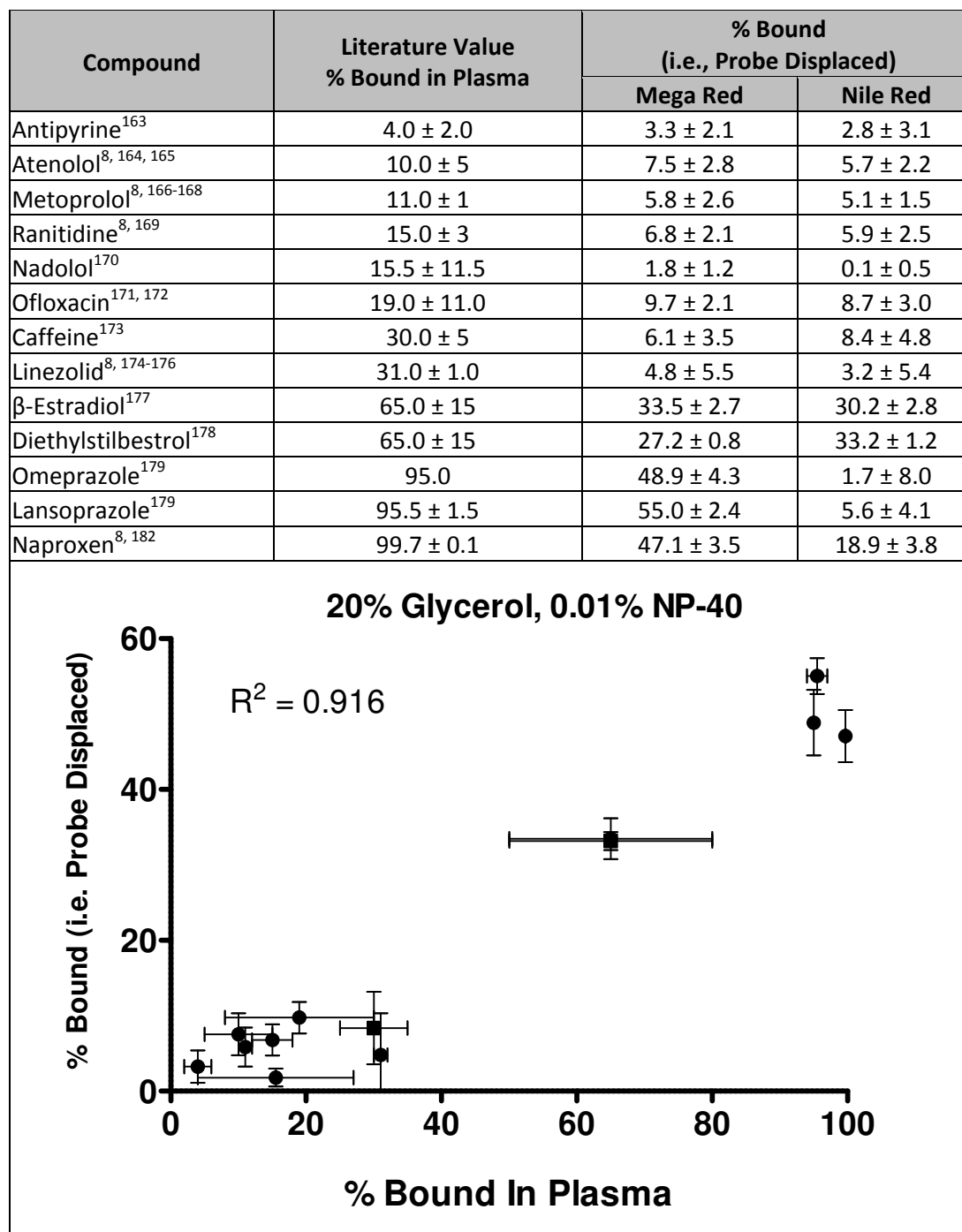


Figure 74. Standard small molecule displacement of 500 nM Mega Red and Nile Red in PBS with 20% glycerol and 0.01% NP-40 by volume in the presence of 0.2 mg/mL HSA (n=3). Averages of literature values for *in vivo* plasma protein binding are given in comparison. Larger % bound values used for the plot.

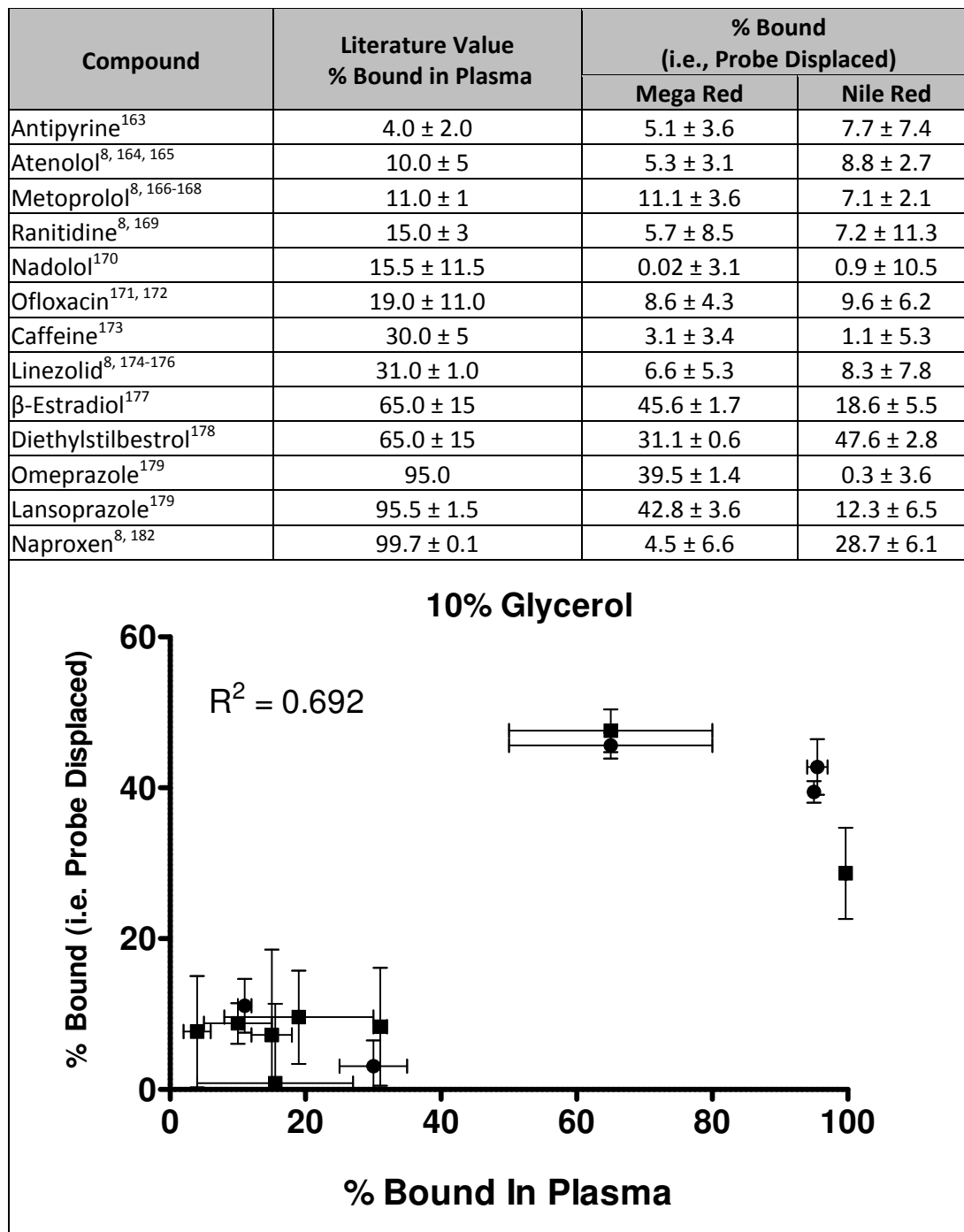


Figure 75. Standard small molecule displacement of 500 nM Mega Red and Nile Red in PBS with 10% glycerol by volume in the presence of 0.2 mg/mL HSA (n=3). Averages of literature values for *in vivo* plasma protein binding are given in comparison. Larger % bound values used for the plot.

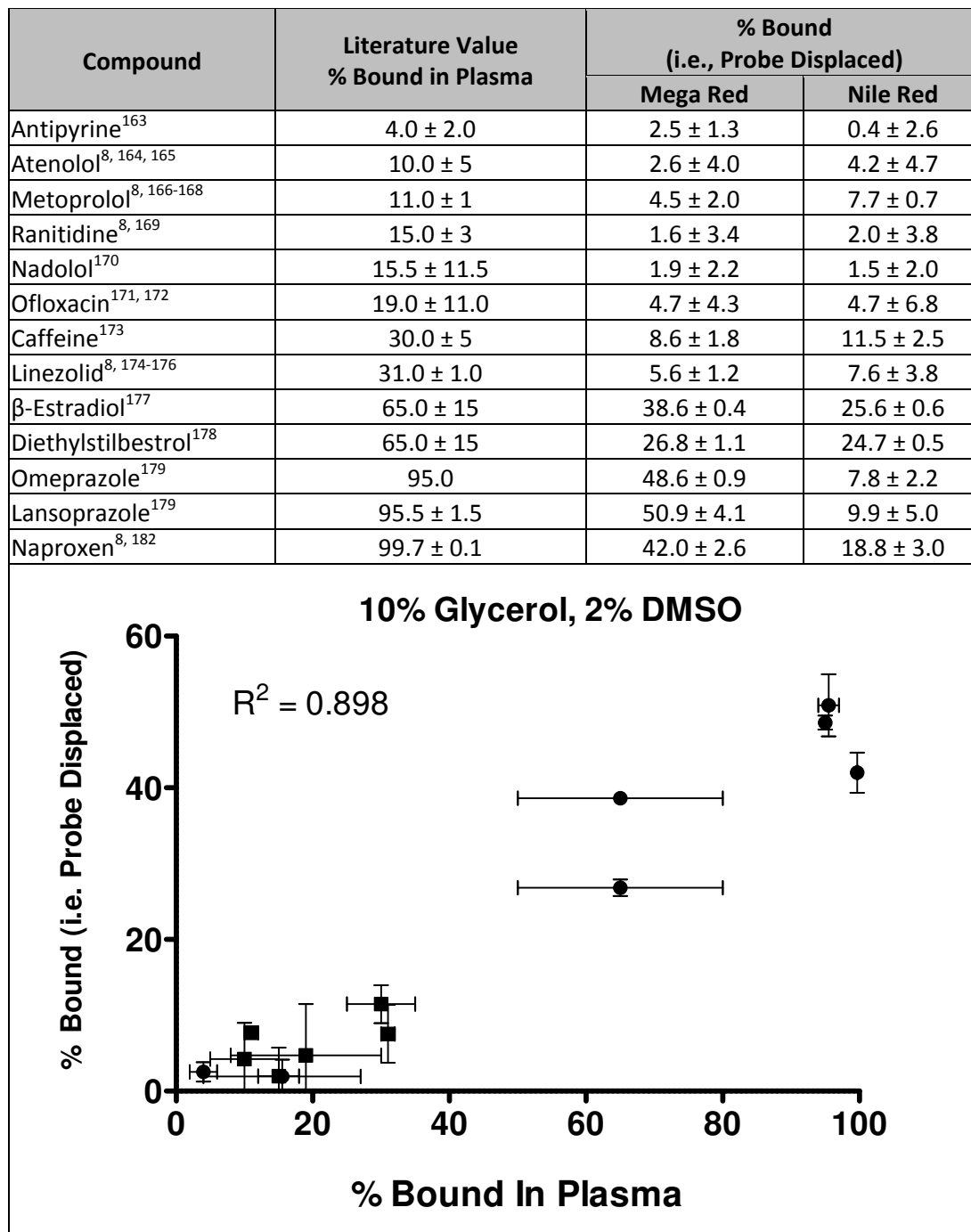


Figure 76. Standard small molecule displacement of 500 nM Mega Red and Nile Red in PBS with 10% glycerol and 2% DMSO by volume in the presence of 0.2 mg/mL HSA (n=3). Averages of literature values for *in vivo* plasma protein binding are given in comparison. Larger % bound values used for the plot.

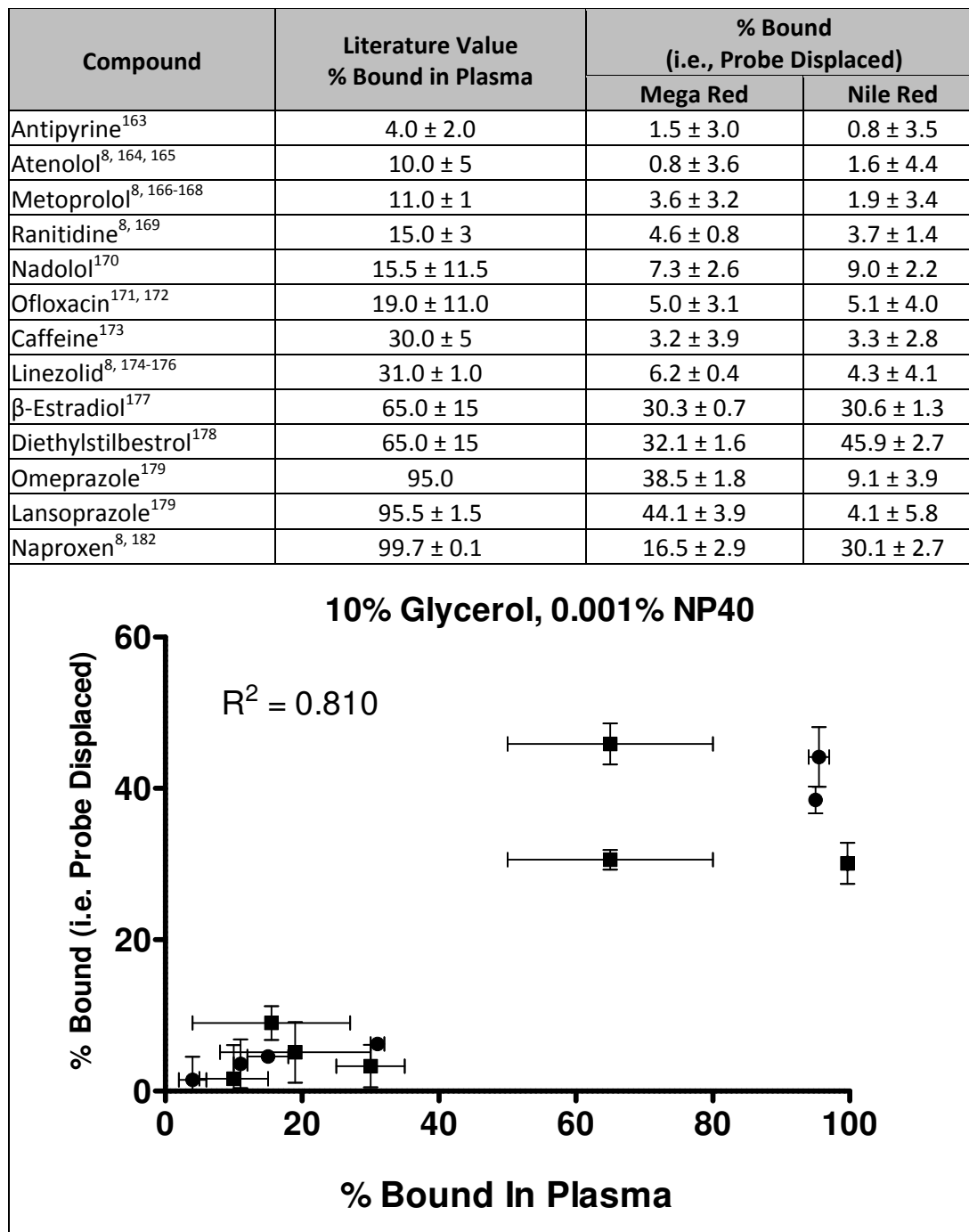


Figure 77. Standard small molecule displacement of 500 nM Mega Red and Nile Red in PBS with 10% glycerol and 0.001% NP-40 by volume in the presence of 0.2 mg/mL HSA (n=3). Averages of literature values for *in vivo* plasma protein binding are given in comparison. Larger % bound values used for the plot.

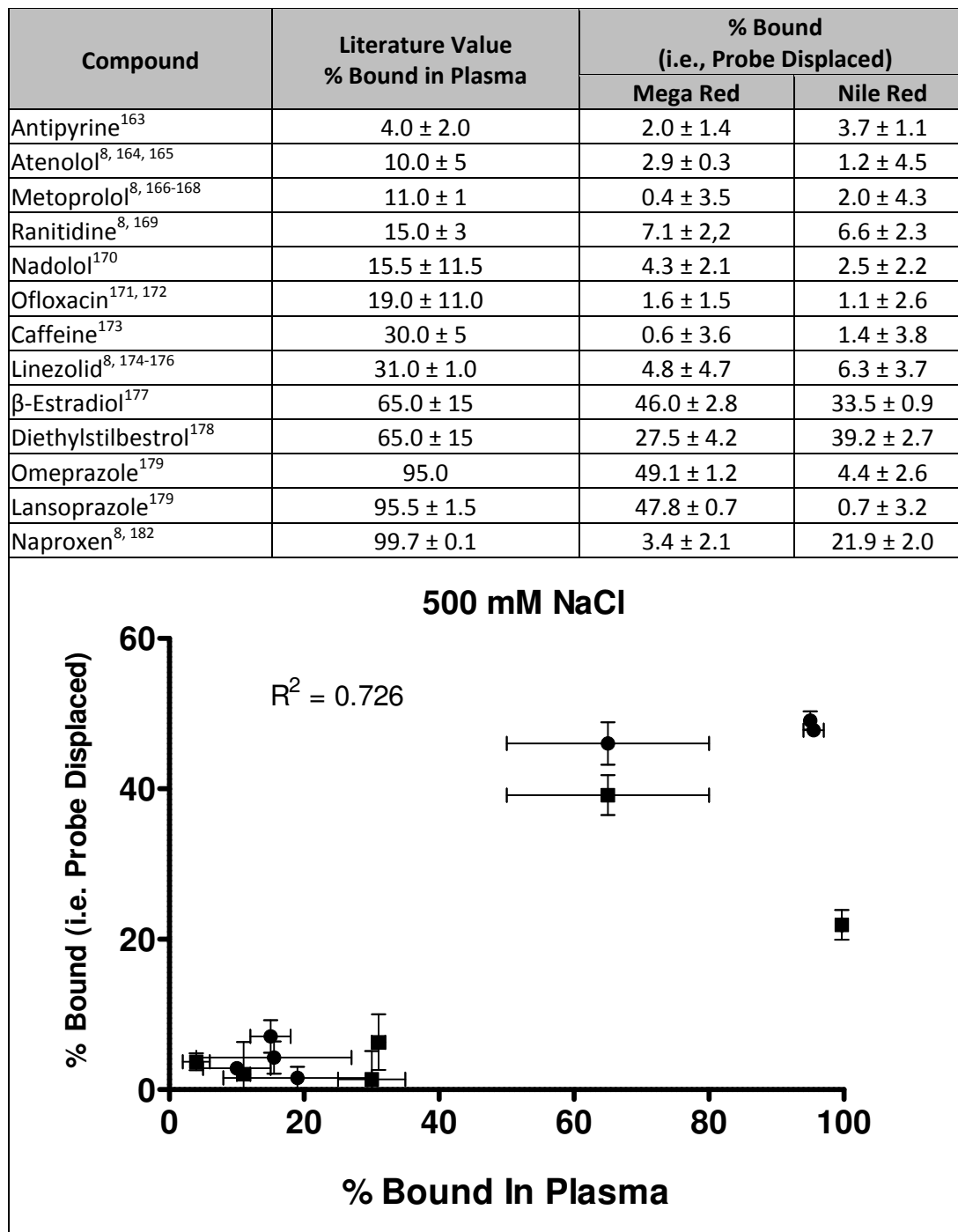


Figure 78. Standard small molecule displacement of 500 nM Mega Red and Nile Red in PBS with 500 mM NaCl in the presence of 0.2 mg/mL HSA (n=3). Averages of literature values for *in vivo* plasma protein binding are given in comparison. Larger % bound values used for the plot.

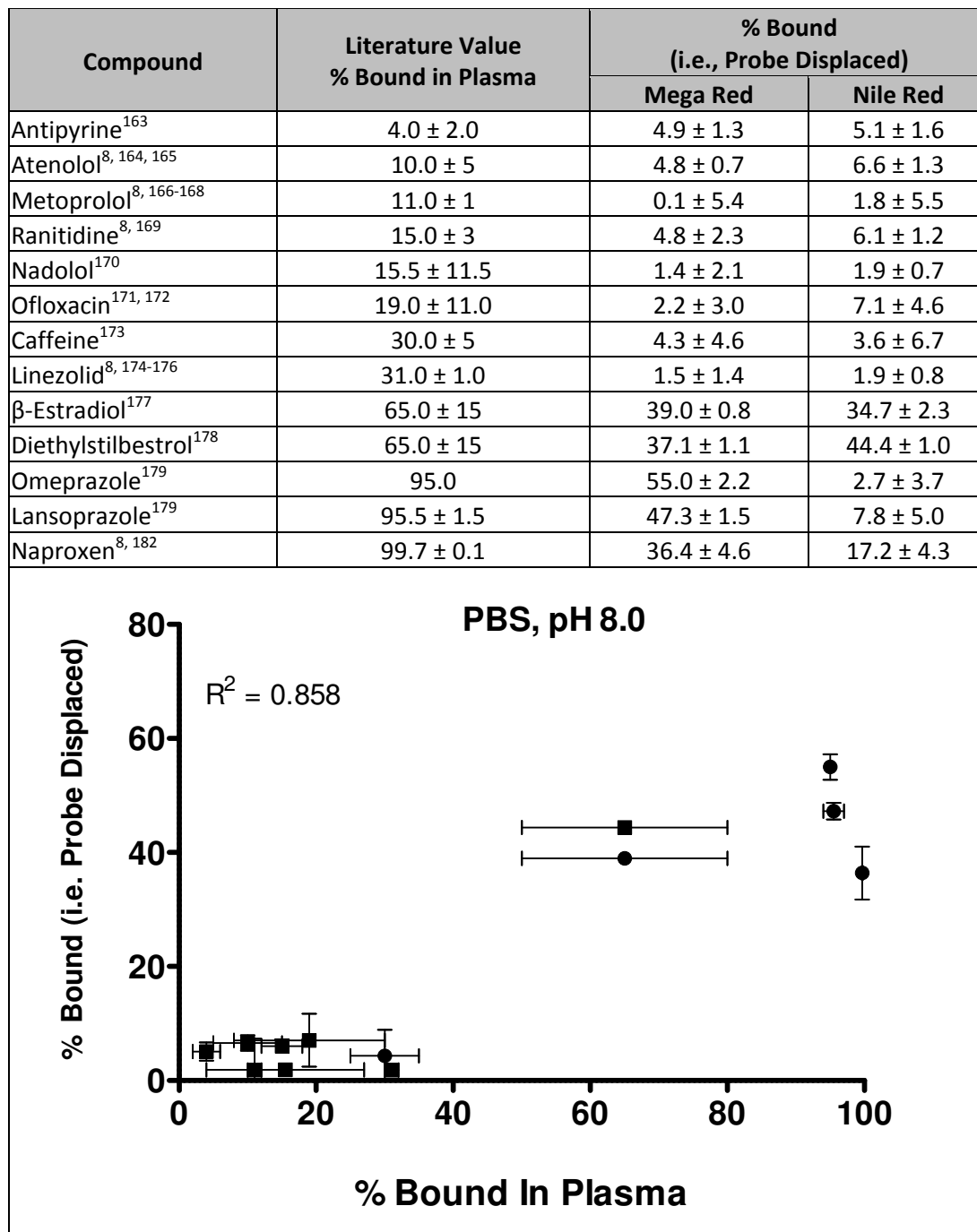


Figure 79. Standard small molecule displacement of 500 nM Mega Red and Nile Red in PBS at pH 8.0 in the presence of 0.2 mg/mL HSA (n=3). Averages of literature values for *in vivo* plasma protein binding are given in comparison. Larger % bound values used for the plot.

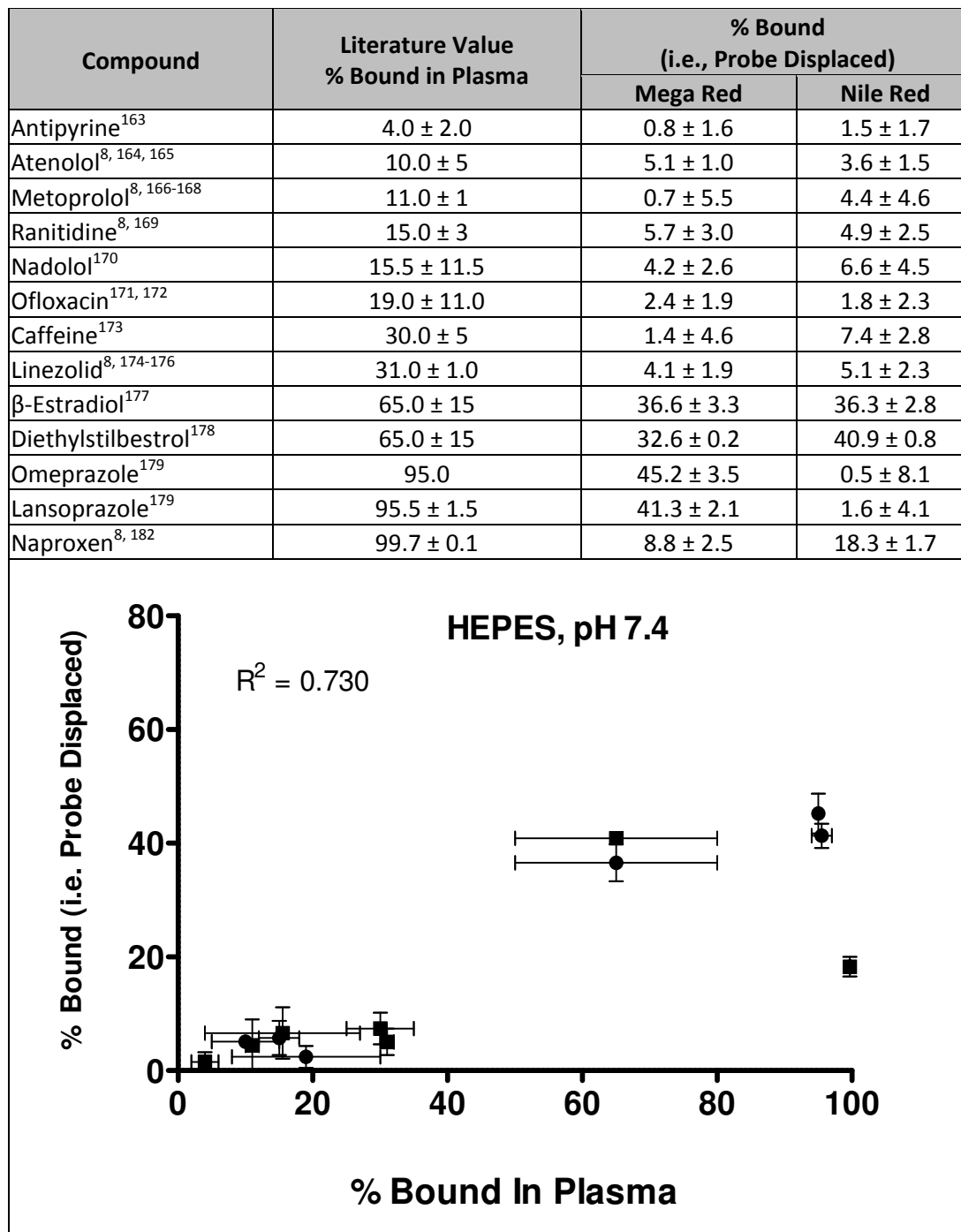
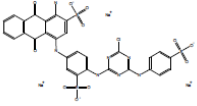
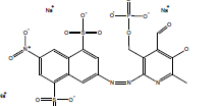
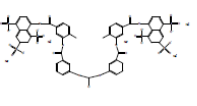
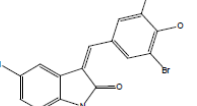
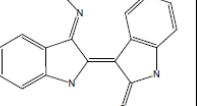
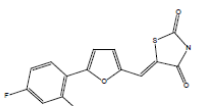
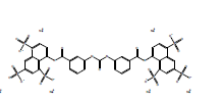
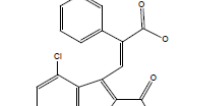
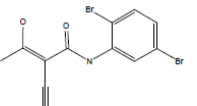
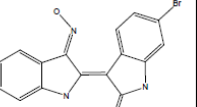
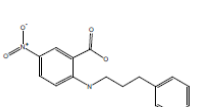
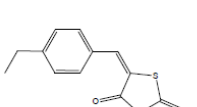
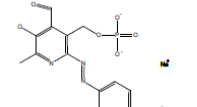
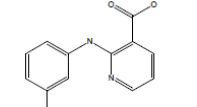
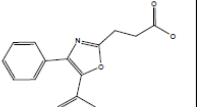
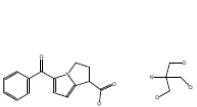
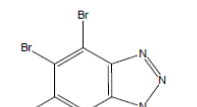
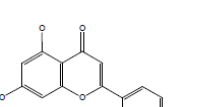
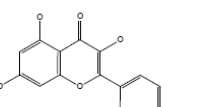
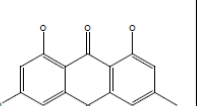
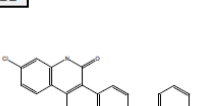
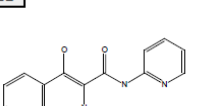
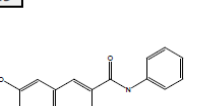
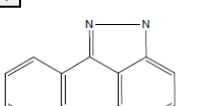
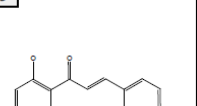
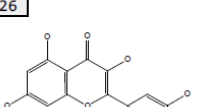
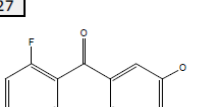
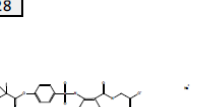
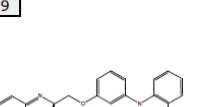
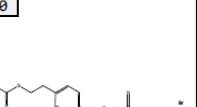
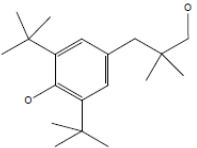
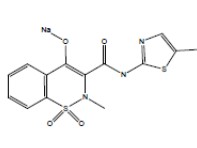
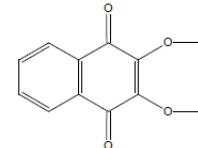
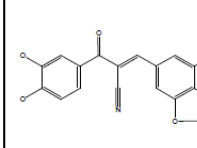
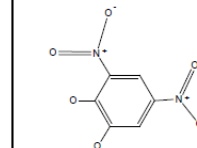
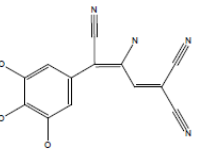
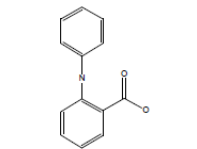
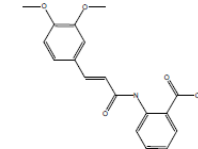
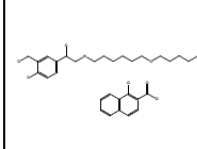
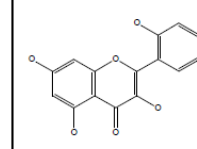
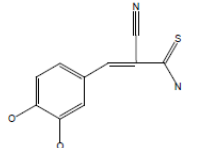
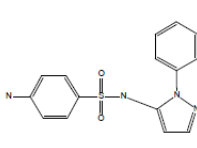
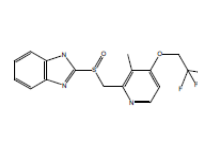
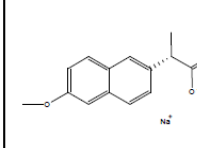
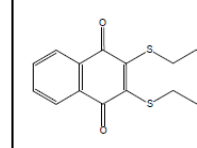
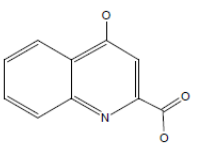
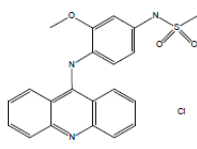
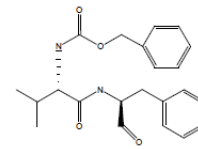
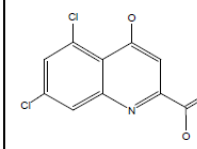
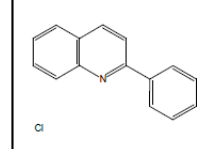
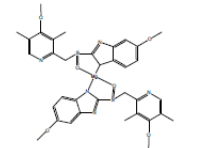
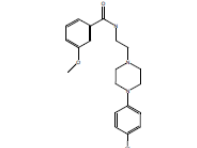
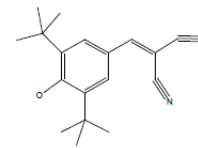
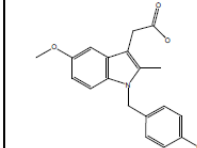
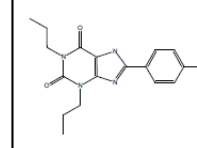
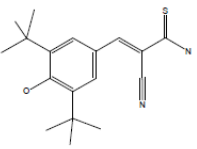
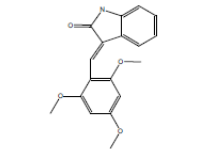
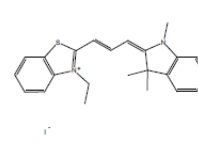
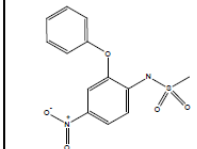
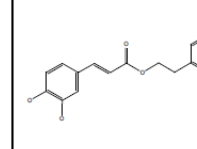


Figure 80. Standard small molecule displacement of 500 nM Mega Red and Nile Red in 200 mM HEPES buffer at pH 7.4 in the presence of 0.2 mg/mL HSA (n=3). Averages of literature values for *in vivo* plasma protein binding are given in comparison. Larger % bound values used for the plot.

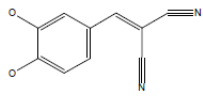
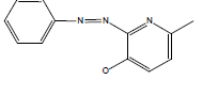
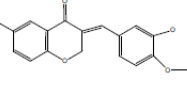
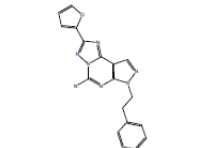
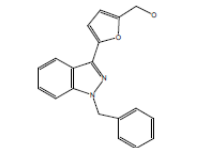
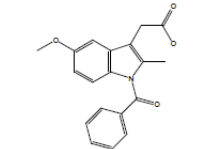
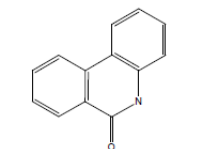
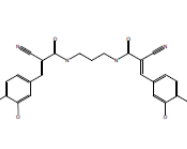
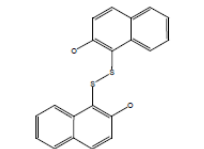
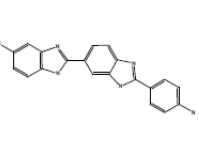
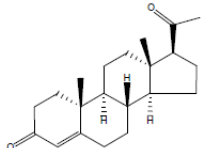
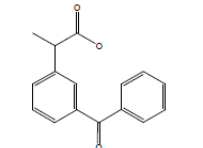
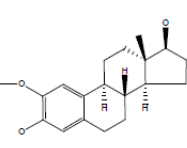
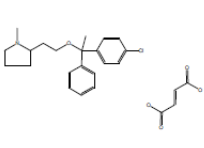
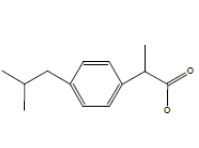
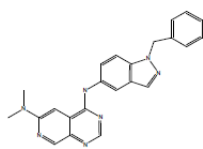
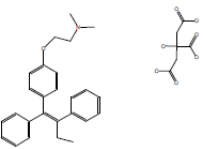
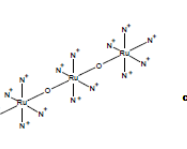
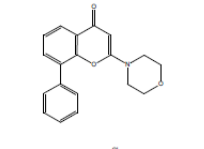
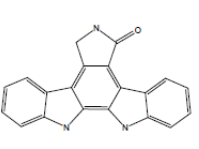
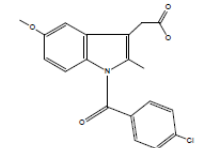
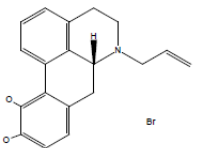
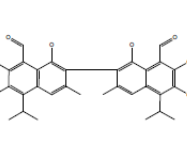
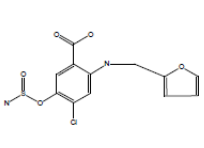
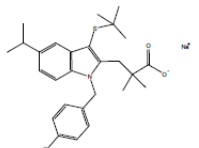
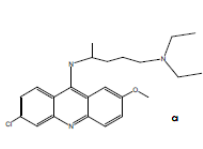
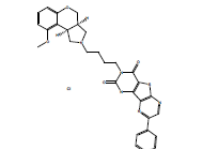
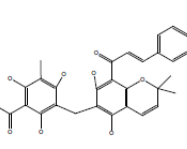
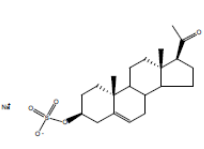
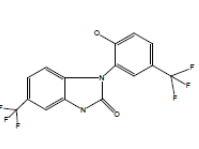
Table 22. Results of fluorescence-based drug-protein binding screen of the LOPAC library. Values are percent of Mega Red and Nile Red displaced. (n=3)

 Avg. % MegaRed: 98.7 Avg. % NileRed: 93.0	 Avg. % MegaRed: 96.6 Avg. % NileRed: 42.1	 Avg. % MegaRed: 90.4 Avg. % NileRed: 19.4	 Avg. % MegaRed: 89.3 Avg. % NileRed: 75.9	 Avg. % MegaRed: 86.1 Avg. % NileRed: 57.3
 Avg. % MegaRed: 84.0 Avg. % NileRed: 58.5	 Avg. % MegaRed: 81.9 Avg. % NileRed: 33.4	 Avg. % MegaRed: 80.8 Avg. % NileRed: 10.2	 Avg. % MegaRed: 77.2 Avg. % NileRed: 2.44	 Avg. % MegaRed: 77.1 Avg. % NileRed: 51.3
 Avg. % MegaRed: 77.1 Avg. % NileRed: 22.8	 Avg. % MegaRed: 73.2 Avg. % NileRed: 14.0	 Avg. % MegaRed: 70.5 Avg. % NileRed: 8.17	 Avg. % MegaRed: 70.0 Avg. % NileRed: 15.5	 Avg. % MegaRed: 69.2 Avg. % NileRed: 42.8
 Avg. % MegaRed: 68.7 Avg. % NileRed: 28.7	 Avg. % MegaRed: 68.4 Avg. % NileRed: 4.50	 Avg. % MegaRed: 68.3 Avg. % NileRed: 7.34	 Avg. % MegaRed: 68.2 Avg. % NileRed: 37.3	 Avg. % MegaRed: 65.7 Avg. % NileRed: 13.2
 Avg. % MegaRed: 65.5 Avg. % NileRed: 21.6	 Avg. % MegaRed: 65.5 Avg. % NileRed: 22.1	 Avg. % MegaRed: 64.4 Avg. % NileRed: 3.16	 Avg. % MegaRed: 62.6 Avg. % NileRed: 10.8	 Avg. % MegaRed: 62.5 Avg. % NileRed: 7.12
 Avg. % MegaRed: 61.7 Avg. % NileRed: 57.4	 Avg. % MegaRed: 61.4 Avg. % NileRed: 6.38	 Avg. % MegaRed: 60.8 Avg. % NileRed: 24.7	 Avg. % MegaRed: 60.2 Avg. % NileRed: 40.1	 Avg. % MegaRed: 59.7 Avg. % NileRed: 2.64

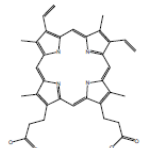

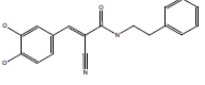
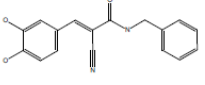
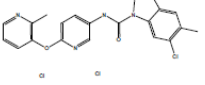
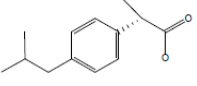
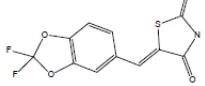
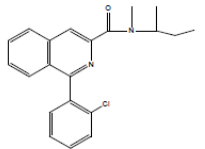
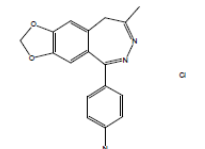
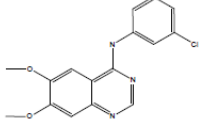
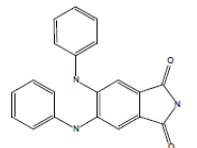
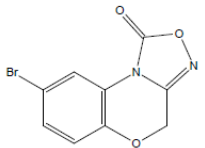
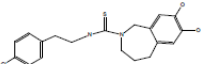
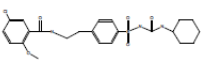
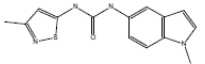
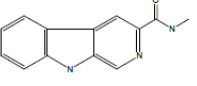
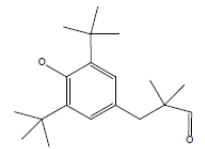
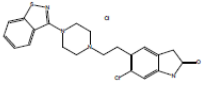
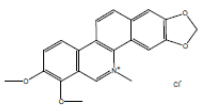
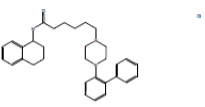
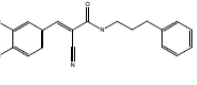
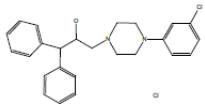
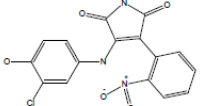
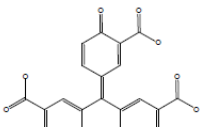
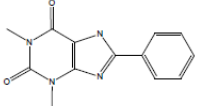
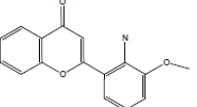
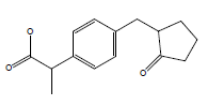
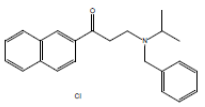
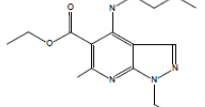
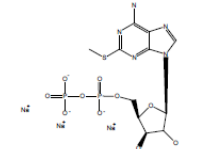
Continued, Table 22. Results of fluorescence-based drug-protein binding screen of the LOPAC library. Values are percent of Mega Red and Nile Red displaced. (n=3)

31		32		33		34		35	
Avg. % MegaRed: 56.9 Avg. % NileRed: 3.04	Avg. % MegaRed: 56.3 Avg. % NileRed: 2.83	Avg. % MegaRed: 54.7 Avg. % NileRed: 11.4	Avg. % MegaRed: 54.0 Avg. % NileRed: 29.2	Avg. % MegaRed: 53.2 Avg. % NileRed: 18.0					
36		37		38		39		40	
Avg. % MegaRed: 53.2 Avg. % NileRed: 18.4	Avg. % MegaRed: 53.2 Avg. % NileRed: 11.9	Avg. % MegaRed: 52.3 Avg. % NileRed: 30.2	Avg. % MegaRed: 52.0 Avg. % NileRed: 18.4	Avg. % MegaRed: 51.5 Avg. % NileRed: 29.2					
41		42		43		44		45	
Avg. % MegaRed: 50.0 Avg. % NileRed: 23.2	Avg. % MegaRed: 49.9 Avg. % NileRed: 12.1	Avg. % MegaRed: 49.0 Avg. % NileRed: 3.30	Avg. % MegaRed: 47.8 Avg. % NileRed: 24.9	Avg. % MegaRed: 47.8 Avg. % NileRed: 2.73					
46		47		48		49		50	
Avg. % MegaRed: 47.2 Avg. % NileRed: 29.0	Avg. % MegaRed: 46.5 Avg. % NileRed: 3.81	Avg. % MegaRed: 46.4 Avg. % NileRed: 9.68	Avg. % MegaRed: 45.8 Avg. % NileRed: 28.4	Avg. % MegaRed: 45.3 Avg. % NileRed: 8.47					
51		52		53		54		55	
Avg. % MegaRed: 45.3 Avg. % NileRed: 19.2	Avg. % MegaRed: 45.2 Avg. % NileRed: 12.4	Avg. % MegaRed: 45.1 Avg. % NileRed: 55.6	Avg. % MegaRed: 44.1 Avg. % NileRed: 8.10	Avg. % MegaRed: 43.9 Avg. % NileRed: 2.80					
56		57		58		59		60	
Avg. % MegaRed: 43.4 Avg. % NileRed: 73.7	Avg. % MegaRed: 42.8 Avg. % NileRed: 2.09	Avg. % MegaRed: 42.7 Avg. % NileRed: 0.00	Avg. % MegaRed: 42.3 Avg. % NileRed: 2.62	Avg. % MegaRed: 42.0 Avg. % NileRed: 25.5					

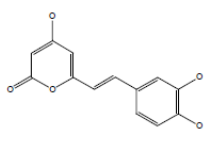
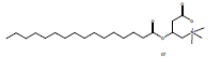
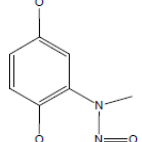
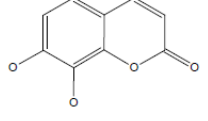
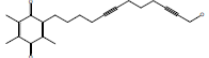
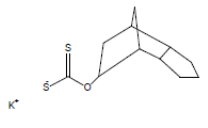
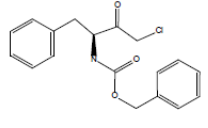
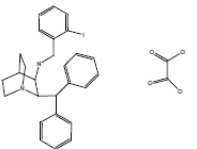
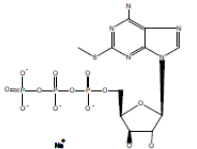
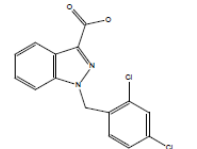
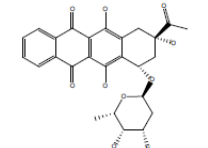
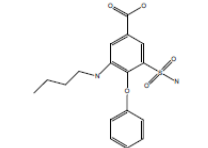
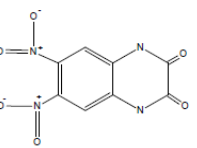
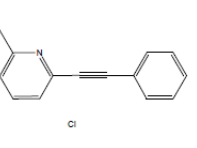
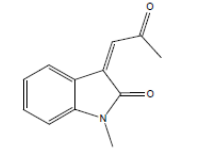
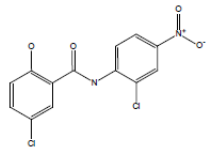
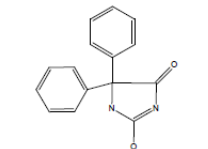
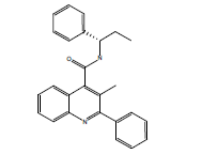
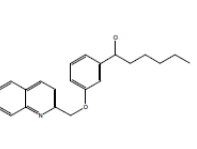
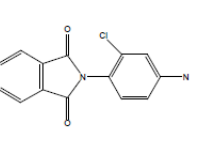
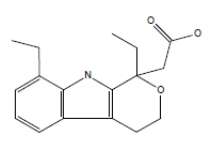
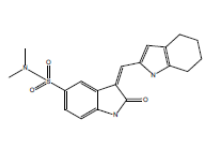
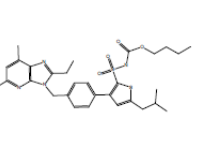
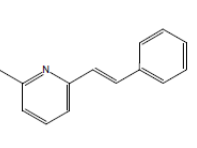
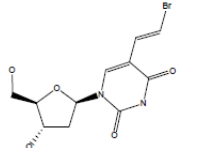
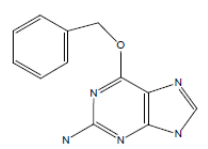
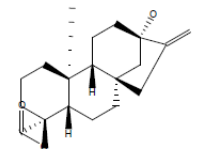
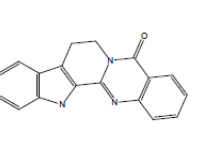
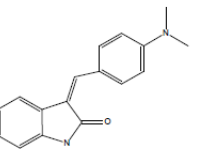
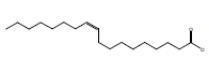
Continued, Table 22. Results of fluorescence-based drug-protein binding screen of the LOPAC library. Values are percent of Mega Red and Nile Red displaced. (n=3)

61	62	63	64	65
				
Avg. % MegaRed: 41.9 Avg. % NileRed: 31.6	Avg. % MegaRed: 41.2 Avg. % NileRed: 11.3	Avg. % MegaRed: 41.0 Avg. % NileRed: 2.66	Avg. % MegaRed: 40.1 Avg. % NileRed: 16.6	Avg. % MegaRed: 39.9 Avg. % NileRed: 6.69
66	67	68	69	70
				
Avg. % MegaRed: 38.5 Avg. % NileRed: 3.15	Avg. % MegaRed: 38.1 Avg. % NileRed: 9.29	Avg. % MegaRed: 37.9 Avg. % NileRed: 12.1	Avg. % MegaRed: 37.7 Avg. % NileRed: 62.3	Avg. % MegaRed: 37.5 Avg. % NileRed: 17.6
71	72	73	74	75
				
Avg. % MegaRed: 37.3 Avg. % NileRed: 20.5	Avg. % MegaRed: 37.2 Avg. % NileRed: 17.8	Avg. % MegaRed: 37.1 Avg. % NileRed: 25.9	Avg. % MegaRed: 37.1 Avg. % NileRed: 5.82	Avg. % MegaRed: 36.8 Avg. % NileRed: 10.0
76	77	78	79	80
				
Avg. % MegaRed: 36.6 Avg. % NileRed: 61.1	Avg. % MegaRed: 36.5 Avg. % NileRed: 16.0	Avg. % MegaRed: 35.7 Avg. % NileRed: 13.0	Avg. % MegaRed: 34.8 Avg. % NileRed: 21.2	Avg. % MegaRed: 34.7 Avg. % NileRed: 51.4
81	82	83	84	85
				
Avg. % MegaRed: 34.1 Avg. % NileRed: 2.73	Avg. % MegaRed: 33.7 Avg. % NileRed: 4.50	Avg. % MegaRed: 33.6 Avg. % NileRed: 65.5	Avg. % MegaRed: 33.6 Avg. % NileRed: 24.3	Avg. % MegaRed: 33.5 Avg. % NileRed: 25.9
86	87	88	89	90
				
Avg. % MegaRed: 33.2 Avg. % NileRed: 17.1	Avg. % MegaRed: 33.1 Avg. % NileRed: 20.1	Avg. % MegaRed: 33.1 Avg. % NileRed: 45.8	Avg. % MegaRed: 33.1 Avg. % NileRed: 3.12	Avg. % MegaRed: 33.0 Avg. % NileRed: 14.6

Continued, Table 22. Results of fluorescence-based drug-protein binding screen of the LOPAC library. Values are percent of Mega Red and Nile Red displaced. (n=3)

91		92		93		94		95	
	Avg. % MegaRed: 32.8 Avg. % NileRed: 43.7		Avg. % MegaRed: 32.2 Avg. % NileRed: 31.6		Avg. % MegaRed: 31.9 Avg. % NileRed: 9.70		Avg. % MegaRed: 31.9 Avg. % NileRed: 3.80		Avg. % MegaRed: 31.8 Avg. % NileRed: 6.29
96		97		98		99		100	
	Avg. % MegaRed: 31.3 Avg. % NileRed: 10.3		Avg. % MegaRed: 31.1 Avg. % NileRed: 18.7		Avg. % MegaRed: 30.9 Avg. % NileRed: 14.0		Avg. % MegaRed: 30.8 Avg. % NileRed: 17.8		Avg. % MegaRed: 30.8 Avg. % NileRed: 12.7
101		102		103		104		105	
	Avg. % MegaRed: 30.5 Avg. % NileRed: 32.7		Avg. % MegaRed: 30.2 Avg. % NileRed: 15.1		Avg. % MegaRed: 30.2 Avg. % NileRed: 16.4		Avg. % MegaRed: 30.1 Avg. % NileRed: 24.0		Avg. % MegaRed: 29.8 Avg. % NileRed: 27.5
106		107		108		109		110	
	Avg. % MegaRed: 29.5 Avg. % NileRed: 39.5		Avg. % MegaRed: 28.6 Avg. % NileRed: 5.62		Avg. % MegaRed: 28.5 Avg. % NileRed: 14.6		Avg. % MegaRed: 27.8 Avg. % NileRed: 4.53		Avg. % MegaRed: 27.6 Avg. % NileRed: 5.30
111		112		113		114		115	
	Avg. % MegaRed: 27.6 Avg. % NileRed: 12.3		Avg. % MegaRed: 27.4 Avg. % NileRed: 14.5		Avg. % MegaRed: 27.4 Avg. % NileRed: 1.33		Avg. % MegaRed: 27.3 Avg. % NileRed: 8.09		Avg. % MegaRed: 27.2 Avg. % NileRed: 32.4
116		117		118		119		120	
	Avg. % MegaRed: 27.2 Avg. % NileRed: 5.32		Avg. % MegaRed: 25.8 Avg. % NileRed: 7.82		Avg. % MegaRed: 25.7 Avg. % NileRed: 28.3		Avg. % MegaRed: 25.6 Avg. % NileRed: 2.02		Avg. % MegaRed: 25.5 Avg. % NileRed: 12.5

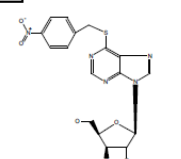
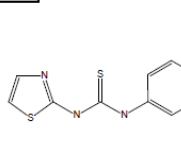
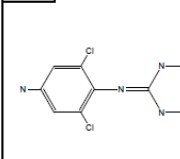
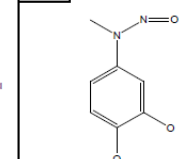
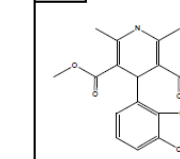
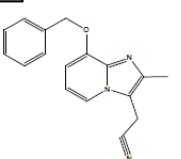
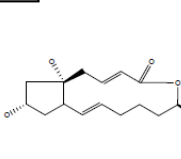
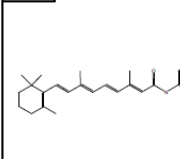
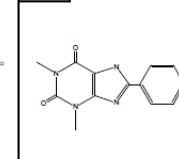
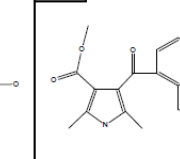
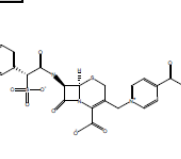
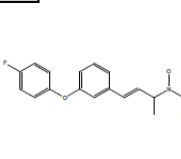
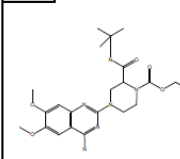
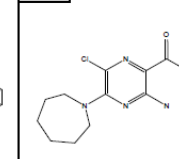
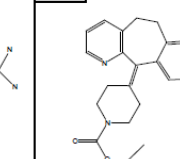
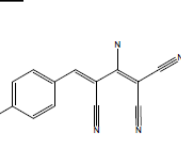
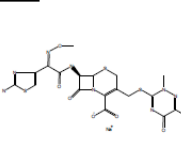
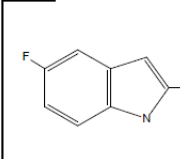
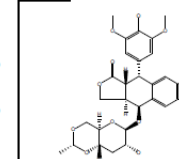
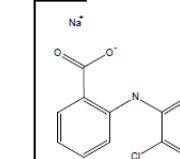
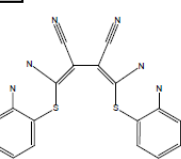
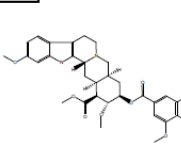
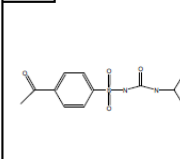
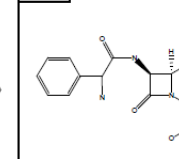
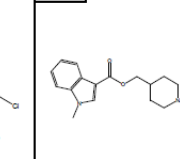
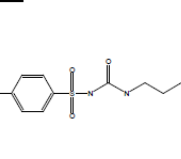
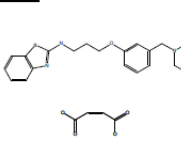
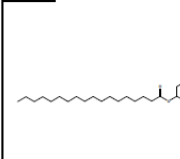
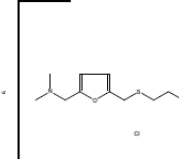
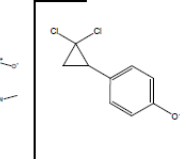
Continued, Table 22. Results of fluorescence-based drug-protein binding screen of the LOPAC library. Values are percent of Mega Red and Nile Red displaced. (n=3)

121	122	123	124	125
				
Avg. % MegaRed: 25.5 Avg. % NileRed: 3.25	Avg. % MegaRed: 25.3 Avg. % NileRed: 24.4	Avg. % MegaRed: 25.1 Avg. % NileRed: 0.43	Avg. % MegaRed: 25.1 Avg. % NileRed: 10.7	Avg. % MegaRed: 24.7 Avg. % NileRed: 21.9
126	127	128	129	130
				
Avg. % MegaRed: 24.5 Avg. % NileRed: 10.7	Avg. % MegaRed: 24.3 Avg. % NileRed: 10.9	Avg. % MegaRed: 23.9 Avg. % NileRed: 4.36	Avg. % MegaRed: 23.9 Avg. % NileRed: 14.7	Avg. % MegaRed: 23.7 Avg. % NileRed: 23.1
131	132	133	134	135
				
Avg. % MegaRed: 23.5 Avg. % NileRed: 1.71	Avg. % MegaRed: 23.3 Avg. % NileRed: 8.30	Avg. % MegaRed: 23.3 Avg. % NileRed: 7.11	Avg. % MegaRed: 23.2 Avg. % NileRed: 17.5	Avg. % MegaRed: 23.1 Avg. % NileRed: 15.3
136	137	138	139	140
				
Avg. % MegaRed: 23.0 Avg. % NileRed: 14.9	Avg. % MegaRed: 22.9 Avg. % NileRed: 3.42	Avg. % MegaRed: 22.6 Avg. % NileRed: 12.9	Avg. % MegaRed: 22.6 Avg. % NileRed: 6.12	Avg. % MegaRed: 22.5 Avg. % NileRed: 11.5
141	142	143	144	145
				
Avg. % MegaRed: 22.3 Avg. % NileRed: 6.48	Avg. % MegaRed: 22.3 Avg. % NileRed: 3.08	Avg. % MegaRed: 22.2 Avg. % NileRed: 16.1	Avg. % MegaRed: 22.2 Avg. % NileRed: 20.0	Avg. % MegaRed: 22.2 Avg. % NileRed: 4.45
146	147	148	149	150
				
Avg. % MegaRed: 22.1 Avg. % NileRed: 40.7	Avg. % MegaRed: 22.0 Avg. % NileRed: 26.8	Avg. % MegaRed: 21.8 Avg. % NileRed: 9.46	Avg. % MegaRed: 21.8 Avg. % NileRed: 4.97	Avg. % MegaRed: 21.8 Avg. % NileRed: 4.40

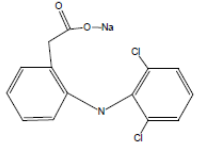
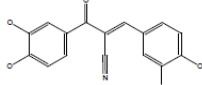
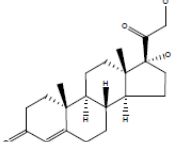
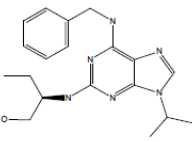
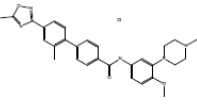
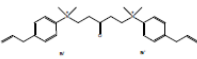
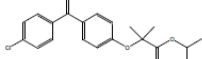
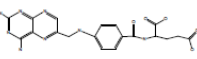
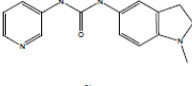
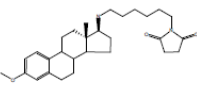
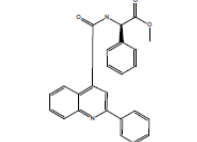
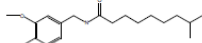
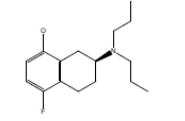
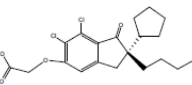
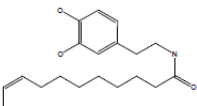
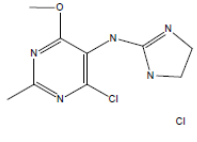
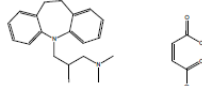
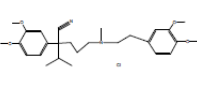
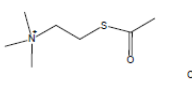
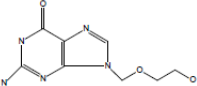
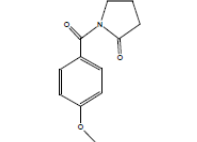
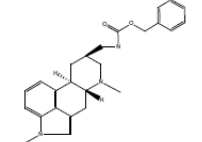
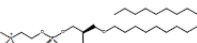

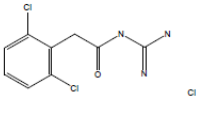
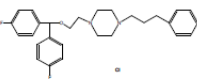
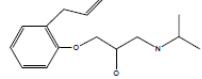
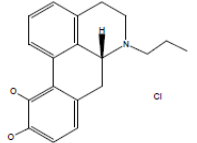
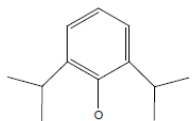
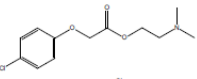
Continued, Table 22. Results of fluorescence-based drug-protein binding screen of the LOPAC library. Values are percent of Mega Red and Nile Red displaced. (n=3)

151	152	153	154	155
Avg. % MegaRed: 21.7 Avg. % NileRed: 10.4	Avg. % MegaRed: 21.4 Avg. % NileRed: 15.6	Avg. % MegaRed: 21.4 Avg. % NileRed: 70.2	Avg. % MegaRed: 20.9 Avg. % NileRed: 38.9	Avg. % MegaRed: 20.8 Avg. % NileRed: 15.5
156	157	158	159	160
Avg. % MegaRed: 20.8 Avg. % NileRed: 1.60	Avg. % MegaRed: 20.6 Avg. % NileRed: 5.46	Avg. % MegaRed: 20.6 Avg. % NileRed: 59.1	Avg. % MegaRed: 20.4 Avg. % NileRed: 7.02	Avg. % MegaRed: 20.3 Avg. % NileRed: 13.2
161	162	163	164	165
Avg. % MegaRed: 20.2 Avg. % NileRed: 5.38	Avg. % MegaRed: 20.2 Avg. % NileRed: 13.6	Avg. % MegaRed: 19.9 Avg. % NileRed: 4.42	Avg. % MegaRed: 19.5 Avg. % NileRed: 3.65	Avg. % MegaRed: 19.5 Avg. % NileRed: 10.6
166	167	168	169	170
Avg. % MegaRed: 19.4 Avg. % NileRed: 10.2	Avg. % MegaRed: 19.2 Avg. % NileRed: 14.3	Avg. % MegaRed: 19.1 Avg. % NileRed: 21.4	Avg. % MegaRed: 19.0 Avg. % NileRed: 13.8	Avg. % MegaRed: 19.0 Avg. % NileRed: 8.05
171	172	173	174	175
Avg. % MegaRed: 18.9 Avg. % NileRed: 15.6	Avg. % MegaRed: 18.8 Avg. % NileRed: 3.20	Avg. % MegaRed: 18.6 Avg. % NileRed: 14.8	Avg. % MegaRed: 18.6 Avg. % NileRed: 8.67	Avg. % MegaRed: 18.6 Avg. % NileRed: 4.86
176	177	178	179	180
Avg. % MegaRed: 18.4 Avg. % NileRed: 65.6	Avg. % MegaRed: 18.4 Avg. % NileRed: 17.1	Avg. % MegaRed: 18.2 Avg. % NileRed: 66.4	Avg. % MegaRed: 18.1 Avg. % NileRed: 3.99	Avg. % MegaRed: 17.8 Avg. % NileRed: 10.3

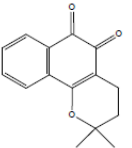
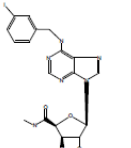
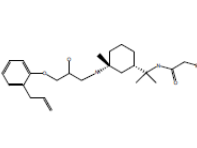
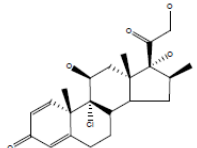
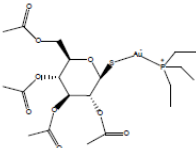
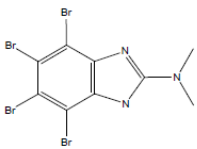
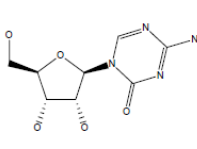
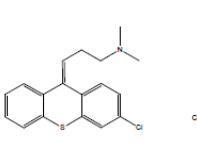
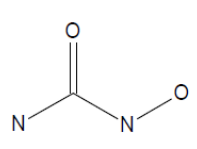
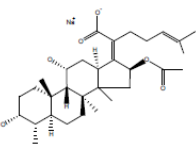
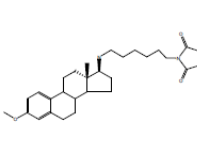
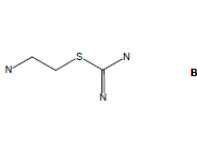
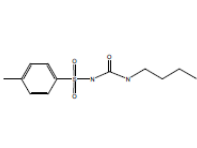
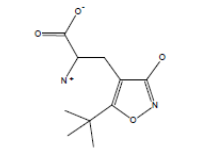
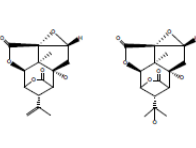
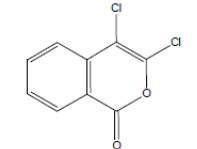
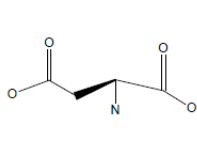
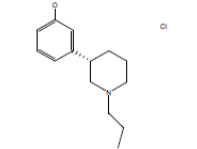
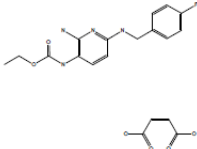
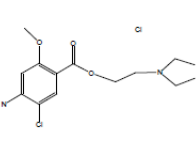
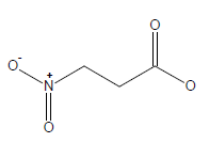
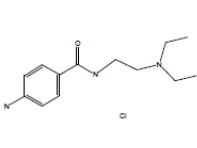
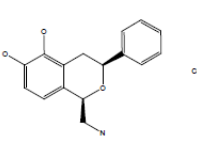
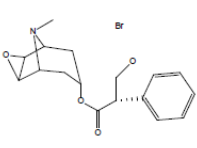
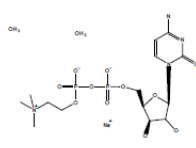
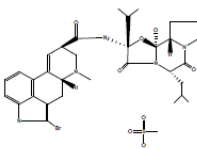
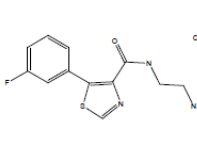
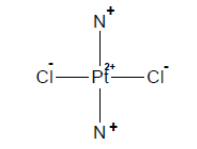
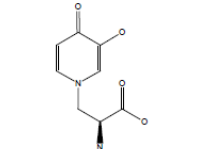
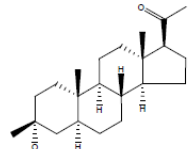
Continued, Table 22. Results of fluorescence-based drug-protein binding screen of the LOPAC library. Values are percent of Mega Red and Nile Red displaced. (n=3)

181	182	183	184	185
				
Avg. % MegaRed: 17.7 Avg. % NileRed: 12.0	Avg. % MegaRed: 17.6 Avg. % NileRed: 15.5	Avg. % MegaRed: 17.4 Avg. % NileRed: 6.24	Avg. % MegaRed: 17.0 Avg. % NileRed: 7.70	Avg. % MegaRed: 16.8 Avg. % NileRed: 27.1
186	187	188	189	190
				
Avg. % MegaRed: 16.8 Avg. % NileRed: 30.3	Avg. % MegaRed: 16.7 Avg. % NileRed: 1.89	Avg. % MegaRed: 16.7 Avg. % NileRed: 25.6	Avg. % MegaRed: 16.5 Avg. % NileRed: 4.22	Avg. % MegaRed: 16.5 Avg. % NileRed: 2.19
191	192	193	194	195
				
Avg. % MegaRed: 16.5 Avg. % NileRed: 24.9	Avg. % MegaRed: 16.4 Avg. % NileRed: 3.34	Avg. % MegaRed: 16.4 Avg. % NileRed: 4.48	Avg. % MegaRed: 16.4 Avg. % NileRed: 5.05	Avg. % MegaRed: 16.3 Avg. % NileRed: 2.22
197	198	199	200	201
				
Avg. % MegaRed: 16.2 Avg. % NileRed: 1.46	Avg. % MegaRed: 16.2 Avg. % NileRed: 18.3	Avg. % MegaRed: 16.1 Avg. % NileRed: 33.4	Avg. % MegaRed: 16.1 Avg. % NileRed: 1.46	Avg. % MegaRed: 16.1 Avg. % NileRed: 24.8
202	203	204	205	206
				
Avg. % MegaRed: 16.1 Avg. % NileRed: 3.13	Avg. % MegaRed: 16.0 Avg. % NileRed: 2.78	Avg. % MegaRed: 16.0 Avg. % NileRed: 1.49	Avg. % MegaRed: 15.7 Avg. % NileRed: 16.0	Avg. % MegaRed: 15.6 Avg. % NileRed: 12.6
207	208	209	210	211
				
Avg. % MegaRed: 15.5 Avg. % NileRed: 13.4	Avg. % MegaRed: 15.4 Avg. % NileRed: 15.9	Avg. % MegaRed: 15.3 Avg. % NileRed: 9.21	Avg. % MegaRed: 15.2 Avg. % NileRed: 2.11	Avg. % MegaRed: 15.2 Avg. % NileRed: 16.8

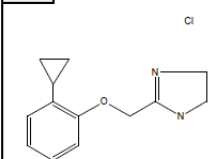
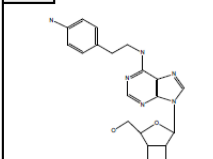
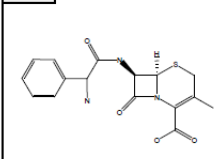
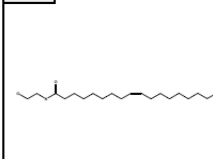
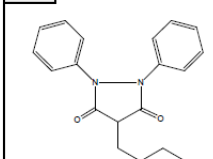
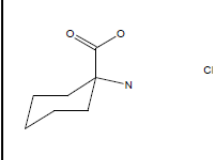
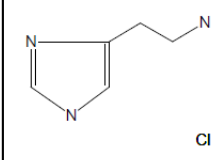
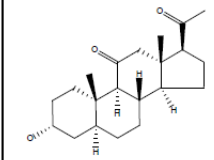
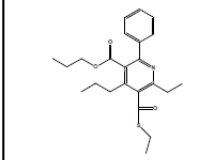
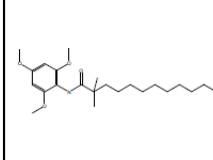
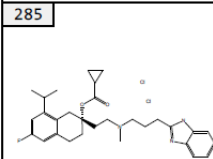
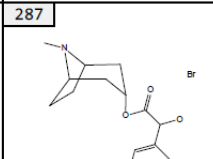
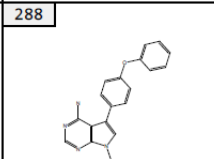
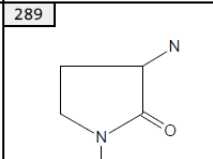
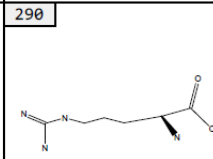
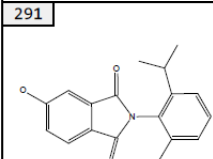
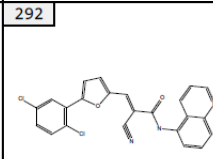
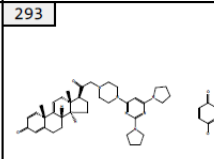
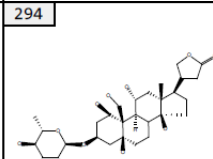
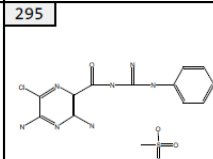
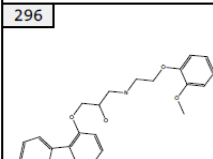
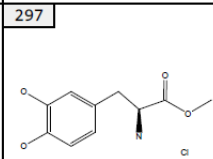
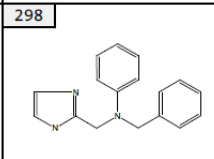
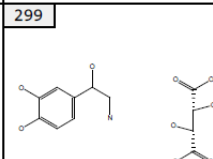
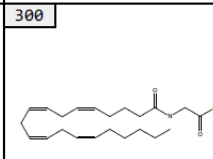
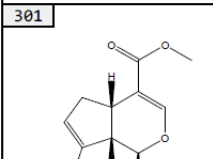
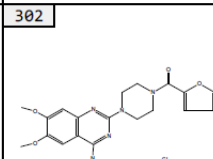
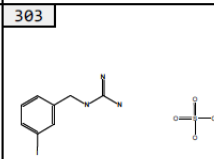
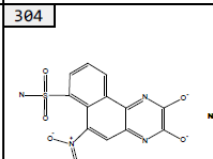
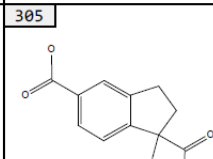
Continued, Table 22. Results of fluorescence-based drug-protein binding screen of the LOPAC library. Values are percent of Mega Red and Nile Red displaced. (n=3)

212	213	214	215	216
				
Avg. % MegaRed: 15.2 Avg. % NileRed: 43.8	Avg. % MegaRed: 15.1 Avg. % NileRed: 4.31	Avg. % MegaRed: 15.0 Avg. % NileRed: 15.3	Avg. % MegaRed: 14.9 Avg. % NileRed: 2.61	Avg. % MegaRed: 14.9 Avg. % NileRed: 8.05
217	218	219	221	222
				
Avg. % MegaRed: 14.9 Avg. % NileRed: 4.69	Avg. % MegaRed: 14.6 Avg. % NileRed: 2.81	Avg. % MegaRed: 14.6 Avg. % NileRed: 19.4	Avg. % MegaRed: 14.6 Avg. % NileRed: 4.01	Avg. % MegaRed: 14.3 Avg. % NileRed: 6.83
223	224	225	226	227
				
Avg. % MegaRed: 14.3 Avg. % NileRed: 2.48	Avg. % MegaRed: 14.2 Avg. % NileRed: 17.3	Avg. % MegaRed: 14.2 Avg. % NileRed: 11.9	Avg. % MegaRed: 14.2 Avg. % NileRed: 13.0	Avg. % MegaRed: 14.2 Avg. % NileRed: 33.3
228	229	230	231	232
				
Avg. % MegaRed: 14.1 Avg. % NileRed: 1.51	Avg. % MegaRed: 14.1 Avg. % NileRed: 11.1	Avg. % MegaRed: 14.1 Avg. % NileRed: 12.1	Avg. % MegaRed: 14.1 Avg. % NileRed: 1.98	Avg. % MegaRed: 14.1 Avg. % NileRed: 8.61
233	234	235	236	238
				
Avg. % MegaRed: 13.8 Avg. % NileRed: 5.35	Avg. % MegaRed: 13.8 Avg. % NileRed: 2.57	Avg. % MegaRed: 13.7 Avg. % NileRed: 22.0	Avg. % MegaRed: 13.6 Avg. % NileRed: 4.10	Avg. % MegaRed: 13.6 Avg. % NileRed: 10.6
239	240	241	242	243
				
Avg. % MegaRed: 13.5 Avg. % NileRed: 13.5	Avg. % MegaRed: 13.4 Avg. % NileRed: 12.1	Avg. % MegaRed: 13.4 Avg. % NileRed: 5.03	Avg. % MegaRed: 13.3 Avg. % NileRed: 7.58	Avg. % MegaRed: 13.1 Avg. % NileRed: 6.28

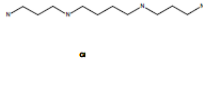
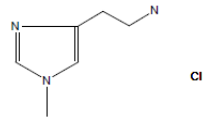
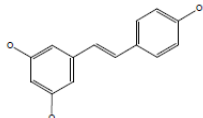
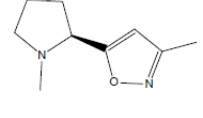
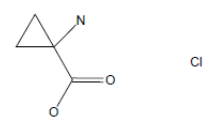
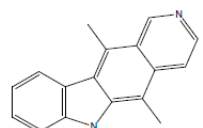
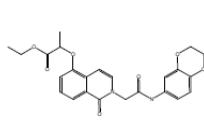
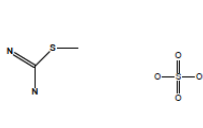
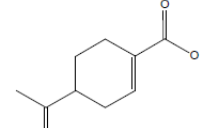
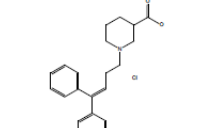
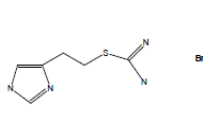
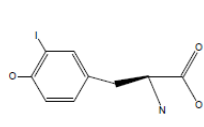
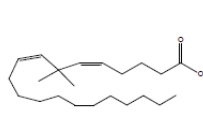
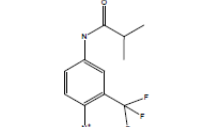
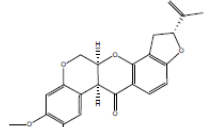
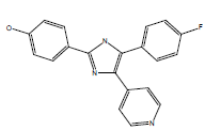
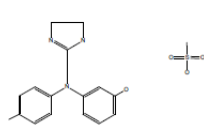
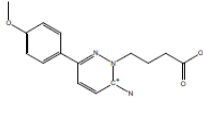
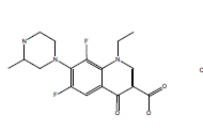
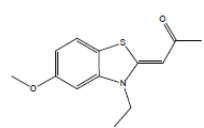
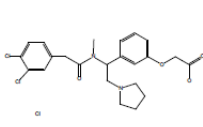
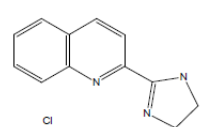
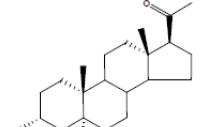
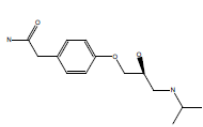
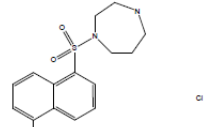
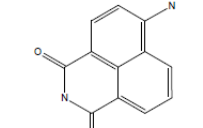
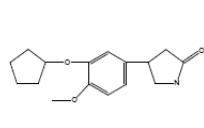
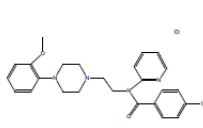
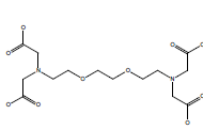
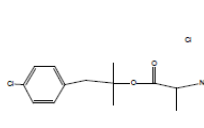
Continued, Table 22. Results of fluorescence-based drug-protein binding screen of the LOPAC library. Values are percent of Mega Red and Nile Red displaced. (n=3)

244		245		246		247		248	
	Avg. % MegaRed: 13.1 Avg. % NileRed: 7.50		Avg. % MegaRed: 13.1 Avg. % NileRed: 3.15		Avg. % MegaRed: 13.0 Avg. % NileRed: 3.48		Avg. % MegaRed: 13.0 Avg. % NileRed: 43.9		Avg. % MegaRed: 12.9 Avg. % NileRed: 2.18
249		250		251		253		254	
	Avg. % MegaRed: 12.9 Avg. % NileRed: 3.66		Avg. % MegaRed: 12.9 Avg. % NileRed: 7.76		Avg. % MegaRed: 12.9 Avg. % NileRed: 4.90		Avg. % MegaRed: 12.8 Avg. % NileRed: 8.82		Avg. % MegaRed: 12.8 Avg. % NileRed: 7.61
255		256		257		258		259	
	Avg. % MegaRed: 12.7 Avg. % NileRed: 12.2		Avg. % MegaRed: 12.6 Avg. % NileRed: 6.55		Avg. % MegaRed: 12.5 Avg. % NileRed: 23.0		Avg. % MegaRed: 12.5 Avg. % NileRed: 2.34		Avg. % MegaRed: 12.4 Avg. % NileRed: 11.9
260		261		262		263		264	
	Avg. % MegaRed: 12.4 Avg. % NileRed: 5.00		Avg. % MegaRed: 12.4 Avg. % NileRed: 2.04		Avg. % MegaRed: 12.3 Avg. % NileRed: 2.96		Avg. % MegaRed: 12.3 Avg. % NileRed: 7.74		Avg. % MegaRed: 12.2 Avg. % NileRed: 15.0
265		266		267		268		269	
	Avg. % MegaRed: 12.2 Avg. % NileRed: 12.5		Avg. % MegaRed: 12.1 Avg. % NileRed: 4.25		Avg. % MegaRed: 12.1 Avg. % NileRed: 12.0		Avg. % MegaRed: 12.0 Avg. % NileRed: 1.80		Avg. % MegaRed: 12.0 Avg. % NileRed: 2.82
270		271		272		273		274	
	Avg. % MegaRed: 12.0 Avg. % NileRed: 23.0		Avg. % MegaRed: 11.8 Avg. % NileRed: 2.51		Avg. % MegaRed: 11.8 Avg. % NileRed: 25.0		Avg. % MegaRed: 11.8 Avg. % NileRed: 10.6		Avg. % MegaRed: 11.8 Avg. % NileRed: 6.02

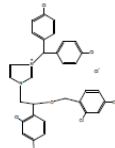
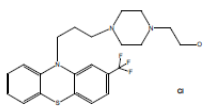
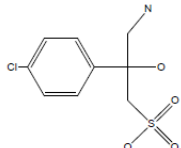
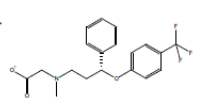
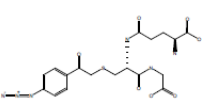
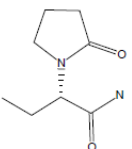
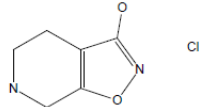
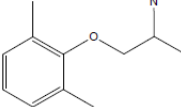
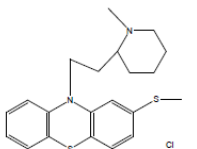
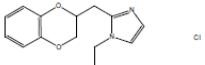
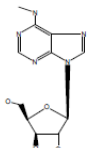
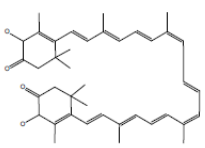
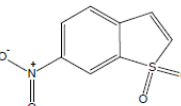
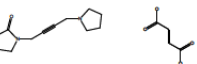
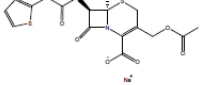
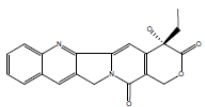
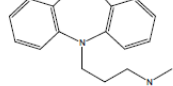
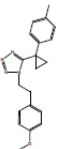
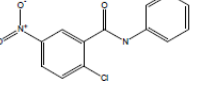
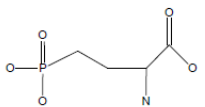
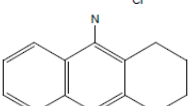
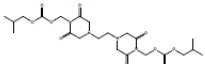
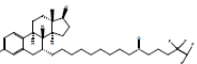
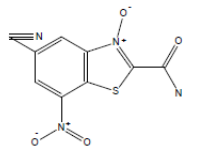
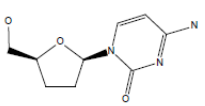
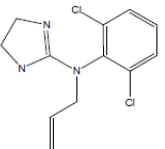
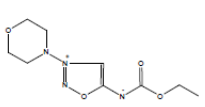
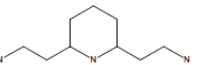
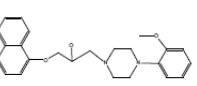
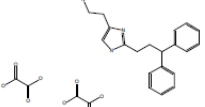
Continued, Table 22. Results of fluorescence-based drug-protein binding screen of the LOPAC library. Values are percent of Mega Red and Nile Red displaced. (n=3)

275	276	277	278	279
				
Avg. % MegaRed: 11.8 Avg. % NileRed: 2.33	Avg. % MegaRed: 11.7 Avg. % NileRed: 4.63	Avg. % MegaRed: 11.7 Avg. % NileRed: 2.95	Avg. % MegaRed: 11.7 Avg. % NileRed: 6.76	Avg. % MegaRed: 11.7 Avg. % NileRed: 5.32
280	281	282	283	284
				
Avg. % MegaRed: 11.6 Avg. % NileRed: 7.79	Avg. % MegaRed: 11.6 Avg. % NileRed: 10.3	Avg. % MegaRed: 11.5 Avg. % NileRed: 1.43	Avg. % MegaRed: 11.5 Avg. % NileRed: 3.64	Avg. % MegaRed: 11.5 Avg. % NileRed: 44.4
285	287	288	289	290
				
Avg. % MegaRed: 11.4 Avg. % NileRed: 5.96	Avg. % MegaRed: 11.4 Avg. % NileRed: 14.6	Avg. % MegaRed: 11.4 Avg. % NileRed: 3.95	Avg. % MegaRed: 11.4 Avg. % NileRed: 2.01	Avg. % MegaRed: 11.4 Avg. % NileRed: 4.85
291	292	293	294	295
				
Avg. % MegaRed: 11.3 Avg. % NileRed: 2.89	Avg. % MegaRed: 11.3 Avg. % NileRed: 3.45	Avg. % MegaRed: 11.3 Avg. % NileRed: 10.0	Avg. % MegaRed: 11.3 Avg. % NileRed: 0.81	Avg. % MegaRed: 11.3 Avg. % NileRed: 0.79
296	297	298	299	300
				
Avg. % MegaRed: 11.3 Avg. % NileRed: 4.76	Avg. % MegaRed: 11.2 Avg. % NileRed: 3.17	Avg. % MegaRed: 11.1 Avg. % NileRed: 1.99	Avg. % MegaRed: 11.1 Avg. % NileRed: 2.71	Avg. % MegaRed: 11.1 Avg. % NileRed: 3.40
301	302	303	304	305
				
Avg. % MegaRed: 11.1 Avg. % NileRed: 12.4	Avg. % MegaRed: 11.0 Avg. % NileRed: 3.63	Avg. % MegaRed: 11.0 Avg. % NileRed: 1.29	Avg. % MegaRed: 11.0 Avg. % NileRed: 12.5	Avg. % MegaRed: 11.0 Avg. % NileRed: 7.12

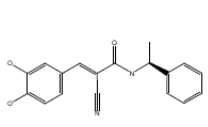
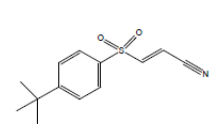
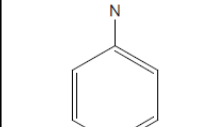
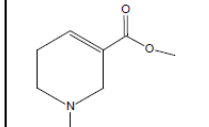
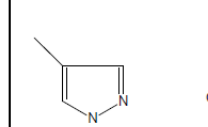
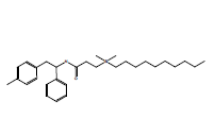
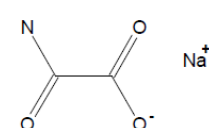
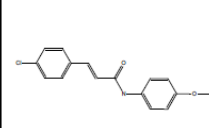
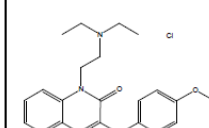
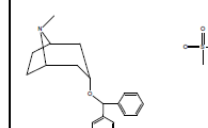
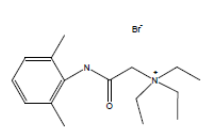
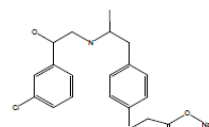
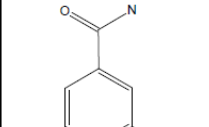
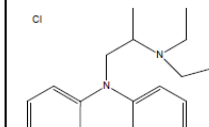
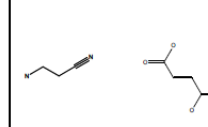
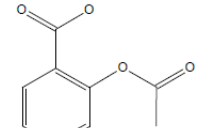
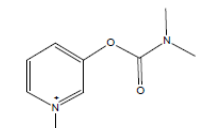
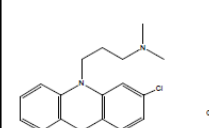
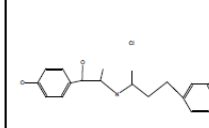
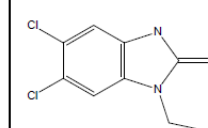
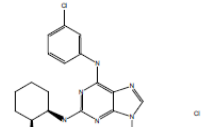
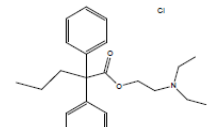
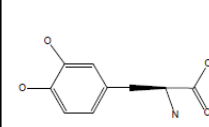
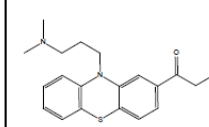
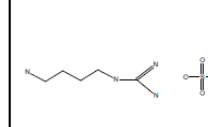
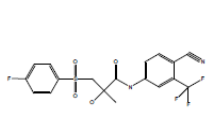
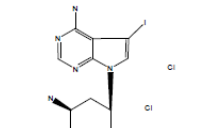
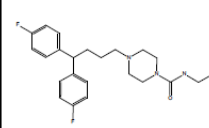
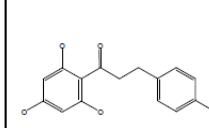
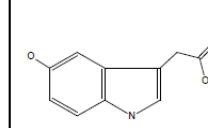
Continued, Table 22. Results of fluorescence-based drug-protein binding screen of the LOPAC library. Values are percent of Mega Red and Nile Red displaced. (n=3)

306	307	308	309	311
				
Avg. % MegaRed: 11.0 Avg. % NileRed: 2.44	Avg. % MegaRed: 10.9 Avg. % NileRed: 2.45	Avg. % MegaRed: 10.9 Avg. % NileRed: 31.0	Avg. % MegaRed: 10.8 Avg. % NileRed: 16.0	Avg. % MegaRed: 10.8 Avg. % NileRed: 12.0
312	313	314	315	316
				
Avg. % MegaRed: 10.7 Avg. % NileRed: 3.71	Avg. % MegaRed: 10.7 Avg. % NileRed: 2.26	Avg. % MegaRed: 10.7 Avg. % NileRed: 2.41	Avg. % MegaRed: 10.7 Avg. % NileRed: 22.1	Avg. % MegaRed: 10.6 Avg. % NileRed: 9.08
317	318	319	320	321
				
Avg. % MegaRed: 10.6 Avg. % NileRed: 3.15	Avg. % MegaRed: 10.6 Avg. % NileRed: 1.81	Avg. % MegaRed: 10.6 Avg. % NileRed: 8.89	Avg. % MegaRed: 10.6 Avg. % NileRed: 14.3	Avg. % MegaRed: 10.6 Avg. % NileRed: 10.7
322	323	324	325	326
				
Avg. % MegaRed: 10.6 Avg. % NileRed: 4.46	Avg. % MegaRed: 10.6 Avg. % NileRed: 3.46	Avg. % MegaRed: 10.4 Avg. % NileRed: 11.9	Avg. % MegaRed: 10.4 Avg. % NileRed: 1.60	Avg. % MegaRed: 10.4 Avg. % NileRed: 14.8
327	328	329	330	331
				
Avg. % MegaRed: 10.4 Avg. % NileRed: 1.97	Avg. % MegaRed: 10.3 Avg. % NileRed: 2.69	Avg. % MegaRed: 10.3 Avg. % NileRed: 21.4	Avg. % MegaRed: 10.3 Avg. % NileRed: 5.77	Avg. % MegaRed: 10.3 Avg. % NileRed: 6.39
332	333	335	336	337
				
Avg. % MegaRed: 10.3 Avg. % NileRed: 2.68	Avg. % MegaRed: 10.2 Avg. % NileRed: 4.86	Avg. % MegaRed: 10.1 Avg. % NileRed: 1.63	Avg. % MegaRed: 10.1 Avg. % NileRed: 14.8	Avg. % MegaRed: 10.1 Avg. % NileRed: 7.48

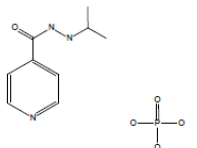
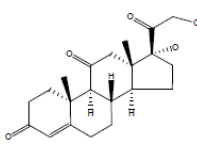
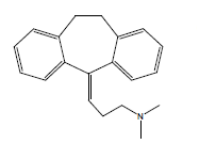
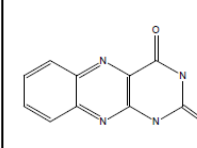
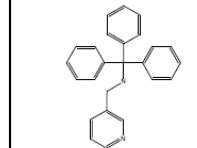
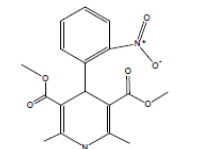
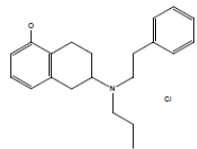
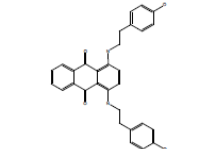
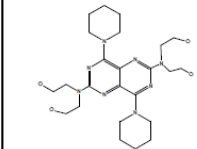
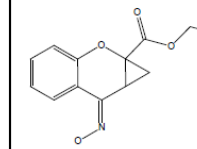
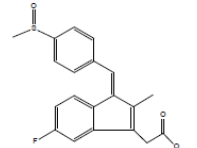
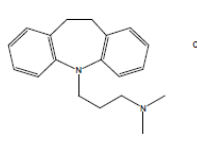
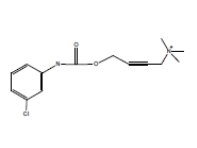
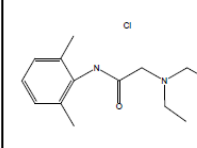
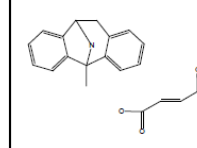
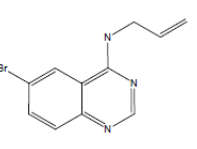
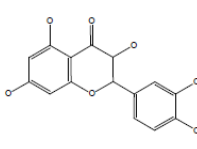
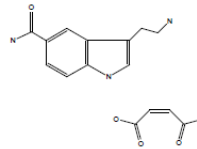
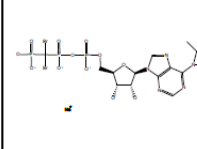
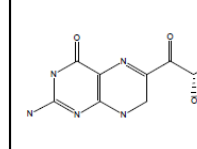
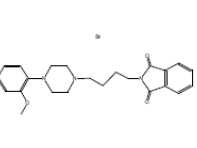
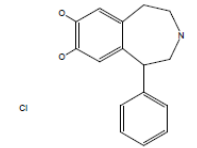
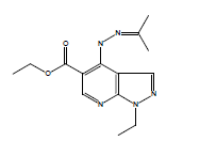
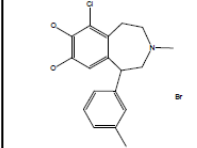
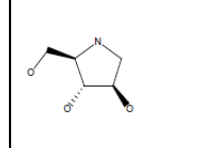
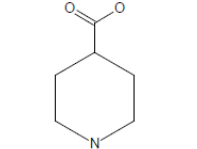
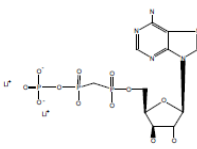
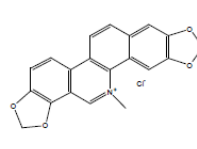
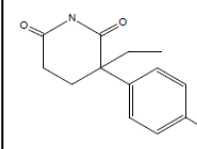
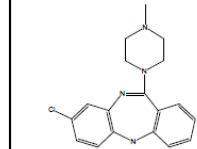
Continued, Table 22. Results of fluorescence-based drug-protein binding screen of the LOPAC library. Values are percent of Mega Red and Nile Red displaced. (n=3)

338	 Avg. % MegaRed: 10.1 Avg. % NileRed: 12.9	339	 Avg. % MegaRed: 10.1 Avg. % NileRed: 2.45	340	 Avg. % MegaRed: 10.0 Avg. % NileRed: 5.76	341	 Avg. % MegaRed: 10.0 Avg. % NileRed: 5.87	342	 Avg. % MegaRed: 9.98 Avg. % NileRed: 3.99
343	 Avg. % MegaRed: 9.94 Avg. % NileRed: 13.9	344	 Avg. % MegaRed: 9.94 Avg. % NileRed: 14.0	345	 Avg. % MegaRed: 9.90 Avg. % NileRed: 1.74	346	 Avg. % MegaRed: 9.87 Avg. % NileRed: 1.51	347	 Avg. % MegaRed: 9.87 Avg. % NileRed: 2.00
348	 Avg. % MegaRed: 9.85 Avg. % NileRed: 2.78	349	 Avg. % MegaRed: 9.81 Avg. % NileRed: 2.49	350	 Avg. % MegaRed: 9.75 Avg. % NileRed: 6.18	351	 Avg. % MegaRed: 9.75 Avg. % NileRed: 12.0	352	 Avg. % MegaRed: 9.74 Avg. % NileRed: 12.3
353	 Avg. % MegaRed: 9.71 Avg. % NileRed: 7.85	354	 Avg. % MegaRed: 9.70 Avg. % NileRed: 2.75	356	 Avg. % MegaRed: 9.68 Avg. % NileRed: 8.36	357	 Avg. % MegaRed: 9.63 Avg. % NileRed: 2.27	358	 Avg. % MegaRed: 9.59 Avg. % NileRed: 0.98
359	 Avg. % MegaRed: 9.54 Avg. % NileRed: 5.89	360	 Avg. % MegaRed: 9.49 Avg. % NileRed: 5.46	361	 Avg. % MegaRed: 9.48 Avg. % NileRed: 1.57	362	 Avg. % MegaRed: 9.48 Avg. % NileRed: 3.66	363	 Avg. % MegaRed: 9.48 Avg. % NileRed: 4.96
364	 Avg. % MegaRed: 9.45 Avg. % NileRed: 12.3	365	 Avg. % MegaRed: 9.42 Avg. % NileRed: 1.20	366	 Avg. % MegaRed: 9.36 Avg. % NileRed: 14.0	367	 Avg. % MegaRed: 9.29 Avg. % NileRed: 13.3	368	 Avg. % MegaRed: 9.27 Avg. % NileRed: 9.91

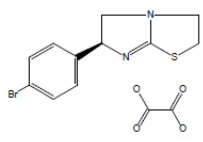
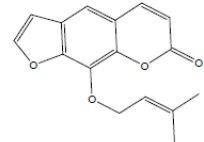
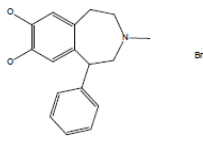
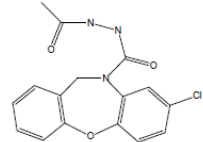
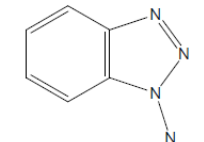
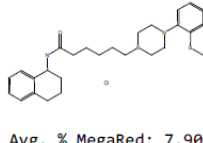
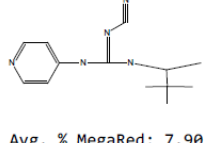
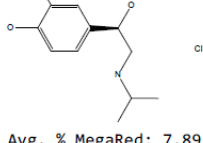
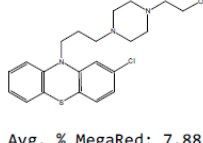
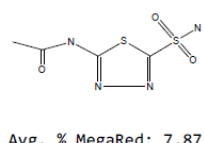
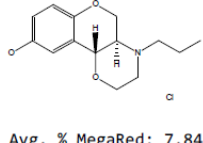
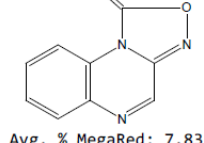
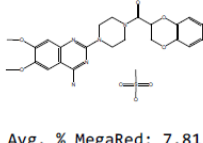
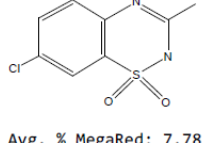
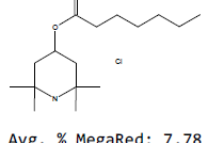
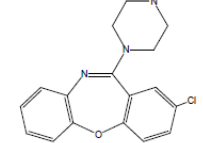
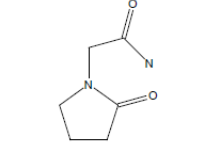
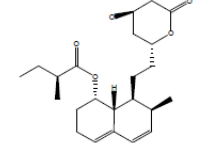
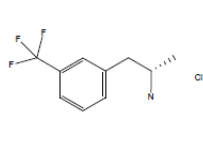
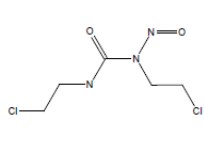
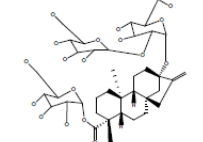
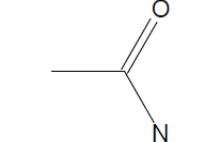
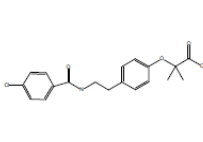
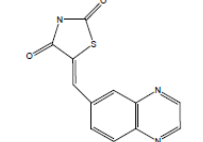
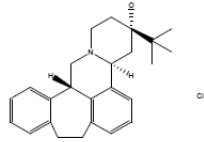
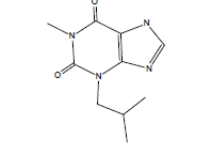
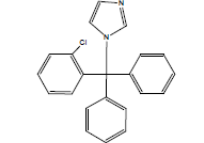
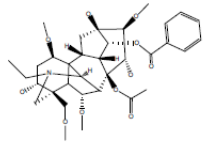
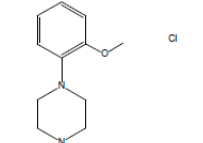
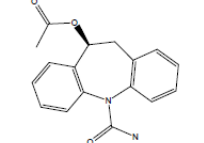
Continued, Table 22. Results of fluorescence-based drug-protein binding screen of the LOPAC library. Values are percent of Mega Red and Nile Red displaced. (n=3)

369	370	371	372	373
				
Avg. % MegaRed: 9.25 Avg. % NileRed: 9.89	Avg. % MegaRed: 9.22 Avg. % NileRed: 3.71	Avg. % MegaRed: 9.22 Avg. % NileRed: 12.9	Avg. % MegaRed: 9.21 Avg. % NileRed: 5.27	Avg. % MegaRed: 9.14 Avg. % NileRed: 1.83
374	375	376	377	378
				
Avg. % MegaRed: 9.14 Avg. % NileRed: 1.63	Avg. % MegaRed: 9.12 Avg. % NileRed: 12.4	Avg. % MegaRed: 9.10 Avg. % NileRed: 3.03	Avg. % MegaRed: 9.04 Avg. % NileRed: 5.11	Avg. % MegaRed: 9.03 Avg. % NileRed: 20.0
379	380	381	382	383
				
Avg. % MegaRed: 9.00 Avg. % NileRed: 2.19	Avg. % MegaRed: 8.99 Avg. % NileRed: 11.2	Avg. % MegaRed: 8.98 Avg. % NileRed: 9.12	Avg. % MegaRed: 8.93 Avg. % NileRed: 11.2	Avg. % MegaRed: 8.87 Avg. % NileRed: 3.42
384	386	387	388	389
				
Avg. % MegaRed: 8.85 Avg. % NileRed: 8.61	Avg. % MegaRed: 8.83 Avg. % NileRed: 3.09	Avg. % MegaRed: 8.82 Avg. % NileRed: 5.99	Avg. % MegaRed: 8.78 Avg. % NileRed: 16.6	Avg. % MegaRed: 8.77 Avg. % NileRed: 5.40
390	391	392	393	394
				
Avg. % MegaRed: 8.73 Avg. % NileRed: 11.8	Avg. % MegaRed: 8.73 Avg. % NileRed: 8.34	Avg. % MegaRed: 8.69 Avg. % NileRed: 3.45	Avg. % MegaRed: 8.69 Avg. % NileRed: 4.48	Avg. % MegaRed: 8.59 Avg. % NileRed: 2.25
395	396	397	398	399
				
Avg. % MegaRed: 8.58 Avg. % NileRed: 26.9	Avg. % MegaRed: 8.57 Avg. % NileRed: 6.30	Avg. % MegaRed: 8.56 Avg. % NileRed: 1.20	Avg. % MegaRed: 8.50 Avg. % NileRed: 16.5	Avg. % MegaRed: 8.50 Avg. % NileRed: 11.2

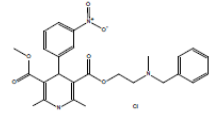
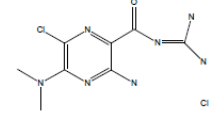
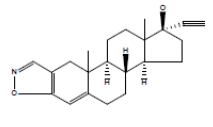
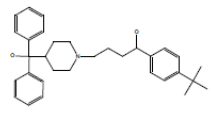
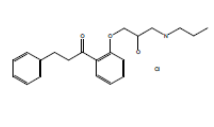
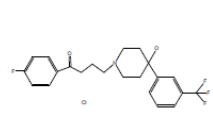
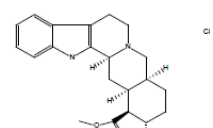
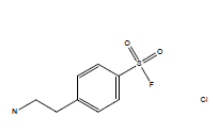
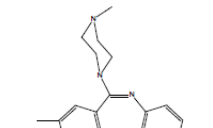
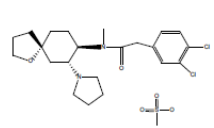
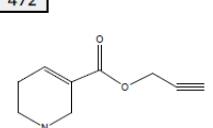
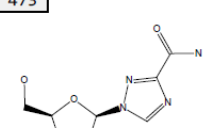
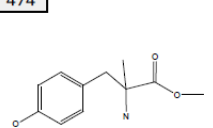
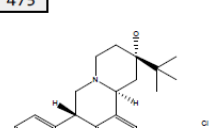
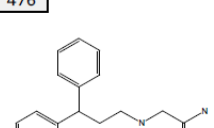
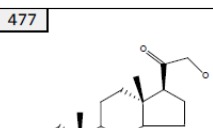
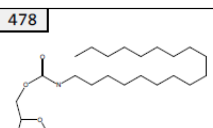
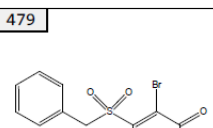
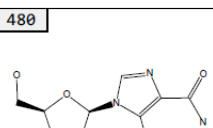
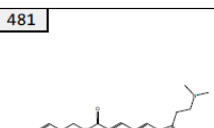
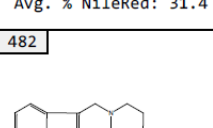
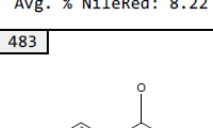
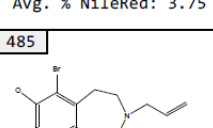
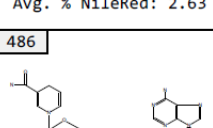
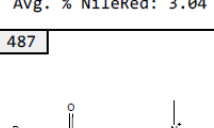
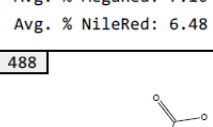
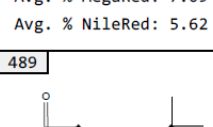
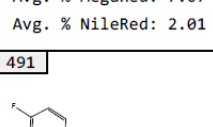
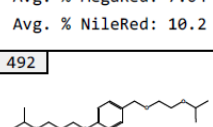
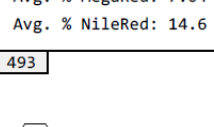
Continued, Table 22. Results of fluorescence-based drug-protein binding screen of the LOPAC library. Values are percent of Mega Red and Nile Red displaced. (n=3)

400	401	402	403	404
				
Avg. % MegaRed: 8.49 Avg. % NileRed: 1.03	Avg. % MegaRed: 8.48 Avg. % NileRed: 6.57	Avg. % MegaRed: 8.46 Avg. % NileRed: 13.0	Avg. % MegaRed: 8.45 Avg. % NileRed: 3.16	Avg. % MegaRed: 8.45 Avg. % NileRed: 1.39
405	406	407	408	409
				
Avg. % MegaRed: 8.44 Avg. % NileRed: 5.63	Avg. % MegaRed: 8.41 Avg. % NileRed: 6.25	Avg. % MegaRed: 8.39 Avg. % NileRed: 22.8	Avg. % MegaRed: 8.38 Avg. % NileRed: 2.78	Avg. % MegaRed: 8.34 Avg. % NileRed: 8.99
410	411	412	413	414
				
Avg. % MegaRed: 8.34 Avg. % NileRed: 19.4	Avg. % MegaRed: 8.34 Avg. % NileRed: 2.53	Avg. % MegaRed: 8.31 Avg. % NileRed: 14.4	Avg. % MegaRed: 8.31 Avg. % NileRed: 2.98	Avg. % MegaRed: 8.30 Avg. % NileRed: 11.8
415	416	417	418	419
				
Avg. % MegaRed: 8.24 Avg. % NileRed: 3.53	Avg. % MegaRed: 8.22 Avg. % NileRed: 8.09	Avg. % MegaRed: 8.21 Avg. % NileRed: 8.57	Avg. % MegaRed: 8.21 Avg. % NileRed: 7.98	Avg. % MegaRed: 8.20 Avg. % NileRed: 11.2
420	421	422	423	424
				
Avg. % MegaRed: 8.18 Avg. % NileRed: 11.6	Avg. % MegaRed: 8.17 Avg. % NileRed: 1.82	Avg. % MegaRed: 8.17 Avg. % NileRed: 4.60	Avg. % MegaRed: 8.16 Avg. % NileRed: 8.24	Avg. % MegaRed: 8.15 Avg. % NileRed: 6.09
425	426	427	428	429
				
Avg. % MegaRed: 8.11 Avg. % NileRed: 1.03	Avg. % MegaRed: 8.10 Avg. % NileRed: 4.31	Avg. % MegaRed: 8.10 Avg. % NileRed: 14.7	Avg. % MegaRed: 8.09 Avg. % NileRed: 9.84	Avg. % MegaRed: 8.07 Avg. % NileRed: 9.41

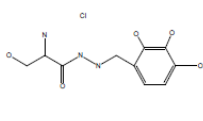
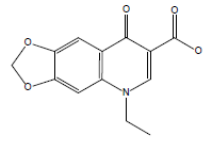
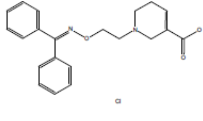
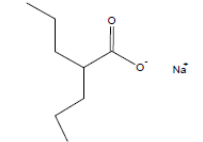
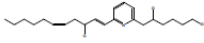
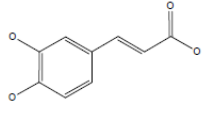
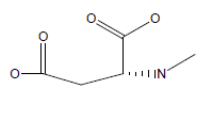
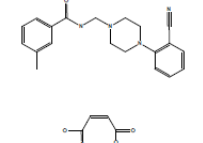
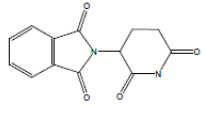
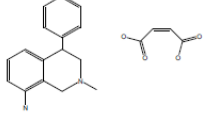
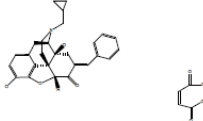
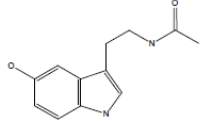
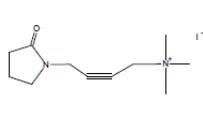
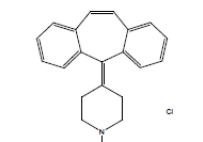
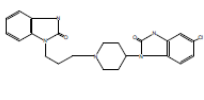
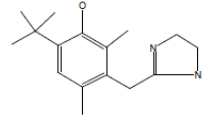
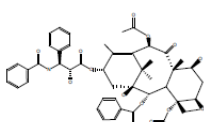
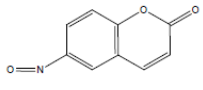
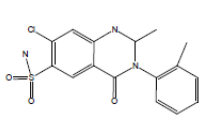
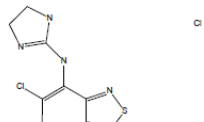
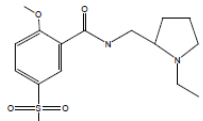
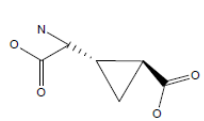
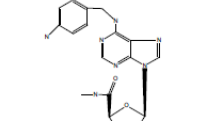
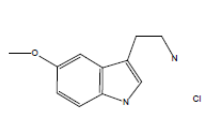
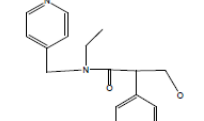
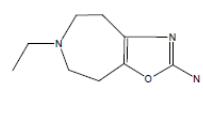
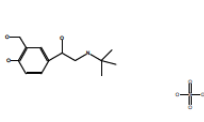
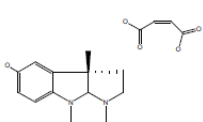
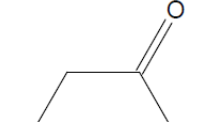
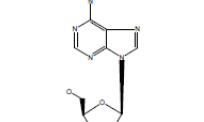
Continued, Table 22. Results of fluorescence-based drug-protein binding screen of the LOPAC library. Values are percent of Mega Red and Nile Red displaced. (n=3)

430	431	432	433	434
				
Avg. % MegaRed: 8.04 Avg. % NileRed: 9.43	Avg. % MegaRed: 8.01 Avg. % NileRed: 4.74	Avg. % MegaRed: 7.96 Avg. % NileRed: 5.40	Avg. % MegaRed: 7.95 Avg. % NileRed: 2.76	Avg. % MegaRed: 7.93 Avg. % NileRed: 3.80
435	436	437	438	439
				
Avg. % MegaRed: 7.90 Avg. % NileRed: 5.85	Avg. % MegaRed: 7.90 Avg. % NileRed: 2.12	Avg. % MegaRed: 7.89 Avg. % NileRed: 8.64	Avg. % MegaRed: 7.88 Avg. % NileRed: 1.69	Avg. % MegaRed: 7.87 Avg. % NileRed: 2.73
440	441	442	443	444
				
Avg. % MegaRed: 7.84 Avg. % NileRed: 3.84	Avg. % MegaRed: 7.83 Avg. % NileRed: 14.1	Avg. % MegaRed: 7.81 Avg. % NileRed: 21.4	Avg. % MegaRed: 7.78 Avg. % NileRed: 4.30	Avg. % MegaRed: 7.78 Avg. % NileRed: 5.63
445	446	447	448	449
				
Avg. % MegaRed: 7.77 Avg. % NileRed: 2.14	Avg. % MegaRed: 7.77 Avg. % NileRed: 9.85	Avg. % MegaRed: 7.74 Avg. % NileRed: 2.01	Avg. % MegaRed: 7.74 Avg. % NileRed: 7.94	Avg. % MegaRed: 7.74 Avg. % NileRed: 9.27
450	451	452	453	454
				
Avg. % MegaRed: 7.71 Avg. % NileRed: 2.20	Avg. % MegaRed: 7.70 Avg. % NileRed: 6.72	Avg. % MegaRed: 7.70 Avg. % NileRed: 1.72	Avg. % MegaRed: 7.69 Avg. % NileRed: 13.2	Avg. % MegaRed: 7.69 Avg. % NileRed: 7.23
456	457	458	459	460
				
Avg. % MegaRed: 7.65 Avg. % NileRed: 5.49	Avg. % MegaRed: 7.65 Avg. % NileRed: 2.90	Avg. % MegaRed: 7.63 Avg. % NileRed: 6.04	Avg. % MegaRed: 7.61 Avg. % NileRed: 14.0	Avg. % MegaRed: 7.60 Avg. % NileRed: 2.30

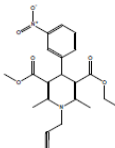
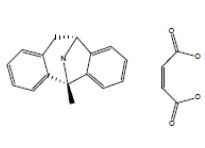
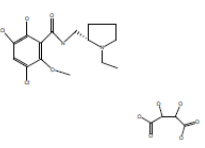
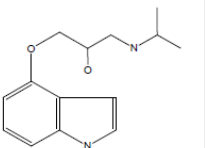
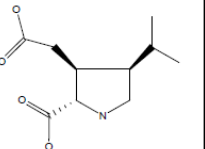
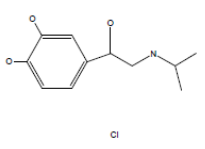
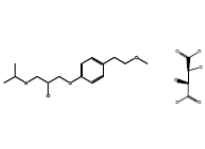
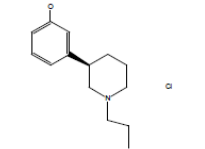
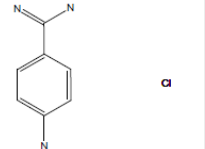
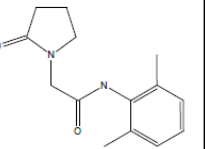
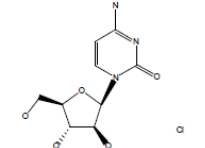
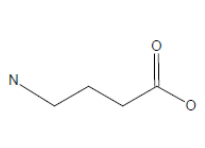
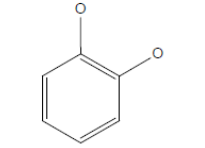
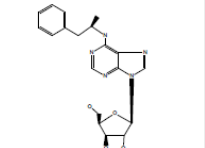
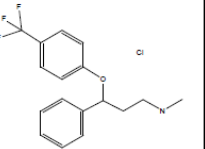
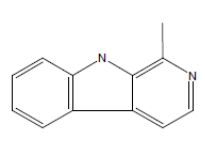
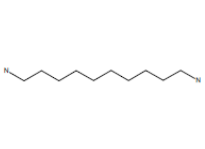
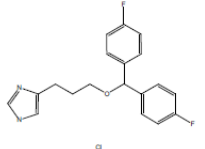
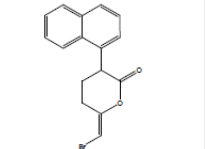
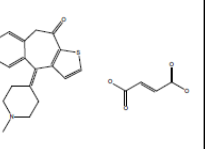
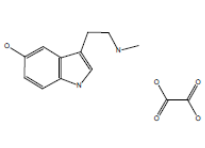
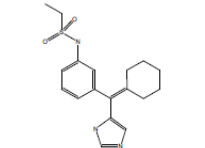
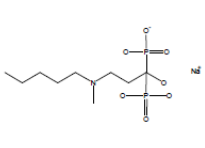
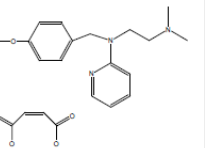
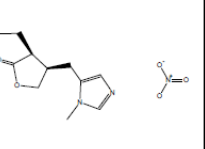
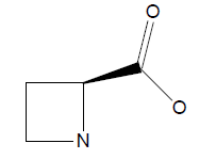
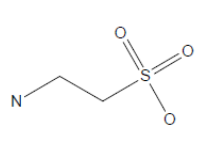
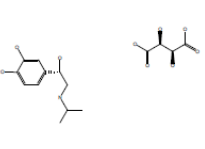
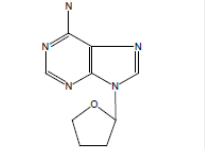
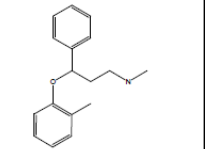
Continued, Table 22. Results of fluorescence-based drug-protein binding screen of the LOPAC library. Values are percent of Mega Red and Nile Red displaced. (n=3)

462	 Avg. % MegaRed: 7.58 Avg. % NileRed: 11.7	463	 Avg. % MegaRed: 7.57 Avg. % NileRed: 1.35	464	 Avg. % MegaRed: 7.56 Avg. % NileRed: 21.7	465	 Avg. % MegaRed: 7.54 Avg. % NileRed: 8.54	466	 Avg. % MegaRed: 7.49 Avg. % NileRed: 12.6
467	 Avg. % MegaRed: 7.45 Avg. % NileRed: 9.19	468	 Avg. % MegaRed: 7.44 Avg. % NileRed: 6.22	469	 Avg. % MegaRed: 7.44 Avg. % NileRed: 4.70	470	 Avg. % MegaRed: 7.41 Avg. % NileRed: 3.47	471	 Avg. % MegaRed: 7.40 Avg. % NileRed: 5.66
472	 Avg. % MegaRed: 7.33 Avg. % NileRed: 1.87	473	 Avg. % MegaRed: 7.32 Avg. % NileRed: 3.87	474	 Avg. % MegaRed: 7.30 Avg. % NileRed: 2.08	475	 Avg. % MegaRed: 7.30 Avg. % NileRed: 2.10	476	 Avg. % MegaRed: 7.28 Avg. % NileRed: 4.71
477	 Avg. % MegaRed: 7.21 Avg. % NileRed: 31.4	478	 Avg. % MegaRed: 7.20 Avg. % NileRed: 8.22	479	 Avg. % MegaRed: 7.13 Avg. % NileRed: 3.75	480	 Avg. % MegaRed: 7.13 Avg. % NileRed: 2.63	481	 Avg. % MegaRed: 7.12 Avg. % NileRed: 3.04
482	 Avg. % MegaRed: 7.10 Avg. % NileRed: 6.48	483	 Avg. % MegaRed: 7.09 Avg. % NileRed: 5.62	485	 Avg. % MegaRed: 7.07 Avg. % NileRed: 2.01	486	 Avg. % MegaRed: 7.04 Avg. % NileRed: 10.2	487	 Avg. % MegaRed: 7.04 Avg. % NileRed: 14.6
488	 Avg. % MegaRed: 7.00 Avg. % NileRed: 13.4	489	 Avg. % MegaRed: 6.97 Avg. % NileRed: 2.71	491	 Avg. % MegaRed: 6.94 Avg. % NileRed: 3.56	492	 Avg. % MegaRed: 6.92 Avg. % NileRed: 14.0	493	 Avg. % MegaRed: 6.91 Avg. % NileRed: 11.6

Continued, Table 22. Results of fluorescence-based drug-protein binding screen of the LOPAC library. Values are percent of Mega Red and Nile Red displaced. (n=3)

494	495	496	497	498
				
Avg. % MegaRed: 6.89 Avg. % NileRed: 16.3	Avg. % MegaRed: 6.86 Avg. % NileRed: 14.2	Avg. % MegaRed: 6.85 Avg. % NileRed: 7.28	Avg. % MegaRed: 6.82 Avg. % NileRed: 5.12	Avg. % MegaRed: 6.80 Avg. % NileRed: 3.87
499	500	501	502	503
				
Avg. % MegaRed: 6.80 Avg. % NileRed: 3.74	Avg. % MegaRed: 6.79 Avg. % NileRed: 0.78	Avg. % MegaRed: 6.75 Avg. % NileRed: 0.68	Avg. % MegaRed: 6.74 Avg. % NileRed: 6.31	Avg. % MegaRed: 6.73 Avg. % NileRed: 11.2
504	505	506	507	508
				
Avg. % MegaRed: 6.70 Avg. % NileRed: 3.63	Avg. % MegaRed: 6.68 Avg. % NileRed: 9.31	Avg. % MegaRed: 6.68 Avg. % NileRed: 14.2	Avg. % MegaRed: 6.64 Avg. % NileRed: 3.74	Avg. % MegaRed: 6.64 Avg. % NileRed: 0.45
509	510	511	512	513
				
Avg. % MegaRed: 6.64 Avg. % NileRed: 8.18	Avg. % MegaRed: 6.63 Avg. % NileRed: 10.4	Avg. % MegaRed: 6.63 Avg. % NileRed: 3.08	Avg. % MegaRed: 6.61 Avg. % NileRed: 1.02	Avg. % MegaRed: 6.60 Avg. % NileRed: 3.04
514	515	516	517	518
				
Avg. % MegaRed: 6.56 Avg. % NileRed: 2.16	Avg. % MegaRed: 6.56 Avg. % NileRed: 4.01	Avg. % MegaRed: 6.56 Avg. % NileRed: 3.24	Avg. % MegaRed: 6.55 Avg. % NileRed: 2.49	Avg. % MegaRed: 6.55 Avg. % NileRed: 10.7
519	520	521	522	523
				
Avg. % MegaRed: 6.53 Avg. % NileRed: 8.10	Avg. % MegaRed: 6.53 Avg. % NileRed: 7.17	Avg. % MegaRed: 6.53 Avg. % NileRed: 13.8	Avg. % MegaRed: 6.50 Avg. % NileRed: 3.30	Avg. % MegaRed: 6.49 Avg. % NileRed: 9.17

Continued, Table 22. Results of fluorescence-based drug-protein binding screen of the LOPAC library. Values are percent of Mega Red and Nile Red displaced. (n=3)

524	525	526	527	528
				
Avg. % MegaRed: 6.48 Avg. % NileRed: 17.8	Avg. % MegaRed: 6.48 Avg. % NileRed: 14.3	Avg. % MegaRed: 6.47 Avg. % NileRed: 4.52	Avg. % MegaRed: 6.47 Avg. % NileRed: 11.1	Avg. % MegaRed: 6.46 Avg. % NileRed: 2.91
529	530	531	532	533
				
Avg. % MegaRed: 6.45 Avg. % NileRed: 14.6	Avg. % MegaRed: 6.44 Avg. % NileRed: 2.23	Avg. % MegaRed: 6.43 Avg. % NileRed: 3.38	Avg. % MegaRed: 6.43 Avg. % NileRed: 3.86	Avg. % MegaRed: 6.43 Avg. % NileRed: 6.43
534	535	536	537	538
				
Avg. % MegaRed: 6.42 Avg. % NileRed: 14.4	Avg. % MegaRed: 6.42 Avg. % NileRed: 6.29	Avg. % MegaRed: 6.40 Avg. % NileRed: 5.04	Avg. % MegaRed: 6.40 Avg. % NileRed: 11.1	Avg. % MegaRed: 6.40 Avg. % NileRed: 8.85
539	540	541	542	543
				
Avg. % MegaRed: 6.39 Avg. % NileRed: 14.8	Avg. % MegaRed: 6.39 Avg. % NileRed: 6.34	Avg. % MegaRed: 6.38 Avg. % NileRed: 7.44	Avg. % MegaRed: 6.37 Avg. % NileRed: 7.04	Avg. % MegaRed: 6.35 Avg. % NileRed: 0.99
544	545	546	547	548
				
Avg. % MegaRed: 6.33 Avg. % NileRed: 5.33	Avg. % MegaRed: 6.33 Avg. % NileRed: 4.73	Avg. % MegaRed: 6.33 Avg. % NileRed: 4.06	Avg. % MegaRed: 6.32 Avg. % NileRed: 3.77	Avg. % MegaRed: 6.31 Avg. % NileRed: 6.40
549	550	551	552	553
				
Avg. % MegaRed: 6.31 Avg. % NileRed: 3.83	Avg. % MegaRed: 6.31 Avg. % NileRed: 9.41	Avg. % MegaRed: 6.30 Avg. % NileRed: 3.56	Avg. % MegaRed: 6.29 Avg. % NileRed: 12.2	Avg. % MegaRed: 6.29 Avg. % NileRed: 9.98

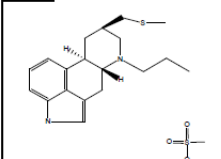
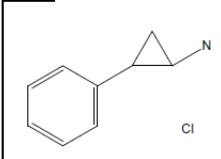
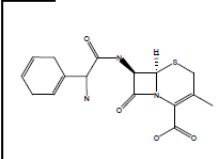
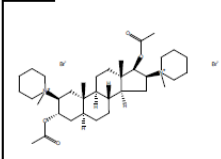
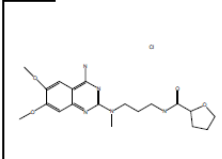
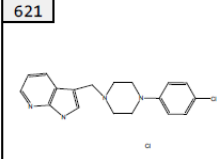
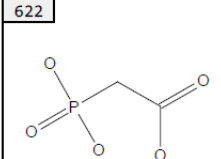
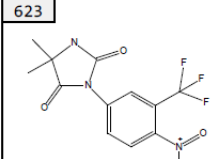
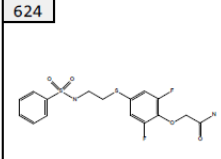
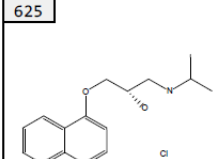
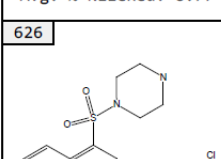
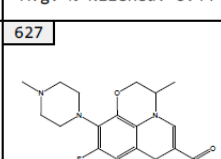
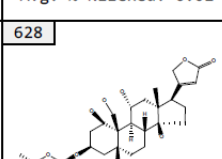
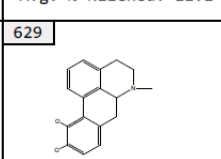
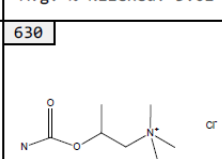
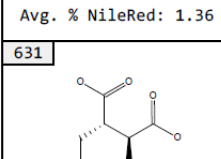
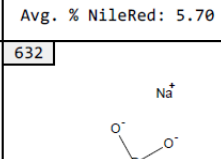
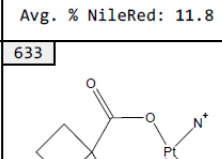
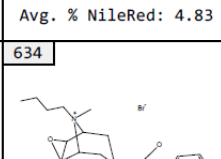
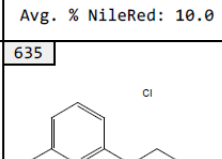
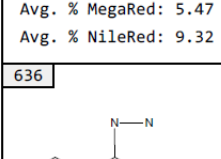
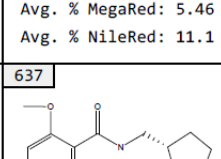
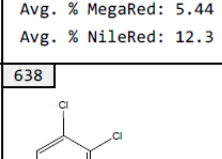
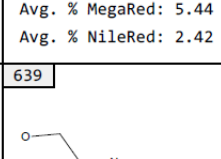
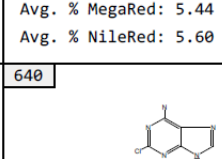
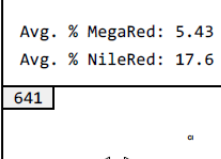
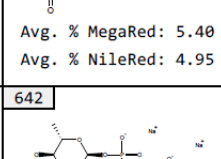
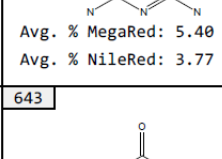
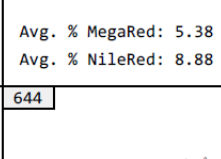
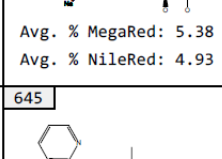
Continued, Table 22. Results of fluorescence-based drug-protein binding screen of the LOPAC library. Values are percent of Mega Red and Nile Red displaced. (n=3)

554	555	556	557	558
Avg. % MegaRed: 6.29 Avg. % NileRed: 19.7	Avg. % MegaRed: 6.29 Avg. % NileRed: 2.33	Avg. % MegaRed: 6.27 Avg. % NileRed: 20.7	Avg. % MegaRed: 6.27 Avg. % NileRed: 3.97	Avg. % MegaRed: 6.22 Avg. % NileRed: 16.0
559	560	561	562	563
Avg. % MegaRed: 6.20 Avg. % NileRed: 13.1	Avg. % MegaRed: 6.19 Avg. % NileRed: 11.7	Avg. % MegaRed: 6.16 Avg. % NileRed: 0.77	Avg. % MegaRed: 6.15 Avg. % NileRed: 4.03	Avg. % MegaRed: 6.15 Avg. % NileRed: 3.74
564	565	566	567	568
Avg. % MegaRed: 6.15 Avg. % NileRed: 4.01	Avg. % MegaRed: 6.13 Avg. % NileRed: 15.6	Avg. % MegaRed: 6.12 Avg. % NileRed: 11.7	Avg. % MegaRed: 6.11 Avg. % NileRed: 4.22	Avg. % MegaRed: 6.07 Avg. % NileRed: 1.98
569	570	571	572	573
Avg. % MegaRed: 6.04 Avg. % NileRed: 11.8	Avg. % MegaRed: 6.03 Avg. % NileRed: 6.98	Avg. % MegaRed: 6.03 Avg. % NileRed: 6.39	Avg. % MegaRed: 6.02 Avg. % NileRed: 6.53	Avg. % MegaRed: 6.00 Avg. % NileRed: 16.1
574	575	576	577	578
Avg. % MegaRed: 6.00 Avg. % NileRed: 3.34	Avg. % MegaRed: 6.00 Avg. % NileRed: 7.72	Avg. % MegaRed: 5.99 Avg. % NileRed: 7.36	Avg. % MegaRed: 5.97 Avg. % NileRed: 13.7	Avg. % MegaRed: 5.96 Avg. % NileRed: 7.67
579	580	581	582	583
Avg. % MegaRed: 5.94 Avg. % NileRed: 22.8	Avg. % MegaRed: 5.94 Avg. % NileRed: 4.17	Avg. % MegaRed: 5.93 Avg. % NileRed: 3.01	Avg. % MegaRed: 5.93 Avg. % NileRed: 4.57	Avg. % MegaRed: 5.92 Avg. % NileRed: 5.51

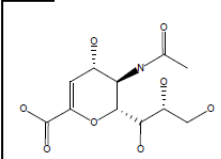
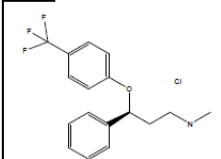
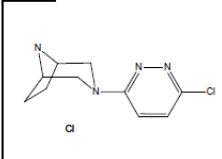
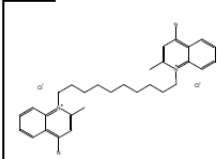
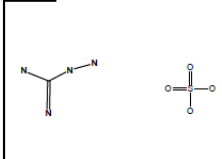
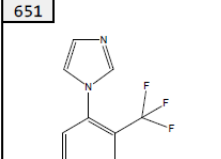
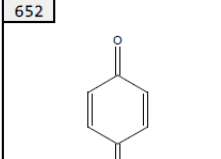
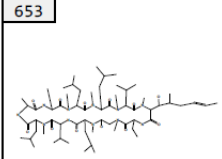
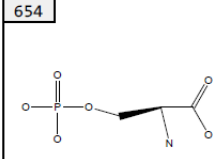
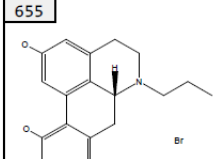
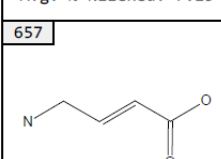
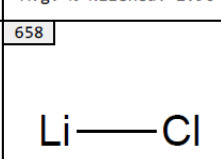
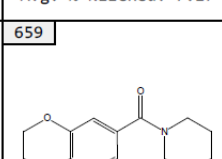
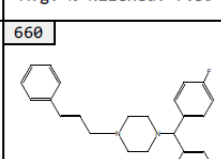
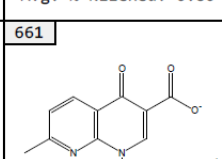
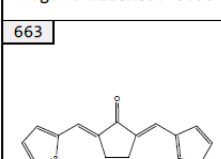
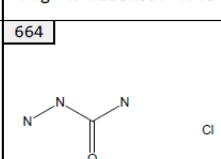
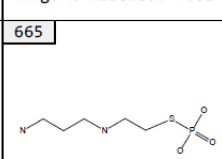
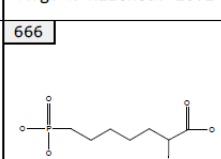
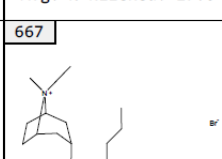
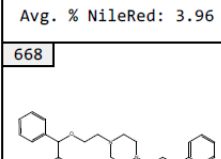
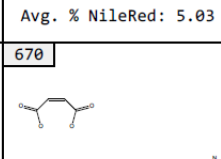
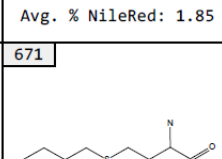
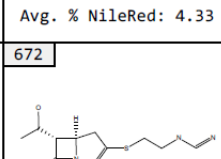
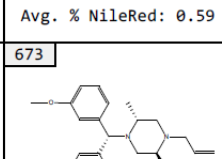
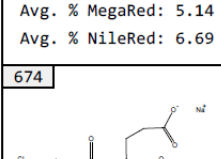
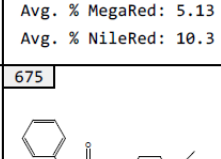
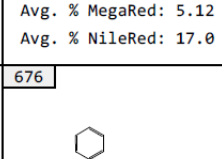
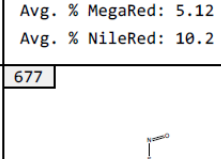
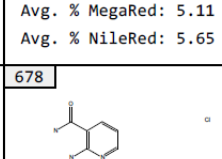
Continued, Table 22. Results of fluorescence-based drug-protein binding screen of the LOPAC library. Values are percent of Mega Red and Nile Red displaced. (n=3)

584	585	586	587	588
Avg. % MegaRed: 5.91 Avg. % NileRed: 11.5	Avg. % MegaRed: 5.91 Avg. % NileRed: 10.9	Avg. % MegaRed: 5.90 Avg. % NileRed: 0.94	Avg. % MegaRed: 5.90 Avg. % NileRed: 3.83	Avg. % MegaRed: 5.90 Avg. % NileRed: 3.13
589	590	591	592	593
Avg. % MegaRed: 5.89 Avg. % NileRed: 6.34	Avg. % MegaRed: 5.88 Avg. % NileRed: 16.4	Avg. % MegaRed: 5.87 Avg. % NileRed: 4.06	Avg. % MegaRed: 5.86 Avg. % NileRed: 2.08	Avg. % MegaRed: 5.84 Avg. % NileRed: 19.5
594	596	597	598	599
Avg. % MegaRed: 5.82 Avg. % NileRed: 1.20	Avg. % MegaRed: 5.81 Avg. % NileRed: 22.1	Avg. % MegaRed: 5.80 Avg. % NileRed: 8.91	Avg. % MegaRed: 5.79 Avg. % NileRed: 2.47	Avg. % MegaRed: 5.76 Avg. % NileRed: 6.75
600	601	602	603	604
Avg. % MegaRed: 5.75 Avg. % NileRed: 6.41	Avg. % MegaRed: 5.74 Avg. % NileRed: 12.1	Avg. % MegaRed: 5.74 Avg. % NileRed: 10.2	Avg. % MegaRed: 5.73 Avg. % NileRed: 2.88	Avg. % MegaRed: 5.73 Avg. % NileRed: 13.1
605	606	607	609	610
Avg. % MegaRed: 5.73 Avg. % NileRed: 10.1	Avg. % MegaRed: 5.70 Avg. % NileRed: 1.96	Avg. % MegaRed: 5.69 Avg. % NileRed: 4.27	Avg. % MegaRed: 5.68 Avg. % NileRed: 2.72	Avg. % MegaRed: 5.68 Avg. % NileRed: 3.09
611	612	613	614	615
Avg. % MegaRed: 5.67 Avg. % NileRed: 3.79	Avg. % MegaRed: 5.67 Avg. % NileRed: 5.27	Avg. % MegaRed: 5.67 Avg. % NileRed: 7.91	Avg. % MegaRed: 5.66 Avg. % NileRed: 14.7	Avg. % MegaRed: 5.65 Avg. % NileRed: 5.39

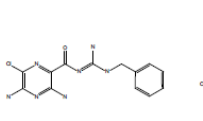
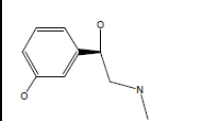
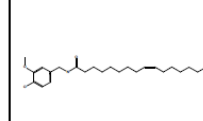
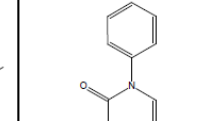
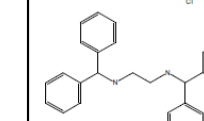
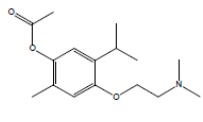
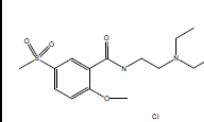
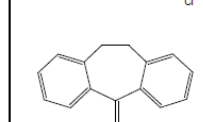
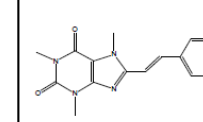
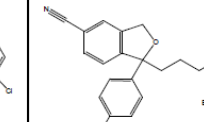
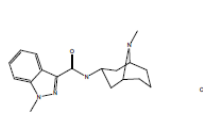
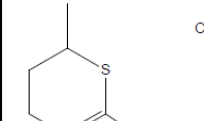
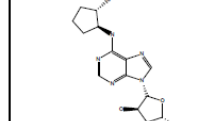
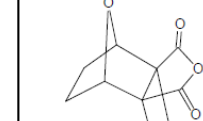
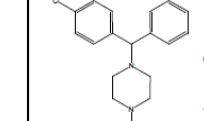
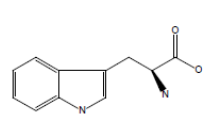
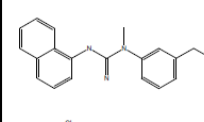
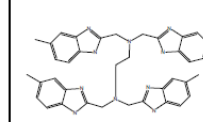
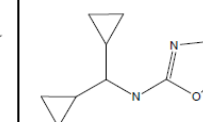
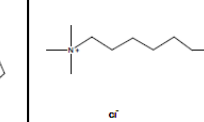
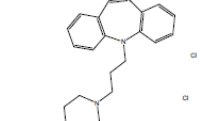
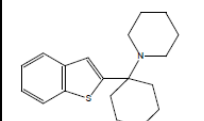
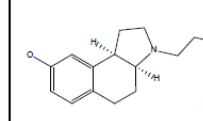
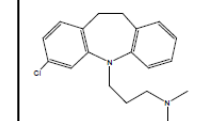
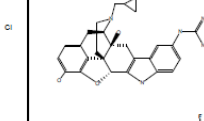
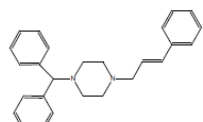
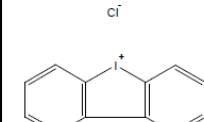
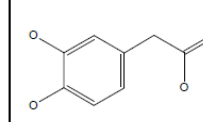
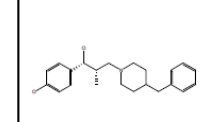
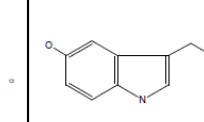
Continued, Table 22. Results of fluorescence-based drug-protein binding screen of the LOPAC library. Values are percent of Mega Red and Nile Red displaced. (n=3)

616	617	618	619	620
				
Avg. % MegaRed: 5.65 Avg. % NileRed: 6.65	Avg. % MegaRed: 5.64 Avg. % NileRed: 3.53	Avg. % MegaRed: 5.64 Avg. % NileRed: 5.11	Avg. % MegaRed: 5.59 Avg. % NileRed: 10.4	Avg. % MegaRed: 5.59 Avg. % NileRed: 9.52
621	622	623	624	625
				
Avg. % MegaRed: 5.58 Avg. % NileRed: 8.77	Avg. % MegaRed: 5.58 Avg. % NileRed: 8.44	Avg. % MegaRed: 5.57 Avg. % NileRed: 6.02	Avg. % MegaRed: 5.56 Avg. % NileRed: 11.2	Avg. % MegaRed: 5.56 Avg. % NileRed: 3.61
626	627	628	629	630
				
Avg. % MegaRed: 5.54 Avg. % NileRed: 1.36	Avg. % MegaRed: 5.52 Avg. % NileRed: 5.70	Avg. % MegaRed: 5.51 Avg. % NileRed: 11.8	Avg. % MegaRed: 5.49 Avg. % NileRed: 4.83	Avg. % MegaRed: 5.47 Avg. % NileRed: 10.0
631	632	633	634	635
				
Avg. % MegaRed: 5.47 Avg. % NileRed: 9.32	Avg. % MegaRed: 5.46 Avg. % NileRed: 11.1	Avg. % MegaRed: 5.44 Avg. % NileRed: 12.3	Avg. % MegaRed: 5.44 Avg. % NileRed: 2.42	Avg. % MegaRed: 5.44 Avg. % NileRed: 5.60
636	637	638	639	640
				
Avg. % MegaRed: 5.43 Avg. % NileRed: 17.6	Avg. % MegaRed: 5.40 Avg. % NileRed: 4.95	Avg. % MegaRed: 5.40 Avg. % NileRed: 3.77	Avg. % MegaRed: 5.38 Avg. % NileRed: 8.88	Avg. % MegaRed: 5.38 Avg. % NileRed: 4.93
641	642	643	644	645
				
Avg. % MegaRed: 5.36 Avg. % NileRed: 9.84	Avg. % MegaRed: 5.36 Avg. % NileRed: 3.32	Avg. % MegaRed: 5.35 Avg. % NileRed: 10.5	Avg. % MegaRed: 5.35 Avg. % NileRed: 3.65	Avg. % MegaRed: 5.34 Avg. % NileRed: 22.1

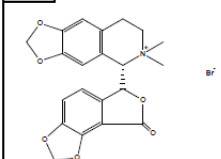
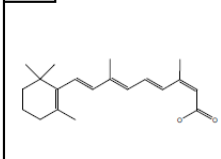
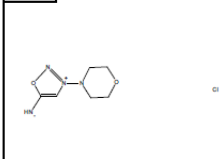
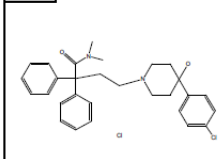
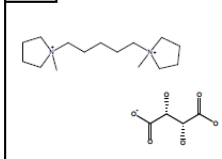
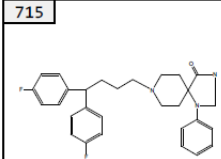
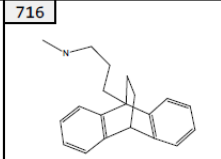
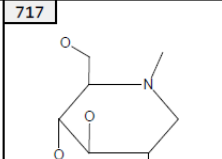
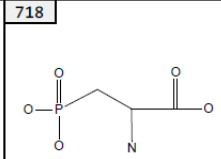
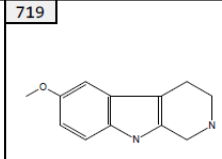
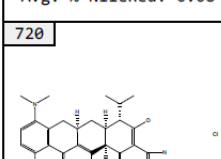
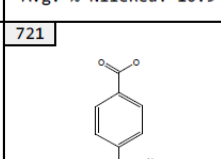
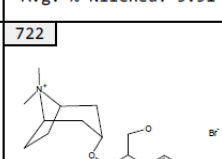
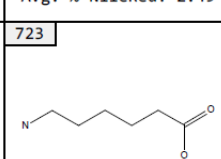
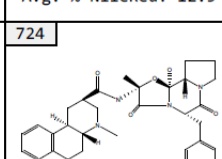
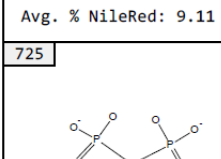
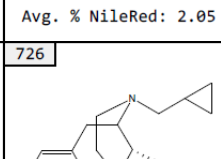
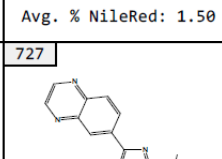
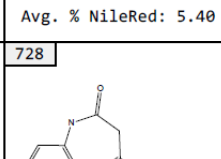
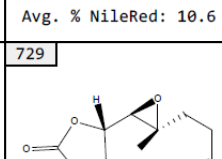
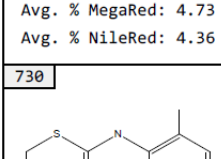
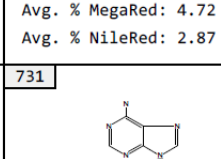
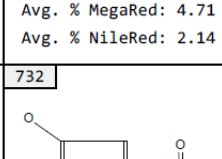
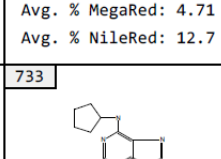
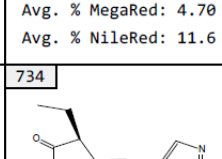
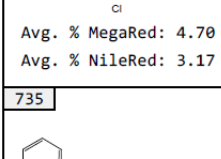
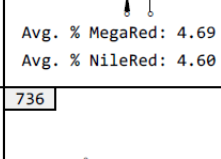
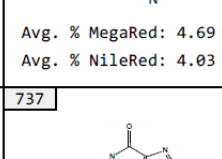
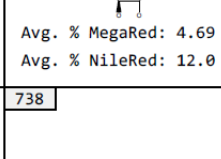
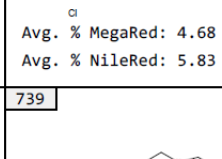
Continued, Table 22. Results of fluorescence-based drug-protein binding screen of the LOPAC library. Values are percent of Mega Red and Nile Red displaced. (n=3)

646	647	648	649	650
				
Avg. % MegaRed: 5.34 Avg. % NileRed: 3.28	Avg. % MegaRed: 5.34 Avg. % NileRed: 8.41	Avg. % MegaRed: 5.33 Avg. % NileRed: 2.59	Avg. % MegaRed: 5.33 Avg. % NileRed: 5.65	Avg. % MegaRed: 5.31 Avg. % NileRed: 4.49
651	652	653	654	655
				
Avg. % MegaRed: 5.30 Avg. % NileRed: 7.15	Avg. % MegaRed: 5.30 Avg. % NileRed: 2.96	Avg. % MegaRed: 5.29 Avg. % NileRed: 7.17	Avg. % MegaRed: 5.27 Avg. % NileRed: 7.39	Avg. % MegaRed: 5.25 Avg. % NileRed: 6.80
657	658	659	660	661
				
Avg. % MegaRed: 5.21 Avg. % NileRed: 6.80	Avg. % MegaRed: 5.21 Avg. % NileRed: 4.48	Avg. % MegaRed: 5.20 Avg. % NileRed: 4.81	Avg. % MegaRed: 5.19 Avg. % NileRed: 10.2	Avg. % MegaRed: 5.18 Avg. % NileRed: 17.6
663	664	665	666	667
				
Avg. % MegaRed: 5.18 Avg. % NileRed: 3.96	Avg. % MegaRed: 5.17 Avg. % NileRed: 5.03	Avg. % MegaRed: 5.17 Avg. % NileRed: 1.85	Avg. % MegaRed: 5.17 Avg. % NileRed: 4.33	Avg. % MegaRed: 5.16 Avg. % NileRed: 0.59
668	670	671	672	673
				
Avg. % MegaRed: 5.14 Avg. % NileRed: 6.69	Avg. % MegaRed: 5.13 Avg. % NileRed: 10.3	Avg. % MegaRed: 5.12 Avg. % NileRed: 17.0	Avg. % MegaRed: 5.12 Avg. % NileRed: 10.2	Avg. % MegaRed: 5.11 Avg. % NileRed: 5.65
674	675	676	677	678
				
Avg. % MegaRed: 5.11 Avg. % NileRed: 10.5	Avg. % MegaRed: 5.11 Avg. % NileRed: 1.59	Avg. % MegaRed: 5.10 Avg. % NileRed: 3.47	Avg. % MegaRed: 5.10 Avg. % NileRed: 5.23	Avg. % MegaRed: 5.09 Avg. % NileRed: 9.52

Continued, Table 22. Results of fluorescence-based drug-protein binding screen of the LOPAC library. Values are percent of Mega Red and Nile Red displaced. (n=3)

679	680	681	682	683
				
Avg. % MegaRed: 5.09 Avg. % NileRed: 12.1	Avg. % MegaRed: 5.09 Avg. % NileRed: 8.03	Avg. % MegaRed: 5.09 Avg. % NileRed: 8.34	Avg. % MegaRed: 5.09 Avg. % NileRed: 8.34	Avg. % MegaRed: 5.08 Avg. % NileRed: 4.41
684	685	686	687	688
				
Avg. % MegaRed: 5.07 Avg. % NileRed: 2.15	Avg. % MegaRed: 5.07 Avg. % NileRed: 8.58	Avg. % MegaRed: 5.06 Avg. % NileRed: 7.85	Avg. % MegaRed: 5.06 Avg. % NileRed: 3.49	Avg. % MegaRed: 5.03 Avg. % NileRed: 10.5
689	690	691	692	693
				
Avg. % MegaRed: 5.03 Avg. % NileRed: 8.40	Avg. % MegaRed: 5.02 Avg. % NileRed: 7.24	Avg. % MegaRed: 5.01 Avg. % NileRed: 7.62	Avg. % MegaRed: 5.00 Avg. % NileRed: 4.65	Avg. % MegaRed: 5.00 Avg. % NileRed: 1.98
694	695	696	697	698
				
Avg. % MegaRed: 4.98 Avg. % NileRed: 13.3	Avg. % MegaRed: 4.98 Avg. % NileRed: 18.1	Avg. % MegaRed: 4.98 Avg. % NileRed: 10.0	Avg. % MegaRed: 4.97 Avg. % NileRed: 6.53	Avg. % MegaRed: 4.97 Avg. % NileRed: 6.78
699	700	701	702	703
				
Avg. % MegaRed: 4.96 Avg. % NileRed: 7.52	Avg. % MegaRed: 4.96 Avg. % NileRed: 11.5	Avg. % MegaRed: 4.95 Avg. % NileRed: 5.67	Avg. % MegaRed: 4.92 Avg. % NileRed: 10.5	Avg. % MegaRed: 4.92 Avg. % NileRed: 10.6
704	705	706	707	708
				
Avg. % MegaRed: 4.91 Avg. % NileRed: 15.2	Avg. % MegaRed: 4.90 Avg. % NileRed: 3.26	Avg. % MegaRed: 4.90 Avg. % NileRed: 6.00	Avg. % MegaRed: 4.89 Avg. % NileRed: 1.89	Avg. % MegaRed: 4.88 Avg. % NileRed: 7.22

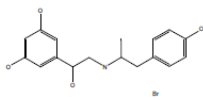
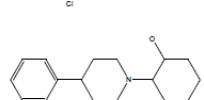
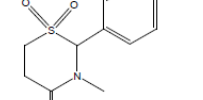
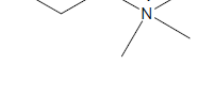
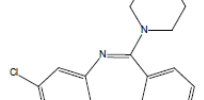
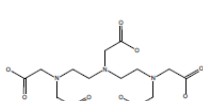
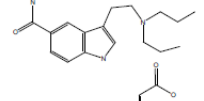
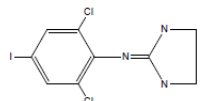
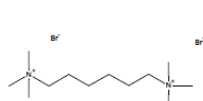
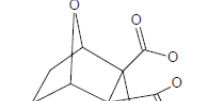
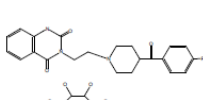
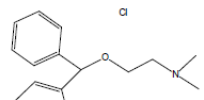
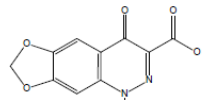
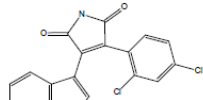
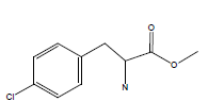
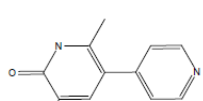
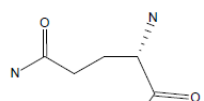
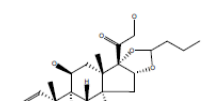
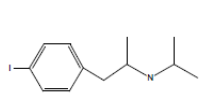
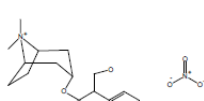
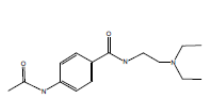
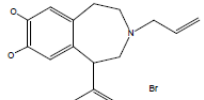
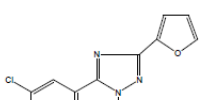
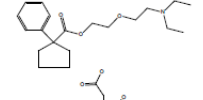
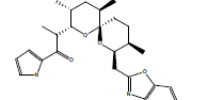
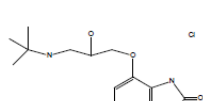
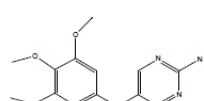
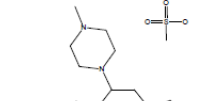
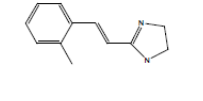
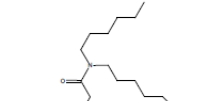
Continued, Table 22. Results of fluorescence-based drug-protein binding screen of the LOPAC library. Values are percent of Mega Red and Nile Red displaced. (n=3)

709	710	711	712	714
				
Avg. % MegaRed: 4.87 Avg. % NileRed: 8.77	Avg. % MegaRed: 4.87 Avg. % NileRed: 0.82	Avg. % MegaRed: 4.83 Avg. % NileRed: 3.23	Avg. % MegaRed: 4.82 Avg. % NileRed: 2.55	Avg. % MegaRed: 4.81 Avg. % NileRed: 3.88
715	716	717	718	719
				
Avg. % MegaRed: 4.81 Avg. % NileRed: 6.68	Avg. % MegaRed: 4.80 Avg. % NileRed: 10.9	Avg. % MegaRed: 4.80 Avg. % NileRed: 5.51	Avg. % MegaRed: 4.80 Avg. % NileRed: 2.49	Avg. % MegaRed: 4.80 Avg. % NileRed: 12.5
720	721	722	723	724
				
Avg. % MegaRed: 4.79 Avg. % NileRed: 9.11	Avg. % MegaRed: 4.78 Avg. % NileRed: 2.05	Avg. % MegaRed: 4.77 Avg. % NileRed: 1.50	Avg. % MegaRed: 4.76 Avg. % NileRed: 5.40	Avg. % MegaRed: 4.74 Avg. % NileRed: 10.6
725	726	727	728	729
				
Avg. % MegaRed: 4.73 Avg. % NileRed: 4.36	Avg. % MegaRed: 4.72 Avg. % NileRed: 2.87	Avg. % MegaRed: 4.71 Avg. % NileRed: 2.14	Avg. % MegaRed: 4.71 Avg. % NileRed: 12.7	Avg. % MegaRed: 4.70 Avg. % NileRed: 11.6
730	731	732	733	734
				
Avg. % MegaRed: 4.70 Avg. % NileRed: 3.17	Avg. % MegaRed: 4.69 Avg. % NileRed: 4.60	Avg. % MegaRed: 4.69 Avg. % NileRed: 4.03	Avg. % MegaRed: 4.69 Avg. % NileRed: 12.0	Avg. % MegaRed: 4.68 Avg. % NileRed: 5.83
735	736	737	738	739
				
Avg. % MegaRed: 4.68 Avg. % NileRed: 2.84	Avg. % MegaRed: 4.66 Avg. % NileRed: 10.4	Avg. % MegaRed: 4.62 Avg. % NileRed: 3.13	Avg. % MegaRed: 4.62 Avg. % NileRed: 11.0	Avg. % MegaRed: 4.62 Avg. % NileRed: 7.48

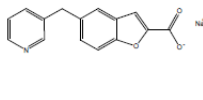
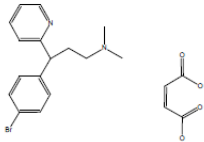
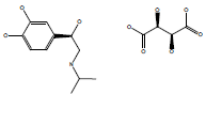
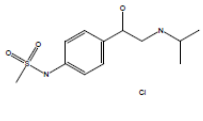
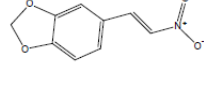
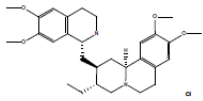
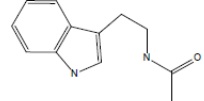
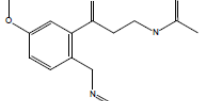
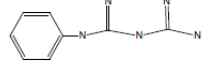
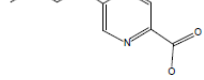
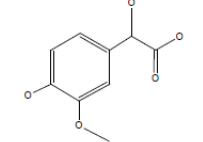
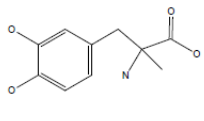
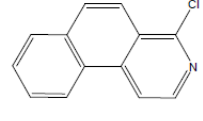
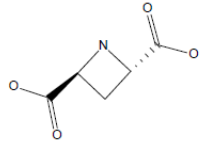
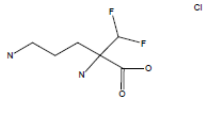
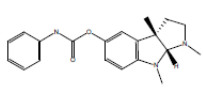
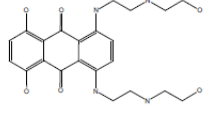
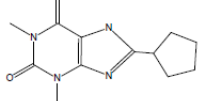
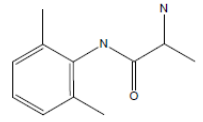
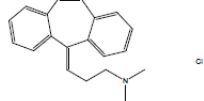
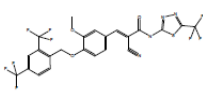
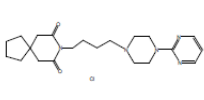
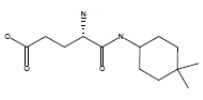
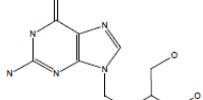
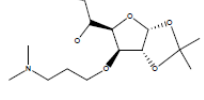
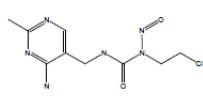
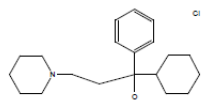
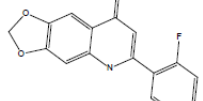
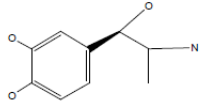
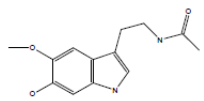
Continued, Table 22. Results of fluorescence-based drug-protein binding screen of the LOPAC library. Values are percent of Mega Red and Nile Red displaced. (n=3)

740 Avg. % MegaRed: 4.62 Avg. % NileRed: 12.4	741 Avg. % MegaRed: 4.61 Avg. % NileRed: 5.25	742 Avg. % MegaRed: 4.57 Avg. % NileRed: 1.78	743 Avg. % MegaRed: 4.57 Avg. % NileRed: 13.9	744 Avg. % MegaRed: 4.57 Avg. % NileRed: 3.86
745 Avg. % MegaRed: 4.56 Avg. % NileRed: 6.72	746 Avg. % MegaRed: 4.56 Avg. % NileRed: 3.18	747 Avg. % MegaRed: 4.55 Avg. % NileRed: 2.30	748 Avg. % MegaRed: 4.52 Avg. % NileRed: 1.36	749 Avg. % MegaRed: 4.51 Avg. % NileRed: 3.39
750 Avg. % MegaRed: 4.50 Avg. % NileRed: 16.8	751 Avg. % MegaRed: 4.48 Avg. % NileRed: 1.62	752 Avg. % MegaRed: 4.48 Avg. % NileRed: 12.5	753 Avg. % MegaRed: 4.48 Avg. % NileRed: 9.72	754 Avg. % MegaRed: 4.47 Avg. % NileRed: 2.07
755 Avg. % MegaRed: 4.47 Avg. % NileRed: 4.90	756 Avg. % MegaRed: 4.46 Avg. % NileRed: 6.39	757 Avg. % MegaRed: 4.46 Avg. % NileRed: 10.7	758 Avg. % MegaRed: 4.46 Avg. % NileRed: 3.04	759 Avg. % MegaRed: 4.44 Avg. % NileRed: 1.70
760 Avg. % MegaRed: 4.44 Avg. % NileRed: 10.3	761 Avg. % MegaRed: 4.43 Avg. % NileRed: 12.0	762 Avg. % MegaRed: 4.43 Avg. % NileRed: 6.76	763 Avg. % MegaRed: 4.41 Avg. % NileRed: 3.93	764 Avg. % MegaRed: 4.41 Avg. % NileRed: 6.79
765 Avg. % MegaRed: 4.40 Avg. % NileRed: 2.73	766 Avg. % MegaRed: 4.40 Avg. % NileRed: 5.20	767 Avg. % MegaRed: 4.39 Avg. % NileRed: 3.44	768 Avg. % MegaRed: 4.38 Avg. % NileRed: 4.09	769 Avg. % MegaRed: 4.38 Avg. % NileRed: 5.86

Continued, Table 22. Results of fluorescence-based drug-protein binding screen of the LOPAC library. Values are percent of Mega Red and Nile Red displaced. (n=3)

770	771	772	773	774
				
Avg. % MegaRed: 4.37 Avg. % NileRed: 9.73	Avg. % MegaRed: 4.37 Avg. % NileRed: 3.02	Avg. % MegaRed: 4.37 Avg. % NileRed: 2.54	Avg. % MegaRed: 4.36 Avg. % NileRed: 9.61	Avg. % MegaRed: 4.36 Avg. % NileRed: 26.9
775	776	778	779	780
				
Avg. % MegaRed: 4.36 Avg. % NileRed: 10.8	Avg. % MegaRed: 4.35 Avg. % NileRed: 3.88	Avg. % MegaRed: 4.33 Avg. % NileRed: 3.94	Avg. % MegaRed: 4.31 Avg. % NileRed: 12.0	Avg. % MegaRed: 4.30 Avg. % NileRed: 13.1
781	782	783	784	785
				
Avg. % MegaRed: 4.30 Avg. % NileRed: 14.1	Avg. % MegaRed: 4.30 Avg. % NileRed: 3.86	Avg. % MegaRed: 4.30 Avg. % NileRed: 15.4	Avg. % MegaRed: 4.29 Avg. % NileRed: 3.83	Avg. % MegaRed: 4.29 Avg. % NileRed: 21.0
786	787	788	789	790
				
Avg. % MegaRed: 4.28 Avg. % NileRed: 1.43	Avg. % MegaRed: 4.27 Avg. % NileRed: 1.96	Avg. % MegaRed: 4.27 Avg. % NileRed: 10.6	Avg. % MegaRed: 4.27 Avg. % NileRed: 1.96	Avg. % MegaRed: 4.26 Avg. % NileRed: 10.4
791	793	794	795	796
				
Avg. % MegaRed: 4.23 Avg. % NileRed: 7.43	Avg. % MegaRed: 4.22 Avg. % NileRed: 6.32	Avg. % MegaRed: 4.21 Avg. % NileRed: 0.48	Avg. % MegaRed: 4.20 Avg. % NileRed: 13.4	Avg. % MegaRed: 4.19 Avg. % NileRed: 2.92
797	798	799	800	801
				
Avg. % MegaRed: 4.19 Avg. % NileRed: 4.44	Avg. % MegaRed: 4.18 Avg. % NileRed: 8.90	Avg. % MegaRed: 4.15 Avg. % NileRed: 7.73	Avg. % MegaRed: 4.12 Avg. % NileRed: 4.20	Avg. % MegaRed: 4.11 Avg. % NileRed: 6.57

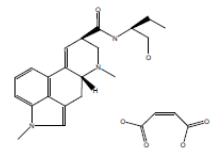
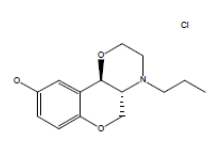
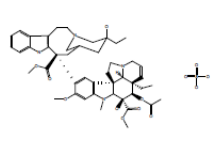
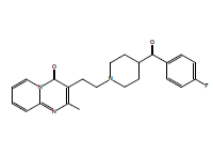
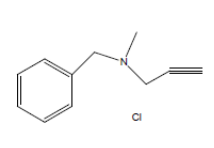
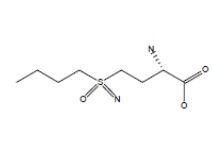
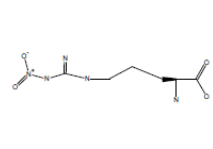
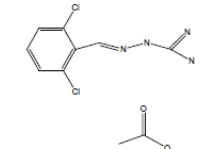
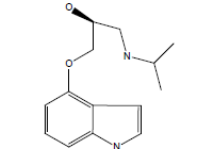
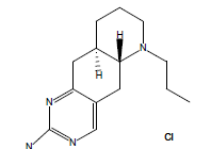
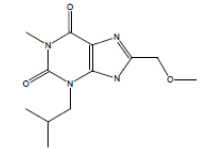
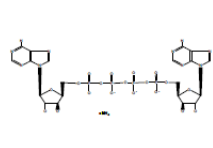
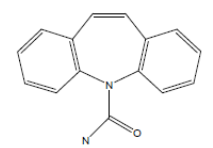
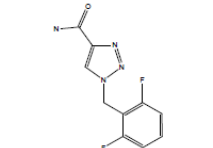
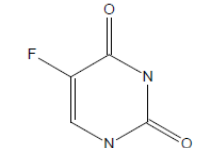
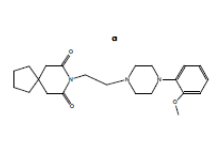
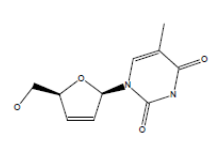
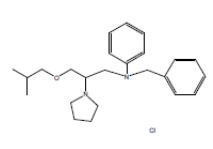
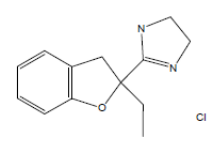
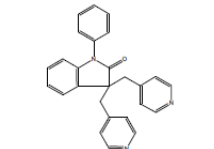
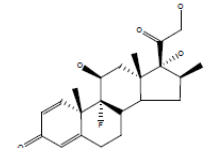
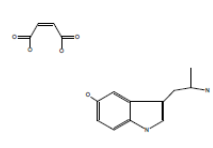
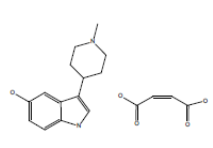
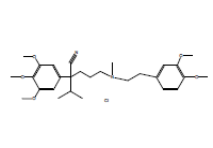
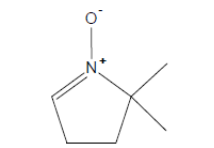
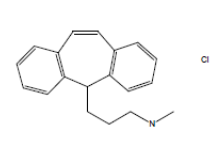
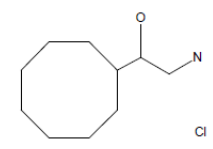
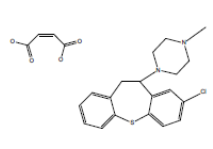
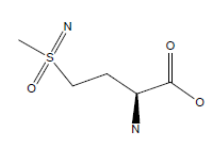
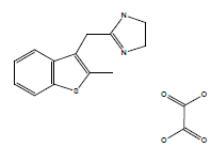
Continued, Table 22. Results of fluorescence-based drug-protein binding screen of the LOPAC library. Values are percent of Mega Red and Nile Red displaced. (n=3)

802	803	804	805	806
				
Avg. % MegaRed: 4.11 Avg. % NileRed: 14.6	Avg. % MegaRed: 4.11 Avg. % NileRed: 12.4	Avg. % MegaRed: 4.08 Avg. % NileRed: 4.08	Avg. % MegaRed: 4.07 Avg. % NileRed: 3.08	Avg. % MegaRed: 4.07 Avg. % NileRed: 12.4
807	808	809	810	811
				
Avg. % MegaRed: 4.07 Avg. % NileRed: 4.09	Avg. % MegaRed: 4.06 Avg. % NileRed: 10.7	Avg. % MegaRed: 4.06 Avg. % NileRed: 7.97	Avg. % MegaRed: 4.04 Avg. % NileRed: 6.77	Avg. % MegaRed: 4.03 Avg. % NileRed: 13.4
812	813	814	815	816
				
Avg. % MegaRed: 4.02 Avg. % NileRed: 8.43	Avg. % MegaRed: 4.02 Avg. % NileRed: 2.65	Avg. % MegaRed: 4.02 Avg. % NileRed: 19.5	Avg. % MegaRed: 4.01 Avg. % NileRed: 3.24	Avg. % MegaRed: 4.01 Avg. % NileRed: 2.19
817	818	819	820	821
				
Avg. % MegaRed: 4.01 Avg. % NileRed: 5.79	Avg. % MegaRed: 4.00 Avg. % NileRed: 15.9	Avg. % MegaRed: 4.00 Avg. % NileRed: 13.6	Avg. % MegaRed: 4.00 Avg. % NileRed: 4.31	Avg. % MegaRed: 3.99 Avg. % NileRed: 13.6
822	823	824	825	826
				
Avg. % MegaRed: 3.98 Avg. % NileRed: 9.40	Avg. % MegaRed: 3.98 Avg. % NileRed: 17.7	Avg. % MegaRed: 3.98 Avg. % NileRed: 5.92	Avg. % MegaRed: 3.98 Avg. % NileRed: 6.08	Avg. % MegaRed: 3.98 Avg. % NileRed: 4.57
827	828	829	830	831
				
Avg. % MegaRed: 3.97 Avg. % NileRed: 9.59	Avg. % MegaRed: 3.96 Avg. % NileRed: 11.4	Avg. % MegaRed: 3.95 Avg. % NileRed: 13.3	Avg. % MegaRed: 3.95 Avg. % NileRed: 3.23	Avg. % MegaRed: 3.94 Avg. % NileRed: 9.36

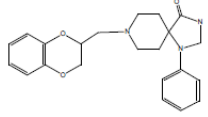
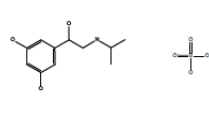
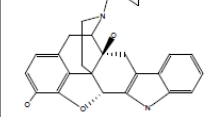
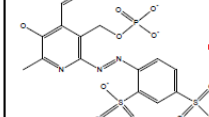
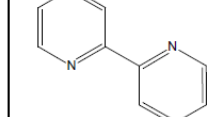
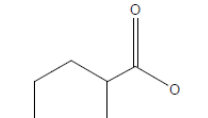
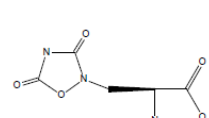
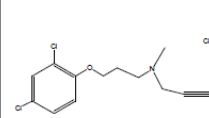
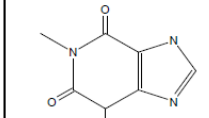
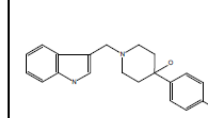
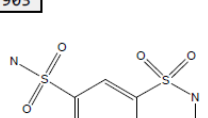
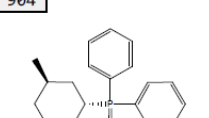
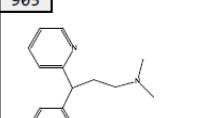
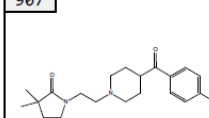
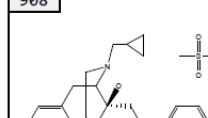
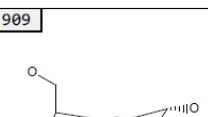
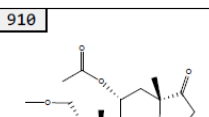
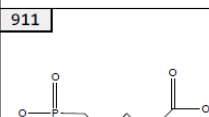
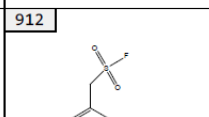
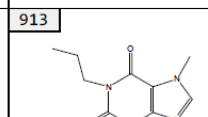
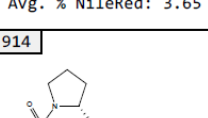
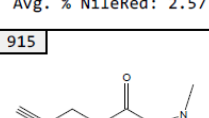
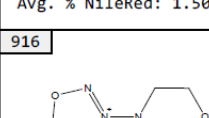
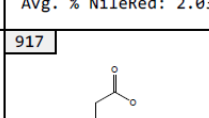
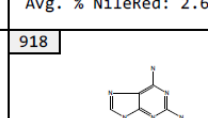
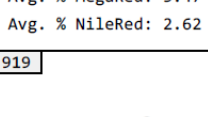
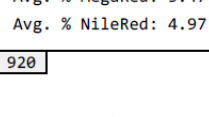
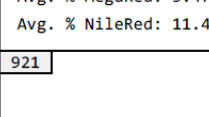
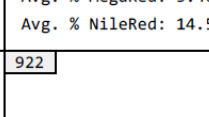
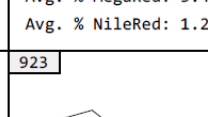
Continued, Table 22. Results of fluorescence-based drug-protein binding screen of the LOPAC library. Values are percent of Mega Red and Nile Red displaced. (n=3)

832	833	834	835	836
Avg. % MegaRed: 3.94 Avg. % NileRed: 6.58	Avg. % MegaRed: 3.93 Avg. % NileRed: 2.15	Avg. % MegaRed: 3.92 Avg. % NileRed: 5.18	Avg. % MegaRed: 3.91 Avg. % NileRed: 9.08	Avg. % MegaRed: 3.90 Avg. % NileRed: 7.62
837	838	839	840	841
Avg. % MegaRed: 3.89 Avg. % NileRed: 11.3	Avg. % MegaRed: 3.89 Avg. % NileRed: 7.23	Avg. % MegaRed: 3.88 Avg. % NileRed: 1.44	Avg. % MegaRed: 3.88 Avg. % NileRed: 7.07	Avg. % MegaRed: 3.88 Avg. % NileRed: 4.45
842	843	844	845	846
Avg. % MegaRed: 3.88 Avg. % NileRed: 6.32	Avg. % MegaRed: 3.87 Avg. % NileRed: 10.1	Avg. % MegaRed: 3.87 Avg. % NileRed: 9.34	Avg. % MegaRed: 3.87 Avg. % NileRed: 2.08	Avg. % MegaRed: 3.87 Avg. % NileRed: 3.23
847	848	849	850	852
Avg. % MegaRed: 3.86 Avg. % NileRed: 9.56	Avg. % MegaRed: 3.86 Avg. % NileRed: 5.89	Avg. % MegaRed: 3.85 Avg. % NileRed: 12.4	Avg. % MegaRed: 3.85 Avg. % NileRed: 5.99	Avg. % MegaRed: 3.84 Avg. % NileRed: 7.07
853	854	855	856	857
Avg. % MegaRed: 3.83 Avg. % NileRed: 2.79	Avg. % MegaRed: 3.82 Avg. % NileRed: 6.86	Avg. % MegaRed: 3.81 Avg. % NileRed: 4.21	Avg. % MegaRed: 3.81 Avg. % NileRed: 6.29	Avg. % MegaRed: 3.80 Avg. % NileRed: 5.77
858	859	860	861	862
Avg. % MegaRed: 3.80 Avg. % NileRed: 8.55	Avg. % MegaRed: 3.79 Avg. % NileRed: 3.25	Avg. % MegaRed: 3.79 Avg. % NileRed: 14.7	Avg. % MegaRed: 3.79 Avg. % NileRed: 8.15	Avg. % MegaRed: 3.78 Avg. % NileRed: 6.64

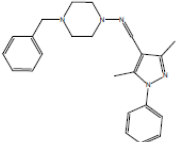
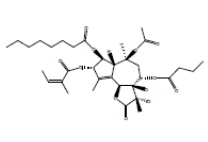
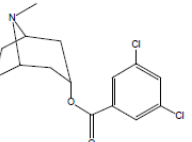
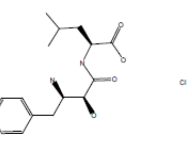
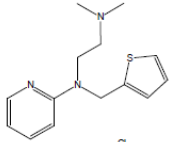
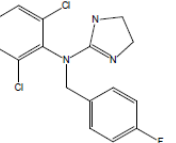
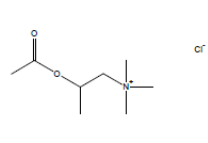
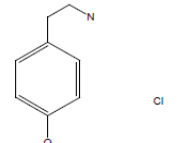
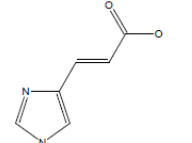
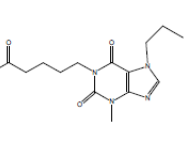
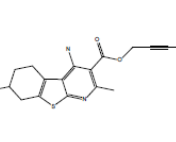
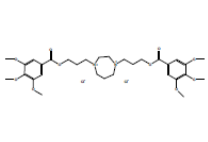
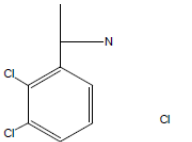
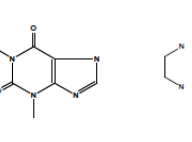
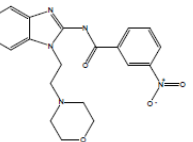
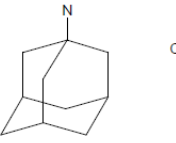
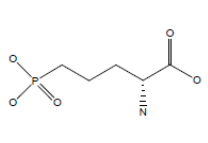
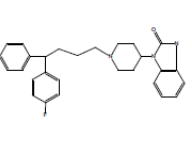
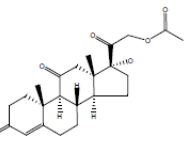
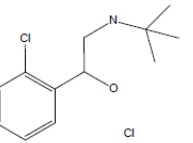
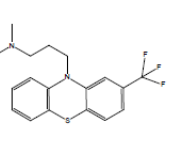
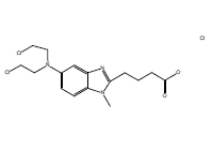
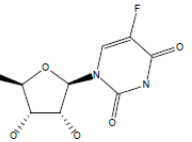
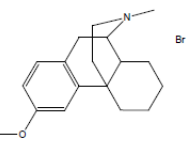
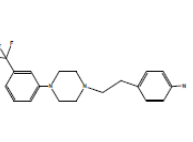
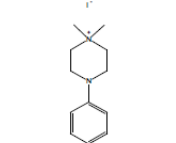
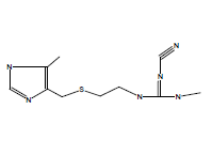
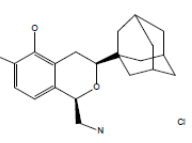
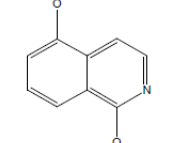
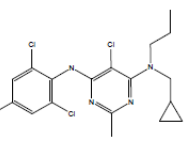
Continued, Table 22. Results of fluorescence-based drug-protein binding screen of the LOPAC library. Values are percent of Mega Red and Nile Red displaced. (n=3)

863	864	865	866	867
				
Avg. % MegaRed: 3.76 Avg. % NileRed: 10.6	Avg. % MegaRed: 3.76 Avg. % NileRed: 2.17	Avg. % MegaRed: 3.76 Avg. % NileRed: 2.17	Avg. % MegaRed: 3.75 Avg. % NileRed: 6.87	Avg. % MegaRed: 3.74 Avg. % NileRed: 1.59
868	869	870	871	872
				
Avg. % MegaRed: 3.74 Avg. % NileRed: 12.3	Avg. % MegaRed: 3.73 Avg. % NileRed: 3.70	Avg. % MegaRed: 3.73 Avg. % NileRed: 14.8	Avg. % MegaRed: 3.72 Avg. % NileRed: 5.74	Avg. % MegaRed: 3.71 Avg. % NileRed: 3.36
873	874	875	876	877
				
Avg. % MegaRed: 3.70 Avg. % NileRed: 3.68	Avg. % MegaRed: 3.70 Avg. % NileRed: 5.19	Avg. % MegaRed: 3.70 Avg. % NileRed: 18.5	Avg. % MegaRed: 3.70 Avg. % NileRed: 2.29	Avg. % MegaRed: 3.69 Avg. % NileRed: 6.66
878	879	880	881	882
				
Avg. % MegaRed: 3.69 Avg. % NileRed: 3.71	Avg. % MegaRed: 3.68 Avg. % NileRed: 2.68	Avg. % MegaRed: 3.67 Avg. % NileRed: 14.4	Avg. % MegaRed: 3.67 Avg. % NileRed: 9.30	Avg. % MegaRed: 3.67 Avg. % NileRed: 2.62
883	884	885	886	887
				
Avg. % MegaRed: 3.66 Avg. % NileRed: 16.3	Avg. % MegaRed: 3.66 Avg. % NileRed: 7.87	Avg. % MegaRed: 3.66 Avg. % NileRed: 5.17	Avg. % MegaRed: 3.63 Avg. % NileRed: 4.11	Avg. % MegaRed: 3.63 Avg. % NileRed: 2.11
888	889	890	891	892
				
Avg. % MegaRed: 3.63 Avg. % NileRed: 2.67	Avg. % MegaRed: 3.62 Avg. % NileRed: 4.02	Avg. % MegaRed: 3.61 Avg. % NileRed: 8.95	Avg. % MegaRed: 3.60 Avg. % NileRed: 2.69	Avg. % MegaRed: 3.60 Avg. % NileRed: 21.8

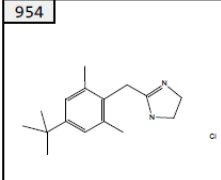
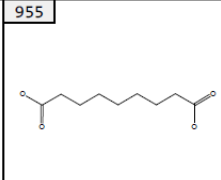
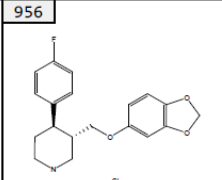
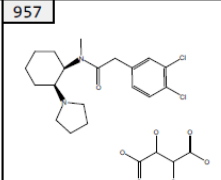
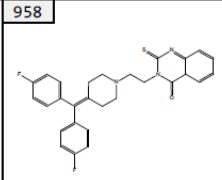
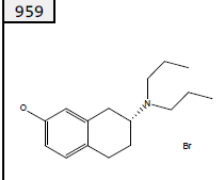
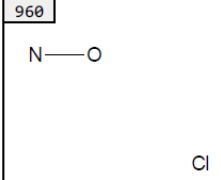
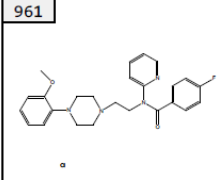
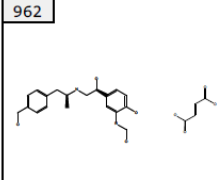
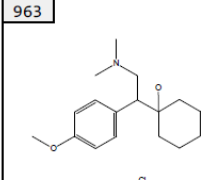
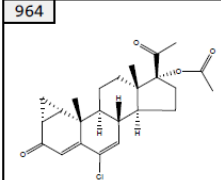
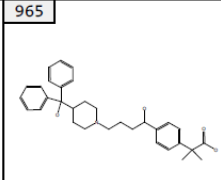
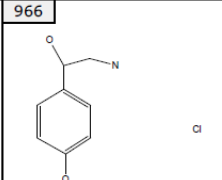
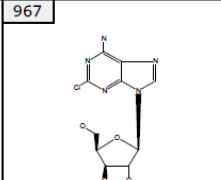
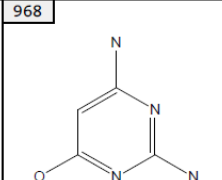
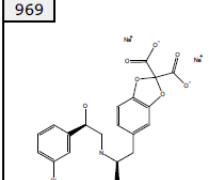
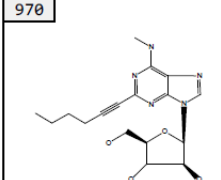
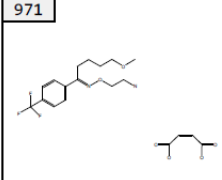
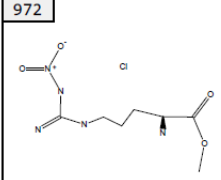
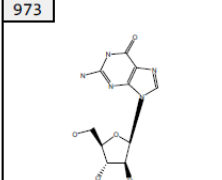
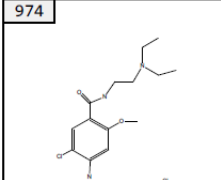
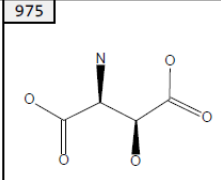
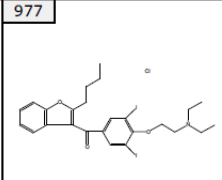
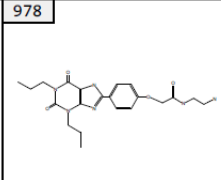
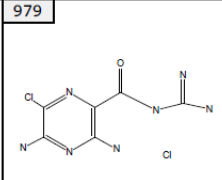
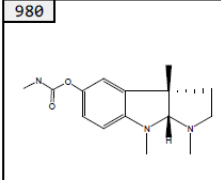
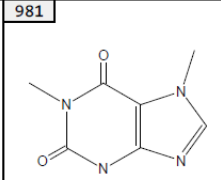
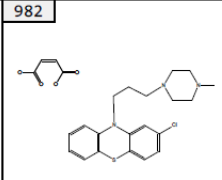
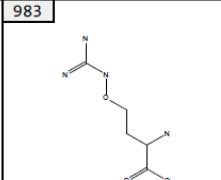
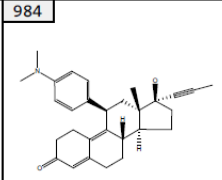
Continued, Table 22. Results of fluorescence-based drug-protein binding screen of the LOPAC library. Values are percent of Mega Red and Nile Red displaced. (n=3)

893	894	895	896	897
				
Avg. % MegaRed: 3.59 Avg. % NileRed: 7.10	Avg. % MegaRed: 3.59 Avg. % NileRed: 5.93	Avg. % MegaRed: 3.59 Avg. % NileRed: 4.73	Avg. % MegaRed: 3.57 Avg. % NileRed: 2.69	Avg. % MegaRed: 3.57 Avg. % NileRed: 13.2
898	899	900	901	902
				
Avg. % MegaRed: 3.55 Avg. % NileRed: 6.48	Avg. % MegaRed: 3.54 Avg. % NileRed: 1.76	Avg. % MegaRed: 3.53 Avg. % NileRed: 11.0	Avg. % MegaRed: 3.53 Avg. % NileRed: 8.16	Avg. % MegaRed: 3.52 Avg. % NileRed: 1.13
903	904	905	907	908
				
Avg. % MegaRed: 3.52 Avg. % NileRed: 12.7	Avg. % MegaRed: 3.51 Avg. % NileRed: 5.54	Avg. % MegaRed: 3.50 Avg. % NileRed: 13.1	Avg. % MegaRed: 3.50 Avg. % NileRed: 4.73	Avg. % MegaRed: 3.50 Avg. % NileRed: 9.46
909	910	911	912	913
				
Avg. % MegaRed: 3.49 Avg. % NileRed: 3.65	Avg. % MegaRed: 3.49 Avg. % NileRed: 2.57	Avg. % MegaRed: 3.49 Avg. % NileRed: 1.50	Avg. % MegaRed: 3.49 Avg. % NileRed: 2.03	Avg. % MegaRed: 3.47 Avg. % NileRed: 2.62
914	915	916	917	918
				
Avg. % MegaRed: 3.47 Avg. % NileRed: 2.62	Avg. % MegaRed: 3.47 Avg. % NileRed: 4.97	Avg. % MegaRed: 3.47 Avg. % NileRed: 11.4	Avg. % MegaRed: 3.46 Avg. % NileRed: 14.5	Avg. % MegaRed: 3.46 Avg. % NileRed: 1.28
919	920	921	922	923
				
Avg. % MegaRed: 3.46 Avg. % NileRed: 10.3	Avg. % MegaRed: 3.45 Avg. % NileRed: 2.76	Avg. % MegaRed: 3.45 Avg. % NileRed: 5.54	Avg. % MegaRed: 3.44 Avg. % NileRed: 22.2	Avg. % MegaRed: 3.44 Avg. % NileRed: 1.37

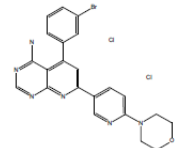
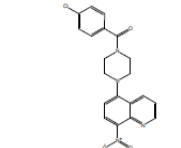
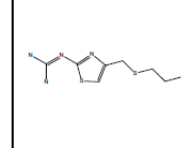
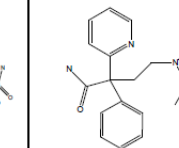
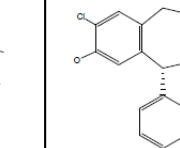
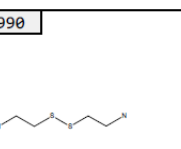
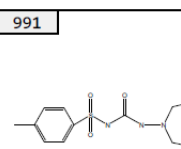
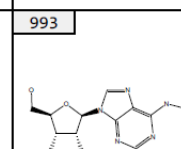
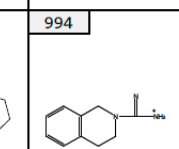
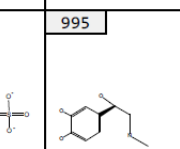
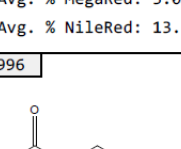
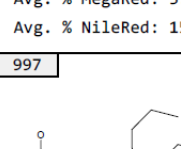
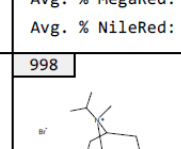
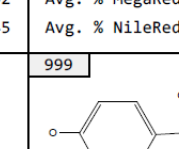
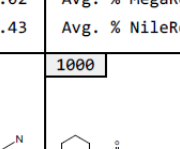
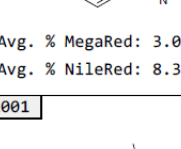
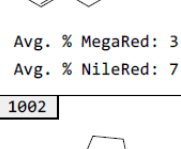
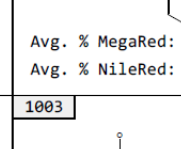
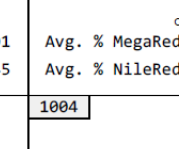
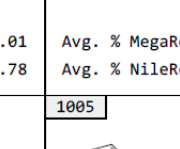
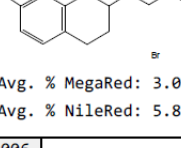
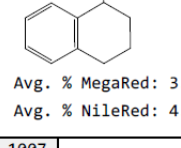
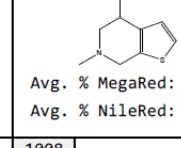
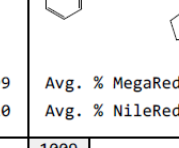
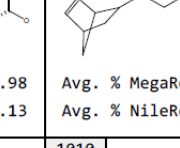
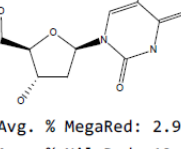
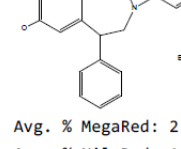
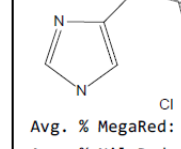
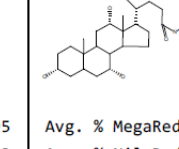
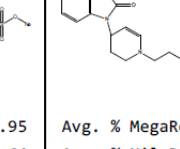
Continued, Table 22. Results of fluorescence-based drug-protein binding screen of the LOPAC library. Values are percent of Mega Red and Nile Red displaced. (n=3)

924	925	926	927	928
				
Avg. % MegaRed: 3.44 Avg. % NileRed: 3.98	Avg. % MegaRed: 3.43 Avg. % NileRed: 2.55	Avg. % MegaRed: 3.42 Avg. % NileRed: 6.09	Avg. % MegaRed: 3.42 Avg. % NileRed: 10.8	Avg. % MegaRed: 3.41 Avg. % NileRed: 10.1
929	930	931	932	933
				
Avg. % MegaRed: 3.41 Avg. % NileRed: 2.75	Avg. % MegaRed: 3.40 Avg. % NileRed: 2.55	Avg. % MegaRed: 3.40 Avg. % NileRed: 7.14	Avg. % MegaRed: 3.39 Avg. % NileRed: 7.39	Avg. % MegaRed: 3.39 Avg. % NileRed: 6.42
934	935	936	937	938
				
Avg. % MegaRed: 3.38 Avg. % NileRed: 18.1	Avg. % MegaRed: 3.38 Avg. % NileRed: 5.73	Avg. % MegaRed: 3.37 Avg. % NileRed: 3.63	Avg. % MegaRed: 3.37 Avg. % NileRed: 2.38	Avg. % MegaRed: 3.37 Avg. % NileRed: 2.56
939	940	941	942	943
				
Avg. % MegaRed: 3.36 Avg. % NileRed: 8.43	Avg. % MegaRed: 3.35 Avg. % NileRed: 2.67	Avg. % MegaRed: 3.35 Avg. % NileRed: 6.27	Avg. % MegaRed: 3.35 Avg. % NileRed: 21.4	Avg. % MegaRed: 3.34 Avg. % NileRed: 1.81
944	945	946	947	948
				
Avg. % MegaRed: 3.33 Avg. % NileRed: 4.83	Avg. % MegaRed: 3.32 Avg. % NileRed: 13.6	Avg. % MegaRed: 3.31 Avg. % NileRed: 5.90	Avg. % MegaRed: 3.30 Avg. % NileRed: 5.11	Avg. % MegaRed: 3.30 Avg. % NileRed: 4.54
949	950	951	952	953
				
Avg. % MegaRed: 3.30 Avg. % NileRed: 2.76	Avg. % MegaRed: 3.30 Avg. % NileRed: 12.5	Avg. % MegaRed: 3.27 Avg. % NileRed: 13.6	Avg. % MegaRed: 3.27 Avg. % NileRed: 0.62	Avg. % MegaRed: 3.27 Avg. % NileRed: 9.56

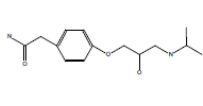
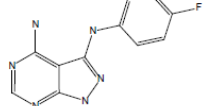
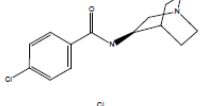
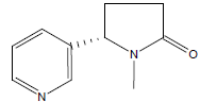
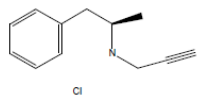
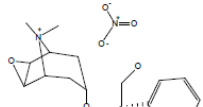
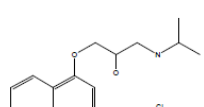
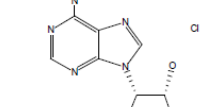
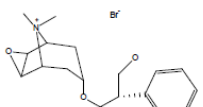
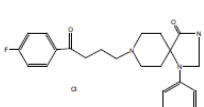
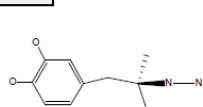
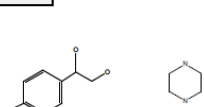
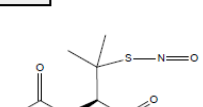
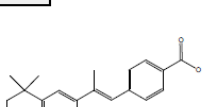
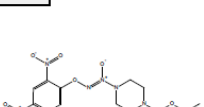
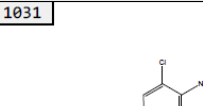
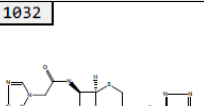
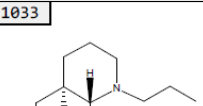
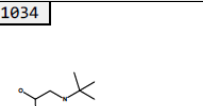

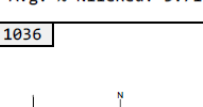
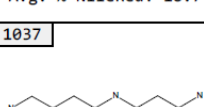
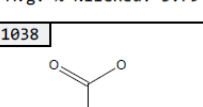
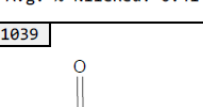
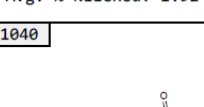
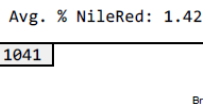
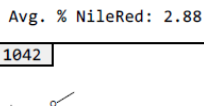
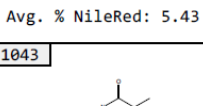
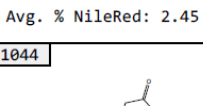
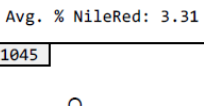
Continued, Table 22. Results of fluorescence-based drug-protein binding screen of the LOPAC library. Values are percent of Mega Red and Nile Red displaced. (n=3)

954	955	956	957	958
				
Avg. % MegaRed: 3.23 Avg. % NileRed: 5.21	Avg. % MegaRed: 3.23 Avg. % NileRed: 9.19	Avg. % MegaRed: 3.22 Avg. % NileRed: 2.56	Avg. % MegaRed: 3.22 Avg. % NileRed: 1.45	Avg. % MegaRed: 3.21 Avg. % NileRed: 13.0
959	960	961	962	963
				
Avg. % MegaRed: 3.20 Avg. % NileRed: 6.66	Avg. % MegaRed: 3.19 Avg. % NileRed: 10.1	Avg. % MegaRed: 3.18 Avg. % NileRed: 6.53	Avg. % MegaRed: 3.17 Avg. % NileRed: 6.80	Avg. % MegaRed: 3.17 Avg. % NileRed: 4.16
964	965	966	967	968
				
Avg. % MegaRed: 3.17 Avg. % NileRed: 15.3	Avg. % MegaRed: 3.16 Avg. % NileRed: 9.06	Avg. % MegaRed: 3.16 Avg. % NileRed: 11.8	Avg. % MegaRed: 3.16 Avg. % NileRed: 10.0	Avg. % MegaRed: 3.15 Avg. % NileRed: 0.96
969	970	971	972	973
				
Avg. % MegaRed: 3.14 Avg. % NileRed: 10.8	Avg. % MegaRed: 3.14 Avg. % NileRed: 6.42	Avg. % MegaRed: 3.13 Avg. % NileRed: 6.33	Avg. % MegaRed: 3.12 Avg. % NileRed: 2.81	Avg. % MegaRed: 3.11 Avg. % NileRed: 4.05
974	975	977	978	979
				
Avg. % MegaRed: 3.11 Avg. % NileRed: 1.47	Avg. % MegaRed: 3.10 Avg. % NileRed: 4.59	Avg. % MegaRed: 3.10 Avg. % NileRed: 18.7	Avg. % MegaRed: 3.09 Avg. % NileRed: 4.22	Avg. % MegaRed: 3.09 Avg. % NileRed: 15.4
980	981	982	983	984
				
Avg. % MegaRed: 3.09 Avg. % NileRed: 11.0	Avg. % MegaRed: 3.08 Avg. % NileRed: 1.14	Avg. % MegaRed: 3.08 Avg. % NileRed: 7.74	Avg. % MegaRed: 3.07 Avg. % NileRed: 3.85	Avg. % MegaRed: 3.06 Avg. % NileRed: 23.0

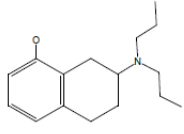
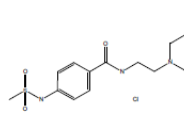
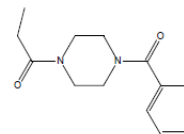
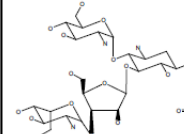
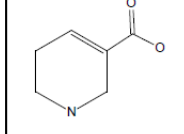
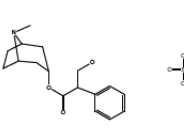
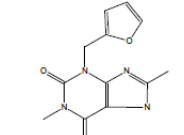
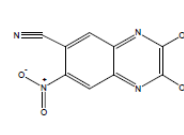
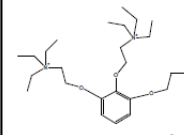
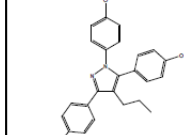
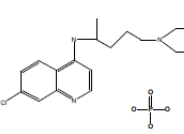
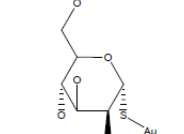
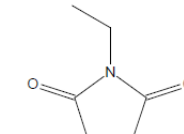
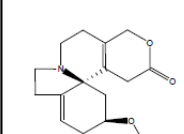
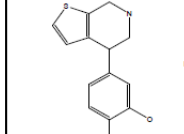
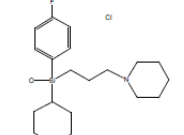
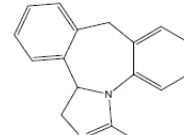
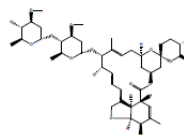
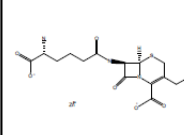
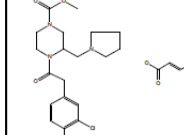
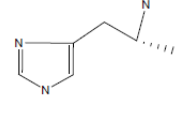
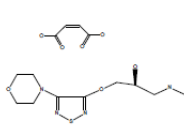
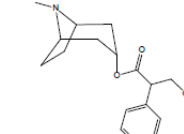
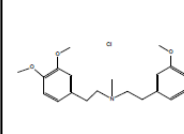
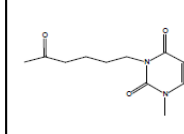
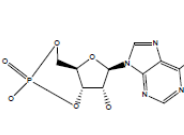
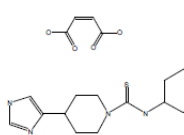
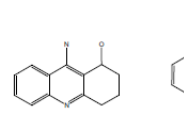
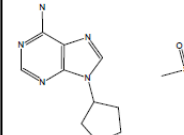
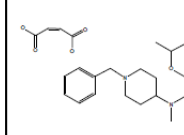
Continued, Table 22. Results of fluorescence-based drug-protein binding screen of the LOPAC library. Values are percent of Mega Red and Nile Red displaced. (n=3)

<p>985</p>  <p>Avg. % MegaRed: 3.05 Avg. % NileRed: 4.24</p>	<p>986</p>  <p>Avg. % MegaRed: 3.05 Avg. % NileRed: 3.90</p>	<p>987</p>  <p>Avg. % MegaRed: 3.04 Avg. % NileRed: 3.10</p>	<p>988</p>  <p>Avg. % MegaRed: 3.04 Avg. % NileRed: 6.23</p>	<p>989</p>  <p>Avg. % MegaRed: 3.03 Avg. % NileRed: 0.48</p>
<p>990</p>  <p>Avg. % MegaRed: 3.03 Avg. % NileRed: 13.5</p>	<p>991</p>  <p>Avg. % MegaRed: 3.03 Avg. % NileRed: 15.0</p>	<p>993</p>  <p>Avg. % MegaRed: 3.02 Avg. % NileRed: 5.45</p>	<p>994</p>  <p>Avg. % MegaRed: 3.02 Avg. % NileRed: 2.43</p>	<p>995</p>  <p>Avg. % MegaRed: 3.02 Avg. % NileRed: 8.10</p>
<p>996</p>  <p>Avg. % MegaRed: 3.01 Avg. % NileRed: 8.36</p>	<p>997</p>  <p>Avg. % MegaRed: 3.01 Avg. % NileRed: 7.71</p>	<p>998</p>  <p>Avg. % MegaRed: 3.01 Avg. % NileRed: 1.45</p>	<p>999</p>  <p>Avg. % MegaRed: 3.01 Avg. % NileRed: 8.78</p>	<p>1000</p>  <p>Avg. % MegaRed: 3.01 Avg. % NileRed: 5.82</p>
<p>1001</p>  <p>Avg. % MegaRed: 3.00 Avg. % NileRed: 5.88</p>	<p>1002</p>  <p>Avg. % MegaRed: 3.00 Avg. % NileRed: 4.03</p>	<p>1003</p>  <p>Avg. % MegaRed: 2.99 Avg. % NileRed: 4.20</p>	<p>1004</p>  <p>Avg. % MegaRed: 2.98 Avg. % NileRed: 4.13</p>	<p>1005</p>  <p>Avg. % MegaRed: 2.98 Avg. % NileRed: 8.37</p>
<p>1006</p>  <p>Avg. % MegaRed: 2.97 Avg. % NileRed: 12.9</p>	<p>1007</p>  <p>Avg. % MegaRed: 2.97 Avg. % NileRed: 1.00</p>	<p>1008</p>  <p>Avg. % MegaRed: 2.95 Avg. % NileRed: 5.63</p>	<p>1009</p>  <p>Avg. % MegaRed: 2.95 Avg. % NileRed: 4.64</p>	<p>1010</p>  <p>Avg. % MegaRed: 2.94 Avg. % NileRed: 3.42</p>
<p>1011</p>  <p>Avg. % MegaRed: 2.94 Avg. % NileRed: 5.79</p>	<p>1012</p>  <p>Avg. % MegaRed: 2.93 Avg. % NileRed: 2.01</p>	<p>1013</p>  <p>Avg. % MegaRed: 2.92 Avg. % NileRed: 4.14</p>	<p>1014</p>  <p>Avg. % MegaRed: 2.92 Avg. % NileRed: 13.1</p>	<p>1015</p>  <p>Avg. % MegaRed: 2.90 Avg. % NileRed: 2.39</p>

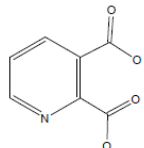
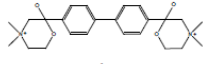
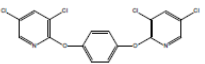
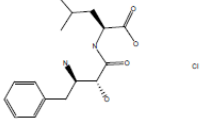
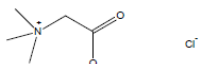
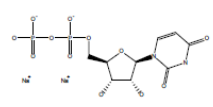
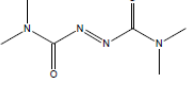
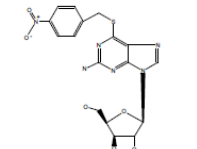
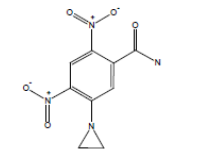
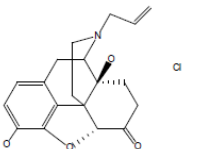
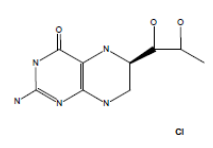
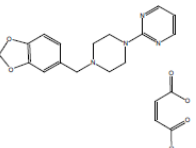
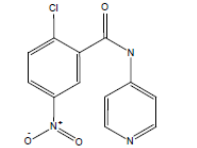
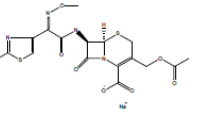
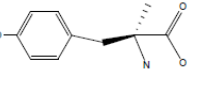
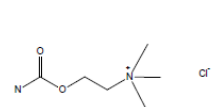
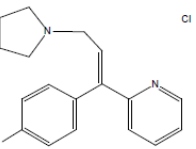
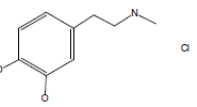
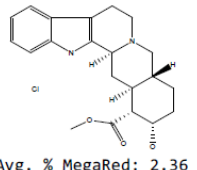
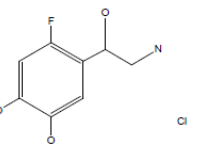
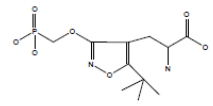
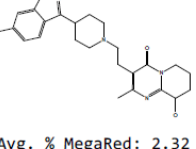
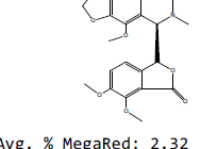
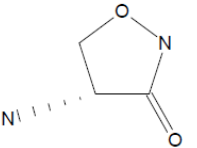
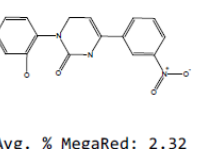
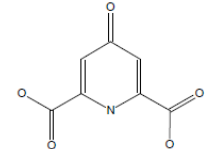
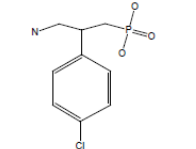
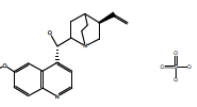
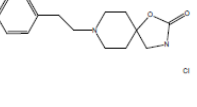
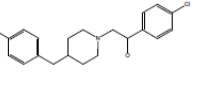
Continued, Table 22. Results of fluorescence-based drug-protein binding screen of the LOPAC library. Values are percent of Mega Red and Nile Red displaced. (n=3)

<p>1016</p>  <p>Avg. % MegaRed: 2.89 Avg. % NileRed: 4.67</p>	<p>1017</p>  <p>Avg. % MegaRed: 2.89 Avg. % NileRed: 3.56</p>	<p>1018</p>  <p>Avg. % MegaRed: 2.89 Avg. % NileRed: 4.75</p>	<p>1019</p>  <p>Avg. % MegaRed: 2.88 Avg. % NileRed: 3.82</p>	<p>1020</p>  <p>Avg. % MegaRed: 2.86 Avg. % NileRed: 9.05</p>
<p>1021</p>  <p>Avg. % MegaRed: 2.86 Avg. % NileRed: 5.52</p>	<p>1022</p>  <p>Avg. % MegaRed: 2.81 Avg. % NileRed: 4.12</p>	<p>1023</p>  <p>Avg. % MegaRed: 2.81 Avg. % NileRed: 5.47</p>	<p>1024</p>  <p>Avg. % MegaRed: 2.81 Avg. % NileRed: 2.09</p>	<p>1025</p>  <p>Avg. % MegaRed: 2.81 Avg. % NileRed: 3.87</p>
<p>1026</p>  <p>Avg. % MegaRed: 2.80 Avg. % NileRed: 4.59</p>	<p>1027</p>  <p>Avg. % MegaRed: 2.79 Avg. % NileRed: 9.38</p>	<p>1028</p>  <p>Avg. % MegaRed: 2.77 Avg. % NileRed: 10.3</p>	<p>1029</p>  <p>Avg. % MegaRed: 2.77 Avg. % NileRed: 10.8</p>	<p>1030</p>  <p>Avg. % MegaRed: 2.77 Avg. % NileRed: 3.85</p>
<p>1031</p>  <p>Avg. % MegaRed: 2.75 Avg. % NileRed: 3.71</p>	<p>1032</p>  <p>Avg. % MegaRed: 2.73 Avg. % NileRed: 18.7</p>	<p>1033</p>  <p>Avg. % MegaRed: 2.73 Avg. % NileRed: 3.79</p>	<p>1034</p>  <p>Avg. % MegaRed: 2.72 Avg. % NileRed: 6.41</p>	<p>1035</p>  <p>Avg. % MegaRed: 2.72 Avg. % NileRed: 1.92</p>
<p>1036</p>  <p>Avg. % MegaRed: 2.70 Avg. % NileRed: 1.42</p>	<p>1037</p>  <p>Avg. % MegaRed: 2.69 Avg. % NileRed: 2.88</p>	<p>1038</p>  <p>Avg. % MegaRed: 2.69 Avg. % NileRed: 5.43</p>	<p>1039</p>  <p>Avg. % MegaRed: 2.68 Avg. % NileRed: 2.45</p>	<p>1040</p>  <p>Avg. % MegaRed: 2.67 Avg. % NileRed: 3.31</p>
<p>1041</p>  <p>Avg. % MegaRed: 2.67 Avg. % NileRed: 2.25</p>	<p>1042</p>  <p>Avg. % MegaRed: 2.67 Avg. % NileRed: 2.62</p>	<p>1043</p>  <p>Avg. % MegaRed: 2.65 Avg. % NileRed: 2.87</p>	<p>1044</p>  <p>Avg. % MegaRed: 2.65 Avg. % NileRed: 32.9</p>	<p>1045</p>  <p>Avg. % MegaRed: 2.64 Avg. % NileRed: 18.2</p>

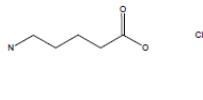
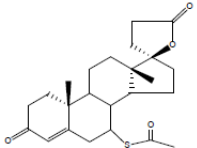
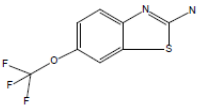
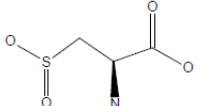
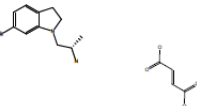
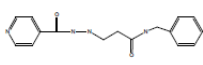
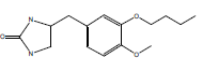
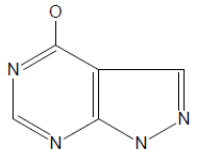
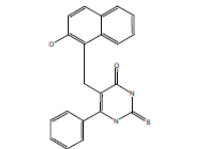
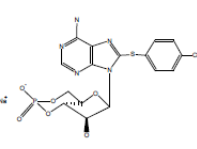
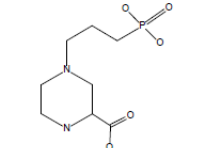
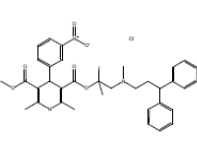
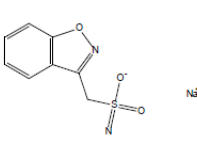
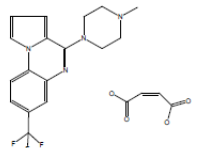
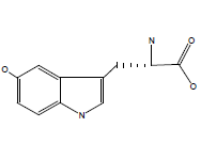
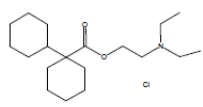
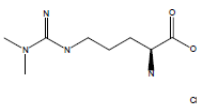
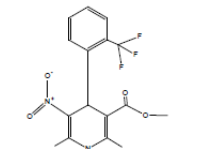
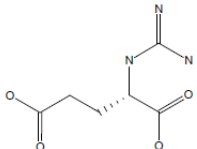
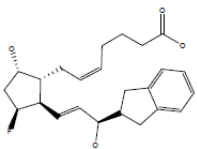
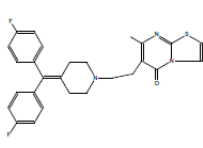
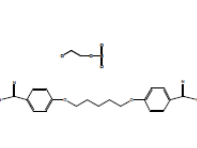
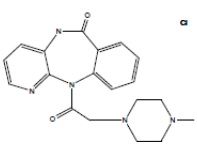
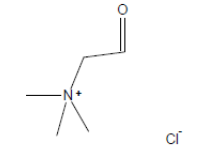
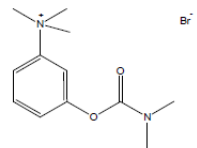
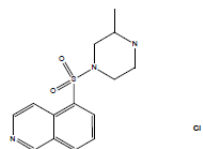
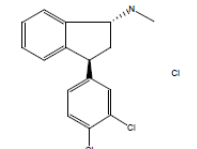
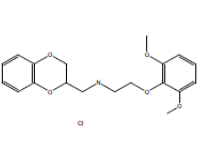
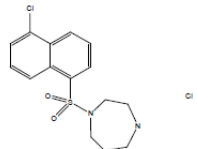
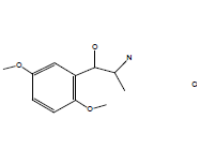
Continued, Table 22. Results of fluorescence-based drug-protein binding screen of the LOPAC library. Values are percent of Mega Red and Nile Red displaced. (n=3)

<p>1046</p>  <p>Avg. % MegaRed: 2.64 Avg. % NileRed: 2.45</p>	<p>1047</p>  <p>Avg. % MegaRed: 2.64 Avg. % NileRed: 4.23</p>	<p>1048</p>  <p>Avg. % MegaRed: 2.61 Avg. % NileRed: 1.27</p>	<p>1049</p>  <p>Avg. % MegaRed: 2.61 Avg. % NileRed: 3.06</p>	<p>1050</p>  <p>Avg. % MegaRed: 2.60 Avg. % NileRed: 12.5</p>
<p>1051</p>  <p>Avg. % MegaRed: 2.58 Avg. % NileRed: 6.36</p>	<p>1052</p>  <p>Avg. % MegaRed: 2.57 Avg. % NileRed: 6.21</p>	<p>1053</p>  <p>Avg. % MegaRed: 2.56 Avg. % NileRed: 2.25</p>	<p>1054</p>  <p>Avg. % MegaRed: 2.56 Avg. % NileRed: 5.17</p>	<p>1055</p>  <p>Avg. % MegaRed: 2.55 Avg. % NileRed: 24.6</p>
<p>1056</p>  <p>Avg. % MegaRed: 2.55 Avg. % NileRed: 6.58</p>	<p>1057</p>  <p>Avg. % MegaRed: 2.55 Avg. % NileRed: 1.57</p>	<p>1058</p>  <p>Avg. % MegaRed: 2.54 Avg. % NileRed: 11.5</p>	<p>1059</p>  <p>Avg. % MegaRed: 2.54 Avg. % NileRed: 3.81</p>	<p>1060</p>  <p>Avg. % MegaRed: 2.54 Avg. % NileRed: 5.37</p>
<p>1061</p>  <p>Avg. % MegaRed: 2.54 Avg. % NileRed: 2.38</p>	<p>1062</p>  <p>Avg. % MegaRed: 2.54 Avg. % NileRed: 9.28</p>	<p>1063</p>  <p>Avg. % MegaRed: 2.53 Avg. % NileRed: 10.4</p>	<p>1064</p>  <p>Avg. % MegaRed: 2.51 Avg. % NileRed: 9.57</p>	<p>1065</p>  <p>Avg. % MegaRed: 2.51 Avg. % NileRed: 9.47</p>
<p>1066</p>  <p>Avg. % MegaRed: 2.50 Avg. % NileRed: 4.42</p>	<p>1067</p>  <p>Avg. % MegaRed: 2.50 Avg. % NileRed: 2.68</p>	<p>1068</p>  <p>Avg. % MegaRed: 2.50 Avg. % NileRed: 7.09</p>	<p>1069</p>  <p>Avg. % MegaRed: 2.49 Avg. % NileRed: 1.91</p>	<p>1070</p>  <p>Avg. % MegaRed: 2.49 Avg. % NileRed: 5.97</p>
<p>1071</p>  <p>Avg. % MegaRed: 2.48 Avg. % NileRed: 6.24</p>	<p>1072</p>  <p>Avg. % MegaRed: 2.48 Avg. % NileRed: 7.01</p>	<p>1073</p>  <p>Avg. % MegaRed: 2.47 Avg. % NileRed: 4.86</p>	<p>1074</p>  <p>Avg. % MegaRed: 2.47 Avg. % NileRed: 13.2</p>	<p>1075</p>  <p>Avg. % MegaRed: 2.46 Avg. % NileRed: 9.56</p>

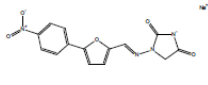
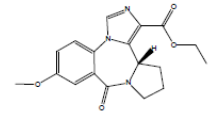
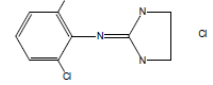
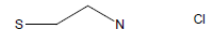
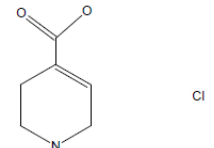
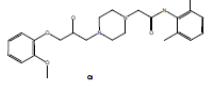
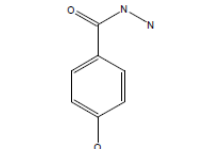
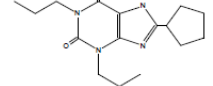
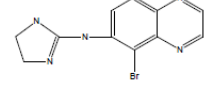
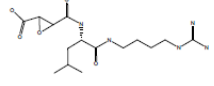
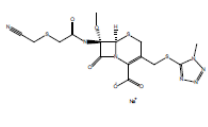
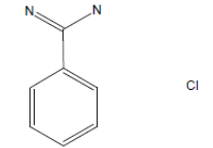
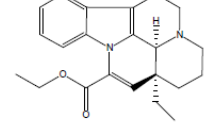
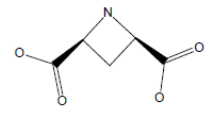
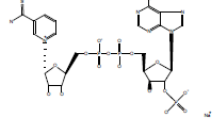
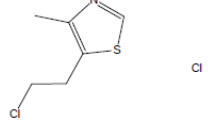
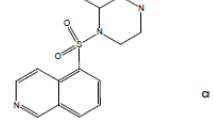
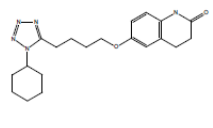
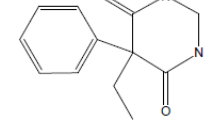
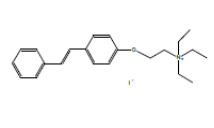
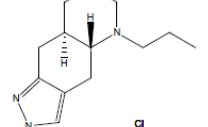
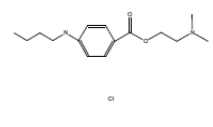
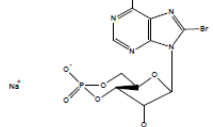
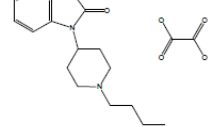
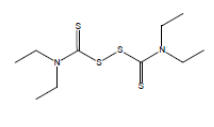
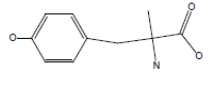
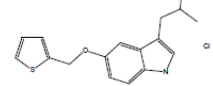
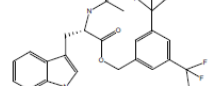
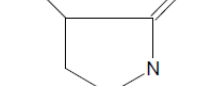
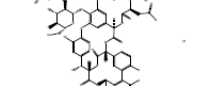
Continued, Table 22. Results of fluorescence-based drug-protein binding screen of the LOPAC library. Values are percent of Mega Red and Nile Red displaced. (n=3)

<p>1076</p>  <p>Avg. % MegaRed: 2.45 Avg. % NileRed: 6.72</p>	<p>1077</p>  <p>Avg. % MegaRed: 2.44 Avg. % NileRed: 3.73</p>	<p>1078</p>  <p>Avg. % MegaRed: 2.44 Avg. % NileRed: 7.58</p>	<p>1079</p>  <p>Avg. % MegaRed: 2.43 Avg. % NileRed: 1.09</p>	<p>1080</p>  <p>Avg. % MegaRed: 2.43 Avg. % NileRed: 15.0</p>
<p>1081</p>  <p>Avg. % MegaRed: 2.42 Avg. % NileRed: 7.31</p>	<p>1082</p>  <p>Avg. % MegaRed: 2.42 Avg. % NileRed: 2.83</p>	<p>1083</p>  <p>Avg. % MegaRed: 2.41 Avg. % NileRed: 6.52</p>	<p>1084</p>  <p>Avg. % MegaRed: 2.40 Avg. % NileRed: 10.0</p>	<p>1085</p>  <p>Avg. % MegaRed: 2.39 Avg. % NileRed: 2.87</p>
<p>1086</p>  <p>Avg. % MegaRed: 2.39 Avg. % NileRed: 4.69</p>	<p>1087</p>  <p>Avg. % MegaRed: 2.39 Avg. % NileRed: 7.71</p>	<p>1088</p>  <p>Avg. % MegaRed: 2.39 Avg. % NileRed: 4.83</p>	<p>1089</p>  <p>Avg. % MegaRed: 2.38 Avg. % NileRed: 14.1</p>	<p>1090</p>  <p>Avg. % MegaRed: 2.38 Avg. % NileRed: 8.23</p>
<p>1091</p>  <p>Avg. % MegaRed: 2.38 Avg. % NileRed: 6.90</p>	<p>1092</p>  <p>Avg. % MegaRed: 2.38 Avg. % NileRed: 5.86</p>	<p>1093</p>  <p>Avg. % MegaRed: 2.37 Avg. % NileRed: 1.36</p>	<p>1094</p>  <p>Avg. % MegaRed: 2.36 Avg. % NileRed: 5.68</p>	<p>1095</p>  <p>Avg. % MegaRed: 2.35 Avg. % NileRed: 4.29</p>
<p>1096</p>  <p>Avg. % MegaRed: 2.33 Avg. % NileRed: 3.74</p>	<p>1097</p>  <p>Avg. % MegaRed: 2.32 Avg. % NileRed: 12.6</p>	<p>1098</p>  <p>Avg. % MegaRed: 2.32 Avg. % NileRed: 12.5</p>	<p>1099</p>  <p>Avg. % MegaRed: 2.32 Avg. % NileRed: 14.8</p>	<p>1100</p>  <p>Avg. % MegaRed: 2.32 Avg. % NileRed: 3.39</p>
<p>1101</p>  <p>Avg. % MegaRed: 2.29 Avg. % NileRed: 10.3</p>	<p>1102</p>  <p>Avg. % MegaRed: 2.28 Avg. % NileRed: 3.57</p>	<p>1103</p>  <p>Avg. % MegaRed: 2.28 Avg. % NileRed: 5.40</p>	<p>1104</p>  <p>Avg. % MegaRed: 2.27 Avg. % NileRed: 6.18</p>	<p>1105</p>  <p>Avg. % MegaRed: 2.27 Avg. % NileRed: 3.49</p>

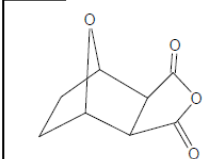
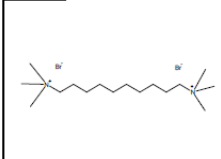
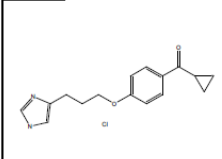
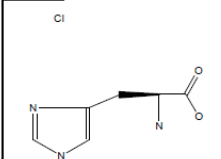
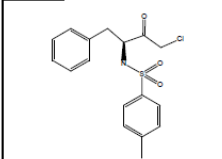
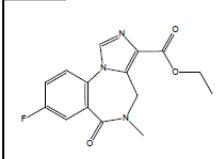
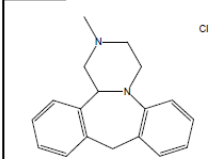
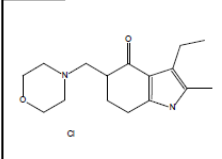
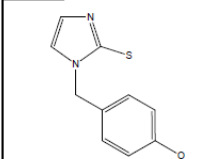
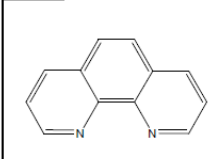
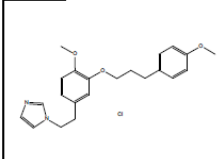
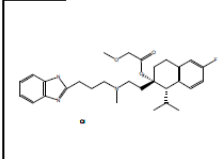
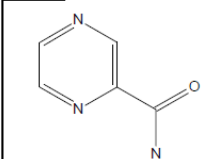
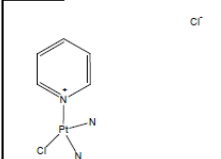
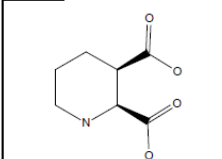
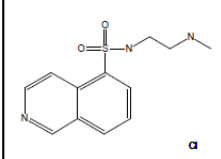
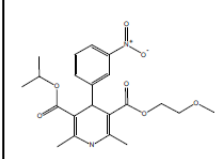
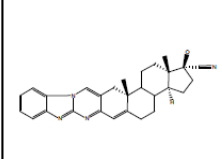
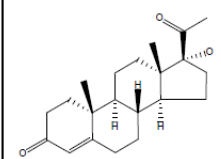
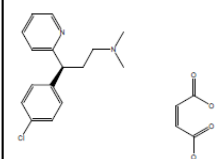
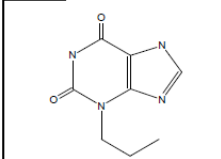
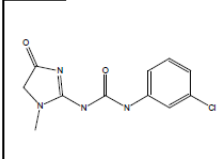
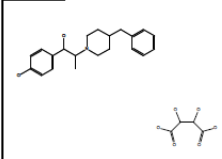
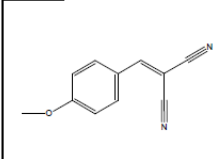
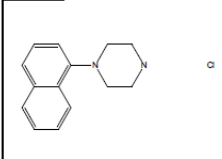
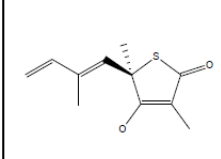
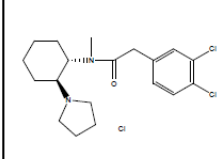
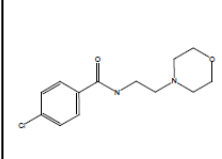
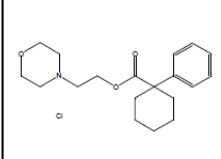
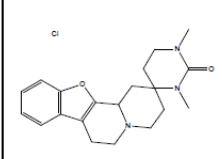
Continued, Table 22. Results of fluorescence-based drug-protein binding screen of the LOPAC library. Values are percent of Mega Red and Nile Red displaced. (n=3)

1106	1107	1108	1109	1110
				
Avg. % MegaRed: 2.27 Avg. % NileRed: 12.8	Avg. % MegaRed: 2.25 Avg. % NileRed: 7.96	Avg. % MegaRed: 2.25 Avg. % NileRed: 7.59	Avg. % MegaRed: 2.24 Avg. % NileRed: 10.6	Avg. % MegaRed: 2.21 Avg. % NileRed: 6.70
1111	1112	1113	1114	1115
				
Avg. % MegaRed: 2.21 Avg. % NileRed: 9.04	Avg. % MegaRed: 2.21 Avg. % NileRed: 3.71	Avg. % MegaRed: 2.20 Avg. % NileRed: 4.21	Avg. % MegaRed: 2.20 Avg. % NileRed: 3.67	Avg. % MegaRed: 2.20 Avg. % NileRed: 13.4
1116	1117	1118	1119	1120
				
Avg. % MegaRed: 2.19 Avg. % NileRed: 7.42	Avg. % MegaRed: 2.17 Avg. % NileRed: 30.3	Avg. % MegaRed: 2.17 Avg. % NileRed: 0.45	Avg. % MegaRed: 2.17 Avg. % NileRed: 2.61	Avg. % MegaRed: 2.17 Avg. % NileRed: 8.53
1121	1122	1123	1124	1125
				
Avg. % MegaRed: 2.16 Avg. % NileRed: 7.29	Avg. % MegaRed: 2.16 Avg. % NileRed: 2.82	Avg. % MegaRed: 2.15 Avg. % NileRed: 4.29	Avg. % MegaRed: 2.14 Avg. % NileRed: 4.04	Avg. % MegaRed: 2.13 Avg. % NileRed: 11.9
1126	1127	1128	1129	1130
				
Avg. % MegaRed: 2.13 Avg. % NileRed: 8.91	Avg. % MegaRed: 2.13 Avg. % NileRed: 5.58	Avg. % MegaRed: 2.12 Avg. % NileRed: 4.71	Avg. % MegaRed: 2.12 Avg. % NileRed: 12.1	Avg. % MegaRed: 2.11 Avg. % NileRed: 7.49
1131	1132	1133	1134	1135
				
Avg. % MegaRed: 2.11 Avg. % NileRed: 1.50	Avg. % MegaRed: 2.10 Avg. % NileRed: 4.39	Avg. % MegaRed: 2.09 Avg. % NileRed: 1.22	Avg. % MegaRed: 2.08 Avg. % NileRed: 4.55	Avg. % MegaRed: 2.08 Avg. % NileRed: 0.46

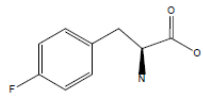
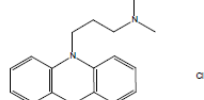
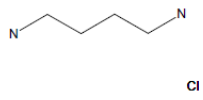
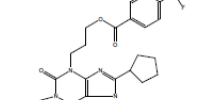
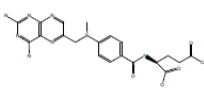
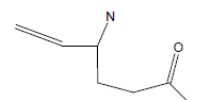
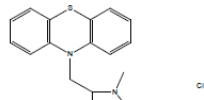
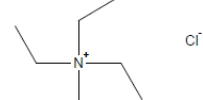
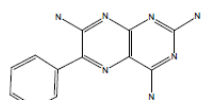
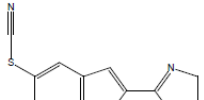
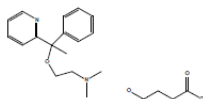
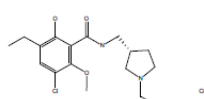
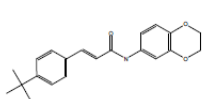
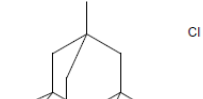
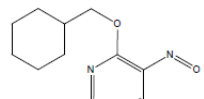
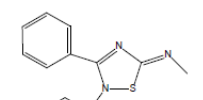
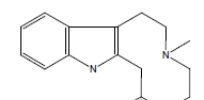
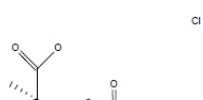
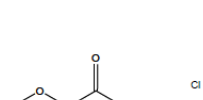
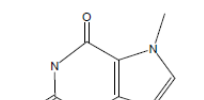
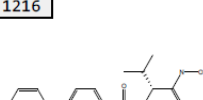
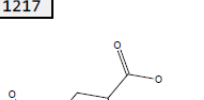
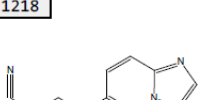
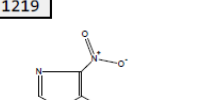
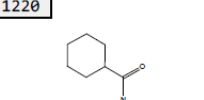
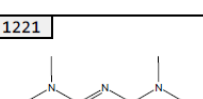
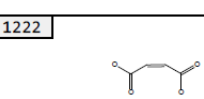
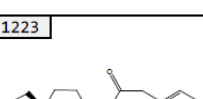

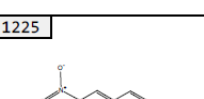
Continued, Table 22. Results of fluorescence-based drug-protein binding screen of the LOPAC library. Values are percent of Mega Red and Nile Red displaced. (n=3)

1136	1137	1138	1139	1140
				
Avg. % MegaRed: 2.05 Avg. % NileRed: 4.39	Avg. % MegaRed: 2.05 Avg. % NileRed: 1.60	Avg. % MegaRed: 2.05 Avg. % NileRed: 10.5	Avg. % MegaRed: 2.03 Avg. % NileRed: 1.74	Avg. % MegaRed: 2.02 Avg. % NileRed: 16.2
1141	1142	1143	1144	1145
				
Avg. % MegaRed: 2.00 Avg. % NileRed: 2.97	Avg. % MegaRed: 1.99 Avg. % NileRed: 4.90	Avg. % MegaRed: 1.99 Avg. % NileRed: 6.61	Avg. % MegaRed: 1.99 Avg. % NileRed: 5.59	Avg. % MegaRed: 1.98 Avg. % NileRed: 3.19
1146	1147	1148	1149	1150
				
Avg. % MegaRed: 1.98 Avg. % NileRed: 10.8	Avg. % MegaRed: 1.96 Avg. % NileRed: 4.58	Avg. % MegaRed: 1.93 Avg. % NileRed: 2.51	Avg. % MegaRed: 1.93 Avg. % NileRed: 5.06	Avg. % MegaRed: 1.92 Avg. % NileRed: 6.54
1151	1152	1153	1154	1155
				
Avg. % MegaRed: 1.92 Avg. % NileRed: 9.72	Avg. % MegaRed: 1.91 Avg. % NileRed: 3.64	Avg. % MegaRed: 1.90 Avg. % NileRed: 15.5	Avg. % MegaRed: 1.90 Avg. % NileRed: 6.81	Avg. % MegaRed: 1.89 Avg. % NileRed: 3.72
1156	1157	1158	1159	1160
				
Avg. % MegaRed: 1.88 Avg. % NileRed: 3.82	Avg. % MegaRed: 1.88 Avg. % NileRed: 7.32	Avg. % MegaRed: 1.87 Avg. % NileRed: 12.0	Avg. % MegaRed: 1.87 Avg. % NileRed: 4.46	Avg. % MegaRed: 1.86 Avg. % NileRed: 4.24
1161	1162	1163	1164	1165
				
Avg. % MegaRed: 1.86 Avg. % NileRed: 3.94	Avg. % MegaRed: 1.84 Avg. % NileRed: 4.85	Avg. % MegaRed: 1.82 Avg. % NileRed: 9.02	Avg. % MegaRed: 1.82 Avg. % NileRed: 9.02	Avg. % MegaRed: 1.81 Avg. % NileRed: 7.43

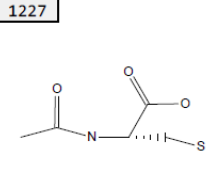
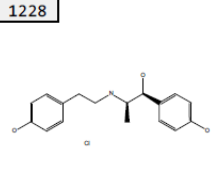
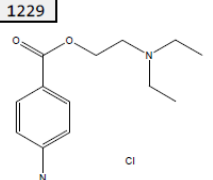
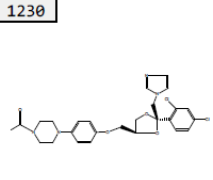
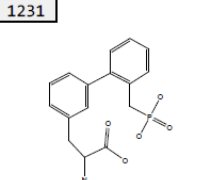
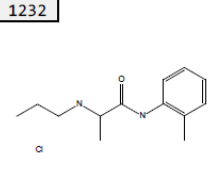
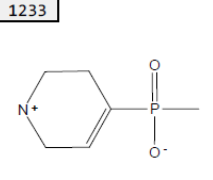
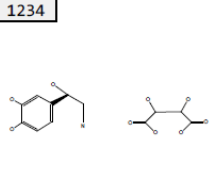
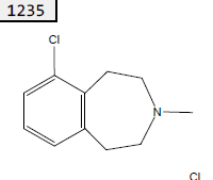
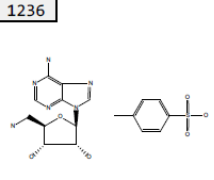
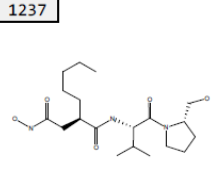
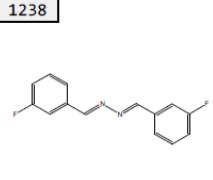
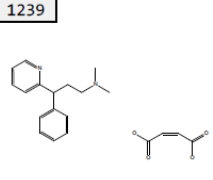
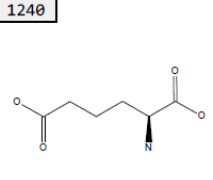
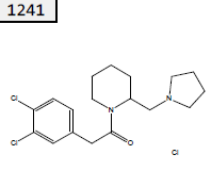
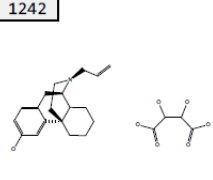
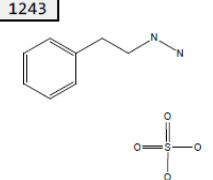
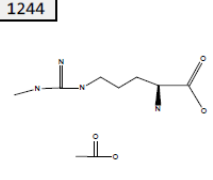
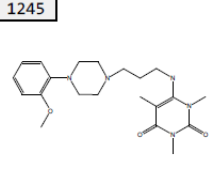
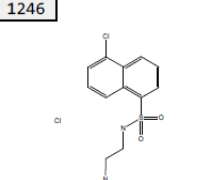
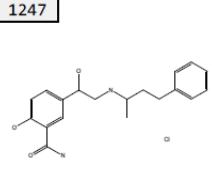
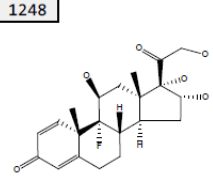
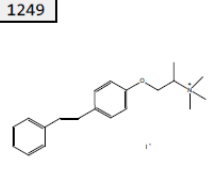
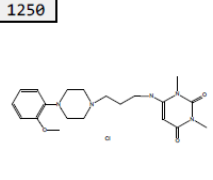
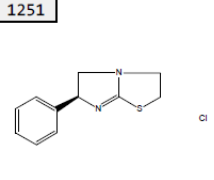
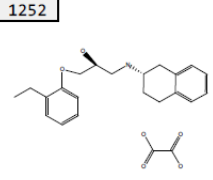
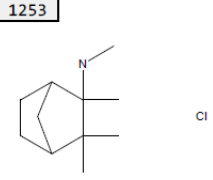
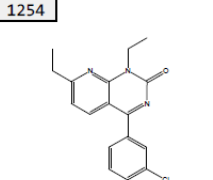
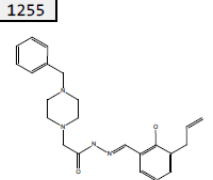
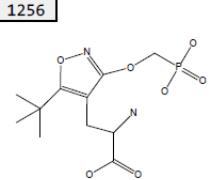
Continued, Table 22. Results of fluorescence-based drug-protein binding screen of the LOPAC library. Values are percent of Mega Red and Nile Red displaced. (n=3)

1166	1167	1168	1169	1170
				
Avg. % MegaRed: 1.80 Avg. % NileRed: 4.81	Avg. % MegaRed: 1.78 Avg. % NileRed: 2.99	Avg. % MegaRed: 1.78 Avg. % NileRed: 4.06	Avg. % MegaRed: 1.77 Avg. % NileRed: 6.39	Avg. % MegaRed: 1.76 Avg. % NileRed: 33.7
1171	1172	1173	1174	1175
				
Avg. % MegaRed: 1.75 Avg. % NileRed: 6.30	Avg. % MegaRed: 1.70 Avg. % NileRed: 3.22	Avg. % MegaRed: 1.69 Avg. % NileRed: 3.96	Avg. % MegaRed: 1.68 Avg. % NileRed: 5.88	Avg. % MegaRed: 1.66 Avg. % NileRed: 2.72
1176	1177	1178	1179	1180
				
Avg. % MegaRed: 1.66 Avg. % NileRed: 2.85	Avg. % MegaRed: 1.64 Avg. % NileRed: 2.96	Avg. % MegaRed: 1.63 Avg. % NileRed: 3.92	Avg. % MegaRed: 1.63 Avg. % NileRed: 13.8	Avg. % MegaRed: 1.62 Avg. % NileRed: 3.39
1181	1182	1183	1184	1185
				
Avg. % MegaRed: 1.62 Avg. % NileRed: 10.7	Avg. % MegaRed: 1.62 Avg. % NileRed: 10.0	Avg. % MegaRed: 1.58 Avg. % NileRed: 6.70	Avg. % MegaRed: 1.58 Avg. % NileRed: 1.95	Avg. % MegaRed: 1.55 Avg. % NileRed: 7.47
1186	1187	1188	1189	1190
				
Avg. % MegaRed: 1.53 Avg. % NileRed: 2.52	Avg. % MegaRed: 1.53 Avg. % NileRed: 11.4	Avg. % MegaRed: 1.52 Avg. % NileRed: 5.18	Avg. % MegaRed: 1.52 Avg. % NileRed: 3.36	Avg. % MegaRed: 1.49 Avg. % NileRed: 9.44
1191	1192	1193	1194	1195
				
Avg. % MegaRed: 1.49 Avg. % NileRed: 5.29	Avg. % MegaRed: 1.48 Avg. % NileRed: 5.43	Avg. % MegaRed: 1.48 Avg. % NileRed: 8.70	Avg. % MegaRed: 1.47 Avg. % NileRed: 4.72	Avg. % MegaRed: 1.45 Avg. % NileRed: 2.76

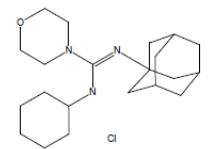
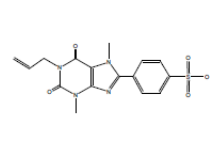
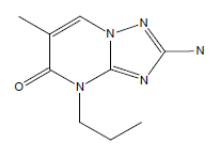
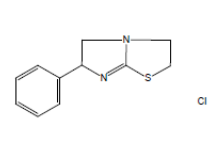
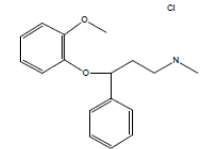
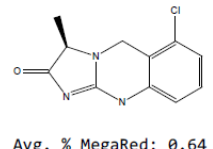
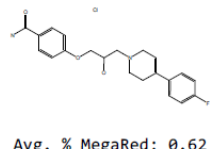
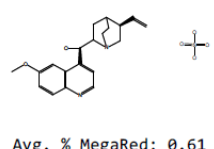
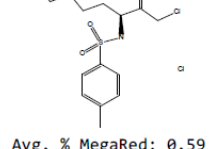
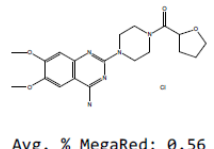
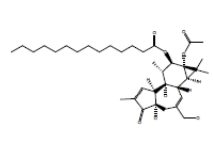
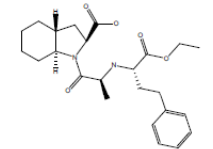
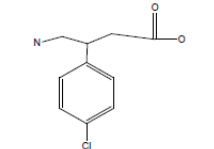
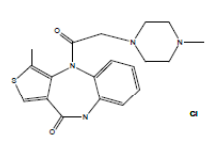
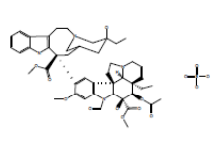
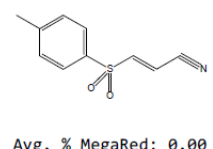
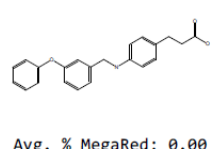
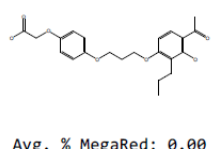
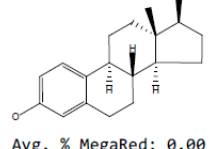
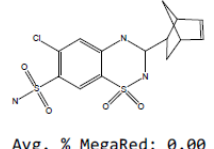
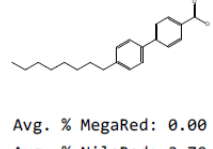
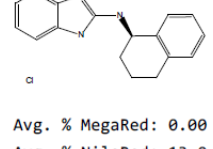
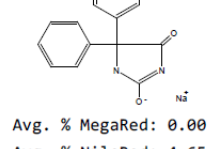
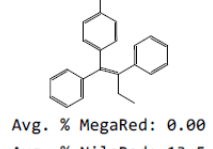
Continued, Table 22. Results of fluorescence-based drug-protein binding screen of the LOPAC library. Values are percent of Mega Red and Nile Red displaced. (n=3)

<p>1196</p>  <p>Avg. % MegaRed: 1.45 Avg. % NileRed: 8.28</p>	<p>1197</p>  <p>Avg. % MegaRed: 1.45 Avg. % NileRed: 7.54</p>	<p>1198</p>  <p>Avg. % MegaRed: 1.44 Avg. % NileRed: 2.18</p>	<p>1199</p>  <p>Avg. % MegaRed: 1.43 Avg. % NileRed: 20.6</p>	<p>1200</p>  <p>Avg. % MegaRed: 1.42 Avg. % NileRed: 8.97</p>
<p>1201</p>  <p>Avg. % MegaRed: 1.42 Avg. % NileRed: 9.10</p>	<p>1202</p>  <p>Avg. % MegaRed: 1.42 Avg. % NileRed: 4.15</p>	<p>1203</p>  <p>Avg. % MegaRed: 1.42 Avg. % NileRed: 8.87</p>	<p>1204</p>  <p>Avg. % MegaRed: 1.40 Avg. % NileRed: 11.3</p>	<p>1205</p>  <p>Avg. % MegaRed: 1.40 Avg. % NileRed: 5.23</p>
<p>1206</p>  <p>Avg. % MegaRed: 1.40 Avg. % NileRed: 5.23</p>	<p>1207</p>  <p>Avg. % MegaRed: 1.39 Avg. % NileRed: 8.83</p>	<p>1208</p>  <p>Avg. % MegaRed: 1.39 Avg. % NileRed: 21.2</p>	<p>1209</p>  <p>Avg. % MegaRed: 1.38 Avg. % NileRed: 8.68</p>	<p>1210</p>  <p>Avg. % MegaRed: 1.36 Avg. % NileRed: 1.89</p>
<p>1211</p>  <p>Avg. % MegaRed: 1.35 Avg. % NileRed: 2.18</p>	<p>1212</p>  <p>Avg. % MegaRed: 1.34 Avg. % NileRed: 3.21</p>	<p>1213</p>  <p>Avg. % MegaRed: 1.33 Avg. % NileRed: 2.72</p>	<p>1214</p>  <p>Avg. % MegaRed: 1.32 Avg. % NileRed: 6.63</p>	<p>1215</p>  <p>Avg. % MegaRed: 1.31 Avg. % NileRed: 5.83</p>
<p>1216</p>  <p>Avg. % MegaRed: 1.30 Avg. % NileRed: 1.40</p>	<p>1217</p>  <p>Avg. % MegaRed: 1.29 Avg. % NileRed: 7.42</p>	<p>1218</p>  <p>Avg. % MegaRed: 1.28 Avg. % NileRed: 4.05</p>	<p>1219</p>  <p>Avg. % MegaRed: 1.27 Avg. % NileRed: 2.48</p>	<p>1220</p>  <p>Avg. % MegaRed: 1.27 Avg. % NileRed: 2.84</p>
<p>1221</p>  <p>Avg. % MegaRed: 1.26 Avg. % NileRed: 6.30</p>	<p>1222</p>  <p>Avg. % MegaRed: 1.23 Avg. % NileRed: 6.89</p>	<p>1223</p>  <p>Avg. % MegaRed: 1.21 Avg. % NileRed: 6.97</p>	<p>1224</p>  <p>Avg. % MegaRed: 1.19 Avg. % NileRed: 2.51</p>	<p>1225</p>  <p>Avg. % MegaRed: 1.15 Avg. % NileRed: 4.84</p>

Continued, Table 22. Results of fluorescence-based drug-protein binding screen of the LOPAC library. Values are percent of Mega Red and Nile Red displaced. (n=3)

1227	1228	1229	1230	1231
				
Avg. % MegaRed: 1.14 Avg. % NileRed: 5.55	Avg. % MegaRed: 1.11 Avg. % NileRed: 6.28	Avg. % MegaRed: 1.09 Avg. % NileRed: 2.42	Avg. % MegaRed: 1.08 Avg. % NileRed: 10.7	Avg. % MegaRed: 1.07 Avg. % NileRed: 4.33
1232	1233	1234	1235	1236
				
Avg. % MegaRed: 1.03 Avg. % NileRed: 4.10	Avg. % MegaRed: 1.02 Avg. % NileRed: 5.18	Avg. % MegaRed: 1.02 Avg. % NileRed: 5.60	Avg. % MegaRed: 1.00 Avg. % NileRed: 4.06	Avg. % MegaRed: 1.00 Avg. % NileRed: 5.01
1237	1238	1239	1240	1241
				
Avg. % MegaRed: 1.00 Avg. % NileRed: 5.27	Avg. % MegaRed: 0.99 Avg. % NileRed: 9.70	Avg. % MegaRed: 0.99 Avg. % NileRed: 3.67	Avg. % MegaRed: 0.98 Avg. % NileRed: 9.18	Avg. % MegaRed: 0.97 Avg. % NileRed: 8.17
1242	1243	1244	1245	1246
				
Avg. % MegaRed: 0.96 Avg. % NileRed: 2.44	Avg. % MegaRed: 0.96 Avg. % NileRed: 7.32	Avg. % MegaRed: 0.95 Avg. % NileRed: 15.0	Avg. % MegaRed: 0.91 Avg. % NileRed: 11.1	Avg. % MegaRed: 0.89 Avg. % NileRed: 5.99
1247	1248	1249	1250	1251
				
Avg. % MegaRed: 0.88 Avg. % NileRed: 3.80	Avg. % MegaRed: 0.87 Avg. % NileRed: 2.86	Avg. % MegaRed: 0.87 Avg. % NileRed: 7.43	Avg. % MegaRed: 0.85 Avg. % NileRed: 13.7	Avg. % MegaRed: 0.84 Avg. % NileRed: 1.32
1252	1253	1254	1255	1256
				
Avg. % MegaRed: 0.83 Avg. % NileRed: 9.83	Avg. % MegaRed: 0.83 Avg. % NileRed: 10.4	Avg. % MegaRed: 0.79 Avg. % NileRed: 7.09	Avg. % MegaRed: 0.78 Avg. % NileRed: 1.92	Avg. % MegaRed: 0.76 Avg. % NileRed: 7.19

Continued, Table 22. Results of fluorescence-based drug-protein binding screen of the LOPAC library. Values are percent of Mega Red and Nile Red displaced. (n=3)

<p>1257</p>  <p>Avg. % MegaRed: 0.72 Avg. % NileRed: 1.46</p>	<p>1258</p>  <p>Avg. % MegaRed: 0.72 Avg. % NileRed: 3.71</p>	<p>1259</p>  <p>Avg. % MegaRed: 0.69 Avg. % NileRed: 1.50</p>	<p>1260</p>  <p>Avg. % MegaRed: 0.69 Avg. % NileRed: 14.1</p>	<p>1261</p>  <p>Avg. % MegaRed: 0.68 Avg. % NileRed: 9.56</p>
<p>1262</p>  <p>Avg. % MegaRed: 0.64 Avg. % NileRed: 1.37</p>	<p>1263</p>  <p>Avg. % MegaRed: 0.62 Avg. % NileRed: 3.00</p>	<p>1264</p>  <p>Avg. % MegaRed: 0.61 Avg. % NileRed: 4.70</p>	<p>1265</p>  <p>Avg. % MegaRed: 0.59 Avg. % NileRed: 2.15</p>	<p>1266</p>  <p>Avg. % MegaRed: 0.56 Avg. % NileRed: 2.30</p>
<p>1267</p>  <p>Avg. % MegaRed: 0.46 Avg. % NileRed: 3.48</p>	<p>1268</p>  <p>Avg. % MegaRed: 0.37 Avg. % NileRed: 1.84</p>	<p>1269</p>  <p>Avg. % MegaRed: 0.24 Avg. % NileRed: 8.59</p>	<p>1270</p>  <p>Avg. % MegaRed: 0.18 Avg. % NileRed: 5.41</p>	<p>1271</p>  <p>Avg. % MegaRed: 0.15 Avg. % NileRed: 3.47</p>
<p>1272</p>  <p>Avg. % MegaRed: 0.00 Avg. % NileRed: 16.8</p>	<p>1273</p>  <p>Avg. % MegaRed: 0.00 Avg. % NileRed: 12.1</p>	<p>1274</p>  <p>Avg. % MegaRed: 0.00 Avg. % NileRed: 4.60</p>	<p>1275</p>  <p>Avg. % MegaRed: 0.00 Avg. % NileRed: 34.2</p>	<p>1276</p>  <p>Avg. % MegaRed: 0.00 Avg. % NileRed: 7.30</p>
<p>1277</p>  <p>Avg. % MegaRed: 0.00 Avg. % NileRed: 2.70</p>	<p>1278</p>  <p>Avg. % MegaRed: 0.00 Avg. % NileRed: 13.0</p>	<p>1279</p>  <p>Avg. % MegaRed: 0.00 Avg. % NileRed: 4.65</p>	<p>1280</p>  <p>Avg. % MegaRed: 0.00 Avg. % NileRed: 13.5</p>	

REFERENCES

1. Young, D. L.; Michelson, S., *Systems Biology in Drug Discovery and Development*. 1st ed.; John Wiley & Sons, Inc.: Hoboken, New Jersey, 2012.
2. Bleicher, K. H.; Böhm, H.-J.; Müller, K.; Alanine, A. I., A guide to drug discovery: Hit and lead generation: beyond high-throughput screening. *Nature Reviews Drug Discovery* **2003**, *2*, 369-378.
3. Kerns, E. H.; Di, L., Pharmaceutical profiling in drug discovery. *Drug Discovery Today* **2003**, *8* (7) 316-323.
4. Kerns, E. H.; Di, L., Automation in Pharmaceutical Profiling. *Journal of the Association for Laboratory Automation* **2005**, *10* (2) 114-123.
5. Waterbeemd, H. v. d.; Testa, B., *Drug Bioavailability: Estimation of Solubility, Permeability, Absorption and Bioavailability*. 2nd ed.; 2009; Vol. 40.
6. Gad, S. C., *Preclinical Development Handbook: ADME and Biopharmaceutical Properties*. John Wiley and Sons: Hoboken, New Jersey, 2008.
7. Hu, M.; Li, X., *Oral Bioavailability: Basic Principles, Advanced Concepts, and Applications*. John Wiley & Sons, Inc.: Hoboken, New Jersey, 2011.
8. Brunton, L.; Chabner, B.; Knollman, B., *Goodman and Gilman's The Pharmacological Basis of Therapeutics*. 12 ed.; McGraw-Hill Professional: 2010; p 1808.
9. Ekins, S.; Nikolsky, Y.; Nikolskaya, T., Techniques: Application of systems biology to absorption, distribution, metabolism, excretion and toxicity. *Trends in Pharmacological Sciences* *26* (4) 202-209.
10. Rogge, M. C.; Taft, D. R., *Preclinical Drug Development*. 2nd ed.; Informa Healthcare USA, Inc.: New York, NY, 2010; Vol. 187.
11. Alsenz, J.; Kansy, M., High throughput solubility measurement in drug discovery and development. *Advanced Drug Delivery Reviews* **2007**, *59*, 546-567.
12. Press, B.; Grandi, D. D., Permeability for Intestinal Absorption: Caco-2 Assay and Related Issues. *Current Drug Metabolism* **2008**, *9*, 893-900.
13. Ruell, J., Membrane-based drug assays. *Modern Drug Discovery* January 2003, 2003, pp 28-30.
14. Millipore, Protocol PC2004EN00, *HDM-PAMPA with the MultiScreen Permeability Filter Plate*; Millipore; PC2004EN00: June 2004, 2004.

15. Millipore, Protocol PC040EN00, *Lipid-PAMPA with the MultiScreen® Filter Plates*; Millipore: 2004.
16. Ong, S.; Liu, H.; Pidgeon, C., Immobilized-artificial-membrane chromatography: measurements of membrane partition coefficient and predicting drug membrane permeability. *Journal of Chromatography A* **1996**, 728 (1-2) 113-128.
17. Sethi, B.; Soni, M.; Kumar, S.; Gupta, G. D.; Mishra, S.; Singh, R., Lipophilicity Measurement Through Newer Techniques. *Journal of Pharmacy Research* **2010**, 3 (2) 345-351.
18. Lipinski, C. A., Drug-like properties and the causes of poor solubility and permeability. *Journal of Pharmacological and Toxicological Methods* **2000**, 44, 235-249.
19. Li, A. P., Preclinical *in vitro* screening assays for drug-like properties. *Drug Discovery Today: Technologies* **2005**, 2 (2) 179-185.
20. Kibbey, C. E.; Poole, S. K.; Robinson, B.; Jackson, J. D.; Durham, D., An integrated process for measuring the physicochemical properties of drug candidates in a preclinical discovery environment. *Journal of Pharmaceutical Sciences* **2001**, 90 (8) 1164–1175.
21. Wright, J. D.; Boudinot, F. D.; Ujhelyi, M. R., Measurement and analysis of unbound drug concentrations. *Clinical Pharmacokinetics* **1996**, 30 (6) 445-462.
22. Wan, H.; Rehngrén, M., High-throughput screening of protein binding by equilibrium dialysis combined with liquid chromatography and mass spectrometry. *Journal of Chromatography A* **2006**, 1102, 125-134.
23. Ballard, P.; Rowland, M., Correction for Nonspecific Binding to Various Components of Ultrafiltration Apparatus and Impact on Estimating *In Vivo* Rat Clearance for a Congeneric Series of 5-Ethyl, 5-n-Alkyl Barbituric Acids. *Drug Metabolism and Disposition* **2011**, 39 (12) 2165-2168.
24. Noctor, T. A. G.; Diaz-Perez, M. J.; Wainer, I. W., Use of a human serum albumin-based stationary phase for high-performance liquid chromatography as a tool for the rapid determination of drug-plasma protein binding. *Journal of Pharmaceutical Sciences* **1993**, 82 (6) 675-676.
25. Karlsson, R., SPR for molecular interaction analysis: a review of emerging application areas. *Journal of Molecular Recognition* **2004**, 17 (3) 151–161.

26. Lázaro, E.; Lowe, P. J.; Briand, X.; Faller, B., New Approach To Measure Protein Binding Based on a Parallel Artificial Membrane Assay and Human Serum Albumin. *Journal of Medicinal Chemistry* **2008**, 51 (7) 2009-2017.
27. Yu, S.; Li, S.; Yang, H.; Lee, F.; Wu, J.-T.; Qian, M. G., A novel liquid chromatography/tandem mass spectrometry based depletion method for measuring red blood cell partitioning of pharmaceutical compounds in drug discovery. *Rapid Communications in Mass Spectrometry* **2005**, 19 (2) 250-254.
28. Han, C.; Davis, C. B.; Wang, B., *Evaluation of Drug Candidates for Preclinical Development*. John Wiley & Sons, Inc.: Hoboken, NJ, 2010.
29. Xu, R.; Manuel, M.; Cramlett, J.; Kassel, D. B., A high throughput metabolic stability screening workflow with automated assessment of data quality in pharmaceutical industry. *Journal of Chromatography A* **2010**, 1217, 1616-1625.
30. Chu, I.; Favreau, L.; Soares, T.; Lin, C.-c.; Nomeir, A. A., Validation of higher-throughput high-performance liquid chromatography/atmospheric pressure chemical ionization tandem mass spectrometry assays to conduct cytochrome P450s CYP2D6 and CYP3A4 enzyme inhibition studies in human liver microsomes. *Rapid Communications in Mass Spectrometry* **2000**, 14 (4) 207-214.
31. Gao, F.; Johnson, D. L.; Ekins, S.; Janiszewski, J.; Kelly, K. G.; Meyer, R. D.; West, M., Optimizing Higher Throughput Methods to Assess Drug-Drug Interactions for CYP1A2, CYP2C9, CYP2C19, CYP2D6, rCYP2D6, and CYP3A4 In Vitro Using a Single Point IC50 *Journal of Biomolecular Screening* **2002**, 7 (4) 373-382.
32. Rodrigues, A. D.; Lin, J. H., Screening of drug candidates for their drug-drug interaction potential. *Current Opinion in Chemical Biology* **2001**, 5, 396-401.
33. Soars, M. G.; Grime, K.; Sproston, J. L.; Webborn, P. J. H.; Riley, R. J., Use of Hepatocytes to Assess the Contribution of Hepatic Uptake to Clearance in Vivo. *Drug Metabolism and Disposition* **2007**, 35 (6) 859-865
34. Cho, M.-H.; Niles, A.; Huang, R.; Inglese, J.; Austin, C. P.; Riss, T.; Xia, M., A Bioluminescent Cytotoxicity Assay for Assessment of Membrane Integrity Using a Proteolytic Biomarker. *Toxicology in Vitro* **2008**, 22 (4) 1099-1106.
35. Wallace, K. B.; Starkov, A. A., Mitochondrial Targets of Drug Toxicity. *Annual Review of Pharmacology and Toxicology* **2000**, 40, 353-388.
36. Repetto, G.; delPeso, A.; Zurita, J. L., Neutral red uptake assay for the estimation of cell viability/cytotoxicity. *Nature Protocols* **2008**, 3, 1125-1131.

37. Aubry, J.-P.; Blaecke, A.; Lecoanet-Henchoz, S.; Jeannin, P.; Herbault, N.; Caron, G.; Moine, V.; Bonnefoy, J.-Y., Annexin V used for measuring apoptosis in the early events of cellular cytotoxicity. *Cytometry* **1999**, 37 (3) 197-204.
38. Gintant, G., An evaluation of hERG current assay performance: Translating preclinical safety studies to clinical QT prolongation. *Pharmacology & Therapeutics* **2011**, 129 (2) 109-119.
39. Ozkan, S. A., Present Applications of Analytical Methods: Prospects for High Throughput Screening of Pharmaceutically Active Compounds (Part 1). *Combinatorial Chemistry & High Throughput Screening* **2010**, 13 (6) 454.
40. Nayar, R.; Manning, M. C., High-Throughput Biopharmaceutical Drug Development. *BioPharm International* February 2002, February 2002, pp 20-28.
41. Chignell, C. F., Spectroscopic Techniques for the Study of Drug Interactions with Biological Systems. *Advances in Drug Research* **1970**, 5, 55-93.
42. Waterbeemd, H. v. d.; Lennernas, H.; Artursson, P., *Drug Bioavailability: Methods and Principles in Medicinal Chemistry*. Wiley - VCH: Germany, 2003; Vol. 18.
43. Cary, H. H.; Beckman, A. O., A quartz photoelectric spectrophotometer. *Journal of the Optical Society of America* **1941**, 31, 682-689.
44. Skoog, D. A.; West, D. M.; Holler, F. J.; Crouch, S. R., *Analytical Chemistry*. 7th ed.; Brooks/Cole, Thomson Learning: 2000.
45. Surveyor PDA Plus Detector. In Thermo Scientific, Instrument Manual: 2009.
46. Lavis, L. D.; Raines, R. T., Bright Ideas for Chemical Biology. *ACS Chemical Biology* **2008**, 3, (3), 142-155.
47. Herschel, J. F. W., On a case of superficial colour presented by a homogenous liquid internally colourless. *Philosophical Transactions of the Royal Society of London* **1845**, 135, 143-145.
48. Stokes, G. G., On the change of refrangibility of light. *Philosophical Transactions of the Royal Society of London* **1852**, 142, 463-562.
49. Lakowicz, J. R., *Principles of Fluorescence*. 3rd ed.; Springer: New York, 2006.
50. Jablonski, A., Efficiency of anti-Stokes fluorescence in dyes. *Nature* **1933**, 131, 839-840.

51. Atkins, P.; dePaula, J., *Physical Chemistry*. 7th ed.; W. H. Freeman: New York, 2002.
52. Udenfriend, S., Development of the spectrophotofluorometer and its commercialization. *Protein Science* **1995**, 4 (3) 542–551.
53. Macek, K.; Deyl, Z.; Janák, J., *Liquid Column Chromatography: A Survey of Modern Techniques and Applications*. Elsevier: 1975.
54. Tswett, M., Adsorptionanalyse und chromatographische Methode. Anwendung auf die Chemie des Chlorophylls (Adsorption analysis and chromatographic method. Application to the chemistry of chlorophyll.). *Berichte der Deutschen botanischen Gesellschaft* **1906**, 24, 384–393.
55. Tswett, M., Physikalisch-Chemische Studien über das Chlorophyll. Die Adsorption. (Physical-chemical studies of chlorophyll. Adsorption.). *Berichte der Deutschen botanischen Gesellschaft* **1906**, 24, 316–326.
56. Kellner, R.; Mermet, J. M.; Otto, M.; Valcarcel, M.; Widmer, H. M., *Analytical Chemistry: A Modern Approach to Analytical Science*. 2nd ed.; Wiley-VCH: 2004.
57. Martin, A. J. P.; Synge, R. L. M., A new form of chromatogram employing two liquid phases. *Biochemical Journal* **1941**, 35, 1358-1368.
58. vanDeemter, J. J.; Zuiderweg, F. J.; Klinkenberg, A., Longitudinal diffusion and resistance to mass transfer as causes of nonideality in chromatography. *Chemical Engineering Science* **1956**, 5 (6) 271–289.
59. HPLC Introduction. In IDEX Corporation: 2010. <<http://webstore.idexhs.com/TechInfo/hplcIntro.asp>>
60. Surveyor MSQ Plus Hardware Manual. In Thermo Fisher Scientific, Instrument Manual: 2007.
61. Bard, B.; Martel, S.; Carrupt, P.-A., High throughput UV method for the estimation of thermodynamic solubility and the determination of the solubility in biorelevant media. *European Journal of Pharmaceutical Sciences* **2008**, 33, 230-240.
62. Loftsson, T., Aqueous solubility of true solutions. *Die Pharmazie* **2010**, 65, (6), 404-407.
63. Di, L.; Kerns, E. H., Biological assay challenges from compound solubility: strategies for bioassay optimization. *Drug Discovery Today* **2006**, 11 (9/10) 446-451.

64. McGovern, S. L.; Caselli, E.; Grigorieff, N.; Shoichet, B. K., A Common Mechanism Underlying Promiscuous Inhibitors from Virtual and High-Throughput Screening. *Journal of Medicinal Chemistry* **2002**, 45 (8) 1712-1722.
65. Battachar, S. N.; Deschenes, L. A.; Wesley, J. A., Solubility: it's not just for physical chemists. *Drug Discovery Today* **2006**, 11 (21/22) 1012-1017.
66. Kerns, E. W.; Di, L., Pharmaceutical profiling in drug discovery. *Drug Discovery Today* **2003**, 8 (7) 316-323.
67. PC2445EN00, Protocol: MultiScreen Solubility Filter Plate - Determination of aqueous compound solubility using a 96-well filter plate to remove precipitated solids prior to UV/Vis spectroscopic analysis. In *Millipore Technical Publications*, Millipore: 2003.
68. Lipinski, C. A., Drug-like properties and the causes of poor solubility and poor permeability. *Journal of Pharmacological and Toxicological Methods* **2000**, 44, 235-249.
69. Hoelke, B.; Gieringer, S.; Arlt, M.; Saal, C., Comparison of Nephelometric, UV-Spectroscopic, and HPLC Methods for High-Throughput Determination of Aqueous Drug Solubility in Microtiter Plates. *Analytical Chemistry* **2009**, 81 (8) 3165-3172.
70. Faller, B., Artificial Membrane Assays to Assess Permeability. *Current Drug Metabolism* **2008**, 9, 886-892.
71. Wohnsland, F.; Faller, B., High-Throughput Permeability pH Profile and High-Throughput Alkane/Water log P with Artificial Membranes. *Journal of Medicinal Chemistry* **2001**, 44, 923-930.
72. Jin, H.; Di, L., Permeability – In Vitro Assays for Assessing Drug Transporter Activity. *Current Drug Metabolism* **2008**, 9, 911-920.
73. Winiwarter, S.; Bonham, N. M.; Ax, F.; Hallberg, A.; Lennernas, H.; Karlen, A., Correlation of Human Jejunal Permeability (in Vivo) of Drugs with Experimentally and Theoretically Derived Parameters. A Multivariate Data Analysis Approach. *Journal of Medicinal Chemistry* **1998**, 41 (25) 4939-4949.
74. Kansy, M.; Senner, F.; Gubernator, K., Physicochemical High Throughput Screening: Parallel Artificial Membrane Permeation Assay in the Description of Passive Absorption Processes. *Journal of Medicinal Chemistry* **1998**, 41 (7) 1007-1010.

75. Mueller, P.; Rudin, D. O.; Tien, H. T.; Wescott, W. C., Methods for the Formation of Single Biomolecular Lipid Membranes in Aqueous Solution. *Journal of Physical Chemistry* **1963**, 67 (2) 534-535.
76. Kellard, L.; Engelstein, M., Automation of cell-based and noncell-based permeability assays. *Journal of the Association for Laboratory Automation* **2007**, 12 (2) 104-109.
77. Sugano, K.; Nabuchi, Y.; Machida, M.; Aso, Y., Prediction of human intestinal permeability using artificial membrane permeability. *International Journal of Pharmaceutics* **2003**, 257, 245-251.
78. Chen, X.; Murawski, A.; Patel, K.; Crespi, C. L.; Balimane, P. V., A Novel Design of Artificial Membrane for Improving the PAMPA Model. *Pharmaceutical Research* **2008**, 25 (7) 1511-1520.
79. Knutson, L.; Odland, B.; Hallgren, R., A New Technique for Segmental Jejunal Perfusion in Man. *The American Journal of Gastroenterology* **1989**, 84, 1278-1284.
80. Lennernas, H., Human Jejunal Effective Permeability and Its Correlation with Preclinical Drug Absorption Models. *Journal of Pharmacy and Pharmacology* **1997**, 49, 627-638.
81. Lennernas, H.; Ahrenstedt, O.; Hallgren, R.; Knutson, L.; Ryde, M.; Paalzow, L. K., Regional Jejunal Perfusion, a New *in Vivo* Approach to Study Oral Drug Absorption in Man. *Pharmaceutical Research* **1992**, 9, 1243-1251.
82. Reddy, B. B. K.; Karunakar, A., Biopharmaceutics Classification System: A Regulatory Approach. *Dissolution Technologies* **2011**, 18 (1) 31-37.
83. Schmidt, D.; Lynch, J. *MultiScreen Filter Plates for PAMPA and Permeability Assays: Data review and optimization of PAMPA and permeability assays*; Millipore Corporation: Billerica, MA, 2003.
84. Pidgeon, C.; Ong, S.; Liu, H.; Qiu, X.; Pidgeon, M.; Dantzig, A. H.; Munroe, J.; Hornback, W. J.; Kasher, J. S.; Glunz, L.; Szczerba, T., IAM Chromatography: An *in Vitro* Screen for Predicting Drug Membrane Permeability. *Journal of Medicinal Chemistry* **1995**, 38 (2) 590-594.
85. Giaginis, C.; Tsantili-Kakoulidou, A., Current State of the Art in HPLC Methodology for Lipophilicity Assessment of Basic Drugs. A Review. *Journal of Liquid Chromatography & Related Technologies* **2008**, 31, 79-96.
86. Fatemi, M. H.; Shamseddin, H., Prediction of immobilized artificial membrane-liquid chromatography retention of some drugs from their

- molecular structure descriptors and LFER parameters. *Journal of Separation Science* **2009**, 32 (20) 3395-3402.
87. Pidgeon, C.; Ong, S.; Choi, H.; Liu, H., Preparation of Mixed Ligand Immobilized Artificial Membranes for Predicting Drug Binding to Membranes. *Analytical Chemistry* **1994**, 66 (17) 2701-2709.
 88. IAM Chromatography. In Regis Technologies: 2008.
<www.registech.com/iam>
 89. Lundahl, P.; Beigi, F., Immobilized liposome chromatography of drugs for model analysis of drug-membrane interactions. *Advanced Drug Delivery Reviews* **1997**, 23 (1-3) 221-227.
 90. Hitzel, L.; Watt, A. P.; Locker, K. L., An Increased Throughput Method for the Determination of Partition Coefficients. *Pharmaceutical Research* **2000**, 17 (11) 1389-1395.
 91. Caldwell, G. W.; Masucci, J. A.; Evangelisto, M.; White, R., Evaluation of the immobilized artificial membrane phosphatidylcholine Drug discovery column for high-performance liquid chromatographic screening of drug-membrane interactions. *Journal of Chromatography A* **1998**, 800 (2) 161-169.
 92. Smith, G. K.; Barrett, D. G.; Blackburn, K.; Cory, M.; Dallas, W. S.; Davis, R.; Hassler, D.; McConnell, R.; Moyer, M.; Weaver, K., Expression, preparation, and high-throughput screening of caspase-8: discovery of redox-based and steroid diacid inhibition. *Arch. Biochem. Biophys.* **2002** (399) 195-205.
 93. Metz, J. T.; Huth, J. R.; Hajduk, P. J., Enhancement of chemical rules for predicting compound reactivity towards protein thiol groups. *Journal of Computer-Aided Molecular Design* **2007** (21) 139-144.
 94. Simeonov, A.; Jadhav, A.; Thomas, C. J.; Wang, Y.; Huang, R.; Southall, N. T.; Shinn, P.; Smith, J.; Austin, C. P.; Auld, D. S.; Inglese, J., Fluorescence Spectroscopic Profiling of Compound Libraries. *Journal of Medicinal Chemistry* **2008**, 51 (8) 2363-2371.
 95. Feng, B. Y.; Shelat, A.; Doman, T. N.; Guy, R. K.; Shoichet, B. K., High-throughput assays for promiscuous inhibitors. *Nature Chemical Biology* **2005**, 1 (3) 146-148.
 96. Lor, L. A.; Schneck, J.; McNulty, D. E.; Diaz, E.; Brandt, M.; Thrall, S. H.; Schwartz, B., A Simple Assay for Detection of Small-Molecule Redox Activity. *Journal of Biomolecular Screening* **2007**, 12 (6) 881-890.

97. Roche, O.; Schneider, P.; Zuegge, J.; Guba, W.; Kansy, M.; Alanine, A.; Bleicher, K.; Danel, F.; Gutknecht, E. M.; Rogers-Evans, M.; Neidhart, W.; Stalder, H.; Dillon, M.; Sjogren, E.; Fotouhi, N.; Gillespie, P.; Goodnow, R.; Harris, W.; Jones, P.; Taniguchi, M.; Tsujii, S.; von der Saal, W.; Zimmermann, G.; Schneider, G., Development of a virtual screening method for identification of "frequent hitters" in compound libraries. *Journal of Medicinal Chemistry* **2002** (45) 137-142.
98. Pearce, B. C.; Sofia, M. J.; Good, A. C.; Drexler, D. M.; Stock, D. A., An empirical process for the design of high-throughput screening deck filters. *Journal of Chemical Information and Modeling* **2006** (46) 1060-1068.
99. Rishton, G. M., Reactive compounds and in vitro false positives in HTS. *Drug Discovery Today* **1997**, 2 (9) 382-384.
100. Hann, M.; Hudson, B.; Lewell, X.; Lively, R.; Miller, L.; Ramsden, N., Strategic pooling of compounds for high-throughput screening. *Journal of Chemical Information and Computer Sciences* **1999** (39) 897-902.
101. Baell, J. B.; Holloway, G. A., New substructure filters for removal of pan assay interference compounds (PAINS) from screening libraries and for their exclusion in bioassays. *Journal of Medicinal Chemistry* **2010** (53) 2719-2740.
102. Coleman, M. D., *Human Drug Metabolism: An Introduction*. John Wiley & Sons Ltd.: West Sussex, England, 2005.
103. Hayes, A. W., *Principles And Methods of Toxicology*. 5th ed.; CRC Press: New York, NY, 2008.
104. Hinson, J. A.; Pohl, L. R.; Monks, T. J.; Gillette, J. R., Acetaminophen-induced hepatotoxicity. *Life Sciences* **1981**, 29 (2) 107-116.
105. Awasthi, Y. C.; Misra, G.; Rassin, D. K.; Srivastava, S. K., Detoxification of xenobiotics by glutathione S-transferases in erythrocytes: the transport of the conjugate of glutathione and 1-chloro-2,4-dinitrobenzene. *British Journal of Haematology* **1983**, 55 (3) 419-425.
106. Epps, D. E.; Taylor, B. M., A Competitive Fluorescence Assay to Measure the Reactivity of Compounds. *Analytical Biochemistry* **2001**, 295 (1) 101-106.
107. Huth, J. R.; Mendoza, R.; Olejniczak, E. T.; Johnson, R. W.; Cothron, D. A.; Liu, Y.; Lerner, C. G.; Chen, J.; Hajduk, P. J., ALARM NMR: A Rapid and Robust Experimental Method To Detect Reactive False Positives in Biochemical Screens. *Journal of The American Chemical Society* **2005**, 127 (1) 217-224.
108. Dickinson, D. A.; Forman, H. J., Cellular glutathione and thiols metabolism. *Biochemical Pharmacology* **2002**, 64, 1019-1026.

109. Reddie, K. G.; Humphries, W. H.; Bain, C. P.; Payne, C. K.; Kemp, M. L.; Murthy, N., Fluorescent Coumarin Thiols Measure Biological Redox Couples. *Organic Letters* **2012**, 14 (3) 680-682.
110. Zhang, J.-H.; Chung, T. D. Y.; Oldenburg, K. R., A simple statistical parameter for use in evaluation and validation of high throughput screening assays. *Journal of Biomolecular Screening* **1999**, 4 (2) 67-73.
111. Ge, Y.; Kazi, A.; Marsilio, F.; Luo, Y.; Jain, S.; Brooks, W.; Daniel, K. G.; Guida, W. C.; Sebti, S. M.; Lawrence, H. R., Discovery and synthesis of hydronaphthoquinones as novel proteasome inhibitors. *Journal of Medicinal Chemistry* **2012** (55) 1978-1998.
112. Nandhikonda, P.; Lynt, W. Z.; McCallum, M. M.; Ara, T.; Baranowski, A. M.; Yuan, N. Y.; Pearson, D.; Bikle, D. D.; Guy, R. K.; Arnold, L. A., Discovery of the First Irreversible Small Molecule Inhibitors of the Interaction between the Vitamin D Receptor and Coactivators. *Journal of Medicinal Chemistry* **2012**, 55 (10) 4640-51.
113. Shin, J. M.; Cho, Y. M.; Sachs, G., Chemistry of covalent inhibition of the gastric (H⁺, K⁺)-ATPase by proton pump inhibitors. *Journal of the American Chemical Society* **2004**, 126 (25) 7800-11.
114. Estebanez-Perpina, E.; Arnold, L. A.; Jouravel, N.; Togashi, M.; Blethrow, J.; Mar, E.; Nguyen, P.; Phillips, K. J.; Baxter, J. D.; Webb, P.; Guy, R. K.; Fletterick, R. J., Structural insight into the mode of action of a direct inhibitor of coregulator binding to the thyroid hormone receptor. *Mol Endocrinol* **2007**, 21 (12) 2919-28.
115. Arnold, L. A.; Estebanez-Perpina, E.; Togashi, M.; Shelat, A.; Ocasio, C. A.; McReynolds, A. C.; Nguyen, P.; Baxter, J. D.; Fletterick, R. J.; Webb, P.; Guy, R. K., A high-throughput screening method to identify small molecule inhibitors of thyroid hormone receptor coactivator binding. *Sci STKE* **2006**, 2006 (341) pl3.
116. Feng, B. Y.; Shoichet, B. K., A Detergent-Based Assay for the Detection of Promiscuous Inhibitors. *Nature Protocols* **2006**, 1 (2) 550-553.
117. Udyardy, A.; Gyulai, Z.; Sipos, A., Extensive study of the autooxidation products of apomorphine and its pharmacologically active derivatives. *Journal of Molecular Structure* **2011** (1002) 37-44.
118. Yasgar, A., Unpublished Observations, National Center for Advancing Translational Sciences, National Institutes of Health, Bethesda, Maryland 20892-3370: 2012.

119. DeVane, C. L., Clinical significance of drug binding, protein binding, and binding displacement drug interactions. *Drug Dispositions and Pharmacokinetics* **2002**, 36 (3) 5-21.
120. Fung, E. N.; Chen, Y.-H.; Lau, Y. Y., Semi-automatic high-throughput determination of plasma protein binding using a 96-well plate filtrate assembly and fast liquid chromatography-tandem mass spectrometry. *Journal of Chromatography B* **2003**, 795, 187-194.
121. Obach, R. S., Nonspecific binding to microsomes: impact on scale-up of in vitro intrinsic clearance to hepatic clearance as assessed through examination of warfarin, imipramine, and propranolol. *Drug Metabolism and Disposition* **1997**, 25 (12) 1359-1369.
122. Peters, T., *All About Albumin: Biochemistry, Genetics and Medical Applications*. Academic Press: San Diego, CA, 1996.
123. Carter, D. C.; Ho, J. X., Structure of serum albumin. *Advances in Protein Chemistry* **1994**, 45, 153-203.
124. He, X. M.; Carter, D. C., Atomic structure and chemistry of human serum albumin. *Nature* **1992**, 358, 209-215.
125. Lindup, W. E.; L'Orme, M. C., Clinical Pharmacology: Plasma protein binding of drugs. *British Medical Journal* **1981**, 282, 212-214.
126. Lee, K. J.; Mower, R.; Hollenbeck, T.; Castelo, J.; Johnson, N.; Gordon, P.; Sinko, P. J.; Holme, K.; Lee, Y. H., Modulation of nonspecific binding in ultrafiltration protein binding studies. *Pharmaceutical Research* **2003**, 20 (7) 1015-1021.
127. Chuang, V. T. G.; Maruyama, T.; Otagiri, M., Updates on Contemporary Protein Binding Techniques. *Drug Metabolism and Pharmacokinetics* **2009**, 24 (4) 358-364.
128. Wan, H.; Bergström, F., High Throughput Screening of Drug-Protein Binding in Drug Discovery. *Journal of Liquid Chromatography & Related Technologies* **2007**, 30, 681-700.
129. Zhang, J.; Musson, D. G., Investigation of high-throughput ultrafiltration for the determination of an unbound compound in human plasma using liquid chromatography and tandem mass spectrometry with electrospray ionization. *Journal of Chromatography B* **2006**, 843, 47-56.
130. Angelakou, A.; Valsami, G.; Macheras, P.; Koupparis, M., Displacement approach for competitive drug-protein binding studies using the potentiometric 1-anilino-8-naphthalene-sulfonate probe technique. *European Journal of Pharmaceutical Sciences* **1999**, 9 (2) 123-130.

131. Boozer, C.; Kim, G.; Cong, S.; Guan, H.; Londergan, T., Looking towards label-free biomolecular interaction analysis in a high-throughput format: a review of new surface plasmon resonance technologies. *Current Opinion in Biotechnology* **2006**, 17 (4) 400-405.
132. Singh, S. S.; Mehta, J., Measurement of drug-protein binding by immobilized human serum albumin-HPLC and comparison with ultrafiltration. *Journal of Chromatography B* **2006**, 834, 108-116.
133. Valko, K. N., S.; Bevan, C.; Abraham, M. H.; Reynolds, D. P., Fast gradient HPLC method to determine compounds binding to human serum albumin. Relationships with octanol/water and immobilized artificial membrane lipophilicity. *Journal of Pharmaceutical Sciences* **2003**, 92, 2236-2248.
134. El-Hady, D.; Kühne, S.; El-Maali, N.; Wätzig, H., Precision in affinity capillary electrophoresis for drug-protein binding studies. *Journal of Pharmaceutical and Biomedical Analysis* **2010**, 55 (2) 232-241.
135. Østergaard, J.; Heegaard, N. H. H., Capillary electrophoresis frontal analysis: Principles and applications for the study of drug-plasma protein binding. *Electrophoresis* **2003**, 24, 2903-2913.
136. Hartmann, T.; Schmitt, J.; Roehring, C.; Nimptsch, D.; Noeller, J.; Mohr, C., ADME related profiling in 96 and 384-well plate format - a novel and robust HT-assay for the determination of lipophilicity and serum albumin binding. *Current Drug Delivery* **2006**, 3 (2) 181-192.
137. Transil XL HSA Binding Kit. <www.admecell.com/transilxl-hsa/>
138. Transil^{XL} HSA Binding Kit. <www.sovicell.com/transil-hsa-binding-kit.asp>
139. AcroPrep Advance Filter Plates. In Pall Life Sciences: 2013.
140. Rehse, K.; Fiedler, B., Determination of the protein binding of drugs by continuous ultrafiltration. 9. Comparison of the binding of nonsteroid antirheumatics to human serum albumin and their interaction with phenprocoumon. *Archiv der Pharmazie (Weinheim)* **1989**, 322 (4) 241-243.
141. Waters, N. J.; Jones, R.; Williams, G.; Sohal, B., Validation of a rapid equilibrium dialysis approach for the measurement of plasma protein binding. *Journal of Pharmaceutical Sciences* **2008**, 97 (10) 4586-4595.
142. *MultiScreen® Filter Plates with Ultracel™-PPB Membrane: For use in the separation of serum protein-bound drug from free drug in plasma protein binding assays*; Millipore Corporation: 2002.

143. Borgå, O.; Borgå, B., Serum protein binding of nonsteroidal antiinflammatory drugs: a comparative study. *Journal of Pharmacokinetics and Biopharmaceutics* **1997**, 25 (1) 63-77.
144. Burton, M. E.; Shaw, L. M.; Schentag, J. J.; Evans, W. E., *Applied Pharmacokinetics & Pharmacodynamics: Principles Of Therapeutic Drug Monitoring*. 4th ed.; Lippincott Williams & Wilkins: Baltimore, MD, 2006.
145. Zhirkov, Y. A.; Piotrovskii, V. K., On the usefulness of ultrafiltration in drug-protein binding studies. *Journal of Pharmacy and Pharmacology* **1984**, 36, 844-845.
146. Gad, S. C., *Preclinical Development Handbook: Toxicology*. John Wiley & Sons: 2008.
147. Hawe, A.; Sutter, M.; Jiskoot, W., Extrinsic Fluorescent Dyes as Tools for Protein Characterization. *Pharmaceutical Research* **2008**, 25 (7) 1487-1499.
148. Muller, N.; Lopicque, F.; Drelon, E.; Netter, P., Binding Sites of Fluorescent Probes on Human Serum Albumin. *Journal of Pharmacy and Pharmacology* **1994**, 46, 300-304.
149. Ercelen, S.; Klymchenko, A. S.; Demchenko, A. P., Novel two-color fluorescence probe with extreme specificity to bovine serum albumin. *FEBS Letters* **2003**, 538, 25-28.
150. Moreno, F.; Cortijo, M.; Gonzalez-Jimenez, J., The Fluorescent Probe Prodan Characterizes the Warfarin Binding Site on Human Serum Albumin. *Photochemistry and Photobiology* **1999**, 69 (1) 8-15.
151. Stryer, L., The interaction of a naphthalene dye with apomyoglobin and apohemoglobin. A fluorescent probe of nonpolar binding sites. *Journal of Molecular Biology* **1965**, 13, (2), 482-495.
152. Rosen, C. G.; Weber, G., Dimer formation from 1-amino-8-naphthalenesulfonate catalyzed by bovine serum albumin. A new fluorescent molecule with exceptional binding properties *Biochemistry* **1969**, 8 (10) 3915-3920.
153. Valsami, G. N.; Macheras, P. E.; Koupparis, M. A., Binding Study of the Fluorescence Probe 1-Anilino-8-naphthalenesulfonate to Human Plasma and Human and Bovine Serum Albumin Using Potentiometric Titration. *Pharmaceutical Research* **1991**, 8 (7) 888-892.
154. Chignell, C. F., Spectroscopic Techniques for the Study of Drug Interactions with Biological Systems. *Advances in Drug Research* **1970**, 5, 55-94.

155. Lakowicz, J. R., *Principles of Fluorescence Spectroscopy*. 3rd ed.; Springer: 2009.
156. Czerney, P.; Wenzel, M.; Schweder, B.; Lehmann, F.; Dyomics GmbH, Germany USA, 2004; Vol. US 7563907 B2; Fluorescent dyes based on polymethines for use in optical measurement. **2004**.
157. Berkelman, T. R.; Bio-Rad Laboratories, Inc., USA: USA, 2009; Vol. US 7625758 B2; Coumari-based cyanine dyes for non-specific protein binding. **2009**.
158. Davis, D. M.; Birch, D. J. S., Extrinsic Fluorescence Probe Study of Human Serum Albumin Using Nile Red. *Journal of Fluorescence* **1996**, 6 (1) 23-32.
159. Sarkar, N.; Das, K.; Nath, D. N.; Bhattacharyya, K., Twisted charge transfer process of Nile Red in homogeneous solution and in faujasite seolite. *Langmuir* **1994**, 10 (326-329) 326.
160. Brown, M. B.; Edmonds, T. E.; Miller, J. N.; Seare, N. J., Use of Nile Red as a long-wave fluorophore in dual-probe studies of ligand-protein interactions. *Journal of Fluorescence* **1993**, 3 (3) 129-130.
161. Tritsch, G. L.; Rathke, C. E.; Tritsch, N. E.; Weiss, C. M., Thyroxine Binding by Human Serum Albumin. *Journal of Biological Chemistry* **1961**, 236 (12) 3163-3167.
162. Tjernberg, A.; Markova, N.; Griffiths, W. J.; Hallén, D., DMSO-Related Effects in Protein Characterization. *Journal of Biomolecular Screening* **2006**, 11 (2) 131-137.
163. Wan, H.; Rehngrén, M., High-throughput screening of protein binding by equilibrium dialysis combined with liquid chromatography and mass spectrometry. *Journal of Chromatography A* **2006**, 1102 (1-2) 125-134.
164. Boyd, R. A.; Chin, S. K.; Don-Pedro, O.; Williams, R. L.; Giacomini, K. M., The pharmacokinetics of the enantiomers of atenolol. *Clinical Pharmacology & Therapeutics* **1989**, 45 (4) 403-410.
165. Mason, W. D.; Winer, N.; Kochak, G.; Cohen, I.; Bell, R., Kinetics and absolute bioavailability of atenolol. *Clinical Pharmacology & Therapeutics* **1979**, 25 (4) 408-415.
166. Dayer, P.; Leemann, T.; Marmy, A.; Rosenthaler, J., Interindividual variation of beta-adrenoceptor blocking drugs, plasma concentration and effect: influence of genetic status on behaviour of atenolol, bopindolol and metoprolol *European Journal of Clinical Pharmacology* **1985**, 28 (2) 149-153.

167. McGourty, J. C.; Silas, J. H.; Lennard, M. S.; Tucker, G. T.; Woods, H. F., Metoprolol metabolism and debrisoquine oxidation polymorphism--population and family studies *British Journal of Clinical Pharmacology* **1985**, 20 (6) 555-566.
168. Lennard, M. S.; Silas, J. H.; Freestone, S.; Ramsay, L. E.; Tucker, G. T.; Woods, H. F., Oxidation phenotype--a major determinant of metoprolol metabolism and response *The New England Journal of Medicine* **1982**, 307 (25) 1558-15560.
169. Gladziwa, U.; Klotz, U., Pharmacokinetics and pharmacodynamics of H₂-receptor antagonists in patients with renal insufficiency *Clinical Pharmacokinetics* **1993**, 24 (4) 319-332.
170. Patel, L.; Johnson, A.; Turner, P., Nadolol binding to human serum proteins. *Journal of Pharmacy and Pharmacology* **1984**, 36 (6) 414-415.
171. Soergel, F.; Kinzig, M., Pharmacokinetics of gyrase inhibitors, part 2: renal and hepatic elimination pathways and drug interactions. *American Journal of Medicine* **1993**, 94 (3A) 56S-69S.
172. Zlotos, G.; Bucker, A.; Kinzig-Schippers, M.; Sorgel, F.; Holzgrabe, U., Plasma Protein Binding of Gyrase Inhibitors. *Journal of Pharmaceutical Sciences* **1998**, 87 (2) 215-220.
173. Blanchard, J., Protein binding of caffeine in young and elderly males. *Journal of Pharmaceutical Sciences* **1982**, 71 (12) 1415-1418.
174. MacGowan, A. P., Pharmacokinetic and pharmacodynamic profile of linezolid in healthy volunteers and patients with Gram-positive infections. *Journal of Antimicrobial Chemotherapy* **2003**, 51 (S2) ii17-ii25.
175. Stalker, D. J.; Jungbluth, G. L., Clinical pharmacokinetics of linezolid, a novel oxazolidinone antibacterial. *Clinical Pharmacokinetics* **2003**, 42 (13) 1129-1140.
176. Lepak, A. J.; Marchillo, K.; Pichereau, S.; Craig, W. A.; Andes, D. R., Comparative pharmacodynamics of the new oxazolidinone tedizolid phosphate and linezolid in a neutropenic murine *Staphylococcus aureus* pneumonia model *Antimicrobial Agents and Chemotherapy* **2012**, 56 (11) 5916-5922.
177. Foye, W. O.; Lemke, T. L., *Foye's Principles of Medicinal Chemistry*. Lippincott Williams & Wilkins: 2008; p 1377.
178. Anderson, B.; Peyster, A. d.; Gad, S.; Hakkinen, P. J.; Kamrin, M.; Locey, B.; Mehendale, H.; Pope, C.; Shugart, L., *Encyclopedia of Toxicology*. 2nd ed.; Elsevier Inc.: 2005.

179. Andersson, T.; Weidolf, L., Stereoselective disposition of proton pump inhibitors. *Clinical Drug Investigation* **2008**, 28 (5) 263-279.
180. Verbeeck, R. K.; Richardson, C. J.; Blocka, K. L., Clinical pharmacokinetics of piroxicam. *The Journal of Rheumatology* **1986**, 13 (4) 789-186.
181. Bree, F.; Urien, S.; Nguyen, P.; Riant, P.; Albengres, E.; Tillement, J. P., A re-evaluation of the HSA-piroxicam interaction. *European Journal of Drug Metabolism and Pharmacokinetics* **1990**, 15 (4) 303-307.
182. Wells, T. G.; Mortensen, M. E.; Dietrich, A.; Walson, P. D.; Blasier, D.; Kearns, G. L., Comparison of the pharmacokinetics of naproxen tablets and suspension in children *Journal of Clinical Pharmacology* **1994**, 34 (1) 30-33.
183. *Molecular Operating Environment (MOE)*, Chemical Computing Group Inc.: 1010 Sherbooke St. West, Suite #910, Montreal, QC, Canada, H3A 2R7, 2011.
184. Willis, J. V.; Kendall, M. J.; Flinn, R. M.; Thornhill, D. P.; Welling, P. G., The pharmacokinetics of diclofenac sodium following intravenous and oral administration. *European Journal of Clinical Pharmacology* **1979**, 16 (6) 405-410.
185. Oberbauer, R.; Krivanek, P.; Turnheim, K., Pharmacokinetics of indomethacin in the elderly *Clinical pharmacokinetics* **1993**, 24 (5) 428-434.
186. Lee, E. J. D.; Williams, K.; Day, R.; Graham, G. C., D. , Stereoselective disposition of ibuprofen enantiomers in man. *British Journal of Clinical Pharmacology* **1985**, 19 (5) 669-674.
187. Lockwood, G. F.; Albert, K. S.; Gillespie, W. R.; Bole, G. G.; Harkcom, T. M.; Szpunar, G. J.; Wagner, J. G., Pharmacokinetics of ibuprofen in man. I. Free and total area/dose relationships. *Clinical Pharmacology & Therapeutics* **1983**, 34 (1) 97-103.
188. Brocks, D. R.; Jamali, F., Clinical pharmacokinetics of ketorolac tromethamine. *Clinical Pharmacokinetics* **1992**, 23 (6) 415-427.

CURRICULUM VITAE
Megan M. McCallum, Ph.D.

EDUCATION:

- **Ph.D. Analytical Chemistry** August 2008 – May 2013
University of Wisconsin – Milwaukee, Milwaukee, WI
Dissertation: “High-throughput approaches for the assessment of factors influencing bioavailability of small molecules in pre-clinical drug development”
Advisor: Dr. Alexander “Leggy” Arnold
- **M.S. Analytical/ Materials Chemistry** August 2006 – August 2008
Central Michigan University, Mount Pleasant, MI
Thesis: “Succinic Based Plasticizers for Poly(Vinyl Chloride)”
Advisor: Dr. Dale J. LeCaptain
- **B.S. Chemistry** August 2002 – May 2006
Central Michigan University, Mount Pleasant, MI
Undergraduate Thesis: “Oxidation of C-C composite aircraft brakes due to runway deicers”

EXPERIENCE:

- **Graduate Research Assistant; University of Wisconsin – Milwaukee; August 2010 - May 2013**
Developed and optimized pre-clinical drug development assays including permeability, solubility, alkylating properties, and protein binding and displacement. Performed high-throughput screening of large drug libraries for ADME properties. Maintained and repaired laboratory instruments (LC-MS, Prep-LC, liquid handling system).
- **Chemistry Teaching Assistant; University of Wisconsin – Milwaukee; August 2008 - May 2013**
General Chemistry, Introductory Biochemistry, and Quantitative Analysis
- **Chemistry Teaching Assistant; Central Michigan University; August 2006 – May 2007**
General Chemistry for both science and non-science majors
- **Graduate Research Assistant; Central Michigan University; May 2006 – August 2008**
Synthesized and tested the properties of succinic ester-based plasticizers for PVC. Performed analysis of the chemical properties of the plasticizers with GC, NMR, IR, and Raman Spectroscopy as well as the mechanical properties of the plasticized PVC with TGA, DSC, Raman, and IR.

- **Undergraduate Research Assistant; Central Michigan University; January 2005 – May 2006**
Researched the effects of acetate and succinate based de-icing solvents on aircraft C-C composite brake pads. The degradation of the material surface was analyzed using SEM and Raman spectroscopy.
- **Laboratory Aide; Central Michigan University; August 2004 – May 2006**
Assisted the instructing professor in the undergraduate laboratories.

MEMBERSHIPS AND EXTRACURRICULAR:

- New Graduate Student Mentor, Department of Chemistry and Biochemistry, University of Wisconsin – Milwaukee; August 2011 – December 2012 and January – May 2013
- Society for Applied Spectroscopy; University of Wisconsin – Milwaukee Student Chapter; 2009 - Present
- American Chemical Society, Member, 2003 - Present
 - Held positions of president, vice president, and treasurer of the Central Michigan University Student Affiliate chapter (2003-2006)

AWARDS:

- *Sosnovsky Award for Excellence in Graduate Research*, University of Wisconsin – Milwaukee (**April 2013**)
- *Graduate School Research Poster Award*, University of Wisconsin – Milwaukee (**April 2013**)
- *Student Travel Award*; Awarded by the Milwaukee, WI section of the American Chemical Society (**March 2013**)
- *Graduate Student Travel Award*; Awarded by the Graduate School at the University of Wisconsin – Milwaukee (**February 2013**)
- *Alumni Poster Award*; University of Wisconsin – Milwaukee Department of Chemistry and Biochemistry (**April 2012**)
- *Chancellor's Graduate Fellowship*; University of Wisconsin – Milwaukee (**2008-2012**)
- *Student Travel Award*; Awarded by the University of Wisconsin – Milwaukee Department of Chemistry and Biochemistry (**April 2011**)
- *Student Travel Award*; Awarded by the Milwaukee, WI section of the American Chemical Society (**March 2011**)
- *Donald R. Wayenberg Memorial Student Travel Grant*; Awarded by the Midland, MI Section of the American Chemical Society (**March 2008**)

- *Outstanding Student Affiliate Chapter of the American Chemical Society*
President, vice president, and treasurer on the executive board which was recognized nationally as an “Outstanding Chapter” for the **2003-2004, 2004-2005, and 2005-2006** academic years

PUBLICATIONS:

1. M. M. McCallum, A. J. Pawlak, A. Simeonov, A. Jadhav, A. Yasgar, D. Maloney, L. A. Arnold, “A Fluorescence-based high throughput method for the quantification of plasma protein binding”, *Journal of Biomolecular Chemistry*, **2013** (In Preparation)
2. P. Nandhikonda, A. Yasgar, A. M. Baranowski, K. Teske, B. Feleke, M. M. McCallum, N. Y. Yuan, C. Kevin, A. J. Pawlak, D. D. Bikle, S. D. Ayers, P. Webb, G. Bantukallu, A. Simeonov, A. Jadhav, D. Maloney, L. A. Arnold; “PPAR δ agonist GW0742 interacts with multiple nuclear receptors including the vitamin D receptor”, *Biochemistry*, **2013** (Submitted)
3. M. M. McCallum, P. Nandhikonda, A. Jadhav, A. Yasgar, D. Maloney, A. Simeonov, J. J. Temmer, L. A. Arnold, “High throughput identification of promiscuous inhibitors among screening libraries with the use of an intrinsically fluorescent probe”, *Journal of Biomolecular Screening*, **2013** (In Press).
4. P. Nandhikonda, W. Z. Lynt, M. M. McCallum, D. Pearson, A. Baranowski, N. Y. Yuan, R. K. Guy, L. A. Arnold, “Discovery of the first irreversible small molecule inhibitors of the interaction between the Vitamin D receptor and coactivators”, *Journal of Medicinal Chemistry*, **2012**, 55(10), 4640-4651.
5. L. Brard, T. S. Lange, K. Robison, K. K. Kim, T. Ara, M. M. McCallum, L. A. Arnold, R. G. Moore, R. K. Singh; “Evaluation of the first Ergocalciferol-derived, non hypercalcemic anti-cancer agent MT19c in ovarian cancer SKOV-3 cell lines”, *Gynecologic Oncology*, **2011**, 123(2), 370-378.
6. Stuart, M. M. McCallum, D. Fan, D. J. LeCaptain, C.Y. Lee, D. K. Mohanty; “Poly(vinyl chloride) plasticized with succinate esters: synthesis and characterization”, *Polymer Bulletin*, **2010**, 65(6), 589-598.
7. M.M. McCallum, D. Fan, C.Y. Lee, D.K. Mohanty, D.J. LeCaptain; “Bio-based plasticizers for poly-vinyl chloride”, *Polymer Preprints*, **2007**, 48(2), 869.

PRESENTATIONS:

1. M. M. McCallum, Alan J. Pawlak, Anton Simeonov, Ajit Jadhav, Adam Yasgar, David Maloney, L. A. Arnold, “A new fluorescence-based high throughput method for the quantification of drug-protein binding” Student Awards Day, University of Wisconsin-Milwaukee, April **2013**.

2. M. M. McCallum, L. A. Arnold, "A new fluorescence-based high-throughput method for the quantification of drug-protein binding" 245th ACS National Meeting & Exposition, New Orleans, LA, April 7-11, **2013**.
3. M. M. McCallum, P. Nandhikonda, J. J. Temmer, L. A. Arnold, "A high-throughput approach for the identification of promiscuous inhibitors among screening libraries with the use of a nucleophilic fluorescent probe" 245th ACS National Meeting & Exposition, New Orleans, LA, April 7-11, **2013**.
4. M. M. McCallum, P. Nandhikonda, L. A. Arnold "High-throughput determination of glutathione binding ability of small molecules with the use of intrinsically fluorescent probes" Student Awards Day, University of Wisconsin-Milwaukee, May **2012**.
5. M. M. McCallum, P. Nandhikonda, L. A. Arnold "High-throughput determination of glutathione binding ability of small molecules with the use of intrinsically fluorescent probes" 243rd ACS National Meeting & Exposition, San Diego, CA, March 25-29, **2012**.
6. M. M. McCallum, L. A. Arnold "Miniaturizing Solubility and Permeability Assays for Small Molecules" Student Awards Day, University of Wisconsin-Milwaukee, May **2011**.
7. M. M. McCallum, L. A. Arnold "Miniaturizing Solubility and Permeability Assays for Small Molecules" 241st ACS National Meeting & Exposition, Anaheim, CA, March 27-31, **2011**.
8. M. M. McCallum, D. Fan, C. Y. Lee, D. K. Mohanty, D. J. LeCaptain, "Determination of molecular interactions between bio-based plasticizers and poly-vinyl chloride" Pittsburgh Conference on Analytical Chemistry and Applied Spectroscopy (PittCon), New Orleans, LA, March **2008**.
9. M. M. McCallum, D. Fan, C. Y. Lee, D. K. Mohanty, D. J. LeCaptain, "Determination of Molecular Interactions of Succinic Based Plasticizers and PVC" Fall Scientific Meeting, Midland, MI, October **2007**.
10. M. M. McCallum, D. Fan, C. Y. Lee, D. K. Mohanty, D. J. LeCaptain, "Bio-based plasticizers for poly-vinyl chloride" 234th ACS National Meeting & Exposition, Boston, MA, August 19-23, **2007**.
11. M. M. McCallum, D. Fan, C. Y. Lee, D. K. Mohanty, D. J. LeCaptain, "Bio-based plasticizers for PVC" Fall Scientific Meeting, Midland, MI, October **2006**.
12. M. M. McCallum, D. Dunuwila, D. J. LeCaptain, "Oxidation of C-C composite aircraft brakes due to runway deicers" 231st ACS National Meeting, Atlanta, GA, March 26-30, **2006**.
13. M. M. McCallum, D. Dunuwila, D. J. LeCaptain, "Oxidation of C-C composite aircraft brakes due to runway deicers" Fall Scientific Meeting, Midland, MI, October **2005**.

14. M. M. McCallum, D. Dunuwila, D. J. LeCaptain, "Oxidation of C-C composite aircraft brakes due to runway deicers" 229th ACS National Meeting & Exposition, San Diego, CA, March 13-17, **2005**.

ACKNOWLEDGEMENTS:

- Acknowledged for input in the review of:
Fahlman, B. D. *Materials Chemistry*; 1st ed.; Springer, 2007.

INVITATIONS:

- Co-moderator for the symposium "Advances in Biopharmaceutical and Pharmaceutical Analysis", ANYL-008, 245th ACS National Meeting & Exposition, New Orleans, LA, April 7-11, 2013.
- Reviewer of the *Journal of Biomolecular Screening*